Towards Automatic Generation of Chemistry Sets for Plasma Modeling Applications

Martin Hanič̆inec

A dissertation submitted in partial fulfillment

of the requirements for the degree of

Doctor of Philosophy

of

University College London

Department of Physics and Astronomy

University College London

January 11, 2022

I, Martin Haničinec, confirm that the work presented in this thesis is my own. Where information has been derived from other sources, I confirm that this has been indicated in the work.

Abstract

Every technique for numerical modeling of low–temperature plasmas usually needs to be centered around a chemistry set (also referred to in the literature as reaction set, reaction mechanism, kinetic mechanism, etc.) Chemistry sets describe the kinetics of volumetric interactions between all the species tracked in the model, and additionally, the kinetics of the interactions between the species, and the surfaces of the modeling domain. Assembling self-consistent chemistry sets is a non-trivial task, mostly addressed by scientists with extensive experience in the field.

This work envisions the *Automatic Chemistry Set Generator*; a method for algorithmic assembling of chemistry sets for low–temperature plasma modeling applications, based on a set of feed gas species and plasma parameters supplied by a user. In particular, two parts of this work detail two distinct steps necessary to be part of such a chemistry generator.

I present a method for fast regression of kinetic parameters for reactions with unknown kinetics, and a method for skeletal reduction of detailed chemistry sets, by identifying redundant species and reactions.

Impact Statement

The present work carries a significant impact for Quantemol Ltd, as the industrial sponsor of my CASE studentship. Both the main outputs of my work described in this thesis, the novel method for fast automated reduction of chemistry sets, and the regression model for fast approximative estimation of rate coefficients of plasma reactions, were developed in direct alignment with the company's interests and product base.

The reduction method is being routinely used already by Quantemol scientists in consultancy projects. In the future, it will likely be embedded in the user interface of the company's database of plasma chemical processes, QDB, together also with the regression model.

Furthermore, the PyGMol plasma global modeling package, which I have written as a part of the reduction method development, has formed the heart of a new Quantemol product, a stand-alone global modeling software currently in development. The global model is now also embedded in the QDB database, triggering positive feedback from Quantemol customers.

Apart from the present thesis, during my PhD project, I also left a lasting impact on other Quantemol products, such as QVT and QEC, where I have coded parts of the graphical user interface.

Finally, as low-temperature plasmas have become an integral part of almost every industry sector, any work aiming to simplify the modeling of plasma physics phenomena has the potential to carry a significant and lasting impact for the field, both in the industry sector and in academia. Both the global modeling package and the chemistry reduction framework, as well as the full regression model for estimation of the plasma reaction kinetics, are published as GitHub repositories.

Acknowledgements

I have received a great deal of support and assistance throughout the years of working on this project and writing this dissertation.

First, I would like to thank my supervisor, Professor Jonathan Tennyson, for his endless insightful feedback and invaluable help with formulating the right research questions.

I would also like to acknowledge my colleagues from Quantemol Ltd. All the presented work is tightly coupled to the company's own research interests and I have received a lot of very helpful advice and feedback, especially from Dr. Sebastian Möhr, who was kind enough to take on the role of my secondary supervisor and mentor.

I could not have completed this dissertation without the support of my wife. You were always there for me, with a sympathetic ear, and ever lifting words of encouragement.

Finally, I would like to thank EPSRC for a CASE studentship under grant EP/N509577/1.

List of Author's Publications

Here, I am listing all the publications I have ever contributed to during my time as a Master's student of Plasma Physics at Masaryk University, as R&D Physicist in the industries of Scanning Electron Microscopy and Plasma Etching, and as a PhD student at UCL. Publications relevant to present work are marked with an asterisk.

* Tennyson, J., Mohr, S., **Hanicinec, M.**, Brown, D., Dzarasova, A., Alves L. L., Bartschat, K., Bogaerts, A., Booth, J. P., Braams, B. J., Bruggemann, P. J., Engelmann, S. U., Gans, T., Goeckner, M. J., Hamaguchi, S., Hamilton, K. R., Hassall, G., Hill, C., Hassouni, K., Krishnakumar, E., Kushner, M. J., Laricchiuta, A., Mason, N. J., Pandey, S., Petrovic, Z. L., Pu, Y. K., Rachimova, T., Ranjan, A., Rauf, S., Schulze, J., Yoon, J. S., Veer, K., Zatsarinny, O., 2021. The 2021 release of the Quantemol database (QDB) of plasma chemistries and reactions. *Manuscript submitted for publication.*

* Mohr, S., Tudorovskaya, M., **Hanicinec, M.**, Tennyson, J., 2021. Targeted Cross-Section Calculations For Plasma Simulations. *Atoms* **9**, 85.

* **Hanicinec, M.**, Mohr, S., Tennyson, J., 2021. Fast species ranking for iterative species-oriented skeletal reduction of chemistry sets. *Plasma Sources Sci. Technol.* **29**, 125024.

  Fulton, H., Ansell, O., Hopkins, J., **Hanicinec, M.**, Nishida, T., Umemoto, T., Li, L., 2020. A Study of Integrated Circuit Dicing Tape When Used in a Plasma Dicing Environment. *IEEE Trans. Compon., Packag. Manufact. Technol.* **10**, 694–703.

Cooper, B., Tudorovskaya, M., Mohr, S., O'Hare, A., **Hanicinec, M.**, Dzarasova, A., Gorfinkiel, J., Benda, J., Mašín, Z., Al-Refaie, A., Knowles, P., Tennyson, J., 2019. Quantemol Electron Collisions (QEC): An Enhanced Expert System for Performing Electron Molecule Collision Calculations Using the R-Matrix Method. *Atoms* **7**, 97.

* Ayilaran, A., **Hanicinec, M.**, Mohr, S., Tennyson, J., 2019. Reduced chemistries with the Quantemol database (QDB). *Plasma Sci. Technol.* **21**, 064006.

Jiruše, J., **Haničinec, M.**, Havelka, M., Hollricher, O., Ibach, W., Spizig, P., 2014. Integrating focused ion beam–scanning electron microscope with confocal Raman microscope into a single instrument. *Journal of Vacuum Science & Technology B, Nanotechnology and Microelectronics: Materials, Processing, Measurement, and Phenomena* **32**, 06FC03.

Jiruše, J., **Haničinec, M.**, Havelka, M., Hollricher, O., Ibach, W., Spizig, P., 2014. FIB-SEM Instrument with Integrated Raman Spectroscopy for Correlative Microscopy. *Microsc. Microanal.* **20**, 990–991.

Jiruše, J., Havelka, M., **Haničinec, M.**, Polster, J., Hrnčíř, T., 2014. New High-Resolution Low-Voltage and High Performance Analytical FIB/SEM System. *Microsc. Microanal.* **20**, 1104–1105.

Skácelová, D., Sládek, P., Sťahel, P., Pawera, L., **Haničinec, M.**, Meichsner, J., Černák, M., 2014. Properties of atmospheric pressure plasma oxidized layers on silicon wafers. *Open Chemistry* **13**.

Pamreddy, A., Skácelová, D., **Haničinec, M.**, Sťahel, P., Stupavská, M., Černák, M., Havel, J., 2013. Plasma cleaning and activation of silicon surface in Dielectric Coplanar Surface Barrier Discharge. *Surface and Coatings Technology* **236**, 326–331.

Contents

Chapter 1

Introduction

Utilizing the unique properties of the low–temperature plasma has become an integral part of almost every industry sector, spanning over a wide range of applications such as medicine, biotechnology, surface modification, microfabrication, harvesting energy, thrusters, ozone generation or abatement systems, to name just a few. As an example of the importance of the low–temperature plasma technologies for our every day lives, it has been estimated that as much as one–third of steps involved in the manufacturing of microelectronic technologies are plasma–based [1]. While providing desirable properties, the very complex nature low–temperature plasma systems also poses challenges for describing and understanding plasma phenomena. Understanding the plasma properties is crucial for the optimization of plasma–based processes and technologies and the only way to acquire an insight of any significant depth is through numerical modeling techniques. It can be argued, that adoption of plasma technologies by various branches of industry is nowhere close to be saturated. In 2019, a patent search using the keywords plasma, cold plasma, non-thermal plasma and gas discharge, revealed more than 1,000,000 granted patents worldwide since 1976, of which about 750,000 have not expired to date [2]. Therefore, any work aiming to simplify modeling of plasma physics phenomena has a potential to carry a very high impact for the field.

There are many methods available for modeling low–temperature plasma properties and behaviour which vary in both accuracy and complexity. No matter what kind of plasma model of whatever spatial dimensionality is considered, each is built

around a chemistry set which describes the volumetric interactions between all the species tracked in the model, and additionally, the interactions between the species and surfaces. A volumetric and surface chemistry set is a very important base for every plasma model, accounting for the majority of sources and sinks of species. Many pre–compiled detailed chemistry sets for various feed gases and applications can be found in the literature, see for example Refs [3; 4; 5; 6; 7; 8; 9]. As a consequence of advances in gas kinetics, published chemistry sets are becoming increasingly larger. For plasma physics modeling applications, chemistry sets may routinely include up to a hundred species and many thousands of reactions. For example, Koelman *et al* [10] provide a chemistry set for the splitting of CO_2 in non-equilibrium plasmas which contains 73 unique species involved in 5724 reactions. In the combustion modeling community, where very large chemistry sets have been used for longer than in the plasma modeling community, some applications require sets that may contain several hundred or even thousands of species and tens of thousands of reactions [11].

1.1 Chemistry reduction

While the more detailed and comprehensive chemistry sets containing many species and reactions might be reasonably universal, they pose challenges with computational resources in multi–dimensional plasma models and as a trade–off, chemistry sets with more manageable sizes are usually optimised for a specific set of plasma conditions and applications.

Any chemistry set might contain redundant species or reactions, which could be removed without compromising any plasma model outputs for the space of model parameters linked to the desired application. In fact, almost all published chemistry sets contain redundant species and reactions [12]. There are two main reasons for this. First, chemistry sets tend to cautiously include species and reactions with uncertain importance for the plasma model built around the given set. Second, even if the importance of each species and reaction is somehow tested, it might be done so for a much wider range of input parameters and conditions, than the range of conditions, the chemistry set is finally utilized over. While large chemistry sets

do not significantly impact the performance of more approximative plasma models with low computational cost, such as volume–averaged 0D models, this is not true for plasma models resolving several spatial dimensions, where the larger chemistry sets (particularly larger numbers of species in the set) means that models can rapidly become prohibitively expensive to run.

While one might come across published chemistry sets which have been reduced to smaller sizes to accurately model only a particular application with a particular set of plasma conditions, such as the chemistry set for plasma in air reduced by Bak and Cappelli [13] from the detailed chemistry set by Kossyi *et al* [14], these published reduced sets are, by design, only valid for a narrow domain of plasma conditions and parameters described in the publications and therefore cannot be readily adopted for a more general case. It follows that methods for identifying and eliminating redundant species (as well as reactions) from very large detailed chemistry sets, or more generally, methods reducing the dimensionality of the underlying systems of partial differential equations are of great importance for more computationally costly plasma models, capable of generating more insight than simple 0D models. The computational cost of solving spatially resolved plasma models increases greatly with the number of species in the chemistry set up to the point, that solving 3D plasma models with more than a few species might become too time–consuming, costly, and impractical. The number of reactions in the chemistry set N_{R} on the other hand does not increase the dimensionality of the system of governing equations but might still increase its stiffness. Then there is also a question of the interpretability of a solution, which might become unclear with very complex chemistry sets.

1.1.1 Existing reduction methods

Several review papers have dealt with the problem of chemistry set reduction, mostly in combustion modeling [15; 16; 17; 18; 19]. Reduction methods might be classified into three main categories: lumping, time-scale analysis, and skeletal reduction [19; 20]. The lumping method [21] may be useful, whenever the species of a chemistry set can be clustered together into groups with very similar chemical properties, and each group can be then treated as one pseudo–species. This method is

used very frequently in plasma modeling, for example for lumping of vibrational levels of species A into few groups [3] or a single lumped pseudo–state A(ν) [22], or for lumping several electronic metastable states into a single compound state A* [22]. Various reduction methods falling under the time-scale analysis category aim to define fast reactions or highly reactive species in the chemistry set and approximate those as partial equilibrium reactions and quasi–steady state species. Their corresponding PDEs can then be solved explicitly as algebraic equations, or their solutions tabulated, decreasing the dimensionality of the whole system of PDEs. Various methods based on time-scale analysis exist, such as quasi-steady state analysis (QSSA) [23], partial equilibrium analysis (PEA), and more systematic approaches including the intrinsic low dimensional manifold method (ILDM) [24; 25] and computational singular perturbation (CSP) method by Lam and Goussis [23; 26; 27; 28] have been widely adopted in the past in plasma and combustion modeling. Finally, skeletal reduction methods seek to identify and eliminate species and reactions unimportant for a given set of particular simulation conditions and applications. As per the scope of this work (further on in section 1.3), the skeletal reduction is an obvious choice for my specific application. Therefore, I concentrate exclusively on skeletal reduction in the present thesis, and ignore the rest.

1.1.2 Skeletal reduction

The skeletal reduction methods can be further categorized as reactions–oriented and species–oriented, based on whether they aim to reduce the number of reactions or species in the kinetic system. Reactions–oriented methods for elimination of reactions from a chemistry set include among others sensitivity analysis [29; 30], and detailed reduction method [31; 32]. The computational cost of running a plasma model is typically mostly driven by the dimensionality of the system of governing PDEs. In a situation, when reaction rate coefficients are treated as known and fixed input parameters, eliminating reactions from a chemistry set does not reduce the system dimensionality. Therefore, decreasing the number of reactions has typically only a marginal effect on the model computation time, due to faster computation of the species sources terms (as well as a possible decrease in stiffness of the system).

It should be noted, that in certain applications of plasma models, rate coefficients might be treated as unknowns (e.g. to be calibrated within the ranges of their uncertainties). In those cases, the number of reactions will play very significant role in the computational costs, however, these cases will not be considered in this work and the species–oriented reduction will be treated with higher importance for the reasons described above.

The simplest method of species–oriented reduction, which is frequently used by the plasma modeling community, is the elimination of species with very low density. This method was used for reduction by, among others, Van Gaens and Bogaerts [6], Liu *et al* [33], and Turner [22], but this method is rather crude and cannot be generalized. More systematic methods for species elimination include, for example, sensitivity analysis [12; 34], Jacobian analysis, CSP [35], principal component analysis (PCA) [36], the simulation error minimization connectivity method (SEM-CM) of Nagy and Turanyi [11], and the directed relation graph method (DRG) of Lu and Law [37; 38; 39] as well as its variations, such the DRG with error propagation (DRGEP) method of Pepiot and Pitsch [40], and DRG–aided sensitivity analysis (DRGASA) [23; 41]. Again, most of the above–mentioned methods were developed and used specifically for combustion modeling, but some were recently also used in plasma–assisted combustion applications (PCA and DRGEP, both by Bellemans *et al* [36; 42]) or even in plasma physics and astrochemistry modeling, such as DRG by Sun *et al* [43], DRGEP by Venot *et al* [44], and sensitivity analysis by Obrusnik *et al* [45]. The majority of the methods mentioned above are even implemented in a single software package by Lebedev *et al* [46].

The existing species–oriented skeletal reduction methods mentioned above all use a thresholding parameter in one form or another, with a somewhat arbitrary value, usually user–determined by the method of trial and error. An example of this might be the threshold value ϵ int the DRG theory, which is a user–defined lower–minimum threshold value for the direct interaction coefficient $w(u, v)$, see (4.3) further in chapter 4, below which the direct interaction between two species u and v is neglected. The fact that the thresholding parameter ϵ is not algorithmically determinable might pose a problem for some automatic applications, such as the chemistry set generator

tool outlined later in section 1.3. The thresholding coefficients ϵ employed in the existing species–oriented skeletal reduction methods generally have a very uncertain mapping to the errors of the model outputs induced by the reduction with given ϵ. The output errors also are not monotonic with ϵ, which forbids the use of binary search to converge towards the optimal ϵ value. Together with the higher computational cost of the existing methods, this fact renders their employment for my intended application somewhat problematic.

1.2 Estimation of reaction kinetics

Another major problem faced by the plasma modeling community is the availability of the reaction kinetic data. Depending on the specific application and the required degree of resolution of the model in question, the chemistry set might be required to contain a very large numbers of reactions. Every single reaction needs to have its kinetic parameters assigned and these data are not always readily available. In chemistry sets for plasma modeling, there are two most common forms of reaction kinetics representation. Kinetics for electron collisions are most commonly represented by their full collisional cross-sections. Heavy species collisions, on the other hand, are typically parametrised by the modified Arrhenius formula (3.5a), although other functional forms are sometimes used.

When compiling a new chemistry set for a given plasma modeling application, a researcher will typically search for the kinetic data in other related chemistry sets, which have already been published, or in one of the databases, compiled and maintained by the plasma modeling community. Publications compiling chemistry sets for various plasma modeling applications, models, and conditions are indeed numerous, and some of them were cited already in chapter 1 above. Moreover, many online databases of plasma kinetic processes are freely accessible. To name a few, there are databases for modeling low-temperature plasmas such as Quantemol Database (QDB) by Tennyson *et al* [9], and LXCat database by Pitchford *et al* [47], the Phys4Entry database by Celiberto *et al* [48] for modeling re–entry plasmas, databases for astrochemical modeling, such as KIDA by Wakelam *et al* [49; 50],

UDfA by McElroy *et al* [51], and BASECOL by Dubernet *et al* [52], or fusion oriented databases by Murakami *et al* [53] of NIFS, Japan, by Park *et al* [54] of Data Center for Plasma Properties, NFRI, Korea, or ALADDIN database maintained by the International Atomic Energy Agency (IAEA) [55].

While numerous, the sources of reaction kinetics data listed above form only a finite and very limited set. A researcher aiming to assemble a new chemistry set (e.g. to model plasma in a novel gas mixture) or to extend an existing chemistry set (e.g. to cover a different range of conditions than what the source chemistry set was published for) will most likely have to tackle the problem of not being able to find any published kinetic data for certain reactions. This problem can be dealt with in several ways. Preferably, the missing kinetics would be either experimentally determined, or calculated from first principles, but accurate results from both are extremely difficult and time–consuming to obtain, and not always possible.

For example experimental determination of electron collision cross sections typically relies on beam attenuation or swarm experiments. Those are generally problematic for collisions with species which can only exist within the plasma state (such as radicals and other unstable species). Experimental methods also pose well–known technical challenges, well summarised in the review papers by Brunger and Buckman [56], and Trajmar *et al* [57]. For those reasons, generally accepted experimental kinetic data for common gases have been around for a long time (e.g. cross sections on molecules of atmospheric gases published in an extensive series of papers by Itikawa *et al*, such as [58]). However, experimental data for more exotic molecules are extremely rare. It has been argued (e.g. by Bartshat and Kushner [59]), that large amounts of data are needed to model electron collisions with sufficient accuracy, and the data cannot be provided by experiments alone. When it comes to experimental measurement of heavy species interactions, the situation is somewhat similar.

Considering the most fundamental and precise level of theory, the accurate description and calculation of even seemingly simple chemical reactions from first principles is a challenging task [60]. Any such calculation requires the knowledge (or pre–calculation) of extended regions of the underlying electronic potential energy

surface (PES) of the molecular system. Very high–dimensional quantum chemical numerical calculations are required to obtain any reliable theoretical predictions. This is reflected by considerable computational complexity, and consequently by many limitations, such as maximal molecule size, and similar.

For the reasons described above, plasma modeling researchers will very often fall back to *estimation by analogy* or an *educated guess*, when confronted with the problem of unavailable kinetic data for certain reactions. In fact, in a typical published chemistry set, a substantial subset of the reactions' kinetics are likely to be estimates. As an example, Turner [22] performed a review of the state–of–the–art chemistry set for helium–oxygen atmospheric pressure plasmas, carefully tracing the primary sources of kinetic data for all the reactions in the set. He found, that 63 out of the total 373 reactions have estimated kinetic data. That is very high fraction considering that He–O_2 is a fairly simple system and might be expected to be better than many, regarding the data availability. The same phenomenon can be observed also in online databases. As an example, I have discovered, that 1298 reactions in the KIDA database, as well as 869 reactions in the UDfA database share the same reaction rate coefficient $k = 7.5 \times 10^{-8}\,(T/300)^{-0.5}$, and the same reference, pointing to the publication by Harada and Herbst [61], which only lists a single reaction[1] with this value of k:

$$\mathrm{C_3N^-} + \mathrm{C^+} \rightarrow \mathrm{C_3N} + \mathrm{C}, \tag{1.1}$$

All the reactions in KIDA and UDfA pointing to this source are *mutual neutralisation* reactions generally in the form of

$$\mathrm{R_1^-} + \mathrm{R_2^+} \rightarrow \mathrm{P_1} + \mathrm{P_2}\ \ (+\mathrm{P_3} + \mathrm{P_4}), \tag{1.2}$$

and their reaction rate coefficients are estimated in the databases by analogy to the reaction (1.1).

Such an estimation practice does have its place in plasma modeling, but it requires a skillful researchers experience, which is difficult to algorithmize and automate. Yet, even a crudely approximative automated and fast–running method for

[1] The paper itself cites a different paper by Smith *et al* [62] as the data source.

estimation of unknown kinetics could be very beneficial for the field, especially for use in automated workflows and applications.

Since the whole part II of this thesis describes my development of a machine learning model for fast regression of unknown kinetic data of binary heavy species reactions, it is only appropriate to dedicate a couple of paragraphs to introduction of the existing methods for computation of reaction kinetics. In the following two sections, I will list some state-of-the-art methods for computation of heavy–species reaction kinetic data, together with some recent advances in the efforts to combine the more traditional computational chemistry with machine learning methods for computational speedup.

1.2.1 Kinetic data calculation

It has been argued (e.g. by Mason and Tennyson in *The 2017 Plasma Roadmap: Low temperature plasma science and technology* [63] or by Bartschat and Kushner [59]), that the majority of atomic and molecular data required by the plasma modeling community for diverse modeling application is expected to be derived from theoretical calculations. Although the equations governing the quantum–mechanical many–body phenomena are believed to be known with a high degree of confidence, their solution with the accuracy needed for reliable quantitative predictions remains a great challenge [59]. A full quantum–mechanical (QM) treatment of, e.g., a heavy particle reaction requires solving the QM potential energy surface (PES) and the Schrodinger equation in $3N - 6$ dimensions, where N is the number of atoms in the molecular target. An effort required to calculate the kinetics from first QM principals for even a single reaction featuring a modest size molecule typically takes the size of an entire PhD project [64]. Furthermore, even with the continuing advances in computational power, the size of the molecules in the reactions that can be described fully quantum–mechanically is severely limited, due to the steep increase in the problem dimensionality with each additional atom in the molecular target. To address these issues, several techniques were devised offering a higher degree of approximation redeemed by lower computational cost. In the space of heavy species processes (relevant to present work), these are mainly the *Molecular dynamics* and

the *Transition–state theory* methods.

The field of *ab initio* molecular dynamics (AIMD) was started with the seminal contribution by Car and Parrinello [65], and since then it has become a cornerstone of modern simulation techniques in many areas of computational science [66]. The AIMD simulation method combines classical molecular dynamics of nuclei with on–the–fly calculation of interaction potentials from electronic structure theory (typically using the method of Kohn–Sham density functional theory [67]). The theory is beyond the scope of this thesis, but several review papers and books have been written addressing AIMD theory in detail, e.g. by Hutter [66], Remler and Madden [68], Galli, and Pasquarello [69], or by Marx and Hutter [70].

In their historical account [71] of the theory, Laidler and King date the origins of the Transition–state theory (TST) to Henry Eyring in 1935 [72]. Since then, TST might be considered a general name for any theory, based in whole or in part on the fundamental assumption, that there exists a or surface in phase space with two properties: (1) it divides space into a reactant region and a product region, and (2) trajectories passing through this surface in the direction of the products originated at reactant region and will not reach the surface again before being thermalized or captured in a product state [73]. TST rate coefficient of a volumetric reaction is then proportional to the total flux of classical trajectories from reactant to product side of the dividing surface and is determined by the transition–state barrier height. Many books and review papers describe the theory to an extent beyond the scope of this thesis, among others e.g. by Pechukas [74], or by Miller [75].

Apart from the more or less sophisticated methods described in the earlier paragraphs, there also exist several very approximative ways of estimating reaction rate coefficients for some specific reaction families, such as the *Langevin* rate coefficients [76] for barrier–less processes of ions and polarizable molecules, calculated classically with the assumption that the reaction occurs upon every collision.

1.2.2 Machine learning in plasma and chemistry

Machine learning (ML) is used nowadays very extensively in plasma physics, processing, and modeling, as well as in computational chemistry. A sizable body of

research has been done on artificial neural network (ANN) models used as *surrogate models* for prediction of macroscopic plasma processing outputs (such as etch rate, deposition rate, etc.) from the processing reactor control variables, such as RF power, pressure, or feed gas flows. Examples from plasma *etch* process modeling and real–time process control include, among others, the extensive work of Kim *et al* on this subject [77; 78; 79; 80], Himmel and May [81], Rietman and Lory [82], Han *et al* [83], Stokes and May [84], or Tudoroiu *et al* [85]. The same is true for other areas of plasma processing. The plasma *deposition* process control modeling researchers have also been using ML, including e.g. Rosen *et al* [86], Bhatikar and Mahajan [87], Chen *et al* [88], or Ko *et al* [89]. ANNs have been further used to model plasma *spray* processes (e.g. by Guessasma *et al* [90], Jean *et al* [91], and Choudhury *et al* [92]), for modeling of plasma *sputtering* (e.g. by Krueger *et al* [93] or Kino *et al* [94]), plasma–assisted *nano–particle synthesis* (e.g. by Leparoux *et al* [95]), or plasma *surface modification* (e.g. by Wang *et al* [96], or Abd Jelil *et al* [97]). Finally, there is also a large amount of work dedicated to the utilization of ANNs in any plasma processing generally, such as by Rietman [98], Salam *et al* [99], Molga [100], Kim *et al* [101; 102], or Mesbah and Graves [103].

Apart from modeling plasma processing, control, and diagnostics, ANNs have also been used to augment some traditional quantum chemistry calculation methods. As examples, one might cite the work of Dral *et al* [104], using ML models for learning the parameters for semi–empirical quantum chemistry calculation methods from molecule structure, or the work of Komp and Valleau [105] using deep ANNs for prediction of quantum reaction rate constants of simple systems trained on calculated data, to overcome the high cost of ab initio calculation. Zhang [106] used ANNs for estimation of standard enthalpies of formation of several kinds of acyclic alkanes, and Hansen *et al* [107] used ML methods for predicting molecular atomization energies. The review paper by Goh *et al* [108] summarizes the use of deep learning in computational chemistry.

Pertinent to the present work, ML techniques were also used in the calculation of chemical kinetics. In the work by Ventura *et al* [109] and Galvan *et al* [110], ANNs were used for curve–fitting complex experimental kinetic data, bypassing ki-

netic models built around chemistry sets altogether. Bas *et al* [111; 112] developed an ANN model for estimation of reaction rate of the catalyzed enzymatic hydrolysis of maltose into glucose, also bypassing a kinetic model. Valeh-e-Sheyda *et al* [113] applied ANN trained on experimental data to estimate the reaction rate of methanol dehydration as a function of temperature, pressure, and the purity of the feed stream. Tumanov and Gaifullin [114] describe ANNs learning the activation energies of reactions of phenyl radicals with hydrocarbons at a single given temperature. Allison [115] trained an ANN to learn to predict rate coefficients of reactions of ·OH radicals from the bonds and bends of the selected set of possible reactants. Choi *et al* [116] discuss the feasibility of activation energy prediction of gas–phase reactions by gradient–boosted trees method from structural and thermodynamical properties of the molecules, as does Grambow *et al* [117] using deep learning. Kuang and Xu [118] showcased the use of a convolutional neural network for the prediction of kinetic triplets for pyrolysis processes from experimental data, more specifically the temperatures at pre–selected values of conversion degrees. Very similar work has also been done by Huang *et al* [119], and Vieira *et al* [120].

In most cases, a research work intersecting ML and chemical kinetics introduces ANNs and other ML model techniques (or *soft* computing) as an alternative to the hard kinetic model of a system, which typically integrates the differential equations governing the species densities to calculate the reaction rates. Inputs to such models are typically absorbance, concentration, temperature, pH, etc. This "soft" approach for chemical kinetics is reviewed nicely in the paper by Amato *et al* [121]. Unfortunately, such methods are not entirely relevant to the work I am aspiring to do in my PhD project, which is to develop a model to estimate kinetic parameters for a chemistry set as an input for a hard kinetic model.

1.3 Scope of this work

In this dissertation, I envision an *Automated Chemistry Set Generator* application, which could be attached to an online database of plasma kinetics. An input for such an application would take the form of the required plasma feed gas mixture,

a set of plasma conditions and simulation parameters, and a set of observables of interest. The output would be an optimized chemistry set of a minimal size, required for accurate modeling of all the observables of interest. A diagram of a possible workflow of such an application is proposed as figure 1.1

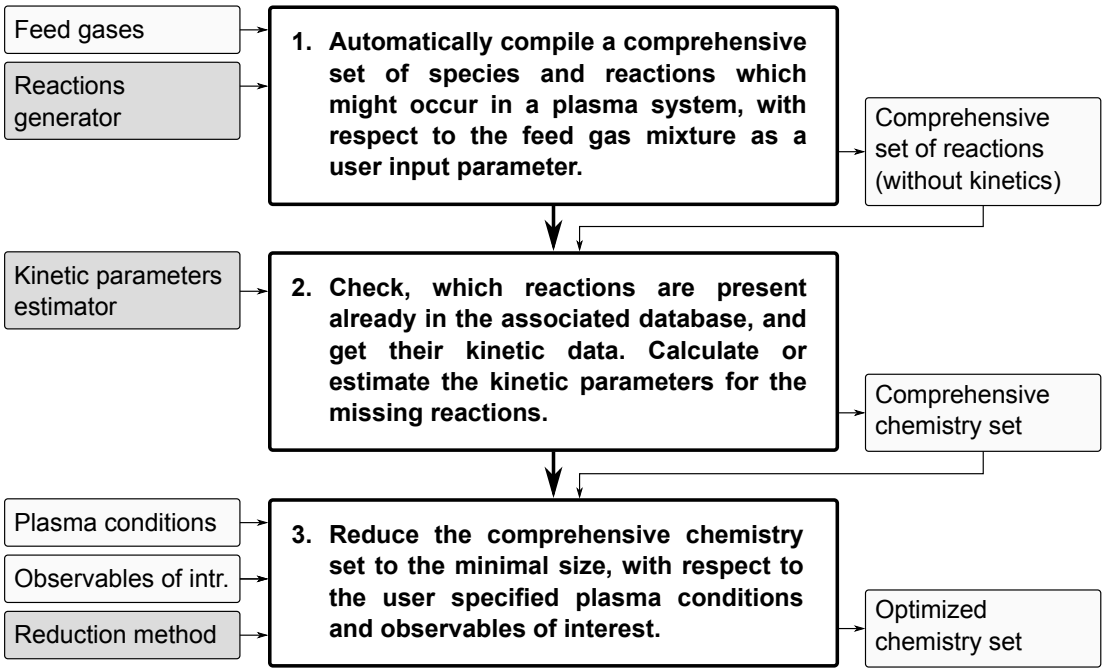

Figure 1.1: A flow diagram of the proposed chemistry set generator application. Three separate stand–alone components are shown, powering the application. Inputs to the components are placed on the left-hand side of the figure, while outputs are on the right. The final output of the proposed chemistry set generator app is the *optimized chemistry set*.

In this implementation, the chemistry set generator app would be powered by three stand–alone automated components.

In *the first step*, the method would identify a comprehensive set of species and reactions which might appear in a plasma for the given mixture of feed gases, with no regard to the kinetic data for the identified reactions. In *the second step*, the kinetics for each reaction identified in the first steps are attached. The kinetic data are either simply retrieved from the attached database, or dynamically computed, where no kinetics are available. This produces a comprehensive chemistry set. Finally, in *the last step* of the algorithm, the comprehensive chemistry set is reduced to an optimal size, based on the user–defined plasma conditions and observables of interest, outputting the optimized chemistry set. In this (rather abstract) definition,

outlined as figure 1.1, all the three stand–alone steps rely on automated methods, depicted as inputs in a slightly darker shade of gray. In the proposed implementation, these methods are called *Reactions generator*, *Kinetic parameters estimator*, and *Reduction method* respectively.

As this topic is far too big to be covered by a single PhD project, I have limited my focus only on the steps no. 2 and 3 from figure 1.1, and their respective automated methods. Additionally, I have limited the scope of the kinetic parameters estimator to predicting kinetics of *binary heavy species reactions* only, in an attempt to further reduce the workload to fit the typical PhD thesis time budget. A novel method for fast skeletal reduction of chemistry sets is presented in part I of the thesis, while in part II, I explore the feasibility of a fast data–based regression model for estimation of unavailable reaction kinetics from accessible data. The ordering of the thesis parts does not align with the order of the steps depicted in figure 1.1, but rather reflects how I have tackled this project chronologically. Both methods detailed in the theses are intended to form the foundation of a chemistry generator add-on module for the QDB database [9]. This, however, does not limit in any way the generality of the ideas presented. Finally, the core of part I of this dissertation, describing the development of a novel skeletal reduction method for reduction of chemistry sets for plasma modeling, has also been published already [122].

1.4 Thesis structure

This thesis is divided into three parts. Part I details the development of the novel *ranking–based species–oriented iterative skeletal reduction method*, together with a thorough assessment of different possible *species ranking schemes*. Part II describes my development of a very fast machine learning–based regression model for crude estimation of reaction kinetics. Finally, in part III, I discuss some conclusions and outline possible future work.

Part I is divided into several chapters. The first chapter after this Introduction, chapter 2, provides an overview of the reduction method I developed during this PhD project. Chapter 3 gives thorough documentation of *PyGMol*, the plasma

global model I have developed specifically for this project. In chapter 4, I present some competing species ranking schemes, based on a graph representation of comprehensive chemistry sets. An appropriate species ranking scheme is a crucial input for the reduction method to perform well. Different methods of chemistry graph edge weight distribution are considered, all based on a single evaluation of a plasma model with the detailed chemistry set and different flavors of the underlining theory. Chapter 5 details several test reduction cases which are used to identify the statistically best–performing ranking scheme, and finally, chapter 6 summarizes the results.

The chapters of part II are as follows: In chapter 7, I build a case for utilizing machine learning to meet my objective of a very fast regression model of reaction kinetics and provide some theory behind the particular machine learning methods used in the work. Chapter 8 describes the raw training dataset and how exactly it was compiled, while the next chapter 9 details the preprocessing of the training dataset and describes in detail how it was trained. In chapter 10, I give all the results of the final trained regression model for predicting the reaction kinetics, such as the generalization error evaluation on a withheld test set, as well as some interesting analysis of the data and the predicting capability of the model.

Finally, part III only contains a single chapter 11, summarizing the conclusions and outlook into some interesting future work possible.

Part I

Automatic Reduction of Chemistry Sets

Chapter 2

Ranking–based iterative reduction method

In this work, I present a simple chemistry set reduction method overcoming the difficulties suffered by other existing reduction methods mentioned in the Introduction (chapter 1). The method is based on ranking all the species in the model based on their importance for modeling densities of a defined set of species of interest and iteratively eliminating the lowest–ranked species, while periodically checking after each iteration, if the reduction error does not exceed a defined maximum threshold value. This way, the validity of the reduced chemistry set is always ensured with respect to the pre–selected species of interest, and the set of reduction conditions. The following section outlines the general framework behind the method and some key concepts, while the species ranking method development is described in chapter 4.

2.1 Introduction of the method

Table 2.1 lists all the key concepts and definitions that are important for this work. The general structure of the reduction method presented is summarized by the flow diagram given as figure 2.1.

The method uses a *plasma model* to generate results used as inputs for a species ranking method and also to check the *reduction error* after each species elimination. Although the reduction framework described here is defined very generally,

Table 2.1: Key concepts and definitions for the ranking–based iterative reduction method.

Concept	Definition
Detailed chemistry set	The set containing all the species and reactions.
Reduced chemistry set	A set with at least one species eliminated from the detailed set.
Species elimination	Removal of all the reactions involving the given species (on either side).
Reduction conditions	A set of application–specific conditions (such as pressure, power, etc.), for which the reduced chemistry set should yield a low *reduction error*.
Reduction error δ	The collective relative difference of *outputs of interest* between the detailed and reduced models.
Allowed error Δ	Maximal δ allowed.
Outputs of interest	Set of outputs, which need to be modeled within Δ using the reduced chemistry set. This can generally be any *plasma model* outputs, but most frequently species' number densities.
Species of interest	Species, whose densities are among the *outputs of interest*.
Species ranking	Species hierarchy reflecting how important each species is for modeling all of the *outputs of interest*. Rank of each species in the chemistry set is determined by its *ranking score*.

throughout this work I used the *PyGMol* 0D global model as a *plasma model*, and the *reduction error* took the form of a *mixed error* function adopted from the work of Nagy and Turanyi [11]

2.1.1 Plasma model

A plasma model plays a crucial role in the reduction process. The validity of a reduced chemistry set is ensured by comparing outputs of interest of the plasma model for the detailed and reduced chemistry set and ensuring their difference is sufficiently small. Outputs of the plasma model are also needed for the species ranking step. Since the plasma model needs to be run in every single iteration of the reduction process, care must be taken to employ sufficiently fast plasma model.

The global model used throughout this work was the *PyGMol* (Python Global Model), which was developed as a part of this work and specifically for the reduction method presented. Although there are several global models available within the

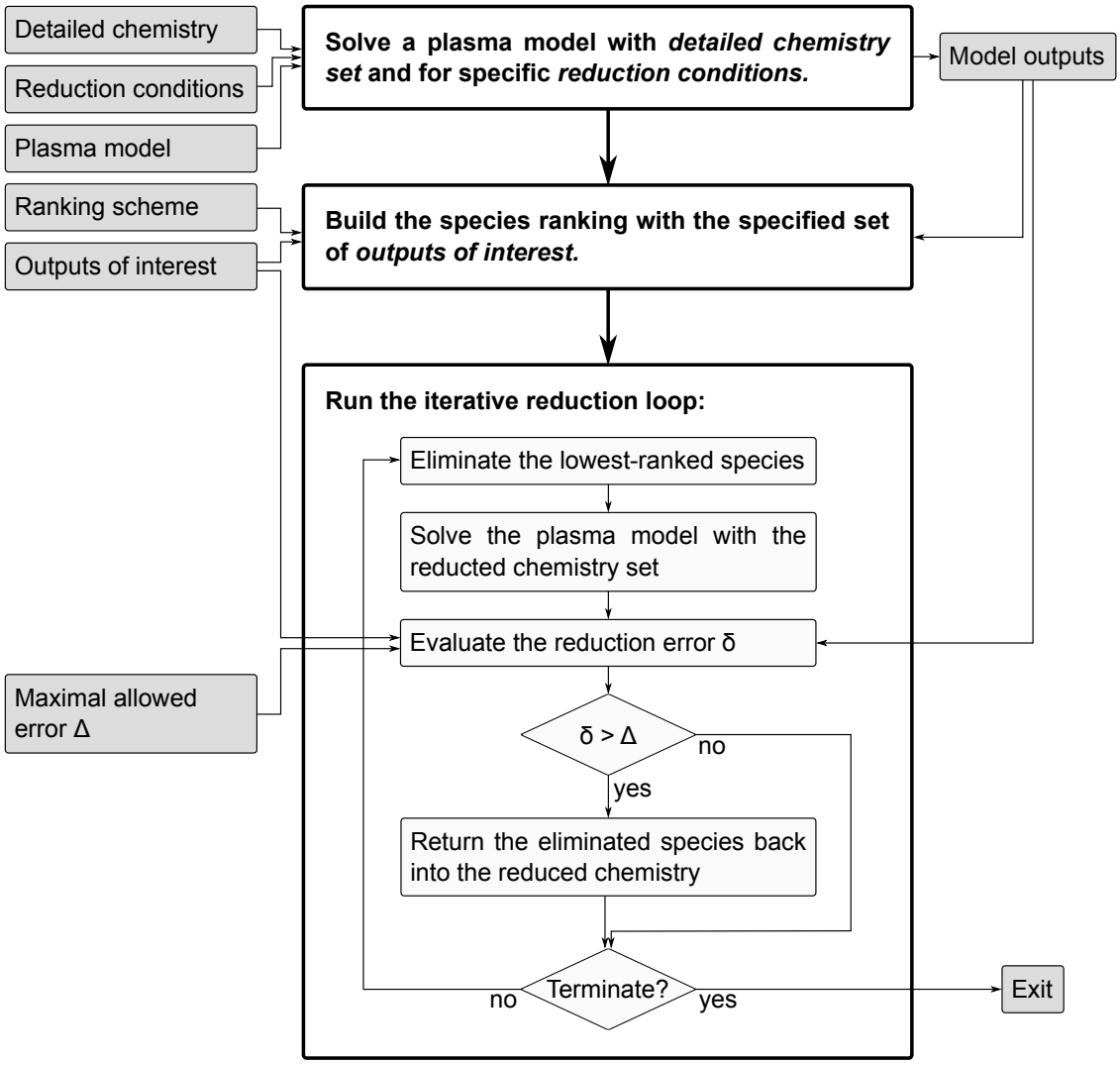

Figure 2.1: Flow diagram outlining the general structure of the species–oriented reduction method framework presented in this work. Inputs to the reduction method are on the left–hand side of the diagram.

plasma modeling community, such as GlobalKin by Kushner [123], Plasma-R by Kokkoris [124] or ZDPlasKin by Pancheshnyi *et al* [125], the choice of developing a new code was driven by the need for Python implementation which allowed seamless integration with the rest of the reduction framework.

A detailed description of the PyGMol global model is given in Chapter 3. While obviously being heavily approximative, the PyGMol model should however suffice here, since the quantitative results of the model are not the aim of the present work; an equally simplistic model was used in a similar study by Turner [22; 126].

It should be noted, that the framework of the iteration–based reduction method

is independent of the plasma model. Any fast–running plasma model will be appropriate, as long as it satisfies the following conditions:

- A set of inputs for the plasma model includes (or can be mapped to) the *reduction conditions*
- A set of outputs of the plasma model includes (or can be mapped to) the defined *outputs of interest*, and allows for creation of the *species ranking*.

2.1.2 Reduction error

In this work, the reduction error δ takes form of a *mixed error* adopted from the work of Nagy and Turanyi [11]. Since the PyGMol global model outputs time–dependent outputs, each output of interest A_i is sampled over a set of pre–selected *times of interest* $\{t_j\}$. The concept of the times of interest is further elaborated on in chapter 4.

Local error $\delta_i(t_j)$ of output of interest A_i at time t_j is expressed by the following error function:

$$\delta_i(t_j) = 2\frac{\mathrm{A}_i^{\mathrm{red}}(t_j) - \mathrm{A}_i^{\mathrm{full}}(t_j)}{\mathrm{A}_i^{\mathrm{full}}(t_j) + \mathrm{A}_{i,\mathrm{max}}^{\mathrm{full}}}, \tag{2.1}$$

where $\mathrm{A}_i^{\mathrm{red}}(t_j)$, and $\mathrm{A}_i^{\mathrm{full}}(t_j)$ are values of the output of interest A_i associated with reduced and detailed chemistry sets respectively evaluated at time t_j, and $\mathrm{A}_{i,\mathrm{max}}^{\mathrm{full}}$ denotes maximum over all the times of interest

$$\mathrm{A}_{i,\mathrm{max}}^{\mathrm{full}} = \max_j \mathrm{A}_i^{\mathrm{full}}(t_j). \tag{2.2}$$

The index i runs over all the outputs of interest A_i, and the index j runs over the *times of interest* $\{t_j\}$. This way, the local reduction error takes form of

$$\delta_i(t_j) = \begin{cases} \dfrac{\mathrm{A}_i^{\mathrm{red}}(t_j) - \mathrm{A}_i^{\mathrm{full}}(t_j)}{\mathrm{A}_i^{\mathrm{full}}(t_j)} & \text{if } \mathrm{A}_i^{\mathrm{full}}(t_j) \sim \mathrm{A}_{i,\mathrm{max}}^{\mathrm{full}}, \\ \\ \dfrac{\mathrm{A}_i^{\mathrm{red}}(t_j) - \mathrm{A}_i^{\mathrm{full}}(t_j)}{\mathrm{A}_{i,\mathrm{max}}^{\mathrm{full}}/2} & \text{if } \mathrm{A}_i^{\mathrm{full}}(t_j) \ll \mathrm{A}_{i,\mathrm{max}}^{\mathrm{full}}, \end{cases} \tag{2.3}$$

which appropriately behaves as a relative error at output values close to the maximal

values over times t_j, but loses significance for values much lower than maximal values, where it behaves as a scaled absolute error.

The global reduction error δ is finally defined as a maximum of local error function over the space of both times and outputs of interest

$$\delta = \max_{i,j} \mid \delta_i(t_j) \mid . \tag{2.4}$$

Although any choice of different error metrics can be generally implemented within the reduction method presented, in this work, error function defined by equations (2.1), and (2.4) was used exclusively.

2.1.3 Termination Condition

The condition for terminating the reduction method from figure 2.1 was set to be N_δ *subsequent* iterations resulting in exceeding the maximal reduction error allowed $\delta > \Delta$. An appropriate value of N_δ must be chosen to balance the trade–off between the number of eliminated species, and the number of plasma model calls. As with other parts of this loosely defined reduction framework, various different termination conditions are of course possible, but this one was used exclusively in this work.

2.2 Influence of species ranking

It is clear, that the method for ranking the species (or the species ranking scheme) is the most important part of the reduction method presented. Good species ranking scores should correlate strongly with the error in the species of interest densities induced by removing the species from a chemistry set. Completed reduction runs may be analyzed by plotting the reduction error as a function of the number of species retained in the chemistry set. As an example, figure 2.2 shows such a reduction plot for an N_2–H_2 chemistry set (described more closely in section 5.2), and plasma model with arbitrary reduction conditions. The solid line starts with the detailed chemistry set containing in total 42 species, and follows all the species eliminated from the set while keeping the reduction error δ below the maximal value

allowed (in this case, $\Delta = 10\%$). The dotted lines show species, which could only be eliminated with an unacceptable reduction error, and were therefore reinstalled back into the chemistry set. The species ranking order coming into the reduction method in this particular case was [N_3^+, N(^{2}D), N(^{2}P), N^+, NH^+, NH_2^+, H^+, NH_3^+, $H_2(B\,^1\Sigma_u^+)$, $H_2(\nu_3)$, $H_2(\nu_2)$, $H_2(a\,^3\Sigma_g^+)$, N_4^+, $N_2(a'\,^1\Sigma_u^-)$, $N_2(\nu_8)$, $N_2(\nu_7)$, $N_2(C\,^3\Pi_u)$, $N_2(\nu_6)$, $N_2(\nu_5)$, $N_2(\nu_4)$, $\cdots$], where subsequent unsuccessful elimination of the three species $N_2(\nu_6)$, $N_2(\nu_5)$ and $N_2(\nu_4)$ triggered the termination condition for $N_\delta = 2$. Figure 2.2 also demonstrates that the reduction error is generally not monotonic with the number of species eliminated.

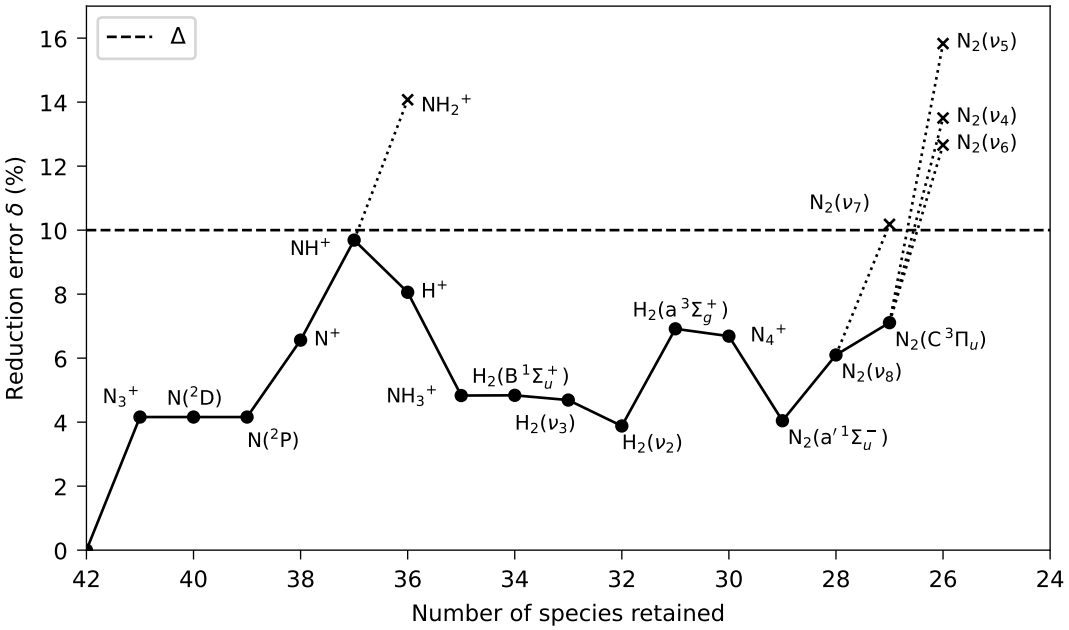

Figure 2.2: A reduction plot for an N_2–H_2 chemistry set and plasma model with arbitrary reduction conditions. The error function is plotted against the number of species retained in the chemistry. The solid line follows all the species eliminated from the chemistry set while keeping the reduction error δ below the maximal value allowed (dashed line). The dotted lines show species that could not be eliminated from the chemistry set with an acceptable reduction error. The species eliminated (or not eliminated) at each iteration are given next to the plotted points.

There will be, of course, potentially large differences between different ranking schemes in the size of the resulting reduced chemistry sets, where better species ranking yields fewer redundant species left in the reduced set. Figure 2.3 shows the same reduction plot as in figure 2.2, this time compared together with 4 other

different ranking schemes (annotation of eliminated species is omitted for clarity). It can be seen, that the number of eliminated species at the end of the reduction procedure differs for each ranking scheme greatly (between 6 and 15). Another thing to note, is that reduction procedures for the two ranking schemes labelled as *rank. #1*, and *rank. #3* are both terminated with 15 eliminated species, but the set of eliminated species is clearly different for both (resulting in a different reduction error). Although this might often be the case, large number of eliminated species will generally be shared between the two ranking schemes in cases like this.

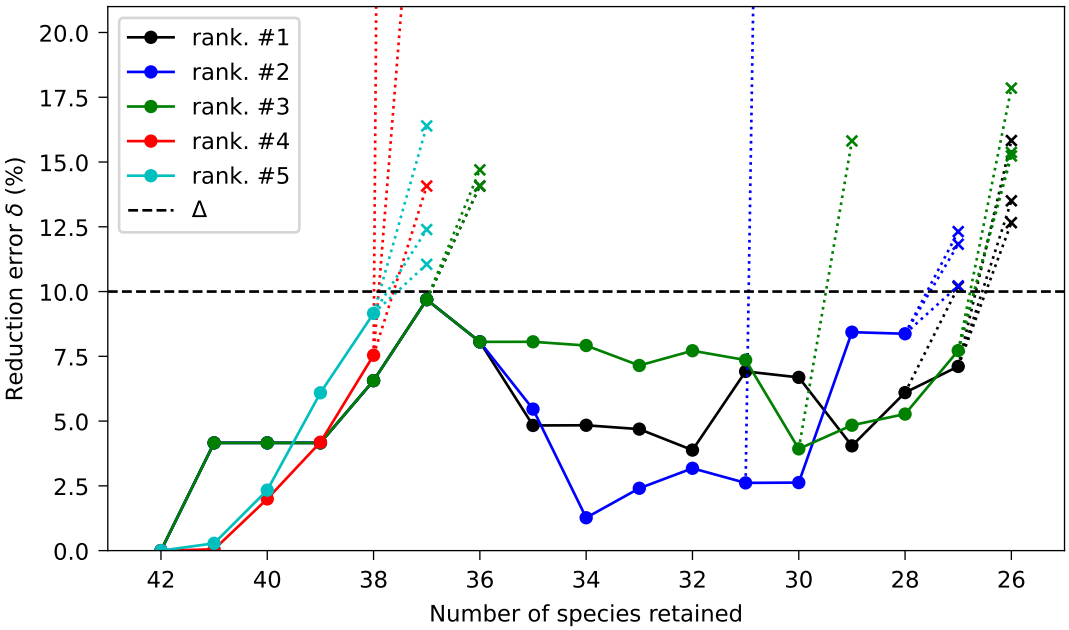

Figure 2.3: Reduction plots for several different arbitrary species ranking schemes for N_2–H_2 chemistry and plasma model with arbitrary reduction conditions. The error function is plotted against the number of species retained in the chemistry. The solid lines follow all the species eliminated from the chemistry set while keeping the reduction error δ below the maximal value allowed (dashed line). The dotted lines show species that could not be eliminated from the chemistry set with an acceptable reduction error.

Some caveats need to be noted regarding the process of species elimination from a chemistry set. The integrity of the chemistry sets needs to be protected at all times. For example, each retained species must have at least one production and consumption channel and at least one positive ion must be retained in the set. This adds extra constraints on species elimination. Similarly, in some cases, elimination of a species upsets the balance of the chemistry set to the point where the plasma

model solution fails. Cases like this are treated as if the iteration resulted in a higher than allowed reduction error. Also, elimination of one species might instantly trigger elimination of another, if the set of reactions associated with the first species contains all the reactions associated with the second. Figure 2.4 shows such a situation during N_2–H_2 chemistry reduction (different reduction conditions than in figures 2.2 and 2.3), where elimination of atomic nitrogen N removes all the reactions involving both excited states N(^{2}P) and N(^{2}D), leaving the chemistry set with 22 species retained at that point. Safeguards against inconsistent chemistry sets after species elimination are coded into the elimination routine of the framework.

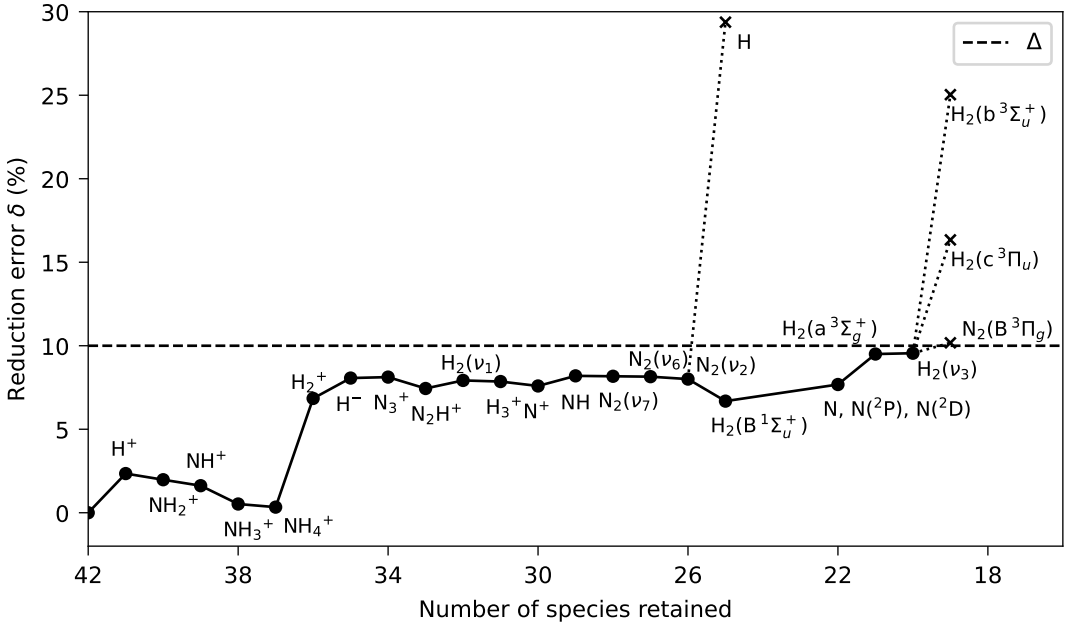

Figure 2.4: A reduction plot for N_2–H_2 chemistry and plasma model with arbitrary reduction conditions, showing that elimination of a single species might trigger other species to be eliminated in the same iteration. The error function is plotted against the number of species retained in the chemistry. The solid line follows all the species eliminated from the chemistry set while keeping the reduction error δ below the maximal value allowed (dashed line). The dotted lines show species that could not be eliminated from the chemistry set with an acceptable reduction error. The species eliminated (or not eliminated) at each iteration are given next to the plotted points.

2.3 Dynamic ranking–based iterative reduction

If it is the case, that the species ranking procedure carries only a marginal computational cost compared to the plasma model evaluation, it can be inserted into the main iterative reduction loop, updating the species ranking inside each iteration. The flow diagram for this *dynamic ranking–based iterative reduction* procedure is given as figure 2.5.

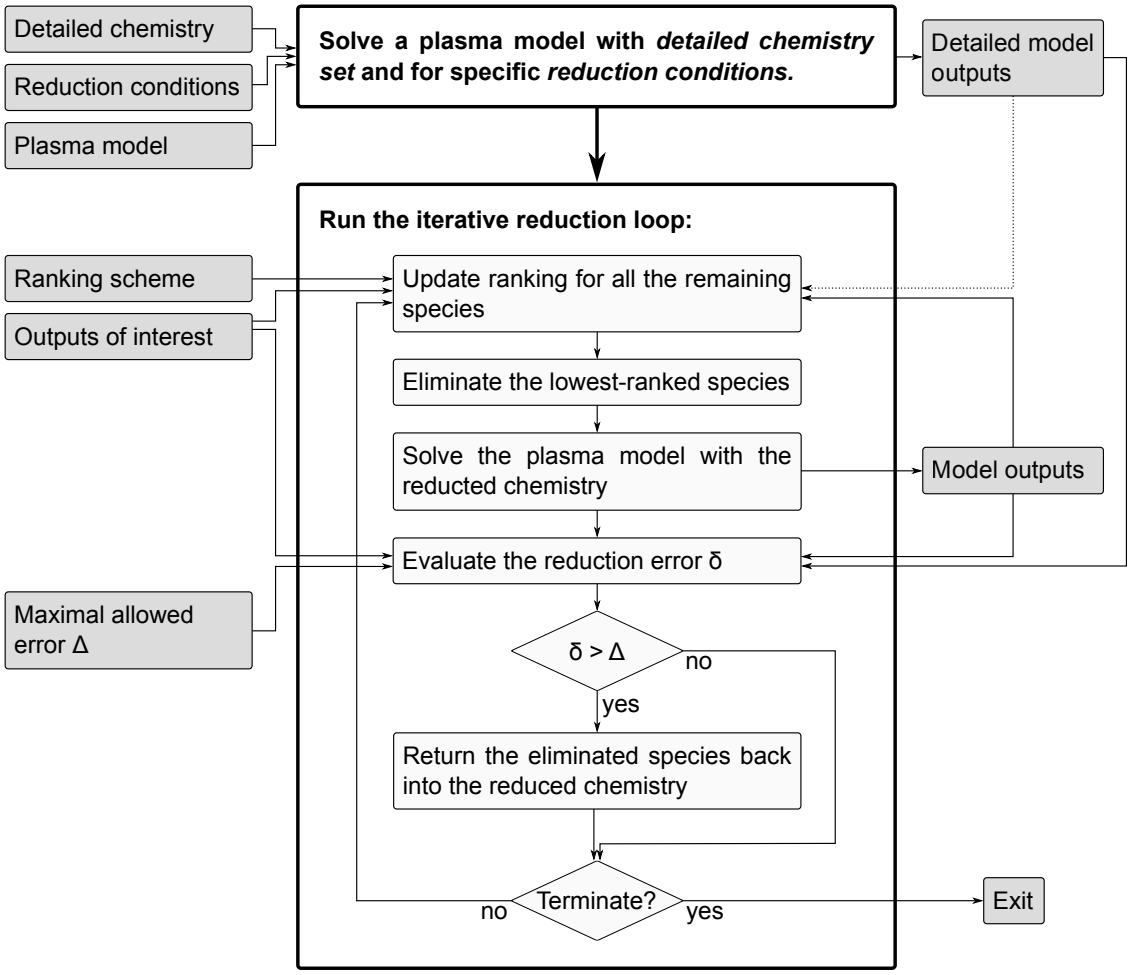

Figure 2.5: A flow diagram outlining the general structure of the dynamic species–oriented reduction method framework. This is a modified method to the *static* method shown on Figure 2.1, with the species ranking being updated inside the iterative reduction loop.

2.4 Reduction validity

Finally, it needs to be noted, that validity of the reduced chemistry set for all the species of interest is strictly ensured within the density error Δ only in the scope of the same plasma model that was used in the reduction method. This plasma model, of course, needs to be sufficiently simple to handle the full detailed chemistry set with very fast run–time, so no reduction is strictly necessary, when using the simple model only. Reduced chemistry sets need to be created for more sophisticated (usually spatially resolved) plasma models where the number of species in the set is of much greater importance. In a case of any *end–application* plasma model (different from the one used in the reduction process), the validity of the reduced chemistry set cannot be readily extrapolated and completely ensured. The use of any reduced chemistry set should therefore always be preceded by careful consideration of the similarity of both the plasma models. As an example, if a reduced set is expected to be used within a plasma model capturing the same *physics* as the plasma model employed in the reduction method, only in multiple dimensions, it might be appropriate to run the reduction method for more than one point of the *reduction conditions* parameter space and/or use lower maximal reduction error Δ within the reduction method, than what is an acceptable accuracy of the end–application model.

By the same token, the validity of the reduced chemistry set is by design only ensured for the single set of plasma conditions that are the reduction conditions. More specifically, if certain model parameters, such as pressure p (or the related total tensity n), or the neutral species temperature T_{g}, are used to calculate the species ranking, and this ranking is used to perform a chemistry set reduction, the reduced chemistry set will *only* be appropriate for modeling plasma with the same p, (n), T_{g}. When performing a chemistry set reduction targeting a specific modeling application, it might be appropriate to run the reduction with multiple sets of reduction conditions sampled from the parameter space, and only eliminate species that are flagged redundant in all of those runs. Such a parameter sweep, however, can be performed on top of the reduction method presented in this work

and therefore will not form part of this work.

In the method as described, the actual species ranking *scores* are not at all taken into account, only the *ordering* of the ranked species. Further speed–up might generally be possible by clustering the ranked species according to their ranking scores and iteratively eliminating whole clusters one–by–one. However, one might imagine a situation, when eliminating one species of such a cluster might distort the outputs of interest completely, while eliminating a second species from the cluster might compensate the kinetic mechanism exactly in the way that the outputs of interest change back close to the ones from before the cluster elimination. If we are interested, for example, in modeling densities of some species of interest, this might be undesirable, since although correct densities of the selected species modeled with the reduced chemistry would still be ensured by the method, the exact pathways of production or consumption of those species might not remain unchanged with the reduction. On the other hand, if only a single species is eliminated in each iteration, and the maximum allowed error Δ is kept sufficiently small, the outputs of interest together with their main pathways should be conserved by the reduced chemistry set.

Chapter 3

Global model

The ranking–based iterative reduction method presented in chapter 2, and in figures 2.1, and 2.5 uses outputs of a plasma model to build the species ranking, and to evaluate the reduction error.

This chapter describes the PyGMol global model, which was used throughout the present work for this purpose. All the equations which are being solved for by the model are shown explicitly, with the intention of providing the most complete and transparent description possible. For a better clarity, Table 3.2 summarizes all the symbols and quantities defined in the PyGMol documentation. The model calculates the number densities n_i (where the index i runs over all the heavy species in the associated chemistry set), as well as the electron temperature T_e, as a function of time by integrating the set of particle density balance and electron energy density balance ordinary differential equations (ODE):

- **Particle density balance equation for heavy species**, including contributions from volumetric reactions, flow and from diffusion sinks and surface sources of n_i.

- **Electron energy density balance equation**, including contributions of power absorbed by the plasma, elastic and inelastic collisions between electrons and heavy species, generation and loss of electrons in volumetric reactions and power lost to the walls by electrons and ions.

The electron density n_e is not solved for explicitly but rather implicitly by enforc-

ing the charge neutrality. The heavy species temperature T_g is treated as a constant input parameter, rather than being solved for self–consistently. The collisional kinetics is not described by cross sections, but rather parametrized for each reaction with the Arrhenius formula, Eq. (3.5a), (3.5b). The model was developed mainly for the purpose of plasma chemistry reduction, which justifies its simplicity and the degree of approximation. For those reasons, the model should only be used with a great care to obtain any sort of quantitative results.

The inputs and outputs of the PyGMol plasma model are summarized in table 3.1. The rest of this chapter describes all the equations in detail.

Table 3.1: Summary of all the inputs and outputs of the PyGMol global model of plasma.

Inputs	
Plasma parameters:	P, p_0, Q_i, R_p, Z_p, $\mathrm{T_g}$
Chemistry parameters:	M_i, q_i, σ_i^LJ, k_j, $\Delta E_{\mathrm{e},j}^\mathrm{inel}$
Outputs	
Number densities:	n_i, n_e
Electron temperature:	T_e

Table 3.2: Overview of symbols used in the description of the presented global modelling framework.

Symbol	Unit	Description
i, k		Index, running over species in a chemistry set
i_0, i_+, i_-		Indices i running over neutral, positive and negative species respectively
j		Index, running over reactions in a chemistry set
N_S		number of species in a chemistry set
n_i	$[\mathrm{m^{-3}}]$	Number density of the i-th species in a chemistry set
n_e	$[\mathrm{m^{-3}}]$	Electron number density
ϱ_e	$[\mathrm{eV{\cdot}m^{-3}}]$	Electron energy density
P	[W]	Absorbed power
p_0	[Pa]	Desired pressure
p	[Pa]	Instantaneous pressure
Q_i	[sccm]	Feed flow for i-th species in a chemistry set
$R_\mathrm{p}, Z_\mathrm{p}$	[m]	Plasma dimensions: radius and length
V	$[\mathrm{m^3}]$	Plasma volume
$\mathrm{T_g}$	[K]	Neutral temperature
$\mathrm{T_i}$	[K]	Positive ion temperature

Continued on next page

Table 3.2 (*Continued*)

Symbol	Unit	Description
$\mathrm{T_e}$	[K]	Electron temperature
T_g	[eV]	Neutral temperature
T_i	[eV]	Positive ion temperature
T_e	[eV]	Electron temperature
k_j	$[\mathrm{m}^{-3+3m}\mathrm{s}^{-1}]$	Reaction rate coefficient of the j-th reaction of an order m in a kinetic scheme
R_j	$[\mathrm{m}^{-3}\mathrm{s}^{-1}]$	Reaction rate of the j-th reaction in a chemistry set
$M_{\mathrm{cp},j}$	[kg]	Mass of the collision partner in j-th electron reaction
M_i	[kg]	Mass of the i-th species
m_e	[kg]	Electron mass
q_i	[e]	Charge of the i-th species
e	[C]	Electron charge
σ_i^LJ	[m]	σ parameter of the Lennard-Jones potential for i-th species
$\Delta E_{\mathrm{e},j}^\mathrm{inel}$	[eV]	Electron energy loss due to an inelastic collision j
a_{ij}^L		Stoichiometric coefficient of i-th distinct species on left-hand side in j-th reaction
a_{ij}^R		Stoichiometric coefficient of i-th distinct species on right-hand side in j-th reaction
a_{ij}		Net stoichiometric coefficient of i-th distinct species in j-th reaction
A_j	$[\mathrm{m}^{-3+3m}\mathrm{s}^{-1}]$	Arrhenius parameter – pre-exponential factor
n_j		Arrhenius parameter – exponent
$E_{\mathrm{a},j}$	[eV]	Arrhenius parameter – activation energy
$\mathrm{E}_{\mathrm{a},j}$	[K]	Arrhenius parameter – activation energy
k_B	$[\mathrm{JK}^{-1}]$	Boltzmann constant
s_i		Sticking coefficient – probability of i-th species sticking to a plasma boundary ($s_i \in [0, 1]$)
r_{ik}		Return coefficient – number of i-th species returned for each *one* of *stuck* k-th species ($r_{ik} \in \mathbf{R}_0^+$)
D_i	$[\mathrm{m}^2\mathrm{s}^{-1}]$	Diffusion coefficient of i-th species
D_a	$[\mathrm{m}^2\mathrm{s}^{-1}]$	Ambipolar diffusion coefficient
Λ	[m]	Characteristic diffusion length
λ_i	[m]	Mean free path of i-th species
$\overline{v}_i$	$[\mathrm{ms}^{-1}]$	Mean speed of i-th species
σ_{ik}^m	$[\mathrm{m}^2]$	Momentum transfer cross section for i-th species scattering on k-th species
$\overline{V_\mathrm{s}}$	[V]	Mean sheath voltage
n_min	$[\mathrm{m}^{-3}]$	Minimal allowed particle density
$\varrho_\mathrm{e,min}$	$[\mathrm{eV{\cdot}m}^{-3}]$	Minimal allowed electron energy density

3.1 Particle density balance

The time derivative of all heavy species densities is expressed as a sum of contributions from volumetric processes, flow sources and sinks and surface (diffusion) processes [127]:

$$\frac{\mathrm{d}n_i}{\mathrm{d}t} = \left(\frac{\delta n_i}{\delta t}\right)_{\mathrm{vol}} + \left(\frac{\delta n_i}{\delta t}\right)_{\mathrm{flow}} + \left(\frac{\delta n_i}{\delta t}\right)_{\mathrm{diff}}. \tag{3.1}$$

3.1.1 Volumetric reactions contribution

The contribution of volumetric reactions is

$$\left(\frac{\delta n_i}{\delta t}\right)_{\mathrm{vol}} = \sum_j G_{ij} - \sum_j L_{ij}, \tag{3.2}$$

where G_{ij}, and L_{ij} are contributions of generation and loss of n_i due to inelastic reaction j. In greater detail, it can be written as

$$\left(\frac{\delta n_i}{\delta t}\right)_{\mathrm{vol}} = \sum_j (a_{ij}^{\mathrm{R}} - a_{ij}^{\mathrm{L}}) R_j, \tag{3.3}$$

$$R_j = k_j \prod_l n_{lj}^{\mathrm{L}}, \tag{3.4}$$

where n_{lj}^{L} is the density of l^{th} species on the left-hand side of reaction j. The reaction rate coefficient k_j in this model takes form of the Arrhenius equation

$$k_j = A_j \left(\frac{\mathrm{T_g}}{300\mathrm{K}}\right)^{n_j} \exp\left(-\frac{\mathrm{E_{a,}}_j}{\mathrm{T_g}}\right) \tag{3.5a}$$

for heavy species reactions j (reactions where all the reactants are heavy species), and

$$k_j = A_j \left(\frac{T_{\mathrm{e}}}{1\mathrm{eV}}\right)^{n_j} \exp\left(-\frac{E_{\mathrm{a},j}}{T_{\mathrm{e}}}\right) \tag{3.5b}$$

for electron processes j (reactions where at least one reactant is an electron). The Arrhenius parameters A_j, n_j, and $E_{\mathrm{a},j}$ (or $\mathrm{E_{a,}}_j$) describe the collisional kinetics of the model.

3.1.2 Flow contribution

The contribution of flow to the time evolution of heavy species densities will consist of inflow and outflow terms as well as a term regulating the pressure.

$$\left(\frac{\delta n_i}{\delta t}\right)_{\text{flow}} = \left(\frac{\delta n_i}{\delta t}\right)^{\text{in}}_{\text{flow}} + \left(\frac{\delta n_i}{\delta t}\right)^{\text{out}}_{\text{flow}} + \left(\frac{\delta n_i}{\delta t}\right)^{\text{reg}}_{\text{flow}} \tag{3.6}$$

Inflow

$$\left(\frac{\delta n_i}{\delta t}\right)^{\text{in}}_{\text{flow}} = \frac{Q'_i}{V}, \tag{3.7}$$

where

$$Q'_i = \frac{N_{\text{A}}}{V_{\text{m}} \cdot 60} Q_i = 4.478 \times 10^{17} \cdot Q_i$$

is the inflow expressed in [particles/sec] rather than in [sccm]. $N_{\text{A}} = 6.022 \times 10^{23}$ mol^{-1} is Avogadro constant and $V_{\text{m}} = 2.241 \times 10^4$ cm^{3}mol^{-1} is the molar volume for the ideal gas at standard temperature and pressure.

Outflow

The outflow term is set in such a way that only neutrals are leaving the plasma region due to the flow, the neutral species flow rate is proportional to the species density, and the total flow rate out of the plasma region is the same as total inflow rate:

$$\left(\frac{\delta n_i}{\delta t}\right)^{\text{out}}_{\text{flow}} = \begin{cases} -\dfrac{\sum Q'_i}{\sum n_{i_0}} \cdot \dfrac{n_i}{V} & \text{neutrals,} \\ 0 & \text{ions,} \end{cases} \tag{3.8}$$

where the index i_0 runs only over neutral species.

Pressure regulation

A term regulating the plasma pressure is added to the particle balance equation, accounting for changes in p due to dissociation/association processes and to diffusion losses and surface sources. This term, similarly to the outflow term, only acts upon the neutral species and can be viewed as an addition to the outflow term, or physically as adjusting a pressure-regulation valve between a plasma chamber and

a pump, based on the instantaneous pressure.

$$\left(\frac{\delta n_i}{\delta t}\right)_{\text{flow}}^{\text{reg}} = \begin{cases} -\dfrac{p - p_0}{p_0}\dfrac{n_i}{\tau_p} & \text{neutrals,} \\ 0 & \text{ions.} \end{cases} \tag{3.9}$$

Here, p is the instantaneous pressure from the state equation for an ideal gas

$$p = k_{\text{B}} T_{\text{g}} \cdot \sum_i n_i, \tag{3.10}$$

and τ_p is a pressure recovery time-scale. In present work, a value of $\tau_p = 10^{-3}$ s was found to yield satisfactory results for a wide range of process parameters.

3.1.3 Diffusion contribution

The diffusion contribution towards the particle balance equation is ultimately controlled by the vector of sticking coefficients s_i, and matrix of return coefficients r_{ik}, and the diffusion model:

$$\left(\frac{\delta n_i}{\delta t}\right)_{\text{diff}} = \left(\frac{\delta n_i}{\delta t}\right)_{\text{diff}}^{\text{out}} + \left(\frac{\delta n_i}{\delta t}\right)_{\text{diff}}^{\text{in}}. \tag{3.11}$$

Diffusion losses

As used (among others) by Kushner in GlobalKin [123], the rate of species loss to the plasma boundaries due to diffusion is expressed as

$$\left(\frac{\delta n_i}{\delta t}\right)_{\text{diff}}^{\text{out}} = -\frac{D_i}{\Lambda^2} n_i s_i, \tag{3.12}$$

where

$$\Lambda = \left[\left(\frac{\pi}{Z_{\text{p}}}\right)^2 + \left(\frac{2.405}{R_{\text{p}}}\right)^2\right]^{-1/2}. \tag{3.13}$$

The diffusion coefficient is calculated separately for neutrals and ions. For positive and negative ions, the diffusion coefficient is the coefficient of ambipolar diffusion

in electronegative plasma, as proposed by Stoeffels *et al* [128].

$$D_i = \begin{cases} D_i^{\text{free}} & \text{neutrals,} \\ D_+^{\text{free}} \dfrac{1+\gamma(1+2\alpha)}{1+\alpha\gamma} & +\text{ions,} \\ 0 & -\text{ions.} \end{cases} \tag{3.14}$$

Here, $\gamma = T_\text{e}/T_\text{i}$, and $\alpha = \sum n_{\text{i}^-}/n_\text{e}$. $D_i = 0$ for negative ions implies that no negative ions are reaching the plasma boundaries and therefore there are no negative ion diffusion losses. This approximation is justified by the positive plasma potential trapping the negative ions in the plasma bulk. It should be noted that the stated ambipolar diffusion coefficients are only valid for the case of $\alpha \ll \mu_\text{e}/\mu_\text{i}$, where μ are mobilities of electrons and ions respectively. The free diffusion coefficient for heavy species is calculated as

$$D_i^{\text{free}} = \frac{\pi}{8}\lambda_i \overline{v}_i. \tag{3.15}$$

The mean free path λ_i for all heavy species is

$$\frac{1}{\lambda_i} = \sum_k n_k \sigma_{ik}^\text{m}(1-\delta_{ik}), \tag{3.16}$$

where σ_{ik}^m is the momentum transfer cross section, and the mean speed $\overline{v}_i$ is the mean thermal speed

$$\overline{v}_i = \begin{cases} \left(\dfrac{8k_\text{B}\text{T}_\text{g}}{\pi M_i}\right)^{1/2} & \text{neutrals,} \\ \left(\dfrac{8k_\text{B}\text{T}_\text{i}}{\pi M_i}\right)^{1/2} & \text{ions,} \end{cases} \tag{3.17}$$

where the ion temperature is approximated, as proposed by Lee and Lieberman in [129],

$$\text{T}_\text{i} = \begin{cases} (5800 - \text{T}_\text{g})\,\dfrac{0.133}{p} + \text{T}_\text{g} & p > 0.133 \text{ Pa}, \\ 5800 & p \leq 0.133 \text{ Pa}. \end{cases} \tag{3.18}$$

The momentum transfer cross section σ_{ik}^m is for the purpose of this model crudely approximated with hard sphere model for neutral–neutral and ion–neutral collisions, and with momentum transfer for Rutherford scattering (as proposed by Lieberman

and Lichtenberg [130]) for the case of ion–ion collisions:

$$\sigma_{ik}^{\mathrm{m}} = \begin{cases} \left(\sigma_i^{\mathrm{LJ}} + \sigma_k^{\mathrm{LJ}}\right)^2 & i = i_+, i_-, i_0, \text{ and } k = k_0, \\ & i = i_0, \text{ and } k = k_+, k_-, \\ \pi b_0^2 \ln\left(\dfrac{2\lambda_{\mathrm{De}}}{b_0}\right) & i = i_+, i_-, \text{ and } k = k_+, k_-, \end{cases} \tag{3.19}$$

with Debye length

$$\lambda_{\mathrm{De}} = \left(\frac{\epsilon_0 T_{\mathrm{e}}}{\mathrm{e} n_{\mathrm{e}}}\right)^{1/2}, \tag{3.20}$$

classical distance of the closest approach

$$b_0 = \frac{q_i q_k \mathrm{e}^2}{2\pi\epsilon_0 m_{\mathrm{R}} v_{\mathrm{R}}^2}, \tag{3.21}$$

reduced mass

$$m_{\mathrm{R}} = \frac{m_i m_k}{m_i + m_k}, \tag{3.22}$$

and the relative speed being approximated by the mean thermal speed

$$v_{\mathrm{R}} = \overline{v}_i. \tag{3.23}$$

The δ_{ik} term filters out self–collisions, as collisions between the same species do not affect the species collective behaviour

$$\delta_{ik} = \begin{cases} 1 & \text{for } i = k, \\ 0 & \text{for } i \neq k. \end{cases} \tag{3.24}$$

Finally, the free diffusion coefficient for positive ions is approximated by

$$D_+^{\mathrm{free}} = \overline{D_{i_+}^{\mathrm{free}}}. \tag{3.25}$$

Boundary sources

Each k-th species which is lost (or *stuck*) to the plasma boundary can get returned as i-th species, introducing the boundary sources

$$\left(\frac{\delta n_i}{\delta t}\right)_{\text{diff}}^{\text{in}} = -\sum_k r_{ik} \left(\frac{\delta n_k}{\delta t}\right)_{\text{diff}}^{\text{out}} = \sum_k \frac{D_k}{\Lambda^2} n_k s_k r_{ik} \tag{3.26}$$

3.1.4 Minimal allowed species density

To prevent the ODE solver from *overshooting* into unphysical negative densities, an additional *artificial* term is added to the right-hand side of Eq. (3.1), ensuring a finite minimal value of particle densities (which can be considered zero). This correction term takes form of

$$\left(\frac{\delta n_i}{\delta t}\right)_{n_{\min}} = \begin{cases} \dfrac{n_{\min} - n_i}{\tau} & n_i < n_{\min}, \\ 0 & n_i \geq n_{\min}. \end{cases} \tag{3.27}$$

In the present work, $n_{\min}$ was set to 1 particle/m^3, and τ to 1.0×10^{-10} s, ensuring an adequately fast response.

3.2 Electron energy density balance

The balance equation for the electron energy density consists of contributions from the absorbed power, elastic and inelastic electron collisions, electron production and consumption and contribution from diffusion losses of electrons and ions [127].

$$\frac{\mathrm{d}\varrho_{\mathrm{e}}}{\mathrm{d}t} = \frac{P}{V\mathrm{e}} - \left(\frac{\delta \varrho_{\mathrm{e}}}{\delta t}\right)_{\text{el/inel}} - \left(\frac{\delta \varrho_{\mathrm{e}}}{\delta t}\right)_{\text{gen/loss}} - \left(\frac{\delta \varrho_{\mathrm{e}}}{\delta t}\right)_{\text{el}\to\text{walls}} - \left(\frac{\delta \varrho_{\mathrm{e}}}{\delta t}\right)_{\text{ion}\to\text{walls}} \tag{3.28}$$

3.2.1 Contribution of elastic and inelastic collisions

Electron energy density loss rate due to electron collisions is described as

$$\left(\frac{\delta \varrho_{\mathrm{e}}}{\delta t}\right)_{\text{el/inel}} = \sum_j R_j \Delta E_{\mathrm{e},j}, \tag{3.29}$$

with the electron energy loss for j-th reaction $\Delta E_{\mathrm{e},j}$ being

$$\Delta E_{\mathrm{e},j} = \begin{cases} \Delta E_{\mathrm{e},j}^{\mathrm{inel}} & \text{inelastic collisions,} \\ 3\dfrac{m_{\mathrm{e}}}{M_{\mathrm{cp},j}}(T_{\mathrm{e}} - T_{\mathrm{g}}) & \text{elastic collisions,} \\ 0 & \text{heavy species collisions or } a_{\mathrm{e}j}^{\mathrm{R}} = 0, \end{cases} \tag{3.30}$$

and

$$T_{\mathrm{e}} = \frac{2}{3}\frac{\varrho_{\mathrm{e}}}{n_{\mathrm{e}}}. \tag{3.31}$$

The electron density n_{e} is not resolved explicitly, but rather calculated from plasma charge neutrality

$$n_{\mathrm{e}} = \sum_i n_i q_i. \tag{3.32}$$

For that reason, T_{e} might reach non-physically low values, when ϱ_{e} governed directly by Eq. (3.28) is much greater than $\sum_i n_i q_i$. A correction is introduced to T_{e} in the form of

$$T_{\mathrm{e}} = \max\left(T_{\mathrm{g}}, \frac{2}{3}\frac{\varrho_{\mathrm{e}}}{n_{\mathrm{e}}}\right), \tag{3.33}$$

to help with the solution stability, as the electron temperature will converge to the neutral gas temperature at low electron energy, due to dominance of elastic processes.

3.2.2 Electron generation and loss contribution

Rate of change of electron energy density due to generation and loss of electrons is described by

$$\left(\frac{\delta \varrho_{\mathrm{e}}}{\delta t}\right)_{\mathrm{gen/loss}} = \frac{3}{2} T_{\mathrm{e}} \sum_j (a_{\mathrm{e}j}^{\mathrm{R}} - a_{\mathrm{e}j}^{\mathrm{L}}) R_j. \tag{3.34}$$

3.2.3 Energy loss by electron transport

Under a Maxwellian energy distribution assumption, each electron lost through the plasma boundary sheath takes away $2k_{\mathrm{B}}\mathrm{T_e}$ of energy with it [130], which gives

$$\left(\frac{\delta \varrho_{\mathrm{e}}}{\delta t}\right)_{\mathrm{el}\to\mathrm{walls}} = -2T_{\mathrm{e}}\left(\frac{\delta n_{\mathrm{e}}}{\delta t}\right)_{\mathrm{walls}}, \tag{3.35}$$

while the total charge flux needs to be zero, yielding

$$\left(\frac{\delta n_\mathrm{e}}{\delta t}\right)_{\mathrm{walls}} = \sum_i q_i \left(\frac{\delta n_i}{\delta t}\right)_{\mathrm{diff}}. \tag{3.36}$$

3.2.4 Energy loss by ion transport

If it is assumed, that ions leave the plasma boundary sheath with the Bohm velocity, each positive ion removed from the plasma takes away $\frac{1}{2}k_\mathrm{B}\mathrm{T_e}$ of kinetic energy, as well as sheath voltage acceleration energy [130]

$$\left(\frac{\delta \varrho_\mathrm{e}}{\delta t}\right)_{\mathrm{ion}\to\mathrm{walls}} = -\frac{1}{2}T_\mathrm{e}\sum_{i_+}\left(\frac{\delta n_{i_+}}{\delta t}\right)_{\mathrm{diff}} - \overline{V_\mathrm{s}}\sum_{i_+} q_{i_+}\left(\frac{\delta n_{i_+}}{\delta t}\right)_{\mathrm{diff}}. \tag{3.37}$$

The last open parameter in the system is the mean sheath voltage $\overline{V_\mathrm{s}}$, which, according to Lieberman and Lichtenberg [130], can be approximated by

$$\overline{V_\mathrm{s}} = T_\mathrm{e}\cdot\ln\left(\frac{\overline{M_{i_+}}}{2\pi m_\mathrm{e}}\right)^{1/2}. \tag{3.38}$$

This value of $\overline{V_\mathrm{s}}$ is only consistent with ICP plasma sources.

3.2.5 Minimal allowed electron energy density

To prevent the ODE solver from *overshooting* into unphysical negative ϱ_e, an additional *artificial* term is added to the right-hand side of Eq. (3.28), ensuring a finite minimal value of electron energy density (which can be considered zero). This correction term takes form of

$$\left(\frac{\delta \varrho_\mathrm{e}}{\delta t}\right)_{\varrho_{\min}} = \begin{cases} \dfrac{\varrho_{\mathrm{e,min}} - \varrho_\mathrm{e}}{\tau} & \varrho_\mathrm{e} < \varrho_{\mathrm{e,min}}, \\ 0 & \varrho_\mathrm{e} \geq \varrho_{\mathrm{e,min}}. \end{cases} \tag{3.39}$$

In the present work, $\varrho_{\mathrm{e,min}}$ was set to 1 eV/m^3, and τ to 1.0×10^{-10} s, ensuring an adequately fast response.

3.3 Implementation

The equations described in the previous sections are implemented in the Python programming language as methods of an `Equations` class. All the methods return convenient array data–structures of the *NumPy* library [131]. The main output of the `Equations` instance is a single *objective function* returning the time derivative of the solution vector $\mathbf{y}$

$$\mathbf{y} = (n_1, n_2, \cdots, n_{N_S-1}, n_{N_S}, \rho_e).$$

The time derivative is primarily the function of the solution vector $\mathbf{y}$, and the time t

$$\frac{\mathrm{d}\mathbf{y}}{\mathrm{d}t} = f(t, \mathbf{y}),$$

with both the $\mathbf{y}$, and t being the parameters to the said objective function. However, being the combination of all the equations defined in sections 3.1, and 3.2, it is also a function of all the model input parameters, and the chemistry set and its kinetics, all stored as the `Equations` instance attributes. The main purpose of the `Equations` class is to build and return the objective function, as summarized in the python code snippet given as figure 3.1

```
from numpy import array
class Equations:
    def __init__(self, chemistry_set, model_parameters):
        self.chemistry_set = chemistry_set
        self.model_parameters = model_parameters
        ...
    def get_objective_function():
        """Objective function factory. Builds and return the
        objective function which can be fed into an ODE solver.
        """
        def objective_function(t: float, y: array) -> array:
            ...
            return dy_dt
        return objective_function
```

Figure 3.1: Python code snippet outlining the implementation of the `Equations` class.

The `objective_function` object built and returned by the `Equations` instance is than fed into the `scipy.integrate.solve_ivp` ODE solver from the *SciPy* library [132]. The PyGMol model uses the BDF integration method backend of the `solve_ivp` function, implementation of which follows the one described by the reference [133], according to the SciPy package documentation. The `solve_ivp` function returns a 2D array of $\mathbf{y}(t)$ for a vector of time–samples determined internally by the solver method.

The PyGMol global model documented in this chapter is published as an open–source python package `pygmol` as part of the project GutHub repository:
`https://github.com/martin-hanicinec-ucl/plaschem`.
The package is available to anyone and the repository contains basic documentation on installation and usage. The `pygmol` package is in fact a *subpackage* of the `pygmo_fwork` (python global modeling framework) package, which also includes the `optichem` subpackage with all the chemistry set reduction functionality. The `pygmo_fwork` package also implements a higher–level wrapper for the `pygmol` functionality. Apart from `pygmo_fwork`, the repository also contains the `plaschem` package with data structures representing species, reactions and chemistry sets, and with additional functionality relevant to chemistry set reduction. All the packages in the repository are synergic and meant to be installed and used together as a single ecosystem.

Chapter 4

Species ranking schemes

The specific method of building the species ranking based on the outputs of interest is the most important part of the reduction framework presented in chapter 2. Several methods of fast species ranking are proposed in this chapter, each based on a single evaluation of a plasma model with the detailed chemistry set, and a graph–theoretical representation of the chemistry. A *chemistry graph* is created, with species as nodes and directed weighted edges between species. The species ranking hierarchy is then built, and it reflects the indirect coupling between each species, and the outputs of interest. The *chemistry graph–based* ranking schemes presented are also compared to two *benchmark* ranking schemes, based on the Morris method of sensitivity analysis and on the detailed chemistry species densities respectively. All the ranking scheme variations are tested empirically in Chapter 6 on a range of different detailed chemistry sets, sets of reduction conditions and sets of outputs of interest, and the best performing ranking scheme is identified.

Section 4.1 outlines the core method of how the species ranking is built using asymmetric coupling coefficients between species and plasma model outputs. The following sections 4.2, and 4.3 then detail calculation of the coupling coefficients for the graph–based ranking, and for the Morris–based benchmark method. Finally, section 4.4 describes the trivial case of ranking the species according their densities modeled with the detailed chemistry set, defining the second (albeit very naive) benchmark ranking scheme.

It should be noted, that the graph–based method uses path search in the chem-

istry graph between nodes co calculate the coupling coefficients, and the nodes are representing the chemistry set species only. This implies that only species densities are acceptable as outputs of interest within the framework of the chemistry graph–based ranking schemes, and the term *species of interest* will be used as synonymous to *outputs of interest* in section 4.2. The other coupling method does not share this limitation and therefore section 4.3 will retain the original nomenclature, using outputs of interest.

4.1 Species ranking

The species ranking method described in this work is built around the idea of an *asymmetric coupling coefficient* W_{AB} between the species A and the model output B. Whatever method is used to obtain W_{AB} values, the species' ranking scores are calculated from the coupling coefficients as described in this section.

An instantaneous ranking score C_i^t for i–th species X_i can be expressed as a maximum coupling coefficient between X_i, and any of the pre–defined *outputs of interest* Y_k at a given simulation time t, such as

$$C_i^t = \max_k W^t_{\mathrm{X}_i\mathrm{Y}_k}, \tag{4.1}$$

where index k runs over all the outputs of interest $\{\mathrm{Y}_k\}$. The instantaneous coupling coefficients C_i^t depend on the plasma model parameters at any given time t. To ensure the reduction validity over the whole simulation time span, C_i^t are sampled over a sufficiently dense set of *times of interest* $\{t\}$, and the species ranking scores C_i are defined as

$$C_i = \max_{k,t} W^t_{\mathrm{X}_i\mathrm{X}_k} = \max_t C_i^t. \tag{4.2}$$

This way, the ranking score of any particular species covers the coupling between its presence in the chemistry set, and all the modeled outputs of interest sampled at all the times of interest – which are exactly the outputs the reduced chemistry set is designed to preserve.

Figure 4.1 demonstrates the importance of choosing an appropriate set of times

of interest $\{t\}$. It shows the time evolution of oxygen radical in an O_2–He atmospheric pressure plasma, comparing the PyGMol outputs with detailed and reduced chemistry for two reduced chemistry sets, each reduced with reduction and species ranking evaluated for a different set of times of interest. In both cases, the reduction was performed with $\Delta = 10\%$, and with only the O atom number density, as a single output of interest. Figure 4.1a is showing data for a chemistry set reduced using a single time sample, coinciding with the end of the power pulse. While the atomic oxygen density agrees with the detailed set sufficiently well for the steady–state phase, the reduction error during the afterglow phase might be unacceptable. Figure 4.1b shows that sampling the reaction rates from a larger times of interest set, spanning the pulsing period, results in a (albeit larger) reduced chemistry set which preserves atomic oxygen density even during the afterglow.

The choice of the sampling times of interest will always depend on the specific application and on the computational time budget. A logarithmic distribution of time samples might be more useful for calculations with a constant external power term, while a linear distribution might be preferred for a time–dependent power source, as shown in figure 4.1. The times of interest might also be sampled based on the detailed chemistry set solution, with the instantaneous sampling frequency proportional to the time derivatives of the densities of species of interest. However, in the case of chemistry graph–based ranking, the computational cost of the ranking algorithm will increase linearly with the size of the samples set, because each time sample will effectively instantiate a separate chemistry graph which needs to be weighted and searched.

4.2 Chemistry graph coupling

Figure 4.2 shows a schematic depiction of such a chemistry graph, with 11 nodes (species), and 17 directed edges. Each directed edge (u, v), leading from u–th species to the v–th species, is weighted by a *direct interaction coefficient* $w(u, v)$, which is generally a function of reaction rates R_j of all the reactions in the detailed chemistry set. By analogy with graph theory nomenclature, when regarding a single edge, or a

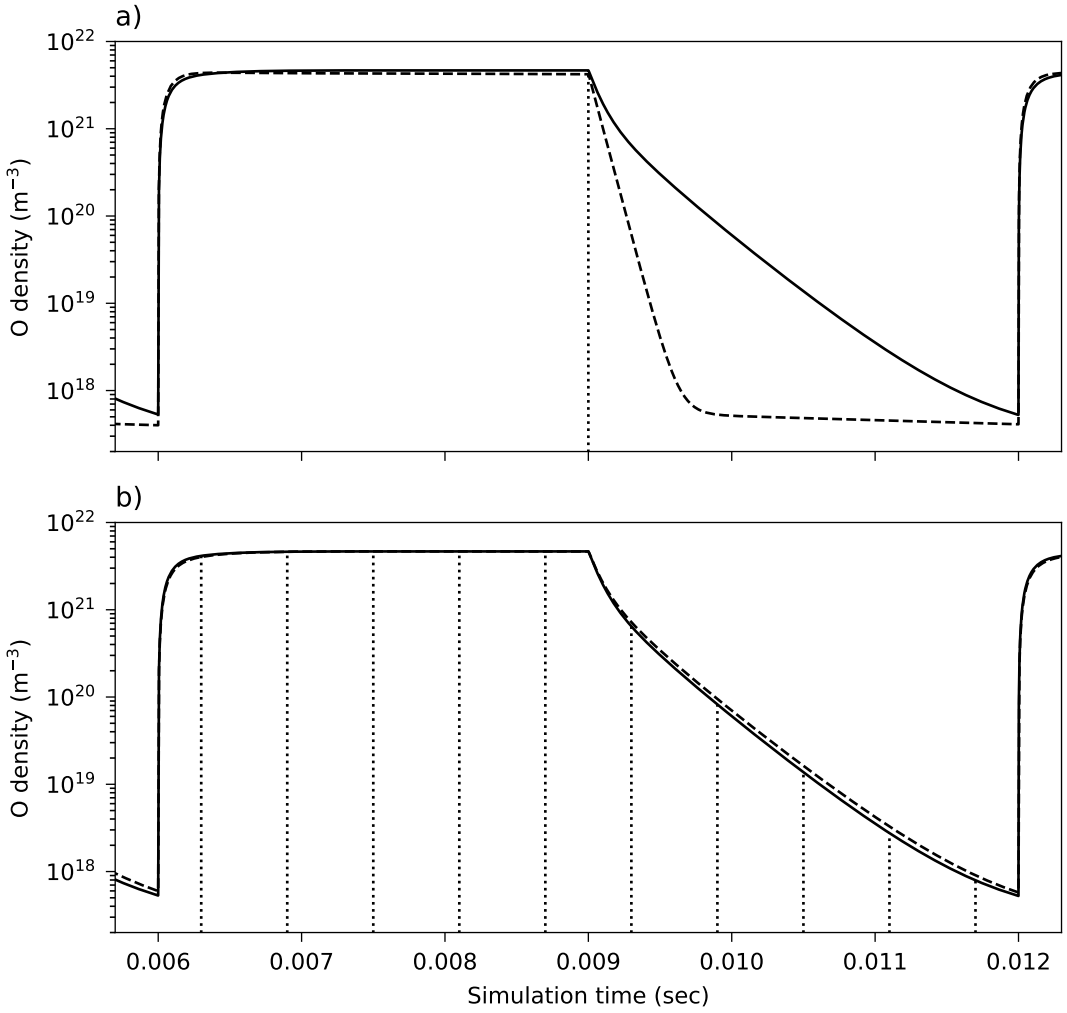

Figure 4.1: Comparison of the time evolution of atomic oxygen species in pulsed O_2–He plasma modeled with the detailed and reduced chemistry sets. a) The reduction was performed for a time of interest, coinciding with the end of the power pulse. b) The reduction was performed for a set of times of interest, spanning over the whole pulsing period. In both cases, atomic oxygen was set as the only species of interest. Solid and dashed lines show O density modeled using detailed and reduced chemistry set respectively, while the dotted lines indicate the times of interest used for species ranking and the iterative reduction.

direct interaction coefficient, u–th and v–th species will be referred to as *tail species*, and *head species* respectively, where the v–th head species is directly affected by the presence of all the reactions involving u–th tail species. Any direct interaction coefficient $w(u, v)$ is a measure of asymmetric coupling between two species that are directly related through some elementary reactions in the detailed chemistry set.

Coupling between two species, however, exists even if they do not share any

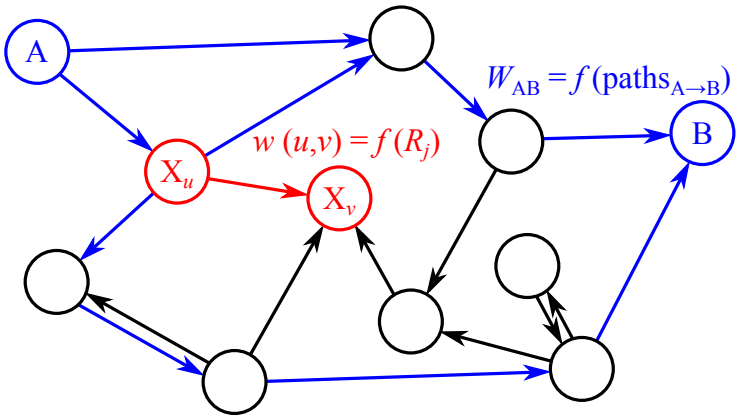

Figure 4.2: Depiction of a *chemistry graph* with nodes representing species and directional edges representing asymmetric direct interactions between species, weighted by the direct interaction coefficients. A direct interaction coefficient $w(u, v)$ between u–th and v–th species is depicted in red, while the asymmetric coupling coefficient W_{AB} between species A and B is hinted in blue, depending on all the paths $p(\text{A} \to \text{B})$ in the chemistry graph leading from A to B.

elementary reactions. The indirect asymmetric *coupling coefficients* W_{AB} between species A and B are therefore defined, reflecting the global (often indirect) effect of the presence of species A (with all its reactions) on the modeled density of the species B. For coupling coefficient W_{AB}, the species A and B will, by convention, be referred to as the *source species*, and *target species*, respectively. A coupling coefficient W_{AB} is generally a function of direct interaction coefficients along all the paths leading from the source species A to the target species B in the chemistry graph. This way, in the resulting species ranking, the rank of each species A will reflect its importance (or rather the collective importance of all the reactions involving the species A) for modeling species B belonging to the set of species of interest; even a species with a very low density will rank relatively high, if it acts as an important intermediate species for production or consumption of the species of interest.

The following section defines several methods for calculating $w(u, v)$, and W_{AB}, and how the species ranking is extracted from the set of coupling coefficients.

4.2.1 Direct interaction coefficients

Several methods for edge weights distribution in chemistry graphs, and for calculating the direct interaction coefficients $w(u, v)$, have been proposed in the literature.

In the original directed relation graph (DRG) theory [37], Lu and Law propose that $w(u,v)$ takes the form of the sum of absolute values of production and consumption rates for head species by all the reactions involving the tail species, with a normalizing factor of the sum of absolute values of production and consumption rates for head species by all the reactions in the chemistry set:

$$w(u,v) = \frac{\sum_{j=1}^{N_\mathrm{R}} |a_{vj} R_j \delta_u^j|}{\sum_{j=1}^{N_\mathrm{R}} |a_{vj} R_j|}. \tag{4.3}$$

The index j runs over all N_R reactions in the chemistry and R_j is the reaction rate of the j–th reaction

$$R_j = k_j \prod_l n_{lj}^\mathrm{L}, \tag{4.4}$$

k_j is a reaction rate coefficient of the j–th reaction (3.5a), (3.5b), and n_{lj}^L is the density of the l–th reactant of the j–th reaction. The term δ_u^j selects only reactions involving the tail species

$$\delta_u^j = \begin{cases} 1 & \text{if } u\text{–th species in } j\text{–th reaction,} \\ 0 & \text{otherwise,} \end{cases} \tag{4.5}$$

and a_{vj} is the net stoichiometric coefficient of head species in j–th reaction

$$a_{vj} = a_{vj}^\mathrm{R} - a_{vj}^\mathrm{L}. \tag{4.6}$$

In their other work [39], Lu and Law propose an alternative definition for the direct interaction coefficient to (4.3), replacing the denomination factor by the absolute value of the total net production rate of the head species

$$w(u,v) = \frac{\sum_{j=1}^{N_\mathrm{R}} |a_{vj} R_j \delta_u^j|}{\left|\sum_{j=1}^{N_\mathrm{R}} a_{vj} R_j\right|}. \tag{4.7}$$

This means, that unlike the direct interaction coefficient defined by (4.3) which is bound between 0 and 1, and (4.7) becomes singular for the head species in equilibrium.

Another definition of the direct interaction coefficient was proposed by Pepiot and Pitch [40] in their DRGEP method. In their definition, the direct interaction coefficients are equal to the absolute value of net production of the head species by all the reactions involving the tail species, normalized by the maximum of total production or consumption of the head species, as

$$w(u,v) = \frac{\left|\sum_{j=1}^{N_\mathrm{R}} a_{vj} R_j \delta_u^j\right|}{\max(P_v, C_v)}. \tag{4.8}$$

The range of the direct interaction coefficient (4.8) can also be shown to be between 0 and 1 [40].

Finally, here I propose another definition of $w(u,v)$ which naturally emerges from (4.3), (4.7), and (4.8) as their combination

$$w(u,v) = \frac{\left|\sum_{j=1}^{N_\mathrm{R}} a_{vj} R_j \delta_u^j\right|}{\left|\sum_{j=1}^{N_\mathrm{R}} a_{vj} R_j\right|}. \tag{4.9}$$

Similar to (4.7), and sharing the same denominator, (4.9) is not bound between 0 and 1 but rather is singular for the head species in equilibrium.

The direct interaction coefficients defined by (4.3), (4.7) – (4.9) only reflect the importance of volumetric reactions involving tail species towards modeling the head species density. While this is appropriate for combustion modeling, where the DRG method and its variants all originated, it is, in fact, blind to the effect of surface reactions and conversions, which are often of great importance in plasma modeling. Therefore, in the present work, modified definitions are proposed, addressing also the production and consumption rates of head species by diffusion losses and surface

conversions, such as

$$w_{\mathrm{DRG}}(u,v) = \frac{\sum_{j=1}^{N_\mathrm{R}} |a_{vj} R_j \delta_u^j| + |S_u r_{uv} - S_v (1 - r_{vv})|}{\sum_{j=1}^{N_\mathrm{R}} |a_{vj} R_j| + \left| \sum_{i=1}^{N_\mathrm{S}} S_i r_{iv} - S_v \right|}, \tag{4.10a}$$

$$w_{\mathrm{DRG'}}(u,v) = \frac{\sum_{j=1}^{N_\mathrm{R}} |a_{vj} R_j \delta_u^j| + |S_u r_{uv} - S_v (1 - r_{vv})|}{\left| \sum_{j=1}^{N_\mathrm{R}} a_{vj} R_j + \sum_{i=1}^{N_\mathrm{S}} S_i r_{iv} - S_v \right|}, \tag{4.10b}$$

$$w_{\mathrm{DRGEP}}(u,v) = \frac{\left| \sum_{j=1}^{N_\mathrm{R}} a_{vj} R_j \delta_u^j + S_u r_{uv} - S_v (1 - r_{vv}) \right|}{\max(P_v, C_v)}, \tag{4.10c}$$

$$w_{\mathrm{DRG''}}(u,v) = \frac{\left| \sum_{j=1}^{N_\mathrm{R}} a_{vj} R_j \delta_u^j + S_u r_{uv} - S_v (1 - r_{vv}) \right|}{\left| \sum_{j=1}^{N_\mathrm{R}} a_{vj} R_j + \sum_{i=1}^{N_\mathrm{S}} S_i r_{iv} - S_v \right|}. \tag{4.10d}$$

Equations (4.10a) – (4.10d) correspond to (4.3), (4.7) – (4.9) respectively, with added species consumption and production rates on surfaces. The index i runs over all N_S species in the chemistry set and S_i is the surface sticking rate of i–th species, defined by (3.12). The total production and consumption rates of the head species P_v, and C_v are

$$P_v = \sum_{j=1}^{N_\mathrm{R}} \max(a_{vj} R_j, 0) + \sum_{i=1}^{N_\mathrm{S}} S_i r_{iv} \left(1 - \delta_v^i\right), \tag{4.11}$$

$$C_v = \sum_{j=1}^{N_\mathrm{R}} \max(-a_{vj} R_j, 0) + S_v (1 - r_{vv}), \tag{4.12}$$

with

$$\delta_v^i = \begin{cases} 1 & \text{if } i = v, \\ 0 & \text{otherwise.} \end{cases} \tag{4.13}$$

These modified direct interaction coefficients also preserve the ranges of the original ones, that means (4.10a) and (4.10c) are bound between 0 and 1, while (4.10b) and (4.10d) are not.

4.2.2 Asymmetric coupling coefficients

With chemistry graph edges weighted by the direct interaction coefficients according to one of (4.10a) – (4.10d), the species coupling coefficients W_{AB} can be defined

between any two species A, B, using some well–established graph search algorithms: *shortest path*, *maximum bottleneck path*, *maximal product path*, and *maximal flow* searches.

In the shortest path approach, the coupling coefficient between source species A and target species B is calculated as a reciprocal of the length of the shortest path leading from A to B, with the individual edges being attributed their own *length* equal to reciprocals of weights $w(u, v)$

$$W_{\mathrm{AB}}^{\mathrm{sh.path}} = \left[\min_{\text{all paths } p(\mathrm{A}\to\mathrm{B})} \sum_{\text{all edges } (u,v)\in p} w^{-1}(u, v) \right]^{-1}. \tag{4.14}$$

Since all the edge weights (lengths) are by definition non-negative, the shortest paths might be calculated very efficiently, using, for example, Dijkstra's algorithm [134] with a very convenient computational complexity $\mathcal{O}(N_{\mathrm{S}}^2)$. The non-negativity of the weights of the edges relies of course on the assumption, that the return coefficient $r_{ii} \leq 1.0$ for any i–th species, meaning the plasma surface does not act as a species multiplier for any species in the chemistry set, as it should not.

Alternatively, one might define the coupling coefficient W_{AB} as the direct interaction coefficient of a rate–limiting step across all the paths $\mathrm{A} \to \mathrm{B}$. For each path $p(\mathrm{A} \to \mathrm{B})$, the path rate–limiting step can be defined as

$$W_{\mathrm{AB},p}^{\mathrm{min}} = \min_{i=1}^{n-1} w(i, i+1), \tag{4.15}$$

with index i running through all the species in any one path p, and with the source and target species A, B corresponding to $i = 0$, and $i = n$ respectively. The coupling coefficient $W_{\mathrm{AB}}^{\mathrm{lim.rate}}$ is then defined as the global rate–limiting step

$$W_{\mathrm{AB}}^{\mathrm{lim.rate}} = \max_{\text{all paths } p} W_{\mathrm{AB},p}^{\mathrm{min}}. \tag{4.16}$$

This is equivalent to the maximum bottleneck path problem, the widest path problem or a maximum capacity route problem from graph theory. As in the case of the shortest path approach, the maximal limiting rate search between any two species

can be performed very efficiently, for example by a modified Dijkstra's algorithm with $\mathcal{O}(N_\mathrm{S}^2)$ complexity [135].

Another option is to define W_AB as a product of all the direct interaction coefficients in a path $p(\mathrm{A} \to \mathrm{B})$ with maximal such a product:

$$W_\mathrm{AB}^\mathrm{err.prop.} = \max_{\text{all paths } p(\mathrm{A}\to\mathrm{B})} \prod_{\text{all edges } (u,v)\in p} w(u,v). \tag{4.17}$$

This definition of the species coupling coefficients only makes sense for direct interaction coefficients bound between 0 and 1, otherwise, the graph search would favour long, *convoluted* paths involving a maximal number of edges with $w(u,v) > 1$. Therefore, this approach only applies to the w_DRG (4.10a), and w_DRGEP (4.10c) definitions of direct interaction coefficients, as $w_\mathrm{DRG'}$ (4.10b), and $w_\mathrm{DRG''}$ (4.10d) are not bound between 0 and 1, but rather become singular for head species in total equilibrium. The maximal propagated error search is inspired by the notion of error propagation proposed by Pepiot and Pitch [40] in their DRGEP method. If the direct interaction coefficients as edges are approximating errors induced to the density of a head species by the elimination of the tail species, the errors propagate along the paths from source to target species introducing geometric damping. The idea is that if some error is introduced to the prediction of the source species A, the longer the error needs to propagate along the path $p(\mathrm{A} \to \mathrm{B})$ to reach the target species B, the smaller the effect will typically be. For edge weights bound between 0 and 1, the maximal product path problem is equivalent to the shortest path problem with modified edge lengths, as the coupling coefficient can be redefined as

$$W_\mathrm{AB}^\mathrm{err.prop.} = \exp\left[-\min_{\text{all paths } p(\mathrm{A}\to\mathrm{B})} \sum_{\text{all edges } (u,v)\in p} -\ln w(u,v)\right], \tag{4.18}$$

which can be solved by any shortest path searching algorithm, which can handle zero–weighted edges, corresponding to $w(u,v) = 1.0$. It needs to be noted that Dijkstra's shortest path algorithm treats edges with zero weight as non-existing edges, which would generally result in an incorrect $W_\mathrm{AB}^\mathrm{err.prop.}$, therefore a different algorithm needs to be used to compute (4.18), e.g. Bellman–Ford algorithm [136],

which would in our case have $\mathcal{O}(N_\mathrm{S}^3)$ asymptotic complexity.

The last option considered in this work for expressing the coupling coefficients W_AB from a chemistry graph is using a maximum flow search. In analogy to the maximum bottleneck path problem (4.16), where the weights of the edges can be imagined as flow capacities and the flow capacity of the maximum–bottleneck path $p^\mathrm{widest}(\mathrm{A} \to \mathrm{B})$ is searched for, in the maximum flow problem, the maximum flow from A to B is sought, without the restriction of only one single path. The species coupling coefficient $W_\mathrm{AB}^\mathrm{max.flow}$ is then defined as a maximal total flow from A to B, while a partial flow through any single edge $f(u, v)$ does not exceed the edge capacity (or value of the direct interaction coefficient)

$$f(u, v) \leq w(u, v),$$

and flow is conserved in around any node

$$\sum_i f(i, v) = \sum_k f(v, k),$$

except for the source and target species. The maximum flow problem may be solved for example employing the Edmonds–Karp algorithm [137] with $\mathcal{O}(VE^2)$ complexity, where V is the number of vertices in the graph, while E is the number of edges. In the asymptotic case of a fully connected graph, the complexity in terms of the size of the chemistry set might be expressed as $\mathcal{O}(N_\mathrm{S}^5)$, for a single pair of (A, B). This makes the maximal flow search relatively slow, in contrast to $W_\mathrm{AB}^\mathrm{sh.path}$, $W_\mathrm{AB}^\mathrm{lim.rate}$, and $W_\mathrm{AB}^\mathrm{err.prop}$ with $\mathcal{O}(N_\mathrm{S}^{2-3})$ complexity for evaluating *all* pairs of $\{(\mathrm{X}_i, \mathrm{B})\}$.

4.3 Species coupling using Morris method

Apart from all the chemistry graph–based ranking scheme variations described in section 4.2, another method of ranking the species in chemistry set according to their importance for plasma model prediction of the outputs of interest was developed based on the Morris method of sensitivity analysis.

4.3.1 Morris method

There are several methods of investigating the sensitivity of outputs of a system towards a perturbation of different inputs. In our case of a plasma model and regarding species–oriented chemistry reduction, we might be interested in the sensitivity of the outputs of interest (such as n_i, T_e) on perturbation of collection of reaction rate coefficients belonging to all the reactions involving i–th species. These sensitivity coefficients will become the basis for asymmetric coupling between species and outputs of interest. The coupling coefficients will yield the species ranking as described in section 4.1, with the idea that if the set of outputs of interest is insensitive to the perturbations of collection of reaction rates belonging to a certain species, this species is more likely to be redundant for our chemistry set, than another species with a greater sensitivity.

One of the methods for sensitivity analysis was described in the work of Morris [138], and in relation to plasma modelling e.g. in the work of Turner [126], and Obrusnik *et al* [45]. Also known as elementary effects method (EEM), the Morris method is a screening method investigating elementary effects of model inputs (called *factors*) on the model *outputs*. In the framework of the Morris method, n factors are distributed in a configuration space of a unit n-dimensional hypercube, defining the *vector of factors* $\mathbf{x} = (x_1, \ldots, x_n)$, with each x_i restricted to a finite number of discrete choices $x_i \in [0, 1]$. The key quantity for the Morris method is the elementary effect $\mathbf{d}_i(\mathbf{x})$ defined as

$$\mathbf{d}_i(\mathbf{x}) = \frac{\mathbf{y}(x_1, \ldots, x_i + \Delta, \ldots, x_n) - \mathbf{y}(x_1, \ldots, x_n)}{\Delta}, \tag{4.19}$$

where $\mathbf{y}(\mathbf{x})$ is a vector of outputs of the plasma model and Δ is a perturbation of the factor x_i. Value of the Δ parameter must be chosen such as the perturbed factor $x_i + \Delta \in [0, 1]$. For convenience, $\Delta = \pm 0.5$ is often used , where only one sign permits the perturbed vector of factors $(x_1, \ldots, x_i + \Delta, \ldots, x_n)$ being kept in the unit hypercube, for whichever value of the unperturbed vector of factors $(x_1, \ldots, x_n)$.

In relation to the plasma global model described in Chapter 3, the vector of outputs could take a form $\mathbf{y}(\mathbf{x}) = (n_1(\mathbf{x}), \ldots, n_{N_\mathrm{S}}(\mathbf{x}), T_\mathrm{e}(\mathbf{x}))$, and in our framework

of species–oriented skeletal reduction method, the vector of factors $\mathbf{x} = (x_1, \ldots, x_{N_\mathrm{S}})$ could be mapped (with some defined ranges and distribution) to a vector of scaling factors $(\alpha_1, \ldots, \alpha_{N_\mathrm{S}})$, where each scaling factor α_i scales the reaction rate coefficients belonging to all the reactions involving the i–th species.

Examining the vectors of elementary effects $\mathbf{d}_i$ for each factor x_i from $\mathbf{x}$, the matrix of elementary effects $\mathbf{D}$ if formed with each element d_i^k denoting an elementary effect of i–th factor on the k–th output. The matrix $\mathbf{D}$ is analogous to a Jacobian matrix with finite differences Δ. Since $\mathbf{D}$ depends (apart from Δ) most crucially on the point $\mathbf{x}$ in the configuration space of the factors, the Morris method investigates $\mathbf{D}$ more than once, each with different $\mathbf{x}$, and collects statistical results. For N separate evaluations of $\mathbf{D}_j$, the two key outputs of the Morris method are the mean elementary effect

$$\mu_i^k = \frac{1}{N} \sum_{j=1}^{N} d_{i,j}^k, \tag{4.20}$$

and the standard deviation of the mean

$$\sigma_i^k = \sqrt{\frac{1}{N} \sum_{j=1}^{N} \left(d_{i,j}^k - \mu_i^k\right)^2}, \tag{4.21}$$

with both metrics μ_i^k, σ_i^k characterising the effect of the i–th factor on the k–th output. Magnitude of the mean elementary effect μ_i^k correlates with an influence of i–th factor on the k–th output and σ_i^k can be used to evaluate the effect of non-linear coupling between factors and model outputs. If, for example, $\sigma_i^k \ll \mu_i^k$, then the dependence of k–th output on the i–th factor is practically linear and independent of the other factors, while $\sigma_i^k > \mu_i^k$ would suggest that the dependence is non–linear or strongly coupled to some other factors (or both).

An efficient process for sampling the elementary effects is employed by the Morris method based on so called *Morris trajectories* through the configuration space of $\mathbf{x}$ definition range. Each Morris trajectory starts with a randomly distributed $\mathbf{x}$ (with uniform distribution for each $x_i \in [0, 1]$), and progresses through n elementary effects evaluations proceeding randomly through elements of $\mathbf{x}$ (where each factors elementary effect is evaluated exactly once). One Morris trajectory can be repre-

sented by a random walk of n steps through the configuration space of factors, where each step has the same length Δ, and is progressed along each single basis vector of the configuration space no more than once. In such a trajectory, each step defines one elementary effect vector $\mathbf{d}_i$ as a normalised difference in model outputs from the previous position in the Morris trajectory, (4.19). The morris metrics μ_i^k (4.20), and σ_i^k (4.21) are compiled from N distinct Morris trajectories.

Just for better clarity, in the present section, the indices i, j, and k are running over the *Morris factors*, *Morris trajectories*, and *model outputs* respectively, as shown in table 4.1, together with their relation to the global model presented in chapter 3.

Table 4.1: Summary of the indices used in section 4.3, with relation to the employed global model, described in chapter 3.

Index	**Running over**	**Ranges**
i	factors	$1, \cdots, n = N_\mathrm{S}$
j	trajectories	$1, \cdots, N$
k	model outputs	$1, \cdots, N_\mathrm{S} + 1$

Each Morris trajectory requires $n + 1$ global model evaluations, where n is the length of the factors vector $\mathbf{x}$ (in our case of species ranking, $n = N_\mathrm{S}$), while it has been shown that with the sampling scheme presented here, a sufficient number of Morris trajectories yielding converged statistics is in the order of 100 [45]. This means that the required number of global model evaluations is roughly $100N_\mathrm{S}$ for analysis of model sensitivity on all species, which renders it impractical as a ranking scheme for a fast ranking–based iterative reduction method, compared to the chemistry graph–based ranking schemes described in section 4.2, which only requires a single global model evaluation. Nevertheless, the species ranking based on the Morris method of sensitivity analysis is included in the assessment in chapter 6 as a benchmark.

4.3.2 Morris–based coupling coefficients

In order to consider species ranking based on the outputs of the Morris method of sensitivity analysis, the precise mapping from the vector of factors

$$\mathbf{x} = (x_1, \ldots, x_{N_\mathrm{S}}) \ \in \ [0,1]^{N_\mathrm{S}}$$

to the set of plasma model inputs needs to be established. In the present work, this mapping takes form of scaling factors for reaction rate coefficients, such as

$$k_j(\mathbf{x}) = \alpha_j(\mathbf{x}) A_j T^{n_j} \exp\left(-\frac{T}{E_{\mathrm{a},j}}\right), \tag{4.22}$$

where A_j, n_j, and $E_{\mathrm{a}j}$ are the nominal kinetic parameters for the j–th reaction, equations (3.5a), (3.5b), and the scaling factors themselves are

$$\alpha_j(\mathbf{x}) = 2 \prod_{i=1}^{N_\mathrm{S}} x_i \delta_i^j, \tag{4.23}$$

with

$$\delta_i^j = \begin{cases} 1 & \text{if the } j\text{–th reaction involves } i\text{–th species,} \\ 0 & \text{otherwise.} \end{cases} \tag{4.24}$$

Such mapping can be interpreted in a way that a single factor $x_i \in [0,1]$, associated with the i–th species, uniformly scales the nominal reaction rate coefficients k_j^0 of all reactions involving the i–th species into new values of $k_j \in [0, 2k_j^0]$. This way, $\mathbf{x} = \mathbf{0.5}$ maps to the nominal reaction rate coefficients $k_j(\mathbf{x}{=}\mathbf{0.5}) = k_j^0$, and for the edge cases, $\mathbf{x} = \mathbf{1}$ maps to $k_j(\mathbf{x}{=}\mathbf{1}) = 2^{N_j} k_j^0$, where N_j is a number of distinct species involved in the j–th reaction and $\mathbf{x} = \mathbf{0}$ (or indeed any of $x_i = 0$) maps to the zero reaction rate coefficient $k_j(\mathbf{x}{=}\mathbf{0}) = 0$.

In practice, the configuration space of Morris factors is discrete and the edge values of $x_i = 0$, and $x_i = 1$ are excluded. Calculations performed in the present work followed the prescription found the work of Campolongo *et al* [139], and Turner [126]. Ten uniformly distributed lattice point on each axis of the Morris configuration space

were chosen, so that each factor takes one of the values $0.05, 0.15, \ldots, 0.85, 0.95$, and it was taken $\Delta = \pm 0.5$, with the sign depending on the starting value of x_i from (4.19), such that $x_i + \Delta$ belongs to the configuration space.

Since both μ_i^k, and σ_i^k are important measures of k–th output dependence (or dependence of k-th species' density, if ignoring the T_e output as with the chemistry graph–based ranking in section 4.2) on the i–th species, the species coupling coefficients between source i–th species A, and target k–th species B are proposed to be the sum of both μ, and σ relative to the output species densities (averaged over all trajectories), or

$$W_{\mathrm{AB}}^{\mathrm{morris}} = W_{\mathrm{S}_i\mathrm{S}_k}^{\mathrm{morris}} = \frac{N}{\sum_{j=1}^{N} \langle n_k \rangle^j} \left(\left| \mu_i^k \right| + \sigma_i^k \right), \tag{4.25}$$

where $\langle n_k \rangle^j$ is the plasma model output density of target k–th species B averaged over the full j–th Morris trajectory. The coupling coefficients are built for each time sample from the set of times of interest, as

$$W_{\mathrm{S}_i\mathrm{S}_k}^{\mathrm{morris},t} = W_{\mathrm{S}_i\mathrm{S}_k}^{\mathrm{morris}}(t). \tag{4.26}$$

Finally, it should be noted, that the Morris–based species ranking method described in this section is inherently stochastic, and its evaluation might differ between several independent runs, even for a fairly large number N of Morris trajectories. As an example, figure 4.3 shows a reduction plot for the same reduction performed with species ranking based on 100 Morris trajectories, compared with 5 distinct reduction runs based on species ranking from 20 Morris trajectories, all random subsets of the same set of 100 trajectories. It is evident, that the species ranking differed slightly for each run.

4.4 Density ranking

The last species ranking scheme considered in this work is the trivial ranking by their densities, as modeled with the detailed chemistry set. The ranking score C_i of

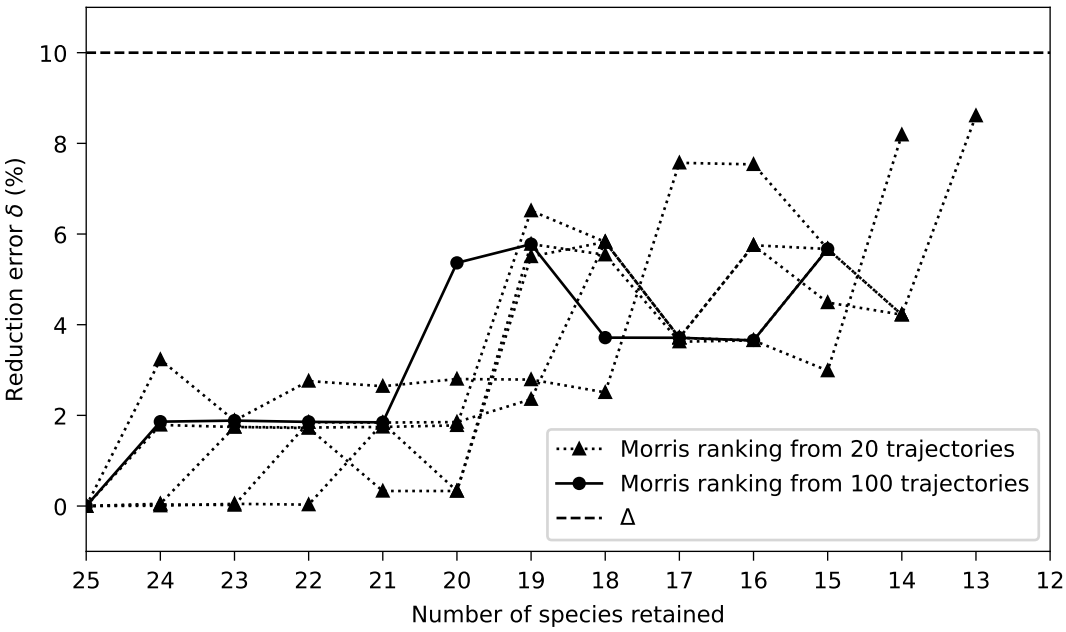

Figure 4.3: A reduction plot for an O_2–He chemistry set and plasma model with arbitrary reduction conditions. Reduction was performed 6 times, each with the same set of species of interest and times of interest. The reduction run with species ranking based on Morris method with 100 Morris trajectories is compared to five runs with species rankings based on 5 random subsets of 20 Morris trajectories (out of the same set of 100 trajectories).

the i–th species is expressed trivially as

$$C_i = \max_t n_i^t, \tag{4.27}$$

where n_i^t is the species density at the time of interest t. It is evident that the density ranking is a very naive method, which is completely blind to any defined outputs of interest. It will, however, serve as a convenient trivial benchmark method to compare the chemistry graph–based and Morris–based methods against.

4.5 Species ranking summary

In section 4.2.1, I proposed 4 alternative definitions of direct interaction coefficients $w(u, v)$ (4.10a) – (4.10d), and in section 4.2.2, I proposed 4 alternative ways to extract the species coupling coefficients W_{AB} out of a chemistry graph, with directional edges weighted by $w(u, v)$. This defines in total 14 alternative methods of

ranking species according to (4.2), with ranking scores being a function of species of interest, times of interest and time–dependent reaction rates simulated by a plasma model with the detailed chemistry set. Two definitions of the direct interaction coefficient (4.10b), (4.10d) are not compatible with the $W_{\mathrm{AB}}^{\mathrm{err.prop.}}$ coupling coefficient (4.17), excluding them from the mix. Two additional methods were proposed as benchmark; a method based on the Morris method of sensitivity analysis in section 4.3, and the naive scheme of ranking species according to their densities (4.4). All 16 methods introduced in this chapter will be assessed on an array of diverse test chemistry sets, later in chapter 6.

Both the ranking schemes based on the chemistry graphs and on the Morris method of sensitivity analysis are coded into the open–source `pygmo_fwork.optichem` subpackage. The `pygmo_fwork` package also contains the `pygmol` subpackage, as well as a higher–level user–friendlier wrapper around the `pygmol` solver, which is also wired into `optichem` as the global model. All the code is published in the project GitHub repository:
`https://github.com/martin-hanicinec-ucl/plaschem`.
The repository is available to anyone and contains basic documentation on installation and usage.

Chapter 5

Test reduction cases

Six test chemistry sets are introduced, to provide the basis for a number of test reduction cases generating the data for a statistical assessment of all the species ranking schemes introduced in chapter 4. Table 5.1 lists all the chosen test chemistry sets with their sizes (number of species and reactions), typical applications and source publications.

Table 5.1: Summary table of test chemistry sets, and associated reduction pressures p considered for testing of the species ranking methods. The number of species and reactions N_S and N_R are listed for each test chemistry set.

ID	Test set	N_S	N_R	Pressure	Typical application	Source
S1	O_2–He	25	373	1 atm	Biomedical plasma	Turner [22]
S2	N_2–H_2	42	408	1 atm	NH_3 synthesis	Hong *et al* [5]
S3	N_2–H_2	42	408	8 Pa	NH_3 synthesis	Hong *et al* [5]
S4	CF_4–CHF_3–H_2–Cl_2–O_2–HBr	67	563	25 Pa	–	QDB [9]
S5	CH_4–N_2	61	521	1 atm	–	QDB [9]
S6	Ar–NF_3–O2	39	310	100 Pa	–	QDB [9]

The first three chemistry sets S1–S3 (O_2–He and N_2–H_2) are taken from published plasma modelling work by Turner [22], and Hong *et al* [5]. Basic validation of the PyGMol model (chapter 3) is performed, to ensure a reasonable match between the outputs of plasma models used in the sets' source publications, and in this work. The species of interest and reduction conditions for the chemistry sets S1–S3 were chosen with consideration for some typical applications of the relevant plasmas. The rest of the test chemistry sets (S4–S6) were imported from the QDB database, without any attempts to verify their validity. The reduction conditions and species

of interest were chosen arbitrarily without consideration for any specific application. This approach is justified, since neither the PyGMol global model, nor the chemistry sets presented here, are the main focus of this work, but rather provide test inputs for the reduction method proposed.

5.1 O_2–He test chemistry set (S1)

The first test chemistry set is one for O_2–He atmospheric pressure plasma taken from the work of Turner [22]. The detailed chemistry set contains 25 species and 373 reactions. Table 5.2 lists all the species included in the detailed chemistry set. While all the reactions, and their kinetics can be found in the cited source publication, together with carefully tracked primary sources, the chemistry set is also reproduced in table A.1 in Appendix A, for consistency with the other test chemistry sets. The kinetics for all the electron as well as heavy species collisions already conveniently take form of the modified Arrhenius equation, (3.5a), (3.5b), and therefore can be input into PyGMol without any further modification.

It is evident that the vibrational kinetics is not treated in great detail in the present model, with a single lumped vibrational state (denoted by ν) present for each neutral molecule. This simplification was justified in the source compilation by very dilute mixtures of oxygen in helium and by much lower densities of those vibrational states compared to their ground states. Reduction conditions for this detailed chemistry set should therefore not increase the oxygen ratio beyond the limit set by the source publication.

Table 5.2: Species included in the O_2–He chemistry set as compiled by Turner [22]. Lumped vibrational states for each neutral molecule are denoted by ν.

Neutrals	He O O_2 O_3
Excited states	He^* He_2^* $O(^1D)$ $O(^1S)$ $O_2(a\,^1\Delta_g)$ $O_2(a\,^1\Delta_g, \nu)$ $O_2(b\,^1\Sigma_g^+)$ $O_2(b\,^1\Sigma_g^+, \nu)$ $O_2(\nu)$ $O_3(\nu)$
Positive ions	He^+ He_2^+ O^+ O_2^+ O_3^+ O_4^+
Negative species	e O^- O_2^- O_3^- O_4^-

Perhaps the most topical use of the O_2–He plasma is for a biomedical application

at atmospheric pressure. The source publication chose to approximate the so–called micro atmospheric pressure plasma jet (μAPPJ) [140], which is in many ways a typical example. The chemistry set source publication uses a device configuration of 1 $\times$ 1 mm^2 channel with a length of 30 mm for its global model and with a constant power of 1 W supplied to the system for 3 ms (which is a residence time of the gas in the channel at a typical flow rate), followed by a further 3 ms of zero power, modeling the afterglow phase. It is not clear if any surface losses or species conversions were considered in the source publication, so a set of *default* surface interaction coefficients was employed for the present work, as shown in table 5.3, for all the species, with exceptions to ions and excited species, without their neutral ground–state counterparts. The sticking coefficient for both He_2^*, and He_2^+ was considered $s = 1.0$, with return species $r_{He} = 2.0$, and similarly, $s_{O_4^+} = s_{O_4^-} = 1.0$, with $r_{O_2} = 2.0$. Identical surface coefficients were considered for both the on/off phases of the power pulsing.

Table 5.3: Default rules for species sticking coefficients s and return species R with return coefficients r considered for detailed chemistry sets and global modeling in present work. The default surface coefficients translate to total quenching of excited species and neutralization of positive ions.

Species	s	**Return species**	r
neutrals	0.0	–	–
exc. states (*excl.* He_2^*)	1.0	ground state	1.0
ions$^+$ (*excl.* He_2^+, O_4^+, O_4^-)	1.0	neutral	1.0
ions$^-$	0.0	–	–

5.1.1 PyGMol validation (O_2–He)

The source publication [22] used a plasma model with kinetic data in the same functional form as used by PyGMol, providing an opportunity to validate the PyGMol global model. Figures 5.1 – 5.8 show mostly very good agreement between the data calculated by Turner [22], and the outputs from PyGMol model, for the same conditions and the same O_2–He chemistry set. The conditions are listed in tables 5.10, and 5.11.

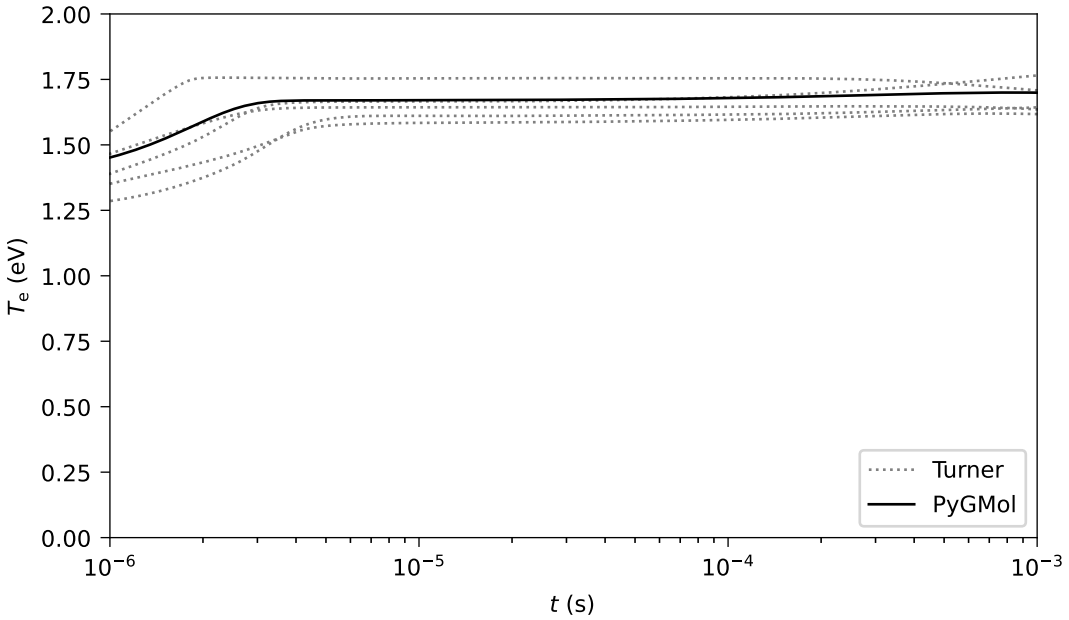

Figure 5.1: Comparison of the time evolution of electron temperature between the solution of PyGMol global model and the results of Turner [22], for the O_2–He chemistry set. Several lines are plotted from Turner which correspond to different random sets of reaction rate coefficients sampled within their uncertainty distributions.

It could be argued that the differences (figures 5.5, and 5.7) observed between the results of PyGMol, and the results of Turner [22] can probably be attributed to possible differences in handling the species surface diffusion losses and sources, and/or possible differences in power dissipation model. Without knowledge of the explicit governing equations of the global model in Turner's work, any conclusions beyond this would be purely speculative. As in Turner's work, results in figures 5.1 – 5.2 were obtained with 0.1 % O_2 ratio in the feedstock gas, while the rest of the results with the O_2 ratio of 0.4 %. The full set of model parameters used in PyGMol simulation is summarized in tables 5.10, and 5.11. The oxygen ratios and the discharge pulsing shape were taken directly from the source publication, while the plasma dimensions were adjusted to fit the PyGMol global model and conserve the plasma volume mentioned in the source publication. The total feedstock gas flow rate as well as the gas temperature was adopted from the work of Schulz-von der Gathen *et al* [140]. The results in the source publication were highly probably obtained with a model considering a μAPPJ CCP plasma reactor, while the PyGMol global model is

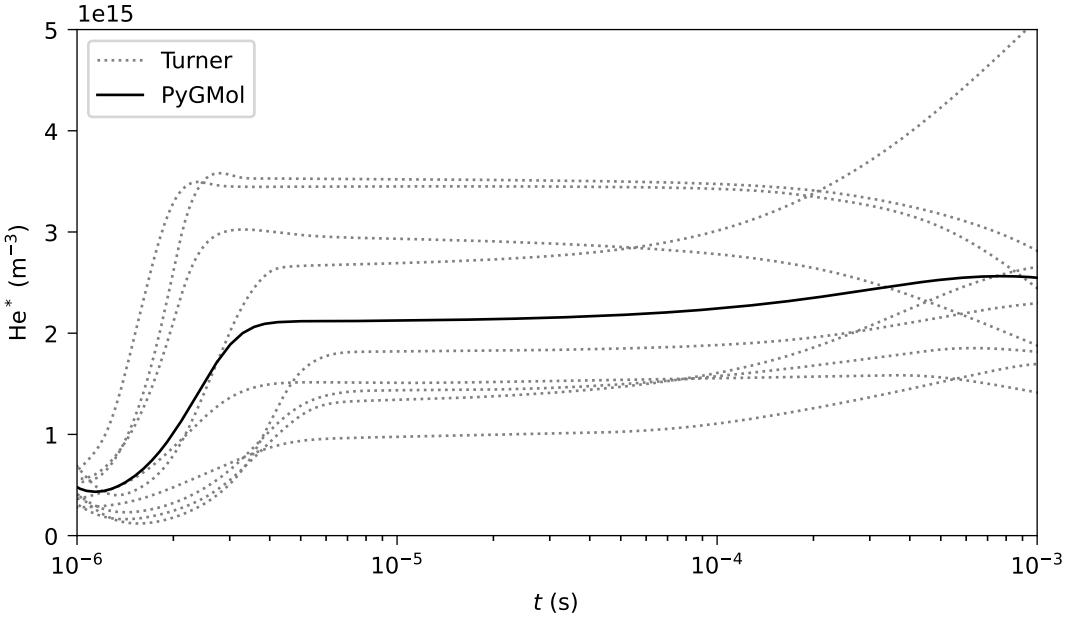

Figure 5.2: Comparison of time evolution of the helium metastable lumped state He^* density between the solution of PyGMol global model and the results of Turner [22], for the O_2–He chemistry set. Several lines are plotted from Turner which correspond to different random sets of reaction rate coefficients sampled within their uncertainty distributions.

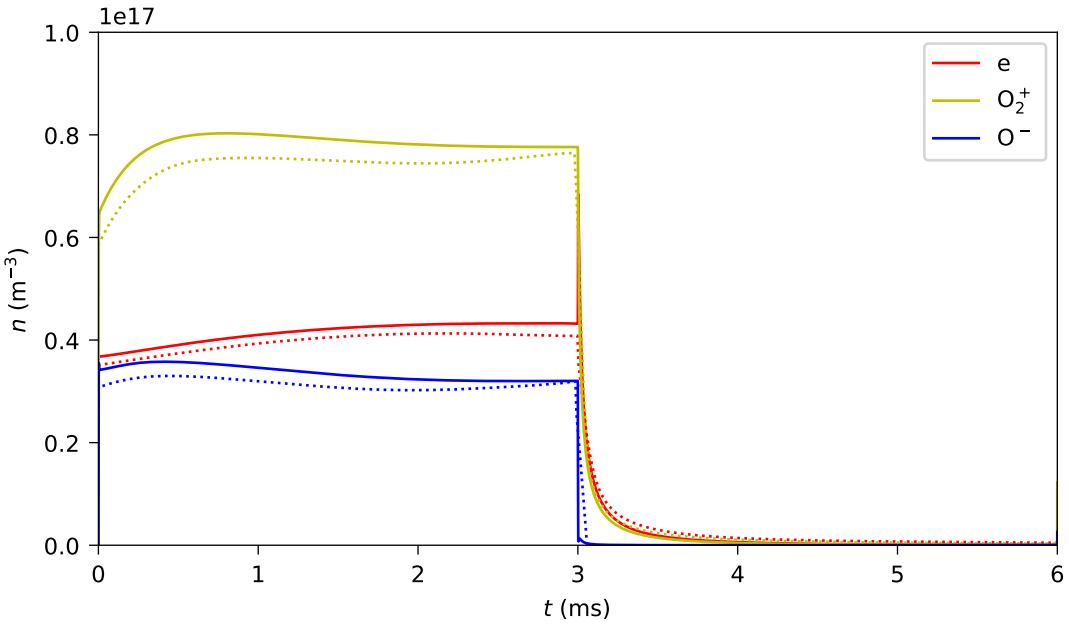

Figure 5.3: Densities of selected charged species during the power cycle for the O_2–He chemistry set: comparison between the PyGMol global model (solid line) and solution by Turner [22] (dotted lines).

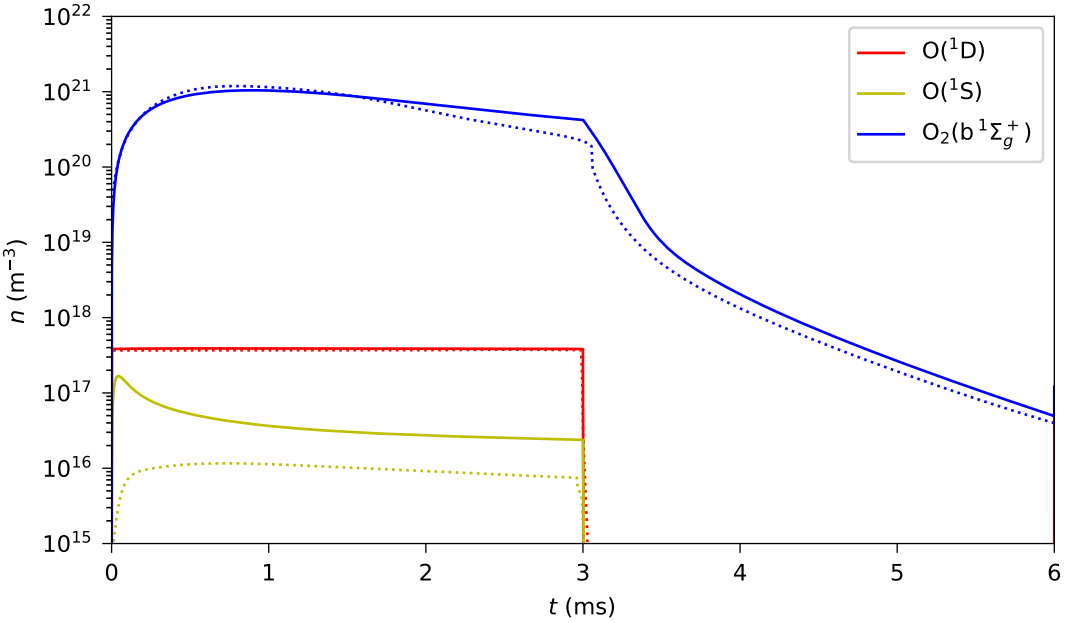

Figure 5.4: Densities of selected short–lived oxygen excited states, formed by a balance of fast processes, for the O_2–He chemistry set. Comparison between the PyGMol global model (solid line) and solution by Turner [22] (dotted lines).

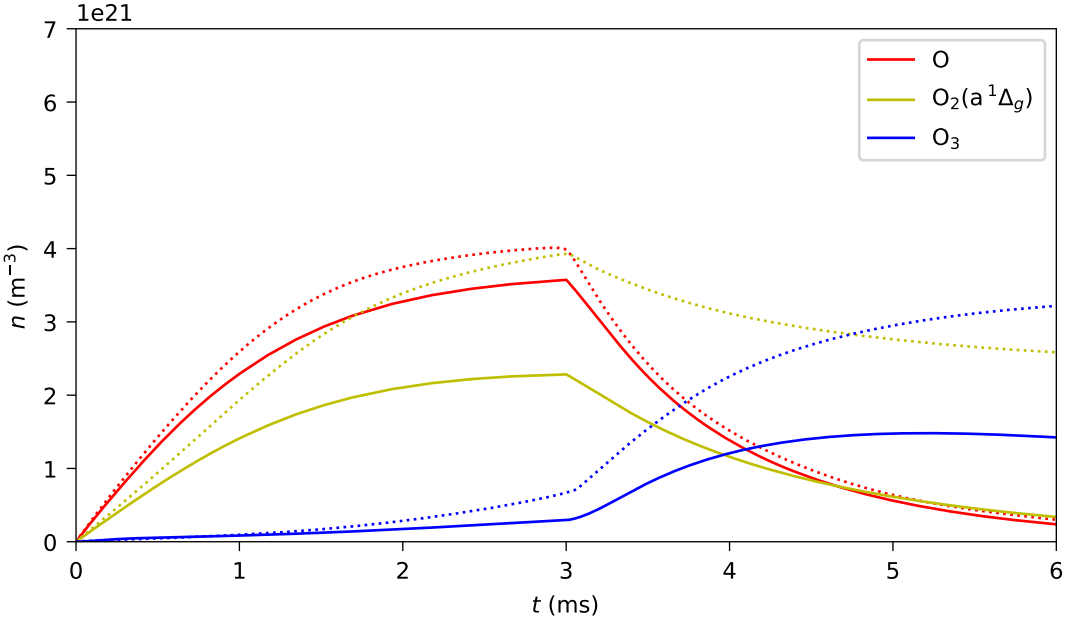

Figure 5.5: Densities of selected relatively long–lived oxygen radicals with slow kinetics for the O_2–He chemistry set. Comparison between the PyGMol global model (solid line) and solution by Turner [22] (dotted lines).

developed for ICP setup with a very different mode of power absorption. In the CCP setup, high fraction of the power is lost to the ions in the sheath with much higher

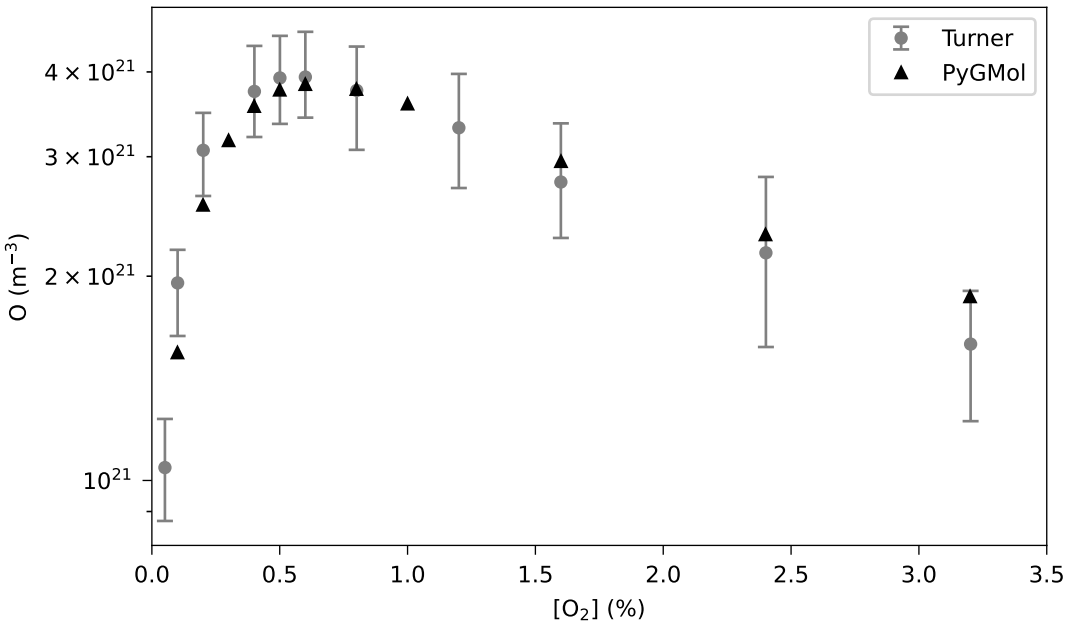

Figure 5.6: Density of atomic oxygen at the end of the discharge pulse, as a function of the fraction of O_2 in the feedstock gas for the O_2–He chemistry set. Comparison between the PyGMol solution and that due to Turner [22].

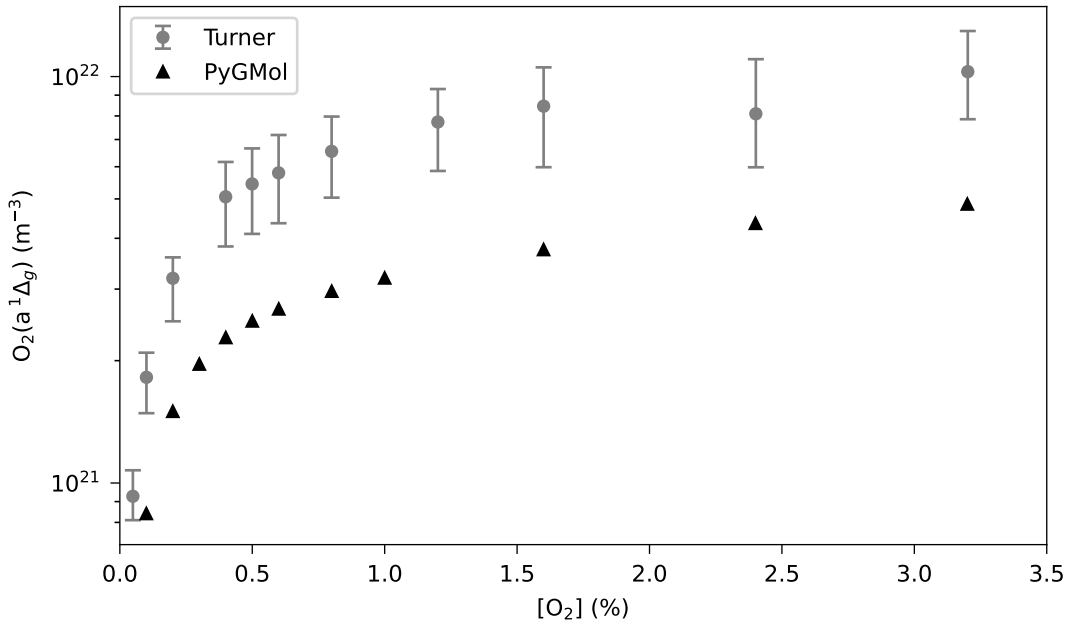

Figure 5.7: Density of molecular oxygen state $O_2(a\,^1\Delta_g)$ at the end of the discharge pulse, as a function of the fraction of O_2 in the feedstock gas for the O_2–He chemistry set. Comparison between the PyGMol solution and that due to Turner [22].

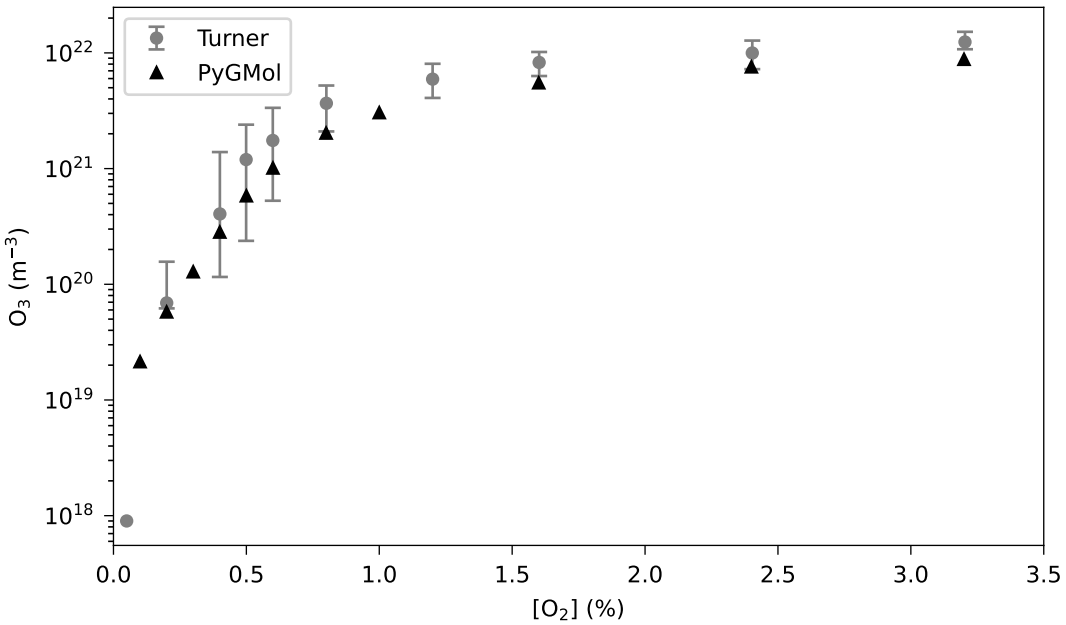

Figure 5.8: Ozone density at the end of the discharge pulse, as a function of the fraction of O_2 in the feedstock gas for the O_2–He chemistry set. Comparison between the PyGMol solution and that due to Turner [22].

voltage than in the case of the ICP setup. Since the sheath voltage is unknown, the power parameter from the source publication was not used, but instead, the power value was calibrated to $P = 0.3$ W, fitting the electron density evolution presented in the source publication.

5.2 N_2–H_2 test chemistry sets (S2 – S3)

The next two test chemistry sets for N_2–H_2 plasma are based on the source publication of Hong *et al* [5]. The source publication compiles a chemistry set containing 42 distinct species and 408 reactions, building on previous work of Gordiets *et al* [141; 142], and adapting it for atmospheric pressure. In contrast to the O_2–He test chemistry set, this set explicitly tracks the first few vibrationally excited states of the most abundant molecular species N_2 and H_2. All the species included are shown in table 5.4, while the reactions can be found in the source publication, together with their original sources.

Perhaps the most topical application for both low–pressure and atmospheric

Table 5.4: Species included in the N_2–H_2 chemistry set as compiled by Hong *et al* [5]

Neutrals	H H_2 N N_2 NH NH_2 NH_3
Excited states	$H_2(b\,^3\Sigma_u^+)$ $H_2(B\,^1\Sigma_u^+)$ $H_2(c\,^3\Pi_u)$ $H_2(a\,^3\Sigma_g^+)$ $H_2(\nu_1)$ – $H_2(\nu_3)$ $N(^2D)$ $N(^2P)$ $N_2(A\,^3\Sigma_u^+)$ $N_2(B\,^3\Pi_g)$ $N_2(a'\,^1\Sigma_u^-)$ $N_2(C\,^3\Pi_u)$ $N_2(\nu_1)$ – $N_2(\nu_8)$
Positive ions	H^+ H_2^+ H_3^+ N^+ N_2^+ N_3^+ N_4^+ NH^+ NH_2^+ NH_3^+ NH_4^+ N_2H^+
Negative species	e H^-

pressure is the ammonia synthesis. However, modeling of N_2–H_2 plasma is also important for a wide range of other applications, such as plasma cutting [143; 144], arcjet thrusters for a satellite propulsion [145; 146], AlN, TiN or SiN film deposition [147; 148; 149], etching of organic low–permittivity layers [150], nitriding [151], and the interaction of puffed N_2 with the H_2 plasma in fusion reactors [152]. In this work, I base two test chemistry sets on the data from Hong *et al*; one for atmospheric pressure conditions (S2), and one for low–pressure conditions (S3), see table 5.1.

5.2.1 N_2–H_2 volumetric reactions

Kinetic data for the volumetric reactions compiled by Hong *et al* are not all compatible with the PyGMol global model. Most of the electron processes in the source publication cite the cross–sectional data from the internal database of ZDPlasKin [125], and many of the heavy species processes follow reaction coefficients described by varying functions of gas temperature, differing from the Arrhenius representation required by PyGMol. The volumetric reaction kinetics were adapted for PyGMol according to the following procedure:

- Electron processes described by cross–sectional data were all fitted to Arrhenius form, assuming the Maxwellian distribution on a grid of electron temperatures. For reproducibility reasons, the cross–sectional data for these processes were adopted from the QDB database. The threshold electron energy for each of the processes was taken to be the electron energy of the first non–zero data–point of the corresponding cross–section.

- For electron processes described in the Arrhenius form, the threshold energy

was adopted from the corresponding processes cross–sections found in QDB, as described in the previous point.

- All the heavy species processes described in the Arrhenius form were left unchanged.

- The heavy species processes following any other functional dependence were all explicitly expressed for a constant gas temperature T_g.

The kinetic data for all the reactions as used in the present work are summarized explicitly in Appendix A. Table A.3 lists the reactions for the atmospheric pressure N_2–H_2 chemistry set (S2), and table A.4 lists the reactions for the low pressure N_2–H_2 chemistry set (S3).

5.2.2 N_2–H_2 surface kinetics

The surface coefficients (sticking and return coefficients s, and r with return species R) are listed in table 5.5 for both atmospheric–pressure and low–pressure test chemistry sets. The surface coefficients for quenching of the excited states and for V–V surface transitions are taken from Hong *et al* (with the original sources listed in table 5.5). Additionally, all the ions are neutralized on surfaces, while ions with their neutral counterparts not present in the system are returned as their most abundant neutral fragments. Finally, a separate category is formed by the species H and H_2. The NH_3 production is reportedly dominated by surface processes both for atmospheric–pressure conditions [5], and for low–pressure conditions [153]. The main channels for NH_3 surface production are reported to be the heterogeneous reactions

$$\begin{aligned} NH_2 + H(s) &\rightarrow NH_3, \\ NH_2(s) + H(s) &\rightarrow NH_3, \\ H_2 + NH(s) &\rightarrow NH_3, \end{aligned}$$

with both the surface–adsorbed $NH_2(s)$, and NH(s) species being predominantly controlled by the surface–adsorbed atomic hydrogen H(s), which is in turn produced

mainly by adsorption of H and H_2[5]

$$H_2 + \text{wall} \rightarrow 2H(s),$$
$$H + \text{wall} \rightarrow H(s).$$

In my work, for the sake of brevity, these NH_3 surface production channels were represented by sticking and return coefficients for H and H_2 only, as shown in table 5.5, with values calibrated to match the modeling results reported by Hong *et al* [5] for atmospheric pressure case and by Carrasco *et al* [153] for the low–pressure conditions, for the plasma conditions and parameters stated in both sources. Surface sticking of the H species was discounted in the case of atmospheric pressure test chemistry set, due to a much lower degree of hydrogen dissociation.

Finally, it needs to be noted that the surface kinetics described by table 5.5 are highly approximative and should not replace the full set of heterogeneous reactions (e.g. [5]) in any work aiming for quantitative modeling results. However, in this work, it will suffice to provide an important test chemistry sets, with some species (mainly NH_x) densities being dominantly controlled by surface diffusion and conversion, rather than volumetric processes.

5.2.3 PyGMol validation (N_2–H_2)

Several figures with results presented in the source publication for the N_2–H_2 chemistry set are reproduced in the present work using PyGMol global model.

PyGMol validation of the atmospheric pressure chemistry set (S2)

The PyGMol results for the atmospheric pressure model are shown in figures 5.9 – 5.13, with table 5.10 listing the PyGMol model inputs. The results presented by Hong *et al* in the source publication were obtained with the ZDPlasKin global model for the same gas temperature, pressure and feedstock gas ratio as shown in table 5.10. The total feed flow was chosen arbitrarily in the present work, as were the plasma dimensions (while preserving the plasma volume $V \simeq 50$ cm^3, reported by the source publication). Finally, the absorbed power, as in case of the O_2–He model,

Table 5.5: Species surface coefficients considered for the N_2–H_2 test chemistry sets: sticking coefficients s, return species R, and return coefficients r. M^+ denotes a general positive ion, with M being its neutral counterpart. The species not included in the table all have sticking coefficient $s = 0$.

Species	s	**R**	r	**Source**
H	[a]0.0			
	[b]4.0×10^{-2}	H_2	0.5	[c]
		NH_3	0.5	[c]
H_2	2.0×10^{-4}	$H_2(\nu_1)$	0.5	[154]
		NH_3	0.5	[d]
$H_2(\nu_i)$	2.0×10^{-4}	$H_2(\nu_{i-1})$	0.5	[154]
		$H_2(\nu_{i+1})$	0.5	[154]
$H_2(\nu_3)$	1.0×10^{-4}	$H_2(\nu_2)$	1.0	[154]
H_2(b), H_2(B), H_2(c), H_2(a)	1.0×10^{-3}	H_2	1.0	[5]
N(D), N(P)	1.0	N	1.0	[141]
N_2	4.5×10^{-4}	$N_2(\nu_1)$	1.0	[155]
$N_2(\nu_i)$	9.0×10^{-4}	$N_2(\nu_{i-1})$	0.5	[155]
		$N_2(\nu_{i+1})$	0.5	[155]
$N_2(\nu_8)$	4.5×10^{-4}	$N_2(\nu_7)$	1.0	[155]
N_2(A)	1.0	N_2	1.0	[141]
N_2(a')	1.0×10^{-3}	N_2	1.0	[141]
H_3^+	1.0	H_2	0.5	
		H	0.5	
N_3^+	1.0	N_2	0.5	
		N	0.5	
N_4^+	1.0	N_2	0.5	
		N_2	0.5	
NH_4^+	1.0	NH_3	0.5	
		H	0.5	
N_2H^+	1.0	N_2	0.5	
		H	0.5	
M^+	1.0	M	1.0	

[a]Only used in the atmospheric–pressure case S2.
[b]Only used in the low–pressure case S3.
[c]Fitted to match the modeling results reported by Carrasco *et al* [153]
[d]Fitted to match the modeling results reported by Hong *et al* [5]

was calibrated to fit the source publication electron energy and density results. The simulation time (table 5.11) was chosen to be long enough to obtain convergent particle densities of all species in the model.

As can be seen on figures 5.9 – 5.13, generally reasonable quantitative and/or

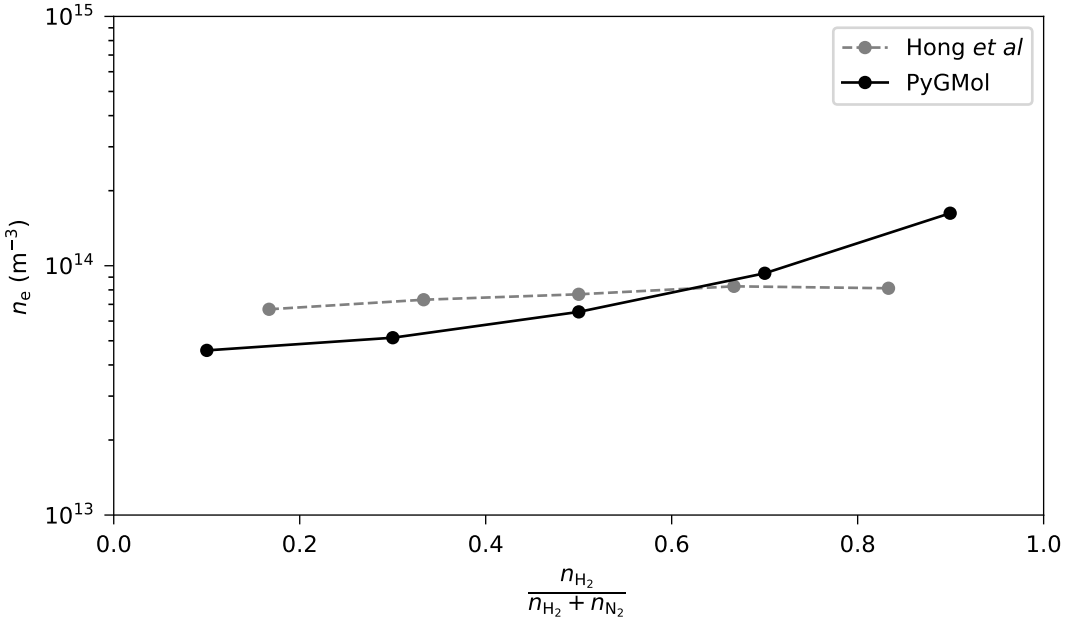

Figure 5.9: Number density of electrons as a function of H_2 fraction in the feedstock gas, modelled with PyGMol global model and detailed N_2–H_2 chemistry set at atmospheric pressure. Comparison with results presented in the source publication of the chemistry set [5].

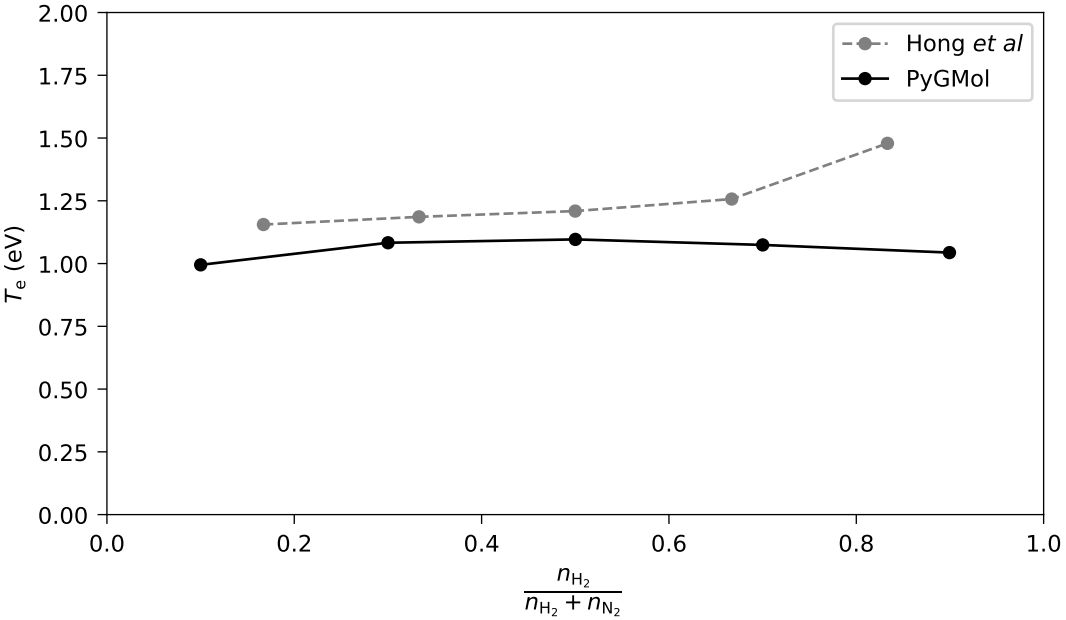

Figure 5.10: Electron temperature as a function of H_2 fraction in the feedstock gas, modelled with PyGMol global model and detailed N_2–H_2 chemistry set at atmospheric pressure. Comparison with results presented in the source publication of the chemistry set [5].

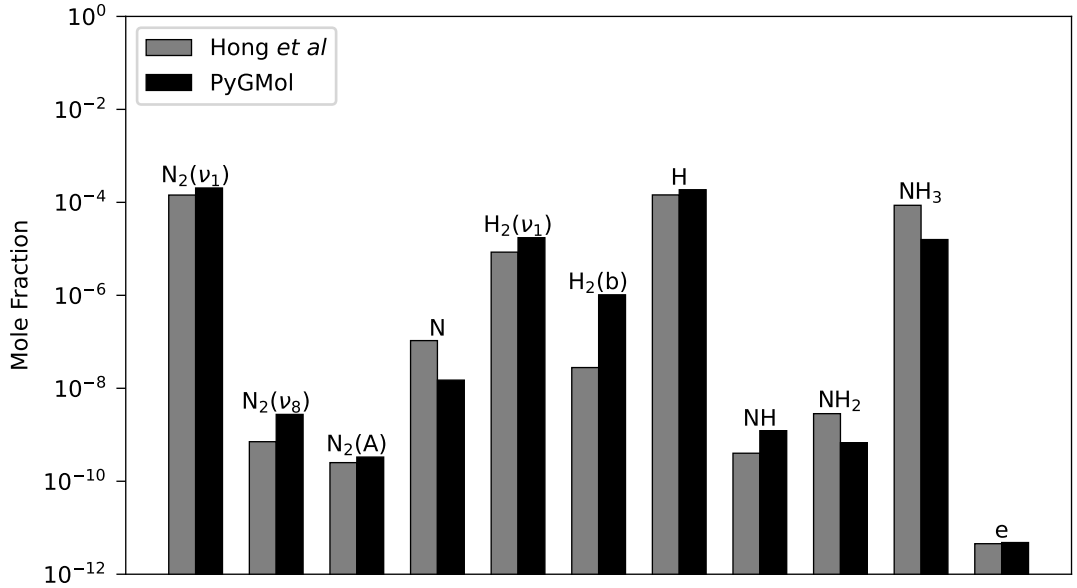

Figure 5.11: Mole fractions of major species, modelled with PyGMol global model and detailed N_2–H_2 chemistry set at atmospheric pressure, considering only wall relaxation of excited species from table 5.5 (excluding the surface conversion of H_2 to NH_3). Comparison to the results presented in the source publication of the chemistry set [5].

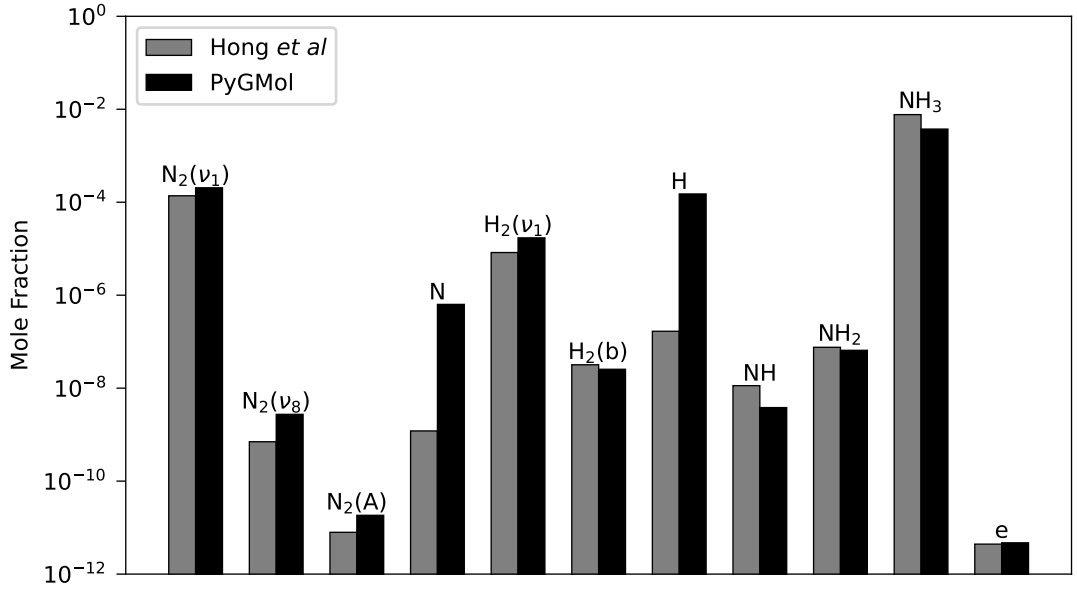

Figure 5.12: Mole fractions of major species, modelled with PyGMol global model and detailed N_2–H_2 chemistry set at atmospheric pressure, considering all the surface kinetics in table 5.5. Comparison to the results presented in the source publication of the chemistry set [5].

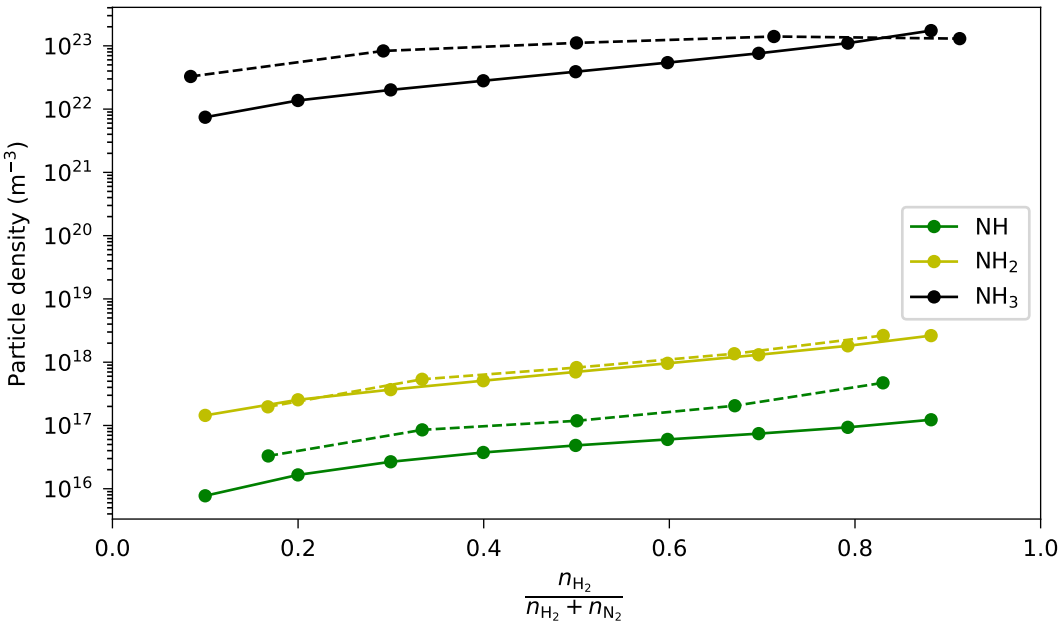

Figure 5.13: Density of the NH_x neutral species as a function of the gas composition, modelled with PyGMol global model and detailed N_2–H_2 chemistry set at atmospheric pressure, considering all the surface kinetics in table 5.5. Comparison to the results presented in the source publication of the chemistry set [5].

qualitative agreement with the source publication results was achieved. The electron temperature and density on figures 5.9, and 5.10, show a reasonably good quantitative agreement, although the qualitative trends with changing feedstock gas ratio are not reproduced very well.

The mole fractions of number of featured species on figures 5.11, and 5.12, also agree reasonably well with the source publication results. The data on figure 5.11 were obtained considering the surface relaxation of excited states only, while the results on figure 5.12 correspond to the full surface kinetics listed in table 5.5. Several species do not match the source publication results very well, such as atomic N and H in the model with $H_2 \rightarrow NH_2$ surface conversion (figure 5.12) or the H_2(b) state in figure 5.11.

Finally, the figure 5.13 shows a nice agreement for NH_x neutrals densities as functions of the gas composition, although the non–monotonic behaviour of NH_3 (consistent also with other publications [156; 157; 158]) was sadly not reproduced by PyGMol global model with its simplified surface model.

The disagreement between modelling results obtained in this work and results obtained by much more sophisticated global model in the source publication is hardly surprising. There are many important differences between PyGMol, and the model used by Hong *et al*, few potentially quite crucial, such as solving for the electron energy distribution function (while assuming Maxwellian EEDF in the present work), and a full treatment of heterogeneous surface reactions with explicit tracking of surface–adsorbed species. Even disregarding the surface interactions, the diffusion of species towards surfaces will likely be very different for both models, since the source publication is working with the packed–bed reactor with much larger A/V ratio and much lower diffusion length Λ, compared to the present work due to PyGMol model limitations. However, it should be reiterated, that the aim of present work is not development of a global model, but development of a reduction technique, which uses global model as one of its inputs. In that regard, the present N_2–H_2 chemistry set will be an important test chemistry set for the developed reduction method, with some species (mainly NH_x) densities being dominantly controlled by surface diffusion and conversion, rather than volumetric processes.

PyGMol validation of the low pressure chemistry set (S3)

For the low pressure case, the surface coefficients were modified slightly compared to the atmospheric pressure case, to reflect higher degree of H_2 dissociation at lower pressure and to loosely match the modeling results presented by Carrasco *et al* [153]. The surface coefficients for the low pressure N_2–H_2 case are also listed in table 5.5 Figure 5.14 shows how the PyGMol solution for some species densities with the low–pressure N_2–H_2 model compares to the modeling results obtained by Carrasco *et al*.

The model parameters used for the low–pressure N_2–H_2 modeling in the present work are summarized in tables 5.10, and 5.11. The pressure, gas temperature, plasma dimensions, and the feedstock gas flow ratio are the same as used by Carrasco *et al*, while the total feed flow has been set to value consistent with the residence time reported by Carrasco *et al*. The electron density is not correctly reported by Carrasco *et al*, so the ICP–equivalent absorbed power could not have been calibrated, as in the case of the previous two chemistry sets. Therefore, the

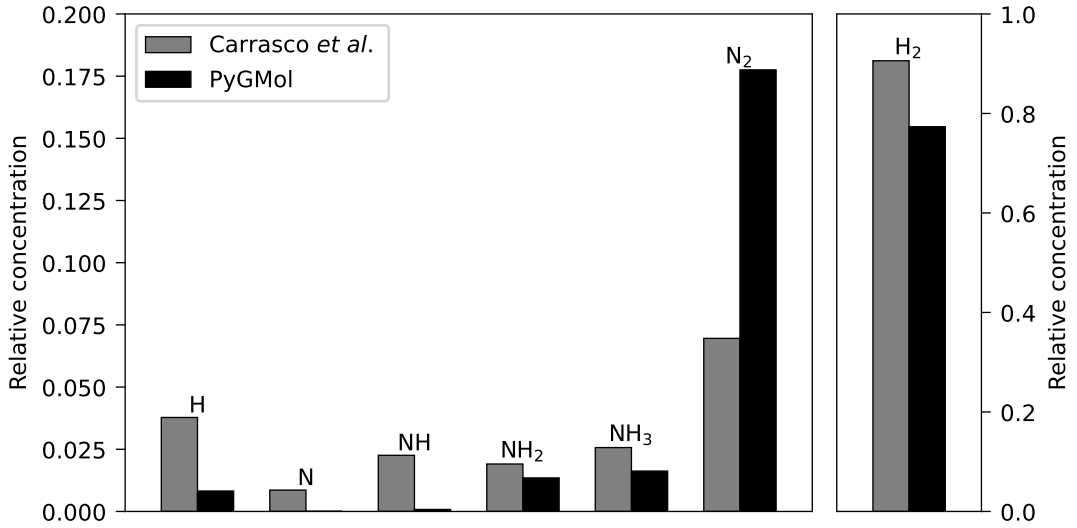

Figure 5.14: Relative concentrations of selected species, modeled with PyGMol model and the detailed N_2–H_2 chemistry set at 8 Pa pressure. Comparison with modeling results presented by Carrasco *et al* [153].

absorbed power was set to a value of 10 W, which corresponds roughly to 20 % of the CCP power reported by Carrasco *et al.* This value of absorbed power yields optimal fit for the relative densities (figure 5.14), with lower power values yielding better fit for the N_2, H_2, NH_2, and NH_3 species but worse fit for H, N, and NH species, and higher power values vice versa. As the chemistry set by Carrasco *et al* does not resolve vibrationally excited states of N_2 and H_2, the results of present work shown in figure 5.14 for N_2 and H_2 are actually sums of densities of ground states and all included vibrational states $N_2(\nu_1 - \nu_8)$ and $H_2(\nu_1 - \nu_3)$.

It can be argued that the agreement between results for the low–pressure N_2–H_2 calculation between the present work and the work by Carrasco *et al* is fairly poor (figure 5.14), but this is understandable, since both models employ very different chemistry set and surface interaction schemes. Nevertheless, the N_2–H_2 chemistry will serve as a good test chemistry set for a low–pressure reduction conditions, with production and consumption rates for some species dominated by surface processes.

Table 5.6: Species included in the test chemistry set for CF_4–CHF_3–H_2–Cl_2–O_2–HBr plasma, taken from the QDB database (chemistry C27). The * symbol denotes the lowest–energy electronically excited states.

Neutrals	H H_2 C O O_2 F F_2 Cl Cl_2 Br CH CH_2 OH H_2O HF HCl HBr CO CO_2 CF CF_2 CF_3 CF_4 FO ClO CHF CHF_2 CHF_3 COF COF_2
Excited states	O^* F^* Cl^* Br^*
Positive ions	H^+ H_2^+ H_3^+ C^+ C_2^+ O^+ O_2^+ F^+ F_2^+ Cl^+ Cl_2^+ Br^+ CH^+ CH_2^+ $C_3H_5^+$ $C_3H_8^+$ H_2O^+ HCl^+ HBr^+ CO^+ CO_2^+ CF^+ CF_2^+ CF_3^+ ClO^+ CHF^+ CHF_2^+
Negative species	e O^- F^- Cl^- Br^- CF_3^-

5.3 Other test chemistry sets (S4 – S6)

Three additional test chemistry sets are used in present work to test the reduction technique: sets for plasma in CF_4–CHF_3–H_2–Cl_2–O_2–HBr, CH_4–N_2, and finally Ar–NF_3–O_2. These chemistry sets were chosen with no regard to any specific target application, and they were adopted directly from the pre–compiled plasma chemistries given by the QDB database [9]; their consistency and validity was not verified in the present work. They can be regarded as mere *generators* of non–linear outputs needed for analysis of the species ranking methods defined in chapter 4. Tables 5.6 – 5.8 summarize all the species included in these chemistry sets.

The full lists of reactions and their kinetic can be found in the QDB database. In the instances of reactions described by cross–sectional kinetics, the data from QDB were fitted to the Arrhenius form on a grid on Maxwellian temperatures. For better clarity and less ambiguity, the reaction kinetics data for all the three additional test chemistry sets from QDB are also provided in tables A.5, A.6, and A.7 in Appendix A, together with data sources cited in QDB database. Default surface coefficients were used for all the QDB test chemistry sets, as defined in table 5.3.

5.4 Reduction cases

Six *test reduction cases* are considered for each test chemistry set, each with a different set of species of interest. This makes 36 reduction cases, each case specified

Table 5.7: Species included in the test chemistry set for CH_4–N_2 plasma, taken from the QDB database (chemistry C28). The * symbol denotes the lowest–energy electronically excited states.

Neutrals	H H_2 C C_2 N N_2 CH CH_2 CH_3 CH_4 CN C_2H C_2H_2 C_2H_3 C_2H_4 C_2H_5 C_2H_6 C_3H_5 C_3H_6 C_3H_7 C_3H_8 C_4H_2 NH NH_2 NH_3 N_2H N_2H_2 N_2H_3 N_2H_4 HCN H_2CN M
Excited states	H^* H_2^* N^* N_2^*
Positive ions	H^+ H_2^+ H_3^+ C^+ C_2^+ N^+ N_2^+ N_3^+ N_4^+ CH^+ CH_2^+ CH_3^+ CH_4^+ CH_5^+ C_2H^+ $C_2H_2^+$ $C_2H_3^+$ $C_2H_4^+$ $C_2H_5^+$ $C_2H_6^+$ NH^+ NH_2^+ NH_3^+ NH_4^+
Negative species	e H^-

Table 5.8: Species included in the test chemistry set for Ar–NF_3–O_2 plasma, taken from the QDB database (chemistry C33). The * and ** symbols denote the electronically excited states with the lowest energies.

Neutrals	Ar O O_2 O_3 N N_2 F F_2 NO N_2O NO_2 NF NF_2 NF_3 FO FNO
Excited states	Ar^* Ar^{**} O^* O_2^* N^* N_2^*
Positive ions	Ar^+ O^+ O_2^+ N^+ N_2^+ F^+ F_2^+ NO^+ N_2O^+ NF^+ NF_2^+ NF_3^+
Negative species	e O^- O_2^- O_3^- F^-

by the pair

$$\text{reduction case} = \{\text{chemistry set},\ \text{species of interest}\}.$$

All the reduction cases considered in the present work are listed in table 5.9. For each reduction case, the species of interest consist of a set of selected negative species (always including an electron), two sets of selected positive species (with higher and lower densities), and three sets of selected neutrals (including one consisting purely of selected excited states.) In some cases, the choice of the species interest is inspired by the chemistry set source publication (such as in the reduction cases C1.4 and C1.5, which feature species identified as important radicals and transient species respectively by Turner [22]), but in most cases, the choice was made purely arbitrarily.

The reduction conditions for each reduction case are summarized in table 5.10.

Table 5.9: Summary of all the 36 test reduction cases addressed in the present work. Six sets of species of interest were considered for each test chemistry set.

Case ID	Test chemistry set	Species of interest
C1.1	O_2–He	e O^- O_3^-
C1.2		O_2^+ O_4^+
C1.3		O^+ He^+
C1.4		O $O_2(a\,^1\Delta_g)$ O_3
C1.5		$O(^1D)$ $O(^1S)$ $O_2(b\,^1\Sigma_g^+)$
C1.6		$O_3(\nu)$ $O_2(\nu)$ He^*
C2.1	N_2–H_2 (atm)	e H^-
C2.2		NH_4^+
C2.3		NH_3^+ H_2^+
C2.4		NH NH_2 NH_3
C2.5		$N_2(\nu_1)$ $H_2(\nu_1)$
C2.6		$N_2(A\,^3\Sigma_u^+)$ $H_2(B\,^1\Sigma_u^+)$
C3.1	N_2–H_2 (low)	e H^-
C3.2		NH_4^+
C3.3		NH_3^+ H_2^+
C3.4		NH, NH_2 NH_3
C3.5		$N_2(\nu_1)$ $H_2(\nu_1)$
C3.6		$N_2(A\,^3\Sigma_u^+)$ $H_2(B\,^1\Sigma_u^+)$
C4.1	CF_4–CHF_3–H_2–Cl_2–O_2–HBr	e O^-
C4.2		Cl^+ Br^+
C4.3		CF^+ CO^+
C4.4		OH CH
C4.5		F Cl
C4.6		O^* F^*
C5.1	CH_4–N_2	e H^-
C5.2		NH_4^+ CH_3^+
C5.3		N_2^+ H_2^+
C5.4		C_2H_3 C_2H_6
C5.5		CH_2 CH_3
C5.6		N_2^* H_2^*
C6.1	Ar–NF_3–O_2	e F^- O^-
C6.2		O_2^+ NO^+ O^+
C6.3		NF^+ NF_2^+ NF_3^+
C6.4		NF NF_2 NF_3
C6.5		O F
C6.6		O^* N^* Ar^*

The reduction conditions were kept the same for each reduction case belonging to any single chemistry set. For the first three chemistry sets, the reduction conditions are taken from Turner *et al* [22], Hong *et al* [5], and Carrasco *et al* [153] respectively. For the chemistry sets sourced from QDB (C4.1 – C6.6), the reduction conditions were set arbitrarily, with exception to the Ar–NF_3–O_2 chemistry set, which adopts the conditions presented in the validation notes in QDB.

Table 5.10: Summary of the reduction conditions for all the chemistry sets considered: pressure p, gas temperature T_g, absorbed power P, the reactor dimensions r and z, the total feedstock gas flow Q and the ratio of the feedstock gases.

Test set	$\boldsymbol{p}$ (Pa)	$\boldsymbol{T_g}$ (K)	$\boldsymbol{P}$ (W)	$\boldsymbol{r}$ (mm)	$\boldsymbol{z}$ (mm)	$\boldsymbol{Q}$ (sccm)	**Ratio**
O_2–He	10^5	305	0.3	0.564	30	300	1:250
N_2–H_2 (atm)	10^5	400	35	25	25	60	1:2
N_2–H_2 (low)	8	300	10	50	340	15	1:9
CF_4–…–HBr	25	300	500	100	100	600	1:1:1:1:1:1
CH_4–N_2	10^5	300	5000	20	100	110	1:10
Ar–NF_3–O_2	100	1500	400	40	200	1150	1:2:20

Table 5.11: Simulation time t_{end}, power pulse duration Δt_{pulse}, and the sets of the times of interest for each one chemistry set considered. Power pulsing was only done for the O_2–He chemistry set, with the pulsing period of 6 ms; the remaining sets were modeled using constant power.

Test set	$\boldsymbol{\Delta t_{pulse}}$ (ms)	$\boldsymbol{t_{end}}$ (s)	**Times of interest**
O_2–He	3	1.2×10^{-2}	6.3×10^{-3}, 6.9×10^{-3}, $\cdots$, 11.7×10^{-3}
N_2–H_2 (atm)	–	100	10^{-3}, 10^{-2}, 10^{-1}, 10^{0}, 10^{1}, 10^{2}
N_2–H_2 (low)	–	10	10^{-3}, 10^{-2}, 10^{-1}, 10^{0}, 10^{1}
CF_4–…–HBr	–	100	10^{-3}, 10^{-2}, 10^{-1}, 10^{0}, 10^{1}, 10^{2}
CH_4–N_2	–	100	10^{-3}, 10^{-2}, 10^{-1}, 10^{0}, 10^{1}, 10^{2}
Ar–NF_3–O_2	–	0.2	10^{-4}, 10^{-3}, 10^{-2}, 10^{-1}

Table 5.11 lists the times of interest used to build the species rankings from the test chemistry sets and to evaluate the reduction error within the iterative reduction algorithm. The same times of interest were used for all reduction cases belonging to any single chemistry set. In the case of the pulsed–power reduction cases with the O_2–He chemistry set (C1.1 – C1.6), the times of interest are distributed linearly,

covering the whole power cycle. In the remaining cases of constant–power reduction conditions, the times of interest are distributed logarithmically, to capture not only the steady–state conditions but also the evolution from the initial conditions. The simulation times t_{end} (also shown in table 5.11) were chosen to be sufficiently long for each reduction case to reach a steady state.

Chapter 6

Chemistry reduction results

Altogether, 14 different species ranking methods were introduced in chapter 4, section 4.2, based on path searches in graphs representing chemistry. These ranking methods are built around 4 separate ways to calculate direct interaction coefficients w (4.10a) – (4.10d), together with 4 separate methods of devising coupling coefficients W between any two species, based on different graph path search algorithms, introduced in section 4.2.2; (4.10b), and (4.10d) yield direct interaction coefficients which are not bound between 0 and 1, excluding the chemistry graphs from the use of the maximal propagated error search method. Apart from the graph–based species ranking methods, two additional methods were proposed as benchmarks, based on the Morris method of sensitivity analysis (section 4.3), and the species density ranking (section 4.4).

All the 16 species ranking schemes presented were tested with the species–oriented iterative skeletal reduction method introduced in chapter 2 on an array of 36 test reduction cases listed in table 5.9, and with further plasma conditions and model parameters listed in tables 5.10 and 5.11. The same maximal reduction error $\Delta = 10$ % was considered in the reduction method with all the test reduction cases. The species ranking scheme yielding the best results with the ranking–based iterative reduction method was identified statistically.

Apart from the *static* iterative reduction method (section 2.1, figure 2.1), a *dynamic* ranking–based iterative reduction method (section 2.3, figure 2.5), was also tested on all the reduction cases, with most of the graph–based species ranking meth-

ods. The graph–based ranking scheme using the *maximal error flow search* method for calculation the species coupling coefficients was not tested with the dynamic reduction method, because the computational expanse of the ranking algorithm is much higher than the expense of the global model, and reduction error evaluation. The benchmark ranking scheme based on the Morris method of sensitivity analysis was also not tested with the dynamic reduction method for the very same reason. Table 6.1 summarizes all the instances of ranking–based iterative reduction method runs performed in the present work.

Table 6.1: Summary of the instances of the ranking-based iterative reduction method runs, performed in the present work.

	Instances tested
Chemistry sets	6
Sets of species of interest (per chemistry set)	6
Reduction cases	36
Ranking schemes	16
Static reduction runs	576
Dynamic reduction runs	360
Reduction runs	936

The following sections define the performance metrics used to assess the performance (or *fitness*) of each ranking scheme, and the final results for all the performed chemistry reduction runs.

6.1 Species ranking performance metrics

To compare the competing species ranking schemes, some performance metrics are introduced, quantifying the ranking schemes' performance with the ranking–based iterative reduction method. The most straightforward measure of ranking method performance is the number of eliminated species N_ϵ from any chemistry set. Aside from a *suitability* of any species ranking scheme for the chemistry reduction method with any given reduction case, the main parameter affecting the N_ϵ will be the maximum allowed number of consequent unsuccessful species eliminations N_δ, as the termination condition of the reduction algorithm (section 2.1.3). Generally, higher N_δ will result in higher N_ϵ, and more significant reduction of any chemistry

set. At the same time, however, the number of plasma model calls N_μ will also increase with N_δ. It is evident, that N_μ is also a very important metric, since it almost fully determines the computational cost of the reduction algorithm.

Clearly, for a given species ranking method, both N_ϵ, and N_μ will vary between reduction cases, with different number of species in each chemistry set N_S, and different sets of species of interest. Therefore, appropriate metrics of performed reduction performance with any species ranking scheme might be defined as

$$\eta = \frac{N_\epsilon}{N_\mu}, \tag{6.1a}$$

$$\eta' = \frac{N_\epsilon}{N_\mathrm{S}}. \tag{6.1b}$$

For a direct comparison of the competing species ranking schemes, I define the number of eliminated species by the j–th ranking scheme in the k–th reduction case as $N^j_{\epsilon,k}$. This is followed with the number of eliminated species by the best–performing ranking scheme in the k–th reduction case, as

$$N^{\max}_{\epsilon,k} = \max_j N^j_{\epsilon,k}. \tag{6.2}$$

For any j–th ranking scheme, the value of

$$\Delta^{\max,j}_k = N^{\max}_{\epsilon,k} - N^j_{\epsilon,k} \tag{6.3}$$

will determine how well it performs against the best ranking scheme in the k–th reduction case. Any well–performing ranking scheme should have consistently low values of $\Delta^{\max,j}_k$ for any reduction case. To assess the performance of the j–th ranking scheme on the whole array of test reduction cases (table 5.9), the *deviation from the best* parameter σ^j can be evaluated as

$$\sigma^j = \left[\frac{1}{N}\sum_k (\Delta^{\max,j}_k)^2\right]^{\frac{1}{2}}, \tag{6.4}$$

where $N = 36$ is the number of reduction cases considered. The σ value is a good measure of a *performance* of a single method in a pool of other species ranking methods, since it quantifies how many more species were eliminated on average by the reduction using *the best* ranking method for every reduction case. A lower value of σ translates to a better species ranking scheme for species reduction, while the lower bound for σ is 0, for a hypothetical j–th ranking scheme, which would result in an elimination of the highest number of species (compared to all the other competing ranking schemes), for every single reduction case, or

$$\sigma^j = 0 \iff \forall k : \left(N^j_{\epsilon,k} = N^{\max}_{\epsilon,k} \text{ and } \Delta^{\max,j}_k = 0\right).$$

In reality, there is a distribution of $\Delta^{\max,j}$ across the different reduction cases.

Of course both $\Delta^{\max,j}_k$, and σ^j will be influenced not only by how well the j–th ranking scheme performs in the reduction method, but also by the chosen value of N_δ, or the maximal allowed streak of unsuccessful species eliminations, as the algorithm termination condition. The results were studied for different values of N_δ, however, it was found that $N_\delta = 2$ offers a good balance between the number of eliminated species, and the number of plasma model calls, for the majority of the ranking methods.

Finally, the last measure of performance of a ranking scheme considered here is a correlation between the ranking scores C_i for any given i–th species in the chemistry set, and the reduction error δ_i induced by elimination of the species from the chemistry set. For each k–th reduction case and j–th ranking scheme, the Spearman's correlation coefficient r is evaluated on a sample of paired data $\{(C_i, \delta_i)\}$ Each sample $\left\{\left(C^j_{k,i}, \delta^j_{k,i}\right)\right\}$ consists only of data belonging to one reduction case and one ranking scheme, where ranking scores C_i are calculated with the detailed chemistry set and each reduction error δ_i is the reduction error induced by eliminating a *single* i–th species from the detailed chemistry set. A mean correlation coefficient is defined for each j–th ranking scheme as the mean over all the reduction cases,

weighted by the sample sizes N_k^{s}

$$r_{C\delta}^{j} = \frac{\sum_{k=1}^{N_{\mathrm{c}}} N_k^{\mathrm{s}} r_{C\delta,k}^{j}}{\sum_{k=1}^{N_{\mathrm{c}}} N_k^{\mathrm{s}}}, \tag{6.5}$$

where N_{c} is the number of reduction cases.

Considering the definition of the reduction error δ, (2.1), (2.4), and the simplest case of a single species of interest A, and a single time of interest, it is clear that δ value is highly asymmetric in the sign of the expression

$$\frac{\mathrm{A}^{\mathrm{red}} - \mathrm{A}^{\mathrm{full}}}{\mathrm{A}^{\mathrm{full}}},$$

and it follows that

$$\delta \in \begin{cases} [0,1] & \text{for } \mathrm{A}^{\mathrm{red}} \leq \mathrm{A}^{\mathrm{full}}, \\ (0,\infty) & \text{for } \mathrm{A}^{\mathrm{red}} > \mathrm{A}^{\mathrm{full}}. \end{cases} \tag{6.6}$$

This asymmetry would skew the correlation coefficients and therefore separate samples are formed for both cases and a pair of distinct correlation coefficients, $r_{C\delta}^{+}$, and $r_{C\delta}^{-}$, was considered for each j–th ranking scheme, with

$$r_{C\delta}^{j} = \begin{cases} r_{C\delta}^{-,j} & \text{for } \delta^j = \max_{l,m} \mid \delta_l^j(t_m) \mid = \max_{l,m} \delta_l^j(t_m), \\ r_{C\delta}^{+,j} & \text{for } \delta^j = \max_{l,m} \mid \delta_l^j(t_m) \mid = -\min_{l,m} \delta_l^j(t_m), \end{cases} \tag{6.7}$$

The indices l, m are in this occasion running over the species of interest and times of interest, respectively (see section 2.1.2).

The choice of the Spearman's coefficient as a measure of the C_i–δ_i correlation is convenient, because it does not assume any specific relation and distribution, but rather it assesses only how well the relationship between the two variables can be described as a monotonic function.

The different ranking performance measures introduced in this chapter might be loosely divided into two groups: *computational* metrics, such as (6.1), with regards to the computational cost of the reduction method, and the *physical* metrics, such as (6.4), (6.5), which relate to the *fitness* of the output reduced chemistry set.

As the computational metrics are not really comparable between the individual test reduction cases, it would be problematic to use them for selection of the best performing ranking scheme. Instead, the computation metrics were used informally to select the appropriate N_δ value, which is on its own a purely computational parameter and influences the balance between the computational time and the *size* of the reduction. On the other hand, the physical metrics parameters are better suited for comparison of different ranking schemes across the different test reduction cases, and as such were used to identify the best performing ranking scheme (measured in terms of reduction size, *not* the computational cost).

6.2 Comparison of ranking schemes

Firstly, the correlation coefficients $r_{C\delta}$, (6.5), between the species ranking scores C, and reduction errors δ induced by the species elimination, was investigated. Figure 6.1 shows $r_{C\delta}$ for each ranking scheme introduced in chapter 4, averaged over all the test reduction cases (chapter 5). It is evident, that in the set of reduction cases investigated, all the ranking schemes based on chemistry graphs with DRG and DRGEP direct interaction coefficients (see section 4.2.1), together with the Morris method ranking (section 4.3.2), correlated better with errors induced than the rest.

For all the ranking schemes, however, there was a significant spread in the correlation coefficients between the individual reduction cases. To illustrate the point, figure 6.2 shows the relationship between C, and δ for the method with the highest average $r_{C\delta}$ ($\mathrm{DRGEP}_{\mathrm{max.flow}}$), and for two individual reduction cases with highest and lowest value of $r^{-}_{C\delta} + r^{+}_{C\delta}$ among all the reduction cases. The best–correlating reduction case for this ranking method was the reduction case C1.3 (O_2–He chemistry set with species of interest O^+, He^+), and the case with the worst correlation was the reduction case C2.2 (N_2–H_2 atmospheric–pressure chemistry set with species of interest NH_4^+).

Next, the data from the actual ranking–based iterative reduction method runs on all the reduction cases were analysed. To establish the optimal N_δ parameter

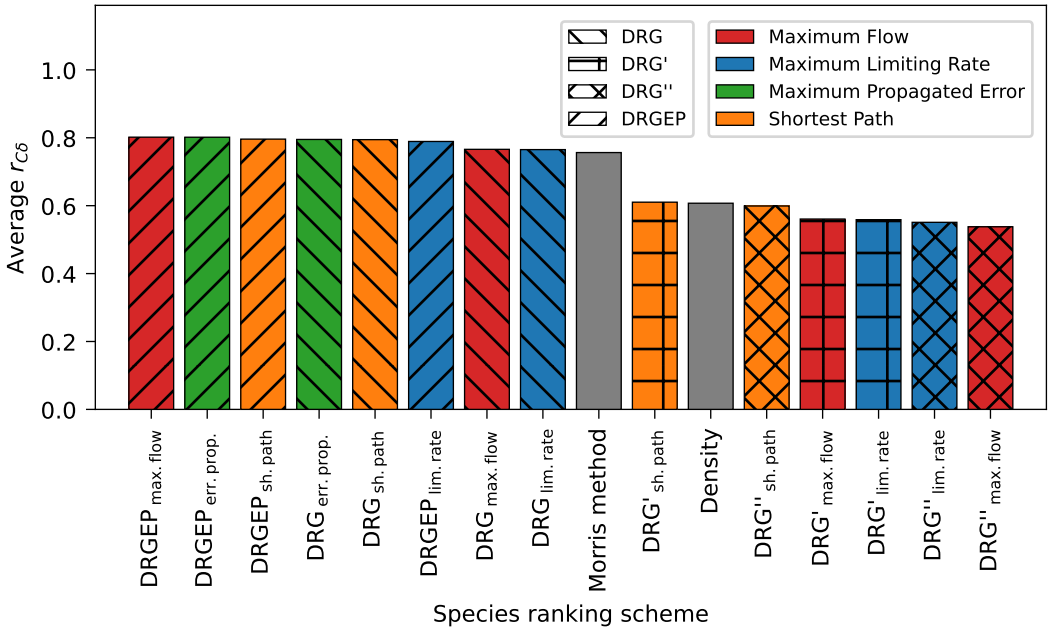

Figure 6.1: Spearman's coefficient of correlation between species ranking scores C and reduction errors δ induced by the species elimination. The correlation coefficients shown for each ranking method are averaged over all the reduction cases. For better clarity, the bars for the ranking schemes based on the chemistry graph are color–coded to distinguish the different graph search algorithms (or species coupling coefficients), and pattern–coded according to the different different graph edge weighting methods (or direct interaction coefficients).

(maximal allowed number of successive unsuccessful species elimination), the trade–off between the number of species eliminated, and the number of plasma model calls (associated with the computational cost) was investigated. Although there was once again a large spread across different reduction cases and species ranking schemes, a typical illustration of this trade–off can be seen in figure 6.3, which shows η, and η', (6.1), for a single (arbitrarily chosen) reduction case C1.5, and for the set of best–performing species ranking schemes (DRG, DRGRP and Morris method ranking). Along with the individual ranking schemes, also their mean is plotted, and an ideal case, modeled on the maximal number of eliminated species across all the ranking schemes and choices of N_δ (in the case of figure 6.3, it was 11) all being eliminated during the first iterations. It appears that $N_\delta = 2$ might be considered a good choice of the N_δ parameter value, bringing η' (together with the number of eliminated species) reasonably close to the maximal value. Additional increase of N_δ

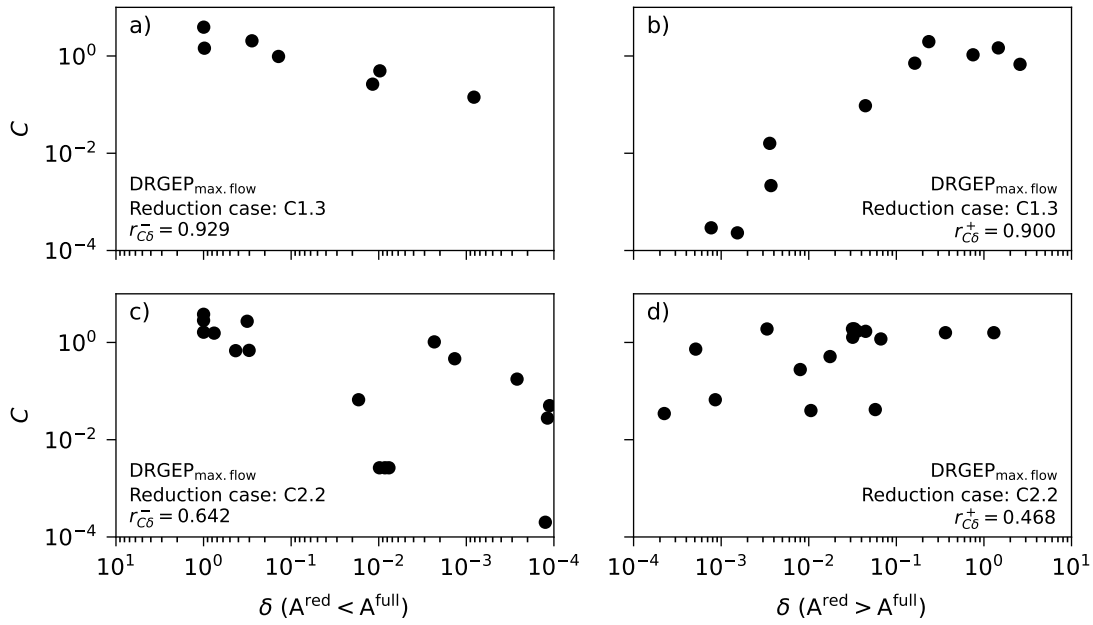

Figure 6.2: Relationship between C and δ for the DRGEP$_{\text{max.flow}}$ ranking method and for two reduction cases with the highest (a, b) and the lowest (c, d) error correlation. The samples with $A^{\text{red}} < A^{\text{full}}$ (a, c) and $A^{\text{red}} > A^{\text{full}}$ (b, d) are plotted separately.

decreases η (increasing computational time) with a minimal benefit to η'. Although figure 6.3 only shows data for a single reduction case, this was true for most of the reduction cases considered in present work.

In order to compare the static and dynamic ranking–based iterative reduction methods (sections 2.1 and 2.3 respectively), the *deviation from the best* parameter σ, (6.4), was compared for both static and dynamic methods, and for most of the chemistry graph–based species ranking schemes. The σ value is a good measure of a method *fitness* in a pool of other species ranking methods, since it quantifies how many more species were eliminated on average by the reduction, which used *the best* ranking scheme per each reduction case. Figure 6.4 shows the difference in σ between the static and dynamic reduction for every ranking scheme which was used in a dynamic reduction and for three different choices of N_δ. Oddly, the figure shows that for the best–performing ranking schemes (DRG and DRGEP–based), the dynamic reduction method appears to be, with some consistency, performing marginally worse than the static reduction method, which certainly should not be

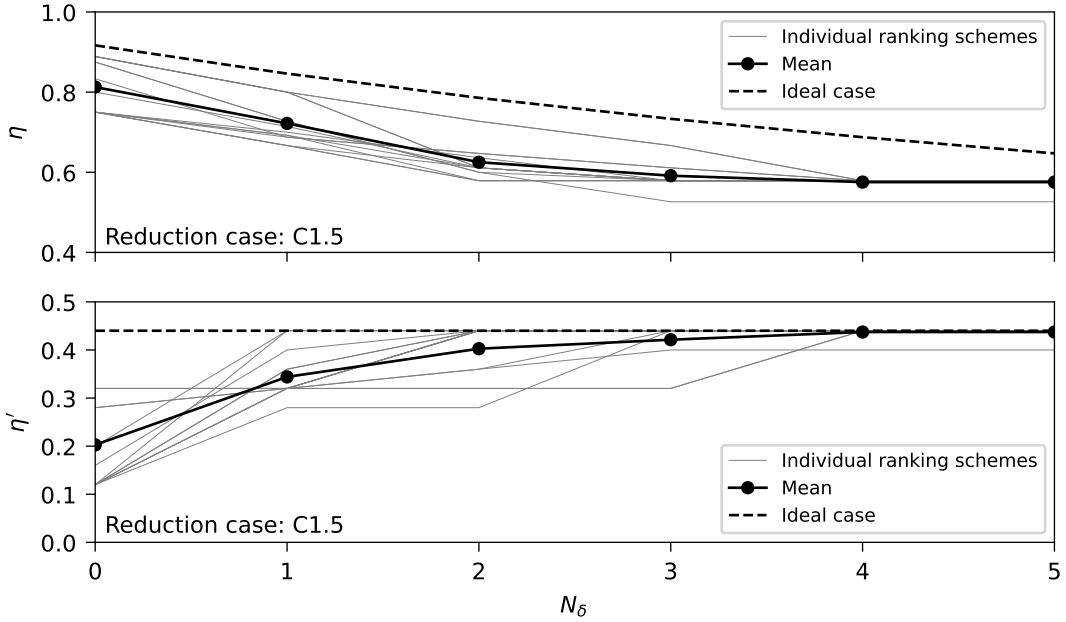

Figure 6.3: Reduction parameters η and η' for a single reduction case C1.5 and a set of best–performing species ranking schemes for this reduction case. The data for the individual ranking schemes are plotted, together with their mean and the data modeled on the ideal case (with the maximum number of species eliminated during the first iterations).

the case. The difference between static and dynamic reduction is, however, indeed marginal only, and might be due to a statistical noise. The dynamic re–evaluation of the species ranking inside the reduction iteration loop (as in the dynamic reduction method) might be of greater importance if allowing for larger maximal reduction error Δ, but with $\Delta = 10$ % used in present work, it appears that the changes to the system induced by species elimination are not large enough to significantly modify the ranking of the set of retained species. Figure 6.4 also shows that σ rises with N_δ consistently for each species ranking scheme. This is due to larger statistical differences between ranking schemes for lower N_δ; for the case of $N_\delta = 0$, a single species with an underestimated ranking score for any one of the ranking schemes can terminate the reduction very early and therefore increase its σ value, while for higher N_δ, more adjacent species with an underestimated ranking score need to appear in the species ranking to terminate the reduction, which is statistically less likely, especially with better performing ranking schemes.

A comparison of the σ values for the static reduction with all the ranking schemes

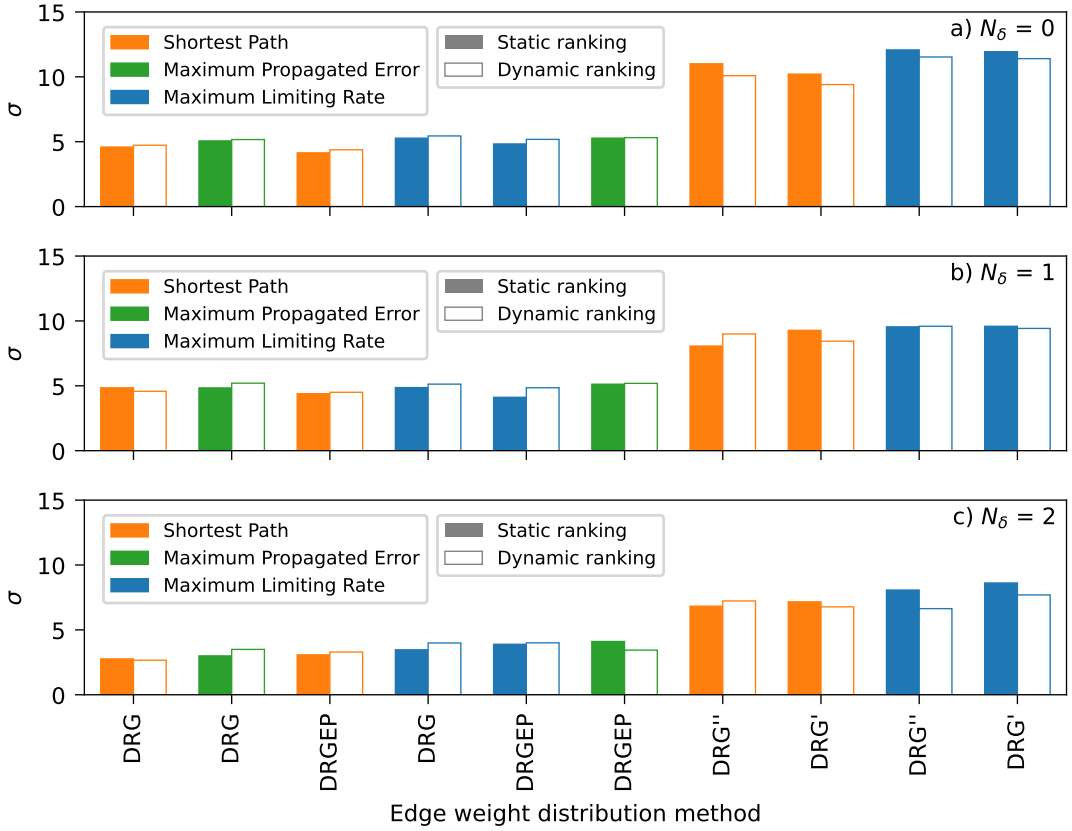

Figure 6.4: Comparison of the σ values for most of the chemistry graph–based species ranking methods and for three choices of $N_\delta \in \{0, 1, 2\}$. The ranking schemes are ordered with increasing σ with static ranking reduction and with $N_\delta = 2$. The bars are color–coded consistently with figure 6.1 by different graph search algorithms (different species coupling coefficients) used in the ranking schemes.

considered in this work is shown in figure 6.5, for three different choices of N_δ. The species ranking scheme using the DRG definition of direct interaction coefficients w_{DRG} (4.10a), and the shortest path approach for the calculation of the coupling coefficients $W_{\mathrm{AB}}^{\mathrm{sh.path}}$ (4.14) can be identified as providing species rankings which perform consistently well with the ranking–based iterative reduction method for $N_\delta = 2$. Regarding constructing the chemistry graph, the DRG (4.10a), and DRGEP (4.10c) methods for direct interaction coefficients give significantly better results than DRG' (4.10b), and DRG" (4.10d) methods, while the *shortest path* method for species coupling coefficients $W_{\mathrm{AB}}^{\mathrm{sh.path}}$ appears to yield marginally better results than the rest.

Finally, the histograms in figure 6.6 show the distribution of $\Delta^{\max}$ (6.3), over all

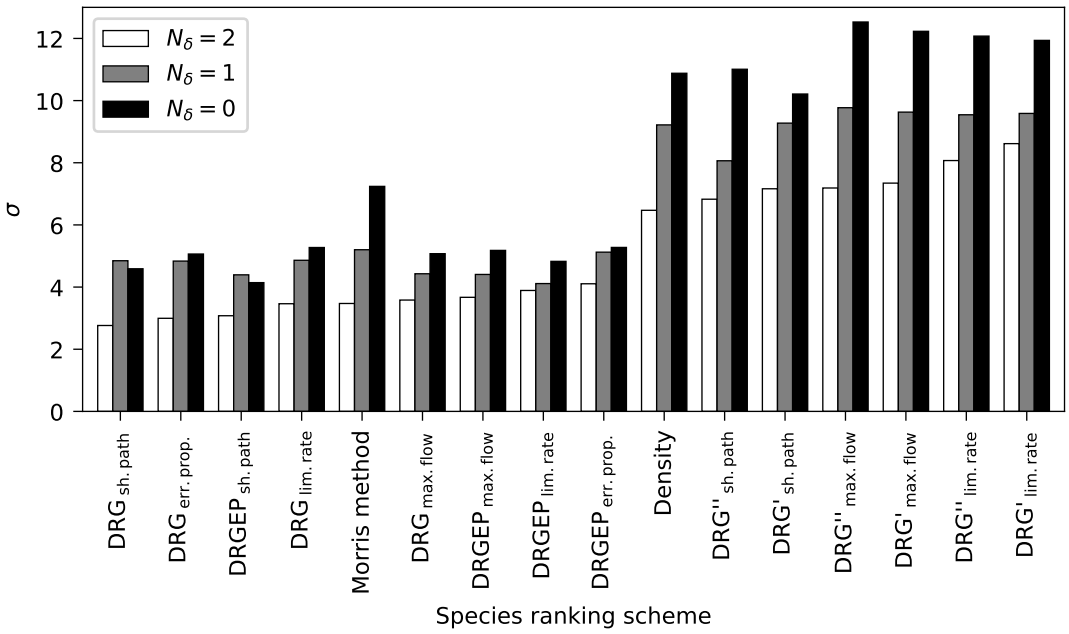

Figure 6.5: Comparison of the σ values (6.4) for all of the species ranking schemes considered in the present work and for three choices of $N_\delta \in \{0, 1, 2\}$. The ranking schemes are ordered with increasing σ for $N_\delta = 2$. The bars are color-coded by different values of N_δ used for the ranking–based iterative reduction method. The ranking schemes are labeled with the different methods of calculating the direct interaction coefficients w and the coupling coefficients W; e.g. the method labeled $\mathrm{DRG}_{\mathrm{sh.path}}$ uses w_{DRG} (4.10a) and $W_{\mathrm{AB}}^{\mathrm{sh.path}}$ (4.14) respectively. The *density* species ranking scheme simply ranks the species according to their density as modeled by the plasma model employed with the detailed chemistry set.

the reduction cases, and for 3 different choices of N_δ. Histograms for the *optimal* $\mathrm{DRG}_{\mathrm{sh.path}}$ species ranking scheme are plotted, together with the Density ranking scheme benchmark. The distribution for the $\mathrm{DRG}_{\mathrm{sh.path}}$ species ranking scheme is centered reasonably tightly around the optimal value of $\Delta^{\max} = 0$, however, there are some instances of reduction cases, where this ranking scheme performs significantly worse than the best–performing ranking scheme. By contrast, the ranking scheme based simply on species density values shows distribution with a significantly wider spread.

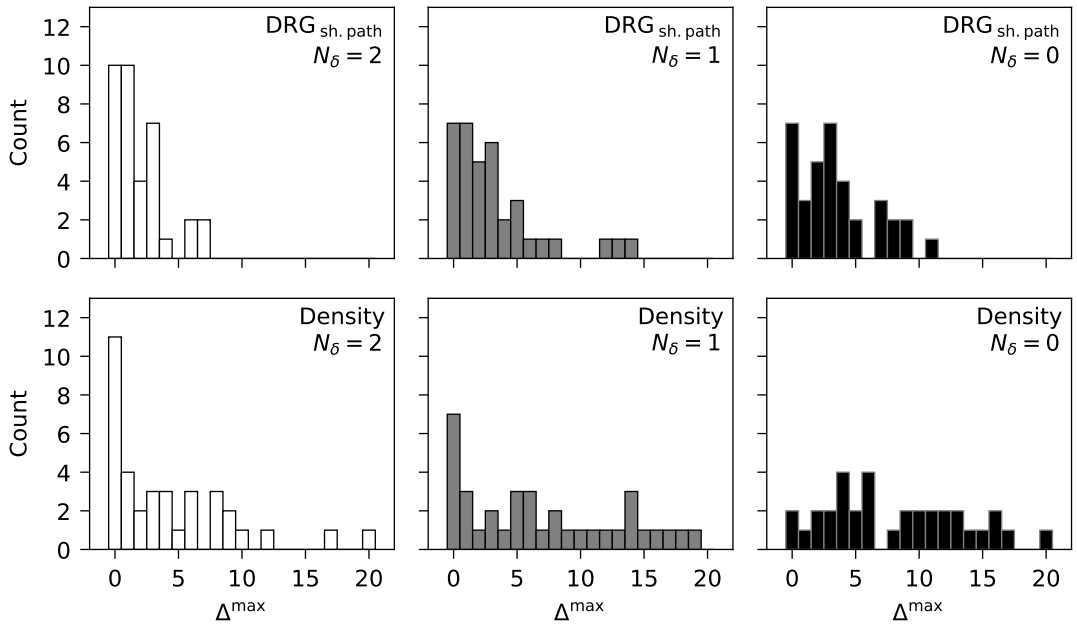

Figure 6.6: Distribution of $\Delta^{\max}$, i.e. the difference in the number of eliminated species between each ranking scheme and the best–performing ranking scheme (6.3), over all the reduction cases. In the first row, histograms for the $\mathrm{DRG}_{\mathrm{sh.path}}$ ranking scheme are shown, in comparison to the trivial benchmark of ranking species by their densities, shown in the second row. Three columns of plots correspond to three different choices of $N_\delta = 2, 1, 0$, with the same color–coding as in figure 6.5.

6.3 Reduced test chemistry sets

To give an idea of typical sizes of reduced chemistry sets as compared with the detailed ones, table 6.2 shows the number of species and reactions in sets reduced using the $\mathrm{DRG}_{\mathrm{sh.path}}$ ranking scheme for each reduction case from table 5.9. The table also shows for each reduction case all the *best ranking schemes* resulting in the greatest reduction (in a number of species), and the number of species corresponding to those, if the ranking scheme $\mathrm{DRG}_{\mathrm{sh.path}}$ is not among them. The reduction parameters were $\Delta = 10$ %, and $N_\delta = 2$ for each of the reduction cases, and the reduction conditions were as described in tables 5.10 and 5.11.

In some cases, such as reduction cases C2.5 or C6.5, the reduced chemistry set was significantly smaller than the detailed set. In other cases, such as C4.3, the reduction was far less significant. The difference in size between the detailed chemistry sets and any reduced sets depends on many factors, such as reduction

Table 6.2: Chemistry set sizes (the number of species and reactions) of sets reduced using the $DRG_{sh.path}$ species ranking scheme for all the reduction cases from table 5.9, compared to the sizes of the detailed chemistry sets. For reference, the last two columns list the *best ranking schemes*, which yielded the most significant reduction in the number of species together with their species reduction magnitude (if different from the $DRG_{sh.path}$ scheme). The reduction cases, where the $DRG_{sh.path}$ ranking scheme was among the best–performing ones, are listed in **bold**.

Case	$DRG_{sh.path}$ **Species**	$DRG_{sh.path}$ **Reactions**	**Best ranking schemes**	*best scheme* **Species**
C1.1	15/25	167/373	$DRG'_{max.flow,\,sh.path}$ DRG''_{all} $DRGEP_{max.flow,\,lim.rate}$ $DRG_{max.flow}$	14/25
C1.2	15/25	163/373	DRG'_{all} DRG''_{all} $DRGEP_{max.flow,\,lim.rate}$ $DRG_{max.flow}$	14/25
C1.3	18/25	247/373	DRG''_{all} $DRGEP_{all}$ $DRG_{max.flow}$	17/25
C1.4	13/25	118/373	$DRGEP_{lim.rate,\,err.prop.,\,sh.path}$	12/25
C1.5	**14/25**	**133/373**	DRG'_{all} $DRG''_{lim.rate,\,sh.path}$ $DRGEP_{all}$ $DRG_{max.flow,\,sh.path}$	
C1.6	**13/25**	**117/373**	$DRGEP_{lim.rate,\,err.prop.,\,sh.path}$ $DRG_{max.flow,\,sh.path}$	
C2.1	26/42	236/408	$DRGEP_{max.flow,\,lim.rate}$ $DRG_{max.flow,\,lim.rate,\,err.prop.}$	25/42
C2.2	21/42	118/408	$DRG_{max.flow}$	20/42
C2.3	26/42	193/408	$DRGEP_{max.flow}$	24/42
C2.4	26/42	236/408	$DRGEP_{max.flow}$ $DRG_{max.flow,\,err.prop.}$	24/42
C2.5	**10/42**	**73/408**	$DRG'_{max.flow,\,sh.path}$ $DRG''_{max.flow,\,sh.path}$ $DRG_{err.prop.,\,sh.path}$	
C2.6	26/42	210/408	$DRG_{err.prop.}$	25/42
C3.1	23/42	101/408	$DRG_{max.flow}$	22/42
C3.2	25/42	198/408	$DRG_{lim.rate}$	19/42
C3.3	36/42	377/408	$DRG'_{max.flow,\,sh.path}$	33/42
C3.4	**19/42**	**91/408**	$DRGEP_{lim.rate,\,err.prop.,\,sh.path}$ $DRG_{err.prop.,\,sh.path}$	
C3.5	19/42	131/408	$DRG'_{sh.path}$ $DRG_{err.prop.}$	18/42
C3.6	28/42	214/408	$DRGEP_{all}$ $DRG_{err.prop.}$	27/42
C4.1	51/67	300/563	$DRG'_{max.flow}$ $DRG''_{max.flow}$	50/67
C4.2	**43/67**	**165/563**	$DRGEP_{all}$ $DRG_{max.flow,\,err.prop.,\,sh.path}$	
C4.3	61/67	475/563	DRG''_{all}	55/67
C4.4	40/67	147/563	$DRGEP_{sh.path}$	34/67
C4.5	44/67	187/563	$DRG_{err.prop.}$	37/67
C4.6	49/67	246/563	$DRGEP_{err.prop.}$	47/67
C5.1	**36/61**	**255/521**	$DRGEP_{all}$ DRG_{all}	
C5.2	48/61	380/521	$DRGEP_{max.flow,\,lim.rate,\,sh.path}$	46/61
C5.3	27/61	140/521	$DRG''_{lim.rate}$	25/61
C5.4	**24/61**	**168/521**	$DRG''_{sh.path}$ $DRGEP_{max.flow,\,sh.path}$ DRG_{all}	
C5.5	**21/61**	**121/521**	$DRGEP_{max.flow,\,sh.path}$ DRG_{all}	
C5.6	26/61	165/521	$DRG'_{max.flow}$ $DRGEP_{lim.rate}$	24/61
C6.1	**20/39**	**79/310**	$DRGEP_{lim.rate,\,sh.path}$ $DRG_{lim.rate,\,err.prop.,\,sh.path}$	
C6.2	30/39	176/310	$DRG_{err.prop.}$	27/39
C6.3	24/39	116/310	$DRG'_{lim.rate,\,sh.path}$ DRG''_{all}	21/39
C6.4	**15/39**	**43/310**	$DRG'_{max.flow}$ DRG''_{all} $DRGEP_{all}$ DRG_{all}	
C6.5	14/39	32/310	$DRG_{max.flow,\,err.prop.}$	13/39
C6.6	26/39	138/310	$DRG'_{max.flow}$ $DRG''_{max.flow}$	25/39

conditions, species of interest, or how well refined the detailed chemistry set is in

the first place.

Since it is impractical to analyze every reduction case in this work, a single reduction case, C1.4 – O_2–He chemistry set with O, $O_2(a\,^1\Delta_g)$ and O_3 as species of interest, was chosen as an example and is elaborated further in greater detail.

6.3.1 The C1.4 O_2–He reduction case

Table 6.3 lists all the species retained in the reduced O_2–He chemistry set, as well as all the species eliminated, after running the reduction algorithm with the $DRG_{sh.path}$ species ranking scheme for the reduction case C1.4. For completeness, all the reactions associated with the species retained in this reduced chemistry set are listed in table A.2 in Appendix A, together with their kinetic data.

Figure 6.7 shows the PyGMol global model solutions for species of interest densities belonging to the same reduced chemistry set. The density evolution is compared to the model with the detailed chemistry set. It is evident, that the reduced chemistry set indeed preserves the densities of species of interest from the detailed set very well inside the allowed error Δ. Some other facts can be noted about the eliminated species listed in table 6.3. The He^+ ion has been eliminated by the reduction algorithm despite being the most abundant ion of one of the feed gases. This is due to a relatively large ionization potential of helium atoms and consequently the very low helium ionization degree ($\approx 10^{-13}$ at the end of a power pulse, as modeled by PyGMol with the detailed chemistry set). The He_2^+ species, on the other hand, has *not* been eliminated by the reduction method, despite being even less abundant than the He^+ species. This is simply a shortcoming of the species ranking scheme employed ($DRG_{sh.path}$), where He_2^+ is ranked above He^+, and more importantly, above all of O^-, He^* and O_2^+, none of which can be eliminated from the chemistry set with an acceptable reduction error δ. He_2^+ can indeed be removed from the reduced set without changing the reduction error significantly and would have been, if $N_\delta \geq 3$, or if one of the DRGEP species ranking schemes was employed (see table 6.2). However, for the reduction parameters presented with $N_\delta = 2$, and the ranking scheme $DRG_{sh.path}$, the reduction algorithm was terminated just before the He_2^+ iteration. Also, all the vibrationally excited species were eliminated except the $O_3(\nu)$ species.

This is because $O_3(\nu)$ is a part of the dominant channel for the consumption of O via the reaction

$$O + He + O_2 \rightarrow He + O_3(\nu).$$

Table 6.3: Species retained and eliminated for the reduced O_2–He chemistry set and the C1.4 reduction case (with species of interest O, $O_2(a\,^1\Delta_g)$ and O_3). The reduction was performed with the $DRG_{sh.path}$ species ranking scheme, $\Delta = 10$ %, $N_\delta = 2$, and with the reduction conditions from tables 5.10 and 5.11.

	Species retained	**Species eliminated**
Neutrals	He O O_2 O_3	
Excited	He^* $O(^1D)$	He_2^* $O(^1S)$
	$O_2(a\,^1\Delta_g)$ $O_2(b\,^1\Sigma_g^+)$ $O_3(\nu)$	$O_2(a\,^1\Delta_g, \nu)$ $O_2(b\,^1\Sigma_g^+, \nu)$ $O_2(\nu)$
Positive	He_2^+ O_2^+	He^+ O^+ O_3^+ O_4^+
Negative	e O^-	O_2^- O_3^- O_4^-

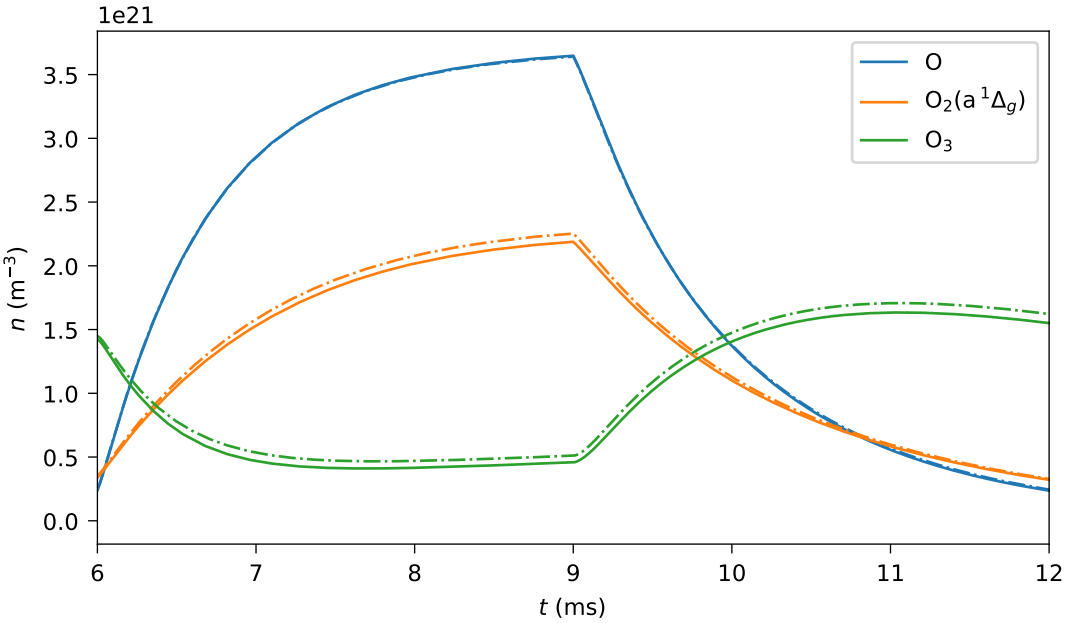

Figure 6.7: Global model solutions for densities of the species of interest O, $O_2(a\,^1\Delta_g)$ and O_3. Comparison between the reduced chemistry set (reduction case C1.4) and the detailed set. The species ranking scheme used for the reduction was $DRG_{sh.path}$. The densities obtained with the detailed chemistry set are plotted with solid lines, while the reduced set results are plotted with dash–dotted lines.

Figure 6.8 shows the relative differences of some other global model outputs between the reduced chemistry set (C1.4), and the detailed set. The outputs plotted

are the densities of the species other than pre–selected species of interest, as well as the electron temperature. It can be seen that the density error induced by the reduction for some species, such as $O(^1D)$ and all the charged species e, O^-, O_2^+, He_2^+, is fairly significant. This is unsurprising, since both the species ranking coming into the reduction method, and the reduction error (2.1) were completely blind to all the global model outputs except the densities of the species of interest. Other outputs, such as densities of He^*, $O_2(b\,^1\Sigma_g^+)$, $O_3(\nu)$, and the electron temperature T_e are well replicated with the reduced chemistry set. This is, however, not guaranteed by the reduction method presented, but rather can be considered a side effect of preserving the dominant production and consumption channels of the species of interest.

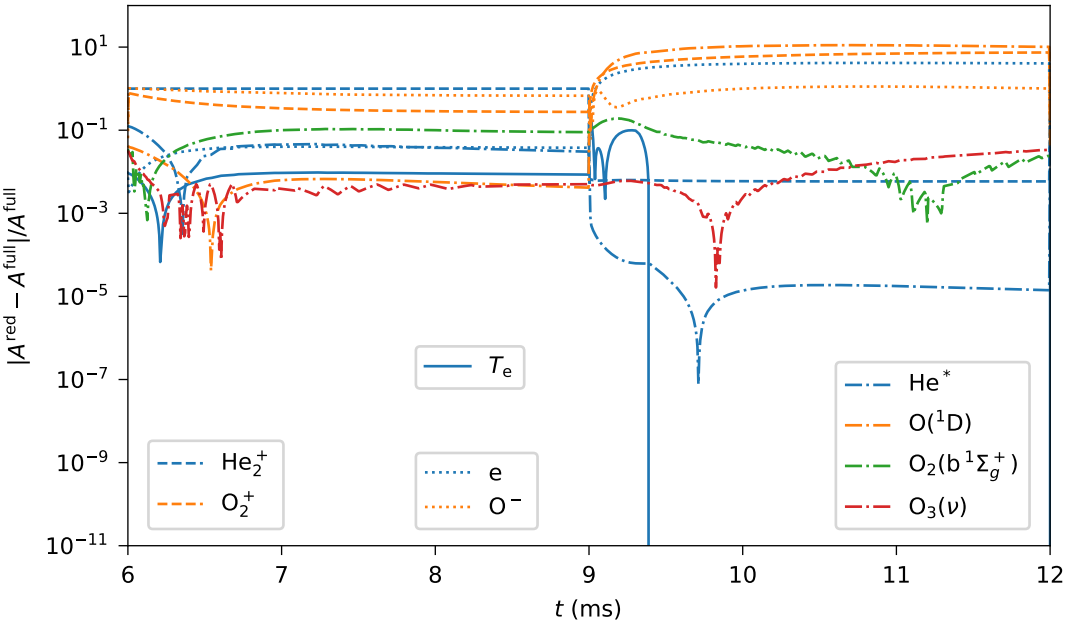

Figure 6.8: Relative differences of global model outputs between the reduced chemistry set (C1.4) and the detailed set. Outputs plotted are electron temperature and densities of the other species than the selected species of interest. The positive ions are plotted with dashed lines, negative species with dotted lines, the excited states with dash–dotted lines, and the electron temperature is plotted with a solid line.

Finally, figures 6.9 - 6.12 show the production and consumption rates of each species of interest via the 5 most prominent processes, for both detailed and reduced chemistry sets described in table 6.3. The values are showed for both the end

of the power pulse (figures 6.9, 6.10), and for the beginning of the afterglow (figures 6.11, 6.12), sampled 0.1 ms before and after the end of power pulse respectively. It can be seen, that while some channels are lost due to the species eliminated, these are generally much less significant channels, with rates lower than the most prominent channel by about 2 orders of magnitude or more. As an example, the channels for O_3 consumption during the end of the power pulse and the beginning of the afterglow, via the reactions

$$O_3 + e \rightarrow e + O + O_2(\nu)$$
$$O_3 + O \rightarrow 2O_2(\nu)$$

respectively, are both lost in the reduced chemistry set due to the elimination of the $O_2(\nu)$ species. The most dominant O_3 loss channel for both cases, via the reaction

$$O_3 + O_2(b\,^1\Sigma_g^+) \rightarrow O + 2O_2,$$

is preserved, however, with a very similar rate.

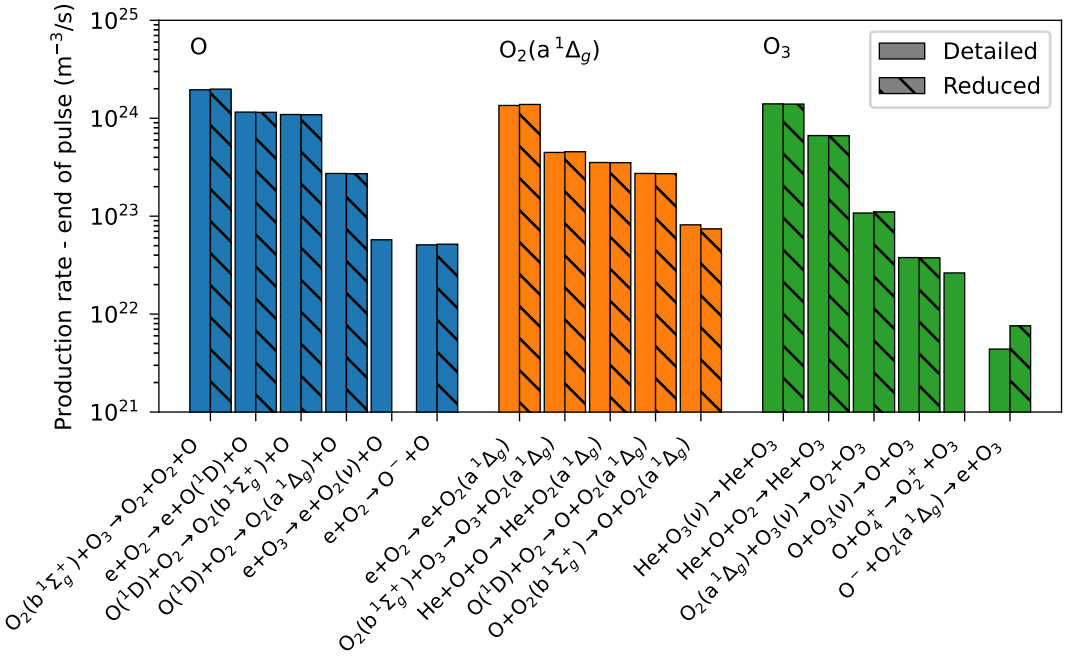

Figure 6.9: Production rates of the species of interest by the most dominant processes for both detailed and reduced chemistry sets (reduction case C1.4). Values sampled 0.1 ms before the end of the power pulse. The species are color–coded consistently with figure 6.7.

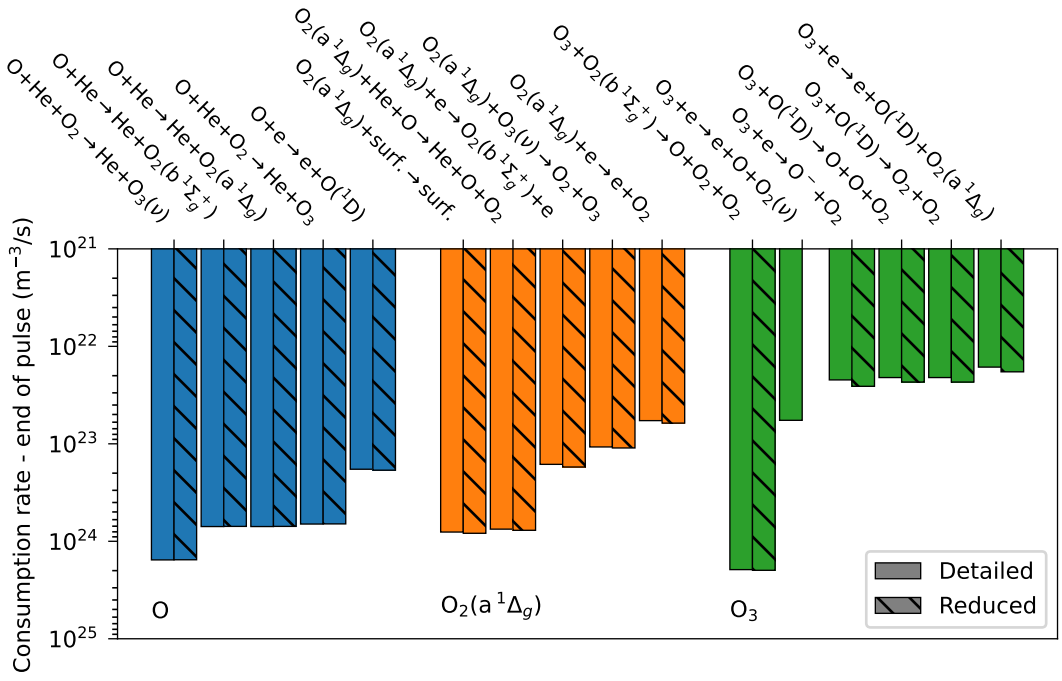

Figure 6.10: Consumption rates of the species of interest by the most dominant processes for both detailed and reduced chemistry sets (reduction case C1.4). Values sampled 0.1 ms before the end of the power pulse. The species are color–coded consistently with figure 6.7.

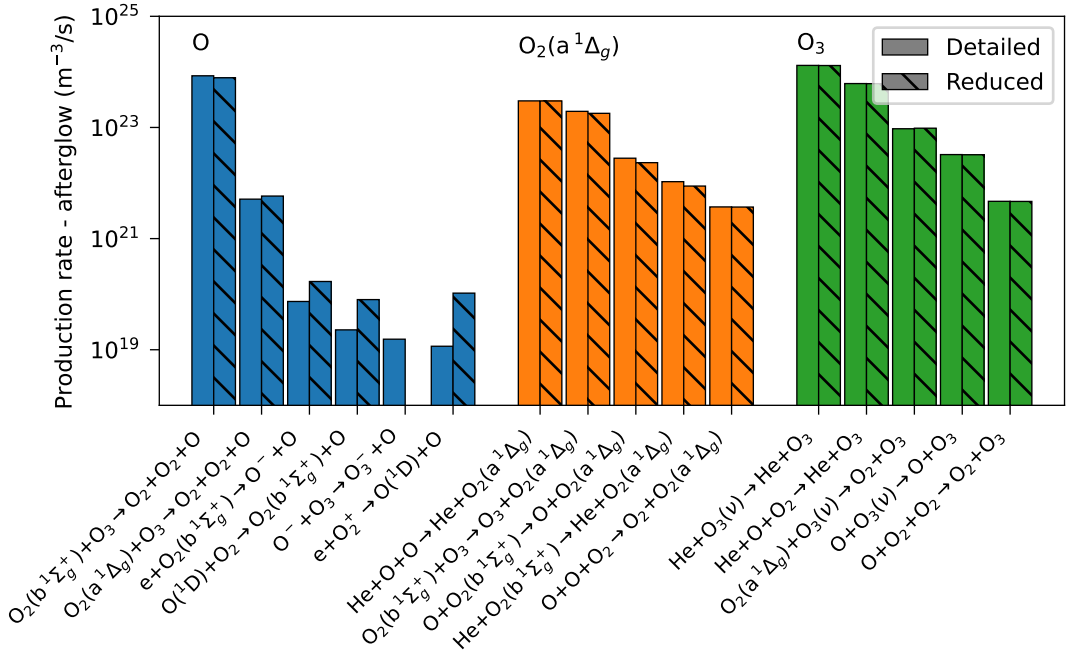

Figure 6.11: Production rates of the species of interest by the most dominant processes for both detailed and reduced chemistry sets (reduction case C1.4). Values sampled 0.1 ms after the end of the power pulse (beginning of the afterglow). The species are color–coded consistently with figure 6.7.

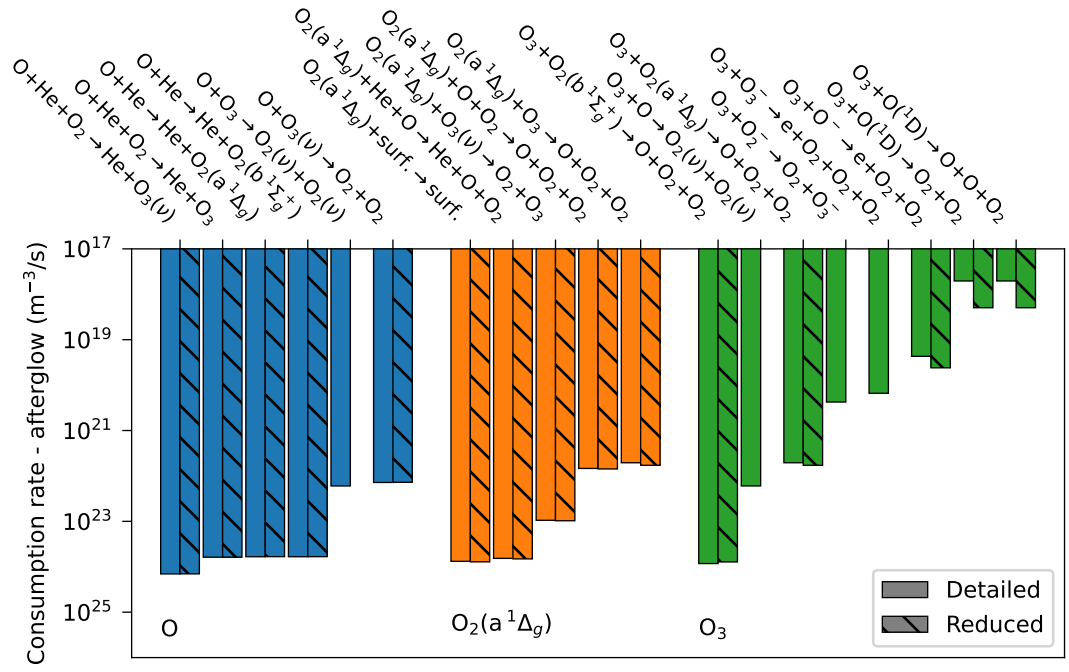

Figure 6.12: Consumption rates of the species of interest by the most dominant processes for both detailed and reduced chemistry sets (reduction case C1.4). Values sampled 0.1 ms after the end of the power pulse (beginning of the afterglow). The species are color–coded consistently with figure 6.7.

Part II

Automatic Estimation of Kinetic Data

Chapter 7

Fast regression of kinetic data

The rigorous state–of–the–art methods of calculating plasma chemistry kinetics, as outlined in the Introduction (chapter 1), are often computationally relatively very expensive, and/or use as inputs data which are not always readily available. This makes it very problematic to use such methods for estimation of missing kinetic data in the framework of the *automatic chemistry generator* I have envisioned in in Introduction, which might need to estimate reaction rate coefficients for a very large number of reactions preferably in real time. As discussed in section 1.2.2, there has been a lot of development recently incorporating machine learning (ML) methods into computational chemistry in order to speed up the calculations. But none of the published work aligns well with my objective of the fast kinetic parameters estimator foreshadowed in section 1.3 for similar reasons: computational cost, input data availability, and generality.

This chapter provides some background and theory behind the *kinetics regression model* I have developed in the present work. I am using machine learning techniques to perform a very fast (albeit crudely approximative) regression of reaction kinetics. The model is trained on publicly available data scraped from online databases of kinetic data. In the following sections, I describe some basics of machine learning regression, as well as different classes of regression models used in this work.

7.1 Regression with machine learning

In his excellent book on machine learning [159], Aurélien Géron quotes two definitions of machine learning. One is more general:

> (Machine Learning is the) field of study that gives computers the ability to learn without being explicitly programmed.
>
> Arthur Samuel, 1959

And one slightly more engineering–oriented:

> A computer program is said to learn from experience E with respect to some task T and some performance measure P, if its performance on T, as measured by P, improves with experience E.
>
> Tom Mitchell, 1997

There is no shortage of machine learning resources available. Over recent years, machine learning has dominated the scientific publishing landscape. In 2019, machine learning (or more specifically *deep learning*) themed papers took the first four spots in the ranking of most highly cited publications, released annually by Google Scholar. Classic textbooks by Mitchell [160], and by Witten *et al* [161] give a very detailed overview of machine learning methods, and earlier cited Géron [159] offers a somewhat higher–level hands–on oriented approach. Out of many topical reviews, Domingos' paper [162] can be cited as a very nice and concise collection of useful machine learning tips, tricks and key insights.

Most of the cutting–edge machine learning research is done nowadays on *deep learning* and *neural networks*. In the present work, however, I have used some more traditional ML techniques. Artificial neural networks (ANN) frequently outperform other ML techniques on very large and complex problems, with huge quantities of data available [159]. The size of my training dataset and the input space dimensionality are not high enough to fully take advantage of ANN. In the following section, I will limit my overview of machine learning theory solely to methods, which I actually used in this work. More specifically, I am trying to solve a problem of *univariate regression* (predicting a single dependent target variable from multiple independent

variables) by *supervised learning* (defined by its use of a training dataset with known target values).

If it can be done, utilizing machine learning is an obvious choice for a problem such as estimation of reaction kinetic data from a set of readily available data encoding each reaction. Machine learning shines for problems where traditional approaches are either too complex for the available resources, or have no known algorithms [159]. Furthermore, although they may take some significant computational time to train, trained machine learning models typically return new predictions based on different sets of inputs with a very high speed. This is well in line with my intended use case of the automatic chemistry set generator.

It needs to be noted, however, that machine learning regression models can potentially suffer from numerous problems. The most pertinent ones are tied to the quality of training data instances (or *samples*), the regression model is trained on. There are many challenges connected to the training data set, such as non–representative training data, poor quality data containing errors, outliers and noise, or dataset with irrelevant features [159]. This machine learning aspect is well embodied by the GIGO (*garbage in, garbage out*) principle. Another major factor is the quantity of the training data. In their very famous paper [163], researchers Banko and Brill show that even very different machine learning algorithms, varying from simple to fairly sophisticated ones, exhibit almost identical performance on a specific problem within the natural language processing domain, once the training data set gets large enough. This idea that data might matter more than the algorithm was further popularized by Halevy *et al* [164] in a paper titled *The unreasonable effectiveness of data*[1]. Other challenges of the machine learning approach are discussed in great lengths in any ML textbook or review paper, and include among others e.g. *overfitting* and *underfitting* the training data. Overfitting occurs when the model performs very well on the data it was trained on, but generalizes poorly to

[1]Paying homage to the classic Eugene Wigner's paper *The unreasonable effectiveness of mathematics in the natural sciences* [165] has became rather popular in computer science circles. Other examples include papers, such as *The unreasonable effectiveness of deep learning in artificial intelligence* [166] by Sejnowski, *Dow Jones trading with deep learning: The unreasonable effectiveness of recurrent neural networks* [167] by Fabbri and Moro, or the talk about Julia programming language titled *The unreasonable effectiveness of multiple dispatch*, given by the Julia co-creator Stephan Karpinski on JuliaCon 2019.

novel data instances. Overfitting normally happens when the model is too complex relative to the amount and noisiness of the training data [159]. Typical way to deal with overfitting issues (short of gathering more training data instances and reducing their noise) is *regularization*. Regularization techniques vary between different ML model classes, but generally involve constraining the model in a way to make it less complex and reduce the risk of overfitting. Underfitting, as one might guess, is the opposite of overfitting: this occurs when the model is too simple to learn the underlying structure of the data and is bound to be inaccurate, even on the training samples [159].

Because of the various challenges, the traditional quantum chemistry methods of calculating the reaction kinetics from the first principles can not, naturally, be fully substituted by machine learning models, which usually offer great computational speed only as a trade–off for accuracy, and the scepticism needed while interpreting the results. This *speed over accuracy* quality of the ML approach is, however, also well aligned with my intended use case of automatic chemistry set generator application, as discussed in the Introduction (chapter 1) and further in section 7.3.

In supervised learning, the training set which gets fed into the ML model includes a set of *features*, and the set of desired solutions, also called *targets*. In univariate regression, the targets take the form of a single numeric value per data sample, and the final task for the trained regression model is to predict target values for new data instances, or new feature values, which were not part of the data set the model was trained on (or the *training set*). Here, predicting reaction kinetics in plasmas, the targets could be the reaction rate coefficients, while the features could include, among others, e.g. masses, charges, or enthalpies of formation for the individual reactants and products of the reactions, as well as categorical features, such as if any given reaction includes any charges or not. *Feature engineering*, or processing data samples into meaningful features and features selection, is easily the most important factor determining if a given ML project succeeds or fails [162]. The features selection for my regression model will be discussed in depth in chapter 9.

A univariate regression model is a non–linear operator f, which takes a vector of features $\mathbf{x}_i$ and produces a target value y. Or more conveniently, it can accept

multiple feature vectors in the form of a features matrix $\mathbf{X}$, and return a vector of target values $\mathbf{y}$

$$f\left(\mathbf{X}, \theta, \phi\right) = \mathbf{y}. \tag{7.1}$$

Apart from the features matrix $\mathbf{X}$, a machine learning regression model typically also accepts a vector of parameters θ, and a vector of *hyperparameters* ϕ. Training of a regression model f on the training data set $\mathbf{X}^{\text{train}}, \mathbf{y}^{\text{train}}$ is simply a search for optimal parameters θ, which maximize some performance measure P for the given set of hyperparameters ϕ. Most commonly, the performance of a model is inversely proportional to the prediction error $\text{diff}(\mathbf{y}, \mathbf{y}^{\text{train}})$ on the training data set, and the prediction error measure usually takes the form of either the root mean square error (RMSE), or the mean absolute error (MAE). The process of model training then can be expressed simply as a minimization problem

$$\underset{\theta}{\text{argmin}} \quad \text{diff}\left(f(\mathbf{X}^{\text{train}}, \theta, \phi), \quad \mathbf{y}^{\text{train}}\right). \tag{7.2}$$

While the parameters optimization is typically taken care of automatically by the training algorithm, under the hood of the given regression model implementation, the optimization of the hyperparameters must be done by the machine learning engineer.

Every decent machine learning package contains many different classes of regression models, each with its distinct set of hyperparameters. Next to feature engineering, the selection of an appropriate model class, together with hyperparameters optimization, make up the bulk of any ML engineer's work. It has been demonstrated that without any assumption about the data, there is no reason to prefer one model class over any other. This has become known as the *No Free Lunch* (NFL) theorem, first demonstrated by Wolpert in his now famous 1996 paper [168]. The implication is that the only way to know for sure which model class will perform the best is to try them all out. The techniques I have used for hyperparameter tuning and to prevent overfitting (such as randomized search in the hyperparameter space and n-fold cross–validation) are discussed further in chapter 9.

In this work, I have used the *Scikit-learn* [169] Python library for all the machine

learning exclusively. Naturally, adhering to the NFL theorem, I have tested almost all regressor classes offered by the Scikit-learn package. On my dataset, three of the regressor classes showed noticeably better performance than the rest. In the following section, I will introduce briefly a theory behind each one of the three regression model classes used in this work, and I will explain how multiple trained regression models can be combined into a single regressor using methods of *ensemble learning*. The theory presented here is significantly simplified. The full theory behind the introduced models is beyond the scope of this work and can be found in any of the textbooks cited earlier, e.g. [159].

7.2 Regression model classes

The three regression model classes used in this work are the *Support Vector Machine* regression model, the *Random Forest* regression model, and the *Gradient–boosted Trees* regression model.

7.2.1 Support vector machine regressor

A support vector machine (SVM) is a class of powerful and versatile algorithms capable of performing linear and non–linear classification and regression. The SVMs were developed by Boser *et al* [170] in 1992 originally for *classification* problems. In great simplification, an SVM *classifier* fits a decision boundary in the features space, separating as well as possible different category labels with the widest possible margin. Different hyperparameters can apply, including the regularization parameter C, the loss function, or the kernel function, which determines the possible non–linearity and the shape of the decision boundary by performing the *kernel trick*. The most common kernels used with SVMs are the linear kernel, polynomial kernel, and the Gaussian *Radial Basis Function* (RBF), each kernel having its own set of hyperparameters.

To use SVMs for regression problems, instead of for classification, the objective reversed. Instead of fitting the widest possible decision boundary between two classes, the SVM regressor fits as many data samples as possible *on* the boundary (or

regression function), while limiting margin violations. A hyperparameter ϵ is used to limit the margin size around the boundary and thus to control the sensitivity to outlier samples. It is often helpful to demonstrate the different model classes on a simplified example dataset. Figure 7.1 shows an artificial single–feature example dataset fitted with two SVM regression models with linear and RBF kernels.

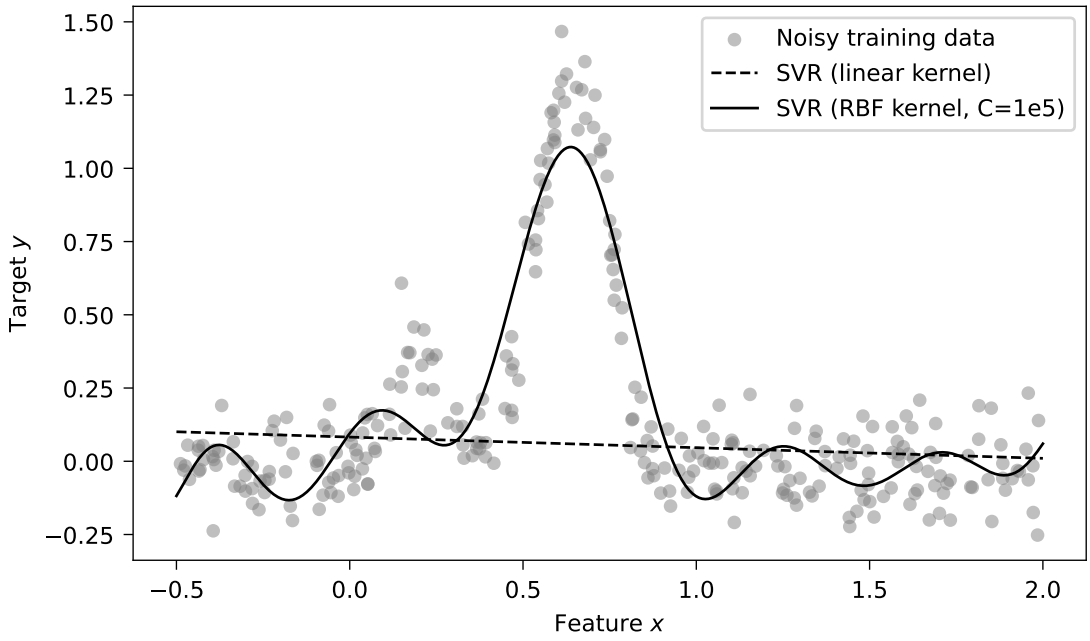

Figure 7.1: Two SVM regression model with different kernels fitting an artificial example dataset in a single–feature space.

The dataset in figure 7.1 was created artificially for this purpose. The target values form two sine–like centre peaks on a flat background in a single–feature space. Some normally distributed noise is added to the samples. As one would expect, the linear kernel naturally does not recover the non–linear peaks in the dataset. The RBF kernel does a better job with the centre peak, but the fit exhibits some artefacts in the background areas. A very high C value (corresponding to a very low regularization) was needed to recover the centre peak.

The full theory behind SVM regression and kernel trick is beyond the scope of this work and can be found in any of the previously cited textbooks. One additional thing to note is that SVMs are sensitive to feature scaling, and work best if all the features are of a similar scale. This is in contrast with the *decision tree* based

regressors discussed next.

7.2.2 Random forest regressor

Random forests are among the most powerful and versatile regression and classification ML algorithms available today [159]. In order to explain random forest regressor, one has to start with a *decision tree* regression model, which forms a fundamental component of random forests.

Decision tree

Decision trees [171; 172] are a class of ML algorithms that can perform both classification and regression. To understand decision trees, it is best to build one on an example dataset and inspect how it makes predictions. Figure 7.2 shows a demonstration example of a decision tree model trained on the same example dataset as shown in section 7.2.1. The decision tree recursively splits the dataset into two subsets, building a binary tree of such splits all the way down to the *leaf nodes*. Each leaf node then corresponds to its range in the feature space and fits all the targets inside this range with a single value y. This process can also be visualized conceptually as a *flow diagram* of *decisions* about the data. Figure 7.3 shows such a flow diagram for the decision tree regression model plotted in figure 7.2.

The decision nodes are built greedily from the root down, and the decision feature and the decision threshold for each decision node are determined by the CART algorithm (*Classification and Regression Tree*) [171]. For each decision node, the CART algorithm finds the feature and the threshold, which minimizes the weighted mean square error (MSE) for both subsets created by splitting the dataset by that feature and threshold. The equation 7.3 shows the cost function which gets minimized in each split:

$$J = \frac{m_{\text{left}}}{m}\text{MSE}_{\text{left}} + \frac{m_{\text{right}}}{m}\text{MSE}_{\text{right}}, \tag{7.3}$$

where

$$\text{MSE}_{\text{subset}} = \sum_{i \in \text{ subset}} \left(\bar{y}_{\text{subset}} - y^{(i)}\right)^2, \tag{7.4}$$

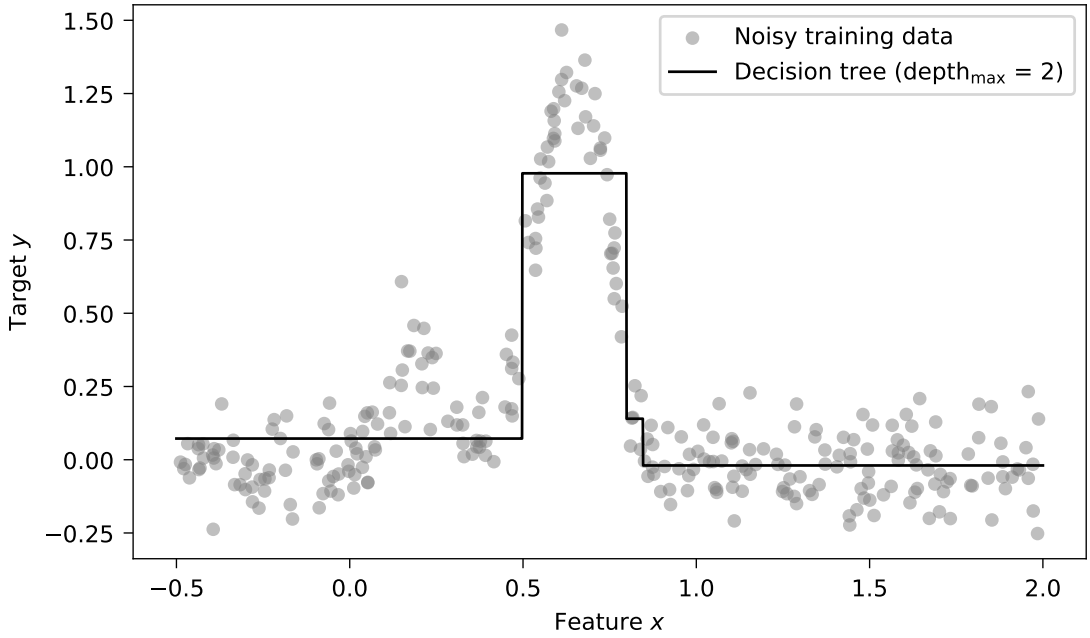

Figure 7.2: An example of a decision tree model trained on the identical dataset, as shown in figure 7.1. For better explanation value, the depth of the decision tree was limited to 2 layers.

$$\bar{y}_{\text{subset}} = \frac{1}{m_{\text{subset}}} \sum_{i \in \text{subset}} y^{(i)}. \tag{7.5}$$

In equations (7.3) – (7.5), m refers to the number of samples, the *left* and *right* subsets refer to the two subsets with the given decision feature values lower and higher than the decision threshold value, and the index i runs over all the sample values y in a given subset.

The test example dataset from figure 7.2 is a single–feature dataset. In a real dataset with multidimensional feature space, each decision node might find a threshold for a different feature axis. The fit on figure 7.2 is naturally not very good, as the decision tree was limited in this example to a maximal depth of 2. Higher maximum depth limit leads to a better fit, but a care must be taken, as unconstrained maximal depth leads to a perfect fit, resembling a *nearest neighbour* regression model. In such a case, there is one leaf node for each training data instance. Figure 7.4 shows how this deep, unrestricted tree fits the data. This is, of course, an example of gross overfitting and such a model will likely not generalize well for new data instances, especially near the outlier samples in the training set. For better generalization, the

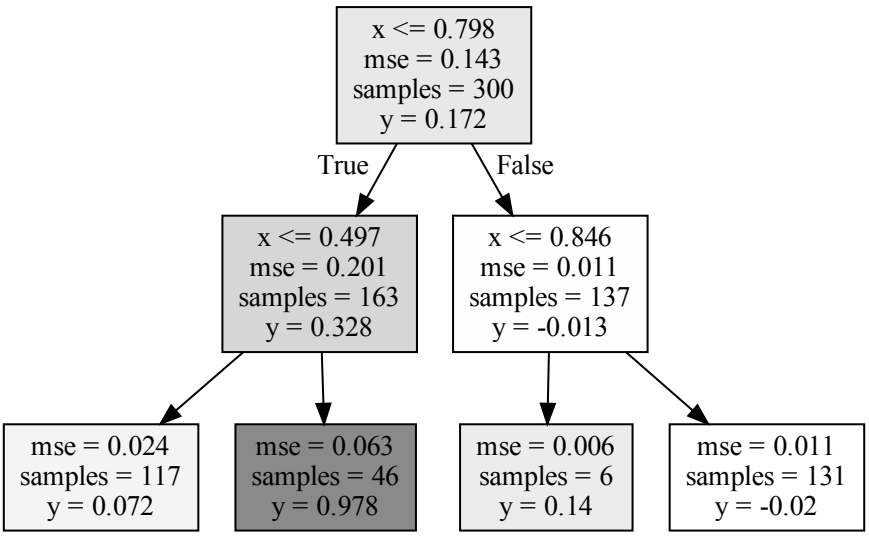

Figure 7.3: The flow diagram summarizing the process of how a trained decision tree model predicts the y values. This flow diagram corresponds to the decision tree model fit shown in figure 7.2. The fill shade of each node corresponds to the y value predicted by the node. Apart from the feature value threshold and y, each node also shows the number of samples and the mean square error of the prediction in the corresponding subset.

model can to be regularized by one of the hyperparameters, such as maximal depth, minimal number of samples in a leaf, or maximal number of leaf nodes.

Random forest

Instead of training a single decision tree on the whole training dataset, it is possible to train many separate decision tree regressors on random subsets of the training dataset and aggregate the predictions. This type of ML model is called random forest [173] and it is usually one of the best performing ML models available [159]. The samples for each tree in the forest are drawn from the whole training dataset, typically *with* replacement. This allows for training instances to be sampled several times across multiple trees, as well as within a single tree. Apart from the hyperparameters of their trees, which they share, random forests can also tune the number of trees, or the maximal number of training instances sampled per each tree. The aggregated prediction is typically the average of predictions of all the constituent

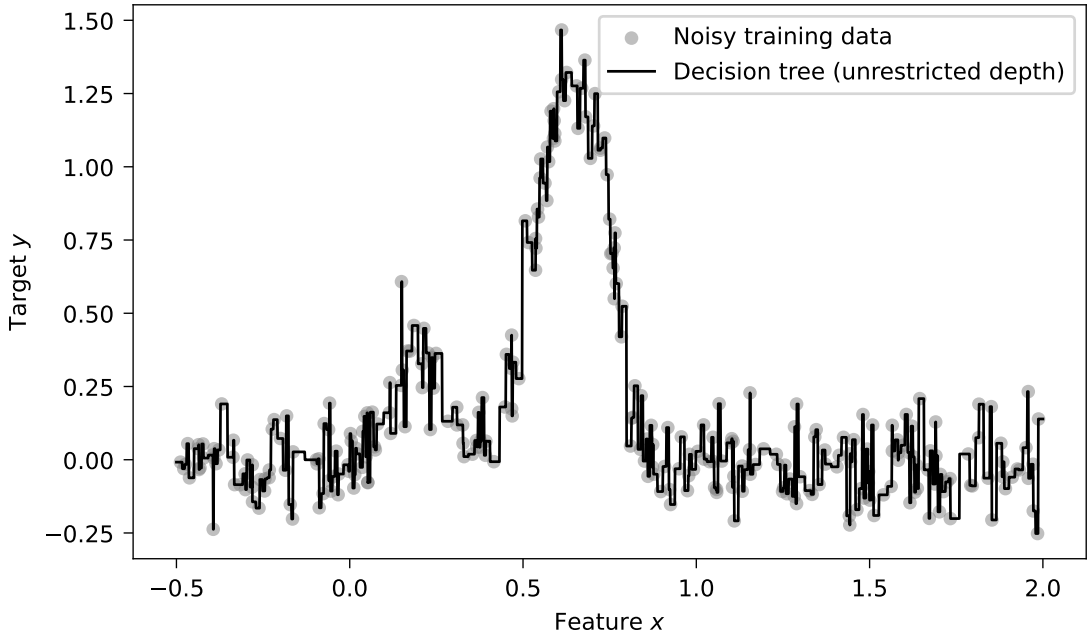

Figure 7.4: An example of a decision tree trained without any restrictions on depth or number of leaf nodes. This is an example of overfitting the data down to a level of its noise. The same dataset is used as in all previous regression model examples shown in this section.

trees. Figure 7.5 shows an example of the random forest regressor trained on the familiar dataset. In can be seen that the model recovers the two peaks feature from the noisy data qualitatively very well. This random forest consisted of 1,000 individual trees, each limited to the maximum of 30 training instances. Amazingly, the individual trees in this random forest were grown without any restriction, similar to the decision tree in figure 7.4. But even while the individual trees undoubtedly overfitted their subsets of training samples, the resulting random forest model is very well regularized. It is also worth mentioning, that the random forest regressor trains itself without any assumptions about the nature of the training data whatsoever.

In datasets with multiple features, important features (those which correlate more strongly with the target values) will generally appear closer to the root of the decision tree. In contrast, the unimportant features will appear closer to the leaves, if at all. By evaluating an average depth of feature appearances across all the trees, the random forests can offer an assessment of the feature importance. This can be used to eliminate redundant features in a dataset, or to refine the particularly

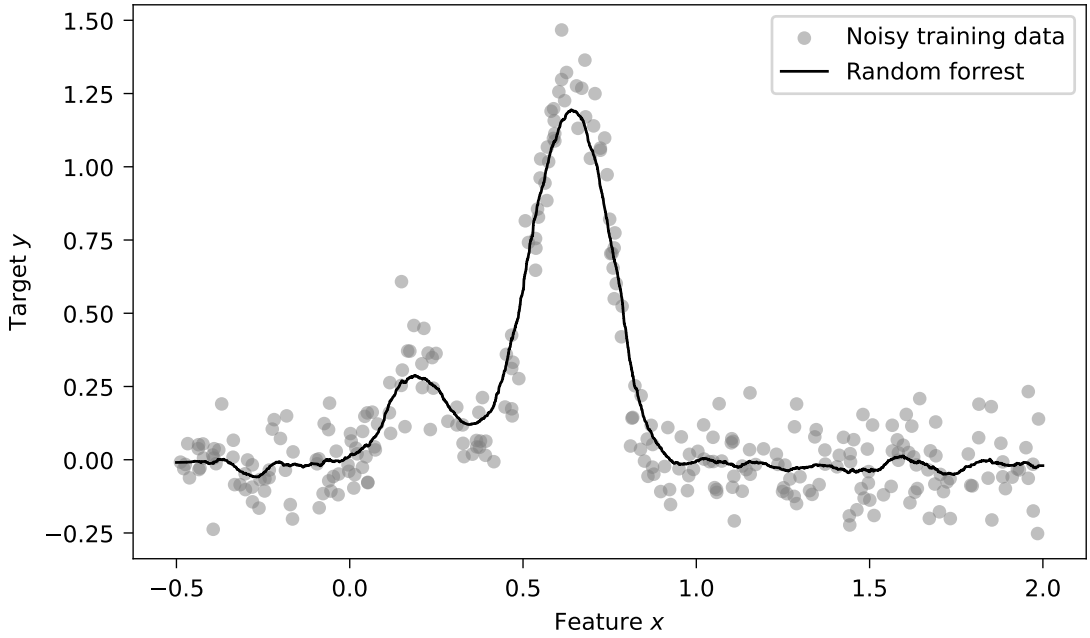

Figure 7.5: An example of a random forest regression model trained on the same dataset as was used in all the previous regression model examples shown in this section. This model was trained with 1,000 decision trees, each limited to maximum of 30 training instances sampled randomly from the dataset.

important features.

7.2.3 Gradient–boosted trees regressor

Gradient boosting as a method was first introduced in 1997 by Brieman [174] and further developed two years later by Friedman [175]. Gradient–boosted trees regressor follows a similar idea as random forests, that is, to combine many *weak–learning* trees to form a single powerful regressor. But instead of building many trees on different subsets of the training dataset, in the gradient–boosting method the trees are added in a sequence, and each additional tree is trained on the residual errors of the previous tree. The first tree in the sequence tries to predict the full dataset targets, the second tree is predicting the prediction errors of the first tree, the third predicts errors of the second (or the errors of the errors of the first), etc. All the predictions of the individual gradient boosted trees are simply summed, resulting in the final strong predictor. Regularization is usually achieved by severely limiting the constituent trees (usually to maximal depth of 2–3), and by limiting the number

of trees in the sequence (also known as *early stopping*).

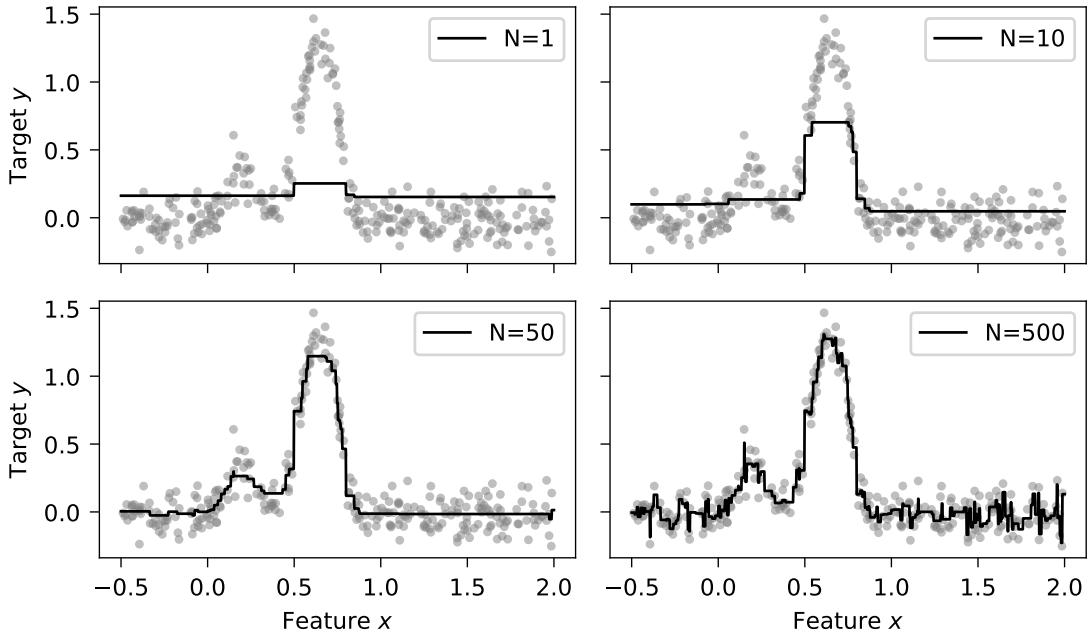

Figure 7.6: Four different gradient–boosted trees trained with increasing number of constituent trees. It can be seen that the model with 50 trees produces a reasonable good fit, while the models with less and more trees are underfitting, and overfitting the data. The dataset used is the same as previously used to illustrate all the regression model classes in this section.

Figure 7.6 shows, for completeness, several gradient–boosted tree regressors in action, each trained with different number of constituent trees. While the model trained with 500 trees clearly overfits the data, the one with 50 trees shows a reasonably good fit. In all four cases, the gradient–boosted trees models were trained using trees with maximal depth of 2.

7.2.4 Ensemble learning

The general idea behind the last ML technique used in this work has been introduced already. It is to combine a number of trained models into a single model, aggregating the predictions from the individual constituent models. The group of the original models is called *ensemble*, thus this technique is called *ensemble learning*, and an ensemble learning algorithm is called *ensemble method* [159]. Both random forest and gradient–boosted trees are examples of ensemble learning.

Ensemble methods are also often used near the end of an ML project, when it is often a good idea to combine a few shortlisted ML models which have already been optimized, into a single, usually stronger ensemble model [159; 162]. There are different ensemble methods available. The most basic one is the *voting regressor* [176], which simply averages the weighted predictions of its models. The weights of the constituent models are treated as hyperparameter of the voting regressor and need to be optimized. In this work, I have used a voting regressor ensemble method to combine optimized SVR, random forest, and gradient–boosted trees regression models into the final regression model for reaction kinetics.

7.3 Kinetics regression model

In this work, I have used the techniques introduced above and attempted to develop an ML regression model, which would regress the reaction rate coefficients of plasma processes from some accessible data known about the reactions, such as masses, charges, or enthalpies of formation of all the reactants and products. As discussed briefly in section 7.1 already, it is quite clear that one can not have very high expectations from such a model. Perhaps the strongest reason for such a scepticism is the feature selection. By design (and in alignment with the intended application of the model) the feature space contains only easily accessible data, which might not correlate at all with the rate coefficients (or targets). This might lead to the typical GIGO scenario. After all, there is a reason why the state-of-the-art quantum chemistry calculation methods need inputs which are coupled much more closely to the outputs via the laws of nature; inputs, such as potential energy surfaces (PES), which are relatedly much less accessible.

Another quite clear problem is the one of the data availability and of various biases in the available data. For example, comparatively much more experimental data can be found on processes involving closed species, than on the ones involving e.g. radical–radical reactions. This will inevitably lead to a biased training dataset and consequently to various biases in the model predictions.

It is my strong belief, however, that such a project should still be attempted

as it offers very high gains if successful. Furthermore, the nature of the intended application of the automated chemistry set generator allows for even a very imprecise model to make a difference. In particular, one might imagine a synergy with the automatic chemistry set reduction method, presented in part I of this thesis, where the unavailable kinetic parameters might get estimated by the regression model, multiplied by some safety factor and finally flagged for further attention only if their reactions survive the reduction process.

The regression model developed is described fully in chapter 9, right after chapter 8 which details the training dataset.

Chapter 8

Acquisition of the training data set

Many different classes of machine learning based models for automatic data regression exist. Every single one of them relies heavily on its training data set. As a rule of thumb, a mediocre algorithm trained on lots and lots of data instances will outperform a clever, better learning algorithm, with only a modest amount of data [162]. Another rule of thumb very widely used in the machine learning community is that the sample size (or the number of training data instances) needs to be at least a factor 10 times the number of free parameters of the model [177]. And naturally, if one aspires to predict some class of complex behaviour, as in my case, the problem of plasma kinetics certainly is, models with high dimensionality are often needed to capture the behaviour. It is therefore evident that the collection of as much as possible of high quality data was a crucial step in the development of my regression model for prediction of reaction kinetics.

In this chapter, I will describe in detail all the sources I acquired my training data from, as well as all the relevant criteria for for data selection, consistency checks, filtering, and finally the methodology for merging all the data into a single unified training data set.

Two things are very important when considering searching for, and collection, of training data instances. One needs to be able to derive from the dataset the future outputs of the model (data which the model will aim to predict), and (as many as possible of) the future inputs of the model (or *features*). Given the large size of the training data set required, the data collection process also needs to be automated.

As discussed in section 1.2, kinetic parameters for plasma reactions can most often be found in scientific publications and in online databases. For convenience and with regard to the limited time span of this project, I have focused solely on the extraction of data from online databases, as automatic extraction of data directly from scientific papers is very difficult and requires much more time.

Section 1.2 lists some of the well-known databases of plasma kinetics. In this work, all the data used for training and testing the regression models were automatically scraped from the following databases: QDB [9], NFRI [54], KIDA [49], and UDfA [51]. I have found that these four databases in particular could provide good amounts of data aligned with the limited scope of my project, i.e. kinetic data for binary heavy–species collisions in room–temperature plasmas.

As I had access to the source code of the QDB database, I could simply query its underlying relational database structure, which made the data extraction fairly simple. The UDfA database provides its raw data as a simple ASCII text file, with a very clear structure, documented in the accompanying paper [51]. This made the UDfA data extraction as simple as writing a short text parser. The data from NFRI and KIDA databases were extracted using web scraping techniques directly from the web user interface. I have used the python package *Scrapy* to automate the web scraping job. Scrapy [178] is an open–source web–crawling platform implemented in Python.

8.1 Reaction criteria

As foreshadowed in the previous chapter already, the regression model developed in this project will describe binary heavy–species collisions only. In addition to that, several other data–filtering criteria were established, to further limit the scope of the project. This was done to decrease the workload required in order to better fit this project for the typical PhD thesis time budget. These criteria naturally make the resulting trained regression model only applicable to a fairly narrow set of cases. The full set of criteria for the training/test data set acquisition are summarised as follows.

1. **Only heavy–species reactions are considered.** Electron collisions and heavy–species collisions follow completely different dynamics, which would make it impractical to mix them in a single model. Further more, electron collisions are usually required for plasma simulations in the form of cross–section, which is much more dimensional output than the reaction rate coefficients, which are typically enough for heavy–species collisions.

2. **Only binary reactions are considered.** This is another practical choice, as the reaction rate coefficient changes its unit with the number of reactants in the reaction.

3. **Only reactions with two products are considered.** As a part of the dataset feature–space will be directly describing the species of the reactions (both reactants and products) and their physical properties, limiting the dataset to only reactions with the same number of reactants and products prevents all the problems one has to face, when the dataset has inherently missing values.

4. **Reactions involving photons are not considered.** All the databases used to source the data support photons as species in their reactions. These, however, make up only a small fraction of the reactions listed, and were therefore excluded from the dataset.

5. **Only reactions involving *stateless* species are considered.** This choice disallows great many reactions from entering the dataset, and limits the applicability of the resulting model considerably. However, this criterion was necessary to introduce, to keep the project to a manageable size.

It is worth re-iterating, that the dataset selection criteria described in this section severely limit the domain of applicability of the resulting regression model as a sole source of kinetic data. For example, discounting the reactions involving photons might pose less of a problem for low–temperature technological plasma models, but for modeling astrochemical plasmas the data for such reactions will likely have to be searched for in a different source. Similarly, exclusion of reactions involving electrons means that such reactions, which are of absolutely vital importance for low–

temperature plasma models, must be sourced from elsewhere, and the final regression model simply cannot suffice as the only data source, no matter how precise.

While adhering to the criteria listed above, my data collection strategy also completely ignored any reactions which did not conserve charge, or elemental stoichiometry. The data were collected from all four databases, taking into account all the criteria listed above. Sections 8.2 – 8.5 discuss some additional considerations related to the data collection from the specific databases.

8.2 QDB database

The kinetics for heavy–species collisions are represented in QDB by the coefficients of the modified Arrhenius formula, parametrizing the temperature dependence of the reaction rate coefficient by three parameters, α, β, and γ, as

$$k\left(T\right) = \alpha \left(\frac{T}{300}\right)^{\beta} \exp\left(-\frac{\gamma}{T}\right). \tag{8.1}$$

The pre–exponential factor α is required to exist for each reaction, while the parameters β and γ are optional. The β and γ parameters are indeed missing in many QDB reaction instances. In those cases, the reaction rate coefficient is simply described as a constant, without any temperature dependence.

In the QDB object model, the reactants and products of each reaction are instances of the species object, which can hold its own properties. The following data were collected per each reaction stored in QDB: the kinetic coefficients α, β, and γ, and for each reactant and product of the reaction their formula, charge, and their enthalpy of formation at normal temperature, if available.

As QDB does not provide any validity ranges for its reactions, simply every reaction adhering to the criteria listed in section 8.1 is collected. In some cases, QDB might contain multiple data for the same reaction. This might happen, e.g. if different data from different publications were added into the database at some points. In such cases, such a reaction was added multiple times, as there exists no fast automated way to determine which rate coefficients are more correct than

others.

8.3 NFRI database

In contrast to QDB, the NFRI database does not offer the Arrhenius parameters for its heavy–species reactions, but rather it represents the reaction kinetics for each reaction as discrete points of either reaction rate coefficient, or cross–section, as a function of temperature. As this work is focussed on cold plasma applications, only those reactions were collected, whose kinetic dataset definition range overlapped with a close range around the room temperature of $T = 300$ K $\pm$ 10%. With this filtering criterion applied, only a handful of reactions remained in the cross–sectional form, which were excluded.

Unlike QDB, the NFRI database does not provide any additional structure around its reactions' species, therefore only the species names (formulas) were collected, together with the reaction kinetics in the form of one or more $[T, k]$ pairs.

With the NFRI database, I also faced an additional challenge with the units of the reaction rate coefficient points. The units declared by the database proved to be very unreliable and, in some cases, clearly erroneous. Two different units for reaction rate coefficient data appeared in the database: $\mathrm{cm^3{\cdot}s^{-1}}$, and $\mathrm{cm^3{\cdot}mol^{-1}{\cdot}s^{-1}}$. The distributions of rate coefficient values for the two units should be both fairly similar and only shifted to each other by the Avogadro number. But the plot on figure 8.1 shows otherwise, implying that some of the reactions in the NFRI database must have incorrect rate coefficients units.

For example, reaction rate coefficients as high as $k = 10^{13}$ do not make any sense for the unit of $[\mathrm{cm^3{\cdot}s^{-1}}]$. And the values shown for the unit of $[\mathrm{cm^3{\cdot}mol^{-1}{\cdot}s^{-1}}]$ clearly follow a very similar distribution as for the unit of $[\mathrm{cm^3{\cdot}s^{-1}}]$, apart from the range of $k = 10^6 - 10^{15}$ $\mathrm{cm^3{\cdot}mol^{-1}{\cdot}s^{-1}}$, which might be the only reactions with the unit of $[\mathrm{cm^3{\cdot}mol^{-1}{\cdot}s^{-1}}]$ actually correctly assigned. Based on the histogram shown in figure 8.1, I have re–assigned the units myself, following the simple rules:

- if the value of $k(300\ \mathrm{K}) < 10^{-6}$, then k is in $\mathrm{cm^3{\cdot}s^{-1}}$,

- if the values of $k(300\ \mathrm{K}) > 10^4$, the unit is $\mathrm{cm^3{\cdot}mol^{-1}{\cdot}s^{-1}}$,

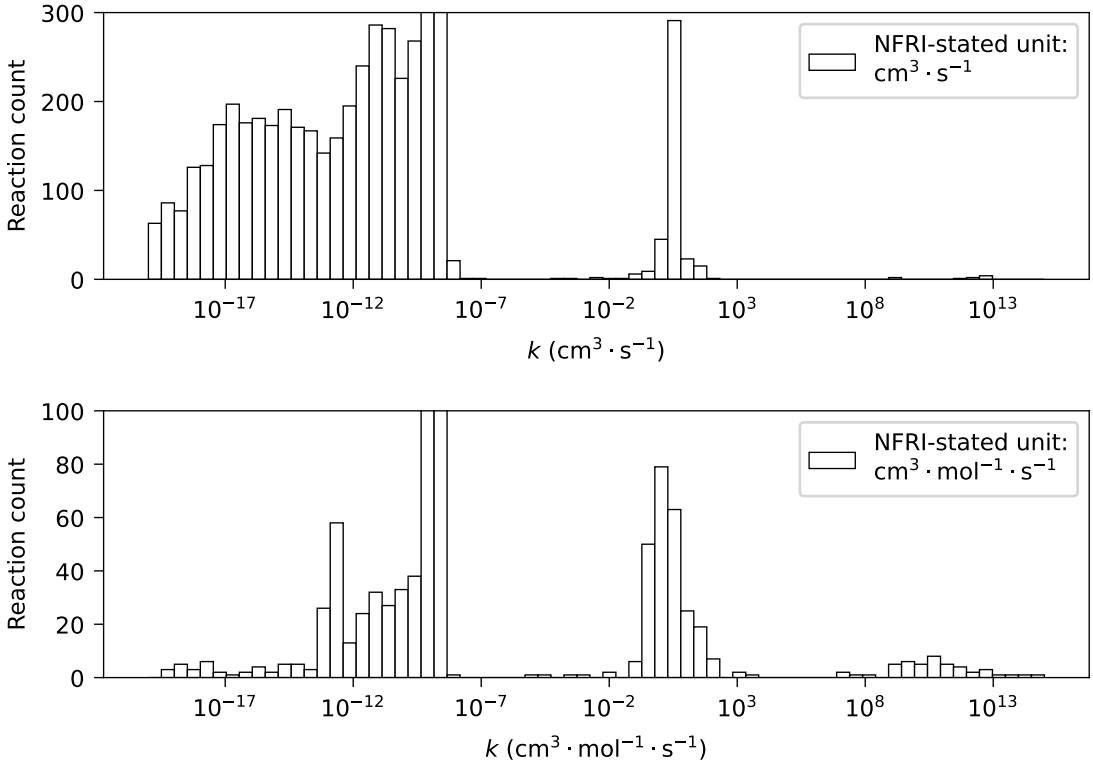

Figure 8.1: Distributions of the reaction rate coefficient values (interpolated for $T = 300$ K) for all reaction collected, with their original units, as present in the NFRI database. Separate histogram is plotted for each one of the two units supported by the database.

- if $10^{-6} \leq k(300\ \mathrm{K}) \leq 10^{4}$, the unit cannot be trusted and the reaction is removed.

Another source of data rejection was reactions involving species with ambiguous formulas and charges. Although I have dedicated a great amount of work to parsing as many species from NFRI reactions as possible, due to the fact that species are only represented by their formula string in this database, many species formulas could not be parsed and correctly identified.

The last two paragraphs also illustrate a very important point: every database contains erroneous data, which will inevitably find a way into my training dataset. Each of the four databases contained some reactions, which did not conserve charge, or elemental stoichiometry. Other errors, such as a wrong unit or incorrect sign of one of the Arrhenius coefficients, were in my case impossible to catch, due to the amount of data to process. But if the amount of erroneous data is low enough, and

more or less uniformly distributed, the regression model trained on the data will not be greatly effected.

8.4 KIDA database

Similar to QDB, the KIDA database also represents the heavy–species kinetics by three parameters, α, β, and γ. This database, however, supports three different temperature dependence functions for its reaction rate coefficients: the kinetics are parametrized either by the modified Arrhenius formula (8.1), or by one of the formulas for Ion–Polar systems, describing the rate coefficients for unmeasured reactions between ions and neutral species with a dipole moment, computed using the Su-Chesnavich capture approach [49; 179; 180]:

$$k\left(T\right) = \alpha\beta\left(0.62 + 0.4767\gamma\left(\frac{300}{T}\right)^{0.5}\right), \tag{8.2}$$

or

$$k\left(T\right) = \alpha\beta\left(1 + 0.0967\gamma\left(\frac{300}{T}\right)^{0.5} + \frac{\gamma^2}{10.526}\frac{300}{T}\right). \tag{8.3}$$

Each of the reactions (8.2), and (8.3) is defined for a different temperature range, α represents the branching ration of the reaction, β is the Lanagevin rate, while γ determines the temperature dependence for the given temperature range.

The KIDA database also has a species model, and stores additional attributes for each reactant and product of any reaction. For each eligible KIDA reaction, the following data were collected: the kinetic parameters α, β, and γ, the type of reaction rate temperature dependence formula to interpret those parameters, and finally, for each reactant and product of the reaction, mass and charge were collected, and if present, also the enthalpy of formation at the normal temperature, polarizability of the species and its dipole moment.

KIDA also provides 4 tiers of data evaluation, assigning to each reaction one of the following values: *Not recommended value*, *Not rated value*, *Valid value*, and *Recommended value*. The reactions labeled with *Not recommended value* evaluation were completely ignored and not added to my dataset, while the reactions with all

the other evaluation labels were added and treated equally. Also, KIDA often lists multiple sets of kinetic parameters for a single reaction, and as in the case of QDB, these were all preserved and added into the dataset as individual data instances. And finally, each reaction in KIDA has a valid temperature range attached, and only reactions where this range of validity overlaps with the range of $T = 300$ K $\pm 10\%$ are added to the dataset, as in the case of the NFRI database.

8.5 UDfA database

The last database scraped for data was the UMIST Database for Astrochemistry. The kinetics of reactions in the UDfA database is described exclusively by the modified Arrhenius formula (8.1). Each reaction also has a temperature range of validity, and the criterion for adding the reactions into the datasets was the same as in the case of QDB (section 8.2) and KIDA (section 8.4); the temperature range must overlap with a range around the room temperature. No additional species data are provided by UDfA, only strings representing their formulas. This means that the species charges, elemental stoichiometry, and possible states had to be parsed from the formulas.

8.6 Dataset unification

The structure of the final unified dataset, aggregating the data from all the four databases, can be summarized by the entity relationship (ER) diagram given in figure 8.2 (only the relevant parameters are shown). In this model, every reaction is uniquely identified by two species as reactants, two species as products, and the set of kinetic parameter values, α, and optionally β, and γ. Each species is then uniquely identified by its elemental stoichiometry and a charge.

Following this model, and for simplicity, different isomers having the same elemental composition and charge were collapsed to a single species, characterised by its stoichiometry and charge. As an example, the following three species collected from KIDA with their unique formulas of HNCCC, HCCNC, and HCNCC, were all

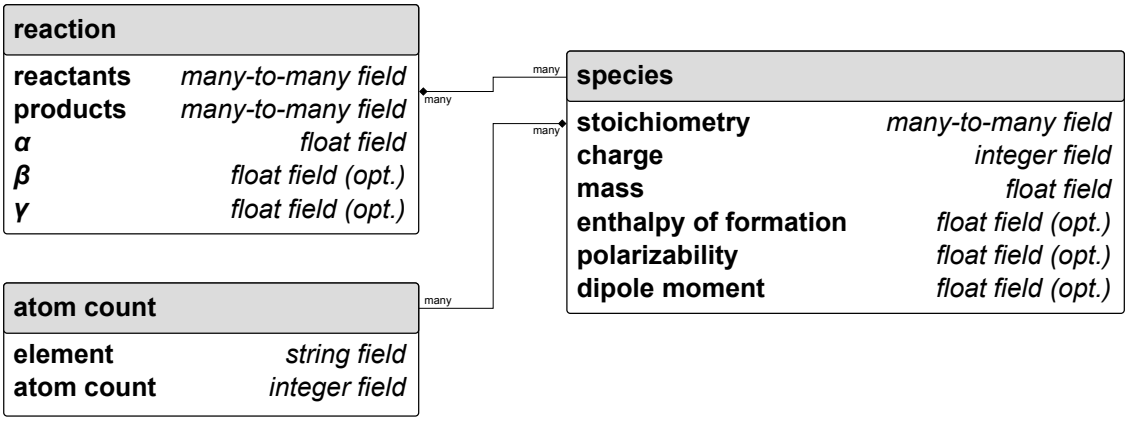

Figure 8.2: ER diagram showing the relevant attributes of the unified dataset aggregating the data instances collected from all four databases.

unified into a single species characterised by the elemental stoichiometry of {"H": 1, "C": 3, "N": 1}, and the charge $q = 0$. If the enthalpy of formation $\Delta_\mathrm{f}H^\circ$, the polarizability α, or the dipole moment p was found in KIDA or in QDB for more than one such isomer, the resulting species got assigned the parameters of the isomer with the lowest $\Delta_\mathrm{f}H^\circ$.

Species from all four databases were identified by parsing the (database–specific) species formulas and extracting the elemental stoichiometry and charges from the formula strings. The species were also further validated with the help of the *pyvalem* python package by Hill [181], and by checking the charge and stoichiometry conservation of the reactions they appear in. The species masses were determined from the elemental stoichiometry and checked against the masses scraped from the databases, adding an additional layer of confidence in correct parsing of the species formulas. This way, I managed to remove all the ambiguity in species names caused by different naming conventions in different databases.

The polarizability and dipole moment species parameters were populated exclusively from the KIDA database, where present. The enthalpy of formation values were being searched for, in order, in the KIDA database, the QDB database, and the NIST-JANAF [182] and ATcT [183] tables, which were previously scraped by Bingqing Lu [184].

Finally, apart from the reaction criteria listed in section 8.1, I have introduced two additional criteria for reactions elimination, based on the first analysis of the

unified dataset. When creating a training dataset, it makes sense to eliminate some obvious fringe and outlying data instances from the set, to increase the data coherence [159]. These additional criteria were:

1. **Only reactions with *neutral* or *single–ionized* species are kept.** Doubly ionized species made up only less than 0.3% of all the species in the dataset.

2. **Only reactions *without electrons* are kept.** The *associative electron detachment* reactions made up only about 1.7% of all the reactions in the dataset, and were therefore eliminated for sake of the dataset coherence.

All together, the final dataset consists of 9,470 reactions involving 1080 distinct species. That is after removing duplicate reactions by the methodology discussed in chapter 9. Table 8.1 provides the number of reactions in the final dataset sourced from each one of the four databases. The final dataset, following the relational structure depicted in figure 8.2, is given as `data_final.yaml` file in the project GitHub repository `https://github.com/martin-hanicinec-ucl/regreschem`.

Table 8.1: The sums of reactions in the final dataset per source database.

Source database	**Number of reactions**
QDB [9]	1586
NFRI [54]	1171
KIDA [49; 50]	4862
UDfA [51]	1851

In the next chapter, I will discuss in more detail the regression model I have developed in this project. More specifically, I will describe which model features are selected, which outputs the model predicts, and I will discuss in detail training of the model on the training subset of the dataset presented.

Chapter 9

Kinetics regression model

This chapter gives a detailed description of the development of my final regression model. In the first two sections, I describe the final processing of the training dataset into the features matrix $\mathbf{X}$ and the targets vector $\mathbf{y}$ (see section 7.1). The final section then focuses on training the regression model and the techniques I used to optimize the hyperparameters for each one of the model classes described in chapter 7.

9.1 Targets

The first thing to do is selecting the outputs the model will aim to regress. In most plasma modeling scenarios, the kinetics for heavy species reactions are most commonly described by the modified Arrhenius formula (8.1), which parameterizes the temperature dependence of reaction rate coefficient $k(T)$ by three parameters α, β, and γ. Ideally, these three parameters could be predicted by a *multivariate regression* model (a model which outputs more than a single value, see e.g. [159]).

In the real case, however, all the three parameters also need to be present in the training dataset as targets for supervised learning. It is very common for sources of plasma kinetics not to give the full set of Arrhenius coefficients. Some sources might only list two Arrhenius coefficients, and in fact, the majority of reactions from my sources only had a single reaction rate *constant* attached. In the NFRI database [54], the kinetic data are served as a series of reaction rate coefficient values for different

temperatures. In theory, the desired Arrhenius coefficients could be fitted on such data, this would require, however, at least three data points present, preferably many more. In reality, less than 4% of the NFRI reactions offer 3 data points and more. Instead, more than 90% of NFRI reactions only a single data point: the reaction rate constant for a temperature within 10% margin around 300 K (otherwise they would not have been selected for my dataset, see chapter 8). In the case of QDB [9], KIDA [49; 50], and UDfA [51] databases, which offer kinetic data already in Arrhenius form, only about 3% of the reactions selected for my dataset actually contained all the three Arrhenius parameters.

I therefore decided to limit my regression model to a single–value prediction of a reaction rate constant expressed for $T = 300$ K, or more precisely to its logarithm, as the rate coefficients need to be well resolved in a range of many orders of magnitude (the trick of target values logarithmization has been used e.g. by Komp and Valleau in their work [105] on a similar topic). As the targets vector $\mathbf{y}$, I used the vector of $\log_{10} k(300\mathrm{K})$ values expressed for all the reactions in the dataset, with k in $\mathrm{cm^3 s^{-1}}$.

Two more things regarding the targets deserve a mention: duplicate reactions, and target capping.

9.1.1 Duplicate reactions

The same kinetic data describing a particular reaction appeared in many cases in more than one database. These duplicate data instances needed to be removed. The duplicates were detected based solely on the set of reactants, set of products, and $k(300\mathrm{K})$, or the target. While iterating over the dataset, each reaction was removed if it had the same two reactants, the same two products, and the $k(300\mathrm{K})$ value within 10% to another reaction present already.

9.1.2 Target capping

As discussed previously in chapter 7, the regression models train to minimize the error measure between the vector of predicted values and the vector of targets, usually RMSE, or MAE (see e.g. [159]). With the logarithmic targets, however, it

would be a bad strategy to treat two data instances with the identical prediction error equally, if one target is very high, and another one very low. Predicting e.g. $k_1^{\text{pred}} = 10^{-5}$ cm^{3}s^{-1} for a data instance with the target of $k_1 = 10^{-7}$ cm^{3}s^{-1} is clearly a much bigger deal, than predicting e.g. $k_2^{\text{pred}} = 10^{-25}$ cm^{3}s^{-1} for a data instance with the target $k_2 = 10^{-27}$ cm^{3}s^{-1}, even if the two instances will share the same square (and absolute) error in the logarithmic target space. This is, naturally, because reactions with relatively low rate coefficients will impact solutions of plasma models typically much less than reactions with relatively high rate coefficients. My workaround is to define an *effective minimal* rate coefficient k_{min}. The targets of all reactions with $k < k_{\text{min}}$ were capped to the minimal value of $\log_{10} k_{\text{min}}$. The predicted values were capped the same way, when evaluating different model classes, or when optimizing the model hyperparameters.

I have chosen the value of $k_{\text{min}} = 10^{-20}$ cm^{3}s^{-1}. This was a somewhat arbitrary choice, but based on plasma modeling experience, both mine and my supervisors'. Figure 9.1 shows histograms of all the dataset targets before, and after capping to k_{min}. The bimodal distribution of k values will be discussed in section 9.3.

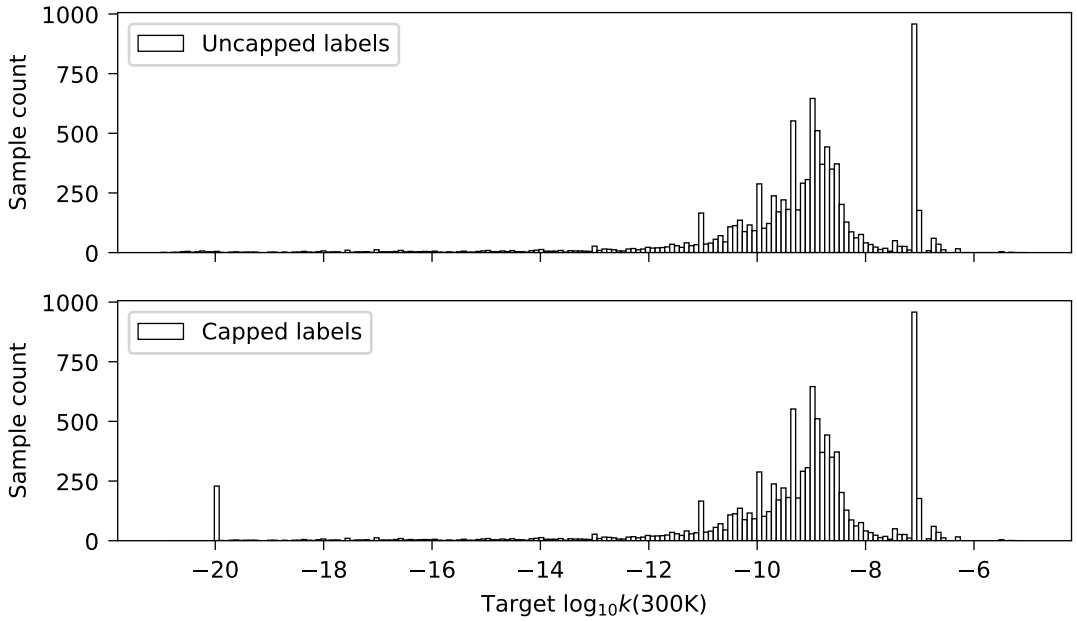

Figure 9.1: Histograms of all the dataset target values before (top) and after (bottom) capping to k_{min}

.

9.2 Features

In my dataset, I have tried to collect as much easily accessible data as possible, which might possibly correlate with the reaction rate coefficients being predicted. This data form the *raw dataset*.

9.2.1 Raw dataset table

The data collected in the raw dataset could be divided into two categories:

1. **Data describing the individual species:** 26 attributes were collected for each species, totaling 104 columns in the raw dataset table (26 per 2 reactants and 2 products). These attributes are:

   - mass m in [amu],
   - charge q in [e],
   - standard enthalpy of formation $\Delta_\mathrm{f}H^\circ$ in [kJ·mol^{-1}]
   - enthalpy of formation of a neutral $\Delta_\mathrm{f}H^\circ_{n_0}$ describing $\Delta_\mathrm{f}H^\circ$ of the neutral counterparts to charged species,
   - polarizability α in [Å^3],
   - dipole moment p in [D],
   - number of atoms summed per each *block* of the periodic table (total of 4 attributes, for 4 blocks: *s*, *p*, *d*, *f*),
   - number of atoms summed per each *group* of the periodic table (total of 16 attributes, for 16 groups: *IA*, *IB*, *IIA*, ..., *VIIB*, *VIIIA*, *VIIIB*).

   The standard enthalpy of formation $\Delta_\mathrm{f}H^\circ$ is at room temperature $T = 298.15$ K. For neutral reactants and products, $\Delta_\mathrm{f}H^\circ_{n_0} = \Delta_\mathrm{f}H^\circ$. The m and q values are naturally fully populated, but the rest of the values are not present in each data instance. The atom counts per block and group are an attempt to encode the elemental composition of the species into the data instances.

2. **Data describing the *exchanged fragment*:** This category of raw dataset table columns regards species fragments exchanged between reactants, in order to create the products. As an example, in the reaction

$$\mathrm{H} + \mathrm{NH} \rightarrow \mathrm{H_2} + \mathrm{N},$$

a single H atom is exchanged. The attributes encoding the exchange fragments are the mass, the number of atoms, and the number of atoms per block and group of the periodic table, as in the previous point. This makes in total 22 columns. In some cases, a single fragment is not enough to turn reactants into products, and the values simply sum all the fragments exchanged. In most cases, multiple ways exist to turn reactants into products, and the passed fragments with the lowest total mass are picked. As another example, in the reaction

$$\mathrm{OH^-} + \mathrm{CCl_4} \rightarrow \mathrm{OCl^-} + \mathrm{CHCl_3},$$

the fragments Cl (passed from $\mathrm{CCl_4}$ to $\mathrm{OH^-}$), and H (passed from $\mathrm{OH^-}$ to $\mathrm{CCl_4}$) are selected in favor of fragments O, and $\mathrm{CCl_3}$. In this example, the mass and number of atoms are calculated from (1H + 1Cl).

The entire raw dataset table is available in the project repository `https://github.com/martin-hanicinec-ucl/regreschem` as `dataset_raw.csv`. Apart from the columns described already, several additional columns exist, containing some metadata about the data instances, such as the reaction strings (e.g. `"SF4 + SF6- -> SF5 + SF5-"`), the name of the database the reaction instance belonged to (`"qdb"`, `"kida"`, `"umist"`, or `"nfri"`), the *doi* identifier of the primary source, where available in the database, or the names and source databases for the individual species in each reaction (data instance) line. Those columns are not used in any way to construct features for the regression models.

9.2.2 Data imputation

ML algorithms typically can not accept missing data [159]. This is a problem, as a fraction of instances is missing at least one of the $\Delta_f H^\circ$, $\Delta_f H^\circ_{n_0}$, α, or p values, for at least one reactant of product. Limiting the dataset to only instances with all the values present would decrease the dataset size considerably. Figure 9.2 gives an overview of how many data instances are missing which attributes. As an example, well over half of the instances are missing e.g. α for a *single* one of its species, but hardly any instances are missing α for *every* one of its species. To prevent decreasing the dataset size to less than a half, the missing values must be imputed.

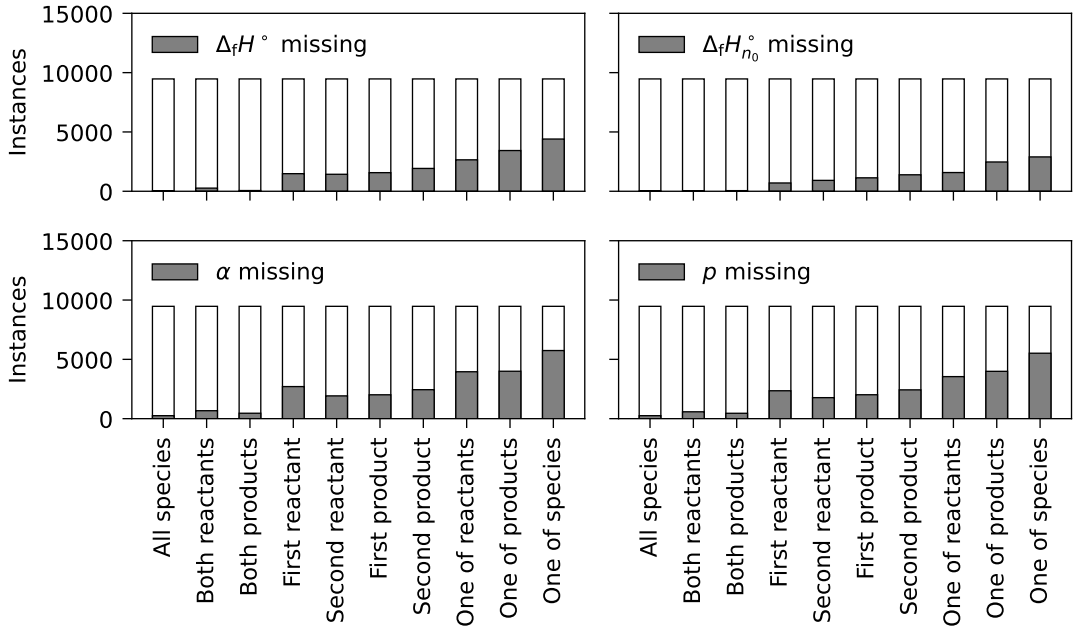

Figure 9.2: Bar plots showing fraction of instances in the dataset, with missing $\Delta_f H^\circ$, $\Delta_f H^\circ_{n_0}$, α, or p for its reactants and products.

I have used the `IterativeImputer` class available in the `sklearn.impute` python module [169]. The `IterativeImputer` basically regresses the missing data in a dataset from all the other attributes. In each iteration, a single column containing some missing data gets filled by an imputation regression model, which is trained on all the other completely populated columns. In this way, the imputation model is just another regression model, which is trained to predict the missing values, in order to produce a complete features matrix, on which the main regression model

could be trained. The `IterativeImputer` model can use different regression model classes to perform the imputation. I have used the default *Bayesian Ridge* regressor. The Scikit-learn implementation, the `BayesianRidge` regression model, is based on an algorithm described by Tipping [185] and MacKey [186], but the full theory is beyond the scope of this work. For illustration, figure 9.3 shows histograms of the polarizability α before and after imputation of the missing values.

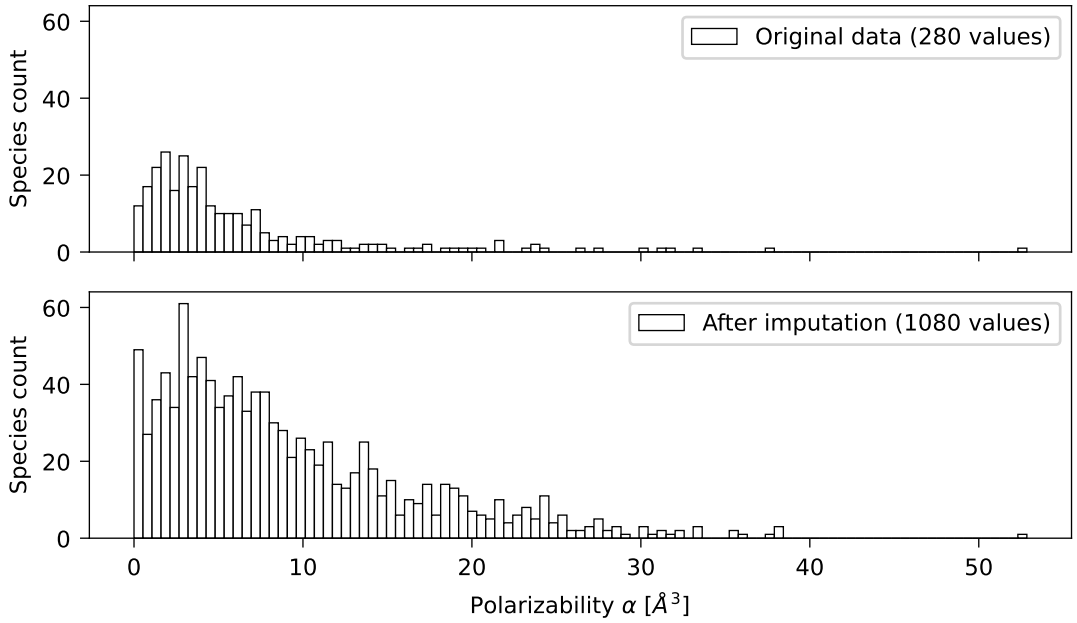

Figure 9.3: Histograms showing the distribution of α values in the dataset before and after the imputation of missing values.

All the data instance attributes described in section 9.2.1 do not yet form the feature matrix for the regression models. Typically, it makes sense to manipulate the values in a way so that the final features utilize some heuristics already known about the system, or some more sensible representations [159]. This manipulation is referred to as *feature engineering* and it is the key to a successful ML model [162].

9.2.3 Feature engineering

As with model selection and hyperparameters tuning, feature engineering is domain–specific and the features matrix $\mathbf{X}$ needs to be optimized, often iteratively by trial and error [162]. In this section, I will describe my final set of features, as a result of

a lengthy process of optimization for the lowest prediction errors.

As the order of reactants and products in any reaction is purely a matter of chance or convention, the features encoding attributes of reactants and products should be symmetric with respect to swapping the two reactants (or products). The features encoding the reaction species were engineered as follows:

- **Masses** m of both reactants were replaced by the reduced mass μ of the left–hand–side (LHS) of the reaction. For a generic reaction

$$\mathrm{A} + \mathrm{B} \rightarrow \mathrm{C} + \mathrm{D}, \tag{9.1}$$

$$\mu_{\mathrm{LHS}} = \frac{m_{\mathrm{A}} m_{\mathrm{B}}}{m_{\mathrm{A}} + m_{\mathrm{B}}}. \tag{9.2}$$

  The same was done for the products, and the right–hand–side (RHS) of any reaction.

- **Charges** q of both reactants were replaced by a series of *one–hot encoded* charge combinations. For the reaction left–hand–side, this resulted in three *boolean–valued* features: Q^{00}_{LHS}, Q^{+0}_{LHS}, and Q^{+-}_{LHS}. As an example, for the generic reaction (9.1),

$$Q^{+0}_{\mathrm{LHS}} = \begin{cases} 1 & \text{if}(q_{\mathrm{A}} = 0 \text{ and } q_{\mathrm{B}} = 1) \text{ or } (q_{\mathrm{A}} = 1 \text{ and } q_{\mathrm{B}} = 0) \\ 0 & \text{otherwise.} \end{cases} \tag{9.3}$$

  The reactant charges are converted by the same token in the features Q^{00}_{RHS}, and Q^{+0}_{RHS}. The only two other charge combinations appearing in the dataset, characterized by the features Q^{-0}_{LHS} and Q^{-0}_{RHS}, have been dropped from the dataset, as nearly all values for these features were zero (very few collisions between neutrals and negative ions are present in the dataset).

- **Enthalpy of formation** $\Delta_{\mathrm{f}}H^{\circ}$ values for both reactants and products were turned into the enthalpy of formation of each side of the reaction. For the

generic reaction (9.1), this made two features

$$\Delta_{\mathrm{f}} H^{\circ}_{\mathrm{LHS}} = \Delta_{\mathrm{f}} H^{\circ}_{\mathrm{A}} + \Delta_{\mathrm{f}} H^{\circ}_{\mathrm{B}}, \tag{9.4a}$$

$$\Delta_{\mathrm{f}} H^{\circ}_{\mathrm{RHS}} = \Delta_{\mathrm{f}} H^{\circ}_{\mathrm{C}} + \Delta_{\mathrm{f}} H^{\circ}_{\mathrm{D}}. \tag{9.4b}$$

Additionally, the total enthalpy of formation for the whole reaction was explicitly added as a feature

$$\Delta_{\mathrm{f}} H^{\circ}_{\mathrm{total}} = \Delta_{\mathrm{f}} H^{\circ}_{\mathrm{RHS}} - \Delta_{\mathrm{f}} H^{\circ}_{\mathrm{LHS}}. \tag{9.5}$$

The $\Delta_{\mathrm{f}} H^{\circ}_{n_0}$ values were manipulated exactly the same way.

- **Polarizability** values α were turned into 2 distinct features

$$F^{\alpha}_{\mathrm{LHS}} = \alpha_{\mathrm{A}} |q_{\mathrm{B}}| + \alpha_{\mathrm{B}} |q_{\mathrm{A}}|, \tag{9.6a}$$

$$F^{\alpha}_{\mathrm{RHS}} = \alpha_{\mathrm{C}} |q_{\mathrm{D}}| + \alpha_{\mathrm{D}} |q_{\mathrm{C}}|, \tag{9.6b}$$

following the species naming convention from the generic reaction (9.1). The choice of these features is motivated by the fact that the electrostatic force between a charged and a polar particle will, in the first approximation, be proportional to the product of the charge and the polarizability of the particles.

- **Dipole moment** values p of all the reactants and products were turned into the features F^{p}_{LHS} and F^{p}_{RHS}, following the same line of reasoning as in the case of polarizability: the electrostatic force between a charged particle and a particle with a dipole moment will be roughly proportional to the product of p and square of the charge, therefore

$$F^{p}_{\mathrm{LHS}} = |p_{\mathrm{A}}| q^2_{\mathrm{B}} + |p_{\mathrm{B}}| q^2_{\mathrm{A}}, \tag{9.7a}$$

$$F^{p}_{\mathrm{RHS}} = |p_{\mathrm{C}}| q^2_{\mathrm{D}} + |p_{\mathrm{D}}| q^2_{\mathrm{C}}. \tag{9.7b}$$

- And finally, the species attributes describing the **elemental composition**

of the reactants and products were all collapsed into just 7 features: $N^{\text{bl.=s}}$, $N^{\text{bl.=p}}$, $N^{\text{gr.=IA}}$, $N^{\text{gr.=IVA}}$, $N^{\text{gr.=VA}}$, $N^{\text{gr.=VIA}}$, $N^{\text{gr.=VIIA}}$. For an explanation by example, $N^{\text{bl.=s}}$ is the number of atoms appearing on the LHS of the reaction, which belong to the *s* block of the periodic table of elements. There are very few species in the dataset made of elements belonging to the block *d* and none of elements belonging to the block *f*. Therefore, only the features describing the blocks *s* and *p* were kept in the features matrix. Similarly, the vast majority of species in the dataset are composed of elements belonging to one of the *IA, IVA, VA, VIA, VIIA* groups of the periodic table. All the other groups were dropped from the features space. All the 7 features described are evaluating the numbers of atoms found on the LHS of any reaction only. As each reaction conserves the species stoichiometry between sides, the features belonging to RHS would be identical and do not have to be present.

Apart from the features encoding the reactants and products, there are 9 more features describing the elements exchanged between the two reactants in order to create the two products. Following the same nomenclature as in the list above, these features are fairly self–evident: m_{X}, N_{X}, $N_{\text{X}}^{\text{bl.=s}}$, $N_{\text{X}}^{\text{bl.=p}}$, $N_{\text{X}}^{\text{gr.=IA}}$, $N_{\text{X}}^{\text{gr.=IVA}}$, $N_{\text{X}}^{\text{gr.=VA}}$, $N_{\text{X}}^{\text{gr.=VIA}}$, $N_{\text{X}}^{\text{gr.=VIIA}}$. Here, X refers to a hypothetical particle made of the exchanged elements (see section 9.2.1), and N_{X} is simply a number of atoms of X, no matter which block or group.

Table 9.1 shows the final list of features forming the features matrix $\mathbf{X}$ in this work. Also shown are the feature names consistent with the code in the project repository, and the features data types. In total, 33 features were used.

The final note about the features should cover the feature scaling. As foreshadowed already in chapter 7, some regression model classes will work sub–optimally if different features are on vastly different scales. This applies to the SVM regressor in particular [159]. Scale sensitivity is typically handled by applying *standard scaling* to all the numeric features [159]. I have done it by adding the `StandardScaler` instance from `sklearn.preprocessing` module [169] into my data transformation pipeline. The standard scaler subtracts the mean from each feature column and scales all the values to unit variance. Figure 9.4 shows the distribution of the final

Table 9.1: The final list of features, relating the nomenclature used throughout this chapter to the feature names used in the project repository code, and to the data types of all the features values.

Symbol	Feature name	Data type
$\Delta_{\mathrm{f}} H^{\circ}_{\mathrm{total}}$	`delta_hform`	`real`
$\Delta_{\mathrm{f}} H^{\circ}_{n_0,\mathrm{total}}$	`delta_hform_neutral`	`real`
Q^{00}_{LHS}	`lhs_charge_00`	`boolean`
Q^{+0}_{LHS}	`lhs_charge_+0`	`boolean`
Q^{+-}_{LHS}	`lhs_charge_+-`	`boolean`
μ_{LHS}	`lhs_mu`	`real`
$\Delta_{\mathrm{f}} H^{\circ}_{\mathrm{LHS}}$	`lhs_hform`	`real`
$\Delta_{\mathrm{f}} H^{\circ}_{n_0,\mathrm{LHS}}$	`lhs_hform_neutral`	`real`
$F^{\alpha}_{\mathrm{LHS}}$	`lhs_polarizability_factor`	`real`
F^{p}_{LHS}	`lhs_dipole_moment_factor`	`real`
$N^{\mathrm{bl.=s}}$	`lhs_block_s`	`integer`
$N^{\mathrm{bl.=p}}$	`lhs_block_p`	`integer`
$N^{\mathrm{gr.=IA}}$	`lhs_group_IA`	`integer`
$N^{\mathrm{gr.=IVA}}$	`lhs_group_IVA`	`integer`
$N^{\mathrm{gr.=VA}}$	`lhs_group_VA`	`integer`
$N^{\mathrm{gr.=VIA}}$	`lhs_group_VIA`	`integer`
$N^{\mathrm{gr.=VIIA}}$	`lhs_group_VIIA`	`integer`
Q^{00}_{RHS}	`rhs_charge_00`	`boolean`
Q^{+0}_{RHS}	`rhs_charge_+0`	`boolean`
μ_{RHS}	`rhs_mu`	`real`
$\Delta_{\mathrm{f}} H^{\circ}_{\mathrm{RHS}}$	`rhs_hform`	`real`
$\Delta_{\mathrm{f}} H^{\circ}_{n_0,\mathrm{RHS}}$	`rhs_hform_neutral`	`real`
$F^{\alpha}_{\mathrm{RHS}}$	`rhs_polarizability_factor`	`real`
F^{p}_{RHS}	`rhs_dipole_moment_factor`	`real`
m_{X}	`exchanged_mass`	`integer`
N_{X}	`exchanged_atoms`	`integer`
$N^{\mathrm{bl.=s}}_{\mathrm{X}}$	`exchanged_block_s`	`integer`
$N^{\mathrm{bl.=p}}_{\mathrm{X}}$	`exchanged_block_p`	`integer`
$N^{\mathrm{gr.=IA}}_{\mathrm{X}}$	`exchanged_group_IA`	`integer`
$N^{\mathrm{gr.=IVA}}_{\mathrm{X}}$	`exchanged_group_IVA`	`integer`
$N^{\mathrm{gr.=VA}}_{\mathrm{X}}$	`exchanged_group_VA`	`integer`
$N^{\mathrm{gr.=VIA}}_{\mathrm{X}}$	`exchanged_group_VIA`	`integer`
$N^{\mathrm{gr.=VIIA}}_{\mathrm{X}}$	`exchanged_group_VIIA`	`integer`

$\Delta_f H^\circ_{total}$ feature (using the $\Delta_f H^\circ$ values after imputation) with different horizontal axes belonging to the original and standard–scaled feature data.

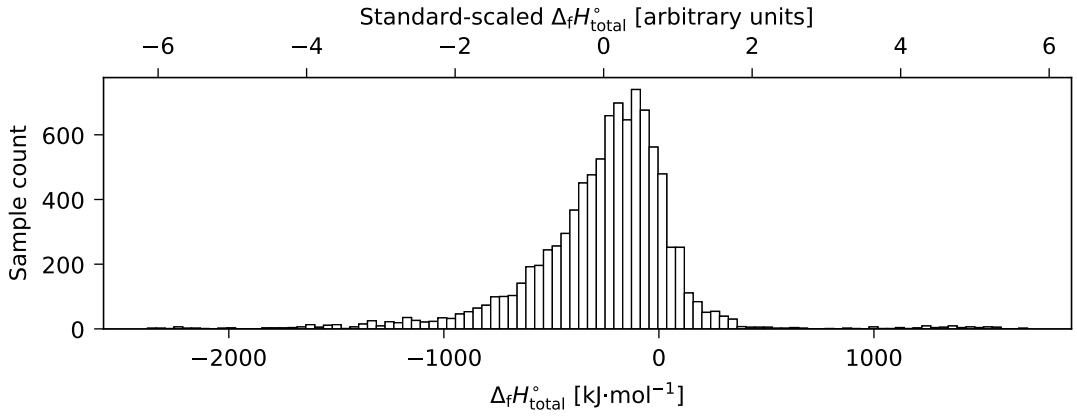

Figure 9.4: Histogram showing the distribution of the $\Delta_f H^\circ_{total}$ feature values in the original unit space (bottom horizontal axis), and in the rescaled space (top horizontal axis).

9.3 Dataset analysis

As mentioned in section 9.1.1, duplicate reactions were identified as identical reactions with very close reaction rate coefficients and were filtered out of the dataset. However, the dataset still contains many different samples which share the same reactants and products, while having very different reaction rate coefficients. Those might be sourced either from different databases, or from the same database, but from different source publications. In some cases, the reaction rate coefficients for identical reactions differ vastly across different data samples. Figure 9.5 shows different target values found in the dataset per each one of three chosen reactions. As the data samples belonging to a single reaction will share the features vector, those form conflicting data samples in the dataset.

It can be seen from figure 9.5, that the difference in reaction rate coefficient k between two conflicting training data samples can in some instances be even higher than 10 orders of magnitude. Figure 9.6 quantifies further the differences between conflicting training data points across the dataset. Per each reaction having more conflicting reaction rate coefficients in the dataset, the difference between the

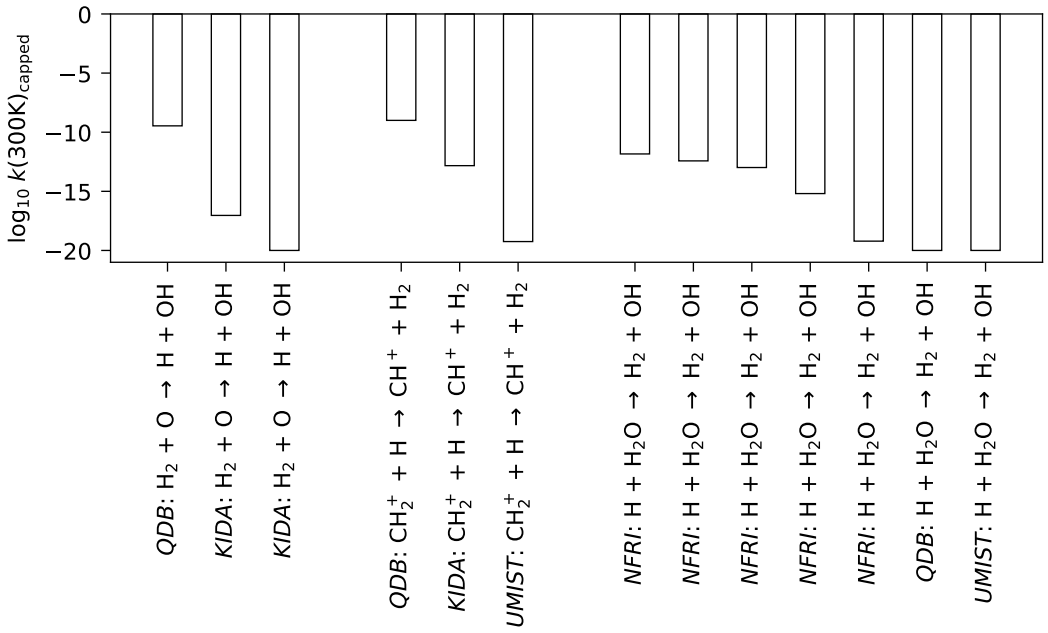

Figure 9.5: All the different target values found in the dataset per each one of three chosen reactions. This plot is shown to illustrate the level of consistency of the training data and to point out the conflicting data samples.

maximal and minimal value is evaluated. As can be seen in figure 9.6, out of the total of 1,916 reactions with multiple k values, the vast majority of reactions have fairly consistent k values within a single order of magnitude. There are, however, a significant number of samples with a much wider spread. This naturally has implications for the limits of how well any regression model can actually perform.

Another thing worth analyzing is the distribution of target values. Figure 9.1 showed the overall distribution of k values across the dataset with a distinct bimodal appearance. The individual peaks of the bimodal distribution correlate with the charge combinations of reactants or with the features Q^{00}_{LHS}, Q^{+0}_{LHS}, Q^{+-}_{LHS}, as can be seen in figure 9.7. The rate coefficients belonging to reactions of two neutrals ($Q^{00}_{\mathrm{LHS}} = 1$) and to neutral–ion reactions ($Q^{+0}_{\mathrm{LHS}} = 1$) together form the first, broader peak, while the reactions between positive and negative ions ($Q^{+-}_{\mathrm{LHS}} = 1$) form the second, tighter peak. Most of the anion–cation collisions in the dataset are mutual neutralization reactions.

A closer look at the *anion–cation* collisions samples reveal two quite populous mono–valued peaks. This is shown in figure 9.8. First, 953 reactions share the same

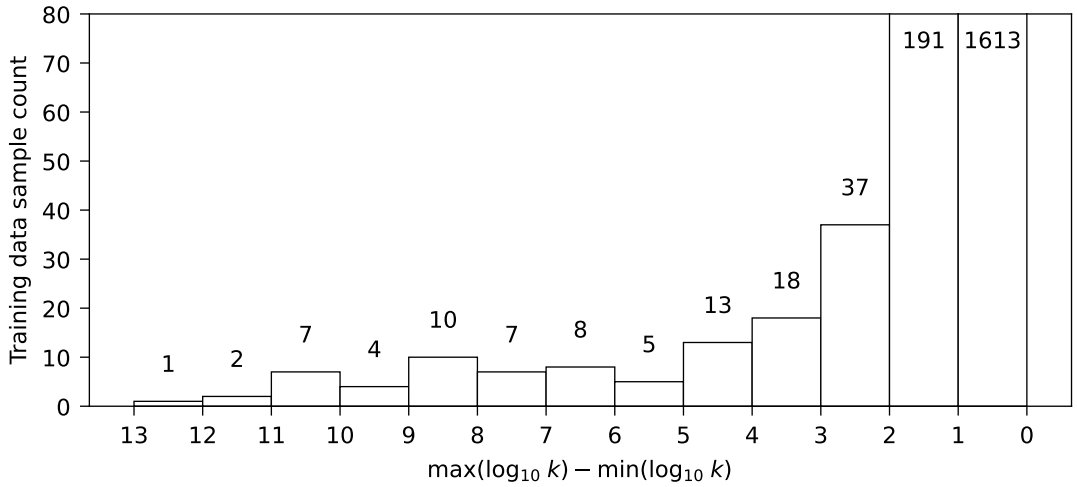

Figure 9.6: Histogram showing the spread of conflicting data samples target values. Per each identical reaction, the minimal and maximal target value is extracted from the dataset, and their difference is plotted as a histogram. This plot is shown to illustrate the level of consistency of the training data and to point out the conflicting data samples.

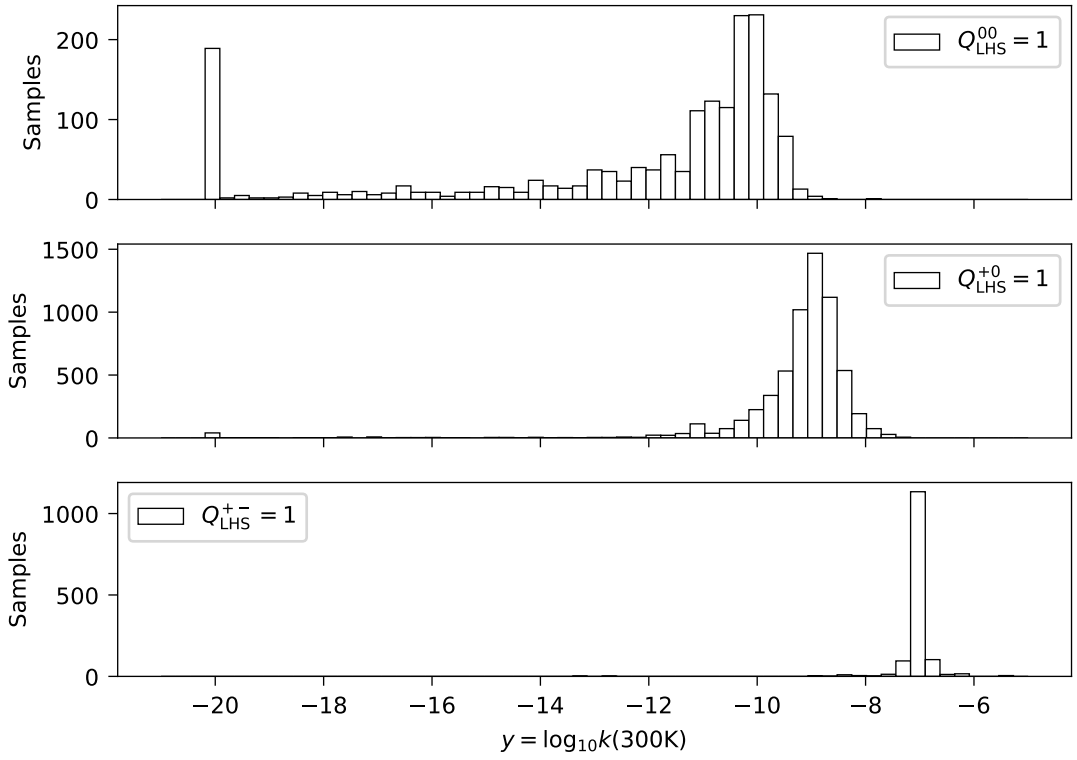

Figure 9.7: Distributions of k values in the dataset shown on three separate histograms for neutral–neutral collisions ($Q^{00}_{\mathrm{LHS}} = 1$), neutral–cation collisions ($Q^{+0}_{\mathrm{LHS}} = 1$), and finally anion–cation collisions ($Q^{+-}_{\mathrm{LHS}} = 1$).

target value, corresponding to the reaction rate coefficient

$$k(T) = 7.5 \times 10^{-8}\ (T/300)^{-0.5}\mathrm{cm}^3\mathrm{s}^{-1},$$

and all appear to be a generalization of a single mutual neutralization reaction (1.1) sourced from Harada and Herbst [61], discussed already in section 1.2. Second, 166 reactions, all acquired from QDB, share the same value of $k = 1.0 \times 10^{-7}\mathrm{cm}^3\mathrm{s}^{-1}$, and cite the same publication by Harada and Herbst. Unfortunately, no reaction rate coefficient with such a value is present in the publication.

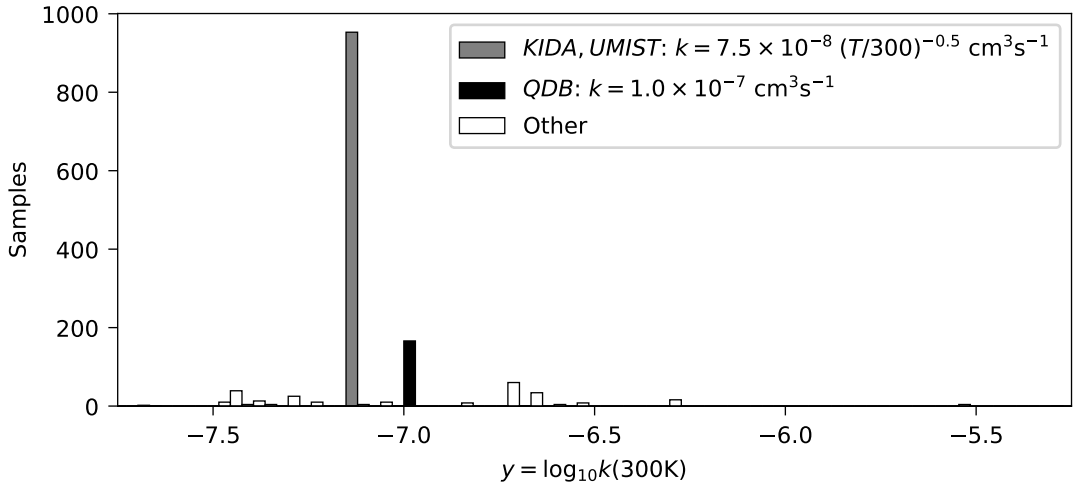

Figure 9.8: Histogram showing distribution of target values for all the anion–cation reactions in the dataset, with the two dominant mono–valued peaks highlighted.

9.4 Training the model

The performance of a trained ML model is typically measured as a prediction error scored on a set of data samples [159]. As mentioned before, the most widely used error functions are RMSE and MAE functions, and I have used these two throughout this work. As discussed in section 9.1.2, the predicted target values were capped to y_{min}, corresponding to $k_{\mathrm{min}} = 1 \times 10^{-20}\ \mathrm{cm}^3\mathrm{s}^{-1}$, for the error metrics evaluation,

resulting in the following definition of both error functions:

$$\mathrm{RMSE}\left(\mathbf{y}, \mathbf{y}^{\mathrm{pred}}\right) = \sqrt{\frac{\sum_{i=1}^{N}\left[y_i - \mathrm{cap}\left(y_i^{\mathrm{pred}}\right)\right]^2}{N}}, \tag{9.8}$$

$$\mathrm{MAE}\left(\mathbf{y}, \mathbf{y}^{\mathrm{pred}}\right) = \frac{\sum_{i=1}^{N}\left|y_i - \mathrm{cap}\left(y_i^{\mathrm{pred}}\right)\right|}{N}, \tag{9.9}$$

where

$$\mathrm{cap}\left(y\right) = \begin{cases} y_{\min} = -20 & \text{if } \; y < y_{\min}, \\ y & \text{otherwise.} \end{cases} \tag{9.10}$$

There, $\mathbf{y}$ and y_i refer to the known target values, while $\mathbf{y}^{\mathrm{pred}}$ and y_i^{pred} are the values predicted by the model. N is the number of data samples the prediction error is evaluated on. Note that the known target values $\mathbf{y}$ are already capped at $y_{\min}$.

9.4.1 Train–test split

As illustrated e.g. in figure 7.4, given enough free parameters in a model and no regularization, the model can easily fit the training data *perfectly*, resulting in the prediction error RMSE = MAE = 0, when evaluated on the training dataset $\mathbf{X}^{\mathrm{train}}, \mathbf{y}^{\mathrm{train}}$. Instead of how well it fits the training data, it is *generalization* that counts [162]. In other words, it is much more important how well the model fits additional data, which the training algorithm never saw.

A standard practice is to split the whole dataset into the *training* and *test* subsets [159]. The training dataset is used for the hyperparameters tuning on different regression models, while the test set is used for the final evaluation of the optimized regression model. No data used to train the model are then used to evaluate it. By evaluating the final model on the test set of withheld data, one can quantify the expected error of the model when predicting the rate coefficients for brand new data instances. This is called *generalization error*, or *out-of-sample error* [159]. By the same token, the prediction error on the training set is called a *training error*. If the training error is low while the generalization error is high, this suggests overfitting [159]. In this work, I have withheld 20% of randomly selected samples as the

test set. This led to the training set of 7,576 instances and the test set of size 1,894.

9.4.2 Cross–validation

Any given ML model class contains some hyperparameters that control the model. The hyperparameters need to be tuned to optimize the model for the given problem represented by the training and test datasets. One approach to hyperparameters optimization is to evaluate alternative models defined by different hyperparameters on the test set and then select the model with the lowest generalization error. This is, however, a very bad practice, as this optimizes the model's hyperparameters for the given test set, and the model becomes essentially *tailored* to the particular train/test split. Such a model is naturally not likely to generalize very well [159]. To prevent this issue, the test set should not be touched in any way during the optimization process. Only then will the test set prediction error approximate the generalization error well. A workaround is to split the full dataset three–way into training, *validation*, and test subsets. The models are trained on the training set and their hyperparameters are optimized by minimizing the validation error. Only once the final model to be used is fully specified, it should be applied to the test set to estimate the generalization error and performance. At this point, crucially, a researcher needs to resist any urge to go back to the optimization process in order to increase the test set performance some more. Despite the best efforts of statistical methodologists, users frequently invalidate their results by inadvertently peeking at the test data [187].

Reserving data samples for the validation set decreases the amount of data that can be used for training. To overcome this problem, the *n-fold cross–validation* technique [188] is very often (and in this work also) used. In n-fold cross–validation, the training set is split into n non–overlapping subsets, and each subset is used both as a training and validation set, in a sequence of n trials. This process is represented visually by figure 9.9, showing schematically how 5-fold cross–validation might be carried out.

Each of the n trials in the n-fold cross–validation produces its own validation error and their mean can be used as the target metric to minimize during the hy-

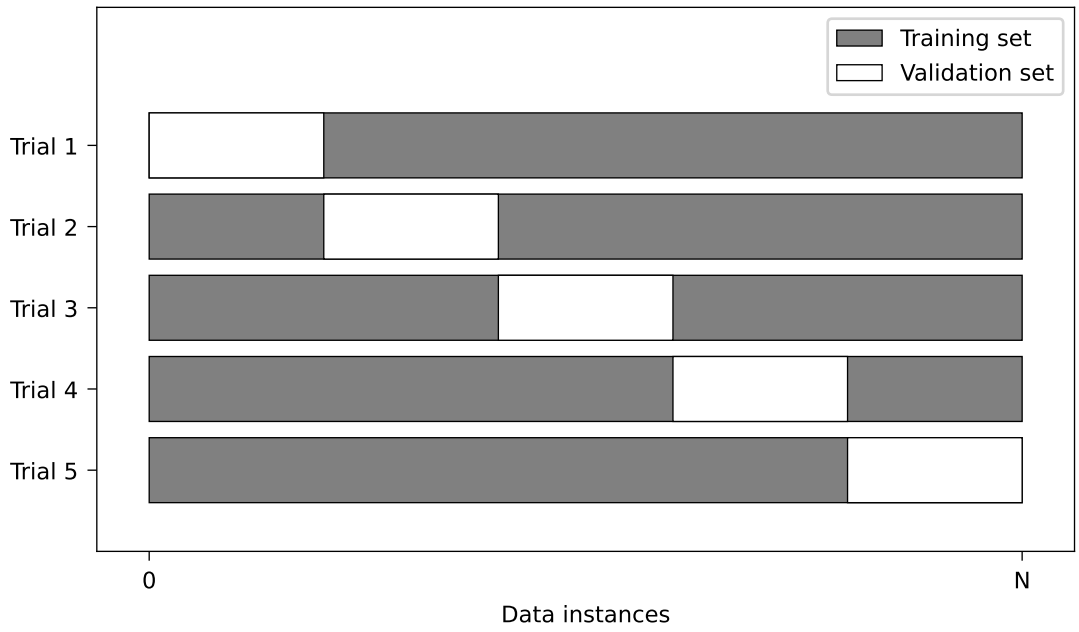

Figure 9.9: A schematic representation of 5-fold cross–validation technique example.

perparameters optimization of any ML model.

9.4.3 Hyperparameters tuning

In this work, I have optimized the hyperparameters for the selected model classes (chapter 7) by minimizing the mean validation error of 5-fold cross–validation. Two techniques were used predominantly: grid search and randomized search.

In the grid search, the hyperparameters space is discretized into a grid (with some defined borders) and the ML model is instantiated many times with sets of hyperparameters belonging to each point of the grid, then trained and evaluated. The whole grid is explored exhaustively. In some cases, when the number of hyperparameters is large, it makes sense to optimize iteratively in lower–dimensional subspaces of the full hyperparameters space. Another relevant technique is the iterative refinement of the grid in narrower regions around the suspected optimum. When the number of hyperparameters is very large and/or the computational complexity of the given ML model is too high, the randomized search can be utilized [159]. In this approach, the sets of hyperparameters are drawn randomly (with defined distributions and ranges) from the hyperparameters space, evaluated one by one,

and ranked dynamically. This technique can often show various trends across the hyperparameters space fairly fast and is often useful as a first step to identify the most promising regions for a thorough grid search.

As an example, figure 9.10 shows the mean MAE errors over 5-fold cross–validation performed on the gradient–boosted trees [175] regression model (see section 7.2.3). The errors are plotted against a single selected hyperparameter of this model class: the number of trees. Both mean training and validation errors are plotted in figure 9.10. It can be seen, that for the selected model and for the given values of other hyperparameters, the minimal mean validation error is achieved for around 100 decision trees in the gradient–boosted trees regressor. At the same time, the mean training error diverges in this region from the validation error significantly, suggesting that some level of overfitting to the training subsets is happening. It might therefore be a more appropriate and conservative strategy to use a lower number of trees, e.g. 50 in this case, to minimize the chance of overfitting to the training set and high generalization error on the withheld test set. In such decisions, the researcher's own experience and intuition must be applied during the hyperparameters tuning.

I have optimized the hyperparameters for all three shortlisted regression models (support vector regressor, random forest regressor, and gradient–boosted trees regressor) using the methods described above. The optimization was carried out using the mean MAE error (9.9) over 5-fold cross–validation, with some attention to the difference between training and validation errors. I have chosen to optimize for MAE, as RMSE (9.8) is more sensitive to outlier samples, which are definitely present in the dataset, as shown in figures 9.5 and 9.6. Finally, the three optimized models were combined into a single voting regression model, with the optimized vector of weights of the constituent models, as the only hyperparameter. For the full reproducibility, I am giving the optimized regression models and their hyperparameters as a code snippet in figure 9.11.

The mean cross–validation MAE errors μ_{MAE} for each model are listed in table 9.2, together with the standard deviations σ_{MAE} over the 5-fold cross–validation trials. Results for two more models are listed as benchmarks. `LinearRegression`

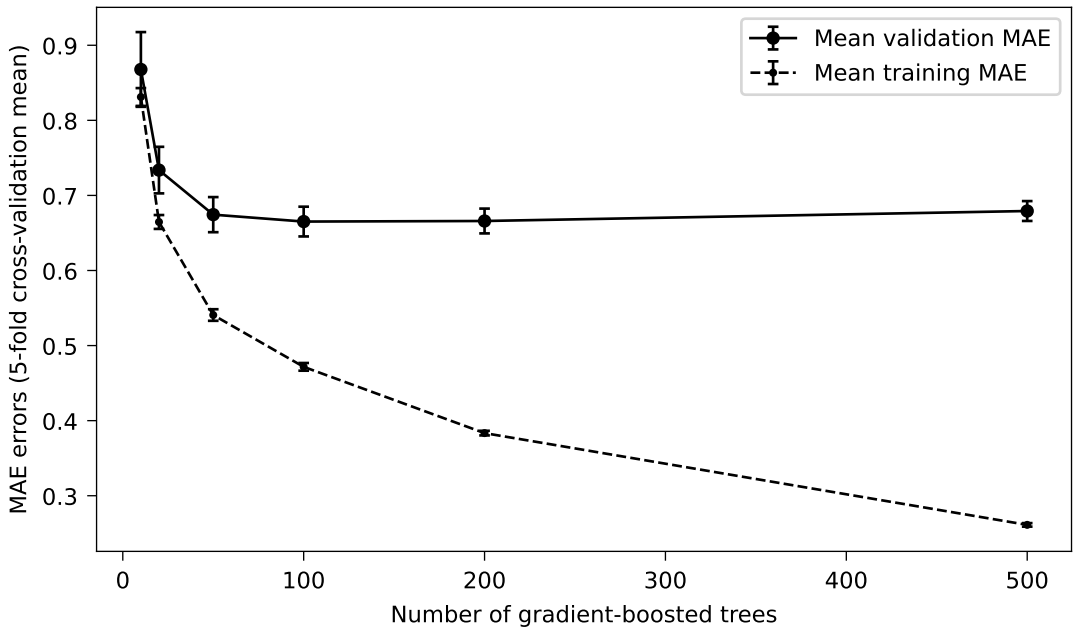

Figure 9.10: An example of a single hyperparameter optimization process for a gradient–boosted trees regression model class. Mean training MAE and mean validation MEA over 5-fold cross–validation are plotted against the number of gradient–boosted trees in the model, as a single hyperparameter being tuned. The vertical error bars show the standard deviation σ around each mean value. The mean validation error shows the expected non–monotonic behavior suggesting underfitting and overfitting of the model in regions around the optimal value. The growing divergence between training and validation errors also suggests overfitting behavior for high numbers of gradient–boosted trees.

model [169] simply performs a linear regression in the features space. `MedianEstimator` model is an extremely naive custom estimator, which simply assigns each sample from the validation set (or test set) with the unknown target value the value of the median of all the known target values from the training set (while completely ignoring the features matrix). The results in table 9.2 were obtained with `scikit-learn` version 0.24.2 and with random (but repeatable) train/test, and train/validation splits. All the code is available as a Jupyter notebook [189] in the project repository `https://github.com/martin-hanicinec-ucl/regreschem` for full reproducibility.

In the next chapter, I will evaluate the generalization error of the final regression model on the withheld test dataset and perform some final analysis on the test set and the full dataset.

```
from sklearn.svm import SVR
from sklearn.ensemble import RandomForestRegressor
from sklearn.ensemble import GradientBoostingRegressor
from sklearn.ensemble import VotingRegressor

model_svr = SVR(
    C=5,
    epsilon=0.2
)
model_rfr = RandomForestRegressor(
    max_depth=14,
    max_leaf_nodes=512,
    min_samples_split=2,
    min_samples_leaf=10,
    n_estimators=200,
    random_state=42
)
model_gbr = GradientBoostingRegressor(
    max_depth=8,
    max_leaf_nodes=32,
    max_features=9,
    min_samples_split=6,
    min_samples_leaf=15,
    n_estimators=50,
    random_state=42
)
# ------------------------------------------------- #
model_final = VotingRegressor(
    estimators=[('svr', model_svr),
                ('rfr', model_rfr),
                ('gbr', model_gbr)],
    weights=[5, 2, 4]
)
```

Figure 9.11: Python code snippet showing instantiation of the three regression model classes with their optimized hyperparameters, together with the final voting regressor combining them into a single regression model. Where not stated explicitly, the default values of hyperparameters were used.

Table 9.2: Table of mean MAE cross–validation errors and their standard deviations for all the three shortlisted optimized models, as well as the final voting regressor model and two naive benchmark models.

Model	μ_{MAE}	σ_{MAE}
`MedianEstimator`	1.329	0.031
`sklearn.linear_model.LinearRegression`	0.992	0.021
`sklearn.svm.SVR`	0.673	0.021
`sklearn.ensemble.RandomForestRegressor`	0.679	0.017
`sklearn.ensemble.GradientBoostingRegressor`	0.668	0.020
`sklearn.ensemble.VotingRegressor`	0.646	0.018

Chapter 10

Results and discussion

With the regression model optimized in its final form (figure 9.11), it is time to evaluate the generalization error of the model, as the MAE error measure (9.9) on the withheld *test set* (20% of the whole dataset, instances of which were never used during the model training or hyperparameters tuning). Table 10.1 shows the MAE^{test} error evaluated on the test set. For reference and comparison, also the error measures of the two benchmark estimators are listed in the table: the *Median estimator* refers to the `MedianEstimator` model introduced in section 9.4.3, and the *Linear regression* model refers to the `LinearRegression` benchmark model. Lastly, the *Final model* refers to the `VotingRegressor` instance with the optimal hyperparameters. Also shown for comparison next to the MAE^{test} values are the mean cross–validation errors $\mu_{\text{MAE}^{\text{val}}}$ from table 9.2. As a reminder, the fact that $\text{MAE}^{\text{test}} = 0.593$ can be interpreted in the way that there is a bit more than half order of magnitude *average* difference between the reaction rate coefficients for the reactions of the test set predicted by the final model, and their known target values.

Table 10.1: The final MAE generalization error evaluated on the withheld test set shown for the final regression model together with two basic models shown as benchmarks. The values are shown in comparison to the mean cross–validation errors, listed in table 9.2 already.

Model	$\mu_{\text{MAE}^{\text{val}}}$	MAE^{test}
Median estimator	1.329	1.278
Linear regression	0.992	0.955
Final model	0.646	0.592

It can be seen that the test errors are relatively significantly lower than the mean cross–validation errors. This is extremely surprising and very improbable. The thorough hyperparameters tuning will typically overfit to the training subset data instances, making the cross–validation errors (evaluated on the training set) typically lower than the test set error [159]. It is a hallmark of a well–trained and optimized model, that the test error is very close to the validation error (while both being as low as possible), but the test error typically *is higher* than the validation error. This anomaly can be explained in my case by looking at not just the mean cross–validation error $\mu_{\mathrm{MAE}^{\mathrm{val}}}$, but at the individual validation errors of the cross–validation folds $\mathrm{MAE}_1^{\mathrm{val}}$ – $\mathrm{MAE}_5^{\mathrm{val}}$. The individual folds validation errors are shown in figure 10.1, together with the test error $\mathrm{MAE}^{\mathrm{test}}$.

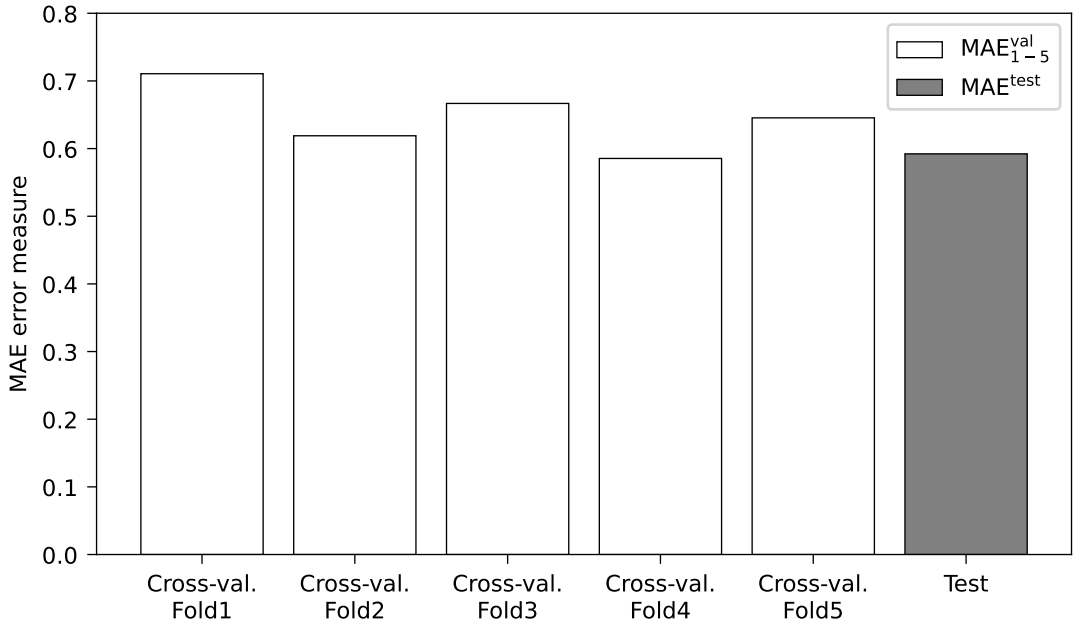

Figure 10.1: Comparison of the final generalization MAE error measure on the withheld test set with errors of the individual cross–validation folds.

The MAE errors for individual cross–validation folds differ considerably just between folds, which are trained on subsets randomly drawn from the same training set. It is possible, that the hyperparameters of the final voting regressor (and its constituent models) were optimized conservatively enough not to cause overfitting to the training set, and at the same time, the withheld test just by chance consists of data instances responding to the final trained model exceptionally well. I will

show later in this chapter, that the whole test (and training) dataset can be split into various subsets, each with significantly different own test (and validation) errors. For a concrete example, the *neutral–neutral* reactions subset of the test set has much higher MAE than the *cation–anion* reactions subset, reactions of which get predicted by the final model relatively precisely. In this case, the final MAE error measure might be quite sensitive to the ratio of neutral–neutral reactions and cation–anion reactions among the data instances, which can be more favorable for the test set than for the training set, just by the act of the random train/test split.

10.1 Analysis of reactants charge combinations

As hinted before, I have found the average prediction error of the model different for different charge combinations of the reactants. This is demonstrated with table 10.2, which shows the mean absolute error on the test evaluated separately for neutral–neutral collisions, ion–neutral collisions, and cation–anion collisions. Figure 10.2 further illustrates the fact with distributions of prediction errors plotted for each of the subsets from table 10.2.

Table 10.2: The MAE errors evaluated on different subsets of the test set. It can be seen that the combination of charges among the two reactants has a great influence on the mean absolute prediction error.

Test subset	**Instances**	**MAE**
All	1849	0.592
Neutral–neutral	336	1.289
Ion–neutral	1271	0.509
Cation–anion	287	0.143

It is evident that different charge combinations among the reactants translated into different mean prediction errors. The very low MAE error measure for the cation–anion reactions is hardly a surprise. This subset had a very tight distribution of target values in the first place, tightly centered around a single value, as discussed in section 9.3 and shown in figures 9.7 and 9.8. The final regression model evidently recovered this tight distribution fairly well. It is less clear why the neutral–neutral collision reaction rate coefficients get predicted by the model with much higher errors

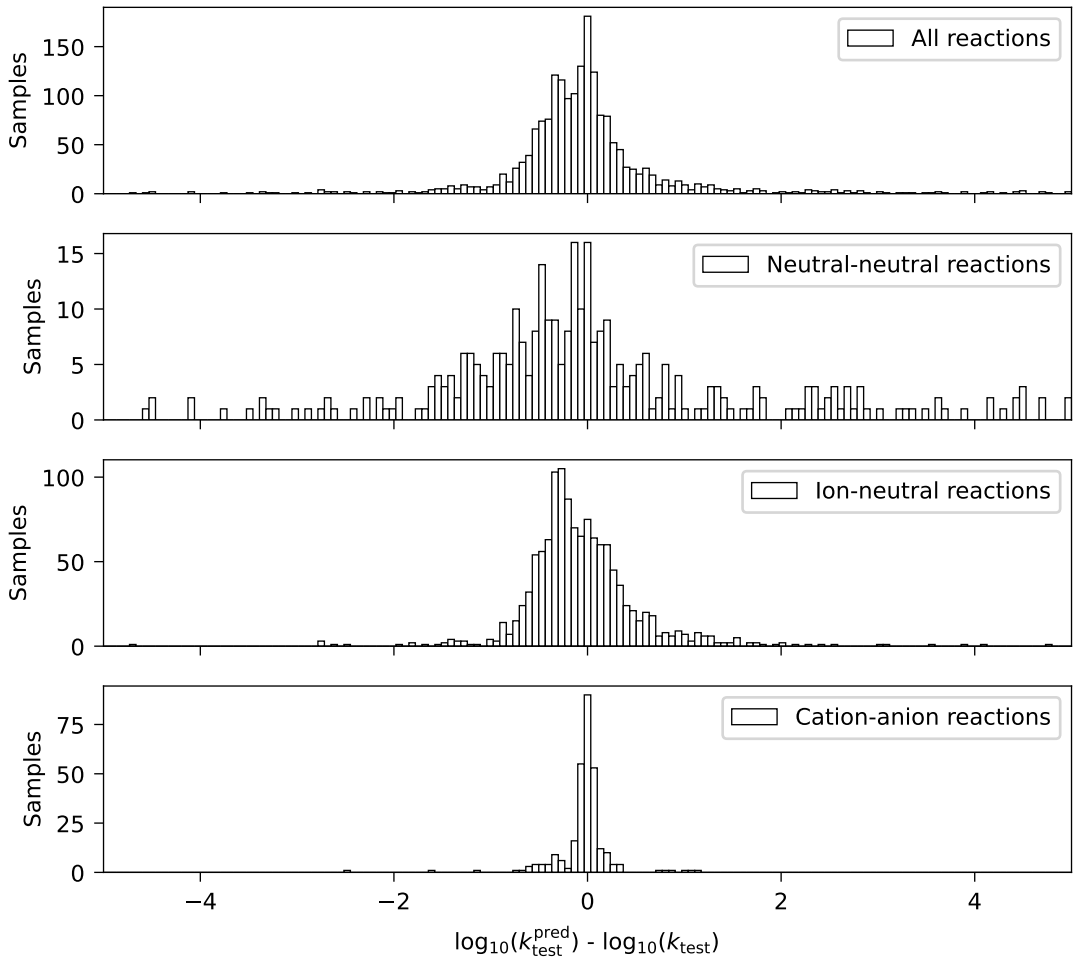

Figure 10.2: The distribution of prediction errors plotted for different subsets of the test set. It can be seen that the combination of charges among the two reactants has a great influence on the prediction errors.

than the ion–neutral collisions. The different physical mechanisms of ion–neutral reactions may make their rate coefficients more correlated with the set of features selected for the model.

As the neutral–neutral, ion–neutral, and ion–ion collisions have such obviously different prediction error distributions, as well as target values distributions (figure 9.7), it was worth exploring the idea of training a dedicated regression model for each of those subsets. Unfortunately, this did not lead to any lower prediction errors.

Figures 9.1 and 9.7 in chapter 9 showed the distribution of the target values of the whole dataset, and its subsets of different reactant charge combinations. These

distributions are naturally present also in the test set (as the test set is just a randomized subset of the whole set), and were recovered fairly well even in the predicted values, as shown in figures 10.3 and 10.4.

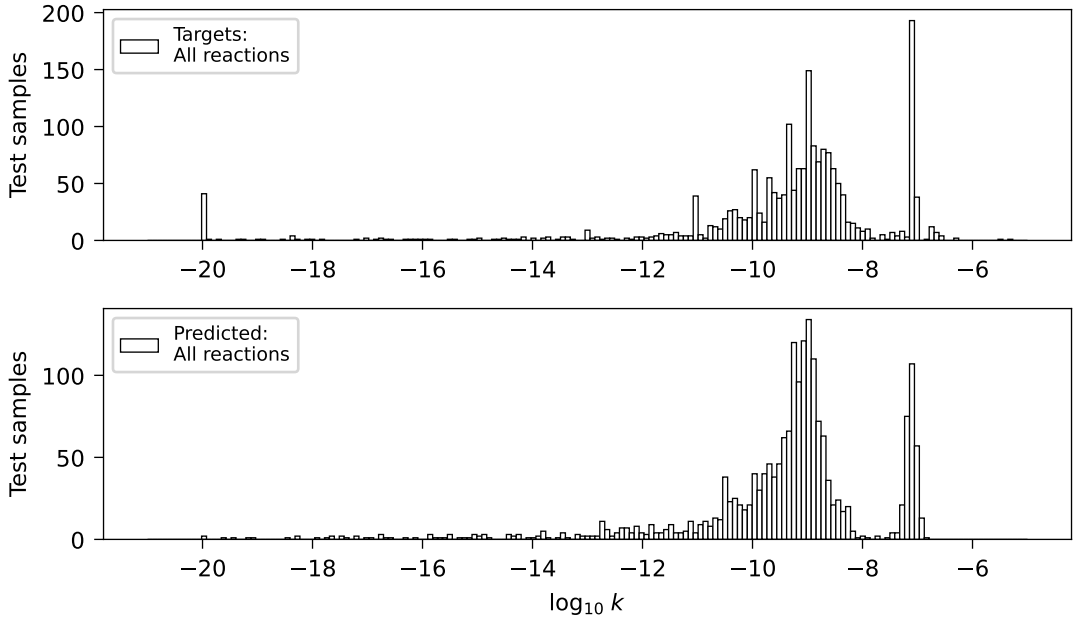

Figure 10.3: The top plot shows the distribution of the target values for the whole test set. This are equivalent to plot in figure 9.1, which shows the same histogram for the full (training & test) set. The bottom plot shows the same distribution histogram for values predicted by the final regression model.

10.2 Analysis of feature importance

As discussed in section 7.2.2, the regression models based on decision trees (random forest and gradient–boosted trees in my case) offer a measure of feature importance as the average depth any particular feature appears as a decision node across all the constituent trees of the ensemble. Figure 10.5 shows the feature importance measure for every single feature in my dataset, as assessed by two parts of the final voting regressor: the random forest regressor and the gradient–boosted trees regressor.

Three interesting facts can be noted about the feature importance values shown in figure 10.5. Firstly, the features encoding the properties of *reactants* (`lhs_` prefix) appear to be more relevant for predicting the reaction rate coefficients, than the features encoding the properties of *products* (`rhs_` prefix). Notably, the

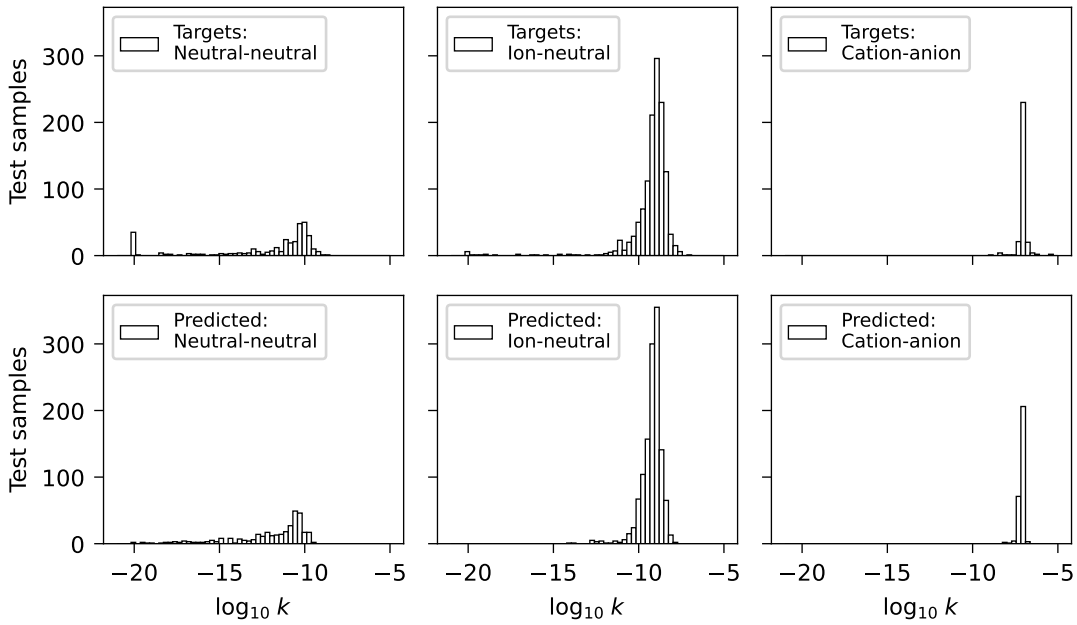

Figure 10.4: The top row shows the distribution of the target values for three test subsets belonging to different reactant charge combinations. Those are equivalent to the plots in figure 9.7, which show similar histograms for the full (training & test) set. The bottom row shows the same distribution histograms for values predicted by the final regression model.

`rhs_polarizability_factor` ($F^{\alpha}_{\mathrm{RHS}}$) and the `rhs_dipole_moment_factor` ($F^{p}_{\mathrm{RHS}}$) features, see (9.6), (9.7), both appear to be completely irrelevant for predicting the rate coefficients, while their reactants counterparts ($F^{\alpha}_{\mathrm{LHS}}$, F^{p}_{LHS}) proved to be somewhat important. As a reminder, see table 9.1 listing all the features of the dataset. Further to note is that the features designed to encode the *fragments exchanged* between reactants (`exchanged_` prefix, see section 9.2.3 and table 9.1) all appear to be almost completely ignored by the model when predicting rate coefficients. And lastly, it can be seen that the boolean features explicitly encoding the charge combinations among reactants and products, `lhs_charge_00`, `lhs_charge_+0`, `lhs_charge_+-`, `rhs_charge_00`, `rhs_charge_+0` (or Q^{00}_{LHS}, Q^{+0}_{LHS}, Q^{+-}_{LHS}, Q^{00}_{RHS}, Q^{+0}_{RHS} respectively), are being completely ignored by the random forest and gradient–boosted trees regressors. And yet, the distinct distributions of rate coefficients for categories represented by different values of those features were correctly recovered in the predicted rate coefficient values, as shown in figure 10.4. This implies, that the same information (distinguishing the $Q^{00}_{\mathrm{LHS}} = 1$, $Q^{+0}_{\mathrm{LHS}} = 1$, and

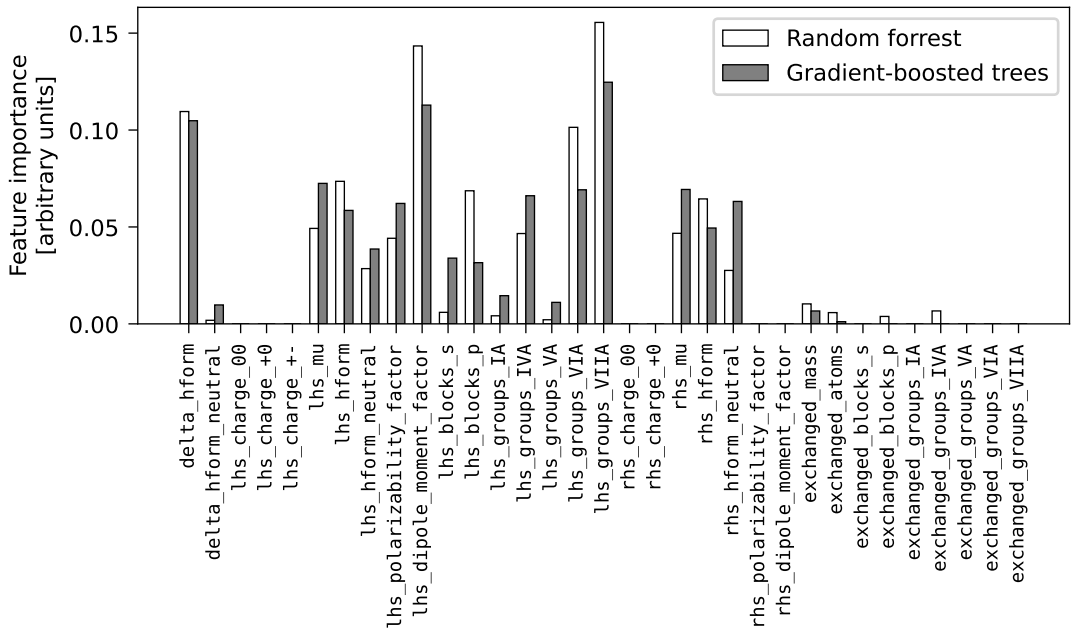

Figure 10.5: The feature importances for all the model features, pulled out of the random forest (section 7.2.2) and gradient–boosted trees (section 7.2.3) regressors (as two constituent models of the final voting regressor model). For better clarity the feature names from the project github repository are used, as listed in table 9.1.

$Q^{+-}_{\mathrm{LHS}} = 1$ cases) must have been encoded implicitly by other features, assessed as more important by the final regression model, such as $F^{\alpha}_{\mathrm{LHS}}$ (9.6) or F^{p}_{LHS} (9.7).

10.3 Analysis of the biggest outliers

Figure 10.2 clearly showed that some of the test set instances (mainly belonging to the neutral–neutral category) were predicted by the model with some significant prediction errors. Tables 10.3 and 10.4 show the top ten reactions with the most overestimated and underestimated rate coefficient predictions respectively. This time, just to have access to more model predictions, both tables show reaction instances from the full dataset, not only the test set. The *prediction error* in the tables refers to the test errors for instances of the test set and training errors for the instances of the training set. Or in other words, the regression model was trained on the training set, and its predictions for the whole dataset were compared to the target values. Apart from the prediction errors and predicted and target values of

reaction rate coefficients, also alternative rate coefficient target values are shown for every reaction where any exist in the dataset.

Table 10.3: Top ten reactions with the most overestimated predicted rate coefficients. For each reaction, the prediction error is listed as well as the predicted value of the reaction rate coefficient and the target value. If there exist alternative rate coefficient targets in the dataset, those are also shown.

ID	Reaction	Prediction error	Prediction	Target		
		$\log k_{\text{pred}} - \log k_{\text{target}}$	k_{pred} (cm^3s^{-1})	k_{target} (cm^3s^{-1})	$k^{(2)}_{\text{target}}$ (cm^3s^{-1})	$k^{(3)}_{\text{target}}$ (cm^3s^{-1})
7800	$C_4H_3^+ + HCN \rightarrow C_4H_2 + HCNH^+$	10.72	5.19e-10	1.00e-20		
213	$H^+ + HCN \rightarrow H^+ + HCN$	10.57	3.72e-10	1.00e-20	1.00e-09	1.47e-08
2569	$CH_3 + HCO^+ \rightarrow CH_4^+ + CO$	10.06	1.14e-10	1.00e-20		
5105	$C_3H_2 + HCNH^+ \rightarrow C_3H_3^+ + HCN$	9.84	6.92e-11	1.00e-20	1.96e-09	
9044	$C_8H_2 + HCNH^+ \rightarrow C_8H_3^+ + HCN$	9.68	4.77e-11	1.00e-20		
5041	$N_2 + NH_4^+ \rightarrow N_2H^+ + NH_3$	9.56	3.61e-11	1.00e-20		
3540	$H_2O + HCNH^+ \rightarrow H_3O^+ + HCN$	9.55	3.51e-11	1.00e-20	1.00e-20	8.80e-13
5403	$HCO^+ + N_2 \rightarrow CO + N_2H^+$	9.50	3.13e-11	1.00e-20	6.70e-10	2.00e-09
8560	$C_6H_2 + HCNH^+ \rightarrow C_6H_3^+ + HCN$	9.45	2.79e-11	1.00e-20		
5192	$C_2H_4 + C_3H_3^+ \rightarrow C_5H_5^+ + H_2$	9.39	2.73e-10	1.10e-19	5.50e-10	1.10e-09

Table 10.4: Top ten reactions with the most underestimated predicted rate coefficients. For each reaction, the prediction error is listed as well as the predicted value of the reaction rate coefficient and the target value. If there exist alternative rate coefficient targets in the dataset, those are also shown.

ID	Reaction	Prediction error	Prediction	Target		
		$\log k_{\text{pred}} - \log k_{\text{target}}$	k_{pred} (cm^3s^{-1})	k_{target} (cm^3s^{-1})	$k^{(2)}_{\text{target}}$ (cm^3s^{-1})	$k^{(3)}_{\text{target}}$ (cm^3s^{-1})
7041	$CH_3CHCH_2 + H_3^+ \rightarrow C_3H_7^+ + H_2$	-17.89	9.36e-09	7.26e+09		
3837	$C_3H_2 + H_3O^+ \rightarrow C_3H_3^+ + H_2O$	-8.78	1.66e-09	1.00e+00	4.60e-09	3.00e-09
7495	$C_4H + S^+ \rightarrow C_3H^+ + CS$	-8.59	1.28e-09	4.98e-01		
7494	$C_4H + S^+ \rightarrow C_4S^+ + H$	-8.24	2.85e-09	4.98e-01	3.17e-09	1.00e-09
5114	$C_2H_4 + H \rightarrow C_2H_3 + H_2$	-7.28	4.70e-17	9.00e-10	1.00e-20	
97	$H + OCN \rightarrow CN + OH$	-6.69	2.04e-17	1.00e-10		
4427	$C_2H_2 + H \rightarrow C_2H + H_2$	-6.39	4.11e-17	1.00e-10	1.00e-20	1.00e-20
949	$C + H_2 \rightarrow CH + H$	-5.87	2.00e-16	1.50e-10	1.00e-20	
2690	$H_2 + O \rightarrow H + OH$	-5.87	4.63e-16	3.44e-10	9.16e-18	1.00e-20
7848	$CH_2F_2 + H \rightarrow CHF_2 + H_2$	-5.56	4.11e-16	1.49e-10		

It is very encouraging to see, that in all the cases where any alternative target values exist, they agree with the predicted value much closer than the most diverging target value responsible for flagging these predictions as outliers. Even without inspecting the sources and credibility of the data instances, it could be argued that the data instances with the very low target values of $k < 10^{-20}\text{cm}^3\text{s}^{-1}$ from table 10.3 are very probably erroneous, as the same reactions can in many cases be found in the dataset with rate coefficients about 10 orders of magnitude lower. The cases from

table 10.3 could then be considered erroneous data samples, rather than erroneous predictions.

Taking as an example the elastic reaction

$$\mathrm{H^+ + HCN \rightarrow H^+ + HCN} \tag{10.1}$$

labeled with ID **213**, it can be seen in table 10.3 that it has 3 data samples in the dataset:

1. The first comes from KIDA [50] with $k = 10^{-9} \exp\left(-7850/T\right)$ $\mathrm{cm^3 s^{-1}}$, which evaluates for $T = 300$ K as 4.32×10^{-21}, and gets capped to the value of $k = 10^{-20}$ listed in table 10.3. This value is very low and a careful examination of the entry in KIDA database reveals the reason: KIDA lists it as the $\mathrm{H^+ + HCN \rightarrow H^+ + HNC}$ reaction, therefore the low rate coefficient belongs to a reaction changing the isomer from hydrogen cyanide HCN, to hydrogen isocyanide HNC, rather than the elastic reaction (10.1) appearing in the dataset, which does not resolve different species isomers, as discussed in section 8.6. The rate coefficient of $k = 10^{-20}$ therefore does not apply for the reaction (10.1) and the model was right to regress much higher value. KIDA cites Harada *et al* [190] as the data source, but unfortunately, I could not find such a reaction explicitly in the cited publication.

2. The second was sourced from UDfA [51], which lists the reaction with the coefficient value of $k^{(2)} = 10^{-9}$ $\mathrm{cm^3 s^{-1}}$, without any temperature dependence (and without any citation).

3. Lastly, the third available data sample connected to the reaction (10.1) was found also in KIDA, which lists it with rate coefficient in the form of one of the formulas for ion–polar systems (8.2), evaluating to $k^{(3)} = 1.47 \times 10^{-8}$ $\mathrm{cm^3 s^{-1}}$. UDfA cites work by Woon and Herbst [179] for this coefficient value, where the authors performed quantum–chemical calculations for neutral molecules, among others for HCN. This data sample could be considered the most reliable out of the three, just by the fact that it actually contains the citation to a paper

relevant for the reaction. The prediction error compared to this data instance is still about 1.6 orders of magnitude, but this is well within the main peak of the prediction errors distribution shown in figure 10.2.

Similar conclusions could be drawn about the most diverging data samples from table 10.4. For example, in the case of the first four reactions in table 10.4, it is obvious that the target values responsible for such high prediction errors are way too high and clearly incorrect. In the case of reactions with IDs **3837** and **7494** in table 10.4, the alternative target values are very close to the predicted one, validating the predictions. And in the case of the first reaction (ID **7041**) in table 10.4, with the highest prediction error of the whole dataset, the data sourced from KIDA is also very obviously wrong. KIDA cites Hickson *et al* [191] as the source publication for the value of the reaction rate coefficient described by the functional dependence (8.3). KIDA lists the parameter β (which corresponds to the Langevin rate in $\mathrm{cm^3 s^{-1}}$) as $\beta = 3.5 \times 10^{9}$ when it clearly should have been $\beta = 3.5 \times 10^{-9}$. This typo[1] in the source database resulted in the absurdly high and incorrect target value, while the value predicted by the model looks much more reasonable.

10.4 Analysis of missing features

It can be seen in figure 10.5, that the features $\Delta_\mathrm{f} H^\circ_\mathrm{total}$, F^α_LHS, and F^p_LHS appear on average fairly high in the decision trees of the random forest and the gradient–boosted trees regression models, which signals their relatively high importance for the prediction of reaction rate coefficients. These three features are also among those derived from values that were not present for all the data samples. More specifically, dipole moment p and polarizability α of both reactants were used to evaluate these features, as were the enthalpies of formation $\Delta_\mathrm{f} H^\circ$ of all the reactants and products in any reaction (see section 9.2.3). The missing species data had to be imputed, as described in section 9.2.2, and it might be interesting to see how the prediction

[1] The value was in fact corrected in KIDA database in February 2021, after I have scraped all the training data for this project, but I have decided to leave this sample in the thesis, just to demonstrate the capability of the model to handle noisy and incorrect training instances. With the correct β coefficient, the rate coefficient for this sample evaluates to $k = 3.76 \times 10^{-9}$ $\mathrm{cm^3 s^{-1}}$, which is fairly close to the predicted value.

error correlates with features data availability. Such a correlation is shown as a bar plot in figure 10.6.

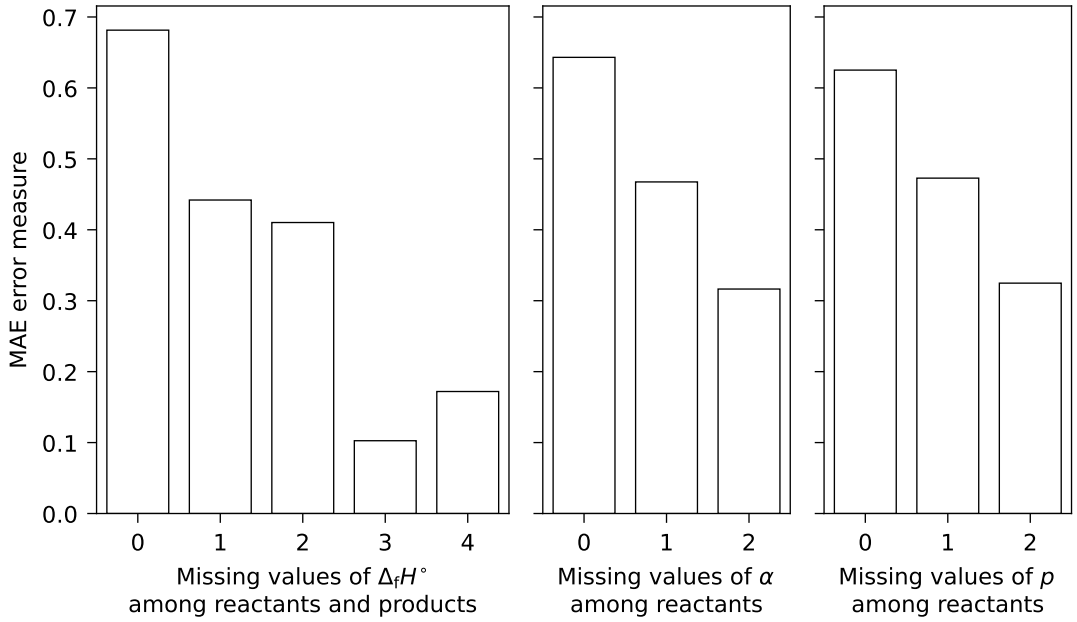

Figure 10.6: Correlation of mean absolute errors (MAE) and a number of missing values of enthalpy of formation $\Delta_f H^\circ$ among reactants and products, and polarizability α and dipole moment p among reactants. These values are used to evaluate the features $\Delta_f H^\circ_{\text{total}}$, F^{α}_{LHS} and F^{p}_{LHS}, that were found to be important for the prediction of rate coefficients (figure 10.5).

At the first glance, there appears to be a negative correlation between the number of values missing relevant for the features discussed, and the MAE error measure, where one might expect (if any) a positive correlation. After all, the imputation process will likely be fairly crude in guessing e.g. the missing polarizability of a species from its other attributes, and if a feature derived from e.g. the said polarizability is important for estimation of rate coefficient (as F^{α}_{LHS} evidently is), such a fact should be reflected in higher MAE error measure for the subset of samples with polarizability of one (or both) of its reactants imputed with imprecise value. However, the correlation is in fact caused by a bias in the dataset, as shown in figure 10.7. The subsets of samples with more species attributes values missing tend to have a higher ratio of cation–anion reactions, and a lower ratio of neutral–neutral reactions. This greatly affects the prediction errors, as the neutral–neutral reactions get predicted with much lower accuracy than the cation–anion reactions, as shown in table 10.2

and figure 10.2. If similar data as in figure 10.6 are plotted for e.g. ion–neutral reactions only, the negative correlation disappears and the MAE error measure appears to be independent of the number of missing values. This could indicate, that the imputation process is fairly effective in recovering the missing data.

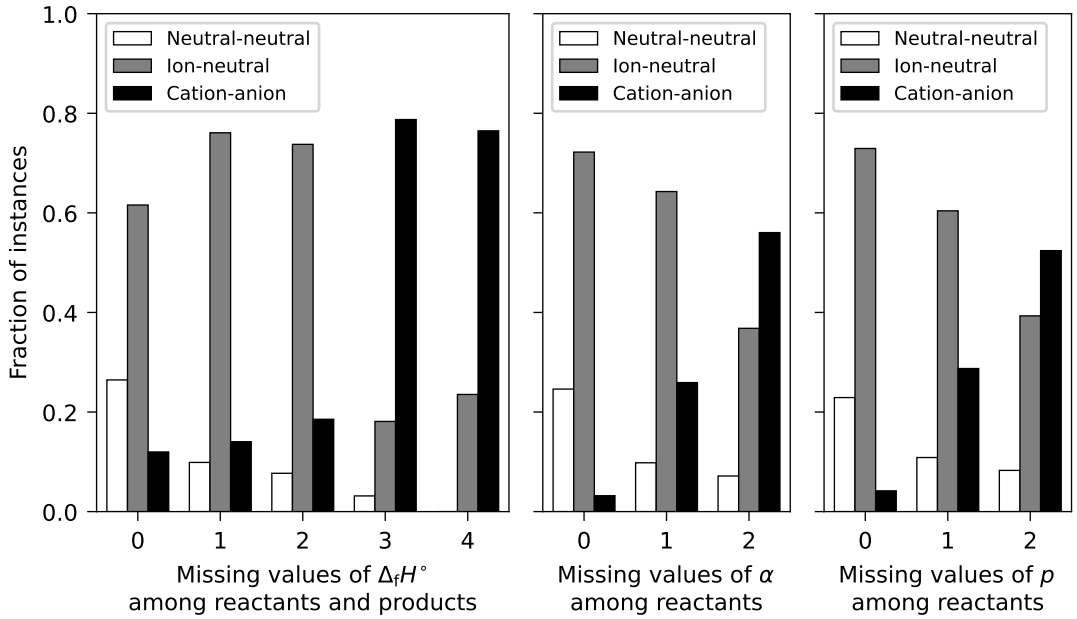

Figure 10.7: Correlation of fraction of instances with a particular combination of reactant charges, and the number of missing values of enthalpy of formation $\Delta_f H^\circ$ among reactants and products, and polarizability α and dipole moment p among reactants. Reactant charges combination greatly affects the prediction error (figure 10.2, table 10.2).

10.5 Packaging of the final regression model

As the final step in the regression model development, I have wrapped the final optimized regression model into a custom `Regressor` class, which takes care of capping the predicted data to the minimal value $y_{\min} = \log_{10} k_{\min} = -20$ after prediction, and recovers the reaction rate coefficients in the original units of $\mathrm{cm^3 s^{-1}}$ by exponentiating the predicted values back to $k^{\mathrm{pred}} = 10^{y^{\mathrm{pred}}}$. I have chained this custom regressor behind the data transformation pipeline, which takes care of missing data imputation, features engineering, and scaling (and which is described in section 9.2.3). The resulting *final regression model pipeline* was trained on the *whole* dataset and

persistently saved as `final_regression_pipeline.joblib` by the `joblib` module from Python standard library. This ready–to–use trained regression model can be easily imported to any python code from the `utils` module in the project repository, by calling the `get_final_regression_pipeline` function.

The model needs to be fed by a `pandas.DataFrame` [192] instance, with rows representing the reactions for which the rate coefficients should be estimated. The project repository provides a *sample input* as `sample_input.csv` which can be read by `pandas` into the `DataFrame` required as the input for the trained model. Figure 10.8 shows a jupyter notebook python snippet detailing how the `example_input DataFrame` is instantiated from the `sample_input.csv` table and showing all the `DataFrame` columns required by the model. All the columns required are given as the header in the `sample_input.csv` table, while the first column of the table indexes the rows by their unique IDs. All the `DataFrame` values are required in units described in section 9.2.1.

Finally, figure 10.9 gives a continuation of the code from figure 10.8, showing how the ready–to–use trained regression model can be imported from the `utils` python module. To obtain the predicted rate coefficients for all the reactions described by the input `DataFrame`, the `predict` method of the regression model instance must be called with the input table as a single parameter, as detailed by figure 10.9. This returns a `NumPy` array of reaction rate coefficients in $\mathrm{cm^3 s^{-1}}$.

Next to the ready–to–use trained regression model, the project repository at `https://github.com/martin-hanicinec-ucl/regreschem` all the data relevant to the project, together with clear documentation.

10.6 Impact on the plasma modeling community

Availability of reaction rate data is a problem frequently tackled by almost any numerical plasma physicist, and presents an ongoing hurdle for the whole plasma modeling community. A reasonably well–performing model regressing reaction rate coefficients of binary reactions from readily available data might therefore be very exciting prospect for the members of the community. However, although the mean

[1]:
```
# Imports:
import pandas as pd
import numpy as np
```

[2]:
```
example_input = pd.read_csv('sample_input.csv', index_col=0, header=0)
# (the left-most index values are unique ids identifying the reaction rows)

example_input  # (truncated view)
```

[2]:

	reactant_1_name	reactant_1_mass	...	exchanged_groups_VIA	exchanged_groups_VIIA
1824	CH	13.019	...	0.0	0.0
409	H+	1.008	...	0.0	0.0
4506	C2H2	26.038	...	0.0	0.0
4012	C2+	24.022	...	0.0	0.0
3657	H2O+	18.015	...	0.0	0.0
2286	CH2	14.027	...	0.0	0.0
1679	C+	12.011	...	0.0	0.0
8935	C8	96.088	...	0.0	0.0
1424	C+	12.011	...	0.0	0.0
6912	Ar+	39.950	...	0.0	0.0

[10 rows x 72 columns]

[3]:
```
np.array(example_input.columns)
```

[3]:
```
array(['reactant_1_name', 'reactant_1_mass', 'reactant_1_charge', 'reactant_1_hform'
       'reactant_1_hform_neutral', 'reactant_1_polarizability', 'reactant_1_dipole_moment',
       'reactant_2_name', 'reactant_2_mass', 'reactant_2_charge', 'reactant_2_hform',
       'reactant_2_hform_neutral', 'reactant_2_polarizability', 'reactant_2_dipole_moment',
       'product_1_name', 'product_1_mass', 'product_1_charge', 'product_1_hform',
       'product_1_hform_neutral', 'product_1_polarizability', 'product_1_dipole_moment',
       'product_2_name', 'product_2_mass', 'product_2_charge', 'product_2_hform',
       'product_2_hform_neutral', 'product_2_polarizability', 'product_2_dipole_moment',
       'exchanged_mass', 'exchanged_atoms', 'lhs_mu', 'rhs_mu',
       'lhs_charge_00', 'lhs_charge_+0', 'lhs_charge_+-', 'rhs_charge_00', 'rhs_charge_+0',
       'reactant_1_blocks_s', 'reactant_1_blocks_p', 'reactant_2_blocks_s', 'reactant_2_blocks_p',
       'product_1_blocks_s', 'product_1_blocks_p', 'product_2_blocks_s', 'product_2_blocks_p',
       'exchanged_blocks_s', 'exchanged_blocks_p',
       'reactant_1_groups_IA', 'reactant_1_groups_IVA', 'reactant_1_groups_VA',
       'reactant_1_groups_VIA', 'reactant_1_groups_VIIA',
       'reactant_2_groups_IA', 'reactant_2_groups_IVA', 'reactant_2_groups_VA',
       'reactant_2_groups_VIA','reactant_2_groups_VIIA',
       'product_1_groups_IA', 'product_1_groups_IVA', 'product_1_groups_VA',
       'product_1_groups_VIA', 'product_1_groups_VIIA',
       'product_2_groups_IA', 'product_2_groups_IVA', 'product_2_groups_VA',
       'product_2_groups_VIA','product_2_groups_VIIA', 'exchanged_groups_IA',
       'exchanged_groups_IVA', 'exchanged_groups_VA',
       'exchanged_groups_VIA', 'exchanged_groups_VIIA'],
      dtype=object)
```

Figure 10.8: A jupyter notebook python code snippet detailing the required form of input for the trained regression model. The code in the figure shows how an example input `DataFrame` is instantiated from the `csv` table provided by the project repository. The regression model requires a `DataFrame` with 72 columns, given as the output of the cell `[3]`.

absolute error on the whole test set of under 0.6 orders of magnitude might look fairly promising on the first glance, table 10.2 and figure 10.2 show some very high individual prediction errors, especially for the neutral–neutral reaction family. It could be argued, that the prediction error of the model is not quite reaching the standard required for synthesizing input data for predictive and quantitative plasma

```
[4]: # import the trained regression model:
     from utils import get_final_regression_pipeline
     regression_model = get_final_regression_pipeline()

     # predict the reaction rate coefficients for the 10 reactions
     # described by the example_input DataFrame:
     k_predicted = regression_model.predict(example_input)

     k_predicted

[4]: array([1.18797400e-09, 5.29729997e-09, 9.87500861e-11, 3.15630581e-10,
            1.89232973e-09, 8.37593678e-10, 6.48672484e-08, 1.77991274e-09,
            9.38216266e-10, 1.66151833e-10])
```

Figure 10.9: A continuation of the jupyter notebook python code snippet from figure 10.8, showing how the ready–to–use trained regression model can be imported from the `utils` python module. The regression model is then fed by the previously built `example_input` `DataFrame` instance (see figure 10.8) to predict the reaction rate coefficients in cm^3s^{-1}.

models, at least not without some further rigorous testing of limitations of the model.

That said, the regression model presented can still be utilised for wide range of different purposes, such as initial estimation of some rate coefficients, as a basis for some further refinement, or as an automated safeguard tool, flagging some obviously erroneous data in existing published chemistry sets or databases, concept of which was proven in section 10.3.

Part III

Conclusion

Chapter 11

Conclusions and outlook

In part I of the thesis, I presented a method of ranking the species in a chemistry set according to their importance for modeling densities of a pre–defined set of species of interest. The ranking scheme formed a crucial component of the species–oriented method for the skeletal reduction of chemistry sets. I compared several competing fast algorithms for species ranking, based on a graph–theoretical representation of chemistry sets. In all the species–ranking methods presented, weights of the edges between species in the chemistry graphs (or the direct interaction coefficients) were distributed according to the different flavors of the *directed relation graph* (DRG) theory, with modifications to include effects of surface interactions, and several species rankings were proposed, built around different well–established search algorithms from the graph theory. I identified the $\mathrm{DRG}_{\mathrm{sh.path}}$ species ranking method, which uses the definition of direct interaction coefficients from the original DRG theory [37], with Dijkstra's search for the shortest path [134] in the chemistry graph, as the most suited for species–oriented skeletal reduction of chemistry sets, statistically on an array of diverse test chemistry sets and plasma conditions. The $\mathrm{DRG}_{\mathrm{sh.path}}$ species ranking method led to reductions of between 10 and 75% in the number of species compared to the original detailed chemistry sets, depending on the specific test set and plasma conditions.

The complete reduction framework also containing a purpose–developed global plasma model is published as a GitHub repository:
`https://github.com/martin-hanicinec-ucl/plaschem`.

While I demonstrate successful utilization of the reduction method for reducing the number of species in several test chemistry sets, the resulting reduced sets likely still retain some redundant reactions. As future work, it could be desirable in the future to devise a reaction–ranking scheme which would assess the importance of the *reactions* retained for modeling the set of species of interest, and thus to expand the chemistry set reduction framework with a reaction–oriented skeletal reduction method.

Additionally, regarding the reduction method presented in this work, the validity of each chemistry set reduced using this method is strictly ensured only for the set of plasma model parameters that are the user–specified reduction conditions. It is often the case in a modeling application, that the chemistry set needs to be valid over a *range* of input parameters. Although this might be achieved by running the reduction method on a set of samples from the parameter space, as proposed in section 2.1, this kind of parameter sweep might be unnecessarily inefficient. Therefore, modifying the species–ranking method along with the reduction error function δ, so they reflect a range of reduction conditions rather than a single set, could be an important area of future research.

Related to the previous point, the validity of the reduced chemistry set is strictly ensured by the method only for the plasma model used for building the species ranking and for the iterative validations. In the case of my work, this was a 0D global model, which is by design very fast and can handle even very large chemistry sets without reduction. As a point of future work, it could be investigated how chemistry sets reduced using a fast global model can be used in higher–dimensional, more sophisticated plasma models, which could benefit the most from the reduction, and if (and at what conditions) do the reduced sets stay valid.

Finally, a significant shortcoming of the species–ranking method presented is that the ranking only takes into account the species' importance for modeling *densities* of a set of pre–selected species of interest. The species ranking is blind to any coupling between the presence of the species in the chemistry set and any other possible plasma model outputs, such as electron temperature. Also, when it comes to the

electron as a species of interest, the coupling between a species in the chemistry set and electron density only captures the production and consumption of electrons via volumetric and surface reactions involving the species, without taking into account collisional energy loss of electrons, which is itself tightly coupled to the electron density. More sophisticated plasma models can also resolve some additional outputs, such as the gas temperature or particle fluxes at the surface, and certain applications might depend on the reduced chemistry set preserving those outputs as well. As an aim for future research, nodes representing other possible plasma model outputs could be inserted into the chemistry graph with appropriate weights distributed among edges connecting them to the other graph nodes. This will allow for the species ranking to reflect species coupling to the said additional model outputs and the notion of *species of interest* will be expanded to a more general notion of *outputs of interest*.

In part II of the thesis, I presented a machine learning–based regression model for fast approximation of unknown plasma reaction rate constants at $T = 300$ K from commonly available species data. Due to the limited time budget of the project, the model was restricted only to binary reactions of heavy species, not involving any excited states on either side of the reaction. The room–temperature rate coefficients are regressed from features built from masses, charges, enthalpies of formation, polarizabilities, dipole moments, and elemental data of both reactants and products. The final model is a voting regressor consisting of three distinct optimized regression models: a support vector regressor[170], random forest regressor [172], and a gradient–boosted trees regressor [174]. The model was trained on a training set of over 7,500 data instances acquired from four popular databases of plasma processes.

The final generalization MAE error (9.9) of the reaction rate coefficient prediction, evaluated on a withheld test set of around 1,900 instances, was just under 0.6 orders of magnitude, compared to about 0.95 orders of magnitude for a benchmark case of a simple linear regression (table 10.1). The overall distribution of the reaction rate coefficients from the test set was recovered very well in the predicted values, as were the distributions for distinct subsets of neutral–neutral, ion–ion, and neutral–ion reactions.

I also demonstrated the ability of the model to flag erroneous data instances, as it was shown that out of the ten most underestimated and overestimated predictions, the majority could be attributed to erroneous training targets, rather than incorrect predictions.

The trained model was packaged as an importable python data structure and published as a GitHub repository

`https://github.com/martin-hanicinec-ucl/regreschem`

together with a jupyter notebook [189] detailing the training and optimization process, the full training dataset, and example input data.

The most obvious potential for future work is the expansion of the model applicability space. The model presented was trained exclusively on reactions of two heavy–species reactants, and two heavy–species products, without any excited states, which makes the model apply only to such reactions. As a subject of future research, the model could be expanded to also handle three–body collisions, dissociative or associative processes with different numbers of reactants and products, ionization processes with electrons among the products, and similar. Furthermore, the model could be expanded to handle excited states among reactants and products. Such an expansion will require redesigning the feature space of the model to capture state–specific properties of species, and to allow features built from more than two species per reaction side.

Electron collisions form a somewhat distinct category of plasma reactions, as full collisional cross–sections are usually required to model low–temperature plasma phenomena. This, with the fact that electron collisions are driven by underlying physics than the heavy–species reactions, would probably make the task of expanding the current model to also handle electron collisions unrealistic. Instead, the development and training of a separate model for electron collisions might be a more sensible approach and another topic of possible future research.

The model presented only regresses rate coefficients expressed for the room temperature, while a much more valuable output of the model would be a temperature dependence $k(T)$ in some form, e.g. as the triplet of parameters for the modified Arrhenius formula (8.1). Training such a model would, however, require training

data instances with temperature–dependent target values of rate coefficients, which were very uncommon in my data sources.

Building a higher–quality training dataset is also worthy of some future research efforts. I have shown in section 9.3, that the training dataset for my regression model contained a fair number of reactions with multiple data instances with diverging target values, sometimes differing by many orders of magnitude. Curating the training dataset such that it contains *only* trustworthy data instances might be a very costly effort, but one which would undoubtedly also improve the quality and performance of any regression model trained on such a curated dataset.

As rejecting untrustworthy data might significantly reduce the size of the training dataset, an exploration of additional training data sources makes for another significant direction of future work. Other databases to scrape the data from could be identified, or high–quality training data could also be mined directly from research publications. The training dataset could also benefit from an analysis of the biases present, as the selection of data sources inevitably influences which reaction classes, or which rate coefficient calculation methods, experimental techniques, etc, are dominant in the dataset. A careful bias analysis helps to understand how the biases in the training dataset translate to the expected prediction accuracies for, e.g., different reaction classes.

Some additional and perhaps more relevant features to regress the rate coefficients from could be identified as part of future work, in an effort to further drive down the prediction error of the regression model.

Finally, testing the regression model on various well–established published chemistry sets (e.g. the ones presented in part I of this thesis) by replacing a fraction of *real* rate coefficients with data synthesized by the model and comparing the model results, presents itself perhaps as another logical next step in this research.

Part IV

Appendices

Appendix A

Test chemistry sets

Table A.1: Detailed chemistry set for all the O_2–He reduction cases. Kinetic data are directly as taken from the source publication [22]. The reactions ID numbers are consistent with the source publication. The reaction rate coefficients k of order-m reactions are in $[m^{3(m-1)}s^{-1}]$. Gas temperature T_g is in [K].The electron temperature T_e and electron energy loss ΔE_e are in [eV].
[a] Not the original source.

ID	Reaction	k	ΔE_e	Source
1	$2e + He^+ \rightarrow He^* + e$	$1.74 \times 10^{-39} T_e^{-4.5}$		[22] [a]
2	$2e + He_2^+ \rightarrow He^* + He + e$	$1.62 \times 10^{-38} T_e^{-4}$		[22] [a]
3	$e + He + He^+ \rightarrow He^* + He$	$2.5 \times 10^{-39} T_e^{-2.5}$		[22] [a]
4	$e + He + He_2^+ \rightarrow 3He$	$2.5 \times 10^{-39} T_e^{-2.5}$		[22] [a]
5	$e + He \rightarrow e + He$	$7.77 \times 10^{-14} T_e^{0.02} \exp(-0.5/T_e)$		[22] [a]
6	$e + He \rightarrow 2e + He^+$	$4.45 \times 10^{-15} T_e^{0.42} \exp(-26.9/T_e)$	24.6	[22] [a]
7	$e + He \rightarrow He^* + e$	$3.3 \times 10^{-15} T_e^{0.33} \exp(-21.6/T_e)$	19.8	[22] [a]
8	$e + He^* \rightarrow 2e + He^+$	$2.51 \times 10^{-13} T_e^{-0.07} \exp(-5.98/T_e)$	4.78	[22] [a]
9	$e + He^+ \rightarrow He^*$	$4.26 \times 10^{-19} T_e^{-0.63}$		[22] [a]
10	$e + He_2^* \rightarrow He_2^+ + 2e$	$3.78 \times 10^{-13} T_e^{-0.19} \exp(-5.6/T_e)$	3.9	[22] [a]
11	$e + He_2^+ \rightarrow He + He^*$	$9.6 \times 10^{-17} T_e^{-0.5}$		[22] [a]
12	$e + O \rightarrow 2e + O^+$	$4.93 \times 10^{-15} T_e^{0.72} \exp(-13.2/T_e)$	13.6	[22] [a]
13	$e + O \rightarrow e + O(^1D)$	$8.45 \times 10^{-15} T_e^{-0.31} \exp(-3.13/T_e)$	1.96	[22] [a]
14	$e + O \rightarrow e + O(^1D)$	$1.04 \times 10^{-15} T_e^{-0.13} \exp(-4.91/T_e)$	4.18	[22] [a]
15	$e + O(^1D) \rightarrow 2e + O^+$	$4.93 \times 10^{-15} T_e^{0.72} \exp(-11.64/T_e)$	11.65	[22] [a]
16	$e + O(^1D) \rightarrow e + O$	$8.45 \times 10^{-15} T_e^{0.31} \exp(-1.17/T_e)$	-1.96	[22] [a]
17	$e + O(^1D) \rightarrow 2e + O^+$	$4.93 \times 10^{-15} T_e^{0.72} \exp(-9.42/T_e)$	9.43	[22] [a]
18	$e + O(^1D) \rightarrow e + O$	$1.04 \times 10^{-15} T_e^{-0.13} \exp(-0.73/T_e)$	-4.18	[22] [a]
19	$e + O^- \rightarrow 2e + O$	$9.33 \times 10^{-14} T_e^{0.18} \exp(-3.13/T_e)$	3.44	[22] [a]
20	$e + O_2 \rightarrow 2e + O + O^+$	$8.6 \times 10^{-16} T_e^{1.11} \exp(-19.84/T_e)$	18.73	[22] [a]
21	$e + O_2 \rightarrow 2e + O_2^+$	$2.32 \times 10^{-15} T_e^{0.99} \exp(-12.51/T_e)$	12.06	[22] [a]
22	$e + O_2 \rightarrow e + O + O(^1D)$	$3.12 \times 10^{-14} T_e^{0.02} \exp(-8.05/T_e)$	8.5	[22] [a]
23	$e + O_2 \rightarrow e + O + O(^1D)$	$1.56 \times 10^{-17} T_e^{1.5} \exp(-4.68/T_e)$	9.97	[22] [a]
24	$e + O_2 \rightarrow e + O_2$	$4.15 \times 10^{-14} T_e^{0.6} \exp(-0.02/T_e)$		[22] [a]
25	$e + O_2 \rightarrow e + O_2$	$3.88 \times 10^{-17} T_e^{-1.22} \exp(-0.55/T_e)$	0.02	[22] [a]
26	$e + O_2 \rightarrow e + O_2(\nu)$	$4.32 \times 10^{-16} T_e^{-1.57} \exp(-0.59/T_e)$	0.19	[22] [a]
27	$e + O_2 \rightarrow e + O_2(\nu)$	$2.76 \times 10^{-14} T_e^{-1.03} \exp(-6.96/T_e)$	0.19	[22] [a]
28	$e + O_2 \rightarrow e + O_2(\nu)$	$5.4 \times 10^{-15} T_e^{-0.92} \exp(-6.6/T_e)$	0.57	[22] [a]
29	$e + O_2 \rightarrow e + O_2(\nu)$	$1.64 \times 10^{-16} T_e^{-1.41} \exp(-0.72/T_e)$	0.38	[22] [a]
30	$e + O_2 \rightarrow e + O_2(\nu)$	$1.2 \times 10^{-14} T_e^{-1.01} \exp(-6.9/T_e)$	0.38	[22] [a]

Continued on next page

Table A.1 (*Continued*)

ID	Reaction	k	ΔE_e	Source
31	$e + O_2 \rightarrow e + O_2(\nu)$	$5.27 \times 10^{-15} T_e^{-1.13} \exp(-7.57/T_e)$	0.75	[22] [a]
32	$e + O_2 \rightarrow e + O_2(a\,^1\Delta_g)$	$2.1 \times 10^{-15} T_e^{-0.23} \exp(-2.87/T_e)$	0.98	[22] [a]
33	$e + O_2 \rightarrow e + O_2(b\,^1\Sigma_g^+)$	$3.97 \times 10^{-16} T_e^{-0.09} \exp(-2.67/T_e)$	1.63	[22] [a]
34	$e + O_2 \rightarrow e + O_2(b\,^1\Sigma_g^+)$	$1.28 \times 10^{-14} T_e^{-1.16} \exp(-7/T_e)$	4.5	[22] [a]
35	$e + O_2 \rightarrow e + O_2(b\,^1\Sigma_g^+)$	$1.98 \times 10^{-14} T_e^{-0.78} \exp(-7.36/T_e)$	6	[22] [a]
36	$e + O_2 \rightarrow O + O^-$	$1.32 \times 10^{-15} T_e^{-1.4} \exp(-6.63/T_e)$		[22] [a]
37	$e + O_2(a\,^1\Delta_g) \rightarrow 2e + O + O^+$	$8.6 \times 10^{-16} T_e^{1.1} \exp(-18.86/T_e)$	17.75	[22] [a]
38	$e + O_2(a\,^1\Delta_g) \rightarrow 2e + O_2^+$	$2.32 \times 10^{-15} T_e^{0.99} \exp(-11.53/T_e)$	11.08	[22] [a]
39	$e + O_2(a\,^1\Delta_g) \rightarrow e + O + O(^1D)$	$3.12 \times 10^{-14} T_e^{0.02} \exp(-7.07/T_e)$	7.52	[22] [a]
40	$e + O_2(a\,^1\Delta_g) \rightarrow e + O + O(^1D)$	$1.56 \times 10^{-17} T_e^{1.5} \exp(-3.7/T_e)$	9	[22] [a]
41	$e + O_2(a\,^1\Delta_g) \rightarrow e + O_2$	$2.1 \times 10^{-15} T_e^{-0.23} \exp(-1.89/T_e)$	-0.98	[22] [a]
42	$e + O_2(a\,^1\Delta_g) \rightarrow e + O_2(a\,^1\Delta_g)$	$4.15 \times 10^{-14} T_e^{0.6} \exp(-0.02/T_e)$		[22] [a]
43	$e + O_2(a\,^1\Delta_g) \rightarrow e + O_2(a\,^1\Delta_g)$	$3.88 \times 10^{-17} T_e^{-1.22} \exp(-0.55/T_e)$	0.02	[22] [a]
44	$e + O_2(a\,^1\Delta_g) \rightarrow e + O_2(a\,^1\Delta_g, \nu)$	$4.32 \times 10^{-16} T_e^{-1.57} \exp(-0.59/T_e)$	0.19	[22] [a]
45	$e + O_2(a\,^1\Delta_g) \rightarrow e + O_2(a\,^1\Delta_g, \nu)$	$2.76 \times 10^{-14} T_e^{-1.03} \exp(-6.96/T_e)$	0.19	[22] [a]
46	$e + O_2(a\,^1\Delta_g) \rightarrow e + O_2(a\,^1\Delta_g, \nu)$	$1.64 \times 10^{-16} T_e^{-1.41} \exp(-0.72/T_e)$	0.38	[22] [a]
47	$e + O_2(a\,^1\Delta_g) \rightarrow e + O_2(a\,^1\Delta_g, \nu)$	$1.2 \times 10^{-15} T_e^{-1.01} \exp(-6.9/T_e)$	0.38	[22] [a]
48	$e + O_2(a\,^1\Delta_g) \rightarrow e + O_2(a\,^1\Delta_g, \nu)$	$5.4 \times 10^{-15} T_e^{-0.92} \exp(-6.6/T_e)$	0.57	[22] [a]
49	$e + O_2(a\,^1\Delta_g) \rightarrow e + O_2(a\,^1\Delta_g, \nu)$	$5.27 \times 10^{-15} T_e^{-1.13} \exp(-7.57/T_e)$	0.75	[22] [a]
50	$e + O_2(a\,^1\Delta_g) \rightarrow O_2(b\,^1\Sigma_g^+) + e$	$5.25 \times 10^{-15} T_e^{-0.44} \exp(-1.49/T_e)$	0.66	[22] [a]
51	$e + O_2(a\,^1\Delta_g) \rightarrow e + O_2(b\,^1\Sigma_g^+)$	$1.28 \times 10^{-14} T_e^{-1.16} \exp(-6.02/T_e)$	3.52	[22] [a]
52	$e + O_2(a\,^1\Delta_g) \rightarrow e + O_2(b\,^1\Sigma_g^+)$	$1.98 \times 10^{-14} T_e^{-0.78} \exp(-6.38/T_e)$	5.02	[22] [a]
53	$e + O_2(a\,^1\Delta_g) \rightarrow O + O^-$	$4.14 \times 10^{-15} T_e^{-1.34} \exp(-5.15/T_e)$	3	[22] [a]
54	$e + O_2(a\,^1\Delta_g) \rightarrow O(^1D) + O^-$	$9.2 \times 10^{-16} T_e^{-1.26} \exp(-6.55/T_e)$	3	[22] [a]
55	$e + O_2(b\,^1\Sigma_g^+) \rightarrow 2e + O + O^+$	$8.6 \times 10^{-16} T_e^{1.11} \exp(-18.21/T_e)$	17.1	[22] [a]
56	$e + O_2(b\,^1\Sigma_g^+) \rightarrow 2e + O_2^+$	$2.32 \times 10^{-15} T_e^{0.99} \exp(-10.88/T_e)$	10.43	[22] [a]
57	$e + O_2(b\,^1\Sigma_g^+) \rightarrow e + O + O(^1D)$	$3.12 \times 10^{-14} T_e^{0.02} \exp(-6.42/T_e)$	6.87	[22] [a]
58	$e + O_2(b\,^1\Sigma_g^+) \rightarrow e + O + O(^1D)$	$1.56 \times 10^{-17} T_e^{1.5} \exp(-3.05/T_e)$	8.34	[22] [a]
59	$e + O_2(b\,^1\Sigma_g^+) \rightarrow e + O_2$	$3.97 \times 10^{-16} T_e^{-0.09} \exp(-1.04/T_e)$	-1.63	[22] [a]
60	$e + O_2(b\,^1\Sigma_g^+) \rightarrow e + O_2(a\,^1\Delta_g)$	$5.25 \times 10^{-15} T_e^{-0.44} \exp(-0.83/T_e)$	-0.66	[22] [a]
61	$e + O_2(b\,^1\Sigma_g^+) \rightarrow e + O_2(b\,^1\Sigma_g^+)$	$4.15 \times 10^{-14} T_e^{0.6} \exp(-0.02/T_e)$		[22] [a]
62	$e + O_2(b\,^1\Sigma_g^+) \rightarrow e + O_2(b\,^1\Sigma_g^+)$	$3.88 \times 10^{-17} T_e^{-1.22} \exp(-0.55/T_e)$	0.02	[22] [a]
63	$e + O_2(b\,^1\Sigma_g^+) \rightarrow e + O_2(b\,^1\Sigma_g^+, \nu)$	$4.32 \times 10^{-16} T_e^{-1.57} \exp(-0.59/T_e)$	0.19	[22] [a]
64	$e + O_2(b\,^1\Sigma_g^+) \rightarrow e + O_2(b\,^1\Sigma_g^+, \nu)$	$2.76 \times 10^{-14} T_e^{-1.03} \exp(-6.96/T_e)$	0.19	[22] [a]
65	$e + O_2(b\,^1\Sigma_g^+) \rightarrow e + O_2(b\,^1\Sigma_g^+, \nu)$	$1.64 \times 10^{-16} T_e^{-1.41} \exp(-0.72/T_e)$	0.38	[22] [a]
66	$e + O_2(b\,^1\Sigma_g^+) \rightarrow e + O_2(b\,^1\Sigma_g^+, \nu)$	$1.2 \times 10^{-15} T_e^{-1.01} \exp(-6.9/T_e)$	0.38	[22] [a]
67	$e + O_2(b\,^1\Sigma_g^+) \rightarrow e + O_2(b\,^1\Sigma_g^+, \nu)$	$5.4 \times 10^{-15} T_e^{-0.92} \exp(-6.6/T_e)$	0.57	[22] [a]
68	$e + O_2(b\,^1\Sigma_g^+) \rightarrow e + O_2(b\,^1\Sigma_g^+, \nu)$	$5.27 \times 10^{-15} T_e^{-1.13} \exp(-7.57/T_e)$	0.75	[22] [a]
69	$e + O_2(b\,^1\Sigma_g^+) \rightarrow e + O_2(b\,^1\Sigma_g^+)$	$1.28 \times 10^{-14} T_e^{-1.16} \exp(-5.37/T_e)$	2.87	[22] [a]
70	$e + O_2(b\,^1\Sigma_g^+) \rightarrow e + O_2(b\,^1\Sigma_g^+)$	$1.98 \times 10^{-14} T_e^{-0.78} \exp(-5.73/T_e)$	4.37	[22] [a]
71	$e + O_2(b\,^1\Sigma_g^+) \rightarrow O + O^-$	$7.11 \times 10^{-16} T_e^{-1.04} \exp(-0.23/T_e)$		[22] [a]
72	$e + O_2^- \rightarrow 2e + O_2$	$1.57 \times 10^{-14} T_e^{1.01} \exp(-1.77/T_e)$	4.68	[22] [a]
73	$e + O_3 \rightarrow e + O + O_2(\nu)$	$1.7 \times 10^{-14} T_e^{-0.57} \exp(-2.48/T_e)$	2.6	[22] [a]
74	$e + O_3 \rightarrow e + O(^1D) + O_2(a\,^1\Delta_g)$	$3.22 \times 10^{-13} T_e^{-1.18} \exp(-9.17/T_e)$	5.72	[22] [a]
75	$e + O_3 \rightarrow O + O_2^-$	$1.02 \times 10^{-15} T_e^{-1.3} \exp(-1.03/T_e)$		[22] [a]
76	$e + O_3 \rightarrow O^- + O_2$	$3.45 \times 10^{-15} T_e^{-0.96} \exp(-1/T_e)$		[22] [a]
77	$e + O_3 \rightarrow 2e + O_3^+$	$5.96 \times 10^{-15} T_e^{-0.98} \exp(-12.55/T_e)$	12.43	[22] [a]
78	$e + O_3^+ \rightarrow 3O$	$2.07 \times 10^{-13} T_e^{-0.55}$	-6.27	[22] [a]
79	$e + O_3^+ \rightarrow 2O + O(^1D)$	$6.69 \times 10^{-13} T_e^{-0.55}$	-4.3	[22] [a]
80	$e + O_3^+ \rightarrow O + 2O(^1D)$	$1.55 \times 10^{-13} T_e^{-0.55}$	-2.33	[22] [a]
81	$e + O_3^- \rightarrow 2e + O_3$	$2.12 \times 10^{-14} T_e^{0.51} \exp(-5.87/T_e)$	2.1	[22] [a]
82	$e + O_3^- \rightarrow 2e + O + O_2$	$7.12 \times 10^{-14} T_e^{-0.13} \exp(-5.94/T_e)$	3.2	[22] [a]
83	$e + O_3^- \rightarrow 2e + 3O$	$1.42 \times 10^{-14} T_e^{-0.52} \exp(-9.3/T_e)$	8.4	[22] [a]
84	$2He + He^* \rightarrow He_2^* + He$	1.5×10^{-46}		[22] [a]
85	$2He + He^+ \rightarrow He_2^+ + He$	$1.3 \times 10^{-43} \left(T_g/300\right)^{-0.6}$		[22] [a]
86	$2He^* \rightarrow e + He + He^+$	4.5×10^{-16}	-16.6	[22] [a]
87	$2He^* \rightarrow e + He_2^+$	1.05×10^{-15}	-19	[22] [a]
88	$He^* + He_2^* \rightarrow e + He^+ + 2He$	5×10^{-16}	-15	[22] [a]
89	$He^* + He_2^* \rightarrow e + He + He_2^+$	2×10^{-15}	-15	[22] [a]
90	$2He_2^* \rightarrow e + He^+ + 3He$	3×10^{-16}	-15	[22] [a]

Continued on next page

Table A.1 (*Continued*)

ID	Reaction	k	ΔE_e	Source
91	$2He_2^* \rightarrow e + 2He + He_2^+$	1.2×10^{-15}	-15	[22] [a]
92	$3O \rightarrow O + O_2$	$3.8 \times 10^{-44} \left(T_g/300\right)^{-1} \exp\left(-17/T_g\right)$		[22] [a]
93	$3O \rightarrow O + O_2(b\,^1\Sigma_g^+)$	$1.4 \times 10^{-42} \exp\left(-65/T_g\right)$		[22] [a]
94	$2O + O_2 \rightarrow O + O_3$	$4.2 \times 10^{-47} \exp\left(1056/T_g\right)$		[22] [a]
95	$2O + O_2 \rightarrow O + O_3(\nu)$	$9.8 \times 10^{-47} \exp\left(1056/T_g\right)$		[22] [a]
96	$2O + O_2 \rightarrow O_2(a\,^1\Delta_g) + O_2$	$6.5 \times 10^{-45} \left(T_g/300\right)^{-1} \exp\left(-17/T_g\right)$		[22] [a]
97	$2O + O_2 \rightarrow O_2(b\,^1\Sigma_g^+) + O_2$	$6.5 \times 10^{-45} \left(T_g/300\right)^{-1} \exp\left(-17/T_g\right)$		[22] [a]
98	$O + O(^1D) \rightarrow 2O$	2×10^{-18}		[22] [a]
99	$O + O(^1D) \rightarrow 2O$	$2.5 \times 10^{-17} \exp\left(-3/T_g\right)$		[22] [a]
100	$O + O(^1D) \rightarrow O + O(^1D)$	$2.5 \times 10^{-17} \exp\left(-3/T_g\right)$		[22] [a]
101	$O + 2O_2 \rightarrow O_2 + O_3$	$1.8 \times 10^{-46} \left(T_g/300\right)^{-2.6}$		[22] [a]
102	$O + 2O_2 \rightarrow O_2 + O_3(\nu)$	$4.2 \times 10^{-46} \left(T_g/300\right)^{-2.6}$		[22] [a]
103	$O + O_2 + O_2(a\,^1\Delta_g) \rightarrow O + 2O_2$	1.1×10^{-44}		[22] [a]
104	$O + O_2 + O_3 \rightarrow 2O_3$	$1.4 \times 10^{-47} \exp\left(-105/T_g\right)$		[22] [a]
105	$O + O_2 + O_3 \rightarrow O_3 + O_3(\nu)$	$3.27 \times 10^{-47} \exp\left(-105/T_g\right)$		[22] [a]
106	$O + O_2(a\,^1\Delta_g) \rightarrow O + O_2$	1×10^{-22}	-2.14	[22] [a]
107	$O + O_2(b\,^1\Sigma_g^+) \rightarrow O + O_2(a\,^1\Delta_g)$	8×10^{-20}	-0.65	[22] [a]
108	$O + O_3 \rightarrow 2O + O_2$	$1.2 \times 10^{-15} \exp\left(-114/T_g\right)$		[22] [a]
109	$O + O_3 \rightarrow 2O_2(\nu)$	$8 \times 10^{-18} \exp\left(-206/T_g\right)$		[22] [a]
110	$O + O_3(\nu) \rightarrow 2O_2$	4.5×10^{-18}		[22] [a]
111	$O + O_3(\nu) \rightarrow O_3 + O$	1.05×10^{-17}		[22] [a]
112	$O(^1D) + O_2 \rightarrow O + O_2(b\,^1\Sigma_g^+)$	$2.64 \times 10^{-17} \exp\left(55/T_g\right)$		[22] [a]
113	$O(^1D) + O_2 \rightarrow O + O_2(a\,^1\Delta_g)$	$6.6 \times 10^{-18} \exp\left(55/T_g\right)$		[22] [a]
114	$O(^1D) + O_3 \rightarrow 2O + O_2$	1.2×10^{-16}		[22] [a]
115	$O(^1D) + O_3 \rightarrow 2O_2$	1.2×10^{-16}		[22] [a]
116	$O(^1D) + O_2 \rightarrow O + O_2$	$3 \times 10^{-18} \exp\left(-85/T_g\right)$		[22] [a]
117	$O(^1D) + O_2 \rightarrow O(^1D) + O_2$	$1.3 \times 10^{-18} \exp\left(-85/T_g\right)$		[22] [a]
118	$O(^1D) + O_2(a\,^1\Delta_g) \rightarrow 3O$	3.2×10^{-17}		[22] [a]
119	$O(^1D) + O_2(a\,^1\Delta_g) \rightarrow O + O_2(b\,^1\Sigma_g^+)$	1.3×10^{-16}		[22] [a]
120	$O(^1D) + O_2(a\,^1\Delta_g) \rightarrow O(^1D) + O_2$	3.6×10^{-17}		[22] [a]
121	$O(^1D) + O_3 \rightarrow O + O(^1D) + O_2$	1.93×10^{-16}		[22] [a]
122	$O(^1D) + O_3 \rightarrow 2O_2$	1.93×10^{-16}		[22] [a]
123	$O(^1D) + O_3 \rightarrow 2O + O_2$	1.93×10^{-16}		[22] [a]
124	$2O_2 \rightarrow 2O + O_2$	$6.6 \times 10^{-15} \left(T_g/300\right)^{-1.5} \exp\left(-59/T_g\right)$		[22] [a]
125	$O_2 + O_2(\nu) \rightarrow 2O_2$	2×10^{-20}	-0.19	[22] [a]
126	$O_2 + O_2(a\,^1\Delta_g) \rightarrow 2O_2$	$3.6 \times 10^{-24} \exp\left(-22/T_g\right)$		[22] [a]
127	$O_2 + O_2(a\,^1\Delta_g, \nu) \rightarrow O_2(\nu) + O_2(a\,^1\Delta_g)$	5×10^{-17}	-0.19	[22] [a]
128	$O_2 + O_2(b\,^1\Sigma_g^+) \rightarrow O_2 + O_2(a\,^1\Delta_g)$	3.9×10^{-23}		[22] [a]
129	$O_2 + O_2(b\,^1\Sigma_g^+, \nu) \rightarrow O_2(\nu) + O_2(b\,^1\Sigma_g^+)$	1.5×10^{-17}	-0.19	[22] [a]
130	$O_2 + O_3 \rightarrow O + 2O_2$	$7.26 \times 10^{-16} \exp\left(-11435/T_g\right)$		[22] [a]
131	$O_2 + O_3(\nu) \rightarrow O_2 + O_3$	4×10^{-20}		[22] [a]
132	$2O_2(a\,^1\Delta_g) \rightarrow O_2 + O_2(b\,^1\Sigma_g^+)$	2.7×10^{-23}		[22] [a]
133	$O_2(a\,^1\Delta_g) + O_2(b\,^1\Sigma_g^+) \rightarrow O_2 + O_2(b\,^1\Sigma_g^+)$	2.7×10^{-23}		[22] [a]
134	$2O_2(b\,^1\Sigma_g^+) \rightarrow O_2 + O_2(b\,^1\Sigma_g^+)$	2.7×10^{-23}		[22] [a]
135	$O_2(a\,^1\Delta_g) + O_3 \rightarrow O + 2O_2$	$5.2 \times 10^{-17} \exp\left(-284/T_g\right)$		[22] [a]
136	$O_2(a\,^1\Delta_g) + O_3(\nu) \rightarrow O_2 + O_3$	5×10^{-17}		[22] [a]
137	$O_2(b\,^1\Sigma_g^+) + O_3 \rightarrow O + 2O_2$	$2.4 \times 10^{-17} \exp\left(-135/T_g\right)$		[22] [a]
138	$O_2(b\,^1\Sigma_g^+) + O_3 \rightarrow O_2 + O_3$	$5.5 \times 10^{-18} \exp\left(-135/T_g\right)$		[22] [a]
139	$O_2(b\,^1\Sigma_g^+) + O_3 \rightarrow O_2(a\,^1\Delta_g) + O_3$	$5.5 \times 10^{-18} \exp\left(-135/T_g\right)$		[22] [a]
140	$2O_3 \rightarrow O + O_2 + O_3$	$1.65 \times 10^{-15} \exp\left(-11435/T_g\right)$		[22] [a]
141	$O_3 + O_3(\nu) \rightarrow 2O_3$	1×10^{-19}		[22] [a]
142	$2e + O^+ \rightarrow e + O$	$2 \times 10^{-39} T_e^{-4.5}$		[22] [a]
143	$2e + O_2^+ \rightarrow e + O_2$	$2 \times 10^{-39} T_e^{-4.5}$		[22] [a]
144	$2e + O_4^+ \rightarrow e + 2O_2$	$2 \times 10^{-39} T_e^{-4.5}$		[22] [a]
145	$e + O + O_2 \rightarrow O + O_2^-$	1×10^{-43}		[22] [a]
146	$e + O^+ \rightarrow O(^1D)$	$2.7 \times 10^{-19} T_e^{-0.7}$		[22] [a]
147	$e + O^+ + O_2 \rightarrow O + O_2$	$3.3 \times 10^{-44} T_e^{-2.5}$		[22] [a]
148	$e + 2O_2 \rightarrow O_2 + O_2^-$	$3.62 \times 10^{-43} T_e^{-1} \exp\left(-0.05/T_e\right)$		[22] [a]
149	$e + O_2 + O_2^+ \rightarrow 2O_2$	$3.3 \times 10^{-44} T_e^{-2.5}$		[22] [a]
150	$e + O_2 + O_3 \rightarrow O_2 + O_3^-$	$3.62 \times 10^{-43} T_e^{-1} \exp\left(-0.05/T_e\right)$		[22] [a]

Continued on next page

Table A.1 (*Continued*)

ID	Reaction	k	ΔE_e	Source
151	$e + O_2^+ \rightarrow O + O(^1D)$	$9.1 \times 10^{-15} T_e^{-0.7}$		[22] [a]
152	$e + O_2^+ \rightarrow O(^1D)$	$6 \times 10^{-15} T_e^{-0.7}$		[22] [a]
153	$e + O_4^+ \rightarrow O + O(^1D) + O_2$	$2.02 \times 10^{-14} T_e^{-0.48}$		[22] [a]
154	$e + O_4^+ \rightarrow O(^1D) + O_2$	$1.35 \times 10^{-14} T_e^{-0.48}$		[22] [a]
155	$O + O^- \rightarrow e + O_2$	$2.3 \times 10^{-16} \left(T_g/300\right)^{-1.3}$		[22] [a]
156	$O + O_2^- \rightarrow O^- + O_2$	$8.5 \times 10^{-17} \left(T_g/300\right)^{-1.8}$		[22] [a]
157	$O + O_2^- \rightarrow e + O_3$	$8.5 \times 10^{-17} \left(T_g/300\right)^{-1.8}$		[22] [a]
158	$O + O_3^- \rightarrow e + 2O_2$	1×10^{-17}		[22] [a]
159	$O + O_3^- \rightarrow O_2 + O_2^-$	2.5×10^{-16}		[22] [a]
160	$O + O_4^+ \rightarrow O_3 + O_2^+$	3×10^{-16}		[22] [a]
161	$O + O_4^- \rightarrow O_2 + O_3^-$	4×10^{-16}		[22] [a]
162	$O(^1D) + O^- \rightarrow 2O + e$	7.4×10^{-16}		[22] [a]
163	$O(^1D) + O_2^- \rightarrow e + O_3$	$8.5 \times 10^{-17} \left(T_g/300\right)^{-1.8}$		[22] [a]
164	$O(^1D) + O_2^- \rightarrow O^- + O_2$	$8.5 \times 10^{-17} \left(T_g/300\right)^{-1.8}$		[22] [a]
165	$O(^1D) + O_3^+ \rightarrow 2O + O_2^+$	3×10^{-16}		[22] [a]
166	$O(^1D) + O_3^- \rightarrow O + O_2 + O^-$	3×10^{-16}		[22] [a]
167	$O(^1D) + O_3^- \rightarrow O + O_3 + e$	3×10^{-16}		[22] [a]
168	$O(^1D) + O_4^+ \rightarrow O + O_2 + O_2^+$	3×10^{-16}		[22] [a]
169	$O(^1D) + O_4^+ \rightarrow O_3 + O_2^+$	3×10^{-16}		[22] [a]
170	$O(^1D) + O_4^- \rightarrow e + O + 2O_2$	2×10^{-16}		[22] [a]
171	$O(^1D) + O_4^- \rightarrow O + O_2 + O_2^-$	2×10^{-16}		[22] [a]
172	$O(^1D) + O_4^- \rightarrow 2O_2 + O^-$	2×10^{-16}		[22] [a]
173	$O(^1D) + O^- \rightarrow e + 2O$	7.4×10^{-16}		[22] [a]
174	$O(^1D) + O_2^- \rightarrow O^- + O_2$	$8.5 \times 10^{-17} \left(T_g/300\right)^{-1.8}$		[22] [a]
175	$O(^1D) + O_2^- \rightarrow e + O_3$	$8.5 \times 10^{-17} \left(T_g/300\right)^{-1.8}$		[22] [a]
176	$O(^1D) + O_3^+ \rightarrow 2O + O_2^+$	2×10^{-16}		[22] [a]
177	$O(^1D) + O_3^- \rightarrow e + O + O_3$	2×10^{-16}		[22] [a]
178	$O(^1D) + O_3^- \rightarrow 2O + O_2^-$	2×10^{-16}		[22] [a]
179	$O(^1D) + O_3^- \rightarrow O + O^- + O_2$	2×10^{-16}		[22] [a]
180	$O(^1D) + O_4^+ \rightarrow O + O_2 + O_2^+$	3×10^{-16}		[22] [a]
181	$O(^1D) + O_4^+ \rightarrow O_2^+ + O_3$	3×10^{-16}		[22] [a]
182	$O(^1D) + O_4^- \rightarrow e + O + 2O_2$	2×10^{-16}		[22] [a]
183	$O(^1D) + O_4^- \rightarrow O + O_2 + O_2^-$	2×10^{-16}		[22] [a]
184	$O(^1D) + O_4^- \rightarrow O^- + 2O_2$	2×10^{-16}		[22] [a]
185	$O^+ + O + O_2 \rightarrow O_2 + O_2^+$	$4 \times 10^{-42} \left(T_g/300\right)^{-2.93}$		[22] [a]
186	$O^+ + O^- \rightarrow 2O$	$3.1 \times 10^{-14} \left(T_g/300\right)^{-1.1}$		[22] [a]
187	$O^+ + O^- + O_2 \rightarrow 2O + O_2$	$1 \times 10^{-37} \left(T_g/300\right)^{-2.5}$		[22] [a]
188	$O^+ + O^- + O_2 \rightarrow 2O_2$	$1 \times 10^{-37} \left(T_g/300\right)^{-2.5}$		[22] [a]
189	$O^+ + O_2 \rightarrow O + O_2^+$	$2.1 \times 10^{-17} \left(T_g/300\right)^{-0.4}$		[22] [a]
190	$O^+ + O_2^- \rightarrow O + O_2$	$3.22 \times 10^{-14} \left(T_g/300\right)^{-1.1}$		[22] [a]
191	$O^+ + O_2^- + O_2 \rightarrow O + 2O_2$	$1 \times 10^{-37} \left(T_g/300\right)^{-2.5}$		[22] [a]
192	$O^+ + O_2^- + O_2 \rightarrow O_2 + O_3$	$1 \times 10^{-37} \left(T_g/300\right)^{-2.5}$		[22] [a]
193	$O^+ + O_3 \rightarrow O_2 + O_2^+$	1.2×10^{-15}		[22] [a]
194	$O^+ + O_3^- \rightarrow O + O_3$	$7.33 \times 10^{-14} \left(T_g/300\right)^{-0.9}$		[22] [a]
195	$O^+ + O_3^- + O_2 \rightarrow O + O_2 + O_3$	$2 \times 10^{-37} \left(T_g/300\right)^{-2.5}$		[22] [a]
196	$O^+ + O_4^- \rightarrow O + 2O_2$	$7.87 \times 10^{-14} \left(T_g/300\right)^{-0.9}$		[22] [a]
197	$O^+ + O_4^- + O_2 \rightarrow O + 3O_2$	$2 \times 10^{-37} \left(T_g/300\right)^{-2.5}$		[22] [a]
198	$O^- + O_2 \rightarrow O_3 + e$	1×10^{-18}		[22] [a]
199	$O^- + O_2 \rightarrow O_2^- + O$	1×10^{-18}		[22] [a]
200	$O^- + 2O_2 \rightarrow O_2 + O_3^-$	1.1×10^{-42}		[22] [a]
201	$O^- + O_2 + O_3^+ \rightarrow O + O_2 + O_3$	$2 \times 10^{-37} \left(T_g/300\right)^{-2.5}$		[22] [a]
202	$O^- + O_2 + O_4^+ \rightarrow O + 3O_2$	$2 \times 10^{-37} \left(T_g/300\right)^{-2.5}$		[22] [a]
203	$O^- + O_2(a\,^1\Delta_g) \rightarrow O + O_2^-$	$7.9 \times 10^{-16} \exp\left(-89/T_g\right)$		[22] [a]
204	$O^- + O_2(a\,^1\Delta_g) \rightarrow O_3 + e$	6.1×10^{-17}		[22] [a]
205	$O^- + O_2(b\,^1\Sigma_g^+) \rightarrow O + O_2^-$	$7.9 \times 10^{-16} \exp\left(-89/T_g\right)$		[22] [a]
206	$O^- + O_2(b\,^1\Sigma_g^+) \rightarrow O_3 + e$	6.1×10^{-17}		[22] [a]
207	$O^- + O_2^+ \rightarrow 3O$	$1.61 \times 10^{-14} \left(T_g/300\right)^{-1.1}$		[22] [a]
208	$O^- + O_2^+ \rightarrow O + O_2$	$1.61 \times 10^{-14} \left(T_g/300\right)^{-1.1}$		[22] [a]
209	$O^- + O_3 \rightarrow e + 2O_2$	3×10^{-16}		[22] [a]
210	$O^- + O_3 \rightarrow O + O_3^-$	2×10^{-16}		[22] [a]

Continued on next page

Table A.1 (*Continued*)

ID	Reaction	k	ΔE_e	Source
211	$O^- + O_3 \rightarrow O_2 + O_2^-$	1×10^{-17}		[22] [a]
212	$O^- + O_3^+ \rightarrow 2O_2$	$3.07 \times 10^{-14} \left(T_g/300\right)^{-1.1}$		[22] [a]
213	$O^- + O_4^+ \rightarrow O + 2O_2$	$1.54 \times 10^{-14} \left(T_g/300\right)^{-0.9}$		[22] [a]
214	$O^- + O_4^+ \rightarrow O_2 + O_3$	$1.54 \times 10^{-14} \left(T_g/300\right)^{-0.9}$		[22] [a]
215	$2O_2 + O_2^+ \rightarrow O_2 + O_4^+$	$4 \times 10^{-42} \left(T_g/300\right)^{-2.93}$		[22] [a]
216	$2O_2 + O_2^- \rightarrow O_2 + O_4^-$	$3.5 \times 10^{-43} \left(T_g/300\right)^{-1}$		[22] [a]
217	$O_2 + O_2^- \rightarrow e + 2O_2$	$2.7 \times 10^{-16} \left(T_g/300\right)^{-0.5} \exp\left(-559/T_g\right)$		[22] [a]
218	$O_2 + O_2^- \rightarrow O + O_3^-$	3.5×10^{-21}		[22] [a]
219	$O_2 + O_2^- + O_3^+ \rightarrow 2O_2 + O_3$	$2 \times 10^{-37} \left(T_g/300\right)^{-2.5}$		[22] [a]
220	$O_2 + O_2^- + O_4^+ \rightarrow 4O_2$	$2 \times 10^{-37} \left(T_g/300\right)^{-2.5}$		[22] [a]
221	$O_2 + O_3^+ \rightarrow O_2^+ + O_3$	6.7×10^{-16}		[22] [a]
222	$O_2 + O_4^+ \rightarrow 2O_2 + O_2^+$	$1 \times 10^{-11} \left(T_g/300\right)^{-4.2} \exp\left(-54/T_g\right)$		[22] [a]
223	$O_2 + O_3^+ + O_3^- \rightarrow O_2 + 2O_3$	$2 \times 10^{-37} \left(T_g/300\right)^{-2.5}$		[22] [a]
224	$O_2 + O_3^+ + O_4^- \rightarrow 3O_2 + O_3$	$2 \times 10^{-37} \left(T_g/300\right)^{-2.5}$		[22] [a]
225	$O_2 + O_3^- + O_4^+ \rightarrow 3O_2 + O_3$	$2 \times 10^{-37} \left(T_g/300\right)^{-2.5}$		[22] [a]
226	$O_2 + O_4^+ + O_4^- \rightarrow 5O_2$	$2 \times 10^{-37} \left(T_g/300\right)^{-2.5}$		[22] [a]
227	$O_2 + O_4^- \rightarrow 2O_2 + O_2^-$	$2.2 \times 10^{-11} \left(T_g/300\right)^{-1} \exp\left(-63/T_g\right)$		[22] [a]
228	$O_2(a\,^1\Delta_g) + O_2^- \rightarrow e + 2O_2$	7×10^{-16}		[22] [a]
229	$O_2(a\,^1\Delta_g) + O_4^+ \rightarrow 2O_2 + O_2^+$	6×10^{-16}		[22] [a]
230	$O_2(a\,^1\Delta_g) + O_4^- \rightarrow 3O_2 + e$	3×10^{-16}		[22] [a]
231	$O_2(a\,^1\Delta_g) + O_4^- \rightarrow 2O_2 + O_2^-$	3×10^{-16}		[22] [a]
232	$O_2(b\,^1\Sigma_g^+) + O_2^- \rightarrow e + 2O_2$	7×10^{-16}		[22] [a]
233	$O_2(b\,^1\Sigma_g^+) + O_3^- \rightarrow O^- + 2O_2$	$6.7 \times 10^{-16} \exp\left(-13/T_g\right)$		[22] [a]
234	$O_2(b\,^1\Sigma_g^+) + O_4^+ \rightarrow 2O_2 + O_2^+$	6×10^{-16}		[22] [a]
235	$O_2(b\,^1\Sigma_g^+) + O_4^- \rightarrow e + 3O_2$	3×10^{-16}		[22] [a]
236	$O_2(b\,^1\Sigma_g^+) + O_4^- \rightarrow 2O_2 + O_2^-$	3×10^{-16}		[22] [a]
237	$O_2^+ + O^- + O_2 \rightarrow O + 2O_2$	$1 \times 10^{-37} \left(T_g/300\right)^{-2.5}$		[22] [a]
238	$O_2^+ + O^- + O_2 \rightarrow O_2 + O_3$	$1 \times 10^{-37} \left(T_g/300\right)^{-2.5}$		[22] [a]
239	$O_2^+ + O_2^- + O_2 \rightarrow 3O_2$	$2 \times 10^{-37} \left(T_g/300\right)^{-2.5}$		[22] [a]
240	$O_2^+ + O_3^- + O_2 \rightarrow 2O_2 + O_3$	$2 \times 10^{-37} \left(T_g/300\right)^{-2.5}$		[22] [a]
241	$O_2^+ + O_4^- + O_2 \rightarrow 4O_2$	$2 \times 10^{-37} \left(T_g/300\right)^{-2.5}$		[22] [a]
242	$O_2^+ + O_2^- \rightarrow O_2 + 2O$	$1.6 \times 10^{-14} \left(T_g/300\right)^{-1.1}$		[22] [a]
243	$O_2^+ + O_2^- \rightarrow 2O_2$	$1.6 \times 10^{-14} \left(T_g/300\right)^{-1.1}$		[22] [a]
244	$O_2^+ + O_3^- \rightarrow 2O + O_3$	$2.9 \times 10^{-14} \left(T_g/300\right)^{-0.9}$		[22] [a]
245	$O_2^+ + O_3^- \rightarrow O_2 + O_3$	$2.9 \times 10^{-14} \left(T_g/300\right)^{-0.9}$		[22] [a]
246	$O_2^+ + O_4^- \rightarrow 3O_2$	$6.07 \times 10^{-14} \left(T_g/300\right)^{-0.9}$		[22] [a]
247	$O_2^- + O_3 \rightarrow O_2 + O_3^-$	6×10^{-16}		[22] [a]
248	$O_2^- + O_3^+ \rightarrow O_2 + O_3$	$3.29 \times 10^{-14} \left(T_g/300\right)^{-1.1}$		[22] [a]
249	$O_2^- + O_4^+ \rightarrow 2O + 2O_2$	$1.6 \times 10^{-14} \left(T_g/300\right)^{-1.1}$		[22] [a]
250	$O_2^- + O_4^+ \rightarrow 3O_2$	$1.6 \times 10^{-14} \left(T_g/300\right)^{-1.1}$		[22] [a]
251	$O_3 + O_4^- \rightarrow 2O_2 + O_3^-$	8×10^{-16}		[22] [a]
252	$O_3^+ + O_3^- \rightarrow 2O_3$	$5.19 \times 10^{-14} \left(T_g/300\right)^{-0.9}$		[22] [a]
253	$O_3^+ + O_4^- \rightarrow 2O_2 + O_3$	$5.37 \times 10^{-14} \left(T_g/300\right)^{-0.9}$		[22] [a]
254	$O_3^- + O_3 \rightarrow e + 3O_2$	8.5×10^{-16}		[22] [a]
255	$O_3^- + O_4^+ \rightarrow O + 3O_2$	$2.43 \times 10^{-14} \left(T_g/300\right)^{-0.9}$		[22] [a]
256	$O_3^- + O_4^+ \rightarrow 2O_2 + O_3$	$2.43 \times 10^{-14} \left(T_g/300\right)^{-0.9}$		[22] [a]
257	$O_4^+ + O_4^- \rightarrow 4O_2$	$4.97 \times 10^{-14} \left(T_g/300\right)^{-0.9}$		[22] [a]
258	$He + He^* + O \rightarrow e + 2He + O^+$	1.6×10^{-43}		[22] [a]
259	$He + He^* + O(^1D) \rightarrow e + 2He + O^+$	1.6×10^{-43}		[22] [a]
260	$He + He^* + O(^1D) \rightarrow e + 2He + O^+$	1.6×10^{-43}		[22] [a]
261	$He + He^* + O_2 \rightarrow e + 2He + O_2^+$	1.6×10^{-43}		[22] [a]
262	$He + He^* + O_2(a\,^1\Delta_g) \rightarrow e + 2He + O_2^+$	1.6×10^{-43}		[22] [a]
263	$He + He^* + O_2(b\,^1\Sigma_g^+) \rightarrow e + 2He + O_2^+$	1.6×10^{-43}		[22] [a]
264	$He + He^* + O_3 \rightarrow e + 2He + O + O_2^+$	1.6×10^{-43}		[22] [a]
265	$He + 2O \rightarrow He + O_2(a\,^1\Delta_g)$	$2 \times 10^{-45} \left(T_g/300\right)^{-1} \exp\left(-17/T_g\right)$		[22] [a]
266	$He + 2O \rightarrow He + O_2(b\,^1\Sigma_g^+)$	$2 \times 10^{-45} \left(T_g/300\right)^{-1} \exp\left(-17/T_g\right)$		[22] [a]
267	$He + O + O_2 \rightarrow He + O_3$	$9 \times 10^{-47} \left(T_g/300\right)^{-2.6}$		[22] [a]
268	$He + O + O_2 \rightarrow He + O_3(\nu)$	$2.1 \times 10^{-46} \left(T_g/300\right)^{-2.6}$		[22] [a]
269	$He + O + O_2(a\,^1\Delta_g) \rightarrow He + O + O_2$	4×10^{-45}		[22] [a]
270	$He + O(^1D) \rightarrow He + O$	1×10^{-21}		[22] [a]

Continued on next page

Table A.1 (*Continued*)

ID	Reaction	k	ΔE_e	Source
271	$He + O(^1D) \rightarrow He + O$	1×10^{-21}		[22] [a]
272	$He + O_2(\nu) \rightarrow He + O_2$	2×10^{-17}	-0.19	[22] [a]
273	$He + O_2(a\,^1\Delta_g) \rightarrow He + O_2$	5×10^{-27}		[22] [a]
274	$He + O_2(a\,^1\Delta_g, \nu) \rightarrow He + O_2(a\,^1\Delta_g)$	2×10^{-17}	-0.19	[22] [a]
275	$He + O_2(b\,^1\Sigma_g^+) \rightarrow He + O_2(a\,^1\Delta_g)$	4.3×10^{-24}		[22] [a]
276	$He + O_2(b\,^1\Sigma_g^+, \nu) \rightarrow He + O_2(b\,^1\Sigma_g^+)$	6×10^{-19}	-0.19	[22] [a]
277	$He + O_3 \rightarrow He + O + O_2$	$5.61 \times 10^{-16} \exp(-114/T_g)$		[22] [a]
278	$He + O_3(\nu) \rightarrow He + O_3$	6×10^{-20}		[22] [a]
279	$He^* + O \rightarrow e + He + O^+$	2.6×10^{-16}		[22] [a]
280	$He^* + O(^1D) \rightarrow e + He + O^+$	2.6×10^{-16}		[22] [a]
281	$He^* + O(^1D) \rightarrow e + He + O^+$	2.6×10^{-16}		[22] [a]
282	$He^* + O_2 \rightarrow e + He + O_2^+$	2.6×10^{-16}		[22] [a]
283	$He^* + O_2(a\,^1\Delta_g) \rightarrow e + He + O_2^+$	2.6×10^{-16}		[22] [a]
284	$He^* + O_2(b\,^1\Sigma_g^+) \rightarrow e + He + O_2^+$	2.6×10^{-16}		[22] [a]
285	$He^* + O_3 \rightarrow e + He + O + O_2^+$	2.6×10^{-16}		[22] [a]
286	$He_2^* + O \rightarrow e + 2He + O^+$	3.6×10^{-16}		[22] [a]
287	$He_2^* + O(^1D) \rightarrow e + 2He + O^+$	3.6×10^{-16}		[22] [a]
288	$He_2^* + O(^1D) \rightarrow e + 2He + O^+$	3.6×10^{-16}		[22] [a]
289	$He_2^* + O_2 \rightarrow e + 2He + O_2^+$	3.6×10^{-16}		[22] [a]
290	$He_2^* + O_2(a\,^1\Delta_g) \rightarrow e + 2He + O_2^+$	3.6×10^{-16}		[22] [a]
291	$He_2^* + O_2(b\,^1\Sigma_g^+) \rightarrow e + 2He + O_2^+$	3.6×10^{-16}		[22] [a]
292	$He_2^* + O_3 \rightarrow e + 2He + O + O_2^+$	3.6×10^{-16}		[22] [a]
293	$e + He + O \rightarrow He + O^-$	$1 \times 10^{-44} T_e^{-0.5}$		[22] [a]
294	$e + He + O_2 \rightarrow He + O_2^-$	$1 \times 10^{-44} T_e^{-0.5}$		[22] [a]
295	$e + He + O_3 \rightarrow He + O_3^-$	$1 \times 10^{-44} T_e^{-0.5}$		[22] [a]
296	$He + He^+ + O^- \rightarrow 2He + O$	$2 \times 10^{-37} (T_g/300)^{-2.5}$		[22] [a]
297	$He + He^+ + O_2^- \rightarrow 2He + O_2$	$2 \times 10^{-37} (T_g/300)^{-2.5}$		[22] [a]
298	$He + He^+ + O_3^- \rightarrow 2He + O_3$	$2 \times 10^{-37} (T_g/300)^{-2.5}$		[22] [a]
299	$He + He^+ + O_4^- \rightarrow 2He + 2O_2$	$2 \times 10^{-37} (T_g/300)^{-2.5}$		[22] [a]
300	$He + He_2^+ + O^- \rightarrow 3He + O$	$2 \times 10^{-37} (T_g/300)^{-2.5}$		[22] [a]
301	$He + He_2^+ + O_2 \rightarrow 3He + O_2^+$	3.5×10^{-41}		[22] [a]
302	$He + He_2^+ + O_2^- \rightarrow 3He + O_2$	$2 \times 10^{-37} (T_g/300)^{-2.5}$		[22] [a]
303	$He + He_2^+ + O_3^- \rightarrow 3He + O_3$	$2 \times 10^{-37} (T_g/300)^{-2.5}$		[22] [a]
304	$He + He_2^+ + O_4^- \rightarrow 3He + 2O_2$	$2 \times 10^{-37} (T_g/300)^{-2.5}$		[22] [a]
305	$He + O + O^+ \rightarrow He + O_2^+$	$5.5 \times 10^{-43} (T_g/300)^{-2.7}$		[22] [a]
306	$He + O^+ + O^- \rightarrow He + 2O$	$2 \times 10^{-37} (T_g/300)^{-2.5}$		[22] [a]
307	$He + O^+ + O_2^- \rightarrow He + O + O_2$	$2 \times 10^{-37} (T_g/300)^{-2.5}$		[22] [a]
308	$He + O^+ + O_3^- \rightarrow He + O + O_3$	$2 \times 10^{-37} (T_g/300)^{-2.5}$		[22] [a]
309	$He + O^+ + O_4^- \rightarrow He + O + 2O_2$	$2 \times 10^{-37} (T_g/300)^{-2.5}$		[22] [a]
310	$He + O^- \rightarrow e + He + O$	$2.5 \times 10^{-24} (T_g/300)^{-0.6}$		[22] [a]
311	$He + O^- + O_2 \rightarrow He + O_3^-$	$3.7 \times 10^{-43} (T_g/300)^{-1}$		[22] [a]
312	$He + O^- + O_2^+ \rightarrow He + O + O_2$	$2 \times 10^{-37} (T_g/300)^{-2.5}$		[22] [a]
313	$He + O^- + O_3^+ \rightarrow He + O + O_3$	$2 \times 10^{-37} (T_g/300)^{-2.5}$		[22] [a]
314	$He + O^- + O_4^+ \rightarrow He + O + 2O_2$	$2 \times 10^{-37} (T_g/300)^{-2.5}$		[22] [a]
315	$He + O_2 + O_2^+ \rightarrow He + O_4^+$	$5.5 \times 10^{-43} (T_g/300)^{-2.7}$		[22] [a]
316	$He + O_2 + O_2^- \rightarrow He + O_4^-$	$1.2 \times 10^{-43} (T_g/300)^{-2.7}$		[22] [a]
317	$He + O_2^+ + O_2^- \rightarrow He + 2O_2$	$2 \times 10^{-37} (T_g/300)^{-2.5}$		[22] [a]
318	$He + O_2^+ + O_3^- \rightarrow He + O_2 + O_3$	$2 \times 10^{-37} (T_g/300)^{-2.5}$		[22] [a]
319	$He + O_2^+ + O_4^- \rightarrow He + 3O_2$	$2 \times 10^{-37} (T_g/300)^{-2.5}$		[22] [a]
320	$He + O_2^- \rightarrow e + He + O_2$	$3.9 \times 10^{-16} \exp(-74/T_g)$		[22] [a]
321	$He + O_2^- + O_3^+ \rightarrow He + O_2 + O_3$	$2 \times 10^{-37} (T_g/300)^{-2.5}$		[22] [a]
322	$He + O_2^- + O_4^+ \rightarrow He + 3O_2$	$2 \times 10^{-37} (T_g/300)^{-2.5}$		[22] [a]
323	$He + O_3^+ + O_3^- \rightarrow He + 2O_3$	$2 \times 10^{-37} (T_g/300)^{-2.5}$		[22] [a]
324	$He + O_3^+ + O_4^- \rightarrow He + 2O_2 + O_3$	$2 \times 10^{-37} (T_g/300)^{-2.5}$		[22] [a]
325	$He + O_3^- + O_4^+ \rightarrow He + 2O_2 + O_3$	$2 \times 10^{-37} (T_g/300)^{-2.5}$		[22] [a]
326	$He + O_4^+ \rightarrow He + O_2 + O_2^+$	3.6×10^{-20}		[22] [a]
327	$He + O_4^+ + O_4^- \rightarrow He + 4O_2$	$2 \times 10^{-37} (T_g/300)^{-2.5}$		[22] [a]
328	$He + O_4^- \rightarrow He + O_2 + O_2^-$	$2.2 \times 10^{-11} (T_g/300)^{-1} \exp(-63/T_g)$		[22] [a]
329	$He^* + O^- \rightarrow 2e + He + O^+$	8.7×10^{-15}		[22] [a]
330	$He^* + O_2^+ \rightarrow He + O + O^+$	8.2×10^{-15}		[22] [a]

Continued on next page

Table A.1 (*Continued*)

ID	Reaction	k	ΔE_e	Source
331	$He^* + O_2^- \rightarrow 2e + He + O_2^+$	8.3×10^{-15}		[22] [a]
332	$He^* + O_3^+ \rightarrow He + O + O_2^+$	8.1×10^{-15}		[22] [a]
333	$He^* + O_3^- \rightarrow 2e + He + O + O_2^+$	8.1×10^{-15}		[22] [a]
334	$He^* + O_4^+ \rightarrow He + O_2 + O_2^+$	8×10^{-15}		[22] [a]
335	$He^* + O_4^- \rightarrow 2e + He + O_2 + O_2^+$	8×10^{-15}		[22] [a]
336	$He^+ + O \rightarrow He + O^+$	5.8×10^{-16}		[22] [a]
337	$He^+ + O(^1D) \rightarrow He + O^+$	5.8×10^{-16}		[22] [a]
338	$He^+ + O(^1D) \rightarrow He + O^+$	5.8×10^{-16}		[22] [a]
339	$He^+ + O^- \rightarrow He + O$	$3.12 \times 10^{-14} \left(T_g/300\right)^{-1.1}$		[22] [a]
340	$He^+ + O^- + O_2 \rightarrow He + O_2 + O$	$2 \times 10^{-37} \left(T_g/300\right)^{-2.5}$		[22] [a]
341	$He^+ + O_2 \rightarrow He + O + O^+$	9.7×10^{-16}		[22] [a]
342	$He^+ + O_2 \rightarrow He + O_2^+$	3×10^{-17}		[22] [a]
343	$He^+ + O_2 + O_4^- \rightarrow He + 3O_2$	$2 \times 10^{-37} \left(T_g/300\right)^{-2.5}$		[22] [a]
344	$He^+ + O_2(a\,^1\Delta_g) \rightarrow He + O + O^+$	9.7×10^{-16}		[22] [a]
345	$He^+ + O_2(a\,^1\Delta_g) \rightarrow He + O_2^+$	3×10^{-17}		[22] [a]
346	$He^+ + O_2(b\,^1\Sigma_g^+) \rightarrow He + O + O^+$	9.7×10^{-16}		[22] [a]
347	$He^+ + O_2(b\,^1\Sigma_g^+) \rightarrow He + O_2^+$	3×10^{-17}		[22] [a]
348	$He^+ + O_2^- \rightarrow He + O_2$	$3.26 \times 10^{-14} \left(T_g/300\right)^{-1.1}$		[22] [a]
349	$He^+ + O_3 \rightarrow He + O_2 + O^+$	2.2×10^{-15}		[22] [a]
350	$He^+ + O_3^- \rightarrow He + O_3$	$1.32 \times 10^{-13} \left(T_g/300\right)^{-0.9}$		[22] [a]
351	$He^+ + O_4^- \rightarrow He + 2O_2$	$1.45 \times 10^{-13} \left(T_g/300\right)^{-0.9}$		[22] [a]
352	$He_2^* + O^- \rightarrow e + 2He + O$	6.7×10^{-15}		[22] [a]
353	$He_2^* + O_2^+ \rightarrow 2He + O + O^+$	6.2×10^{-15}		[22] [a]
354	$He_2^* + O_2^- \rightarrow 2e + 2He + O_2^+$	6.1×10^{-15}		[22] [a]
355	$He_2^* + O_3^- \rightarrow 2e + 2He + O + O_2^+$	6×10^{-15}		[22] [a]
356	$He_2^* + O_4^+ \rightarrow 2He + 2O + O_2^+$	5.8×10^{-15}		[22] [a]
357	$He_2^* + O_4^- \rightarrow 2e + 2He + O_2 + O_2^+$	5.8×10^{-15}		[22] [a]
358	$He_2^+ + O \rightarrow 2He + O^+$	9×10^{-16}		[22] [a]
359	$He_2^+ + O(^1D) \rightarrow 2He + O^+$	9×10^{-16}		[22] [a]
360	$He_2^+ + O(^1D) \rightarrow 2He + O^+$	9×10^{-16}		[22] [a]
361	$He_2^+ + O^- \rightarrow 2He + O$	$3.1 \times 10^{-14} \left(T_g/300\right)^{-1.1}$		[22] [a]
362	$He_2^+ + O^- + O_2 \rightarrow 2He + O_2 + O$	$2 \times 10^{-37} \left(T_g/300\right)^{-2.5}$		[22] [a]
363	$He_2^+ + O_2 \rightarrow 2He + O + O^+$	1×10^{-16}		[22] [a]
364	$He_2^+ + O_2 \rightarrow 2He + O_2^+$	9×10^{-16}		[22] [a]
365	$He_2^+ + O_2 + O_2^- \rightarrow 2He + 2O_2$	$2 \times 10^{-37} \left(T_g/300\right)^{-2.5}$		[22] [a]
366	$He_2^+ + O_2 + O_4^- \rightarrow 2He + 3O_2$	$2 \times 10^{-37} \left(T_g/300\right)^{-2.5}$		[22] [a]
367	$He_2^+ + O_2(a\,^1\Delta_g) \rightarrow 2He + O_2^+$	1.2×10^{-15}		[22] [a]
368	$He_2^+ + O_2(b\,^1\Sigma_g^+) \rightarrow 2He + O_2^+$	1.2×10^{-15}		[22] [a]
369	$He_2^+ + O_2 + O_3^- \rightarrow 2He + O_2 + O_3$	$2 \times 10^{-37} \left(T_g/300\right)^{-2.5}$		[22] [a]
370	$He_2^+ + O_2^- \rightarrow 2He + O_2$	$3.26 \times 10^{-14} \left(T_g/300\right)^{-1.1}$		[22] [a]
371	$He_2^+ + O_3 \rightarrow 2He + O^+ + O_2$	1.6×10^{-15}		[22] [a]
372	$He_2^+ + O_3^- \rightarrow 2He + O_3$	$1.34 \times 10^{-13} \left(T_g/300\right)^{-0.9}$		[22] [a]
373	$He_2^+ + O_4^- \rightarrow 2He + 2O_2$	$1.45 \times 10^{-13} \left(T_g/300\right)^{-0.9}$		[22] [a]

Table A.2: An example of reduced O_2–He chemistry set, using the $DRG_{sh.path}$ species ranking scheme and reduction conditions from tables 5.10 and 5.11. The reduction was performed with set of species of interest O, $O_2(a\,^1\Delta_g)$ and O_3 (reduction case C1.4, Table 5.9). The reduction performed was only species–oriented, therefore this reduced chemistry set almost certainly still includes some redundant reactions. Kinetic data are directly as taken from the source publication [22] and the reactions ID numbers are consistent with the source publication. The reaction rate coefficients k of order-m reactions are in $[m^{3(m-1)}s^{-1}]$. Gas temperature T_g is in [K]. The electron temperature T_e and electron energy loss ΔE_e are in [eV].
[a] Not the original source.

ID	Reaction	k	ΔE_e	Source
2	$2e + He_2^+ \rightarrow He^* + He + e$	$1.62 \times 10^{-38} T_e^{-4}$		[22] [a]
4	$e + He + He_2^+ \rightarrow 3He$	$2.5 \times 10^{-39} T_e^{-2.5}$		[22] [a]
5	$e + He \rightarrow e + He$	$7.77 \times 10^{-14} T_e^{0.02} \exp(-0.5/T_e)$		[22] [a]
7	$e + He \rightarrow He^* + e$	$3.3 \times 10^{-15} T_e^{0.33} \exp(-21.6/T_e)$	19.8	[22] [a]
11	$e + He_2^+ \rightarrow He + He^*$	$9.6 \times 10^{-17} T_e^{-0.5}$		[22] [a]
13	$e + O \rightarrow e + O(^1D)$	$8.45 \times 10^{-15} T_e^{-0.31} \exp(-3.13/T_e)$	1.96	[22] [a]
16	$e + O(^1D) \rightarrow e + O$	$8.45 \times 10^{-15} T_e^{0.31} \exp(-1.17/T_e)$	-1.96	[22] [a]
19	$e + O^- \rightarrow 2e + O$	$9.33 \times 10^{-14} T_e^{0.18} \exp(-3.13/T_e)$	3.44	[22] [a]
21	$e + O_2 \rightarrow 2e + O_2^+$	$2.32 \times 10^{-15} T_e^{0.99} \exp(-12.51/T_e)$	12.06	[22] [a]
22	$e + O_2 \rightarrow e + O + O(^1D)$	$3.12 \times 10^{-14} T_e^{0.02} \exp(-8.05/T_e)$	8.5	[22] [a]
24	$e + O_2 \rightarrow e + O_2$	$4.15 \times 10^{-14} T_e^{0.6} \exp(-0.02/T_e)$		[22] [a]
25	$e + O_2 \rightarrow e + O_2$	$3.88 \times 10^{-17} T_e^{-1.22} \exp(-0.55/T_e)$	0.02	[22] [a]
32	$e + O_2 \rightarrow e + O_2(a\,^1\Delta_g)$	$2.1 \times 10^{-15} T_e^{-0.23} \exp(-2.87/T_e)$	0.98	[22] [a]
33	$e + O_2 \rightarrow e + O_2(b\,^1\Sigma_g^+)$	$3.97 \times 10^{-16} T_e^{-0.09} \exp(-2.67/T_e)$	1.63	[22] [a]
34	$e + O_2 \rightarrow e + O_2(b\,^1\Sigma_g^+)$	$1.28 \times 10^{-14} T_e^{-1.16} \exp(-7/T_e)$	4.5	[22] [a]
35	$e + O_2 \rightarrow e + O_2(b\,^1\Sigma_g^+)$	$1.98 \times 10^{-14} T_e^{-0.78} \exp(-7.36/T_e)$	6	[22] [a]
36	$e + O_2 \rightarrow O + O^-$	$1.32 \times 10^{-15} T_e^{-1.4} \exp(-6.63/T_e)$		[22] [a]
38	$e + O_2(a\,^1\Delta_g) \rightarrow 2e + O_2^+$	$2.32 \times 10^{-15} T_e^{0.99} \exp(-11.53/T_e)$	11.08	[22] [a]
39	$e + O_2(a\,^1\Delta_g) \rightarrow e + O + O(^1D)$	$3.12 \times 10^{-14} T_e^{0.02} \exp(-7.07/T_e)$	7.52	[22] [a]
40	$e + O_2(a\,^1\Delta_g) \rightarrow e + O + O(^1D)$	$1.56 \times 10^{-17} T_e^{1.5} \exp(-3.7/T_e)$	9	[22] [a]
41	$e + O_2(a\,^1\Delta_g) \rightarrow e + O_2$	$2.1 \times 10^{-15} T_e^{-0.23} \exp(-1.89/T_e)$	-0.98	[22] [a]
42	$e + O_2(a\,^1\Delta_g) \rightarrow e + O_2(a\,^1\Delta_g)$	$4.15 \times 10^{-14} T_e^{0.6} \exp(-0.02/T_e)$		[22] [a]
43	$e + O_2(a\,^1\Delta_g) \rightarrow e + O_2(a\,^1\Delta_g)$	$3.88 \times 10^{-17} T_e^{-1.22} \exp(-0.55/T_e)$	0.02	[22] [a]
50	$e + O_2(a\,^1\Delta_g) \rightarrow O_2(b\,^1\Sigma_g^+) + e$	$5.25 \times 10^{-15} T_e^{-0.44} \exp(-1.49/T_e)$	0.66	[22] [a]
51	$e + O_2(a\,^1\Delta_g) \rightarrow e + O_2(b\,^1\Sigma_g^+)$	$1.28 \times 10^{-14} T_e^{-1.16} \exp(-6.02/T_e)$	3.52	[22] [a]
52	$e + O_2(a\,^1\Delta_g) \rightarrow e + O_2(b\,^1\Sigma_g^+)$	$1.98 \times 10^{-14} T_e^{-0.78} \exp(-6.38/T_e)$	5.02	[22] [a]
53	$e + O_2(a\,^1\Delta_g) \rightarrow O + O^-$	$4.14 \times 10^{-15} T_e^{-1.34} \exp(-5.15/T_e)$	3	[22] [a]
54	$e + O_2(a\,^1\Delta_g) \rightarrow O(^1D) + O^-$	$9.2 \times 10^{-16} T_e^{-1.26} \exp(-6.55/T_e)$	3	[22] [a]
56	$e + O_2(b\,^1\Sigma_g^+) \rightarrow 2e + O_2^+$	$2.32 \times 10^{-15} T_e^{0.99} \exp(-10.88/T_e)$	10.43	[22] [a]
57	$e + O_2(b\,^1\Sigma_g^+) \rightarrow e + O + O(^1D)$	$3.12 \times 10^{-14} T_e^{0.02} \exp(-6.42/T_e)$	6.87	[22] [a]
58	$e + O_2(b\,^1\Sigma_g^+) \rightarrow e + O + O(^1D)$	$1.56 \times 10^{-17} T_e^{1.5} \exp(-3.05/T_e)$	8.34	[22] [a]
59	$e + O_2(b\,^1\Sigma_g^+) \rightarrow e + O_2$	$3.97 \times 10^{-16} T_e^{-0.09} \exp(-1.04/T_e)$	-1.63	[22] [a]
60	$e + O_2(b\,^1\Sigma_g^+) \rightarrow e + O_2(a\,^1\Delta_g)$	$5.25 \times 10^{-15} T_e^{-0.44} \exp(-0.83/T_e)$	-0.66	[22] [a]
61	$e + O_2(b\,^1\Sigma_g^+) \rightarrow e + O_2(b\,^1\Sigma_g^+)$	$4.15 \times 10^{-14} T_e^{0.6} \exp(-0.02/T_e)$		[22] [a]
62	$e + O_2(b\,^1\Sigma_g^+) \rightarrow e + O_2(b\,^1\Sigma_g^+)$	$3.88 \times 10^{-17} T_e^{-1.22} \exp(-0.55/T_e)$	0.02	[22] [a]
69	$e + O_2(b\,^1\Sigma_g^+) \rightarrow e + O_2(b\,^1\Sigma_g^+)$	$1.28 \times 10^{-14} T_e^{-1.16} \exp(-5.37/T_e)$	2.87	[22] [a]
70	$e + O_2(b\,^1\Sigma_g^+) \rightarrow e + O_2(b\,^1\Sigma_g^+)$	$1.98 \times 10^{-14} T_e^{-0.78} \exp(-5.73/T_e)$	4.37	[22] [a]
71	$e + O_2(b\,^1\Sigma_g^+) \rightarrow O + O^-$	$7.11 \times 10^{-16} T_e^{-1.04} \exp(-0.23/T_e)$		[22] [a]
74	$e + O_3 \rightarrow e + O(^1D) + O_2(a\,^1\Delta_g)$	$3.22 \times 10^{-13} T_e^{-1.18} \exp(-9.17/T_e)$	5.72	[22] [a]
76	$e + O_3 \rightarrow O^- + O_2$	$3.45 \times 10^{-15} T_e^{-0.96} \exp(-1/T_e)$		[22] [a]
87	$2He^* \rightarrow e + He_2^+$	1.05×10^{-15}	-19	[22] [a]
92	$3O \rightarrow O + O_2$	$3.8 \times 10^{-44} (T_g/300)^{-1} \exp(-17/T_g)$		[22] [a]
93	$3O \rightarrow O + O_2(b\,^1\Sigma_g^+)$	$1.4 \times 10^{-42} \exp(-65/T_g)$		[22] [a]
94	$2O + O_2 \rightarrow O + O_3$	$4.2 \times 10^{-47} \exp(1056/T_g)$		[22] [a]
95	$2O + O_2 \rightarrow O + O_3(\nu)$	$9.8 \times 10^{-47} \exp(1056/T_g)$		[22] [a]

Continued on next page

Table A.2 (*Continued*)

ID	Reaction	k	ΔE_e	Source
96	$2O + O_2 \rightarrow O_2(a\,^1\Delta_g) + O_2$	$6.5 \times 10^{-45}\,(T_g/300)^{-1} \exp(-17/T_g)$		[22] [a]
97	$2O + O_2 \rightarrow O_2(b\,^1\Sigma_g^+) + O_2$	$6.5 \times 10^{-45}\,(T_g/300)^{-1} \exp(-17/T_g)$		[22] [a]
98	$O + O(^1D) \rightarrow 2O$	2×10^{-18}		[22] [a]
101	$O + 2O_2 \rightarrow O_2 + O_3$	$1.8 \times 10^{-46}\,(T_g/300)^{-2.6}$		[22] [a]
102	$O + 2O_2 \rightarrow O_2 + O_3(\nu)$	$4.2 \times 10^{-46}\,(T_g/300)^{-2.6}$		[22] [a]
103	$O + O_2 + O_2(a\,^1\Delta_g) \rightarrow O + 2O_2$	1.1×10^{-44}		[22] [a]
104	$O + O_2 + O_3 \rightarrow 2O_3$	$1.4 \times 10^{-47} \exp(-105/T_g)$		[22] [a]
105	$O + O_2 + O_3 \rightarrow O_3 + O_3(\nu)$	$3.27 \times 10^{-47} \exp(-105/T_g)$		[22] [a]
106	$O + O_2(a\,^1\Delta_g) \rightarrow O + O_2$	1×10^{-22}	-2.14	[22] [a]
107	$O + O_2(b\,^1\Sigma_g^+) \rightarrow O + O_2(a\,^1\Delta_g)$	8×10^{-20}	-0.65	[22] [a]
108	$O + O_3 \rightarrow 2O + O_2$	$1.2 \times 10^{-15} \exp(-114/T_g)$		[22] [a]
110	$O + O_3(\nu) \rightarrow 2O_2$	4.5×10^{-18}		[22] [a]
111	$O + O_3(\nu) \rightarrow O_3 + O$	1.05×10^{-17}		[22] [a]
112	$O(^1D) + O_2 \rightarrow O + O_2(b\,^1\Sigma_g^+)$	$2.64 \times 10^{-17} \exp(55/T_g)$		[22] [a]
113	$O(^1D) + O_2 \rightarrow O + O_2(a\,^1\Delta_g)$	$6.6 \times 10^{-18} \exp(55/T_g)$		[22] [a]
114	$O(^1D) + O_3 \rightarrow 2O + O_2$	1.2×10^{-16}		[22] [a]
115	$O(^1D) + O_3 \rightarrow 2O_2$	1.2×10^{-16}		[22] [a]
124	$2O_2 \rightarrow 2O + O_2$	$6.6 \times 10^{-15}\,(T_g/300)^{-1.5} \exp(-59/T_g)$		[22] [a]
126	$O_2 + O_2(a\,^1\Delta_g) \rightarrow 2O_2$	$3.6 \times 10^{-24} \exp(-22/T_g)$		[22] [a]
128	$O_2 + O_2(b\,^1\Sigma_g^+) \rightarrow O_2 + O_2(a\,^1\Delta_g)$	3.9×10^{-23}		[22] [a]
130	$O_2 + O_3 \rightarrow O + 2O_2$	$7.26 \times 10^{-16} \exp(-11435/T_g)$		[22] [a]
131	$O_2 + O_3(\nu) \rightarrow O_2 + O_3$	4×10^{-20}		[22] [a]
132	$2O_2(a\,^1\Delta_g) \rightarrow O_2 + O_2(b\,^1\Sigma_g^+)$	2.7×10^{-23}		[22] [a]
133	$O_2(a\,^1\Delta_g) + O_2(b\,^1\Sigma_g^+) \rightarrow O_2 + O_2(b\,^1\Sigma_g^+)$	2.7×10^{-23}		[22] [a]
134	$2O_2(b\,^1\Sigma_g^+) \rightarrow O_2 + O_2(b\,^1\Sigma_g^+)$	2.7×10^{-23}		[22] [a]
135	$O_2(a\,^1\Delta_g) + O_3 \rightarrow O + 2O_2$	$5.2 \times 10^{-17} \exp(-284/T_g)$		[22] [a]
136	$O_2(a\,^1\Delta_g) + O_3(\nu) \rightarrow O_2 + O_3$	5×10^{-17}		[22] [a]
137	$O_2(b\,^1\Sigma_g^+) + O_3 \rightarrow O + 2O_2$	$2.4 \times 10^{-17} \exp(-135/T_g)$		[22] [a]
138	$O_2(b\,^1\Sigma_g^+) + O_3 \rightarrow O_2 + O_3$	$5.5 \times 10^{-18} \exp(-135/T_g)$		[22] [a]
139	$O_2(b\,^1\Sigma_g^+) + O_3 \rightarrow O_2(a\,^1\Delta_g) + O_3$	$5.5 \times 10^{-18} \exp(-135/T_g)$		[22] [a]
140	$2O_3 \rightarrow O + O_2 + O_3$	$1.65 \times 10^{-15} \exp(-11435/T_g)$		[22] [a]
141	$O_3 + O_3(\nu) \rightarrow 2O_3$	1×10^{-19}		[22] [a]
143	$2e + O_2^+ \rightarrow e + O_2$	$2 \times 10^{-39} T_e^{-4.5}$		[22] [a]
149	$e + O_2 + O_2^+ \rightarrow 2O_2$	$3.3 \times 10^{-44} T_e^{-2.5}$		[22] [a]
151	$e + O_2^+ \rightarrow O + O(^1D)$	$9.1 \times 10^{-15} T_e^{-0.7}$		[22] [a]
155	$O + O^- \rightarrow e + O_2$	$2.3 \times 10^{-16}\,(T_g/300)^{-1.3}$		[22] [a]
162	$O(^1D) + O^- \rightarrow 2O + e$	7.4×10^{-16}		[22] [a]
198	$O^- + O_2 \rightarrow O_3 + e$	1×10^{-18}		[22] [a]
204	$O^- + O_2(a\,^1\Delta_g) \rightarrow O_3 + e$	6.1×10^{-17}		[22] [a]
206	$O^- + O_2(b\,^1\Sigma_g^+) \rightarrow O_3 + e$	6.1×10^{-17}		[22] [a]
207	$O^- + O_2^+ \rightarrow 3O$	$1.61 \times 10^{-14}\,(T_g/300)^{-1.1}$		[22] [a]
208	$O^- + O_2^+ \rightarrow O + O_2$	$1.61 \times 10^{-14}\,(T_g/300)^{-1.1}$		[22] [a]
209	$O^- + O_3 \rightarrow e + 2O_2$	3×10^{-16}		[22] [a]
237	$O_2^+ + O^- + O_2 \rightarrow O + 2O_2$	$1 \times 10^{-37}\,(T_g/300)^{-2.5}$		[22] [a]
238	$O_2^+ + O^- + O_2 \rightarrow O_2 + O_3$	$1 \times 10^{-37}\,(T_g/300)^{-2.5}$		[22] [a]
261	$He + He^* + O_2 \rightarrow e + 2He + O_2^+$	1.6×10^{-43}		[22] [a]
262	$He + He^* + O_2(a\,^1\Delta_g) \rightarrow e + 2He + O_2^+$	1.6×10^{-43}		[22] [a]
263	$He + He^* + O_2(b\,^1\Sigma_g^+) \rightarrow e + 2He + O_2^+$	1.6×10^{-43}		[22] [a]
264	$He + He^* + O_3 \rightarrow e + 2He + O + O_2^+$	1.6×10^{-43}		[22] [a]
265	$He + 2O \rightarrow He + O_2(a\,^1\Delta_g)$	$2 \times 10^{-45}\,(T_g/300)^{-1} \exp(-17/T_g)$		[22] [a]
266	$He + 2O \rightarrow He + O_2(b\,^1\Sigma_g^+)$	$2 \times 10^{-45}\,(T_g/300)^{-1} \exp(-17/T_g)$		[22] [a]
267	$He + O + O_2 \rightarrow He + O_3$	$9 \times 10^{-47}\,(T_g/300)^{-2.6}$		[22] [a]
268	$He + O + O_2 \rightarrow He + O_3(\nu)$	$2.1 \times 10^{-46}\,(T_g/300)^{-2.6}$		[22] [a]
269	$He + O + O_2(a\,^1\Delta_g) \rightarrow He + O + O_2$	4×10^{-45}		[22] [a]
270	$He + O(^1D) \rightarrow He + O$	1×10^{-21}		[22] [a]
273	$He + O_2(a\,^1\Delta_g) \rightarrow He + O_2$	5×10^{-27}		[22] [a]
275	$He + O_2(b\,^1\Sigma_g^+) \rightarrow He + O_2(a\,^1\Delta_g)$	4.3×10^{-24}		[22] [a]
277	$He + O_3 \rightarrow He + O + O_2$	$5.61 \times 10^{-16} \exp(-114/T_g)$		[22] [a]
278	$He + O_3(\nu) \rightarrow He + O_3$	6×10^{-20}		[22] [a]
282	$He^* + O_2 \rightarrow e + He + O_2^+$	2.6×10^{-16}		[22] [a]

Continued on next page

Table A.2 (*Continued*)

ID	Reaction	k	ΔE_e	Source
283	$\mathrm{He^* + O_2(a\,^1\Delta_g) \rightarrow e + He + O_2^+}$	2.6×10^{-16}		[22] [a]
284	$\mathrm{He^* + O_2(b\,^1\Sigma_g^+) \rightarrow e + He + O_2^+}$	2.6×10^{-16}		[22] [a]
285	$\mathrm{He^* + O_3 \rightarrow e + He + O + O_2^+}$	2.6×10^{-16}		[22] [a]
293	$\mathrm{e + He + O \rightarrow He + O^-}$	$1 \times 10^{-44} T_\mathrm{e}^{-0.5}$		[22] [a]
300	$\mathrm{He + He_2^+ + O^- \rightarrow 3He + O}$	$2 \times 10^{-37}\,(\mathrm{T_g}/300)^{-2.5}$		[22] [a]
301	$\mathrm{He + He_2^+ + O_2 \rightarrow 3He + O_2^+}$	3.5×10^{-41}		[22] [a]
310	$\mathrm{He + O^- \rightarrow e + He + O}$	$2.5 \times 10^{-24}\,(\mathrm{T_g}/300)^{-0.6}$		[22] [a]
312	$\mathrm{He + O^- + O_2^+ \rightarrow He + O + O_2}$	$2 \times 10^{-37}\,(\mathrm{T_g}/300)^{-2.5}$		[22] [a]
361	$\mathrm{He_2^+ + O^- \rightarrow 2He + O}$	$3.1 \times 10^{-14}\,(\mathrm{T_g}/300)^{-1.1}$		[22] [a]
362	$\mathrm{He_2^+ + O^- + O_2 \rightarrow 2He + O_2 + O}$	$2 \times 10^{-37}\,(\mathrm{T_g}/300)^{-2.5}$		[22] [a]
364	$\mathrm{He_2^+ + O_2 \rightarrow 2He + O_2^+}$	9×10^{-16}		[22] [a]
367	$\mathrm{He_2^+ + O_2(a\,^1\Delta_g) \rightarrow 2He + O_2^+}$	1.2×10^{-15}		[22] [a]
368	$\mathrm{He_2^+ + O_2(b\,^1\Sigma_g^+) \rightarrow 2He + O_2^+}$	1.2×10^{-15}		[22] [a]

Table A.3: Detailed chemistry set for the N_2–H_2 atm. pressure reduction cases. The reactions ID numbers are consistent with the source publication. The reaction rate coefficients k of order-m reactions are in $[\mathrm{m}^{3(m-1)}\mathrm{s}^{-1}]$. Gas temperature $\mathrm{T_g}$ is in [K]. The electron temperature T_e and electron energy loss ΔE_e are in [eV].
[a] Fitted from a cross section on a grid of Maxwellian temperatures.
[b] Original source not listed in QDB.
[c] Not the original source.
[d] Threshold energy ΔE_e taken from QDB.
[e] By detailed balance from the corresponding forward reaction.
[f] Expressed for $\mathrm{T_g} = 400$ K.
[g] Data not present in the source publication.
[h] With the assumption of $T_\mathrm{eff} = \mathrm{T_g}$.

ID	Reaction	k	ΔE_e	Source
1	$\mathrm{e + N_2 \rightarrow e + N_2(A\,^3\Sigma_u^+)}$	$2.19 \times 10^{-14} T_\mathrm{e}^{-0.61} \exp(-9.34/T_\mathrm{e})$	7.6	[9; 193][a]
1.1	$\mathrm{e + N_2 \rightarrow e + N_2(B\,^3\Pi_g)}$	$5.22 \times 10^{-14} T_\mathrm{e}^{-0.85} \exp(-10.5/T_\mathrm{e})$	8.55	[9; 193][a]
1.2	$\mathrm{e + N_2 \rightarrow e + N_2(a'\,^1\Sigma_u^-)}$	$1.97 \times 10^{-14} T_\mathrm{e}^{-0.95} \exp(-12/T_\mathrm{e})$	9.4	[9; 193][a]
1.3	$\mathrm{e + N_2 \rightarrow e + N_2(C\,^3\Pi_u)}$	$1.17 \times 10^{-13} T_\mathrm{e}^{-1.02} \exp(-13.6/T_\mathrm{e})$	11	[9; 193][a]
2	$\mathrm{e + H_2 \rightarrow e + H_2(b\,^3\Sigma_u^+)}$	$1.1 \times 10^{-13} T_\mathrm{e}^{-0.8} \exp(-11.6/T_\mathrm{e})$	8.9	[9][a,b]
2.1	$\mathrm{e + H_2 \rightarrow e + H_2(B\,^1\Sigma_u^+)}$	$3.77 \times 10^{-15} T_\mathrm{e}^{0.51} \exp(-12.5/T_\mathrm{e})$	11.3	[9; 194][a]
2.2	$\mathrm{e + H_2 \rightarrow e + H_2(c\,^3\Pi_u)}$	$9.77 \times 10^{-14} T_\mathrm{e}^{-0.95} \exp(-13.9/T_\mathrm{e})$	11.8	[9][a,b]
2.3	$\mathrm{e + H_2 \rightarrow e + H_2(a\,^3\Sigma_g^+)}$	$3.34 \times 10^{-14} T_\mathrm{e}^{-0.93} \exp(-14.1/T_\mathrm{e})$	11.8	[9][a,b]
3	$\mathrm{e + N_2 \rightarrow 2e + N_2^+}$	$1.08 \times 10^{-14} T_\mathrm{e}^{0.63} \exp(-16.6/T_\mathrm{e})$	15.5	[9; 193][a]
3.1	$\mathrm{e + H_2 \rightarrow 2e + H_2^+}$	$1.09 \times 10^{-14} T_\mathrm{e}^{0.46} \exp(-16/T_\mathrm{e})$	15.5	[9][a,b]
4	$\mathrm{e + N \rightarrow 2e + N^+}$	$3 \times 10^{-15} T_\mathrm{e}^{0.89} \exp(-13.1/T_\mathrm{e})$	14.5	[9; 195][a]
5	$\mathrm{e + H \rightarrow 2e + H^+}$	$6.5 \times 10^{-15} T_\mathrm{e}^{0.49} \exp(-12.89/T_\mathrm{e})$	13.6	[5][c,d]
6	$\mathrm{e + NH \rightarrow 2e + NH^+}$	$9.18 \times 10^{-15} T_\mathrm{e}^{0.72} \exp(-13.9/T_\mathrm{e})$	13.5	[9; 196][a]
7	$\mathrm{e + NH_2 \rightarrow 2e + NH_2^+}$	$2.78 \times 10^{-15} T_\mathrm{e}^{1.07} \exp(-9.27/T_\mathrm{e})$	11.2	[9; 196][a]
8	$\mathrm{e + NH_3 \rightarrow 2e + NH_3^+}$	$2.7 \times 10^{-15} T_\mathrm{e}^{0.88} \exp(-9.84/T_\mathrm{e})$	10.2	[9][a,b]
9	$\mathrm{e + N_2 \rightarrow e + N_2}(\nu_1)$	$3.09 \times 10^{-14} T_\mathrm{e}^{-1.44} \exp(-2.28/T_\mathrm{e})$	0.29	[9][a,b]
9.1	$\mathrm{e + N_2 \rightarrow e + N_2}(\nu_2)$	$1.83 \times 10^{-14} T_\mathrm{e}^{-1.46} \exp(-2.34/T_\mathrm{e})$	0.57	[9][a,b]
9.2	$\mathrm{e + N_2 \rightarrow e + N_2}(\nu_3)$	$1.29 \times 10^{-15} T_\mathrm{e}^{-1.47} \exp(-2.33/T_\mathrm{e})$	0.85	[9][a,b]
9.3	$\mathrm{e + N_2 \rightarrow e + N_2}(\nu_4)$	$9.31 \times 10^{-15} T_\mathrm{e}^{-1.48} \exp(-2.41/T_\mathrm{e})$	1.13	[9][a,b]
9.4	$\mathrm{e + N_2 \rightarrow e + N_2}(\nu_5)$	$8.14 \times 10^{-15} T_\mathrm{e}^{-1.48} \exp(-2.48/T_\mathrm{e})$	1.8	[9][a,b]
9.5	$\mathrm{e + N_2 \rightarrow e + N_2}(\nu_6)$	$7.13 \times 10^{-15} T_\mathrm{e}^{-1.49} \exp(-2.58/T_\mathrm{e})$	1.68	[9][a,b]
9.6	$\mathrm{e + N_2 \rightarrow e + N_2}(\nu_7)$	$4.07 \times 10^{-15} T_\mathrm{e}^{-1.49} \exp(-2.72/T_\mathrm{e})$	1.95	[9][a,b]
9.7	$\mathrm{e + N_2 \rightarrow e + N_2}(\nu_8)$	$1.98 \times 10^{-15} T_\mathrm{e}^{-1.49} \exp(-2.87/T_\mathrm{e})$	2.21	[9][a,b]
9.8	$\mathrm{e + N_2}(\nu_1) \rightarrow \mathrm{e + N_2}$	$3.09 \times 10^{-14} T_\mathrm{e}^{-1.44} \exp(-1.99/T_\mathrm{e})$	-0.29	[e]

Continued on next page

Table A.3 (*Continued*)

ID	Reaction	k	ΔE_e	Source
9.9	$e + N_2(\nu_2) \rightarrow e + N_2$	$1.83 \times 10^{-14} T_e^{-1.46} \exp(-1.77/T_e)$	-0.57	[e]
9.10	$e + N_2(\nu_3) \rightarrow e + N_2$	$1.29 \times 10^{-15} T_e^{-1.47} \exp(-1.48/T_e)$	-0.85	[e]
9.11	$e + N_2(\nu_4) \rightarrow e + N_2$	$9.31 \times 10^{-15} T_e^{-1.48} \exp(-1.28/T_e)$	-1.13	[e]
9.12	$e + N_2(\nu_5) \rightarrow e + N_2$	$8.14 \times 10^{-15} T_e^{-1.48} \exp(-0.68/T_e)$	-1.8	[e]
9.13	$e + N_2(\nu_6) \rightarrow e + N_2$	$7.13 \times 10^{-15} T_e^{-1.49} \exp(-0.9/T_e)$	-1.68	[e]
9.14	$e + N_2(\nu_7) \rightarrow e + N_2$	$4.07 \times 10^{-15} T_e^{-1.49} \exp(-0.77/T_e)$	-1.95	[e]
9.15	$e + N_2(\nu_8) \rightarrow e + N_2$	$1.98 \times 10^{-15} T_e^{-1.49} \exp(-0.66/T_e)$	-2.21	[e]
10	$e + H_2 \rightarrow e + H_2(\nu_1)$	$1.67 \times 10^{-14} T_e^{-0.86} \exp(-2.32/T_e)$	0.52	[9; 197][a]
10.1	$e + H_2 \rightarrow e + H_2(\nu_2)$	$2.62 \times 10^{-15} T_e^{-1.13} \exp(-3.85/T_e)$	1	[9; 197][a]
10.2	$e + H_2 \rightarrow e + H_2(\nu_3)$	$2.42 \times 10^{-16} T_e^{-1.04} \exp(-3.34/T_e)$	1.5	[47; 198][a]
10.3	$e + H_2(\nu_1) \rightarrow e + H_2$	$1.67 \times 10^{-14} T_e^{-0.86} \exp(-1.8/T_e)$	-0.52	[e]
10.4	$e + H_2(\nu_2) \rightarrow e + H_2$	$2.62 \times 10^{-15} T_e^{-1.13} \exp(-2.85/T_e)$	-1	[e]
10.5	$e + H_2(\nu_3) \rightarrow e + H_2$	$2.42 \times 10^{-16} T_e^{-1.04} \exp(-1.84/T_e)$	-1.5	[e]
11	$N_2(\nu_1) + N_2 \rightarrow 2N_2$	2.48×10^{-27}		[5][c,f]
11.1	$N_2(\nu_1) + H_2 \rightarrow N_2 + H_2$	3.94×10^{-22}		[5][c,f]
11.2	$N_2(\nu_1) + N \rightarrow N_2 + N$	9.91×10^{-24}		[5][c,f]
11.3	$N_2(\nu_1) + H \rightarrow N_2 + H$	7.99×10^{-24}		[5][c,f]
11.4	$N_2(\nu_2) + N_2 \rightarrow N_2(\nu_1) + N_2$	9.94×10^{-27}		[5][c,f]
11.5	$N_2(\nu_2) + H_2 \rightarrow N_2(\nu_1) + H_2$	1.34×10^{-21}		[5][c,f]
11.6	$N_2(\nu_2) + N \rightarrow N_2(\nu_1) + N$	1.7×10^{-23}		[5][c,f]
11.7	$N_2(\nu_2) + H \rightarrow N_2(\nu_1) + H$	1.9×10^{-23}		[5][c,f]
11.8	$N_2(\nu_3) + N_2 \rightarrow N_2(\nu_2) + N_2$	1.77×10^{-26}		[5][c,f]
11.9	$N_2(\nu_3) + H_2 \rightarrow N_2(\nu_2) + H_2$	2.02×10^{-21}		[5][c,f]
11.10	$N_2(\nu_3) + N \rightarrow N_2(\nu_2) + N$	2.89×10^{-23}		[5][c,f]
11.11	$N_2(\nu_3) + H \rightarrow N_2(\nu_2) + H$	4.5×10^{-23}		[5][c,f]
11.12	$N_2(\nu_4) + N_2 \rightarrow N_2(\nu_3) + N_2$	2.97×10^{-26}		[5][c,f]
11.13	$N_2(\nu_4) + H_2 \rightarrow N_2(\nu_3) + H_2$	2.86×10^{-21}		[5][c,f]
11.14	$N_2(\nu_4) + N \rightarrow N_2(\nu_3) + N$	4.88×10^{-23}		[5][c,f]
11.15	$N_2(\nu_4) + H \rightarrow N_2(\nu_3) + H$	1.05×10^{-22}		[5][c,f]
11.16	$N_2(\nu_5) + N_2 \rightarrow N_2(\nu_4) + N_2$	4.77×10^{-26}		[5][c,f]
11.17	$N_2(\nu_5) + H_2 \rightarrow N_2(\nu_4) + H_2$	3.88×10^{-21}		[5][c,f]
11.18	$N_2(\nu_5) + N \rightarrow N_2(\nu_4) + N$	8.2×10^{-23}		[5][c,f]
11.19	$N_2(\nu_5) + H \rightarrow N_2(\nu_4) + H$	2.42×10^{-22}		[5][c,f]
11.20	$N_2(\nu_6) + N_2 \rightarrow N_2(\nu_5) + N_2$	7.45×10^{-26}		[5][c,f]
11.21	$N_2(\nu_6) + H_2 \rightarrow N_2(\nu_5) + H_2$	5.13×10^{-21}		[5][c,f]
11.22	$N_2(\nu_6) + N \rightarrow N_2(\nu_5) + N$	1.37×10^{-22}		[5][c,f]
11.23	$N_2(\nu_6) + H \rightarrow N_2(\nu_5) + H$	5.53×10^{-22}		[5][c,f]
11.24	$N_2(\nu_7) + N_2 \rightarrow N_2(\nu_6) + N_2$	1.14×10^{-25}		[5][c,f]
11.25	$N_2(\nu_7) + H_2 \rightarrow N_2(\nu_6) + H_2$	6.65×10^{-21}		[5][c,f]
11.26	$N_2(\nu_7) + N \rightarrow N_2(\nu_6) + N$	2.27×10^{-22}		[5][c,f]
11.27	$N_2(\nu_7) + H \rightarrow N_2(\nu_6) + H$	1.25×10^{-21}		[5][c,f]
11.28	$N_2(\nu_8) + N_2 \rightarrow N_2(\nu_7) + N_2$	1.72×10^{-25}		[5][c,f]
11.29	$N_2(\nu_8) + H_2 \rightarrow N_2(\nu_7) + H_2$	8.47×10^{-21}		[5][c,f]
11.30	$N_2(\nu_8) + N \rightarrow N_2(\nu_7) + N$	3.73×10^{-22}		[5][c,f]
11.31	$N_2(\nu_8) + H \rightarrow N_2(\nu_7) + H$	2.8×10^{-21}		[5][c,f]
11.32	$2N_2 \rightarrow N_2(\nu_1) + N_2$	5.82×10^{-31}		[5][c,f]
11.33	$N_2 + H_2 \rightarrow N_2(\nu_1) + H_2$	9.24×10^{-26}		[5][c,f]
11.34	$N_2 + N \rightarrow N_2(\nu_1) + N$	2.33×10^{-27}		[5][c,f]
11.35	$N_2 + H \rightarrow N_2(\nu_1) + H$	1.88×10^{-27}		[5][c,f]
11.36	$N_2(\nu_1) + N_2 \rightarrow N_2(\nu_2) + N_2$	2.55×10^{-30}		[5][c,f]
11.37	$N_2(\nu_1) + H_2 \rightarrow N_2(\nu_2) + H_2$	3.43×10^{-25}		[5][c,f]
11.38	$N_2(\nu_1) + N \rightarrow N_2(\nu_2) + N$	4.35×10^{-27}		[5][c,f]
11.39	$N_2(\nu_1) + H \rightarrow N_2(\nu_2) + H$	4.88×10^{-27}		[5][c,f]
11.40	$N_2(\nu_2) + N_2 \rightarrow N_2(\nu_3) + N_2$	4.96×10^{-30}		[5][c,f]
11.41	$N_2(\nu_2) + H_2 \rightarrow N_2(\nu_3) + H_2$	5.64×10^{-25}		[5][c,f]
11.42	$N_2(\nu_2) + N \rightarrow N_2(\nu_3) + N$	8.08×10^{-27}		[5][c,f]
11.43	$N_2(\nu_2) + H \rightarrow N_2(\nu_3) + H$	1.26×10^{-26}		[5][c,f]
11.44	$N_2(\nu_3) + N_2 \rightarrow N_2(\nu_4) + N_2$	9.32×10^{-30}		[5][c,f]
11.45	$N_2(\nu_3) + H_2 \rightarrow N_2(\nu_4) + H_2$	8.97×10^{-25}		[5][c,f]
11.46	$N_2(\nu_3) + N \rightarrow N_2(\nu_4) + N$	1.53×10^{-26}		[5][c,f]

Continued on next page

Table A.3 (*Continued*)

ID	Reaction	k	ΔE_e	Source
11.47	$N_2(\nu_3) + H \rightarrow N_2(\nu_4) + H$	3.29×10^{-26}		[5][c,f]
11.48	$N_2(\nu_4) + N_2 \rightarrow N_2(\nu_5) + N_2$	1.63×10^{-29}		[5][c,f]
11.49	$N_2(\nu_4) + H_2 \rightarrow N_2(\nu_5) + H_2$	1.33×10^{-24}		[5][c,f]
11.50	$N_2(\nu_4) + N \rightarrow N_2(\nu_5) + N$	2.81×10^{-26}		[5][c,f]
11.51	$N_2(\nu_4) + H \rightarrow N_2(\nu_5) + H$	8.3×10^{-26}		[5][c,f]
11.52	$N_2(\nu_5) + N_2 \rightarrow N_2(\nu_6) + N_2$	2.87×10^{-29}		[5][c,f]
11.53	$N_2(\nu_5) + H_2 \rightarrow N_2(\nu_6) + H_2$	1.97×10^{-24}		[5][c,f]
11.54	$N_2(\nu_5) + N \rightarrow N_2(\nu_6) + N$	5.26×10^{-26}		[5][c,f]
11.55	$N_2(\nu_5) + H \rightarrow N_2(\nu_6) + H$	2.13×10^{-25}		[5][c,f]
11.56	$N_2(\nu_6) + N_2 \rightarrow N_2(\nu_7) + N_2$	4.78×10^{-29}		[5][c,f]
11.57	$N_2(\nu_6) + H_2 \rightarrow N_2(\nu_7) + H_2$	2.79×10^{-24}		[5][c,f]
11.58	$N_2(\nu_6) + N \rightarrow N_2(\nu_7) + N$	9.51×10^{-26}		[5][c,f]
11.59	$N_2(\nu_6) + H \rightarrow N_2(\nu_7) + H$	5.25×10^{-25}		[5][c,f]
11.60	$N_2(\nu_7) + N_2 \rightarrow N_2(\nu_8) + N_2$	8.09×10^{-29}		[5][c,f]
11.61	$N_2(\nu_7) + H_2 \rightarrow N_2(\nu_8) + H_2$	3.99×10^{-24}		[5][c,f]
11.62	$N_2(\nu_7) + N \rightarrow N_2(\nu_8) + N$	1.76×10^{-25}		[5][c,f]
11.63	$N_2(\nu_7) + H \rightarrow N_2(\nu_8) + H$	1.32×10^{-24}		[5][c,f]
12.1	$H_2(\nu_1) + H_2 \rightarrow 2H_2$	4.38×10^{-22}		[5][c,f]
12.3	$H_2(\nu_1) + H \rightarrow H_2 + H$	6.25×10^{-24}		[5][c,f]
12.5	$H_2(\nu_2) + H_2 \rightarrow H_2(\nu_1) + H_2$	2.14×10^{-21}		[5][c,f]
12.7	$H_2(\nu_2) + H \rightarrow H_2(\nu_1) + H$	2.58×10^{-23}		[5][c,f]
12.9	$H_2(\nu_3) + H_2 \rightarrow H_2(\nu_2) + H_2$	4.67×10^{-21}		[5][c,f]
12.11	$H_2(\nu_3) + H \rightarrow H_2(\nu_2) + H$	8.01×10^{-23}		[5][c,f]
12.13	$2H_2 \rightarrow H_2(\nu_1) + H_2$	1.38×10^{-28}		[5][c,f]
12.15	$H_2 + H \rightarrow H_2(\nu_1) + H$	1.97×10^{-30}		[5][c,f]
12.17	$H_2(\nu_1) + H_2 \rightarrow H_2(\nu_2) + H_2$	1.71×10^{-27}		[5][c,f]
12.19	$H_2(\nu_1) + H \rightarrow H_2(\nu_2) + H$	2.05×10^{-29}		[5][c,f]
12.21	$H_2(\nu_2) + H_2 \rightarrow H_2(\nu_3) + H_2$	2.34×10^{-27}		[5][c,f]
12.23	$H_2(\nu_2) + H \rightarrow H_2(\nu_3) + H$	4.01×10^{-29}		[5][c,f]
13	$2N_2(\nu_1) \rightarrow N_2 + N_2(\nu_2)$	6.51×10^{-20}		[5][c,f]
13.1	$N_2(\nu_1) + N_2(\nu_2) \rightarrow N_2 + N_2(\nu_3)$	7.95×10^{-20}		[5][c,f]
13.2	$N_2(\nu_1) + N_2(\nu_3) \rightarrow N_2 + N_2(\nu_4)$	7.74×10^{-20}		[5][c,f]
13.3	$N_2(\nu_1) + N_2(\nu_4) \rightarrow N_2 + N_2(\nu_5)$	7.53×10^{-20}		[5][c,f]
13.4	$N_2(\nu_1) + N_2(\nu_5) \rightarrow N_2 + N_2(\nu_6)$	6.35×10^{-20}		[5][c,f]
13.5	$N_2(\nu_1) + N_2(\nu_6) \rightarrow N_2 + N_2(\nu_7)$	5.66×10^{-20}		[5][c,f]
13.6	$N_2(\nu_1) + N_2(\nu_7) \rightarrow N_2 + N_2(\nu_8)$	4.47×10^{-20}		[5][c,f]
13.7	$N_2(\nu_2) + N_2 \rightarrow 2N_2(\nu_1)$	8.61×10^{-20}		[5][c,f]
13.8	$2N_2(\nu_2) \rightarrow N_2(\nu_1) + N_2(\nu_3)$	1.98×10^{-19}		[5][c,f]
13.9	$N_2(\nu_2) + N_2(\nu_3) \rightarrow N_2(\nu_1) + N_2(\nu_4)$	1.99×10^{-19}		[5][c,f]
13.10	$N_2(\nu_2) + N_2(\nu_4) \rightarrow N_2(\nu_1) + N_2(\nu_5)$	1.96×10^{-19}		[5][c,f]
13.11	$N_2(\nu_2) + N_2(\nu_5) \rightarrow N_2(\nu_1) + N_2(\nu_6)$	1.67×10^{-19}		[5][c,f]
13.12	$N_2(\nu_2) + N_2(\nu_6) \rightarrow N_2(\nu_1) + N_2(\nu_7)$	1.5×10^{-19}		[5][c,f]
13.13	$N_2(\nu_2) + N_2(\nu_7) \rightarrow N_2(\nu_1) + N_2(\nu_8)$	1.19×10^{-19}		[5][c,f]
13.14	$N_2(\nu_3) + N_2 \rightarrow N_2(\nu_2) + N_2(\nu_1)$	1.26×10^{-19}		[5][c,f]
13.15	$N_2(\nu_3) + N_2(\nu_1) \rightarrow 2N_2(\nu_2)$	2.62×10^{-19}		[5][c,f]
13.16	$2N_2(\nu_3) \rightarrow N_2(\nu_2) + N_2(\nu_4)$	3.74×10^{-19}		[5][c,f]
13.17	$N_2(\nu_3) + N_2(\nu_4) \rightarrow N_2(\nu_2) + N_2(\nu_5)$	3.77×10^{-19}		[5][c,f]
13.18	$N_2(\nu_3) + N_2(\nu_5) \rightarrow N_2(\nu_2) + N_2(\nu_6)$	3.28×10^{-19}		[5][c,f]
13.19	$N_2(\nu_3) + N_2(\nu_6) \rightarrow N_2(\nu_2) + N_2(\nu_7)$	2.96×10^{-19}		[5][c,f]
13.20	$N_2(\nu_3) + N_2(\nu_7) \rightarrow N_2(\nu_2) + N_2(\nu_8)$	2.37×10^{-19}		[5][c,f]
13.21	$N_2(\nu_4) + N_2 \rightarrow N_2(\nu_3) + N_2(\nu_1)$	7.16×10^{-20}		[5][c,f]
13.22	$N_2(\nu_4) + N_2(\nu_1) \rightarrow N_2(\nu_3) + N_2(\nu_2)$	3.18×10^{-19}		[5][c,f]
13.23	$N_2(\nu_4) + N_2(\nu_2) \rightarrow 2N_2(\nu_3)$	5.35×10^{-19}		[5][c,f]
13.24	$2N_2(\nu_4) \rightarrow N_2(\nu_3) + N_2(\nu_5)$	6.75×10^{-19}		[5][c,f]
13.25	$N_2(\nu_4) + N_2(\nu_5) \rightarrow N_2(\nu_3) + N_2(\nu_6)$	6.1×10^{-19}		[5][c,f]
13.26	$N_2(\nu_4) + N_2(\nu_6) \rightarrow N_2(\nu_3) + N_2(\nu_7)$	5.62×10^{-19}		[5][c,f]
13.27	$N_2(\nu_4) + N_2(\nu_7) \rightarrow N_2(\nu_3) + N_2(\nu_8)$	4.57×10^{-19}		[5][c,f]
13.28	$N_2(\nu_5) + N_2 \rightarrow N_2(\nu_4) + N_2(\nu_1)$	5.97×10^{-20}		[5][c,f]
13.29	$N_2(\nu_5) + N_2(\nu_1) \rightarrow N_2(\nu_4) + N_2(\nu_2)$	6.68×10^{-20}		[5][c,f]
13.30	$N_2(\nu_5) + N_2(\nu_2) \rightarrow N_2(\nu_4) + N_2(\nu_3)$	5.79×10^{-20}		[5][c,f]

Continued on next page

Table A.3 (*Continued*)

ID	Reaction	k	ΔE_e	Source
13.31	$N_2(\nu_5) + N_2(\nu_3) \rightarrow 2N_2(\nu_4)$	5.16×10^{-20}		[5][c,f]
13.32	$2N_2(\nu_5) \rightarrow N_2(\nu_4) + N_2(\nu_6)$	3.88×10^{-20}		[5][c,f]
13.33	$N_2(\nu_5) + N_2(\nu_6) \rightarrow N_2(\nu_4) + N_2(\nu_7)$	3.17×10^{-20}		[5][c,f]
13.34	$N_2(\nu_5) + N_2(\nu_7) \rightarrow N_2(\nu_4) + N_2(\nu_8)$	2.23×10^{-20}		[5][c,f]
13.35	$N_2(\nu_6) + N_2 \rightarrow N_2(\nu_5) + N_2(\nu_1)$	9.4×10^{-20}		[5][c,f]
13.36	$N_2(\nu_6) + N_2(\nu_1) \rightarrow N_2(\nu_5) + N_2(\nu_2)$	1.81×10^{-19}		[5][c,f]
13.37	$N_2(\nu_6) + N_2(\nu_2) \rightarrow N_2(\nu_5) + N_2(\nu_3)$	1.62×10^{-19}		[5][c,f]
13.38	$N_2(\nu_6) + N_2(\nu_3) \rightarrow N_2(\nu_5) + N_2(\nu_4)$	1.47×10^{-19}		[5][c,f]
13.39	$N_2(\nu_6) + N_2(\nu_4) \rightarrow 2N_2(\nu_5)$	1.12×10^{-19}		[5][c,f]
13.40	$2N_2(\nu_6) \rightarrow N_2(\nu_5) + N_2(\nu_7)$	9.16×10^{-20}		[5][c,f]
13.41	$N_2(\nu_6) + N_2(\nu_7) \rightarrow N_2(\nu_5) + N_2(\nu_8)$	6.48×10^{-20}		[5][c,f]
13.42	$N_2(\nu_7) + N_2 \rightarrow N_2(\nu_6) + N_2(\nu_1)$	1.5×10^{-19}		[5][c,f]
13.43	$N_2(\nu_7) + N_2(\nu_1) \rightarrow N_2(\nu_6) + N_2(\nu_2)$	2.85×10^{-19}		[5][c,f]
13.44	$N_2(\nu_7) + N_2(\nu_2) \rightarrow N_2(\nu_6) + N_2(\nu_3)$	3.33×10^{-19}		[5][c,f]
13.45	$N_2(\nu_7) + N_2(\nu_3) \rightarrow N_2(\nu_6) + N_2(\nu_4)$	3.08×10^{-19}		[5][c,f]
13.46	$N_2(\nu_7) + N_2(\nu_4) \rightarrow N_2(\nu_6) + N_2(\nu_5)$	2.38×10^{-19}		[5][c,f]
13.47	$N_2(\nu_7) + N_2(\nu_5) \rightarrow 2N_2(\nu_6)$	1.97×10^{-19}		[5][c,f]
13.48	$2N_2(\nu_7) \rightarrow N_2(\nu_6) + N_2(\nu_8)$	1.41×10^{-19}		[5][c,f]
13.49	$N_2(\nu_8) + N_2 \rightarrow N_2(\nu_7) + N_2(\nu_1)$	9.58×10^{-20}		[5][c,f]
13.50	$N_2(\nu_8) + N_2(\nu_1) \rightarrow N_2(\nu_7) + N_2(\nu_2)$	3.9×10^{-19}		[5][c,f]
13.51	$N_2(\nu_8) + N_2(\nu_2) \rightarrow N_2(\nu_7) + N_2(\nu_3)$	6.01×10^{-19}		[5][c,f]
13.52	$N_2(\nu_8) + N_2(\nu_3) \rightarrow N_2(\nu_7) + N_2(\nu_4)$	6.19×10^{-19}		[5][c,f]
13.53	$N_2(\nu_8) + N_2(\nu_4) \rightarrow N_2(\nu_7) + N_2(\nu_5)$	4.98×10^{-19}		[5][c,f]
13.54	$N_2(\nu_8) + N_2(\nu_5) \rightarrow N_2(\nu_7) + N_2(\nu_6)$	4.2×10^{-19}		[5][c,f]
13.55	$N_2(\nu_8) + N_2(\nu_6) \rightarrow 2N_2(\nu_7)$	3.04×10^{-19}		[5][c,f]
14	$2H_2(\nu_1) \rightarrow H_2 + H_2(\nu_2)$			[5][c,g]
14.1	$H_2(\nu_1) + H_2(\nu_2) \rightarrow H_2 + H_2(\nu_3)$			[5][c,g]
14.2	$H_2(\nu_2) + H_2 \rightarrow 2H_2(\nu_1)$			[5][c,g]
14.3	$2H_2(\nu_2) \rightarrow H_2(\nu_1) + H_2(\nu_3)$			[5][c,g]
14.4	$H_2(\nu_3) + H_2 \rightarrow H_2(\nu_2) + H_2(\nu_1)$			[5][c,g]
14.5	$H_2(\nu_3) + H_2(\nu_1) \rightarrow 2H_2(\nu_2)$			[5][c,g]
15	$N_2 + H_2(\nu_1) \rightarrow N_2(\nu_1) + H_2$	4.15×10^{-22}		[5][c,f]
15.1	$N_2 + H_2(\nu_2) \rightarrow N_2(\nu_1) + H_2(\nu_1)$	2.24×10^{-21}		[5][c,f]
15.2	$N_2 + H_2(\nu_3) \rightarrow N_2(\nu_1) + H_2(\nu_2)$	2.1×10^{-21}		[5][c,f]
15.3	$N_2(\nu_1) + H_2(\nu_1) \rightarrow N_2(\nu_2) + H_2$	7.62×10^{-22}		[5][c,f]
15.4	$N_2(\nu_1) + H_2(\nu_2) \rightarrow N_2(\nu_2) + H_2(\nu_1)$	4.12×10^{-21}		[5][c,f]
15.5	$N_2(\nu_1) + H_2(\nu_3) \rightarrow N_2(\nu_2) + H_2(\nu_2)$	3.86×10^{-21}		[5][c,f]
15.6	$N_2(\nu_2) + H_2(\nu_1) \rightarrow N_2(\nu_3) + H_2$	1.05×10^{-21}		[5][c,f]
15.7	$N_2(\nu_2) + H_2(\nu_2) \rightarrow N_2(\nu_3) + H_2(\nu_1)$	5.68×10^{-21}		[5][c,f]
15.8	$N_2(\nu_2) + H_2(\nu_3) \rightarrow N_2(\nu_3) + H_2(\nu_2)$	5.32×10^{-21}		[5][c,f]
15.9	$N_2(\nu_3) + H_2(\nu_1) \rightarrow N_2(\nu_4) + H_2$	1.25×10^{-21}		[5][c,f]
15.10	$N_2(\nu_3) + H_2(\nu_2) \rightarrow N_2(\nu_4) + H_2(\nu_1)$	6.74×10^{-21}		[5][c,f]
15.11	$N_2(\nu_3) + H_2(\nu_3) \rightarrow N_2(\nu_4) + H_2(\nu_2)$	6.31×10^{-21}		[5][c,f]
15.12	$N_2(\nu_4) + H_2(\nu_1) \rightarrow N_2(\nu_5) + H_2$	1.43×10^{-21}		[5][c,f]
15.13	$N_2(\nu_4) + H_2(\nu_2) \rightarrow N_2(\nu_5) + H_2(\nu_1)$	7.73×10^{-21}		[5][c,f]
15.14	$N_2(\nu_4) + H_2(\nu_3) \rightarrow N_2(\nu_5) + H_2(\nu_2)$	7.24×10^{-21}		[5][c,f]
15.15	$N_2(\nu_5) + H_2(\nu_1) \rightarrow N_2(\nu_6) + H_2$	1.53×10^{-21}		[5][c,f]
15.16	$N_2(\nu_5) + H_2(\nu_2) \rightarrow N_2(\nu_6) + H_2(\nu_1)$	8.26×10^{-21}		[5][c,f]
15.17	$N_2(\nu_5) + H_2(\nu_3) \rightarrow N_2(\nu_6) + H_2(\nu_2)$	7.74×10^{-21}		[5][c,f]
15.18	$N_2(\nu_6) + H_2(\nu_1) \rightarrow N_2(\nu_7) + H_2$	1.64×10^{-21}		[5][c,f]
15.19	$N_2(\nu_6) + H_2(\nu_2) \rightarrow N_2(\nu_7) + H_2(\nu_1)$	8.85×10^{-21}		[5][c,f]
15.20	$N_2(\nu_6) + H_2(\nu_3) \rightarrow N_2(\nu_7) + H_2(\nu_2)$	8.29×10^{-21}		[5][c,f]
15.21	$N_2(\nu_7) + H_2(\nu_1) \rightarrow N_2(\nu_8) + H_2$	1.66×10^{-21}		[5][c,f]
15.22	$N_2(\nu_7) + H_2(\nu_2) \rightarrow N_2(\nu_8) + H_2(\nu_1)$	9.01×10^{-21}		[5][c,f]
15.23	$N_2(\nu_7) + H_2(\nu_3) \rightarrow N_2(\nu_8) + H_2(\nu_2)$	8.43×10^{-21}		[5][c,f]
15.24	$N_2(\nu_1) + H_2 \rightarrow N_2 + H_2(\nu_1)$	5.56×10^{-25}		[5][c,f]
15.25	$N_2(\nu_1) + H_2(\nu_1) \rightarrow N_2 + H_2(\nu_2)$	7.61×10^{-24}		[5][c,f]
15.26	$N_2(\nu_1) + H_2(\nu_2) \rightarrow N_2 + H_2(\nu_3)$	4.48×10^{-24}		[5][c,f]
15.27	$N_2(\nu_2) + H_2 \rightarrow N_2(\nu_1) + H_2(\nu_1)$	9.36×10^{-25}		[5][c,f]
15.28	$N_2(\nu_2) + H_2(\nu_1) \rightarrow N_2(\nu_1) + H_2(\nu_2)$	1.28×10^{-23}		[5][c,f]

Continued on next page

Table A.3 (*Continued*)

ID	Reaction	k	ΔE_e	Source
15.29	$N_2(\nu_2) + H_2(\nu_2) \rightarrow N_2(\nu_1) + H_2(\nu_3)$	7.54×10^{-24}		[5][c,f]
15.30	$N_2(\nu_3) + H_2 \rightarrow N_2(\nu_2) + H_2(\nu_1)$	1.18×10^{-24}		[5][c,f]
15.31	$N_2(\nu_3) + H_2(\nu_1) \rightarrow N_2(\nu_2) + H_2(\nu_2)$	1.62×10^{-23}		[5][c,f]
15.32	$N_2(\nu_3) + H_2(\nu_2) \rightarrow N_2(\nu_2) + H_2(\nu_3)$	9.52×10^{-24}		[5][c,f]
15.33	$N_2(\nu_4) + H_2 \rightarrow N_2(\nu_3) + H_2(\nu_1)$	1.25×10^{-24}		[5][c,f]
15.34	$N_2(\nu_4) + H_2(\nu_1) \rightarrow N_2(\nu_3) + H_2(\nu_2)$	1.71×10^{-23}		[5][c,f]
15.35	$N_2(\nu_4) + H_2(\nu_2) \rightarrow N_2(\nu_3) + H_2(\nu_3)$	1.01×10^{-23}		[5][c,f]
15.36	$N_2(\nu_5) + H_2 \rightarrow N_2(\nu_4) + H_2(\nu_1)$	1.31×10^{-24}		[5][c,f]
15.37	$N_2(\nu_5) + H_2(\nu_1) \rightarrow N_2(\nu_4) + H_2(\nu_2)$	1.8×10^{-23}		[5][c,f]
15.38	$N_2(\nu_5) + H_2(\nu_2) \rightarrow N_2(\nu_4) + H_2(\nu_3)$	1.06×10^{-23}		[5][c,f]
15.39	$N_2(\nu_6) + H_2 \rightarrow N_2(\nu_5) + H_2(\nu_1)$	1.25×10^{-24}		[5][c,f]
15.40	$N_2(\nu_6) + H_2(\nu_1) \rightarrow N_2(\nu_5) + H_2(\nu_2)$	1.71×10^{-23}		[5][c,f]
15.41	$N_2(\nu_6) + H_2(\nu_2) \rightarrow N_2(\nu_5) + H_2(\nu_3)$	1.01×10^{-23}		[5][c,f]
15.42	$N_2(\nu_7) + H_2 \rightarrow N_2(\nu_6) + H_2(\nu_1)$	1.23×10^{-24}		[5][c,f]
15.43	$N_2(\nu_7) + H_2(\nu_1) \rightarrow N_2(\nu_6) + H_2(\nu_2)$	1.68×10^{-23}		[5][c,f]
15.44	$N_2(\nu_7) + H_2(\nu_2) \rightarrow N_2(\nu_6) + H_2(\nu_3)$	9.89×10^{-24}		[5][c,f]
15.45	$N_2(\nu_8) + H_2 \rightarrow N_2(\nu_7) + H_2(\nu_1)$	1.11×10^{-24}		[5][c,f]
15.46	$N_2(\nu_8) + H_2(\nu_1) \rightarrow N_2(\nu_7) + H_2(\nu_2)$	1.52×10^{-23}		[5][c,f]
15.47	$N_2(\nu_8) + H_2(\nu_2) \rightarrow N_2(\nu_7) + H_2(\nu_3)$	8.96×10^{-24}		[5][c,f]
16	$H_2 + N_2(\nu_2) \rightarrow H_2(\nu_1) + N_2$	5.03×10^{-22}		[5][c,f]
16.1	$H_2 + N_2(\nu_3) \rightarrow H_2(\nu_1) + N_2(\nu_1)$	1.84×10^{-21}		[5][c,f]
16.2	$H_2 + N_2(\nu_4) \rightarrow H_2(\nu_1) + N_2(\nu_2)$	4.62×10^{-21}		[5][c,f]
16.3	$H_2 + N_2(\nu_5) \rightarrow H_2(\nu_1) + N_2(\nu_3)$	9.66×10^{-21}		[5][c,f]
16.4	$H_2 + N_2(\nu_6) \rightarrow H_2(\nu_1) + N_2(\nu_4)$	1.81×10^{-20}		[5][c,f]
16.5	$H_2 + N_2(\nu_7) \rightarrow H_2(\nu_1) + N_2(\nu_5)$	3.15×10^{-20}		[5][c,f]
16.6	$H_2 + N_2(\nu_8) \rightarrow H_2(\nu_1) + N_2(\nu_6)$	5.19×10^{-20}		[5][c,f]
16.7	$H_2(\nu_1) + N_2(\nu_2) \rightarrow H_2(\nu_2) + N_2$	1.02×10^{-21}		[5][c,f]
16.8	$H_2(\nu_1) + N_2(\nu_3) \rightarrow H_2(\nu_2) + N_2(\nu_1)$	3.75×10^{-21}		[5][c,f]
16.9	$H_2(\nu_1) + N_2(\nu_4) \rightarrow H_2(\nu_2) + N_2(\nu_2)$	9.41×10^{-21}		[5][c,f]
16.10	$H_2(\nu_1) + N_2(\nu_5) \rightarrow H_2(\nu_2) + N_2(\nu_3)$	1.97×10^{-20}		[5][c,f]
16.11	$H_2(\nu_1) + N_2(\nu_6) \rightarrow H_2(\nu_2) + N_2(\nu_4)$	3.68×10^{-20}		[5][c,f]
16.12	$H_2(\nu_1) + N_2(\nu_7) \rightarrow H_2(\nu_2) + N_2(\nu_5)$	6.41×10^{-20}		[5][c,f]
16.13	$H_2(\nu_1) + N_2(\nu_8) \rightarrow H_2(\nu_2) + N_2(\nu_6)$	1.06×10^{-19}		[5][c,f]
16.14	$H_2(\nu_2) + N_2(\nu_2) \rightarrow H_2(\nu_3) + N_2$	1.56×10^{-21}		[5][c,f]
16.15	$H_2(\nu_2) + N_2(\nu_3) \rightarrow H_2(\nu_3) + N_2(\nu_1)$	5.72×10^{-21}		[5][c,f]
16.16	$H_2(\nu_2) + N_2(\nu_4) \rightarrow H_2(\nu_3) + N_2(\nu_2)$	1.44×10^{-20}		[5][c,f]
16.17	$H_2(\nu_2) + N_2(\nu_5) \rightarrow H_2(\nu_3) + N_2(\nu_3)$	3×10^{-20}		[5][c,f]
16.18	$H_2(\nu_2) + N_2(\nu_6) \rightarrow H_2(\nu_3) + N_2(\nu_4)$	5.62×10^{-20}		[5][c,f]
16.19	$H_2(\nu_2) + N_2(\nu_7) \rightarrow H_2(\nu_3) + N_2(\nu_5)$	9.79×10^{-20}		[5][c,f]
16.20	$H_2(\nu_2) + N_2(\nu_8) \rightarrow H_2(\nu_3) + N_2(\nu_6)$	1.61×10^{-19}		[5][c,f]
16.21	$H_2(\nu_1) + N_2 \rightarrow H_2 + N_2(\nu_2)$	9.63×10^{-23}		[5][c,f]
16.22	$H_2(\nu_1) + N_2(\nu_1) \rightarrow H_2 + N_2(\nu_3)$	4.19×10^{-22}		[5][c,f]
16.23	$H_2(\nu_1) + N_2(\nu_2) \rightarrow H_2 + N_2(\nu_4)$	1.29×10^{-21}		[5][c,f]
16.24	$H_2(\nu_1) + N_2(\nu_3) \rightarrow H_2 + N_2(\nu_5)$	3.3×10^{-21}		[5][c,f]
16.25	$H_2(\nu_1) + N_2(\nu_4) \rightarrow H_2 + N_2(\nu_6)$	7.58×10^{-21}		[5][c,f]
16.26	$H_2(\nu_1) + N_2(\nu_5) \rightarrow H_2 + N_2(\nu_7)$	1.62×10^{-20}		[5][c,f]
16.27	$H_2(\nu_1) + N_2(\nu_6) \rightarrow H_2 + N_2(\nu_8)$	3.26×10^{-20}		[5][c,f]
16.28	$H_2(\nu_2) + N_2 \rightarrow H_2(\nu_1) + N_2(\nu_2)$	7.74×10^{-23}		[5][c,f]
16.29	$H_2(\nu_2) + N_2(\nu_1) \rightarrow H_2(\nu_1) + N_2(\nu_3)$	3.37×10^{-22}		[5][c,f]
16.30	$H_2(\nu_2) + N_2(\nu_2) \rightarrow H_2(\nu_1) + N_2(\nu_4)$	1.04×10^{-21}		[5][c,f]
16.31	$H_2(\nu_2) + N_2(\nu_3) \rightarrow H_2(\nu_1) + N_2(\nu_5)$	2.66×10^{-21}		[5][c,f]
16.32	$H_2(\nu_2) + N_2(\nu_4) \rightarrow H_2(\nu_1) + N_2(\nu_6)$	6.1×10^{-21}		[5][c,f]
16.33	$H_2(\nu_2) + N_2(\nu_5) \rightarrow H_2(\nu_1) + N_2(\nu_7)$	1.3×10^{-20}		[5][c,f]
16.34	$H_2(\nu_2) + N_2(\nu_6) \rightarrow H_2(\nu_1) + N_2(\nu_8)$	2.63×10^{-20}		[5][c,f]
16.35	$H_2(\nu_3) + N_2 \rightarrow H_2(\nu_2) + N_2(\nu_2)$	1.88×10^{-22}		[5][c,f]
16.36	$H_2(\nu_3) + N_2(\nu_1) \rightarrow H_2(\nu_2) + N_2(\nu_3)$	8.19×10^{-22}		[5][c,f]
16.37	$H_2(\nu_3) + N_2(\nu_2) \rightarrow H_2(\nu_2) + N_2(\nu_4)$	2.52×10^{-21}		[5][c,f]
16.38	$H_2(\nu_3) + N_2(\nu_3) \rightarrow H_2(\nu_2) + N_2(\nu_5)$	6.45×10^{-21}		[5][c,f]
16.39	$H_2(\nu_3) + N_2(\nu_4) \rightarrow H_2(\nu_2) + N_2(\nu_6)$	1.48×10^{-20}		[5][c,f]
16.40	$H_2(\nu_3) + N_2(\nu_5) \rightarrow H_2(\nu_2) + N_2(\nu_7)$	3.16×10^{-20}		[5][c,f]

Continued on next page

Table A.3 (*Continued*)

ID	Reaction	k	ΔE_e	Source
16.41	$H_2(\nu_3) + N_2(\nu_6) \rightarrow H_2(\nu_2) + N_2(\nu_8)$	6.38×10^{-20}		[5][c,f]
17	$N_2(A\,^3\Sigma_u^+) + N_2(\nu_6) \rightarrow N_2(B\,^3\Pi_g) + N_2$	3×10^{-17}		[5][c]
17.1	$N_2(A\,^3\Sigma_u^+) + N_2(\nu_7) \rightarrow N_2(B\,^3\Pi_g) + N_2(\nu_1)$	3×10^{-17}		[5][c]
17.2	$N_2(A\,^3\Sigma_u^+) + N_2(\nu_8) \rightarrow N_2(B\,^3\Pi_g) + N_2(\nu_2)$	3×10^{-17}		[5][c]
18	$N_2(B\,^3\Pi_g) + N_2 \rightarrow N_2(A\,^3\Sigma_u^+) + N_2(\nu_6)$	3×10^{-17}		[5][c]
18.1	$N_2(B\,^3\Pi_g) + N_2(\nu_1) \rightarrow N_2(A\,^3\Sigma_u^+) + N_2(\nu_7)$	3×10^{-17}		[5][c]
18.2	$N_2(B\,^3\Pi_g) + N_2(\nu_2) \rightarrow N_2(A\,^3\Sigma_u^+) + N_2(\nu_8)$	3×10^{-17}		[5][c]
19	$N_2(B\,^3\Pi_g) \rightarrow N_2(A\,^3\Sigma_u^+)$	1.34×10^{5}		[5][c]
20	$N_2(a'\,^1\Sigma_u^-) \rightarrow N_2$	1×10^{2}		[5][c]
21	$N_2(C\,^3\Pi_u) \rightarrow N_2(B\,^3\Pi_g)$	2.45×10^{7}		[5][c]
22	$e + N_2 \rightarrow 2N + e$	$5.15 \times 10^{-15} T_\mathrm{e}^{0.71} \exp(-14.2/T_\mathrm{e})$	12.5	[9][a,b]
23	$e + H_2 \rightarrow 2H + e$	$1.75 \times 10^{-13} T_\mathrm{e}^{-1.24} \exp(-12.59/T_\mathrm{e})$	11.4	[5][c,d]
24	$e + NH \rightarrow e + N + H$	$5 \times 10^{-14} T_\mathrm{e}^{0.5} \exp(-8.6/T_\mathrm{e})$	5.6	[5][c,d]
25	$e + NH_2 \rightarrow e + N + H_2$	$5 \times 10^{-14} T_\mathrm{e}^{0.5} \exp(-7.6/T_\mathrm{e})$	5.6	[5][c,d]
26	$e + NH_2 \rightarrow e + NH + H$	$5 \times 10^{-14} T_\mathrm{e}^{0.5} \exp(-7.6/T_\mathrm{e})$	5.6	[5][c,d]
27	$e + NH_3 \rightarrow e + NH_2 + H$	$5 \times 10^{-14} T_\mathrm{e}^{0.5} \exp(-4.4/T_\mathrm{e})$	5.6	[5][c,d]
28	$e + NH_3 \rightarrow e + NH + H_2$	$5 \times 10^{-14} T_\mathrm{e}^{0.5} \exp(-5.5/T_\mathrm{e})$	5.6	[5][c,d]
29	$e + N_2 \rightarrow 2e + N + N^+$	$1.31 \times 10^{-15} T_\mathrm{e}^{0.89} \exp(-24/T_\mathrm{e})$	21.3	[9][a,b]
30	$e + H_2 \rightarrow 2e + H + H^+$	$3 \times 10^{-14} T_\mathrm{e}^{0.44} \exp(-37.72/T_\mathrm{e})$	3	[5][c,d]
31	$e + N_2^+ \rightarrow 2N$	$2.17 \times 10^{-14} T_\mathrm{e}^{-0.39}$		[5][c]
32	$e + N_2^+ \rightarrow N + N(^2D)$	$1.95 \times 10^{-14} T_\mathrm{e}^{-0.39}$		[5][c]
33	$e + N_2^+ \rightarrow N + N(^2P)$	$2.17 \times 10^{-15} T_\mathrm{e}^{-0.39}$		[5][c]
34	$e + N_3^+ \rightarrow N_2 + N$	$3.22 \times 10^{-14} T_\mathrm{e}^{-0.5}$		[5][c]
35	$e + N_4^+ \rightarrow 2N_2$	$3.32 \times 10^{-13} T_\mathrm{e}^{-0.53}$		[5][c]
36	$e + H_2^+ \rightarrow 2H$	$4.94 \times 10^{-14} T_\mathrm{e}^{-0.5} \exp(-0.03/T_\mathrm{e})$		[9; 199][a]
37	$e + H_3^+ \rightarrow 3H$	$1.19 \times 10^{-15} T_\mathrm{e}^{-1.03} \exp(-0.08/T_\mathrm{e})$		[6; 9][a]
38	$e + H_3^+ \rightarrow H_2 + H$	$6.42 \times 10^{-14} T_\mathrm{e}^{-0.44} \exp(-0.02/T_\mathrm{e})$		[9; 200][a]
39	$e + NH^+ \rightarrow N + H$	$6.93 \times 10^{-15} T_\mathrm{e}^{-0.5}$		[5][c]
40	$e + NH_2^+ \rightarrow NH + H$	$2.37 \times 10^{-14} T_\mathrm{e}^{-0.4}$		[5][c]
41	$e + NH_2^+ \rightarrow N + 2H$	$4.6 \times 10^{-14} T_\mathrm{e}^{-0.4}$		[5][c]
42	$e + NH_3^+ \rightarrow NH + 2H$	$2.5 \times 10^{-14} T_\mathrm{e}^{-0.5}$		[5][c]
43	$e + NH_3^+ \rightarrow NH_2 + H$	$2.5 \times 10^{-14} T_\mathrm{e}^{-0.5}$		[5][c]
44	$e + NH_4^+ \rightarrow NH_3 + H$	$8.8 \times 10^{-14} T_\mathrm{e}^{-0.6}$		[5][c]
45	$e + NH_4^+ \rightarrow NH_2 + 2H$	$1.35 \times 10^{-14} T_\mathrm{e}^{-0.6}$		[5][c]
46	$e + N_2H^+ \rightarrow N_2 + H$	$5.13 \times 10^{-14} T_\mathrm{e}^{-0.72}$		[5][c]
47	$N_2^+ + H_2 \rightarrow N_2H^+ + H$	2×10^{-15}		[5][c]
48	$N_2^+ + N_2(A\,^3\Sigma_u^+) \rightarrow N_3^+ + N$	3×10^{-16}		[5][c]
49	$N_2^+ + N \rightarrow N^+ + N_2$	$7.2 \times 10^{-19} \left(T_\mathrm{g}/300\right)^{2.2}$		[5][c,h]
50	$N_2^+ + N_2 + N \rightarrow N_3^+ + N_2$	$9 \times 10^{-42} \exp\left(4/T_\mathrm{g}\right)$		[5][c,h]
51	$N_2^+ + 2N_2 \rightarrow N_4^+ + N_2$	$5.2 \times 10^{-41} \left(T_\mathrm{g}/300\right)^{-2.2}$		[5][c,h]
52	$N_2^+ + NH_3 \rightarrow NH_3^+ + N_2$	1.95×10^{-15}		[5][c]
53	$N_3^+ + N \rightarrow N_2^+ + N_2$	6.6×10^{-17}		[5][c]
54	$N_4^+ + N \rightarrow N^+ + 2N_2$	1×10^{-17}		[5][c]
55	$N_4^+ + N_2 \rightarrow N_2^+ + 2N_2$	5.73×10^{-21}		[5][c,f]
56	$N^+ + H_2 \rightarrow NH^+ + H$	5×10^{-16}		[5][c]
57	$N^+ + NH_3 \rightarrow NH_2^+ + NH$	4.7×10^{-16}		[5][c]
58	$N^+ + NH_3 \rightarrow NH_3^+ + N$	1.67×10^{-15}		[5][c]
59	$N^+ + NH_3 \rightarrow N_2H^+ + H_2$	2.12×10^{-16}		[5][c]
60	$H_2^+ + H \rightarrow H_2 + H^+$	6.4×10^{-16}		[5][c]
61	$H_2^+ + H_2 \rightarrow H_3^+ + H$	2×10^{-15}		[5][c]
62	$H_2^+ + NH_3 \rightarrow NH_3^+ + H_2$	5.7×10^{-15}		[5][c]
63	$H_2^+ + N_2 \rightarrow N_2H^+ + H$	2×10^{-15}		[5][c]
64	$H^+ + NH_3 \rightarrow NH_3^+ + H$	5.2×10^{-15}		[5][c]
65	$NH^+ + H_2 \rightarrow H_3^+ + N$	1.85×10^{-16}		[5][c]
66	$NH^+ + H_2 \rightarrow NH_2^+ + H$	1.05×10^{-15}		[5][c]
67	$NH^+ + NH_3 \rightarrow NH_3^+ + NH$	1.8×10^{-15}		[5][c]
68	$NH^+ + NH_3 \rightarrow NH_4^+ + N$	6×10^{-16}		[5][c]
69	$NH^+ + N_2 \rightarrow N_2H^+ + N$	6.5×10^{-16}		[5][c]
70	$NH_2^+ + H_2 \rightarrow NH_3^+ + H$	1.95×10^{-16}		[5][c]
71	$NH_2^+ + NH_3 \rightarrow NH_3^+ + NH_2$	1.15×10^{-15}		[5][c]

Continued on next page

Table A.3 (*Continued*)

ID	Reaction	k	ΔE_e	Source
72	$NH_2^+ + NH_3 \rightarrow NH_4^+ + NH$	1.15×10^{-15}		[5]c
73	$NH_3^+ + NH_3 \rightarrow NH_4^+ + NH_2$	2.1×10^{-15}		[5]c
74	$N_2H^+ + NH_3 \rightarrow NH_4^+ + N_2$	2.3×10^{-15}		[5]c
75	$N_2(A\,^3\Sigma_u^+) + N \rightarrow N_2 + N$	2×10^{-18}		[5]c
76	$N_2(A\,^3\Sigma_u^+) + N \rightarrow N_2 + N(^2P)$	$4 \times 10^{-17}\,(T_g/300)^{-0.66}$		[5]c
77	$N_2(A\,^3\Sigma_u^+) + N_2 \rightarrow 2N_2$	3×10^{-22}		[5]c
78	$2N_2(A\,^3\Sigma_u^+) \rightarrow N_2 + N_2(B\,^3\Pi_g)$	3×10^{-16}		[5]c
79	$2N_2(A\,^3\Sigma_u^+) \rightarrow N_2 + N_2(C\,^3\Pi_u)$	1.5×10^{-16}		[5]c
80	$2N_2(A\,^3\Sigma_u^+) \rightarrow N_2 + 2N$	3×10^{-17}		[5]c
82	$N_2(B\,^3\Pi_g) + N_2 \rightarrow N_2(A\,^3\Sigma_u^+) + N_2$	3×10^{-17}		[5]c
83	$N_2(B\,^3\Pi_g) + N_2 \rightarrow 2N_2$	2×10^{-18}		[5]c
84	$N_2(a'\,^1\Sigma_u^-) + N_2 \rightarrow N_2(B\,^3\Pi_g) + N_2$	1.9×10^{-19}		[5]c
85	$2N_2(a'\,^1\Sigma_u^-) \rightarrow N_2^+ + N_2 + e$	1×10^{-17}		[5]c
86	$2N_2(a'\,^1\Sigma_u^-) \rightarrow N_4^+ + e$	1×10^{-17}		[5]c
87	$N_2(a'\,^1\Sigma_u^-) + N_2(A\,^3\Sigma_u^+) \rightarrow N_4^+ + e$	4×10^{-18}		[5]c
88	$N(^2D) + N_2 \rightarrow N + N_2$	$2.3 \times 10^{-20} \exp(-51/T_g)$		[5]c
89	$N(^2P) + N \rightarrow 2N$	1.8×10^{-18}		[5]c
90	$N(^2P) + N \rightarrow N(^2D) + N$	6×10^{-19}		[5]c
91	$N(^2P) + N_2 \rightarrow N + N_2$	6×10^{-20}		[5]c
92	$N_2(A\,^3\Sigma_u^+) + H \rightarrow N_2 + H$	5×10^{-17}		[5]c
93	$N_2(A\,^3\Sigma_u^+) + H_2 \rightarrow N_2 + 2H$	$2 \times 10^{-16} \exp(-35/T_g)$		[5]c
94	$N_2(A\,^3\Sigma_u^+) + NH_3 \rightarrow N_2 + NH_3$	1.6×10^{-16}		[5]c
95	$N_2(B\,^3\Pi_g) + H_2 \rightarrow N_2(A\,^3\Sigma_u^+) + H_2$	2.5×10^{-17}		[5]c
96	$N_2(a'\,^1\Sigma_u^-) + H \rightarrow N_2 + H$	1.5×10^{-17}		[5]c
97	$N_2(a'\,^1\Sigma_u^-) + H_2 \rightarrow N_2 + 2H$	2.6×10^{-17}		[5]c
98	$N + H_2(\nu_1) \rightarrow H + NH$	$4 \times 10^{-16}\,(T_g/300)^{0.5} \exp(-14803/T_g)$		[5]c
98.1	$N + H_2(\nu_2) \rightarrow H + NH$	$4 \times 10^{-16}\,(T_g/300)^{0.5} \exp(-13118/T_g)$		[5]c
98.2	$N + H_2(\nu_3) \rightarrow H + NH$	$4 \times 10^{-16}\,(T_g/300)^{0.5} \exp(-11377/T_g)$		[5]c
98.3	$N + H_2(b\,^3\Sigma_u^+) \rightarrow H + NH$	$4 \times 10^{-16}\,(T_g/300)^{0.5}$		[5]c
98.4	$N + H_2(B\,^1\Sigma_u^+) \rightarrow H + NH$	$4 \times 10^{-16}\,(T_g/300)^{0.5}$		[5]c
98.5	$N + H_2(c\,^3\Pi_u) \rightarrow H + NH$	$4 \times 10^{-16}\,(T_g/300)^{0.5}$		[5]c
98.6	$N + H_2(a\,^3\Sigma_g^+) \rightarrow H + NH$	$4 \times 10^{-16}\,(T_g/300)^{0.5}$		[5]c
99	$N(^2D) + H_2 \rightarrow H + NH$	2.3×10^{-18}		[5]c
100	$N(^2D) + NH_3 \rightarrow NH + NH_2$	1.1×10^{-16}		[5]c
101	$N(^2P) + H_2 \rightarrow H + NH$	2.5×10^{-20}		[5]c
102	$N + NH \rightarrow H + N_2$	5×10^{-17}		[5]c
103	$H + NH \rightarrow H_2 + N$	$5.4 \times 10^{-17} \exp(-165/T_g)$		[5]c
104	$2NH \rightarrow H_2 + N_2$	$5 \times 10^{-20}\,(T_g/300)^1$		[5]c
105	$2NH \rightarrow N + NH_2$	$1.7 \times 10^{-18}\,(T_g/300)^{1.5}$		[5]c
106	$2NH \rightarrow N_2 + 2H$	8.5×10^{-17}		[5]c
107	$H + NH_2 \rightarrow H_2 + NH$	$6.6 \times 10^{-17} \exp(-184/T_g)$		[5]c
108	$N + NH_2 \rightarrow N_2 + 2H$	1.2×10^{-16}		[5]c
109	$N + NH_2 \rightarrow N_2 + H_2$	1.2×10^{-16}		[5]c
110	$NH + NH_2 \rightarrow NH_3 + N$	1.66×10^{-18}		[5]c
111	$H_2 + NH_2 \rightarrow NH_3 + H$	$5.4 \times 10^{-17} \exp(-6492/T_g)$		[5]c
112	$H + NH_3 \rightarrow NH_2 + H_2$	$8.4 \times 10^{-20}\,(T_g/300)^{4.1} \exp(-476/T_g)$		[5]c
113	$2N + N_2 \rightarrow N_2(A\,^3\Sigma_u^+) + N_2$	4.4×10^{-48}		[5]c
113.1	$2N + H_2 \rightarrow N_2(A\,^3\Sigma_u^+) + H_2$	4.4×10^{-48}		[5]c
114	$3N \rightarrow N_2(A\,^3\Sigma_u^+) + N$	2.6×10^{-47}		[5]c
114.1	$2N + H \rightarrow N_2(A\,^3\Sigma_u^+) + H$	2.6×10^{-47}		[5]c
115	$2N + N_2 \rightarrow N_2(B\,^3\Pi_g) + N_2$	6.2×10^{-48}		[5]c
115.1	$2N + H_2 \rightarrow N_2(B\,^3\Pi_g) + H_2$	6.2×10^{-48}		[5]c
116	$3N \rightarrow N_2(B\,^3\Pi_g) + N$	3.6×10^{-47}		[5]c
116.1	$2N + H \rightarrow N_2(B\,^3\Pi_g) + H$	3.6×10^{-47}		[5]c
117	$2N + N_2 \rightarrow 2N_2$	$2.4 \times 10^{-48} \exp(5/T_g)$		[5]c
117.1	$2N + H_2 \rightarrow N_2 + H_2$	$2.4 \times 10^{-48} \exp(5/T_g)$		[5]c
118	$2H + H_2 \rightarrow 2H_2$	$2.3 \times 10^{-47}\,(T_g/300)^{-0.6}$		[5]c
119	$2H + N_2 \rightarrow H_2 + N_2$	$2.2 \times 10^{-47}\,(T_g/300)^{-1}$		[5]c
120	$N + H + N_2 \rightarrow NH + N_2$	2.6×10^{-48}		[5]c
120.1	$N + H + H_2 \rightarrow NH + H_2$	2.6×10^{-48}		[5]c

Continued on next page

Table A.3 (*Continued*)

ID	Reaction	k	ΔE_e	Source
121	$\mathrm{N + H_2 + N_2 \rightarrow NH_2 + N_2}$	2.6×10^{-49}		[5][c]
121.1	$\mathrm{N + 2H_2 \rightarrow NH_2 + H_2}$	2.6×10^{-49}		[5][c]
122	$\mathrm{H + NH + N_2 \rightarrow NH_2 + N_2}$	2.6×10^{-47}		[5][c]
122.1	$\mathrm{H + NH + H_2 \rightarrow NH_2 + H_2}$	2.6×10^{-47}		[5][c]
123	$\mathrm{H + NH_2 + N_2 \rightarrow NH_3 + N_2}$	1.4×10^{-44}		[5][c]
123.1	$\mathrm{H + NH_2 + H_2 \rightarrow NH_3 + H_2}$	1.4×10^{-44}		[5][c]
124	$\mathrm{NH + H_2 + N_2 \rightarrow NH_3 + N_2}$	$6.5 \times 10^{-50}\,(\mathrm{T_g}/300)^{1}\exp\left(17/\mathrm{T_g}\right)$		[5][c]
124.1	$\mathrm{NH + 2H_2 \rightarrow NH_3 + H_2}$	$6.5 \times 10^{-50}\,(\mathrm{T_g}/300)^{1}\exp\left(17/\mathrm{T_g}\right)$		[5][c]
130	$\mathrm{e + H_2 \rightarrow H + H^-}$	$2.72 \times 10^{-17} T_\mathrm{e}^{-1.14}\exp\left(-9.78/T_\mathrm{e}\right)$		[9; 194][a]
131	$\mathrm{H^- + H_2^+ \rightarrow 3H}$	$2 \times 10^{-13}\,(\mathrm{T_g}/300)^{-1}$		[5][c]
132	$\mathrm{H^- + H_3^+ \rightarrow H_2 + 2H}$	$2 \times 10^{-13}\,(\mathrm{T_g}/300)^{-1}$		[5][c]
133	$\mathrm{H^- + N_2^+ \rightarrow N_2 + H}$	$2 \times 10^{-13}\,(\mathrm{T_g}/300)^{-1}$		[5][c]
134	$\mathrm{H^- + N_4^+ \rightarrow 2N_2 + H}$	$2 \times 10^{-13}\,(\mathrm{T_g}/300)^{-1}$		[5][c]
135	$\mathrm{H^- + N_2H^+ \rightarrow H_2 + N_2}$	$2 \times 10^{-13}\,(\mathrm{T_g}/300)^{-1}$		[5][c]
136	$\mathrm{H^- + H_2^+ + N_2 \rightarrow H_2 + H + N_2}$	$5 \times 10^{-40}\,(\mathrm{T_g}/300)^{-2.5}$		[5][c]
136.1	$\mathrm{H^- + H_2^+ + H_2 \rightarrow 2H_2 + H}$	$5 \times 10^{-40}\,(\mathrm{T_g}/300)^{-2.5}$		[5][c]
137	$\mathrm{H^- + H_3^+ + N_2 \rightarrow 2H_2 + N_2}$	$5 \times 10^{-40}\,(\mathrm{T_g}/300)^{-2.5}$		[5][c]
137.1	$\mathrm{H^- + H_3^+ + H_2 \rightarrow 3H_2}$	$5 \times 10^{-40}\,(\mathrm{T_g}/300)^{-2.5}$		[5][c]
138	$\mathrm{H^- + N_2^+ + N_2 \rightarrow 2N_2 + H}$	$5 \times 10^{-40}\,(\mathrm{T_g}/300)^{-2.5}$		[5][c]
138.1	$\mathrm{H^- + N_2^+ + H_2 \rightarrow N_2 + H + H_2}$	$5 \times 10^{-40}\,(\mathrm{T_g}/300)^{-2.5}$		[5][c]
139	$\mathrm{H^- + N_4^+ + N_2 \rightarrow 3N_2 + H}$	$5 \times 10^{-40}\,(\mathrm{T_g}/300)^{-2.5}$		[5][c]
139.1	$\mathrm{H^- + N_4^+ + H_2 \rightarrow 2N_2 + H + H_2}$	$5 \times 10^{-40}\,(\mathrm{T_g}/300)^{-2.5}$		[5][c]
140	$\mathrm{H^- + N_2H^+ + N_2 \rightarrow H_2 + 2N_2}$	$5 \times 10^{-40}\,(\mathrm{T_g}/300)^{-2.5}$		[5][c]
140.1	$\mathrm{H^- + N_2H^+ + H_2 \rightarrow 2H_2 + N_2}$	$5 \times 10^{-40}\,(\mathrm{T_g}/300)^{-2.5}$		[5][c]

Table A.4: Detailed chemistry set for the N_2–H_2 low pressure reduction cases. The reactions ID numbers are consistent with the source publication. The reaction rate coefficients k of order-m reactions are in $[\mathrm{m}^{3(m-1)}\mathrm{s}^{-1}]$. Gas temperature $\mathrm{T_g}$ is in [K]. The electron temperature T_e and electron energy loss ΔE_e are in [eV].
[a] Fitted from a cross section on a grid of Maxwellian temperatures.
[b] Original source not listed in QDB.
[c] Not the original source.
[d] Threshold energy ΔE_e taken from QDB.
[e] By detailed balance from the corresponding forward reaction.
[f] Expressed for $\mathrm{T_g} = 300$ K.
[g] Data not present in the source publication.
[h] With the assumption of $T_\mathrm{eff} = \mathrm{T_g}$.

ID	Reaction	k	ΔE_e	Source
1	$\mathrm{e + N_2 \rightarrow e + N_2(A\,^3\Sigma_u^+)}$	$2.19 \times 10^{-14} T_\mathrm{e}^{-0.61}\exp\left(-9.34/T_\mathrm{e}\right)$	7.6	[9; 193][a]
1.1	$\mathrm{e + N_2 \rightarrow e + N_2(B\,^3\Pi_g)}$	$5.22 \times 10^{-14} T_\mathrm{e}^{-0.85}\exp\left(-10.5/T_\mathrm{e}\right)$	8.55	[9; 193][a]
1.2	$\mathrm{e + N_2 \rightarrow e + N_2(a'\,^1\Sigma_u^-)}$	$1.97 \times 10^{-14} T_\mathrm{e}^{-0.95}\exp\left(-12/T_\mathrm{e}\right)$	9.4	[9; 193][a]
1.3	$\mathrm{e + N_2 \rightarrow e + N_2(C\,^3\Pi_u)}$	$1.17 \times 10^{-13} T_\mathrm{e}^{-1.02}\exp\left(-13.6/T_\mathrm{e}\right)$	11	[9; 193][a]
2	$\mathrm{e + H_2 \rightarrow e + H_2(b\,^3\Sigma_u^+)}$	$1.1 \times 10^{-13} T_\mathrm{e}^{-0.8}\exp\left(-11.6/T_\mathrm{e}\right)$	8.9	[9][a, b]
2.1	$\mathrm{e + H_2 \rightarrow e + H_2(B\,^1\Sigma_u^+)}$	$3.77 \times 10^{-15} T_\mathrm{e}^{0.51}\exp\left(-12.5/T_\mathrm{e}\right)$	11.3	[9; 194][a]
2.2	$\mathrm{e + H_2 \rightarrow e + H_2(c\,^3\Pi_u)}$	$9.77 \times 10^{-14} T_\mathrm{e}^{-0.95}\exp\left(-13.9/T_\mathrm{e}\right)$	11.8	[9][a, b]
2.3	$\mathrm{e + H_2 \rightarrow e + H_2(a\,^3\Sigma_g^+)}$	$3.34 \times 10^{-14} T_\mathrm{e}^{-0.93}\exp\left(-14.1/T_\mathrm{e}\right)$	11.8	[9][a, b]
3	$\mathrm{e + N_2 \rightarrow 2e + N_2^+}$	$1.08 \times 10^{-14} T_\mathrm{e}^{0.63}\exp\left(-16.6/T_\mathrm{e}\right)$	15.5	[9; 193][a]
3.1	$\mathrm{e + H_2 \rightarrow 2e + H_2^+}$	$1.09 \times 10^{-14} T_\mathrm{e}^{0.46}\exp\left(-16/T_\mathrm{e}\right)$	15.5	[9][a, b]
4	$\mathrm{e + N \rightarrow 2e + N^+}$	$3 \times 10^{-15} T_\mathrm{e}^{0.89}\exp\left(-13.1/T_\mathrm{e}\right)$	14.5	[9; 195][a]
5	$\mathrm{e + H \rightarrow 2e + H^+}$	$6.5 \times 10^{-15} T_\mathrm{e}^{0.49}\exp\left(-12.89/T_\mathrm{e}\right)$	13.6	[5][c, d]
6	$\mathrm{e + NH \rightarrow 2e + NH^+}$	$9.18 \times 10^{-15} T_\mathrm{e}^{0.72}\exp\left(-13.9/T_\mathrm{e}\right)$	13.5	[9; 196][a]

Continued on next page

Table A.4 (*Continued*)

ID	Reaction	k	ΔE_e	Source
7	$e + NH_2 \rightarrow 2e + NH_2^+$	$2.78 \times 10^{-15} T_e^{1.07} \exp(-9.27/T_e)$	11.2	[9; 196][a]
8	$e + NH_3 \rightarrow 2e + NH_3^+$	$2.7 \times 10^{-15} T_e^{0.88} \exp(-9.84/T_e)$	10.2	[9][a, b]
9	$e + N_2 \rightarrow e + N_2(\nu_1)$	$3.09 \times 10^{-14} T_e^{-1.44} \exp(-2.28/T_e)$	0.29	[9][a, b]
9.1	$e + N_2 \rightarrow e + N_2(\nu_2)$	$1.83 \times 10^{-14} T_e^{-1.46} \exp(-2.34/T_e)$	0.57	[9][a, b]
9.2	$e + N_2 \rightarrow e + N_2(\nu_3)$	$1.29 \times 10^{-15} T_e^{-1.47} \exp(-2.33/T_e)$	0.85	[9][a, b]
9.3	$e + N_2 \rightarrow e + N_2(\nu_4)$	$9.31 \times 10^{-15} T_e^{-1.48} \exp(-2.41/T_e)$	1.13	[9][a, b]
9.4	$e + N_2 \rightarrow e + N_2(\nu_5)$	$8.14 \times 10^{-15} T_e^{-1.48} \exp(-2.48/T_e)$	1.8	[9][a, b]
9.5	$e + N_2 \rightarrow e + N_2(\nu_6)$	$7.13 \times 10^{-15} T_e^{-1.49} \exp(-2.58/T_e)$	1.68	[9][a, b]
9.6	$e + N_2 \rightarrow e + N_2(\nu_7)$	$4.07 \times 10^{-15} T_e^{-1.49} \exp(-2.72/T_e)$	1.95	[9][a, b]
9.7	$e + N_2 \rightarrow e + N_2(\nu_8)$	$1.98 \times 10^{-15} T_e^{-1.49} \exp(-2.87/T_e)$	2.21	[9][a, b]
9.8	$e + N_2(\nu_1) \rightarrow e + N_2$	$3.09 \times 10^{-14} T_e^{-1.44} \exp(-1.99/T_e)$	-0.29	[e]
9.9	$e + N_2(\nu_2) \rightarrow e + N_2$	$1.83 \times 10^{-14} T_e^{-1.46} \exp(-1.77/T_e)$	-0.57	[e]
9.10	$e + N_2(\nu_3) \rightarrow e + N_2$	$1.29 \times 10^{-15} T_e^{-1.47} \exp(-1.48/T_e)$	-0.85	[e]
9.11	$e + N_2(\nu_4) \rightarrow e + N_2$	$9.31 \times 10^{-15} T_e^{-1.48} \exp(-1.28/T_e)$	-1.13	[e]
9.12	$e + N_2(\nu_5) \rightarrow e + N_2$	$8.14 \times 10^{-15} T_e^{-1.48} \exp(-0.68/T_e)$	-1.8	[e]
9.13	$e + N_2(\nu_6) \rightarrow e + N_2$	$7.13 \times 10^{-15} T_e^{-1.49} \exp(-0.9/T_e)$	-1.68	[e]
9.14	$e + N_2(\nu_7) \rightarrow e + N_2$	$4.07 \times 10^{-15} T_e^{-1.49} \exp(-0.77/T_e)$	-1.95	[e]
9.15	$e + N_2(\nu_8) \rightarrow e + N_2$	$1.98 \times 10^{-15} T_e^{-1.49} \exp(-0.66/T_e)$	-2.21	[e]
10	$e + H_2 \rightarrow e + H_2(\nu_1)$	$1.67 \times 10^{-14} T_e^{-0.86} \exp(-2.32/T_e)$	0.52	[9; 197][a]
10.1	$e + H_2 \rightarrow e + H_2(\nu_2)$	$2.62 \times 10^{-15} T_e^{-1.13} \exp(-3.85/T_e)$	1	[9; 197][a]
10.2	$e + H_2 \rightarrow e + H_2(\nu_3)$	$2.42 \times 10^{-16} T_e^{-1.04} \exp(-3.34/T_e)$	1.5	[47; 198][a]
10.3	$e + H_2(\nu_1) \rightarrow e + H_2$	$1.67 \times 10^{-14} T_e^{-0.86} \exp(-1.8/T_e)$	-0.52	[e]
10.4	$e + H_2(\nu_2) \rightarrow e + H_2$	$2.62 \times 10^{-15} T_e^{-1.13} \exp(-2.85/T_e)$	-1	[e]
10.5	$e + H_2(\nu_3) \rightarrow e + H_2$	$2.42 \times 10^{-16} T_e^{-1.04} \exp(-1.84/T_e)$	-1.5	[e]
11	$N_2(\nu_1) + N_2 \rightarrow 2N_2$	1.68×10^{-28}		[5][c, f]
11.1	$N_2(\nu_1) + H_2 \rightarrow N_2 + H_2$	1.4×10^{-22}		[5][c, f]
11.2	$N_2(\nu_1) + N \rightarrow N_2 + N$	2.39×10^{-26}		[5][c, f]
11.3	$N_2(\nu_1) + H \rightarrow N_2 + H$	1.79×10^{-26}		[5][c, f]
11.4	$N_2(\nu_2) + N_2 \rightarrow N_2(\nu_1) + N_2$	6.94×10^{-28}		[5][c, f]
11.5	$N_2(\nu_2) + H_2 \rightarrow N_2(\nu_1) + H_2$	4.83×10^{-22}		[5][c, f]
11.6	$N_2(\nu_2) + N \rightarrow N_2(\nu_1) + N$	4.89×10^{-26}		[5][c, f]
11.7	$N_2(\nu_2) + H \rightarrow N_2(\nu_1) + H$	5.7×10^{-26}		[5][c, f]
11.8	$N_2(\nu_3) + N_2 \rightarrow N_2(\nu_2) + N_2$	1.28×10^{-27}		[5][c, f]
11.9	$N_2(\nu_3) + H_2 \rightarrow N_2(\nu_2) + H_2$	7.43×10^{-22}		[5][c, f]
11.10	$N_2(\nu_3) + N \rightarrow N_2(\nu_2) + N$	9.93×10^{-26}		[5][c, f]
11.11	$N_2(\nu_3) + H \rightarrow N_2(\nu_2) + H$	1.79×10^{-25}		[5][c, f]
11.12	$N_2(\nu_4) + N_2 \rightarrow N_2(\nu_3) + N_2$	2.2×10^{-27}		[5][c, f]
11.13	$N_2(\nu_4) + H_2 \rightarrow N_2(\nu_3) + H_2$	1.07×10^{-21}		[5][c, f]
11.14	$N_2(\nu_4) + N \rightarrow N_2(\nu_3) + N$	2×10^{-25}		[5][c, f]
11.15	$N_2(\nu_4) + H \rightarrow N_2(\nu_3) + H$	5.54×10^{-25}		[5][c, f]
11.16	$N_2(\nu_5) + N_2 \rightarrow N_2(\nu_4) + N_2$	3.63×10^{-27}		[5][c, f]
11.17	$N_2(\nu_5) + H_2 \rightarrow N_2(\nu_4) + H_2$	1.48×10^{-21}		[5][c, f]
11.18	$N_2(\nu_5) + N \rightarrow N_2(\nu_4) + N$	3.99×10^{-25}		[5][c, f]
11.19	$N_2(\nu_5) + H \rightarrow N_2(\nu_4) + H$	1.69×10^{-24}		[5][c, f]
11.20	$N_2(\nu_6) + N_2 \rightarrow N_2(\nu_5) + N_2$	5.83×10^{-27}		[5][c, f]
11.21	$N_2(\nu_6) + H_2 \rightarrow N_2(\nu_5) + H_2$	2×10^{-21}		[5][c, f]
11.22	$N_2(\nu_6) + N \rightarrow N_2(\nu_5) + N$	7.89×10^{-25}		[5][c, f]
11.23	$N_2(\nu_6) + H \rightarrow N_2(\nu_5) + H$	5.09×10^{-24}		[5][c, f]
11.24	$N_2(\nu_7) + N_2 \rightarrow N_2(\nu_6) + N_2$	9.18×10^{-27}		[5][c, f]
11.25	$N_2(\nu_7) + H_2 \rightarrow N_2(\nu_6) + H_2$	2.63×10^{-21}		[5][c, f]
11.26	$N_2(\nu_7) + N \rightarrow N_2(\nu_6) + N$	1.55×10^{-24}		[5][c, f]
11.27	$N_2(\nu_7) + H \rightarrow N_2(\nu_6) + H$	1.51×10^{-23}		[5][c, f]
11.28	$N_2(\nu_8) + N_2 \rightarrow N_2(\nu_7) + N_2$	1.42×10^{-26}		[5][c, f]
11.29	$N_2(\nu_8) + H_2 \rightarrow N_2(\nu_7) + H_2$	3.42×10^{-21}		[5][c, f]
11.30	$N_2(\nu_8) + N \rightarrow N_2(\nu_7) + N$	3×10^{-24}		[5][c, f]
11.31	$N_2(\nu_8) + H \rightarrow N_2(\nu_7) + H$	4.42×10^{-23}		[5][c, f]
11.32	$2N_2 \rightarrow N_2(\nu_1) + N_2$	2.44×10^{-33}		[5][c, f]
11.33	$N_2 + H_2 \rightarrow N_2(\nu_1) + H_2$	2.02×10^{-27}		[5][c, f]
11.34	$N_2 + N \rightarrow N_2(\nu_1) + N$	3.46×10^{-31}		[5][c, f]
11.35	$N_2 + H \rightarrow N_2(\nu_1) + H$	2.59×10^{-31}		[5][c, f]

Continued on next page

Table A.4 (*Continued*)

ID	Reaction	k	ΔE_e	Source
11.36	$N_2(\nu_1) + N_2 \rightarrow N_2(\nu_2) + N_2$	1.13×10^{-32}		[5][c,f]
11.37	$N_2(\nu_1) + H_2 \rightarrow N_2(\nu_2) + H_2$	7.86×10^{-27}		[5][c,f]
11.38	$N_2(\nu_1) + N \rightarrow N_2(\nu_2) + N$	7.95×10^{-31}		[5][c,f]
11.39	$N_2(\nu_1) + H \rightarrow N_2(\nu_2) + H$	9.27×10^{-31}		[5][c,f]
11.40	$N_2(\nu_2) + N_2 \rightarrow N_2(\nu_3) + N_2$	2.33×10^{-32}		[5][c,f]
11.41	$N_2(\nu_2) + H_2 \rightarrow N_2(\nu_3) + H_2$	1.36×10^{-26}		[5][c,f]
11.42	$N_2(\nu_2) + N \rightarrow N_2(\nu_3) + N$	1.82×10^{-30}		[5][c,f]
11.43	$N_2(\nu_2) + H \rightarrow N_2(\nu_3) + H$	3.27×10^{-30}		[5][c,f]
11.44	$N_2(\nu_3) + N_2 \rightarrow N_2(\nu_4) + N_2$	4.69×10^{-32}		[5][c,f]
11.45	$N_2(\nu_3) + H_2 \rightarrow N_2(\nu_4) + H_2$	2.29×10^{-26}		[5][c,f]
11.46	$N_2(\nu_3) + N \rightarrow N_2(\nu_4) + N$	4.26×10^{-30}		[5][c,f]
11.47	$N_2(\nu_3) + H \rightarrow N_2(\nu_4) + H$	1.18×10^{-29}		[5][c,f]
11.48	$N_2(\nu_4) + N_2 \rightarrow N_2(\nu_5) + N_2$	8.7×10^{-32}		[5][c,f]
11.49	$N_2(\nu_4) + H_2 \rightarrow N_2(\nu_5) + H_2$	3.55×10^{-26}		[5][c,f]
11.50	$N_2(\nu_4) + N \rightarrow N_2(\nu_5) + N$	9.56×10^{-30}		[5][c,f]
11.51	$N_2(\nu_4) + H \rightarrow N_2(\nu_5) + H$	4.06×10^{-29}		[5][c,f]
11.52	$N_2(\nu_5) + N_2 \rightarrow N_2(\nu_6) + N_2$	1.63×10^{-31}		[5][c,f]
11.53	$N_2(\nu_5) + H_2 \rightarrow N_2(\nu_6) + H_2$	5.58×10^{-26}		[5][c,f]
11.54	$N_2(\nu_5) + N \rightarrow N_2(\nu_6) + N$	2.21×10^{-29}		[5][c,f]
11.55	$N_2(\nu_5) + H \rightarrow N_2(\nu_6) + H$	1.42×10^{-28}		[5][c,f]
11.56	$N_2(\nu_6) + N_2 \rightarrow N_2(\nu_7) + N_2$	2.89×10^{-31}		[5][c,f]
11.57	$N_2(\nu_6) + H_2 \rightarrow N_2(\nu_7) + H_2$	8.27×10^{-26}		[5][c,f]
11.58	$N_2(\nu_6) + N \rightarrow N_2(\nu_7) + N$	4.86×10^{-29}		[5][c,f]
11.59	$N_2(\nu_6) + H \rightarrow N_2(\nu_7) + H$	4.75×10^{-28}		[5][c,f]
11.60	$N_2(\nu_7) + N_2 \rightarrow N_2(\nu_8) + N_2$	5.22×10^{-31}		[5][c,f]
11.61	$N_2(\nu_7) + H_2 \rightarrow N_2(\nu_8) + H_2$	1.25×10^{-25}		[5][c,f]
11.62	$N_2(\nu_7) + N \rightarrow N_2(\nu_8) + N$	1.1×10^{-28}		[5][c,f]
11.63	$N_2(\nu_7) + H \rightarrow N_2(\nu_8) + H$	1.62×10^{-27}		[5][c,f]
12.1	$H_2(\nu_1) + H_2 \rightarrow 2H_2$	1.05×10^{-22}		[5][c,f]
12.3	$H_2(\nu_1) + H \rightarrow H_2 + H$	6.78×10^{-25}		[5][c,f]
12.5	$H_2(\nu_2) + H_2 \rightarrow H_2(\nu_1) + H_2$	5.73×10^{-22}		[5][c,f]
12.7	$H_2(\nu_2) + H \rightarrow H_2(\nu_1) + H$	3.05×10^{-24}		[5][c,f]
12.9	$H_2(\nu_3) + H_2 \rightarrow H_2(\nu_2) + H_2$	1.39×10^{-21}		[5][c,f]
12.11	$H_2(\nu_3) + H \rightarrow H_2(\nu_2) + H$	1.04×10^{-23}		[5][c,f]
12.13	$2H_2 \rightarrow H_2(\nu_1) + H_2$	2.25×10^{-31}		[5][c,f]
12.15	$H_2 + H \rightarrow H_2(\nu_1) + H$	1.45×10^{-33}		[5][c,f]
12.17	$H_2(\nu_1) + H_2 \rightarrow H_2(\nu_2) + H_2$	4.23×10^{-30}		[5][c,f]
12.19	$H_2(\nu_1) + H \rightarrow H_2(\nu_2) + H$	2.25×10^{-32}		[5][c,f]
12.21	$H_2(\nu_2) + H_2 \rightarrow H_2(\nu_3) + H_2$	5.52×10^{-30}		[5][c,f]
12.23	$H_2(\nu_2) + H \rightarrow H_2(\nu_3) + H$	4.12×10^{-32}		[5][c,f]
13	$2N_2(\nu_1) \rightarrow N_2 + N_2(\nu_2)$	4.1×10^{-20}		[5][c,f]
13.1	$N_2(\nu_1) + N_2(\nu_2) \rightarrow N_2 + N_2(\nu_3)$	4.81×10^{-20}		[5][c,f]
13.2	$N_2(\nu_1) + N_2(\nu_3) \rightarrow N_2 + N_2(\nu_4)$	4.41×10^{-20}		[5][c,f]
13.3	$N_2(\nu_1) + N_2(\nu_4) \rightarrow N_2 + N_2(\nu_5)$	4.09×10^{-20}		[5][c,f]
13.4	$N_2(\nu_1) + N_2(\nu_5) \rightarrow N_2 + N_2(\nu_6)$	3.24×10^{-20}		[5][c,f]
13.5	$N_2(\nu_1) + N_2(\nu_6) \rightarrow N_2 + N_2(\nu_7)$	2.75×10^{-20}		[5][c,f]
13.6	$N_2(\nu_1) + N_2(\nu_7) \rightarrow N_2 + N_2(\nu_8)$	2.04×10^{-20}		[5][c,f]
13.7	$N_2(\nu_2) + N_2 \rightarrow 2N_2(\nu_1)$	5.64×10^{-20}		[5][c,f]
13.8	$2N_2(\nu_2) \rightarrow N_2(\nu_1) + N_2(\nu_3)$	1.25×10^{-19}		[5][c,f]
13.9	$N_2(\nu_2) + N_2(\nu_3) \rightarrow N_2(\nu_1) + N_2(\nu_4)$	1.18×10^{-19}		[5][c,f]
13.10	$N_2(\nu_2) + N_2(\nu_4) \rightarrow N_2(\nu_1) + N_2(\nu_5)$	1.12×10^{-19}		[5][c,f]
13.11	$N_2(\nu_2) + N_2(\nu_5) \rightarrow N_2(\nu_1) + N_2(\nu_6)$	8.96×10^{-20}		[5][c,f]
13.12	$N_2(\nu_2) + N_2(\nu_6) \rightarrow N_2(\nu_1) + N_2(\nu_7)$	7.65×10^{-20}		[5][c,f]
13.13	$N_2(\nu_2) + N_2(\nu_7) \rightarrow N_2(\nu_1) + N_2(\nu_8)$	5.71×10^{-20}		[5][c,f]
13.14	$N_2(\nu_3) + N_2 \rightarrow N_2(\nu_2) + N_2(\nu_1)$	7.71×10^{-20}		[5][c,f]
13.15	$N_2(\nu_3) + N_2(\nu_1) \rightarrow 2N_2(\nu_2)$	1.71×10^{-19}		[5][c,f]
13.16	$2N_2(\nu_3) \rightarrow N_2(\nu_2) + N_2(\nu_4)$	2.33×10^{-19}		[5][c,f]
13.17	$N_2(\nu_3) + N_2(\nu_4) \rightarrow N_2(\nu_2) + N_2(\nu_5)$	2.25×10^{-19}		[5][c,f]
13.18	$N_2(\nu_3) + N_2(\nu_5) \rightarrow N_2(\nu_2) + N_2(\nu_6)$	1.84×10^{-19}		[5][c,f]
13.19	$N_2(\nu_3) + N_2(\nu_6) \rightarrow N_2(\nu_2) + N_2(\nu_7)$	1.59×10^{-19}		[5][c,f]

Continued on next page

Table A.4 (*Continued*)

ID	Reaction	k	ΔE_e	Source
13.20	$N_2(\nu_3) + N_2(\nu_7) \rightarrow N_2(\nu_2) + N_2(\nu_8)$	1.19×10^{-19}		[5][c,f]
13.21	$N_2(\nu_4) + N_2 \rightarrow N_2(\nu_3) + N_2(\nu_1)$			[5][c,f]
13.22	$N_2(\nu_4) + N_2(\nu_1) \rightarrow N_2(\nu_3) + N_2(\nu_2)$	1.8×10^{-19}		[5][c,f]
13.23	$N_2(\nu_4) + N_2(\nu_2) \rightarrow 2N_2(\nu_3)$	3.47×10^{-19}		[5][c,f]
13.24	$2N_2(\nu_4) \rightarrow N_2(\nu_3) + N_2(\nu_5)$	4.25×10^{-19}		[5][c,f]
13.25	$N_2(\nu_4) + N_2(\nu_5) \rightarrow N_2(\nu_3) + N_2(\nu_6)$	3.64×10^{-19}		[5][c,f]
13.26	$N_2(\nu_4) + N_2(\nu_6) \rightarrow N_2(\nu_3) + N_2(\nu_7)$	3.2×10^{-19}		[5][c,f]
13.27	$N_2(\nu_4) + N_2(\nu_7) \rightarrow N_2(\nu_3) + N_2(\nu_8)$	2.45×10^{-19}		[5][c,f]
13.28	$N_2(\nu_5) + N_2 \rightarrow N_2(\nu_4) + N_2(\nu_1)$	3.65×10^{-20}		[5][c,f]
13.29	$N_2(\nu_5) + N_2(\nu_1) \rightarrow N_2(\nu_4) + N_2(\nu_2)$	3.81×10^{-20}		[5][c,f]
13.30	$N_2(\nu_5) + N_2(\nu_2) \rightarrow N_2(\nu_4) + N_2(\nu_3)$	3×10^{-20}		[5][c,f]
13.31	$N_2(\nu_5) + N_2(\nu_3) \rightarrow 2N_2(\nu_4)$	2.47×10^{-20}		[5][c,f]
13.32	$2N_2(\nu_5) \rightarrow N_2(\nu_4) + N_2(\nu_6)$	1.68×10^{-20}		[5][c,f]
13.33	$N_2(\nu_5) + N_2(\nu_6) \rightarrow N_2(\nu_4) + N_2(\nu_7)$	1.27×10^{-20}		[5][c,f]
13.34	$N_2(\nu_5) + N_2(\nu_7) \rightarrow N_2(\nu_4) + N_2(\nu_8)$	8.06×10^{-21}		[5][c,f]
13.35	$N_2(\nu_6) + N_2 \rightarrow N_2(\nu_5) + N_2(\nu_1)$	6.33×10^{-20}		[5][c,f]
13.36	$N_2(\nu_6) + N_2(\nu_1) \rightarrow N_2(\nu_5) + N_2(\nu_2)$	1.11×10^{-19}		[5][c,f]
13.37	$N_2(\nu_6) + N_2(\nu_2) \rightarrow N_2(\nu_5) + N_2(\nu_3)$	9.03×10^{-20}		[5][c,f]
13.38	$N_2(\nu_6) + N_2(\nu_3) \rightarrow N_2(\nu_5) + N_2(\nu_4)$	7.58×10^{-20}		[5][c,f]
13.39	$N_2(\nu_6) + N_2(\nu_4) \rightarrow 2N_2(\nu_5)$	5.21×10^{-20}		[5][c,f]
13.40	$2N_2(\nu_6) \rightarrow N_2(\nu_5) + N_2(\nu_7)$	3.96×10^{-20}		[5][c,f]
13.41	$N_2(\nu_6) + N_2(\nu_7) \rightarrow N_2(\nu_5) + N_2(\nu_8)$	2.53×10^{-20}		[5][c,f]
13.42	$N_2(\nu_7) + N_2 \rightarrow N_2(\nu_6) + N_2(\nu_1)$	9.72×10^{-20}		[5][c,f]
13.43	$N_2(\nu_7) + N_2(\nu_1) \rightarrow N_2(\nu_6) + N_2(\nu_2)$	1.92×10^{-19}		[5][c,f]
13.44	$N_2(\nu_7) + N_2(\nu_2) \rightarrow N_2(\nu_6) + N_2(\nu_3)$	1.99×10^{-19}		[5][c,f]
13.45	$N_2(\nu_7) + N_2(\nu_3) \rightarrow N_2(\nu_6) + N_2(\nu_4)$	1.71×10^{-19}		[5][c,f]
13.46	$N_2(\nu_7) + N_2(\nu_4) \rightarrow N_2(\nu_6) + N_2(\nu_5)$	1.2×10^{-19}		[5][c,f]
13.47	$N_2(\nu_7) + N_2(\nu_5) \rightarrow 2N_2(\nu_6)$	9.23×10^{-20}		[5][c,f]
13.48	$2N_2(\nu_7) \rightarrow N_2(\nu_6) + N_2(\nu_8)$	5.94×10^{-20}		[5][c,f]
13.49	$N_2(\nu_8) + N_2 \rightarrow N_2(\nu_7) + N_2(\nu_1)$			[5][c,f]
13.50	$N_2(\nu_8) + N_2(\nu_1) \rightarrow N_2(\nu_7) + N_2(\nu_2)$	2.36×10^{-19}		[5][c,f]
13.51	$N_2(\nu_8) + N_2(\nu_2) \rightarrow N_2(\nu_7) + N_2(\nu_3)$	4.05×10^{-19}		[5][c,f]
13.52	$N_2(\nu_8) + N_2(\nu_3) \rightarrow N_2(\nu_7) + N_2(\nu_4)$	3.78×10^{-19}		[5][c,f]
13.53	$N_2(\nu_8) + N_2(\nu_4) \rightarrow N_2(\nu_7) + N_2(\nu_5)$	2.77×10^{-19}		[5][c,f]
13.54	$N_2(\nu_8) + N_2(\nu_5) \rightarrow N_2(\nu_7) + N_2(\nu_6)$	2.17×10^{-19}		[5][c,f]
13.55	$N_2(\nu_8) + N_2(\nu_6) \rightarrow 2N_2(\nu_7)$	1.42×10^{-19}		[5][c,f]
14	$2H_2(\nu_1) \rightarrow H_2 + H_2(\nu_2)$			[5][c,g]
14.1	$H_2(\nu_1) + H_2(\nu_2) \rightarrow H_2 + H_2(\nu_3)$			[5][c,g]
14.2	$H_2(\nu_2) + H_2 \rightarrow 2H_2(\nu_1)$			[5][c,g]
14.3	$2H_2(\nu_2) \rightarrow H_2(\nu_1) + H_2(\nu_3)$			[5][c,g]
14.4	$H_2(\nu_3) + H_2 \rightarrow H_2(\nu_2) + H_2(\nu_1)$			[5][c,g]
14.5	$H_2(\nu_3) + H_2(\nu_1) \rightarrow 2H_2(\nu_2)$			[5][c,g]
15	$N_2 + H_2(\nu_1) \rightarrow N_2(\nu_1) + H_2$	9.18×10^{-23}		[5][c,f]
15.1	$N_2 + H_2(\nu_2) \rightarrow N_2(\nu_1) + H_2(\nu_1)$	5.78×10^{-22}		[5][c,f]
15.2	$N_2 + H_2(\nu_3) \rightarrow N_2(\nu_1) + H_2(\nu_2)$	5.02×10^{-22}		[5][c,f]
15.3	$N_2(\nu_1) + H_2(\nu_1) \rightarrow N_2(\nu_2) + H_2$	1.66×10^{-22}		[5][c,f]
15.4	$N_2(\nu_1) + H_2(\nu_2) \rightarrow N_2(\nu_2) + H_2(\nu_1)$	1.05×10^{-21}		[5][c,f]
15.5	$N_2(\nu_1) + H_2(\nu_3) \rightarrow N_2(\nu_2) + H_2(\nu_2)$	9.08×10^{-22}		[5][c,f]
15.6	$N_2(\nu_2) + H_2(\nu_1) \rightarrow N_2(\nu_3) + H_2$	2.26×10^{-22}		[5][c,f]
15.7	$N_2(\nu_2) + H_2(\nu_2) \rightarrow N_2(\nu_3) + H_2(\nu_1)$	1.42×10^{-21}		[5][c,f]
15.8	$N_2(\nu_2) + H_2(\nu_3) \rightarrow N_2(\nu_3) + H_2(\nu_2)$	1.23×10^{-21}		[5][c,f]
15.9	$N_2(\nu_3) + H_2(\nu_1) \rightarrow N_2(\nu_4) + H_2$	2.63×10^{-22}		[5][c,f]
15.10	$N_2(\nu_3) + H_2(\nu_2) \rightarrow N_2(\nu_4) + H_2(\nu_1)$	1.65×10^{-21}		[5][c,f]
15.11	$N_2(\nu_3) + H_2(\nu_3) \rightarrow N_2(\nu_4) + H_2(\nu_2)$	1.44×10^{-21}		[5][c,f]
15.12	$N_2(\nu_4) + H_2(\nu_1) \rightarrow N_2(\nu_5) + H_2$	2.98×10^{-22}		[5][c,f]
15.13	$N_2(\nu_4) + H_2(\nu_2) \rightarrow N_2(\nu_5) + H_2(\nu_1)$	1.87×10^{-21}		[5][c,f]
15.14	$N_2(\nu_4) + H_2(\nu_3) \rightarrow N_2(\nu_5) + H_2(\nu_2)$	1.63×10^{-21}		[5][c,f]
15.15	$N_2(\nu_5) + H_2(\nu_1) \rightarrow N_2(\nu_6) + H_2$	3.12×10^{-22}		[5][c,f]
15.16	$N_2(\nu_5) + H_2(\nu_2) \rightarrow N_2(\nu_6) + H_2(\nu_1)$	1.96×10^{-21}		[5][c,f]
15.17	$N_2(\nu_5) + H_2(\nu_3) \rightarrow N_2(\nu_6) + H_2(\nu_2)$	1.7×10^{-21}		[5][c,f]

Continued on next page

Table A.4 (*Continued*)

ID	Reaction	k	ΔE_e	Source
15.18	$N_2(\nu_6) + H_2(\nu_1) \rightarrow N_2(\nu_7) + H_2$	3.29×10^{-22}		[5]c,f
15.19	$N_2(\nu_6) + H_2(\nu_2) \rightarrow N_2(\nu_7) + H_2(\nu_1)$	2.07×10^{-21}		[5]c,f
15.20	$N_2(\nu_6) + H_2(\nu_3) \rightarrow N_2(\nu_7) + H_2(\nu_2)$	1.8×10^{-21}		[5]c,f
15.21	$N_2(\nu_7) + H_2(\nu_1) \rightarrow N_2(\nu_8) + H_2$	3.29×10^{-22}		[5]c,f
15.22	$N_2(\nu_7) + H_2(\nu_2) \rightarrow N_2(\nu_8) + H_2(\nu_1)$	2.07×10^{-21}		[5]c,f
15.23	$N_2(\nu_7) + H_2(\nu_3) \rightarrow N_2(\nu_8) + H_2(\nu_2)$	1.8×10^{-21}		[5]c,f
15.24	$N_2(\nu_1) + H_2 \rightarrow N_2 + H_2(\nu_1)$	1.36×10^{-26}		[5]c,f
15.25	$N_2(\nu_1) + H_2(\nu_1) \rightarrow N_2 + H_2(\nu_2)$	2.94×10^{-25}		[5]c,f
15.26	$N_2(\nu_1) + H_2(\nu_2) \rightarrow N_2 + H_2(\nu_3)$	1.38×10^{-25}		[5]c,f
15.27	$N_2(\nu_2) + H_2 \rightarrow N_2(\nu_1) + H_2(\nu_1)$	2.19×10^{-26}		[5]c,f
15.28	$N_2(\nu_2) + H_2(\nu_1) \rightarrow N_2(\nu_1) + H_2(\nu_2)$	4.74×10^{-25}		[5]c,f
15.29	$N_2(\nu_2) + H_2(\nu_2) \rightarrow N_2(\nu_1) + H_2(\nu_3)$	2.22×10^{-25}		[5]c,f
15.30	$N_2(\nu_3) + H_2 \rightarrow N_2(\nu_2) + H_2(\nu_1)$	2.64×10^{-26}		[5]c,f
15.31	$N_2(\nu_3) + H_2(\nu_1) \rightarrow N_2(\nu_2) + H_2(\nu_2)$	5.73×10^{-25}		[5]c,f
15.32	$N_2(\nu_3) + H_2(\nu_2) \rightarrow N_2(\nu_2) + H_2(\nu_3)$	2.68×10^{-25}		[5]c,f
15.33	$N_2(\nu_4) + H_2 \rightarrow N_2(\nu_3) + H_2(\nu_1)$	2.64×10^{-26}		[5]c,f
15.34	$N_2(\nu_4) + H_2(\nu_1) \rightarrow N_2(\nu_3) + H_2(\nu_2)$	5.72×10^{-25}		[5]c,f
15.35	$N_2(\nu_4) + H_2(\nu_2) \rightarrow N_2(\nu_3) + H_2(\nu_3)$	2.68×10^{-25}		[5]c,f
15.36	$N_2(\nu_5) + H_2 \rightarrow N_2(\nu_4) + H_2(\nu_1)$	2.66×10^{-26}		[5]c,f
15.37	$N_2(\nu_5) + H_2(\nu_1) \rightarrow N_2(\nu_4) + H_2(\nu_2)$	5.76×10^{-25}		[5]c,f
15.38	$N_2(\nu_5) + H_2(\nu_2) \rightarrow N_2(\nu_4) + H_2(\nu_3)$	2.7×10^{-25}		[5]c,f
15.39	$N_2(\nu_6) + H_2 \rightarrow N_2(\nu_5) + H_2(\nu_1)$	2.39×10^{-26}		[5]c,f
15.40	$N_2(\nu_6) + H_2(\nu_1) \rightarrow N_2(\nu_5) + H_2(\nu_2)$	5.18×10^{-25}		[5]c,f
15.41	$N_2(\nu_6) + H_2(\nu_2) \rightarrow N_2(\nu_5) + H_2(\nu_3)$	2.42×10^{-25}		[5]c,f
15.42	$N_2(\nu_7) + H_2 \rightarrow N_2(\nu_6) + H_2(\nu_1)$	2.24×10^{-26}		[5]c,f
15.43	$N_2(\nu_7) + H_2(\nu_1) \rightarrow N_2(\nu_6) + H_2(\nu_2)$	4.87×10^{-25}		[5]c,f
15.44	$N_2(\nu_7) + H_2(\nu_2) \rightarrow N_2(\nu_6) + H_2(\nu_3)$	2.28×10^{-25}		[5]c,f
15.45	$N_2(\nu_8) + H_2 \rightarrow N_2(\nu_7) + H_2(\nu_1)$	1.92×10^{-26}		[5]c,f
15.46	$N_2(\nu_8) + H_2(\nu_1) \rightarrow N_2(\nu_7) + H_2(\nu_2)$	4.16×10^{-25}		[5]c,f
15.47	$N_2(\nu_8) + H_2(\nu_2) \rightarrow N_2(\nu_7) + H_2(\nu_3)$	1.95×10^{-25}		[5]c,f
16	$H_2 + N_2(\nu_2) \rightarrow H_2(\nu_1) + N_2$	2.29×10^{-22}		[5]c,f
16.1	$H_2 + N_2(\nu_3) \rightarrow H_2(\nu_1) + N_2(\nu_1)$	8.64×10^{-22}		[5]c,f
16.2	$H_2 + N_2(\nu_4) \rightarrow H_2(\nu_1) + N_2(\nu_2)$	2.25×10^{-21}		[5]c,f
16.3	$H_2 + N_2(\nu_5) \rightarrow H_2(\nu_1) + N_2(\nu_3)$	4.88×10^{-21}		[5]c,f
16.4	$H_2 + N_2(\nu_6) \rightarrow H_2(\nu_1) + N_2(\nu_4)$	9.49×10^{-21}		[5]c,f
16.5	$H_2 + N_2(\nu_7) \rightarrow H_2(\nu_1) + N_2(\nu_5)$	1.71×10^{-20}		[5]c,f
16.6	$H_2 + N_2(\nu_8) \rightarrow H_2(\nu_1) + N_2(\nu_6)$	2.93×10^{-20}		[5]c,f
16.7	$H_2(\nu_1) + N_2(\nu_2) \rightarrow H_2(\nu_2) + N_2$	4.66×10^{-22}		[5]c,f
16.8	$H_2(\nu_1) + N_2(\nu_3) \rightarrow H_2(\nu_2) + N_2(\nu_1)$	1.76×10^{-21}		[5]c,f
16.9	$H_2(\nu_1) + N_2(\nu_4) \rightarrow H_2(\nu_2) + N_2(\nu_2)$	4.58×10^{-21}		[5]c,f
16.10	$H_2(\nu_1) + N_2(\nu_5) \rightarrow H_2(\nu_2) + N_2(\nu_3)$	9.94×10^{-21}		[5]c,f
16.11	$H_2(\nu_1) + N_2(\nu_6) \rightarrow H_2(\nu_2) + N_2(\nu_4)$	1.93×10^{-20}		[5]c,f
16.12	$H_2(\nu_1) + N_2(\nu_7) \rightarrow H_2(\nu_2) + N_2(\nu_5)$	3.49×10^{-20}		[5]c,f
16.13	$H_2(\nu_1) + N_2(\nu_8) \rightarrow H_2(\nu_2) + N_2(\nu_6)$	5.96×10^{-20}		[5]c,f
16.14	$H_2(\nu_2) + N_2(\nu_2) \rightarrow H_2(\nu_3) + N_2$	7.11×10^{-22}		[5]c,f
16.15	$H_2(\nu_2) + N_2(\nu_3) \rightarrow H_2(\nu_3) + N_2(\nu_1)$	2.68×10^{-21}		[5]c,f
16.16	$H_2(\nu_2) + N_2(\nu_4) \rightarrow H_2(\nu_3) + N_2(\nu_2)$	7×10^{-21}		[5]c,f
16.17	$H_2(\nu_2) + N_2(\nu_5) \rightarrow H_2(\nu_3) + N_2(\nu_3)$	1.52×10^{-20}		[5]c,f
16.18	$H_2(\nu_2) + N_2(\nu_6) \rightarrow H_2(\nu_3) + N_2(\nu_4)$	2.95×10^{-20}		[5]c,f
16.19	$H_2(\nu_2) + N_2(\nu_7) \rightarrow H_2(\nu_3) + N_2(\nu_5)$	5.33×10^{-20}		[5]c,f
16.20	$H_2(\nu_2) + N_2(\nu_8) \rightarrow H_2(\nu_3) + N_2(\nu_6)$	9.11×10^{-20}		[5]c,f
16.21	$H_2(\nu_1) + N_2 \rightarrow H_2 + N_2(\nu_2)$	2.52×10^{-23}		[5]c,f
16.22	$H_2(\nu_1) + N_2(\nu_1) \rightarrow H_2 + N_2(\nu_3)$	1.2×10^{-22}		[5]c,f
16.23	$H_2(\nu_1) + N_2(\nu_2) \rightarrow H_2 + N_2(\nu_4)$	4.1×10^{-22}		[5]c,f
16.24	$H_2(\nu_1) + N_2(\nu_3) \rightarrow H_2 + N_2(\nu_5)$	1.17×10^{-21}		[5]c,f
16.25	$H_2(\nu_1) + N_2(\nu_4) \rightarrow H_2 + N_2(\nu_6)$	2.97×10^{-21}		[5]c,f
16.26	$H_2(\nu_1) + N_2(\nu_5) \rightarrow H_2 + N_2(\nu_7)$	7.04×10^{-21}		[5]c,f
16.27	$H_2(\nu_1) + N_2(\nu_6) \rightarrow H_2 + N_2(\nu_8)$	1.58×10^{-20}		[5]c,f
16.28	$H_2(\nu_2) + N_2 \rightarrow H_2(\nu_1) + N_2(\nu_2)$	1.49×10^{-23}		[5]c,f
16.29	$H_2(\nu_2) + N_2(\nu_1) \rightarrow H_2(\nu_1) + N_2(\nu_3)$	7.09×10^{-23}		[5]c,f

Continued on next page

Table A.4 (*Continued*)

ID	Reaction	k	ΔE_e	Source
16.30	$H_2(\nu_2) + N_2(\nu_2) \rightarrow H_2(\nu_1) + N_2(\nu_4)$	2.42×10^{-22}		[5][c, f]
16.31	$H_2(\nu_2) + N_2(\nu_3) \rightarrow H_2(\nu_1) + N_2(\nu_5)$	6.88×10^{-22}		[5][c, f]
16.32	$H_2(\nu_2) + N_2(\nu_4) \rightarrow H_2(\nu_1) + N_2(\nu_6)$	1.75×10^{-21}		[5][c, f]
16.33	$H_2(\nu_2) + N_2(\nu_5) \rightarrow H_2(\nu_1) + N_2(\nu_7)$	4.16×10^{-21}		[5][c, f]
16.34	$H_2(\nu_2) + N_2(\nu_6) \rightarrow H_2(\nu_1) + N_2(\nu_8)$	9.31×10^{-21}		[5][c, f]
16.35	$H_2(\nu_3) + N_2 \rightarrow H_2(\nu_2) + N_2(\nu_2)$	4.22×10^{-23}		[5][c, f]
16.36	$H_2(\nu_3) + N_2(\nu_1) \rightarrow H_2(\nu_2) + N_2(\nu_3)$	2.01×10^{-22}		[5][c, f]
16.37	$H_2(\nu_3) + N_2(\nu_2) \rightarrow H_2(\nu_2) + N_2(\nu_4)$	6.87×10^{-22}		[5][c, f]
16.38	$H_2(\nu_3) + N_2(\nu_3) \rightarrow H_2(\nu_2) + N_2(\nu_5)$	1.95×10^{-21}		[5][c, f]
16.39	$H_2(\nu_3) + N_2(\nu_4) \rightarrow H_2(\nu_2) + N_2(\nu_6)$	4.97×10^{-21}		[5][c, f]
16.40	$H_2(\nu_3) + N_2(\nu_5) \rightarrow H_2(\nu_2) + N_2(\nu_7)$	1.18×10^{-20}		[5][c, f]
16.41	$H_2(\nu_3) + N_2(\nu_6) \rightarrow H_2(\nu_2) + N_2(\nu_8)$	2.64×10^{-20}		[5][c, f]
17	$N_2(A\,^3\Sigma_u^+) + N_2(\nu_6) \rightarrow N_2(B\,^3\Pi_g) + N_2$	3×10^{-17}		[5][c]
17.1	$N_2(A\,^3\Sigma_u^+) + N_2(\nu_7) \rightarrow N_2(B\,^3\Pi_g) + N_2(\nu_1)$	3×10^{-17}		[5][c]
17.2	$N_2(A\,^3\Sigma_u^+) + N_2(\nu_8) \rightarrow N_2(B\,^3\Pi_g) + N_2(\nu_2)$	3×10^{-17}		[5][c]
18	$N_2(B\,^3\Pi_g) + N_2 \rightarrow N_2(A\,^3\Sigma_u^+) + N_2(\nu_6)$	3×10^{-17}		[5][c]
18.1	$N_2(B\,^3\Pi_g) + N_2(\nu_1) \rightarrow N_2(A\,^3\Sigma_u^+) + N_2(\nu_7)$	3×10^{-17}		[5][c]
18.2	$N_2(B\,^3\Pi_g) + N_2(\nu_2) \rightarrow N_2(A\,^3\Sigma_u^+) + N_2(\nu_8)$	3×10^{-17}		[5][c]
19	$N_2(B\,^3\Pi_g) \rightarrow N_2(A\,^3\Sigma_u^+)$	1.34×10^{5}		[5][c]
20	$N_2(a'\,^1\Sigma_u^-) \rightarrow N_2$	1×10^{2}		[5][c]
21	$N_2(C\,^3\Pi_u) \rightarrow N_2(B\,^3\Pi_g)$	2.45×10^{7}		[5][c]
22	$e + N_2 \rightarrow 2N + e$	$5.15 \times 10^{-15} T_e^{0.71} \exp(-14.2/T_e)$	12.5	[9][a, b]
23	$e + H_2 \rightarrow 2H + e$	$1.75 \times 10^{-13} T_e^{-1.24} \exp(-12.59/T_e)$	11.4	[5][c, d]
24	$e + NH \rightarrow e + N + H$	$5 \times 10^{-14} T_e^{0.5} \exp(-8.6/T_e)$	5.6	[5][c, d]
25	$e + NH_2 \rightarrow e + N + H_2$	$5 \times 10^{-14} T_e^{0.5} \exp(-7.6/T_e)$	5.6	[5][c, d]
26	$e + NH_2 \rightarrow e + NH + H$	$5 \times 10^{-14} T_e^{0.5} \exp(-7.6/T_e)$	5.6	[5][c, d]
27	$e + NH_3 \rightarrow e + NH_2 + H$	$5 \times 10^{-14} T_e^{0.5} \exp(-4.4/T_e)$	5.6	[5][c, d]
28	$e + NH_3 \rightarrow e + NH + H_2$	$5 \times 10^{-14} T_e^{0.5} \exp(-5.5/T_e)$	5.6	[5][c, d]
29	$e + N_2 \rightarrow 2e + N + N^+$	$1.31 \times 10^{-15} T_e^{0.89} \exp(-24/T_e)$	21.3	[9][a, b]
30	$e + H_2 \rightarrow 2e + H + H^+$	$3 \times 10^{-14} T_e^{0.44} \exp(-37.72/T_e)$	3	[5][c, d]
31	$e + N_2^+ \rightarrow 2N$	$2.17 \times 10^{-14} T_e^{-0.39}$		[5][c]
32	$e + N_2^+ \rightarrow N + N(^2D)$	$1.95 \times 10^{-14} T_e^{-0.39}$		[5][c]
33	$e + N_2^+ \rightarrow N + N(^2P)$	$2.17 \times 10^{-15} T_e^{-0.39}$		[5][c]
34	$e + N_3^+ \rightarrow N_2 + N$	$3.22 \times 10^{-14} T_e^{-0.5}$		[5][c]
35	$e + N_4^+ \rightarrow 2N_2$	$3.32 \times 10^{-13} T_e^{-0.53}$		[5][c]
36	$e + H_2^+ \rightarrow 2H$	$4.94 \times 10^{-14} T_e^{-0.5} \exp(-0.03/T_e)$		[9; 199][a]
37	$e + H_3^+ \rightarrow 3H$	$1.19 \times 10^{-15} T_e^{-1.03} \exp(-0.08/T_e)$		[6; 9][a]
38	$e + H_3^+ \rightarrow H_2 + H$	$6.42 \times 10^{-14} T_e^{-0.44} \exp(-0.02/T_e)$		[9; 200][a]
39	$e + NH^+ \rightarrow N + H$	$6.93 \times 10^{-15} T_e^{-0.5}$		[5][c]
40	$e + NH_2^+ \rightarrow NH + H$	$2.37 \times 10^{-14} T_e^{-0.4}$		[5][c]
41	$e + NH_2^+ \rightarrow N + 2H$	$4.6 \times 10^{-14} T_e^{-0.4}$		[5][c]
42	$e + NH_3^+ \rightarrow NH + 2H$	$2.5 \times 10^{-14} T_e^{-0.5}$		[5][c]
43	$e + NH_3^+ \rightarrow NH_2 + H$	$2.5 \times 10^{-14} T_e^{-0.5}$		[5][c]
44	$e + NH_4^+ \rightarrow NH_3 + H$	$8.8 \times 10^{-14} T_e^{-0.6}$		[5][c]
45	$e + NH_4^+ \rightarrow NH_2 + 2H$	$1.35 \times 10^{-14} T_e^{-0.6}$		[5][c]
46	$e + N_2H^+ \rightarrow N_2 + H$	$5.13 \times 10^{-14} T_e^{-0.72}$		[5][c]
47	$N_2^+ + H_2 \rightarrow N_2H^+ + H$	2×10^{-15}		[5][c]
48	$N_2^+ + N_2(A\,^3\Sigma_u^+) \rightarrow N_3^+ + N$	3×10^{-16}		[5][c]
49	$N_2^+ + N \rightarrow N^+ + N_2$	$7.2 \times 10^{-19} \left(T_g/300\right)^{2.2}$		[5][c, h]
50	$N_2^+ + N_2 + N \rightarrow N_3^+ + N_2$	$9 \times 10^{-42} \exp\left(4/T_g\right)$		[5][c, h]
51	$N_2^+ + 2N_2 \rightarrow N_4^+ + N_2$	$5.2 \times 10^{-41} \left(T_g/300\right)^{-2.2}$		[5][c, h]
52	$N_2^+ + NH_3 \rightarrow NH_3^+ + N_2$	1.95×10^{-15}		[5][c]
53	$N_3^+ + N \rightarrow N_2^+ + N_2$	6.6×10^{-17}		[5][c]
54	$N_4^+ + N \rightarrow N^+ + 2N_2$	1×10^{-17}		[5][c]
55	$N_4^+ + N_2 \rightarrow N_2^+ + 2N_2$	2.51×10^{-21}		[5][c, f]
56	$N^+ + H_2 \rightarrow NH^+ + H$	5×10^{-16}		[5][c]
57	$N^+ + NH_3 \rightarrow NH_2^+ + NH$	4.7×10^{-16}		[5][c]
58	$N^+ + NH_3 \rightarrow NH_3^+ + N$	1.67×10^{-15}		[5][c]
59	$N^+ + NH_3 \rightarrow N_2H^+ + H_2$	2.12×10^{-16}		[5][c]
60	$H_2^+ + H \rightarrow H_2 + H^+$	6.4×10^{-16}		[5][c]

Continued on next page

Table A.4 (*Continued*)

ID	Reaction	k	ΔE_e	Source
61	$H_2^+ + H_2 \rightarrow H_3^+ + H$	2×10^{-15}		[5][c]
62	$H_2^+ + NH_3 \rightarrow NH_3^+ + H_2$	5.7×10^{-15}		[5][c]
63	$H_2^+ + N_2 \rightarrow N_2H^+ + H$	2×10^{-15}		[5][c]
64	$H^+ + NH_3 \rightarrow NH_3^+ + H$	5.2×10^{-15}		[5][c]
65	$NH^+ + H_2 \rightarrow H_3^+ + N$	1.85×10^{-16}		[5][c]
66	$NH^+ + H_2 \rightarrow NH_2^+ + H$	1.05×10^{-15}		[5][c]
67	$NH^+ + NH_3 \rightarrow NH_3^+ + NH$	1.8×10^{-15}		[5][c]
68	$NH^+ + NH_3 \rightarrow NH_4^+ + N$	6×10^{-16}		[5][c]
69	$NH^+ + N_2 \rightarrow N_2H^+ + N$	6.5×10^{-16}		[5][c]
70	$NH_2^+ + H_2 \rightarrow NH_3^+ + H$	1.95×10^{-16}		[5][c]
71	$NH_2^+ + NH_3 \rightarrow NH_3^+ + NH_2$	1.15×10^{-15}		[5][c]
72	$NH_2^+ + NH_3 \rightarrow NH_4^+ + NH$	1.15×10^{-15}		[5][c]
73	$NH_3^+ + NH_3 \rightarrow NH_4^+ + NH_2$	2.1×10^{-15}		[5][c]
74	$N_2H^+ + NH_3 \rightarrow NH_4^+ + N_2$	2.3×10^{-15}		[5][c]
75	$N_2(A\,^3\Sigma_u^+) + N \rightarrow N_2 + N$	2×10^{-18}		[5][c]
76	$N_2(A\,^3\Sigma_u^+) + N \rightarrow N_2 + N(^2P)$	$4 \times 10^{-17}\,(T_g/300)^{-0.66}$		[5][c]
77	$N_2(A\,^3\Sigma_u^+) + N_2 \rightarrow 2N_2$	3×10^{-22}		[5][c]
78	$2N_2(A\,^3\Sigma_u^+) \rightarrow N_2 + N_2(B\,^3\Pi_g)$	3×10^{-16}		[5][c]
79	$2N_2(A\,^3\Sigma_u^+) \rightarrow N_2 + N_2(C\,^3\Pi_u)$	1.5×10^{-16}		[5][c]
80	$2N_2(A\,^3\Sigma_u^+) \rightarrow N_2 + 2N$	3×10^{-17}		[5][c]
82	$N_2(B\,^3\Pi_g) + N_2 \rightarrow N_2(A\,^3\Sigma_u^+) + N_2$	3×10^{-17}		[5][c]
83	$N_2(B\,^3\Pi_g) + N_2 \rightarrow 2N_2$	2×10^{-18}		[5][c]
84	$N_2(a'\,^1\Sigma_u^-) + N_2 \rightarrow N_2(B\,^3\Pi_g) + N_2$	1.9×10^{-19}		[5][c]
85	$2N_2(a'\,^1\Sigma_u^-) \rightarrow N_2^+ + N_2 + e$	1×10^{-17}		[5][c]
86	$2N_2(a'\,^1\Sigma_u^-) \rightarrow N_4^+ + e$	1×10^{-17}		[5][c]
87	$N_2(a'\,^1\Sigma_u^-) + N_2(A\,^3\Sigma_u^+) \rightarrow N_4^+ + e$	4×10^{-18}		[5][c]
88	$N(^2D) + N_2 \rightarrow N + N_2$	$2.3 \times 10^{-20} \exp(-51/T_g)$		[5][c]
89	$N(^2P) + N \rightarrow 2N$	1.8×10^{-18}		[5][c]
90	$N(^2P) + N \rightarrow N(^2D) + N$	6×10^{-19}		[5][c]
91	$N(^2P) + N_2 \rightarrow N + N_2$	6×10^{-20}		[5][c]
92	$N_2(A\,^3\Sigma_u^+) + H \rightarrow N_2 + H$	5×10^{-17}		[5][c]
93	$N_2(A\,^3\Sigma_u^+) + H_2 \rightarrow N_2 + 2H$	$2 \times 10^{-16} \exp(-35/T_g)$		[5][c]
94	$N_2(A\,^3\Sigma_u^+) + NH_3 \rightarrow N_2 + NH_3$	1.6×10^{-16}		[5][c]
95	$N_2(B\,^3\Pi_g) + H_2 \rightarrow N_2(A\,^3\Sigma_u^+) + H_2$	2.5×10^{-17}		[5][c]
96	$N_2(a'\,^1\Sigma_u^-) + H \rightarrow N_2 + H$	1.5×10^{-17}		[5][c]
97	$N_2(a'\,^1\Sigma_u^-) + H_2 \rightarrow N_2 + 2H$	2.6×10^{-17}		[5][c]
98	$N + H_2(\nu_1) \rightarrow H + NH$	$4 \times 10^{-16}\,(T_g/300)^{0.5} \exp(-14803/T_g)$		[5][c]
98.1	$N + H_2(\nu_2) \rightarrow H + NH$	$4 \times 10^{-16}\,(T_g/300)^{0.5} \exp(-13118/T_g)$		[5][c]
98.2	$N + H_2(\nu_3) \rightarrow H + NH$	$4 \times 10^{-16}\,(T_g/300)^{0.5} \exp(-11377/T_g)$		[5][c]
98.3	$N + H_2(b\,^3\Sigma_u^+) \rightarrow H + NH$	$4 \times 10^{-16}\,(T_g/300)^{0.5}$		[5][c]
98.4	$N + H_2(B\,^1\Sigma_u^+) \rightarrow H + NH$	$4 \times 10^{-16}\,(T_g/300)^{0.5}$		[5][c]
98.5	$N + H_2(c\,^3\Pi_u) \rightarrow H + NH$	$4 \times 10^{-16}\,(T_g/300)^{0.5}$		[5][c]
98.6	$N + H_2(a\,^3\Sigma_g^+) \rightarrow H + NH$	$4 \times 10^{-16}\,(T_g/300)^{0.5}$		[5][c]
99	$N(^2D) + H_2 \rightarrow H + NH$	2.3×10^{-18}		[5][c]
100	$N(^2D) + NH_3 \rightarrow NH + NH_2$	1.1×10^{-16}		[5][c]
101	$N(^2P) + H_2 \rightarrow H + NH$	2.5×10^{-20}		[5][c]
102	$N + NH \rightarrow H + N_2$	5×10^{-17}		[5][c]
103	$H + NH \rightarrow H_2 + N$	$5.4 \times 10^{-17} \exp(-165/T_g)$		[5][c]
104	$2NH \rightarrow H_2 + N_2$	$5 \times 10^{-20}\,(T_g/300)^{1}$		[5][c]
105	$2NH \rightarrow N + NH_2$	$1.7 \times 10^{-18}\,(T_g/300)^{1.5}$		[5][c]
106	$2NH \rightarrow N_2 + 2H$	8.5×10^{-17}		[5][c]
107	$H + NH_2 \rightarrow H_2 + NH$	$6.6 \times 10^{-17} \exp(-184/T_g)$		[5][c]
108	$N + NH_2 \rightarrow N_2 + 2H$	1.2×10^{-16}		[5][c]
109	$N + NH_2 \rightarrow N_2 + H_2$	1.2×10^{-16}		[5][c]
110	$NH + NH_2 \rightarrow NH_3 + N$	1.66×10^{-18}		[5][c]
111	$H_2 + NH_2 \rightarrow NH_3 + H$	$5.4 \times 10^{-17} \exp(-6492/T_g)$		[5][c]
112	$H + NH_3 \rightarrow NH_2 + H_2$	$8.4 \times 10^{-20}\,(T_g/300)^{4.1} \exp(-476/T_g)$		[5][c]
113	$2N + N_2 \rightarrow N_2(A\,^3\Sigma_u^+) + N_2$	4.4×10^{-48}		[5][c]
113.1	$2N + H_2 \rightarrow N_2(A\,^3\Sigma_u^+) + H_2$	4.4×10^{-48}		[5][c]
114	$3N \rightarrow N_2(A\,^3\Sigma_u^+) + N$	2.6×10^{-47}		[5][c]

Continued on next page

Table A.4 (*Continued*)

ID	Reaction	k	ΔE_e	Source
114.1	$2N + H \rightarrow N_2(A\,^3\Sigma_u^+) + H$	2.6×10^{-47}		[5][c]
115	$2N + N_2 \rightarrow N_2(B\,^3\Pi_g) + N_2$	6.2×10^{-48}		[5][c]
115.1	$2N + H_2 \rightarrow N_2(B\,^3\Pi_g) + H_2$	6.2×10^{-48}		[5][c]
116	$3N \rightarrow N_2(B\,^3\Pi_g) + N$	3.6×10^{-47}		[5][c]
116.1	$2N + H \rightarrow N_2(B\,^3\Pi_g) + H$	3.6×10^{-47}		[5][c]
117	$2N + N_2 \rightarrow 2N_2$	$2.4 \times 10^{-48} \exp(5/T_g)$		[5][c]
117.1	$2N + H_2 \rightarrow N_2 + H_2$	$2.4 \times 10^{-48} \exp(5/T_g)$		[5][c]
118	$2H + H_2 \rightarrow 2H_2$	$2.3 \times 10^{-47} (T_g/300)^{-0.6}$		[5][c]
119	$2H + N_2 \rightarrow H_2 + N_2$	$2.2 \times 10^{-47} (T_g/300)^{-1}$		[5][c]
120	$N + H + N_2 \rightarrow NH + N_2$	2.6×10^{-48}		[5][c]
120.1	$N + H + H_2 \rightarrow NH + H_2$	2.6×10^{-48}		[5][c]
121	$N + H_2 + N_2 \rightarrow NH_2 + N_2$	2.6×10^{-49}		[5][c]
121.1	$N + 2H_2 \rightarrow NH_2 + H_2$	2.6×10^{-49}		[5][c]
122	$H + NH + N_2 \rightarrow NH_2 + N_2$	2.6×10^{-47}		[5][c]
122.1	$H + NH + H_2 \rightarrow NH_2 + H_2$	2.6×10^{-47}		[5][c]
123	$H + NH_2 + N_2 \rightarrow NH_3 + N_2$	1.4×10^{-44}		[5][c]
123.1	$H + NH_2 + H_2 \rightarrow NH_3 + H_2$	1.4×10^{-44}		[5][c]
124	$NH + H_2 + N_2 \rightarrow NH_3 + N_2$	$6.5 \times 10^{-50} (T_g/300)^1 \exp(17/T_g)$		[5][c]
124.1	$NH + 2H_2 \rightarrow NH_3 + H_2$	$6.5 \times 10^{-50} (T_g/300)^1 \exp(17/T_g)$		[5][c]
130	$e + H_2 \rightarrow H + H^-$	$2.72 \times 10^{-17} T_e^{-1.14} \exp(-9.78/T_e)$		[9; 194][a]
131	$H^- + H_2^+ \rightarrow 3H$	$2 \times 10^{-13} (T_g/300)^{-1}$		[5][c]
132	$H^- + H_3^+ \rightarrow H_2 + 2H$	$2 \times 10^{-13} (T_g/300)^{-1}$		[5][c]
133	$H^- + N_2^+ \rightarrow N_2 + H$	$2 \times 10^{-13} (T_g/300)^{-1}$		[5][c]
134	$H^- + N_4^+ \rightarrow 2N_2 + H$	$2 \times 10^{-13} (T_g/300)^{-1}$		[5][c]
135	$H^- + N_2H^+ \rightarrow H_2 + N_2$	$2 \times 10^{-13} (T_g/300)^{-1}$		[5][c]
136	$H^- + H_2^+ + N_2 \rightarrow H_2 + H + N_2$	$5 \times 10^{-40} (T_g/300)^{-2.5}$		[5][c]
136.1	$H^- + H_2^+ + H_2 \rightarrow 2H_2 + H$	$5 \times 10^{-40} (T_g/300)^{-2.5}$		[5][c]
137	$H^- + H_3^+ + N_2 \rightarrow 2H_2 + N_2$	$5 \times 10^{-40} (T_g/300)^{-2.5}$		[5][c]
137.1	$H^- + H_3^+ + H_2 \rightarrow 3H_2$	$5 \times 10^{-40} (T_g/300)^{-2.5}$		[5][c]
138	$H^- + N_2^+ + N_2 \rightarrow 2N_2 + H$	$5 \times 10^{-40} (T_g/300)^{-2.5}$		[5][c]
138.1	$H^- + N_2^+ + H_2 \rightarrow N_2 + H + H_2$	$5 \times 10^{-40} (T_g/300)^{-2.5}$		[5][c]
139	$H^- + N_4^+ + N_2 \rightarrow 3N_2 + H$	$5 \times 10^{-40} (T_g/300)^{-2.5}$		[5][c]
139.1	$H^- + N_4^+ + H_2 \rightarrow 2N_2 + H + H_2$	$5 \times 10^{-40} (T_g/300)^{-2.5}$		[5][c]
140	$H^- + N_2H^+ + N_2 \rightarrow H_2 + 2N_2$	$5 \times 10^{-40} (T_g/300)^{-2.5}$		[5][c]
140.1	$H^- + N_2H^+ + H_2 \rightarrow 2H_2 + N_2$	$5 \times 10^{-40} (T_g/300)^{-2.5}$		[5][c]

Table A.5: Detailed chemistry set for all the CF_4–CHF_3–H_2-Cl_2–O_2–HBr reduction cases. The kinetic data are taken directly from the corresponding precompiled chemistry set in QDB database [9] (QDB chemistry ID: C27). Primary sources are cited, if listed in QDB. The purpose of all the test chemistry sets extracted from QDB in this work is merely to provide input for testing of the presented chemistry reduction method, therefore the consistency of this chemistry set and the validity of the cited sources listed in QDB were not explicitly verified in this work.

[a] Fitted from a cross section on a grid of Maxwellian temperatures.

[b] Original source not listed in QDB.

ID	Reaction	k	ΔE_e	Source
1	$e + Cl^* \rightarrow Cl^* + e$	$2.48 \times 10^{-13} T_e^{0.25} \exp(-1.9/T_e)$		[201][a]
2	$e + CF_4 \rightarrow CF_4 + e$	$6.59 \times 10^{-14} T_e^{0.58} \exp(-0.55/T_e)$		[9][a,b]
3	$e + O \rightarrow e + O^*$	$1.06 \times 10^{-14} T_e^{-0.4} \exp(-3.44/T_e)$	1.95	[202][a]
4	$e + O \rightarrow e + O^*$	$1.16 \times 10^{-15} T_e^{-0.17} \exp(-5.08/T_e)$	4.17	[202][a]
5	$F + e \rightarrow F^* + e$	$5.43 \times 10^{-15} T_e^{-0.77} \exp(-15.2/T_e)$	12.7	[9][a,b]
6	$F + e \rightarrow F^* + e$	$5.2 \times 10^{-15} T_e^{-0.1} \exp(-15.1/T_e)$	12.95	[9][a,b]

Continued on next page

Table A.5 (*Continued*)

ID	Reaction	k	ΔE_e	Source
7	$e + Cl \rightarrow e + Cl^*$	$1.57 \times 10^{-14} T_e^{0.03} \exp(-10.4/T_e)$	8.9	[203][a]
8	$e + Br \rightarrow e + Br^*$	$1.56 \times 10^{-14} T_e^{0.03} \exp(-10.4/T_e)$	8.9	[204][a]
9	$e + Br \rightarrow e + Br^*$	$9.75 \times 10^{-14} T_e^{-0.36} \exp(-10.9/T_e)$	10.4	[204][a]
10	$e + Br \rightarrow e + Br^*$	$2.24 \times 10^{-14} T_e^{0.07} \exp(-11.1/T_e)$	10.9	[204][a]
11	$e + Br \rightarrow e + Br^*$	$3.01 \times 10^{-14} T_e^{-0.39} \exp(-12.5/T_e)$	11.8	[204][a]
12	$e + Br \rightarrow e + Br^*$	$1.16 \times 10^{-14} T_e^{0.07} \exp(-12.1/T_e)$	12	[204][a]
13	$e + Br \rightarrow e + Br^*$	$6.56 \times 10^{-15} T_e^{0.03} \exp(-13/T_e)$	12.4	[204][a]
14	$e + F^* \rightarrow F + e$	$1.9 \times 10^{-15} T_e^{-0.35} \exp(-0.77/T_e)$		[9][a,b]
15	$e + H \rightarrow H^+ + 2e$	$1.04 \times 10^{-14} T_e^{0.37} \exp(-14.8/T_e)$	13.55	[9][a,b]
16	$e + H_2 \rightarrow H_2^+ + 2e$	$1.29 \times 10^{-14} T_e^{0.39} \exp(-16.3/T_e)$	15.35	[9][a,b]
17	$e + C \rightarrow C^+ + 2e$	$6.7 \times 10^{-15} T_e^{0.7} \exp(-11.26/T_e)$	11.26	[205][a]
18	$e + O \rightarrow O^+ + 2e$	$4.82 \times 10^{-15} T_e^{0.73} \exp(-13.1/T_e)$	13.6	[202][a]
19	$e + O^* \rightarrow O^+ + 2e$	$1.56 \times 10^{-14} T_e^{0.29} \exp(-13.3/T_e)$	11.65	[9][a,b]
20	$e + O_2 \rightarrow O_2^+ + 2e$	$7.08 \times 10^{-15} T_e^{0.76} \exp(-13.8/T_e)$	12.05	[9][a,b]
21	$e + F \rightarrow F^+ + 2e$	$2.15 \times 10^{-15} T_e^{0.87} \exp(-16/T_e)$	17.27	[9][a,b]
22	$e + F^* \rightarrow F^+ + 2e$	$1.28 \times 10^{-13} T_e^{0.08} \exp(-6.13/T_e)$	4.7	[9][a,b]
23	$e + F_2 \rightarrow F_2^+ + 2e$	$2.96 \times 10^{-15} T_e^{0.84} \exp(-15.9/T_e)$	15.53	[206][a]
24	$e + Cl \rightarrow Cl^+ + 2e$	$4.36 \times 10^{-14} T_e^{0.53} \exp(-14.4/T_e)$	12.95	[207][a]
25	$e + Cl^* \rightarrow Cl^+ + 2e$	$1.73 \times 10^{-13} T_e^{0.05} \exp(-5.45/T_e)$	4.08	[208][a]
26	$e + Cl_2 \rightarrow Cl_2^+ + 2e$	$3.7 \times 10^{-14} T_e^{0.57} \exp(-12.8/T_e)$	11.45	[207][a]
27	$e + Br \rightarrow Br^+ + 2e$	$4.36 \times 10^{-14} T_e^{0.53} \exp(-14.4/T_e)$	12.95	[204][a]
28	$e + Br^* \rightarrow Br^+ + 2e$	$1.73 \times 10^{-13} T_e^{0.05} \exp(-5.45/T_e)$	4.08	[204][a]
29	$e + CH \rightarrow 2e + CH^+$	$1.82 \times 10^{-14} T_e^{0.42} \exp(-13/T_e)$	11.3	[9][a,b]
30	$e + CH_2 \rightarrow 2e + CH_2^+$	$1.46 \times 10^{-14} T_e^{0.5} \exp(-12/T_e)$	10.4	[9][a,b]
31	$e + H_2O \rightarrow H_2O^+ + 2e$	$8.02 \times 10^{-15} T_e^{0.59} \exp(-13.7/T_e)$	13.5	[209][a]
32	$e + HCl \rightarrow HCl^+ + 2e$	$1.78 \times 10^{-14} T_e^{0.76} \exp(-14/T_e)$	12.7	[210][a]
33	$e + CO \rightarrow CO^+ + 2e$	$6.11 \times 10^{-15} T_e^{0.55} \exp(-13.7/T_e)$	14	[208][a]
34	$e + CF \rightarrow CF^+ + 2e$	$6.08 \times 10^{-15} T_e^{0.66} \exp(-12.1/T_e)$	11	[211][a]
35	$e + CF_2 \rightarrow CF_2^+ + 2e$	$9.59 \times 10^{-15} T_e^{0.48} \exp(-11.2/T_e)$	11	[211][a]
36	$e + CF_3 \rightarrow CF_3^+ + 2e$	$3.29 \times 10^{-15} T_e^{0.5} \exp(-10.8/T_e)$	8.9	[212][a]
37	$e + ClO \rightarrow ClO^+ + 2e$	$9.48 \times 10^{-15} T_e^{-1.85} \exp(-12.24/T_e)$	12.24	[213][a]
38	$e + CHF \rightarrow CHF^+ + 2e$	$2.1 \times 10^{-15} T_e^{1.04} \exp(-8.85/T_e)$	8.85	[9][a,b]
39	$e + O_2 \rightarrow O + O^+ + 2e$	$9.92 \times 10^{-16} T_e^{1.1} \exp(-20.3/T_e)$	16.93	[214][a]
40	$e + CH \rightarrow 2e + C^+ + H$	$5.23 \times 10^{-15} T_e^{0.44} \exp(-18.3/T_e)$	18.35	[9][a,b]
41	$e + CH_2 \rightarrow 2e + CH^+ + H$	$1.28 \times 10^{-14} T_e^{0.29} \exp(-19.3/T_e)$	20.38	[9][a,b]
42	$e + CH_2 \rightarrow 2e + C^+ + H_2$	$8.69 \times 10^{-16} T_e^{0.5} \exp(-20.7/T_e)$	21.38	[9][a,b]
43	$e + CO \rightarrow C + O^+ + 2e$	$2.1 \times 10^{-16} T_e^{0.98} \exp(-24.9/T_e)$	23.75	[208][a]
44	$e + CO \rightarrow C^+ + O + 2e$	$6.84 \times 10^{-15} T_e^{0.33} \exp(-24.7/T_e)$	21.82	[208][a]
45	$e + CF_2 \rightarrow CF^+ + F + 2e$	$2.92 \times 10^{-15} T_e^{0.88} \exp(-13.5/T_e)$	14	[212][a]
46	$e + CF_3 \rightarrow CF^+ + 2F + 2e$	$4.32 \times 10^{-15} T_e^{0.61} \exp(-20.5/T_e)$	19.9	[212][a]
47	$e + CF_3 \rightarrow CF_2^+ + F + 2e$	$8.23 \times 10^{-15} T_e^{0.45} \exp(-17.3/T_e)$	16.93	[212][a]
48	$e + CF_3 \rightarrow F^+ + CF_2 + 2e$	$3.76 \times 10^{-15} T_e^{0.51} \exp(-24.7/T_e)$	19.9	[212][a]
49	$e + CF_4 \rightarrow CF_2^+ + 2F + 2e$	$2.95 \times 10^{-15} T_e^{0.54} \exp(-22.2/T_e)$	19.9	[9][a,b]
50	$e + CF_4 \rightarrow CF^+ + F + F_2 + 2e$	$5.47 \times 10^{-15} T_e^{0.43} \exp(-32.7/T_e)$	3	[9][a,b]
51	$e + CF_4 \rightarrow CF_3^+ + F + 2e$	$2.58 \times 10^{-14} T_e^{0.59} \exp(-18.4/T_e)$	16.23	[9][a,b]
52	$e + CF_4 \rightarrow F^+ + CF_3 + 2e$	$1.92 \times 10^{-15} T_e^{0.72} \exp(-36.5/T_e)$	29.88	[9][a,b]
53	$e + CF_4 \rightarrow CF_3^+ + F^+ + 3e$	$6.5 \times 10^{-17} T_e^{1.07} \exp(-36.6/T_e)$	34.95	[9][a,b]
54	$e + CHF_3 \rightarrow CF_3^+ + H + 2e$	$4.99 \times 10^{-15} T_e^{0.9} \exp(-17.3/T_e)$	15.7	[215; 216][a]
55	$e + CHF_3 \rightarrow CHF^+ + 2F + 2e$	$2.38 \times 10^{-16} T_e^{1.36} \exp(-18.5/T_e)$	19.73	[215; 216][a]
56	$e + CHF_3 \rightarrow CH^+ + F + F_2 + 2e$	$5.56 \times 10^{-16} T_e^{0.33} \exp(-36/T_e)$	33.38	[215; 216][a]
57	$e + CHF_3 \rightarrow CF^+ + HF + F + 2e$	$3.34 \times 10^{-15} T_e^{1.09} \exp(-22.4/T_e)$	20.77	[215; 216][a]
58	$e + CHF_3 \rightarrow CHF_2^+ + F + 2e$	$1.21 \times 10^{-15} T_e^{0.85} \exp(-18.6/T_e)$	16.75	[215; 216][a]
59	$e + CHF_3 \rightarrow F^+ + CHF_2 + 2e$	$8.47 \times 10^{-16} T_e^{0.68} \exp(-38.1/T_e)$	36.88	[215; 216][a]
60	$e + CHF_3 \rightarrow CF_2^+ + HF + 2e$	$2.28 \times 10^{-17} T_e^{1.76} \exp(-14.5/T_e)$	17.45	[215; 216][a]
61	$e + CHF \rightarrow CF^+ + H + 2e$	$3.32 \times 10^{-14} T_e^{-0.33} \exp(-19.61/T_e)$	19.61	[9][a,b]
62	$e + O_2 \rightarrow O^- + O$	$6.74 \times 10^{-16} T_e^{-1.02} \exp(-5.78/T_e)$		[9][a,b]
63	$e + F_2 \rightarrow F + F^-$	$3.82 \times 10^{-15} T_e^{-1.16} \exp(-0.16/T_e)$		[206][a]
64	$e + Cl_2 \rightarrow Cl^- + Cl$	$2.31 \times 10^{-16} T_e^{-0.18} \exp(0.12/T_e)$		[207][a]
65	$e + HCl \rightarrow Cl^- + H$	$1.27 \times 10^{-16} T_e^{-1.48} \exp(-0.9/T_e)$		[217][a]
66	$e + HBr \rightarrow Br^- + H$	$1.83 \times 10^{-15} T_e^{-1.28} \exp(-0.28/T_e)$		[218][a]

Continued on next page

Table A.5 (*Continued*)

ID	Reaction	k	ΔE_e	Source
67	$e + CO_2 \rightarrow O^- + CO$	$1.85 \times 10^{-16} T_e^{-1.31} \exp(-6.44/T_e)$		[219][a]
68	$e + CF_2 \rightarrow F^- + CF$	$2.8 \times 10^{-15} T_e^{-1.44} \exp(-7.47/T_e)$		[9][a,b]
69	$e + CF_3 \rightarrow F^- + CF_2$	$2.8 \times 10^{-15} T_e^{-1.44} \exp(-7.47/T_e)$		[9][a,b]
70	$e + CF_4 \rightarrow F^- + CF_3$	$1.33 \times 10^{-15} T_e^{-1.41} \exp(-6.9/T_e)$		[9][a,b]
71	$e + CHF_3 \rightarrow F^- + CHF_2$	$1.05 \times 10^{-16} T_e^{-1.03} \exp(-7/T_e)$		[215][a]
72	$e + CHF_2 \rightarrow CHF + F^-$	1.3×10^{-19}		[9][b]
73	$e + CHF \rightarrow CH + F^-$	1.3×10^{-19}		[9][b]
74	$e + Cl^- \rightarrow Cl + 2e$	$8.46 \times 10^{-15} T_e^{0.61} \exp(-4.74/T_e)$	3.6	[207][a]
75	$e + Br^- \rightarrow Br + 2e$	$8.5 \times 10^{-15} T_e^{0.61} \exp(-4.75/T_e)$	3.6	[204][a]
76	$e + H_2^+ \rightarrow 2H$	$4.92 \times 10^{-14} T_e^{-0.5} \exp(-0.03/T_e)$		[220][a]
77	$e + H_3^+ \rightarrow H + H_2$	$6.39 \times 10^{-14} T_e^{-0.43} \exp(-0.02/T_e)$		[200][a]
78	$e + O_2^+ \rightarrow 2O$	$1.53 \times 10^{-14} T_e^{-0.51} \exp(-0.01/T_e)$		[221][a]
79	$e + F_2^+ \rightarrow 2F$	$2.26 \times 10^{-13} T_e^{-0.5} \exp(-0.01/T_e)$		[222][a]
80	$e + Cl_2^+ \rightarrow 2Cl$	$2.61 \times 10^{-14} T_e^{-0.65} \exp(-0.02/T_e)$		[221][a]
81	$e + CH^+ \rightarrow C + H$	$3.23 \times 10^{-14} T_e^{-0.42}$		[223]
82	$e + CH_2^+ \rightarrow C + 2H$	$2.36 \times 10^{-14} T_e^{-0.86} \exp(-0.04/T_e)$		[9][a,b]
83	$e + CH_2^+ \rightarrow CH + H$	$9.35 \times 10^{-15} T_e^{-0.86} \exp(-0.04/T_e)$		[9][a,b]
84	$e + CH_2^+ \rightarrow C + H_2$	$4.49 \times 10^{-15} T_e^{-0.86} \exp(-0.04/T_e)$		[9][a,b]
85	$e + HCl^+ \rightarrow Cl + H$	$2.62 \times 10^{-14} T_e^{-0.65} \exp(-0.02/T_e)$		[221][a]
86	$e + HBr^+ \rightarrow Br + H$	$2.61 \times 10^{-14} T_e^{-0.65} \exp(-0.02/T_e)$		[9][a,b]
87	$e + CO_2^+ \rightarrow CO + O$	$2.26 \times 10^{-13} T_e^{-0.5} \exp(-0.01/T_e)$		[222][a]
88	$e + CF_2^+ \rightarrow CF + F$	$6.5 \times 10^{-14} T_e^{-0.5} \exp(-0.01/T_e)$		[9][a,b]
89	$e + CF_3^+ \rightarrow CF_2 + F$	$6.5 \times 10^{-14} T_e^{-0.5} \exp(-0.01/T_e)$		[224][a]
90	$e + H_2 \rightarrow 2H + e$	$1.02 \times 10^{-13} T_e^{-0.54} \exp(-11.5/T_e)$	8.8	[9][a,b]
91	$e + H_2^+ \rightarrow H^+ + H + e$	$9.9 \times 10^{-14} T_e^{0.11} \exp(-0.19/T_e)$		[9][a,b]
92	$e + H_3^+ \rightarrow H^+ + H_2 + e$	$9.91 \times 10^{-14} T_e^{0.37} \exp(-14.5/T_e)$	14.9	[220][a]
93	$e + O_2 \rightarrow e + 2O$	$1.75 \times 10^{-14} T_e^{-1.28} \exp(-7.38/T_e)$	4.5	[9][a,b]
94	$e + O_2 \rightarrow e + 2O$	$2.11 \times 10^{-14} T_e^{-0.78} \exp(-7.45/T_e)$	6	[9][a,b]
95	$e + Cl_2 \rightarrow 2Cl + e$	$5.41 \times 10^{-14} T_e^{0.01} \exp(-4.81/T_e)$	3.1	[207][a]
96	$e + CH \rightarrow e + C + H$	$1.71 \times 10^{-14} T_e^{0.38} \exp(-9.62/T_e)$	6.97	[9][a,b]
97	$e + CH_2 \rightarrow e + CH + H$	$1.43 \times 10^{-14} T_e^{0.44} \exp(-11.3/T_e)$	8.5	[9][a,b]
98	$e + HCl \rightarrow Cl + H + e$	$1.43 \times 10^{-14} T_e^{0.6} \exp(-5.91/T_e)$	5.5	[210][a]
99	$e + CO \rightarrow C + O + e$	$1.05 \times 10^{-14} T_e^{0.38} \exp(-13.5/T_e)$	12.95	[208][a]
100	$e + CF \rightarrow C + F + e$	$3.97 \times 10^{-14} T_e^{-0.16} \exp(-7.48/T_e)$	5.6	[225][a]
101	$e + CF_2 \rightarrow CF + F + e$	$4.43 \times 10^{-15} T_e^{0.65} \exp(-7.87/T_e)$	8.7	[9][a,b]
102	$e + CF_3 \rightarrow CF_2 + F + e$	$4.37 \times 10^{-15} T_e^{0.66} \exp(-7.81/T_e)$	7.7	[9][a,b]
103	$e + CF_4 \rightarrow CF_2 + 2F + e$	$4.45 \times 10^{-15} T_e^{0.03} \exp(-14.1/T_e)$	14	[9][a,b]
104	$e + CF_4 \rightarrow CF + F + F_2 + e$	$8.73 \times 10^{-16} T_e^{0.49} \exp(-15.8/T_e)$	17.98	[9][a,b]
105	$e + CF_4 \rightarrow CF_3 + F + e$	$2.58 \times 10^{-15} T_e^{0.09} \exp(-9.86/T_e)$	12	[9][a,b]
106	$e + CF_4 \rightarrow CF_3^+ + F^- + e$	$4.64 \times 10^{-19} T_e^{1.7} \exp(-6.8/T_e)$	11	[9][a,b]
107	$e + ClO \rightarrow Cl + O + e$	$1.27 \times 10^{-13} T_e^{-1.36} \exp(-6.84/T_e)$	6.84	[213][a]
108	$e + COF_2 \rightarrow COF + F + e$	$2.58 \times 10^{-15} T_e^{0.09} \exp(-9.87/T_e)$	12	[9][a,b]
109	$e + CHF_3 \rightarrow CF + 2F + H + e$	$3 \times 10^{-14} T_e^{0.02} \exp(-21.1/T_e)$	19.38	[9][a,b]
110	$e + CHF_3 \rightarrow CF_2 + F + H + e$	$1.66 \times 10^{-15} T_e^{0.85} \exp(-24.2/T_e)$	23.57	[216][a]
111	$e + CHF_3 \rightarrow CF_3 + H + e$	$3.36 \times 10^{-15} T_e^{0.72} \exp(-8.72/T_e)$	11	[216][a]
112	$e + CHF_3 \rightarrow CHF + 2F + e$	$1.19 \times 10^{-16} T_e^{0.75} \exp(-34.4/T_e)$	34.95	[216][a]
113	$e + CHF_3 \rightarrow CHF_2 + F + e$	$7.66 \times 10^{-18} T_e^{1.79} \exp(-9.45/T_e)$	13	[216][a]
114	$e + CHF_3 \rightarrow F^- + CHF_2^+ + e$	$8.08 \times 10^{-16} T_e^{-1.4} \exp(-14.6/T_e)$	11.5	[215][a]
115	$e + CHF_2 \rightarrow CF + H + F + e$	$2.45 \times 10^{-14} T_e^{-0.36} \exp(-29.6/T_e)$	29.6	[9][a,b]
116	$e + CHF_2 \rightarrow CF_2 + H + e$	$9.31 \times 10^{-15} T_e^{0.2} \exp(-11.4/T_e)$	11.4	[9][a,b]
117	$e + CHF_2 \rightarrow CHF + F + e$	$1.4 \times 10^{-14} T_e^{0.36} \exp(-11.37/T_e)$	11.37	[9][a,b]
118	$e + CHF \rightarrow C + F + H + e$	$2.45 \times 10^{-14} T_e^{-0.36} \exp(-29.6/T_e)$	29.6	[9][a,b]
119	$e + CHF \rightarrow CF + H + e$	$9.31 \times 10^{-15} T_e^{0.2} \exp(-11.42/T_e)$	11.42	[9][a,b]
120	$e + C_3H_8^+ \rightarrow C_3H_5^+ + H_2 + H^+ + 2e$	$3.05 \times 10^{-15} T_e^{0.39} \exp(-29.5/T_e)$	27.7	[9][a,b]
121	$Cl_2 + O^* \rightarrow ClO + Cl$	2.11×10^{-16}		[213]
122	$O^* + H_2O \rightarrow 2OH$	2.2×10^{-17}		[8]
123	$O^* + CF \rightarrow CO + F$	2×10^{-17}		[226]
124	$O^* + CF_2 \rightarrow COF + F$	1.4×10^{-17}		[226]
125	$O^* + CF_3 \rightarrow COF_2 + F$	3.1×10^{-17}		[226]
126	$O^* + CF_4 \rightarrow O + CF_4$	1.8×10^{-19}		[226]

Continued on next page

Table A.5 (*Continued*)

ID	Reaction	k	ΔE_e	Source
127	$O^* + FO \rightarrow O_2 + F$	5×10^{-17}		[226]
128	$O^* + COF \rightarrow CO_2 + F$	9.3×10^{-17}		[226]
129	$O^* + COF_2 \rightarrow COF_2 + O$	5.3×10^{-17}		[226]
130	$O^* + COF_2 \rightarrow CO_2 + F_2$	2.1×10^{-17}		[226]
131	$H + F_2 \rightarrow F + HF$	1.8×10^{-18}		[227]
132	$H + CH \rightarrow C + H_2$	1×10^{-16}		[228]
133	$CH_2 + H \rightarrow CH + H_2$	7.7×10^{-16}		[229]
134	$OH + H \rightarrow O + H_2$	1.48×10^{-16}		[230]
135	$HCl + H \rightarrow Cl + H_2$	1.48×10^{-16}		[9][b]
136	$H + HBr \rightarrow H_2 + Br$	6.5×10^{-18}		[231]
137	$CF + H \rightarrow C + HF$	$3.32 \times 10^{-16} \exp\left(-0.21/T_g\right)$		[232]
138	$H + CF \rightarrow CH + F$	1.9×10^{-17}		[227]
139	$CF_2 + H \rightarrow CF + HF$	$3.32 \times 10^{-16} \exp\left(-0.21/T_g\right)$		[227]
140	$CF_3 + H \rightarrow CF_2 + HF$	9.3×10^{-17}		[227]
141	$H + CHF_3 \rightarrow H_2 + CF_3$	5.2×10^{-25}		[227]
142	$CHF_2 + H \rightarrow CF_2 + H_2$	$6.26 \times 10^{-17} \left(T_g/300\right)^{2.42}$		[227]
143	$CHF + H \rightarrow CH + HF$	3.32×10^{-16}		[227]
144	$C + H_2 \rightarrow CH + H$	1.5×10^{-16}		[228]
145	$O + H_2 \rightarrow OH + H$	3.44×10^{-16}		[230]
146	$F + H_2 \rightarrow H + HF$	$4.8 \times 10^{-16} \left(T_g/300\right)^{0.5} \exp\left(0.11/T_g\right)$		[227]
147	$Cl + H_2 \rightarrow HCl + H$	3.44×10^{-16}		[9][b]
148	$CH + H_2 \rightarrow CH_2 + H$	$3.75 \times 10^{-16} \exp\left(-166/T_g\right)$		[233]
149	$OH + H_2 \rightarrow H_2O + H$	$7.7 \times 10^{-18} \exp\left(-21/T_g\right)$		[8]
150	$C + O_2 \rightarrow O + CO$	1.6×10^{-17}		[226]
151	$O + OH \rightarrow O_2 + H$	$2.3 \times 10^{-17} \exp\left(11/T_g\right)$		[8]
152	$O + CF \rightarrow CO + F$	6.6×10^{-17}		[226]
153	$O + CF_2 \rightarrow COF + F$	3.1×10^{-17}		[226]
154	$O + CF_3 \rightarrow COF_2 + F$	3.3×10^{-17}		[226]
155	$FO + O \rightarrow O_2 + F$	2.7×10^{-17}		[226]
156	$ClO + O \rightarrow O_2 + Cl$	4.8×10^{-20}		[234; 235]
157	$O + COF \rightarrow CO_2 + F$	9.3×10^{-17}		[226]
158	$O_2 + CF \rightarrow COF + O$	3.3×10^{-17}		[226]
159	$CHF_3 + F \rightarrow CF_3 + HF$	$7.47 \times 10^{-17} \exp\left(-0.16/T_g\right)$		[227]
160	$CHF_2 + F \rightarrow CF_2 + HF$	4.98×10^{-17}		[227]
161	$F + CHF \rightarrow CF + HF$	5×10^{-17}		[236]
162	$COF + CF_2 \rightarrow CF_3 + CO$	3×10^{-19}		[226]
163	$COF + CF_2 \rightarrow CF + COF_2$	3×10^{-19}		[226]
164	$COF + CF_3 \rightarrow CF_4 + CO$	1×10^{-17}		[226]
165	$COF + CF_3 \rightarrow CF_2 + COF_2$	1×10^{-17}		[226]
166	$CHF_2 + CF_3 \rightarrow CHF_3 + CF_2$	$4.98 \times 10^{-17} \exp\left(-0.1/T_g\right)$		[227]
167	$2COF \rightarrow COF_2 + CO$	1×10^{-17}		[226]
168	$O + CF_2 \rightarrow CO + 2F$	4×10^{-18}		[226]
169	$O^* + CF_2 \rightarrow CO + 2F$	1.4×10^{-17}		[226]
170	$H + H_2^+ \rightarrow H_2 + H^+$	6.4×10^{-16}		[237]
171	$O^+ + H \rightarrow H^+ + O$	5×10^{-16}		[9][b]
172	$F^+ + H \rightarrow H^+ + F$	5×10^{-16}		[9][b]
173	$F_2^+ + H \rightarrow H^+ + F_2$	5×10^{-16}		[9][b]
174	$CO^+ + H \rightarrow H^+ + CO$	5×10^{-16}		[9][b]
175	$H^+ + C \rightarrow C^+ + H$	5×10^{-16}		[9][b]
176	$H^+ + O_2 \rightarrow O_2^+ + H$	5×10^{-16}		[9][b]
177	$H^+ + Cl \rightarrow Cl^+ + H$	5×10^{-16}		[9][b]
178	$H^+ + Cl_2 \rightarrow Cl_2^+ + H$	5×10^{-16}		[9][b]
179	$H^+ + Br \rightarrow H + Br^+$	1×10^{-17}		[9][b]
180	$H^+ + CH \rightarrow CH^+ + H$	1.89×10^{-15}		[237]
181	$H^+ + CH_2 \rightarrow CH_2^+ + H$	1.39×10^{-15}		[237]
182	$H^+ + HCl \rightarrow HCl^+ + H$	5×10^{-16}		[9][b]
183	$H^+ + HBr \rightarrow H + HBr^+$	1×10^{-17}		[9][b]
184	$H^+ + CO \rightarrow CO^+ + H$	5×10^{-16}		[9][b]
185	$H^+ + CO_2 \rightarrow CO_2^+ + H$	5×10^{-16}		[9][b]
186	$H^+ + CF \rightarrow CF^+ + H$	5×10^{-16}		[9][b]

Continued on next page

Table A.5 (*Continued*)

ID	Reaction	k	ΔE_e	Source
187	$H^+ + CF_2 \rightarrow CF_2^+ + H$	5×10^{-16}		[9][b]
188	$H^+ + CF_3 \rightarrow CF_3^+ + H$	5×10^{-16}		[9][b]
189	$H^+ + ClO \rightarrow ClO^+ + H$	5×10^{-16}		[9][b]
190	$H^+ + CHF_2 \rightarrow CHF_2^+ + H$	5×10^{-16}		[9][b]
191	$H^+ + CHF \rightarrow CHF^+ + H$	5×10^{-16}		[9][b]
192	$F^+ + H_2 \rightarrow H_2^+ + F$	5×10^{-16}		[9][b]
193	$F_2^+ + H_2 \rightarrow H_2^+ + F_2$	5×10^{-16}		[9][b]
194	$H_2^+ + O \rightarrow O^+ + H_2$	5×10^{-16}		[9][b]
195	$H_2^+ + O_2 \rightarrow O_2^+ + H_2$	5×10^{-16}		[9][b]
196	$H_2^+ + Cl \rightarrow Cl^+ + H_2$	5×10^{-16}		[9][b]
197	$H_2^+ + Cl_2 \rightarrow Cl_2^+ + H_2$	5×10^{-16}		[9][b]
198	$Br + H_2^+ \rightarrow H_2 + Br^+$	1×10^{-17}		[9][b]
199	$H_2^+ + CH \rightarrow CH^+ + H_2$	7.1×10^{-16}		[237]
200	$H_2^+ + CH_2 \rightarrow CH_2^+ + H_2$	1×10^{-15}		[237]
201	$H_2^+ + HBr \rightarrow H_2 + HBr^+$	1×10^{-17}		[9][b]
202	$H_2^+ + CF \rightarrow CF^+ + H_2$	5×10^{-16}		[9][b]
203	$H_2^+ + CF_2 \rightarrow CF_2^+ + H_2$	5×10^{-16}		[9][b]
204	$H_2^+ + CF_3 \rightarrow CF_3^+ + H_2$	5×10^{-16}		[9][b]
205	$H_2^+ + CHF_2 \rightarrow CHF_2^+ + H_2$	5×10^{-16}		[9][b]
206	$H_2^+ + CHF \rightarrow CHF^+ + H_2$	5×10^{-16}		[9][b]
207	$O^+ + C \rightarrow C^+ + O$	5×10^{-16}		[9][b]
208	$O_2^+ + C \rightarrow C^+ + O_2$	5×10^{-16}		[9][b]
209	$F^+ + C \rightarrow C^+ + F$	1.17×10^{-15}		[238]
210	$Cl_2^+ + C \rightarrow C^+ + Cl_2$	5×10^{-16}		[9][b]
211	$Br^+ + C \rightarrow C^+ + Br$	5×10^{-16}		[9][b]
212	$H_2O^+ + C \rightarrow C^+ + H_2O$	5×10^{-16}		[9][b]
213	$HCl^+ + C \rightarrow C^+ + HCl$	5×10^{-16}		[9][b]
214	$HBr^+ + C \rightarrow C^+ + HBr$	5×10^{-16}		[9][b]
215	$CO^+ + C \rightarrow C^+ + CO$	5×10^{-16}		[9][b]
216	$CO_2^+ + C \rightarrow C^+ + CO_2$	5×10^{-16}		[9][b]
217	$ClO^+ + C \rightarrow C^+ + ClO$	5×10^{-16}		[9][b]
218	$C^+ + CF \rightarrow CF^+ + C$	3.18×10^{-15}		[238]
219	$C^+ + CF_2 \rightarrow CF_2^+ + C$	5×10^{-16}		[9][b]
220	$C^+ + CF_3 \rightarrow CF_3^+ + C$	5×10^{-16}		[9][b]
221	$C^+ + CHF_2 \rightarrow CHF_2^+ + C$	5×10^{-16}		[9][b]
222	$C^+ + CHF \rightarrow CHF^+ + C$	5×10^{-16}		[9][b]
223	$F^+ + O \rightarrow F + O^+$	1×10^{-16}		[226]
224	$F_2^+ + O \rightarrow O^+ + F_2$	5×10^{-16}		[9][b]
225	$CO^+ + O \rightarrow CO + O^+$	1.4×10^{-16}		[226]
226	$O^+ + O_2 \rightarrow O_2^+ + O$	$2 \times 10^{-17} \left(T_g/300\right)^{-0.4}$		[7]
227	$O^+ + Cl \rightarrow Cl^+ + O$	1×10^{-17}		[9][b]
228	$O^+ + Cl_2 \rightarrow Cl_2^+ + O$	1×10^{-17}		[9][b]
229	$O^+ + Br \rightarrow Br^+ + O$	5×10^{-16}		[9][b]
230	$O^+ + CH \rightarrow CH^+ + O$	5×10^{-16}		[9][b]
231	$O^+ + CH_2 \rightarrow CH_2^+ + O$	5×10^{-16}		[9][b]
232	$O^+ + H_2O \rightarrow H_2O^+ + O$	2.6×10^{-15}		[7]
233	$O^+ + HCl \rightarrow HCl^+ + O$	5×10^{-16}		[9][b]
234	$O^+ + HBr \rightarrow HBr^+ + O$	5×10^{-16}		[9][b]
235	$O^+ + CO_2 \rightarrow CO_2^+ + O$	5×10^{-16}		[9][b]
236	$O^+ + CF \rightarrow CF^+ + O$	5×10^{-16}		[9][b]
237	$O^+ + CF_2 \rightarrow CF_2^+ + O$	5×10^{-16}		[9][b]
238	$O^+ + CF_3 \rightarrow CF_3^+ + O$	5×10^{-16}		[9][b]
239	$O^+ + ClO \rightarrow ClO^+ + O$	4.9×10^{-16}		[213]
240	$O^+ + CHF_2 \rightarrow CHF_2^+ + O$	5×10^{-16}		[9][b]
241	$O^+ + CHF \rightarrow CHF^+ + O$	5×10^{-16}		[9][b]
242	$F^+ + O_2 \rightarrow F + O_2^+$	7.14×10^{-16}		[226]
243	$F_2^+ + O_2 \rightarrow O_2^+ + F_2$	5×10^{-16}		[9][b]
244	$Cl^+ + O_2 \rightarrow O_2^+ + Cl$	5×10^{-16}		[9][b]
245	$Br^+ + O_2 \rightarrow O_2^+ + Br$	5×10^{-16}		[9][b]
246	$H_2O^+ + O_2 \rightarrow O_2^+ + H_2O$	4.1×10^{-16}		[7]

Continued on next page

Table A.5 (*Continued*)

ID	Reaction	k	ΔE_e	Source
247	$HCl^+ + O_2 \rightarrow O_2^+ + HCl$	5×10^{-16}		[9]^b
248	$HBr^+ + O_2 \rightarrow O_2^+ + HBr$	5×10^{-16}		[9]^b
249	$CO^+ + O_2 \rightarrow CO + O_2^+$	1.2×10^{-16}		[226]
250	$CO_2^+ + O_2 \rightarrow CO_2 + O_2^+$	5.3×10^{-17}		[239]
251	$ClO^+ + O_2 \rightarrow O_2^+ + ClO$	5×10^{-16}		[9]^b
252	$O_2^+ + Cl_2 \rightarrow Cl_2^+ + O_2$	2×10^{-17}		[9]^b
253	$O_2^+ + CH \rightarrow CH^+ + O_2$	5×10^{-16}		[9]^b
254	$O_2^+ + CH_2 \rightarrow CH_2^+ + O_2$	5×10^{-16}		[9]^b
255	$O_2^+ + CF \rightarrow CF^+ + O_2$	5×10^{-16}		[9]^b
256	$O_2^+ + CF_2 \rightarrow CF_2^+ + O_2$	5×10^{-16}		[9]^b
257	$O_2^+ + CF_3 \rightarrow CF_3^+ + O_2$	5×10^{-16}		[9]^b
258	$O_2^+ + CHF_2 \rightarrow CHF_2^+ + O_2$	5×10^{-16}		[9]^b
259	$O_2^+ + CHF \rightarrow CHF^+ + O_2$	5×10^{-16}		[9]^b
260	$F^+ + F_2 \rightarrow F_2^+ + F$	7.94×10^{-16}		[238]
261	$F^+ + Cl \rightarrow Cl^+ + F$	5×10^{-16}		[9]^b
262	$F^+ + Cl_2 \rightarrow Cl_2^+ + F$	5×10^{-16}		[9]^b
263	$F^+ + Br \rightarrow Br^+ + F$	5×10^{-16}		[9]^b
264	$F^+ + CH \rightarrow CH^+ + F$	5×10^{-16}		[9]^b
265	$F^+ + CH_2 \rightarrow CH_2^+ + F$	5×10^{-16}		[9]^b
266	$F^+ + H_2O \rightarrow H_2O^+ + F$	5×10^{-16}		[9]^b
267	$F^+ + HCl \rightarrow HCl^+ + F$	5×10^{-16}		[9]^b
268	$F^+ + HBr \rightarrow HBr^+ + F$	5×10^{-16}		[9]^b
269	$F^+ + CO \rightarrow CO^+ + F$	5×10^{-16}		[9]^b
270	$F^+ + CO_2 \rightarrow CO_2^+ + F$	5×10^{-16}		[9]^b
271	$F^+ + CF \rightarrow CF^+ + F$	5×10^{-16}		[219]
272	$F^+ + ClO \rightarrow ClO^+ + F$	5×10^{-16}		[9]^b
273	$F^+ + CHF \rightarrow CHF^+ + F$	5×10^{-16}		[9]^b
274	$F_2^+ + Cl \rightarrow Cl^+ + F_2$	5×10^{-16}		[9]^b
275	$F_2^+ + Cl_2 \rightarrow Cl_2^+ + F_2$	5×10^{-16}		[9]^b
276	$F_2^+ + Br \rightarrow Br^+ + F_2$	5×10^{-16}		[9]^b
277	$F_2^+ + CH \rightarrow CH^+ + F_2$	5×10^{-16}		[9]^b
278	$F_2^+ + CH_2 \rightarrow CH_2^+ + F_2$	5×10^{-16}		[9]^b
279	$F_2^+ + H_2O \rightarrow H_2O^+ + F_2$	5×10^{-16}		[9]^b
280	$F_2^+ + HCl \rightarrow HCl^+ + F_2$	5×10^{-16}		[9]^b
281	$F_2^+ + HBr \rightarrow HBr^+ + F_2$	5×10^{-16}		[9]^b
282	$F_2^+ + CO \rightarrow CO^+ + F_2$	5×10^{-16}		[9]^b
283	$F_2^+ + CO_2 \rightarrow CO_2^+ + F_2$	5×10^{-16}		[9]^b
284	$F_2^+ + CF_2 \rightarrow CF_2^+ + F_2$	1×10^{-15}		[238]
285	$F_2^+ + ClO \rightarrow ClO^+ + F_2$	5×10^{-16}		[9]^b
286	$F_2^+ + CHF_2 \rightarrow CHF_2^+ + F_2$	5×10^{-16}		[9]^b
287	$F_2^+ + CHF \rightarrow CHF^+ + F_2$	5×10^{-16}		[9]^b
288	$Br^+ + Cl \rightarrow Cl^+ + Br$	5×10^{-16}		[9]^b
289	$H_2O^+ + Cl \rightarrow Cl^+ + H_2O$	5×10^{-16}		[9]^b
290	$CO^+ + Cl \rightarrow Cl^+ + CO$	5×10^{-16}		[9]^b
291	$CO_2^+ + Cl \rightarrow Cl^+ + CO_2$	5×10^{-16}		[9]^b
292	$Cl_2 + Cl^+ \rightarrow Cl_2^+ + Cl$	$5.4 \times 10^{-16}\ (T_g/300)^{0.5}$		[240; 241]
293	$Cl^+ + CH \rightarrow CH^+ + Cl$	5×10^{-16}		[9]^b
294	$Cl^+ + CH_2 \rightarrow CH_2^+ + Cl$	5×10^{-16}		[9]^b
295	$Cl^+ + HCl \rightarrow HCl^+ + Cl$	5×10^{-16}		[9]^b
296	$Cl^+ + HBr \rightarrow HBr^+ + Cl$	5×10^{-16}		[9]^b
297	$Cl^+ + ClO \rightarrow ClO^+ + Cl$	4.9×10^{-16}		[9]^b
298	$Cl^+ + CHF_2 \rightarrow CHF_2^+ + Cl$	5×10^{-16}		[9]^b
299	$Cl^+ + CHF \rightarrow CHF^+ + Cl$	5×10^{-16}		[9]^b
300	$Br^+ + Cl_2 \rightarrow Cl_2^+ + Br$	5×10^{-16}		[9]^b
301	$H_2O^+ + Cl_2 \rightarrow Cl_2^+ + H_2O$	5×10^{-16}		[9]^b
302	$HCl^+ + Cl_2 \rightarrow Cl_2^+ + HCl$	5×10^{-16}		[9]^b
303	$HBr^+ + Cl_2 \rightarrow Cl_2^+ + HBr$	5×10^{-16}		[9]^b
304	$CO^+ + Cl_2 \rightarrow Cl_2^+ + CO$	5×10^{-16}		[9]^b
305	$CO_2^+ + Cl_2 \rightarrow Cl_2^+ + CO_2$	5×10^{-16}		[9]^b
306	$ClO^+ + Cl_2 \rightarrow Cl_2^+ + ClO$	5×10^{-16}		[9]^b

Continued on next page

Table A.5 (*Continued*)

ID	Reaction	k	ΔE_e	Source
307	$Cl_2^+ + CH \rightarrow CH^+ + Cl_2$	5×10^{-16}		[9]^b
308	$Cl_2^+ + CH_2 \rightarrow CH_2^+ + Cl_2$	5×10^{-16}		[9]^b
309	$Cl_2^+ + CF \rightarrow CF^+ + Cl_2$	5×10^{-16}		[9]^b
310	$Cl_2^+ + CF_2 \rightarrow CF_2^+ + Cl_2$	5×10^{-16}		[9]^b
311	$Cl_2^+ + CF_3 \rightarrow CF_3^+ + Cl_2$	5×10^{-16}		[9]^b
312	$Cl_2^+ + CHF_2 \rightarrow CHF_2^+ + Cl_2$	5×10^{-16}		[9]^b
313	$Cl_2^+ + CHF \rightarrow CHF^+ + Cl_2$	5×10^{-16}		[9]^b
314	$H_2O^+ + Br \rightarrow Br^+ + H_2O$	5×10^{-16}		[9]^b
315	$CO^+ + Br \rightarrow Br^+ + CO$	5×10^{-16}		[9]^b
316	$CO_2^+ + Br \rightarrow Br^+ + CO_2$	5×10^{-16}		[9]^b
317	$Br^+ + CH \rightarrow CH^+ + Br$	5×10^{-16}		[9]^b
318	$Br^+ + CH_2 \rightarrow CH_2^+ + Br$	5×10^{-16}		[9]^b
319	$Br^+ + HCl \rightarrow HCl^+ + Br$	5×10^{-16}		[9]^b
320	$Br^+ + HBr \rightarrow HBr^+ + Br$	1×10^{-17}		[9]^b
321	$Br^+ + CF \rightarrow CF^+ + Br$	5×10^{-16}		[9]^b
322	$Br^+ + CF_2 \rightarrow CF_2^+ + Br$	5×10^{-16}		[9]^b
323	$Br^+ + CF_3 \rightarrow CF_3^+ + Br$	5×10^{-16}		[9]^b
324	$Br^+ + ClO \rightarrow ClO^+ + Br$	5×10^{-16}		[9]^b
325	$Br^+ + CHF_2 \rightarrow CHF_2^+ + Br$	5×10^{-16}		[9]^b
326	$Br^+ + CHF \rightarrow CHF^+ + Br$	5×10^{-16}		[9]^b
327	$H_2O^+ + CH \rightarrow CH^+ + H_2O$	5×10^{-16}		[9]^b
328	$HCl^+ + CH \rightarrow CH^+ + HCl$	5×10^{-16}		[9]^b
329	$HBr^+ + CH \rightarrow CH^+ + HBr$	5×10^{-16}		[9]^b
330	$CO^+ + CH \rightarrow CH^+ + CO$	5×10^{-16}		[9]^b
331	$CO_2^+ + CH \rightarrow CH^+ + CO_2$	5×10^{-16}		[9]^b
332	$ClO^+ + CH \rightarrow CH^+ + ClO$	5×10^{-16}		[9]^b
333	$CH^+ + CH_2 \rightarrow CH_2^+ + CH$	5×10^{-16}		[9]^b
334	$CH^+ + CF \rightarrow CF^+ + CH$	5×10^{-16}		[9]^b
335	$CH^+ + CF_2 \rightarrow CF_2^+ + CH$	5×10^{-16}		[9]^b
336	$CH^+ + CF_3 \rightarrow CF_3^+ + CH$	5×10^{-16}		[9]^b
337	$CH^+ + CHF_2 \rightarrow CHF_2^+ + CH$	5×10^{-16}		[9]^b
338	$CH^+ + CHF \rightarrow CHF^+ + CH$	5×10^{-16}		[9]^b
339	$H_2O^+ + CH_2 \rightarrow CH_2^+ + H_2O$	5×10^{-16}		[9]^b
340	$HCl^+ + CH_2 \rightarrow CH_2^+ + HCl$	5×10^{-16}		[9]^b
341	$HBr^+ + CH_2 \rightarrow CH_2^+ + HBr$	5×10^{-16}		[9]^b
342	$CO^+ + CH_2 \rightarrow CH_2^+ + CO$	5×10^{-16}		[9]^b
343	$CO_2^+ + CH_2 \rightarrow CH_2^+ + CO_2$	5×10^{-16}		[9]^b
344	$CF_2^+ + CH_2 \rightarrow CH_2^+ + CF_2$	5×10^{-16}		[9]^b
345	$ClO^+ + CH_2 \rightarrow CH_2^+ + ClO$	5×10^{-16}		[9]^b
346	$CHF^+ + CH_2 \rightarrow CH_2^+ + CHF$	5×10^{-16}		[9]^b
347	$CH_2^+ + CF \rightarrow CF^+ + CH_2$	5×10^{-16}		[9]^b
348	$CH_2^+ + CF_3 \rightarrow CF_3^+ + CH_2$	5×10^{-16}		[9]^b
349	$CH_2^+ + CHF_2 \rightarrow CHF_2^+ + CH_2$	5×10^{-16}		[9]^b
350	$CO^+ + H_2O \rightarrow H_2O^+ + CO$	5×10^{-16}		[9]^b
351	$H_2O^+ + HCl \rightarrow HCl^+ + H_2O$	5×10^{-16}		[9]^b
352	$H_2O^+ + HBr \rightarrow HBr^+ + H_2O$	5×10^{-16}		[9]^b
353	$H_2O^+ + CO_2 \rightarrow CO_2^+ + H_2O$	5×10^{-16}		[9]^b
354	$H_2O^+ + CF \rightarrow CF^+ + H_2O$	5×10^{-16}		[9]^b
355	$H_2O^+ + CF_2 \rightarrow CF_2^+ + H_2O$	5×10^{-16}		[9]^b
356	$H_2O^+ + CF_3 \rightarrow CF_3^+ + H_2O$	5×10^{-16}		[9]^b
357	$H_2O^+ + ClO \rightarrow ClO^+ + H_2O$	5×10^{-16}		[9]^b
358	$H_2O^+ + CHF_2 \rightarrow CHF_2^+ + H_2O$	5×10^{-16}		[9]^b
359	$H_2O^+ + CHF \rightarrow CHF^+ + H_2O$	5×10^{-16}		[9]^b
360	$CO^+ + HCl \rightarrow HCl^+ + CO$	5×10^{-16}		[9]^b
361	$CO_2^+ + HCl \rightarrow HCl^+ + CO_2$	5×10^{-16}		[9]^b
362	$HCl^+ + HBr \rightarrow HBr^+ + HCl$	5×10^{-16}		[9]^b
363	$HCl^+ + CF \rightarrow CF^+ + HCl$	5×10^{-16}		[9]^b
364	$HCl^+ + CF_2 \rightarrow CF_2^+ + HCl$	5×10^{-16}		[9]^b
365	$HCl^+ + CF_3 \rightarrow CF_3^+ + HCl$	5×10^{-16}		[9]^b
366	$HCl^+ + ClO \rightarrow ClO^+ + HCl$	5×10^{-16}		[9]^b

Continued on next page

Table A.5 (*Continued*)

ID	Reaction	k	ΔE_e	Source
367	$HCl^+ + CHF_2 \rightarrow CHF_2^+ + HCl$	5×10^{-16}		[9]^b
368	$HCl^+ + CHF \rightarrow CHF^+ + HCl$	5×10^{-16}		[9]^b
369	$CO^+ + HBr \rightarrow HBr^+ + CO$	5×10^{-16}		[9]^b
370	$CO_2^+ + HBr \rightarrow HBr^+ + CO_2$	5×10^{-16}		[9]^b
371	$HBr^+ + CF \rightarrow CF^+ + HBr$	5×10^{-16}		[9]^b
372	$HBr^+ + CF_2 \rightarrow CF_2^+ + HBr$	5×10^{-16}		[9]^b
373	$HBr^+ + CF_3 \rightarrow CF_3^+ + HBr$	5×10^{-16}		[9]^b
374	$HBr^+ + ClO \rightarrow ClO^+ + HBr$	5×10^{-16}		[9]^b
375	$HBr^+ + CHF_2 \rightarrow CHF_2^+ + HBr$	5×10^{-16}		[9]^b
376	$HBr^+ + CHF \rightarrow CHF^+ + HBr$	5×10^{-16}		[9]^b
377	$CO^+ + CO_2 \rightarrow CO + CO_2^+$	1×10^{-15}		[239]
378	$CO^+ + CF \rightarrow CF^+ + CO$	5×10^{-16}		[9]^b
379	$CO^+ + ClO \rightarrow ClO^+ + CO$	5×10^{-16}		[9]^b
380	$CO^+ + CHF_2 \rightarrow CHF_2^+ + CO$	5×10^{-16}		[9]^b
381	$CO^+ + CHF \rightarrow CHF^+ + CO$	5×10^{-16}		[9]^b
382	$CO_2^+ + CF \rightarrow CF^+ + CO_2$	5×10^{-16}		[9]^b
383	$CO_2^+ + CF_2 \rightarrow CF_2^+ + CO_2$	5×10^{-16}		[9]^b
384	$CO_2^+ + CF_3 \rightarrow CF_3^+ + CO_2$	5×10^{-16}		[9]^b
385	$CO_2^+ + ClO \rightarrow ClO^+ + CO_2$	5×10^{-16}		[9]^b
386	$CO_2^+ + CHF_2 \rightarrow CHF_2^+ + CO_2$	5×10^{-16}		[9]^b
387	$CO_2^+ + CHF \rightarrow CHF^+ + CO_2$	5×10^{-16}		[9]^b
388	$ClO^+ + CF \rightarrow CF^+ + ClO$	5×10^{-16}		[9]^b
389	$CHF^+ + CF \rightarrow CF^+ + CHF$	5×10^{-16}		[9]^b
390	$CF^+ + CF_3 \rightarrow CF_3^+ + CF$	1.71×10^{-15}		[242; 243]
391	$CF^+ + CHF_2 \rightarrow CHF_2^+ + CF$	5×10^{-16}		[9]^b
392	$ClO^+ + CF_2 \rightarrow CF_2^+ + ClO$	5×10^{-16}		[9]^b
393	$CHF^+ + CF_2 \rightarrow CF_2^+ + CHF$	5×10^{-16}		[9]^b
394	$CF_2^+ + CF_3 \rightarrow CF_3^+ + CF_2$	1.48×10^{-15}		[242]
395	$CF_2^+ + CHF_2 \rightarrow CHF_2^+ + CF_2$	5×10^{-16}		[9]^b
396	$ClO^+ + CF_3 \rightarrow CF_3^+ + ClO$	5×10^{-16}		[9]^b
397	$CHF_2^+ + CF_3 \rightarrow CF_3^+ + CHF_2$	5×10^{-16}		[244]
398	$CHF^+ + CF_3 \rightarrow CF_3^+ + CHF$	5×10^{-16}		[9]^b
399	$ClO^+ + CHF_2 \rightarrow CHF_2^+ + ClO$	5×10^{-16}		[9]^b
400	$ClO^+ + CHF \rightarrow CHF^+ + ClO$	5×10^{-16}		[9]^b
401	$CHF^+ + CHF_2 \rightarrow CHF_2^+ + CHF$	6.4×10^{-16}		[9]^b
402	$H_3^+ + H \rightarrow H^+ + H_2 + H$	5×10^{-16}		[9]^b
403	$H_3^+ + H_2 \rightarrow H_2^+ + H_2 + H$	5×10^{-16}		[9]^b
404	$H_3^+ + O \rightarrow O^+ + H_2 + H$	5×10^{-16}		[9]^b
405	$H_3^+ + O_2 \rightarrow O_2^+ + H_2 + H$	5×10^{-16}		[9]^b
406	$H_3^+ + F_2 \rightarrow F_2^+ + H_2 + H$	5×10^{-16}		[9]^b
407	$H_3^+ + Cl \rightarrow Cl^+ + H_2 + H$	5×10^{-16}		[9]^b
408	$H_3^+ + Cl_2 \rightarrow Cl_2^+ + H_2 + H$	5×10^{-16}		[9]^b
409	$H_3^+ + Br \rightarrow H_2 + H + Br^+$	1×10^{-17}		[9]^b
410	$H_3^+ + CH_2 \rightarrow CH_2^+ + H_2 + H$	5×10^{-16}		[9]^b
411	$H_3^+ + H_2O \rightarrow H_2O^+ + H_2 + H$	5×10^{-16}		[9]^b
412	$H_3^+ + HCl \rightarrow HCl^+ + H_2 + H$	5×10^{-16}		[9]^b
413	$H_3^+ + HBr \rightarrow H_2 + H + HBr^+$	1×10^{-17}		[9]^b
414	$H_3^+ + CO \rightarrow CO^+ + H_2 + H$	5×10^{-16}		[9]^b
415	$H_3^+ + CO_2 \rightarrow CO_2^+ + H_2 + H$	5×10^{-16}		[9]^b
416	$H_3^+ + CF \rightarrow CF^+ + H_2 + H$	5×10^{-16}		[9]^b
417	$H_3^+ + CF_2 \rightarrow CF_2^+ + H_2 + H$	5×10^{-16}		[9]^b
418	$H_3^+ + CF_3 \rightarrow CF_3^+ + H_2 + H$	5×10^{-16}		[9]^b
419	$H_3^+ + ClO \rightarrow ClO^+ + H_2 + H$	5×10^{-16}		[9]^b
420	$H_3^+ + CHF_2 \rightarrow CHF_2^+ + H_2 + H$	5×10^{-16}		[9]^b
421	$H_3^+ + CHF \rightarrow CHF^+ + H_2 + H$	5×10^{-16}		[9]^b
422	$F_2^+ + CF_3 \rightarrow CF_3^+ + 2F$	1.6×10^{-15}		[238]
423	$CH^+ + H \rightarrow C^+ + H_2$	7.5×10^{-16}		[237]
424	$H^+ + CH_2 \rightarrow CH^+ + H_2$	1.39×10^{-15}		[237]
425	$H_2 + H_2^+ \rightarrow H + H_3^+$	2.08×10^{-15}		[237]
426	$CH^+ + H_2 \rightarrow CH_2^+ + H$	1.2×10^{-15}		[237]

Continued on next page

Table A.5 (*Continued*)

ID	Reaction	k	ΔE_e	Source
427	$H_2^+ + C \rightarrow CH^+ + H$	2.4×10^{-15}		[237]
428	$H_2^+ + CH \rightarrow CH_2^+ + H$	7.1×10^{-16}		[237]
429	$H_3^+ + C \rightarrow CH^+ + H_2$	2×10^{-15}		[237]
430	$H_3^+ + CH \rightarrow CH_2^+ + H_2$	1.2×10^{-15}		[237]
431	$F_2^+ + C \rightarrow CF^+ + F$	1.04×10^{-15}		[238]
432	$CH^+ + C \rightarrow C_2^+ + H$	1.2×10^{-15}		[237]
433	$CF_2^+ + C \rightarrow CF^+ + CF$	1.04×10^{-15}		[238]
434	$O^+ + CF_4 \rightarrow CF_3^+ + FO$	1.4×10^{-15}		[226]
435	$F^+ + O_2 \rightarrow O^+ + FO$	5.04×10^{-17}		[245]
436	$F^+ + CF_2 \rightarrow CF^+ + F_2$	2.28×10^{-15}		[238; 242]
437	$F^+ + CF_3 \rightarrow CF_2^+ + F_2$	2.09×10^{-15}		[238; 242]
438	$F^+ + CF_4 \rightarrow F_2 + CF_3^+$	1×10^{-15}		[238; 242]
439	$F^+ + CHF_2 \rightarrow CHF^+ + F_2$	2.09×10^{-15}		[9][b]
440	$F_2^+ + CF \rightarrow CF_2^+ + F$	2.18×10^{-15}		[238]
441	$F_2^+ + CF_2 \rightarrow CF_3^+ + F$	1.79×10^{-15}		[238]
442	$F_2^+ + CF_4 \rightarrow CF_3^+ + F + F_2$	1×10^{-16}		[238]
443	$CO^+ + CF_2 \rightarrow COF + CF^+$	7×10^{-16}		[226]
444	$CO^+ + CF_3 \rightarrow COF + CF_2^+$	7×10^{-16}		[226]
445	$CO^+ + CF_4 \rightarrow COF + CF_3^+$	7×10^{-16}		[226]
446	$CF_2^+ + CF \rightarrow CF_3^+ + C$	2.06×10^{-15}		[238]
447	$CF^+ + CF_4 \rightarrow CF_3^+ + CF_2$	1.8×10^{-16}		[242; 246]
448	$CF_2^+ + CF_4 \rightarrow CF_3^+ + CF_3$	4×10^{-16}		[242; 246]
449	$O^- + H^+ \rightarrow O + H$	1×10^{-13}		[247]
450	$F^- + H^+ \rightarrow H + F$	2.02×10^{-14}		[248]
451	$Cl^- + H^+ \rightarrow H + Cl$	2.02×10^{-14}		[248]
452	$Br^- + H^+ \rightarrow Br + H$	1×10^{-13}		[9][b]
453	$CF_3^- + H^+ \rightarrow H + CF_3$	2.02×10^{-13}		[248]
454	$O^- + H_2^+ \rightarrow O + H_2$	1×10^{-13}		[247]
455	$F^- + H_2^+ \rightarrow H_2 + F$	1.44×10^{-13}		[248]
456	$Cl^- + H_2^+ \rightarrow H_2 + Cl$	1.44×10^{-13}		[248]
457	$Br^- + H_2^+ \rightarrow Br + H_2$	1×10^{-13}		[9][b]
458	$CF_3^- + H_2^+ \rightarrow H_2 + CF_3$	1.44×10^{-13}		[248]
459	$O^- + C^+ \rightarrow O + C$	3×10^{-13}		[224]
460	$F^- + C^+ \rightarrow F + C$	2.2×10^{-13}		[238]
461	$Cl^- + C^+ \rightarrow C + Cl$	6.27×10^{-15}		[248]
462	$Br^- + C^+ \rightarrow C + Br$	6.27×10^{-15}		[248]
463	$CF_3^- + C^+ \rightarrow CF_3 + C$	3×10^{-13}		[247]
464	$O^- + O^+ \rightarrow 2O$	1×10^{-13}		[247]
465	$O^+ + F^- \rightarrow O + F$	1×10^{-13}		[9][b]
466	$Cl^- + O^+ \rightarrow Cl + O$	5×10^{-20}		[8]
467	$Br^- + O^+ \rightarrow O + Br$	5.56×10^{-15}		[248]
468	$CF_3^- + O^+ \rightarrow CF_3 + O$	2.5×10^{-13}		[224]
469	$O^- + O_2^+ \rightarrow O_2 + O$	1×10^{-13}		[247]
470	$O^- + F^+ \rightarrow O + F$	3×10^{-13}		[224]
471	$O^- + F_2^+ \rightarrow O + F_2$	1.5×10^{-13}		[224]
472	$O^- + Cl^+ \rightarrow O + Cl$	1.7×10^{-19}		[8]
473	$O^- + Cl_2^+ \rightarrow O + Cl_2$	1.7×10^{-19}		[8]
474	$O^- + Br^+ \rightarrow Br + O$	3.3×10^{-15}		[248]
475	$O^- + CH^+ \rightarrow CH + O$	6.06×10^{-14}		[248]
476	$O^- + CH_2^+ \rightarrow CH_2 + O$	5.87×10^{-14}		[248]
477	$O^- + H_2O^+ \rightarrow O + H_2O$	1×10^{-13}		[247]
478	$O^- + HCl^+ \rightarrow HCl + O$	4.1×10^{-14}		[248]
479	$O^- + HBr^+ \rightarrow HBr + O$	3.29×10^{-14}		[248]
480	$O^- + CO^+ \rightarrow O + CO$	2×10^{-13}		[224]
481	$O^- + CO_2^+ \rightarrow CO_2 + O$	3.87×10^{-14}		[248]
482	$O^- + CF^+ \rightarrow O + CF$	2×10^{-13}		[224]
483	$O^- + CF_2^+ \rightarrow O + CF_2$	2×10^{-13}		[224]
484	$O^- + CF_3^+ \rightarrow O + CF_3$	2×10^{-13}		[224]
485	$O^- + ClO^+ \rightarrow ClO + O$	3.69×10^{-14}		[248]
486	$O^- + CHF_2^+ \rightarrow CHF_2 + O$	3.7×10^{-14}		[248]

Continued on next page

Table A.5 (*Continued*)

ID	Reaction	k	ΔE_e	Source
487	$O^- + CHF^+ \rightarrow CHF + O$	4.28×10^{-14}		[248]
488	$O_2^+ + F^- \rightarrow O_2 + F$	1×10^{-13}		[9][b]
489	$Cl^- + O_2^+ \rightarrow Cl + O_2$	5×10^{-20}		[8]
490	$Br^- + O_2^+ \rightarrow O_2 + Br$	4.28×10^{-14}		[248]
491	$CF_3^- + O_2^+ \rightarrow CF_3 + O_2$	2×10^{-13}		[248]
492	$F^- + F^+ \rightarrow 2F$	5×10^{-14}		[124]
493	$Cl^- + F^+ \rightarrow F + Cl$	5.19×10^{-15}		[248]
494	$Br^- + F^+ \rightarrow F + Br$	5.19×10^{-15}		[248]
495	$CF_3^- + F^+ \rightarrow CF_3 + F$	2.5×10^{-13}		[242]
496	$F^- + F_2^+ \rightarrow F + F_2$	5×10^{-14}		[124]
497	$F^- + Cl^+ \rightarrow Cl + F$	4.14×10^{-15}		[248]
498	$F^- + Cl_2^+ \rightarrow Cl_2 + F$	3.39×10^{-14}		[248]
499	$F^- + Br^+ \rightarrow Br + F$	3.3×10^{-15}		[248]
500	$F^- + CH^+ \rightarrow CH + F$	6.06×10^{-14}		[248]
501	$F^- + CH_2^+ \rightarrow CH_2 + F$	5.87×10^{-14}		[248]
502	$F^- + H_2O^+ \rightarrow H_2O + F$	5.3×10^{-14}		[248]
503	$F^- + HCl^+ \rightarrow HCl + F$	4.1×10^{-14}		[248]
504	$F^- + HBr^+ \rightarrow HBr + F$	3.29×10^{-14}		[248]
505	$F^- + CO^+ \rightarrow CO + F$	4.49×10^{-14}		[248]
506	$F^- + CO_2^+ \rightarrow CO_2 + F$	3.87×10^{-14}		[248]
507	$F^- + CF^+ \rightarrow CF + F$	9.8×10^{-14}		[242]
508	$F^- + CF_2^+ \rightarrow F + CF_2$	9.1×10^{-14}		[238; 242]
509	$F^- + CF_3^+ \rightarrow F + CF_3$	3×10^{-13}		[238; 242]
510	$F^- + ClO^+ \rightarrow ClO + F$	3.69×10^{-14}		[248]
511	$F^- + CHF_2^+ \rightarrow CHF_2 + F$	3.7×10^{-14}		[248]
512	$F^- + CHF^+ \rightarrow CHF + F$	4.28×10^{-14}		[248]
513	$Cl^- + F_2^+ \rightarrow F_2 + Cl$	4.05×10^{-14}		[248]
514	$Br^- + F_2^+ \rightarrow F_2 + Br$	4.05×10^{-14}		[248]
515	$CF_3^- + F_2^+ \rightarrow CF_3 + F_2$	2×10^{-13}		[242]
516	$Cl^+ + Cl^- \rightarrow 2Cl$	$1 \times 10^{-13} \left(T_g/300\right)^{0.5}$		[240; 241; 249]
517	$Br^- + Cl^+ \rightarrow Cl + Br$	4.14×10^{-15}		[248]
518	$CF_3^- + Cl^+ \rightarrow Cl + CF_3$	4.14×10^{-14}		[248]
519	$Cl^- + Cl_2^+ \rightarrow Cl_2 + Cl$	1×10^{-13}		[9][b]
520	$Cl^- + Br^+ \rightarrow Br + Cl$	3.3×10^{-15}		[248]
521	$Cl^- + CH^+ \rightarrow CH + Cl$	6.06×10^{-14}		[248]
522	$Cl^- + CH_2^+ \rightarrow CH_2 + Cl$	5.87×10^{-14}		[248]
523	$Cl^- + H_2O^+ \rightarrow H_2O + Cl$	5.3×10^{-14}		[248]
524	$Cl^- + HCl^+ \rightarrow HCl + Cl$	4.1×10^{-14}		[248]
525	$Cl^- + HBr^+ \rightarrow HBr + Cl$	3.29×10^{-14}		[248]
526	$Cl^- + CO^+ \rightarrow CO + Cl$	4.49×10^{-14}		[248]
527	$Cl^- + CO_2^+ \rightarrow CO_2 + Cl$	3.87×10^{-14}		[248]
528	$Cl^- + CF^+ \rightarrow CF + Cl$	4.33×10^{-14}		[248]
529	$Cl^- + CF_2^+ \rightarrow CF_2 + Cl$	3.72×10^{-14}		[248]
530	$Cl^- + CF_3^+ \rightarrow CF_3 + Cl$	3.41×10^{-14}		[248]
531	$Cl^- + ClO^+ \rightarrow ClO + Cl$	3.69×10^{-14}		[248]
532	$Cl^- + CHF_2^+ \rightarrow CHF_2 + Cl$	3.7×10^{-14}		[248]
533	$Cl^- + CHF^+ \rightarrow CHF + Cl$	4.28×10^{-14}		[248]
534	$Br^- + Cl_2^+ \rightarrow Cl_2 + Br$	3.39×10^{-14}		[248]
535	$CF_3^- + Cl_2^+ \rightarrow Cl_2 + CF_3$	3.39×10^{-14}		[248]
536	$Br^- + Br^+ \rightarrow 2Br$	1×10^{-13}		[9][b]
537	$CF_3^- + Br^+ \rightarrow Br + CF_3$	3.3×10^{-14}		[248]
538	$Br^- + CH^+ \rightarrow CH + Br$	6.06×10^{-14}		[248]
539	$Br^- + CH_2^+ \rightarrow CH_2 + Br$	5.87×10^{-14}		[248]
540	$Br^- + HBr^+ \rightarrow HBr + Br$	1×10^{-13}		[9][b]
541	$Br^- + CF^+ \rightarrow CF + Br$	4.33×10^{-14}		[248]
542	$Br^- + CF_2^+ \rightarrow CF_2 + Br$	3.72×10^{-14}		[248]
543	$Br^- + CF_3^+ \rightarrow CF_3 + Br$	3.41×10^{-14}		[248]
544	$Br^- + CHF_2^+ \rightarrow CHF_2 + Br$	3.7×10^{-14}		[248]
545	$Br^- + CHF^+ \rightarrow CHF + Br$	4.28×10^{-14}		[248]
546	$CF_3^- + CH^+ \rightarrow CH + CF_3$	6.06×10^{-14}		[248]

Continued on next page

Table A.5 (*Continued*)

ID	Reaction	k	ΔE_e	Source
547	$CF_3^- + CH_2^+ \rightarrow CH_2 + CF_3$	5.87×10^{-14}		[248]
548	$CF_3^- + H_2O^+ \rightarrow H_2O + CF_3$	5.3×10^{-14}		[248]
549	$CF_3^- + HCl^+ \rightarrow HCl + CF_3$	4.1×10^{-14}		[248]
550	$CF_3^- + HBr^+ \rightarrow HBr + CF_3$	3.29×10^{-14}		[248]
551	$CF_3^- + CO^+ \rightarrow CF_3 + CO$	2×10^{-13}		[248]
552	$CF_3^- + CO_2^+ \rightarrow CO_2 + CF_3$	3.87×10^{-14}		[248]
553	$CF_3^- + CF^+ \rightarrow CF + CF_3$	2×10^{-13}		[242]
554	$CF_3^- + CF_2^+ \rightarrow CF_3 + CF_2$	2×10^{-13}		[242]
555	$CF_3^+ + CF_3^- \rightarrow 2CF_3$	1.5×10^{-13}		[242]
556	$CF_3^- + ClO^+ \rightarrow ClO + CF_3$	3.69×10^{-14}		[248]
557	$CF_3^- + CHF_2^+ \rightarrow CHF_2 + CF_3$	3.7×10^{-14}		[248]
558	$CF_3^- + CHF^+ \rightarrow CHF + CF_3$	4.28×10^{-14}		[248]
559	$O^- + H_3^+ \rightarrow O + H_2 + H$	1×10^{-13}		[247]
560	$H_3^+ + F^- \rightarrow H_2 + H + F$	1.18×10^{-13}		[248]
561	$Cl^- + H_3^+ \rightarrow H_2 + H + Cl$	1.18×10^{-13}		[248]
562	$Br^- + H_3^+ \rightarrow Br + H_2 + H$	1×10^{-13}		[9][b]
563	$CF_3^- + H_3^+ \rightarrow H_2 + H + CF_3$	1.18×10^{-13}		[248]

Table A.6: Detailed chemistry set for all the CH_4–N_2 reduction cases. The kinetic data are taken directly from the corresponding pre-compiled chemistry set in QDB database [9] (QDB chemistry ID: C28). Primary sources are cited, if listed in QDB. The purpose of all the test chemistry sets extracted from QDB in this work is merely to provide input for testing of the presented chemistry reduction method, therefore the consistency of this chemistry set and the validity of the cited sources listed in QDB were not explicitly verified in this work.

[a] Fitted from a cross section on a grid of Maxwellian temperatures.

[b] Original source not listed in QDB.

ID	Reaction	k	ΔE_e	Source
1	$e + H \rightarrow H + e$	$1.81 \times 10^{-13} T_e^{-0.23} \exp(-0.19/T_e)$		[250][a]
2	$e + H^+ \rightarrow H^+ + e$	$1.61 \times 10^{-10} T_e^{-1.22} \exp(-0.04/T_e)$		[197][a]
3	$e + H^- \rightarrow H^- + e$	$1.61 \times 10^{-10} T_e^{-1.22} \exp(-0.04/T_e)$		[9][a,b]
4	$e + H(n=2) \rightarrow e + H(n=2)$	$1.81 \times 10^{-13} T_e^{-0.23} \exp(-0.19/T_e)$		[250][a]
5	$e + H_2 \rightarrow H_2 + e$	$1.76 \times 10^{-13} T_e^{-0.35} \exp(-0.65/T_e)$		[197][a]
6	$e + H_2^+ \rightarrow H_2^+ + e$	$1.61 \times 10^{-10} T_e^{-1.22} \exp(-0.04/T_e)$		[251][a]
7	$e + H_3^+ \rightarrow H_3^+ + e$	$1.61 \times 10^{-10} T_e^{-1.22} \exp(-0.04/T_e)$		[251][a]
8	$e + N \rightarrow N + e$	$6.23 \times 10^{-14} T_e^{0.31} \exp(-0.71/T_e)$		[252][a]
9	$e + N^+ \rightarrow N^+ + e$	$1.61 \times 10^{-10} T_e^{-1.22} \exp(-0.04/T_e)$		[251][a]
10	$e + N^* \rightarrow N^* + e$	$6.23 \times 10^{-14} T_e^{0.31} \exp(-0.71/T_e)$		[252][a]
11	$e + N_2 \rightarrow N_2 + e$	$1.06 \times 10^{-13} T_e^{0.36} \exp(-0.26/T_e)$		[9][a,b]
12	$e + N_2^+ \rightarrow N_2^+ + e$	$1.61 \times 10^{-10} T_e^{-1.22} \exp(-0.04/T_e)$		[251][a]
13	$e + N_2^* \rightarrow N_2^* + e$	$1.07 \times 10^{-13} T_e^{0.36} \exp(-0.26/T_e)$		[9][a,b]
14	$e + N_3^+ \rightarrow e + N_3^+$	$1.61 \times 10^{-10} T_e^{-1.22} \exp(-0.04/T_e)$		[6][a]
15	$e + N_4^+ \rightarrow e + N_4^+$	$1.61 \times 10^{-10} T_e^{-1.22} \exp(-0.04/T_e)$		[6][a]
16	$e + CH_4 \rightarrow CH_4 + e$	$2.48 \times 10^{-13} T_e^{0.17} \exp(-2.11/T_e)$		[9][a,b]
17	$e + C_2H_2 \rightarrow C_2H_2 + e$	$2.65 \times 10^{-13} T_e^{-0.14} \exp(-0.76/T_e)$		[253][a]
18	$e + C_2H_4 \rightarrow C_2H_4 + e$	$1.83 \times 10^{-13} T_e^{0.23} \exp(-0.32/T_e)$		[9][a,b]
19	$e + C_2H_6 \rightarrow C_2H_6 + e$	$2.29 \times 10^{-13} T_e^{0.02} \exp(-1.22/T_e)$		[9][a,b]
20	$e + NH \rightarrow NH + e$	$6.73 \times 10^{-14} T_e^{0.43} \exp(0.19/T_e)$		[9][a,b]
21	$e + H \rightarrow e + H(n=2)$	$1.81 \times 10^{-14} T_e^{0.25} \exp(-11.1/T_e)$	10.05	[197][a]
22	$e + H_2 \rightarrow e + H_2^*$	$3.39 \times 10^{-14} T_e^{-0.59} \exp(-12.1/T_e)$	8.8	[197][a]
23	$e + H_2 \rightarrow e + H_2^*$	$6.42 \times 10^{-14} T_e^{-0.98} \exp(-13.8/T_e)$	11.85	[197][a]
24	$e + N \rightarrow e + N^*$	$2.62 \times 10^{-14} T_e^{-0.3} \exp(-2.97/T_e)$	2.38	[254][a]

Continued on next page

Table A.6 (*Continued*)

ID	Reaction	k	ΔE_e	Source
25	$e + N \rightarrow e + N^*$	$1.04 \times 10^{-14} T_e^{-0.33} \exp(-4.56/T_e)$	3.55	[254][a]
26	$e + N_2 \rightarrow e + N_2^*$	$9.43 \times 10^{-14} T_e^{-0.72} \exp(-8.8/T_e)$	6.15	[255][a]
27	$e + H(n = 2) \rightarrow H + e$	$1.11 \times 10^{-14} T_e^{0.43} \exp(-0.14/T_e)$		[197][a]
28	$H_2^* + e \rightarrow H_2 + e$	$9.46 \times 10^{-15} T_e^{-0.11} \exp(-1.04/T_e)$		[9][a,b]
29	$e + N_2^* \rightarrow N_2 + e$	$4.75 \times 10^{-14} T_e^{-0.45} \exp(-1.51/T_e)$		[255][a]
30	$e + H \rightarrow H^+ + 2e$	$1.04 \times 10^{-14} T_e^{0.37} \exp(-14.8/T_e)$	13.55	[9][a,b]
31	$e + H(n = 2) \rightarrow H^+ + 2e$	$2.42 \times 10^{-13} T_e^{0.02} \exp(-4.76/T_e)$	3.45	[197][a]
32	$e + H_2 \rightarrow H_2^+ + 2e$	$1.29 \times 10^{-14} T_e^{0.39} \exp(-16.3/T_e)$	15.35	[9][a,b]
33	$H_2^* + e \rightarrow H_2^+ + 2e$	$6.02 \times 10^{-14} T_e^{0.15} \exp(-8.17/T_e)$	6.6	[9][a,b]
34	$e + C \rightarrow C^+ + 2e$	$1.87 \times 10^{-14} T_e^{0.52} \exp(-12.3/T_e)$	11.3	[9][a,b]
35	$e + N \rightarrow N^+ + 2e$	$4.46 \times 10^{-15} T_e^{0.79} \exp(-14.6/T_e)$	14.5	[195][a]
36	$e + N_2 \rightarrow N_2^+ + 2e$	$8.76 \times 10^{-15} T_e^{0.76} \exp(-16.4/T_e)$	15.35	[256][a]
37	$e + N_2^* \rightarrow N_2^+ + 2e$	$2.7 \times 10^{-14} T_e^{0.24} \exp(-11/T_e)$	9.3	[208][a]
38	$e + CH \rightarrow 2e + CH^+$	$1.82 \times 10^{-14} T_e^{0.42} \exp(-13/T_e)$	11.3	[9][a,b]
39	$e + CH_2 \rightarrow 2e + CH_2^+$	$1.46 \times 10^{-14} T_e^{0.5} \exp(-12/T_e)$	10.4	[9][a,b]
40	$e + CH_3 \rightarrow 2e + CH_3^+$	$1.13 \times 10^{-14} T_e^{0.58} \exp(-11/T_e)$	10.6	[9][a,b]
41	$e + CH_4 \rightarrow CH_4^+ + 2e$	$1.6 \times 10^{-14} T_e^{0.48} \exp(-14/T_e)$	12.6	[257][a]
42	$e + C_2H \rightarrow C_2H^+ + 2e$	$2.95 \times 10^{-14} T_e^{0.59} \exp(-12.1/T_e)$	10.97	[9][a,b]
43	$e + C_2H_2 \rightarrow C_2H_2^+ + 2e$	$2.32 \times 10^{-14} T_e^{0.71} \exp(-11.9/T_e)$	11.4	[253][a]
44	$e + C_2H_3 \rightarrow C_2H_3^+ + 2e$	$1.51 \times 10^{-14} T_e^{0.64} \exp(-10.6/T_e)$	9.97	[9][a,b]
45	$e + C_2H_4 \rightarrow C_2H_4^+ + 2e$	$1.87 \times 10^{-14} T_e^{0.77} \exp(-12.6/T_e)$	10.5	[9][a,b]
46	$e + C_2H_5 \rightarrow C_2H_5^+ + 2e$	$8.82 \times 10^{-15} T_e^{0.63} \exp(-10.6/T_e)$	8.93	[9][a,b]
47	$e + C_2H_6 \rightarrow C_2H_6^+ + 2e$	$7.11 \times 10^{-15} T_e^{0.34} \exp(-13.1/T_e)$	11.57	[9][a,b]
48	$e + CH \rightarrow 2e + C^+ + H$	$5.23 \times 10^{-15} T_e^{0.44} \exp(-18.3/T_e)$	18.35	[9][a,b]
49	$e + CH_2 \rightarrow 2e + CH^+ + H$	$1.28 \times 10^{-14} T_e^{0.29} \exp(-19.3/T_e)$	20.38	[9][a,b]
50	$e + CH_2 \rightarrow 2e + C^+ + H_2$	$8.69 \times 10^{-16} T_e^{0.5} \exp(-20.7/T_e)$	21.38	[9][a,b]
51	$e + CH_3 \rightarrow 2e + CH_2^+ + H$	$2.25 \times 10^{-14} T_e^{0.26} \exp(-19.1/T_e)$	20.38	[9][a,b]
52	$e + CH_3 \rightarrow 2e + CH^+ + H_2$	$2.62 \times 10^{-15} T_e^{0.4} \exp(-20.2/T_e)$	21.62	[9][a,b]
53	$e + CH_4 \rightarrow CH_3^+ + H + 2e$	$1.35 \times 10^{-14} T_e^{0.46} \exp(-15.5/T_e)$	14.3	[257][a]
54	$e + CH_4 \rightarrow 2e + CH_2^+ + H_2$	$2.02 \times 10^{-15} T_e^{0.65} \exp(-19/T_e)$	18.82	[9][a,b]
55	$e + C_2H_3 \rightarrow C_2H_2^+ + H + 2e$	$6.29 \times 10^{-15} T_e^{0.63} \exp(-13.1/T_e)$	12.3	[9][a,b]
56	$e + C_2H_4 \rightarrow C_2H_3^+ + H + 2e$	$7.59 \times 10^{-15} T_e^{0.66} \exp(-14.4/T_e)$	12.03	[9][a,b]
57	$e + C_2H_4 \rightarrow C_2H_2^+ + H_2 + 2e$	$5.92 \times 10^{-15} T_e^{0.69} \exp(-15.7/T_e)$	14.3	[9][a,b]
58	$e + C_2H_5 \rightarrow C_2H_2^+ + H_2 + H + 2e$	$5.26 \times 10^{-15} T_e^{0.6} \exp(-19.1/T_e)$	16.3	[9][a,b]
59	$e + C_2H_5 \rightarrow C_2H_4^+ + H + 2e$	$6.74 \times 10^{-15} T_e^{0.6} \exp(-12.5/T_e)$	11.47	[9][a,b]
60	$e + C_2H_5 \rightarrow C_2H_3^+ + H_2 + 2e$	$1.15 \times 10^{-14} T_e^{0.6} \exp(-13.6/T_e)$	12.07	[9][a,b]
61	$e + C_2H_6 \rightarrow C_2H_3^+ + H_2 + H + 2e$	$9.19 \times 10^{-15} T_e^{0.58} \exp(-17.2/T_e)$	14.97	[9][a,b]
62	$e + C_2H_6 \rightarrow C_2H_5^+ + H + 2e$	$6.87 \times 10^{-15} T_e^{0.35} \exp(-15.1/T_e)$	12.65	[9][a,b]
63	$e + C_2H_6 \rightarrow C_2H_2^+ + 2H_2 + 2e$	$3.04 \times 10^{-15} T_e^{0.8} \exp(-17.1/T_e)$	16	[9][a,b]
64	$e + C_2H_6 \rightarrow C_2H_4^+ + H_2 + 2e$	$2.38 \times 10^{-14} T_e^{0.48} \exp(-15.3/T_e)$	11.8	[9][a,b]
65	$e + C_2H_6 \rightarrow CH_3^+ + CH_3 + 2e$	$1 \times 10^{-16} \exp(-5/T_e)$		[9][b]
66	$e + C_3H_5 \rightarrow C_2H_3^+ + CH_2 + 2e$	$2.82 \times 10^{-15} T_e^{0.59} \exp(-16.9/T_e)$	13.57	[9][a,b]
67	$e + C_3H_5 \rightarrow C_2H_2^+ + CH_3 + 2e$	$1.61 \times 10^{-15} T_e^{0.58} \exp(-16.7/T_e)$	13.4	[9][a,b]
68	$e + C_3H_5 \rightarrow CH_3^+ + C_2H_2 + 2e$	$1.95 \times 10^{-15} T_e^{0.54} \exp(-15/T_e)$	11.82	[9][a,b]
69	$e + C_3H_6 \rightarrow C_2H_5^+ + CH + 2e$	$1.69 \times 10^{-15} T_e^{0.63} \exp(-18.7/T_e)$	15.28	[9][a,b]
70	$e + C_3H_6 \rightarrow C_2H_4^+ + CH_2 + 2e$	$2.59 \times 10^{-15} T_e^{0.62} \exp(-18.2/T_e)$	14.8	[9][a,b]
71	$e + C_3H_6 \rightarrow C_2H_3^+ + CH_3 + 2e$	$5.03 \times 10^{-15} T_e^{0.56} \exp(-15.8/T_e)$	12.55	[9][a,b]
72	$e + C_3H_6 \rightarrow CH_3^+ + C_2H_3 + 2e$	$1.83 \times 10^{-15} T_e^{0.6} \exp(-17.5/T_e)$	14.12	[9][a,b]
73	$e + C_3H_6 \rightarrow C_2H_2^+ + CH_4 + 2e$	$2.32 \times 10^{-15} T_e^{0.57} \exp(-16/T_e)$	12.72	[9][a,b]
74	$e + C_3H_7 \rightarrow C_2H_5^+ + CH_2 + 2e$	$4.69 \times 10^{-15} T_e^{0.56} \exp(-15.6/T_e)$	12.4	[9][a,b]
75	$e + C_3H_7 \rightarrow C_2H_4^+ + CH_3 + 2e$	$5.96 \times 10^{-15} T_e^{0.53} \exp(-14.7/T_e)$	11.55	[9][a,b]
76	$e + C_3H_7 \rightarrow CH_3^+ + C_2H_4 + 2e$	$3.58 \times 10^{-15} T_e^{0.51} \exp(-13.9/T_e)$	10.88	[9][a,b]
77	$e + C_3H_7 \rightarrow C_2H_3^+ + CH_4 + 2e$	$1.04 \times 10^{-14} T_e^{0.47} \exp(-12.6/T_e)$	9.62	[9][a,b]
78	$e + C_3H_8 \rightarrow C_2H_5^+ + CH_3 + 2e$	$1.26 \times 10^{-14} T_e^{0.44} \exp(-15/T_e)$	13.9	[9][a,b]
79	$e + C_3H_8 \rightarrow C_2H_4^+ + CH_4 + 2e$	$1 \times 10^{-16} \exp(-5/T_e)$		[9][b]
80	$e + NH \rightarrow N^+ + H + 2e$	$8.86 \times 10^{-15} T_e^{0.24} \exp(-17.4/T_e)$	17.62	[196][a]
81	$e + H^- \rightarrow 2e + H$	$5.06 \times 10^{-13} T_e^{0.28} \exp(-4.13/T_e)$	1.55	[6][a]
82	$e + H^+ \rightarrow H$	$6.35 \times 10^{-19} T_e^{-0.5} \exp(-0.01/T_e)$		[258][a]
83	$e + N^+ \rightarrow N$	$4.84 \times 10^{-19} T_e^{-0.5} \exp(-0.01/T_e)$		[9][a,b]
84	$e + H_2^+ \rightarrow 2H$	$4.92 \times 10^{-14} T_e^{-0.5} \exp(-0.03/T_e)$		[220][a]

Continued on next page

Table A.6 (*Continued*)

ID	Reaction	k	ΔE_e	Source
85	$e + H_2^+ \rightarrow H^+ + H^-$	$2.57 \times 10^{-16} T_e^{-0.49} \exp(-0.02/T_e)$		[6][a]
86	$e + H_3^+ \rightarrow 3H$	$1.19 \times 10^{-15} T_e^{-1.03} \exp(-0.08/T_e)$		[6][a]
87	$e + H_3^+ \rightarrow H + H_2$	$6.39 \times 10^{-14} T_e^{-0.43} \exp(-0.02/T_e)$		[200][a]
88	$e + C_2^+ \rightarrow 2C$	$1.19 \times 10^{-14} T_e^{-0.71}$		[259]
89	$e + N_2^+ \rightarrow 2N$	$2.61 \times 10^{-14} T_e^{-0.65} \exp(-0.02/T_e)$		[9][a,b]
90	$e + N_3^+ \rightarrow N_2 + N$	$2.04 \times 10^{-13} T_e^{-0.65} \exp(-0.02/T_e)$		[221][a]
91	$e + N_3^+ \rightarrow N + N_2$	$3.22 \times 10^{-14} T_e^{-0.5}$		[6]
92	$e + N_4^+ \rightarrow N_2 + 2N$	$3.13 \times 10^{-13} T_e^{-0.41}$		[6]
93	$e + N_4^+ \rightarrow 2N_2$	$2.04 \times 10^{-13} T_e^{-0.65} \exp(-0.02/T_e)$		[221][a]
94	$e + N_4^+ \rightarrow 2N_2$	$3.21 \times 10^{-13} T_e^{-0.5}$		[6]
95	$e + CH^+ \rightarrow C + H$	$1.72 \times 10^{-14} T_e^{-0.47} \exp(-0.05/T_e)$		[9][a,b]
96	$e + CH_2^+ \rightarrow C + 2H$	$2.36 \times 10^{-14} T_e^{-0.86} \exp(-0.04/T_e)$		[9][a,b]
97	$e + CH_2^+ \rightarrow CH + H$	$9.35 \times 10^{-15} T_e^{-0.86} \exp(-0.04/T_e)$		[9][a,b]
98	$e + CH_2^+ \rightarrow C + H_2$	$4.49 \times 10^{-15} T_e^{-0.86} \exp(-0.04/T_e)$		[9][a,b]
99	$e + CH_3^+ \rightarrow CH + 2H$	$4.4 \times 10^{-15} T_e^{-0.79} \exp(-0.04/T_e)$		[9][a,b]
100	$e + CH_3^+ \rightarrow C + H_2 + H$	$8.21 \times 10^{-15} T_e^{-0.79} \exp(-0.04/T_e)$		[9][a,b]
101	$e + CH_3^+ \rightarrow CH_2 + H$	$1.09 \times 10^{-14} T_e^{-0.79} \exp(-0.04/T_e)$		[9][a,b]
102	$e + CH_3^+ \rightarrow CH + H_2$	$3.83 \times 10^{-15} T_e^{-0.79} \exp(-0.04/T_e)$		[9][a,b]
103	$e + CH_4^+ \rightarrow CH_2 + 2H$	$9.6 \times 10^{-15} T_e^{-0.83} \exp(-0.04/T_e)$		[9][a,b]
104	$e + CH_4^+ \rightarrow CH + H_2 + H$	$5.57 \times 10^{-15} T_e^{-0.83} \exp(-0.04/T_e)$		[9][a,b]
105	$e + CH_4^+ \rightarrow CH_3 + H$	$4.68 \times 10^{-15} T_e^{-0.83} \exp(-0.04/T_e)$		[9][a,b]
106	$e + CH_5^+ \rightarrow CH_3 + 2H$	$2.57 \times 10^{-13} T_e^{-0.3}$		[259]
107	$e + CH_5^+ \rightarrow CH_2 + H_2 + H$	$6.61 \times 10^{-14} T_e^{-0.3}$		[259]
108	$e + C_2H^+ \rightarrow 2C + H$	$4.29 \times 10^{-15} T_e^{-0.71}$		[259]
109	$e + C_2H^+ \rightarrow C_2 + H$	$1.34 \times 10^{-14} T_e^{-0.71}$		[259]
110	$e + C_2H^+ \rightarrow CH + C$	$1.09 \times 10^{-14} T_e^{-0.71}$		[259]
111	$e + C_2H_2^+ \rightarrow C_2 + 2H$	$1.12 \times 10^{-14} T_e^{-0.71}$		[259]
112	$e + C_2H_2^+ \rightarrow C_2H + H$	$1.87 \times 10^{-14} T_e^{-0.71}$		[259]
113	$e + C_2H_2^+ \rightarrow 2CH$	$4.87 \times 10^{-15} T_e^{-0.71}$		[259]
114	$e + C_2H_3^+ \rightarrow C_2H + 2H$	$2.74 \times 10^{-14} T_e^{-0.71}$		[259]
115	$e + C_2H_3^+ \rightarrow C_2H_2 + H$	$1.34 \times 10^{-14} T_e^{-0.71}$		[259]
116	$e + C_2H_4^+ \rightarrow C_2H_2 + 2H$	$3.43 \times 10^{-14} T_e^{-0.71}$		[259]
117	$e + C_2H_4^+ \rightarrow C_2H + H_2 + H$	$5.53 \times 10^{-15} T_e^{-0.71}$		[259]
118	$e + C_2H_4^+ \rightarrow C_2H_3 + H$	$8.29 \times 10^{-15} T_e^{-0.71}$		[259]
119	$e + C_2H_5^+ \rightarrow C_2H_2 + 3H$	$8.98 \times 10^{-15} T_e^{-0.71}$		[259]
120	$e + C_2H_5^+ \rightarrow C_2H_3 + 2H$	$1.92 \times 10^{-14} T_e^{-0.71}$		[259]
121	$e + C_2H_5^+ \rightarrow C_2H_2 + H_2 + H$	$1.6 \times 10^{-14} T_e^{-0.71}$		[259]
122	$e + C_2H_5^+ \rightarrow C_2H_4 + H$	$7.7 \times 10^{-15} T_e^{-0.71}$		[259]
123	$e + C_2H_5^+ \rightarrow CH_3 + CH_2$	$9.62 \times 10^{-15} T_e^{-0.71}$		[259]
124	$e + C_2H_6^+ \rightarrow C_2H_4 + 2H$	$3.36 \times 10^{-14} T_e^{-0.71}$		[259]
125	$e + C_2H_6^+ \rightarrow C_2H_5 + H$	$2.19 \times 10^{-14} T_e^{-0.71}$		[259]
126	$2e + H^+ \rightarrow e + H$	$8.8 \times 10^{-39} T_e^{-4.5}$		[6]
127	$2e + N^+ \rightarrow N + e$	$5.4 \times 10^{-36} T_e^{-4.5}$		[6]
128	$2e + N_2^+ \rightarrow N_2 + e$	$7.18 \times 10^{-39} T_e^{-4.5}$		[6]
129	$e + N^+ + M \rightarrow N + M$	$2.49 \times 10^{-41} T_e^{-1.5}$		[6]
130	$e + M + N_2^+ \rightarrow N_2 + M$	$4.31 \times 10^{-46} T_e^{-4.5}$		[6]
131	$e + H_2 \rightarrow 2H + e$	$1.02 \times 10^{-13} T_e^{-0.54} \exp(-11.5/T_e)$	8.8	[9][a,b]
132	$e + H_2^+ \rightarrow H^+ + H + e$	$9.9 \times 10^{-14} T_e^{0.11} \exp(-0.19/T_e)$		[9][a,b]
133	$e + H_3^+ \rightarrow e + 2H + H^+$	$1.57 \times 10^{-15} T_e^{0.38} \exp(-15.3/T_e)$	17.8	[6][a]
134	$e + H_3^+ \rightarrow H^+ + H_2 + e$	$9.91 \times 10^{-14} T_e^{0.37} \exp(-14.5/T_e)$	14.9	[220][a]
135	$e + N_2 \rightarrow 2N + e$	$4.78 \times 10^{-15} T_e^{0.72} \exp(-13.8/T_e)$	12.5	[9][a,b]
136	$e + CH \rightarrow e + C + H$	$1.71 \times 10^{-14} T_e^{0.38} \exp(-9.62/T_e)$	6.97	[9][a,b]
137	$e + CH_2 \rightarrow e + CH + H$	$1.43 \times 10^{-14} T_e^{0.44} \exp(-11.3/T_e)$	8.5	[9][a,b]
138	$e + CH_3 \rightarrow e + CH_2 + H$	$1.32 \times 10^{-14} T_e^{0.47} \exp(-12.5/T_e)$	9.5	[9][a,b]
139	$e + CH_3 \rightarrow e + CH + H_2$	$2.05 \times 10^{-15} T_e^{0.49} \exp(-13/T_e)$	9.97	[9][a,b]
140	$e + CH_4 \rightarrow CH + H_2 + H + e$	$6.95 \times 10^{-15} T_e^{0.13} \exp(-11.8/T_e)$	1	[260][a]
141	$e + CH_4 \rightarrow C + 2H_2 + e$	$4.19 \times 10^{-13} T_e^{-1.41} \exp(-10.1/T_e)$	7.5	[260][a]
142	$e + CH_4 \rightarrow CH_2 + H_2 + e$	$1.38 \times 10^{-14} T_e^{0.13} \exp(-11.8/T_e)$	1	[260][a]
143	$e + C_2H \rightarrow C_2 + H + e$	$1.05 \times 10^{-14} T_e^{0.46} \exp(-11.6/T_e)$	8.8	[9][a,b]
144	$e + C_2H_2 \rightarrow C_2H + H + e$	$1.05 \times 10^{-14} T_e^{0.4} \exp(-10.2/T_e)$	7.47	[9][a,b]

Continued on next page

Table A.6 (*Continued*)

ID	Reaction	k	ΔE_e	Source
145	$e + C_2H_2 \rightarrow C_2 + H_2 + e$	$2.98 \times 10^{-15} T_e^{0.45} \exp(-11.6/T_e)$	8.68	[9][a,b]
146	$e + C_2H_3 \rightarrow C_2H_2 + H + e$	$2.04 \times 10^{-14} T_e^{0.27} \exp(-6.75/T_e)$	4.58	[9][a,b]
147	$e + C_2H_3 \rightarrow C_2H + H_2 + e$	$6.64 \times 10^{-15} T_e^{0.32} \exp(-7.94/T_e)$	5.58	[9][a,b]
148	$e + C_2H_4 \rightarrow C_2H_3 + H + e$	$8.87 \times 10^{-15} T_e^{0.38} \exp(-9.5/T_e)$	6.9	[9][a,b]
149	$e + C_2H_4 \rightarrow C_2H_2 + H_2 + e$	$8.32 \times 10^{-15} T_e^{0.33} \exp(-8.2/T_e)$	5.78	[9][a,b]
150	$e + C_2H_5 \rightarrow C_2H_4 + H + e$	$2.25 \times 10^{-14} T_e^{0.27} \exp(-6.56/T_e)$	4.45	[9][a,b]
151	$e + C_2H_5 \rightarrow C_2H_3 + H_2 + e$	$7.87 \times 10^{-15} T_e^{0.31} \exp(-7.67/T_e)$	5.35	[9][a,b]
152	$e + C_2H_6 \rightarrow C_2H_4 + H_2 + e$	$2.85 \times 10^{-14} T_e^{0.24} \exp(-6/T_e)$	4	[9][a,b]
153	$e + C_3H_5 \rightarrow C_2H_2 + CH_3 + e$	$7.24 \times 10^{-15} T_e^{0.24} \exp(-6.02/T_e)$	4	[9][a,b]
154	$e + C_3H_6 \rightarrow C_3H_5 + H + e$	$1.55 \times 10^{-14} T_e^{0.31} \exp(-7.66/T_e)$	5.33	[9][a,b]
155	$e + C_3H_6 \rightarrow C_2H_2 + CH_4 + e$	$2.25 \times 10^{-14} T_e^{0.2} \exp(-5.16/T_e)$	3.35	[9][a,b]
156	$e + C_3H_7 \rightarrow C_3H_6 + H + e$	$3.66 \times 10^{-14} T_e^{0.19} \exp(-4.92/T_e)$	3.15	[9][a,b]
157	$e + C_3H_7 \rightarrow C_3H_5 + H_2 + e$	$5.23 \times 10^{-14} T_e^{0.13} \exp(-3.89/T_e)$	2.4	[9][a,b]
158	$e + C_3H_7 \rightarrow C_2H_4 + CH_3 + e$	$1.5 \times 10^{-14} T_e^{0.19} \exp(-4.86/T_e)$	3.1	[9][a,b]
159	$e + C_3H_7 \rightarrow C_2H_3 + CH_4 + e$	$6.53 \times 10^{-15} T_e^{0.23} \exp(-5.86/T_e)$	3.88	[9][a,b]
160	$e + C_3H_8 \rightarrow C_3H_7 + H + e$	$1.37 \times 10^{-14} T_e^{0.33} \exp(-8.22/T_e)$	5.8	[9][a,b]
161	$e + C_3H_8 \rightarrow C_3H_6 + H_2 + e$	$4.77 \times 10^{-14} T_e^{0.15} \exp(-4.25/T_e)$	2.65	[9][a,b]
162	$e + C_3H_8 \rightarrow C_2H_4 + CH_4 + e$	$5.1 \times 10^{-14} T_e^{0.11} \exp(-3.47/T_e)$	2.1	[9][a,b]
163	$e + NH \rightarrow N + H + e$	$4.1 \times 10^{-14} T_e^{-0.17} \exp(-7.56/T_e)$	5.6	[9][a,b]
164	$2NH \rightarrow N_2H_2$	3.49×10^{-18}		[261]
165	$NH_2 + NH \rightarrow N_2H_3$	1.16×10^{-16}		[262]
166	$2NH_2 \rightarrow N_2H_4$	8×10^{-17}		[263]
167	$H_2 + H \rightarrow 3H$	$4.67 \times 10^{-13} (T_g/300)^{-1} \exp(-55/T_g)$		[6]
168	$H + N_2H_2 \rightarrow N_2 + H_2 + H$	$4.53 \times 10^{-19} (T_g/300)^{2.63} \exp(115/T_g)$		[264]
169	$N_2 + CN \rightarrow N_2 + C + N$	$4.15 \times 10^{-16} \exp(-70538.5/T_g)$		[265]
170	$H_2 + H(n=2) \rightarrow H + H_2$	1×10^{-19}		[6]
171	$N + H(n=2) \rightarrow H + N$	1×10^{-19}		[6]
172	$N_2 + H(n=2) \rightarrow H + N_2$	1×10^{-19}		[6]
173	$H_2^* + H_2 \rightarrow 2H_2$	1×10^{-19}		[6]
174	$N_2^* + H_2 \rightarrow N_2 + H_2$	2.1×10^{-16}		[6]
175	$H_2^* + N \rightarrow H_2 + N$	1×10^{-19}		[6]
176	$H_2^* + N_2 \rightarrow H_2 + N_2$	1×10^{-19}		[6]
177	$N_2^* + N \rightarrow N + N_2$	1×10^{-19}		[266]
178	$N^* + NH_3 \rightarrow NH + NH_2$	5×10^{-17}		[9][b]
179	$N^* + M \rightarrow N + M$	2.4×10^{-20}		[6]
180	$N_2^* + N_2 \rightarrow 2N_2$	3.7×10^{-22}		[6]
181	$2N_2^* \rightarrow N_2 + N_2^*$	1.36×10^{-15}		[266]
182	$H + CH \rightarrow C + H_2$	1×10^{-16}		[228]
183	$CH_2 + H \rightarrow CH + H_2$	7.7×10^{-16}		[229]
184	$CH_3 + H \rightarrow CH_2 + H_2$	$1 \times 10^{-16} \exp(-76/T_g)$		[229]
185	$CH_4 + H \rightarrow CH_3 + H_2$	$5.82 \times 10^{-19} (T_g/300)^3 \exp(-4045/T_g)$		[229]
186	$C_2H_2 + H \rightarrow C_2H + H_2$	1×10^{-16}		[229]
187	$C_2H_3 + H \rightarrow C_2H_2 + H_2$	2×10^{-17}		[229]
188	$C_2H_4 + H \rightarrow C_2H_3 + H_2$	9×10^{-16}		[229]
189	$C_2H_5 + H \rightarrow C_2H_4 + H_2$	3×10^{-18}		[229]
190	$C_2H_5 + H \rightarrow 2CH_3$	6×10^{-17}		[229]
191	$C_2H_6 + H \rightarrow C_2H_5 + H_2$	$1.23 \times 10^{-17} (T_g/300)^{1.5} \exp(-373/T_g)$		[229]
192	$C_3H_6 + H \rightarrow C_3H_5 + H_2$	6.94×10^{-21}		[259]
193	$C_3H_7 + H \rightarrow C_3H_6 + H_2$	3.01×10^{-18}		[259]
194	$C_3H_8 + H \rightarrow C_3H_7 + H_2$	5.15×10^{-23}		[259]
195	$H + NH \rightarrow N + H_2$	1.7×10^{-17}		[8]
196	$NH_2 + H \rightarrow H_2 + NH$	4.81×10^{-18}		[267]
197	$NH_3 + H \rightarrow H_2 + NH_2$	$1.34 \times 10^{-16} \exp(-7325/T_g)$		[268]
198	$H + N_2H_3 \rightarrow 2NH_2$	2.66×10^{-18}		[269]
199	$N_2H_4 + H \rightarrow H_2 + N_2H_3$	$1.17 \times 10^{-19} \exp(-1260.5/T_g)$		[270]
200	$H + H_2CN \rightarrow HCN + H_2$	$5.02 \times 10^{-16} (T_g/300)^{0.5}$		[263]
201	$C + H_2 \rightarrow CH + H$	1.5×10^{-16}		[228]
202	$N + H_2 \rightarrow NH + H$	$2.66 \times 10^{-16} \exp(-12609/T_g)$		[271]
203	$CH + H_2 \rightarrow CH_2 + H$	$3.75 \times 10^{-16} \exp(-166/T_g)$		[233]
204	$CH_2 + H_2 \rightarrow CH_3 + H$	5×10^{-21}		[259]

Continued on next page

Table A.6 (*Continued*)

ID	Reaction	k	ΔE_e	Source
205	$CH_3 + H_2 \rightarrow CH_4 + H$	9.6×10^{-27}		[259]
206	$CN + H_2 \rightarrow HCN + H$	$4.8 \times 10^{-19} \left(T_g/300\right)^{2.6} \exp\left(96/T_g\right)$		[272]
207	$C_2H + H_2 \rightarrow C_2H_2 + H$	$8.95 \times 10^{-19} \left(T_g/300\right)^{2.57} \exp\left(-13/T_g\right)$		[272]
208	$C_2H_3 + H_2 \rightarrow C_2H_4 + H$	9.78×10^{-26}		[259]
209	$C_2H_5 + H_2 \rightarrow C_2H_6 + H$	2.97×10^{-27}		[259]
210	$C_3H_7 + H_2 \rightarrow C_3H_8 + H$	7.12×10^{-27}		[259]
211	$NH_2 + H_2 \rightarrow H + NH_3$	$2.09 \times 10^{-18} \exp\left(-4277/T_g\right)$		[242]
212	$C + N_2 \rightarrow CN + N$	$1.04 \times 10^{-16} \exp\left(-23/T_g\right)$		[265]
213	$CH + N \rightarrow CN + H$	2.1×10^{-17}		[272]
214	$CH_2 + N \rightarrow HCN + H$	8.3×10^{-17}		[272]
215	$CH_2 + N \rightarrow CN + H_2$	1.6×10^{-17}		[272]
216	$CH_3 + N \rightarrow H_2CN + H$	1.3×10^{-16}		[272]
217	$CH_3 + N \rightarrow HCN + H_2$	1.4×10^{-17}		[272]
218	$CN + N \rightarrow C + N_2$	3×10^{-16}		[9][b]
219	$C_2H_2 + N \rightarrow CH + HCN$	2.7×10^{-21}		[263]
220	$N + C_2H_4 \rightarrow HCN + CH_3$	1.66×10^{-20}		[272]
221	$C_3H_6 + N \rightarrow HCN + C_2H_5$	$1.94 \times 10^{-19} \exp\left(-654/T_g\right)$		[263]
222	$N + NH \rightarrow H + N_2$	2.5×10^{-17}		[8]
223	$N_2H_4 + N \rightarrow NH_2 + N_2H_2$	1.25×10^{-19}		[269]
224	$H_2CN + N \rightarrow HCN + NH$	6.7×10^{-16}		[272]
225	$CH_4 + CH \rightarrow C_2H_4 + H$	$5 \times 10^{-17} \exp\left(2/T_g\right)$		[229]
226	$2CH_2 \rightarrow C_2H_2 + H_2$	$2 \times 10^{-17} \exp\left(-4/T_g\right)$		[229]
227	$CH_3 + CH_2 \rightarrow C_2H_4 + H$	7×10^{-17}		[229]
228	$CH_4 + CH_2 \rightarrow 2CH_3$	$7.1 \times 10^{-18} \exp\left(-502/T_g\right)$		[229]
229	$CH_2 + C_2H \rightarrow C_2H_2 + CH$	3×10^{-17}		[229]
230	$CH_2 + C_2H_3 \rightarrow C_2H_2 + CH_3$	3×10^{-17}		[229]
231	$CH_2 + C_2H_5 \rightarrow C_2H_4 + CH_3$	3.01×10^{-17}		[259]
232	$CH_2 + C_3H_6 \rightarrow C_3H_5 + CH_3$	3.65×10^{-23}		[259]
233	$CH_2 + C_3H_7 \rightarrow C_3H_6 + CH_3$	3.01×10^{-18}		[259]
234	$CH_2 + C_3H_7 \rightarrow C_2H_4 + C_2H_5$	3.01×10^{-17}		[259]
235	$CH_2 + C_3H_8 \rightarrow C_3H_7 + CH_3$	1.02×10^{-26}		[259]
236	$2CH_3 \rightarrow C_2H_5 + H$	$5 \times 10^{-17} \exp\left(-68/T_g\right)$		[229]
237	$CH_3 + C_2H_2 \rightarrow CH_4 + C_2H$	7.65×10^{-32}		[259]
238	$CH_3 + C_2H_3 \rightarrow C_2H_2 + CH_4$	6.5×10^{-20}		[229]
239	$CH_3 + C_2H_4 \rightarrow C_2H_3 + CH_4$	1.94×10^{-27}		[259]
240	$CH_3 + C_2H_5 \rightarrow C_2H_4 + CH_4$	1.9×10^{-18}		[229]
241	$C_2H_6 + CH_3 \rightarrow C_2H_5 + CH_4$	$1.75 \times 10^{-22} \left(T_g/300\right)^{6} \exp\left(-3043/T_g\right)$		[229]
242	$CH_3 + C_3H_6 \rightarrow C_3H_5 + CH_4$	1.24×10^{-25}		[259]
243	$CH_3 + C_3H_7 \rightarrow C_3H_6 + CH_4$	3.07×10^{-18}		[259]
244	$CH_3 + C_3H_8 \rightarrow C_3H_7 + CH_4$	1.02×10^{-26}		[259]
245	$CH_4 + CN \rightarrow HCN + CH_3$	$7 \times 10^{-19} \left(T_g/300\right)^{2.3} \exp\left(-16/T_g\right)$		[272]
246	$CH_4 + C_2H \rightarrow C_2H_2 + CH_3$	$3 \times 10^{-18} \exp\left(-25/T_g\right)$		[229]
247	$CH_4 + C_2H_3 \rightarrow C_2H_4 + CH_3$	$1.89 \times 10^{-20} \left(T_g/300\right)^{4} \exp\left(-2754/T_g\right)$		[229]
248	$CH_4 + C_2H_5 \rightarrow C_2H_6 + CH_3$	1.83×10^{-30}		[259]
249	$CH_4 + C_3H_7 \rightarrow C_3H_8 + CH_3$	4.38×10^{-30}		[259]
250	$2C_2H \rightarrow C_2H_2 + C_2$	3.01×10^{-18}		[259]
251	$C_2H + C_2H_2 \rightarrow C_4H_2 + H$	1.3×10^{-16}		[272]
252	$C_2H + C_2H_3 \rightarrow 2C_2H_2$	5×10^{-17}		[233]
253	$C_2H_4 + C_2H \rightarrow C_2H_2 + C_2H_3$	1.4×10^{-16}		[259]
254	$C_2H_5 + C_2H \rightarrow C_2H_4 + C_2H_2$	3×10^{-18}		[229]
255	$C_2H_6 + C_2H \rightarrow C_2H_2 + C_2H_5$	6×10^{-18}		[229]
256	$C_2H + C_3H_6 \rightarrow C_3H_5 + C_2H_2$	5.99×10^{-18}		[259]
257	$C_2H + C_3H_7 \rightarrow C_3H_6 + C_2H_2$	1×10^{-17}		[259]
258	$C_2H + C_3H_8 \rightarrow C_2H_2 + C_3H_7$	5.99×10^{-18}		[259]
259	$2C_2H_3 \rightarrow C_2H_4 + C_2H_2$	1.6×10^{-18}		[259]
260	$C_2H_6 + C_2H_3 \rightarrow C_2H_5 + C_2H_4$	3.39×10^{-27}		[259]
261	$C_2H_3 + C_3H_5 \rightarrow C_3H_6 + C_2H_2$	8×10^{-18}		[259]
262	$C_2H_3 + C_3H_6 \rightarrow C_3H_5 + C_2H_4$	6.58×10^{-25}		[259]
263	$C_2H_3 + C_3H_7 \rightarrow C_3H_8 + C_2H_2$	2.01×10^{-18}		[259]
264	$C_2H_3 + C_3H_7 \rightarrow C_3H_6 + C_2H_4$	2.01×10^{-18}		[259]

Continued on next page

Table A.6 (*Continued*)

ID	Reaction	k	ΔE_e	Source
265	$C_2H_3 + C_3H_8 \rightarrow C_2H_4 + C_3H_7$	3.4×10^{-27}		[259]
266	$2C_2H_5 \rightarrow C_2H_6 + C_2H_4$	2.4×10^{-18}		[229]
267	$C_2H_5 + C_3H_5 \rightarrow C_3H_6 + C_2H_4$	5.36×10^{-18}		[259]
268	$C_2H_5 + C_3H_6 \rightarrow C_3H_5 + C_2H_6$	2.53×10^{-26}		[259]
269	$C_2H_5 + C_3H_7 \rightarrow C_3H_8 + C_2H_4$	1.91×10^{-18}		[259]
270	$C_2H_5 + C_3H_7 \rightarrow C_3H_6 + C_2H_6$	2.41×10^{-18}		[259]
271	$C_2H_5 + C_3H_8 \rightarrow C_2H_6 + C_3H_7$	3.62×10^{-28}		[259]
272	$C_2H_6 + C_3H_7 \rightarrow C_3H_8 + C_2H_5$	3.16×10^{-28}		[259]
273	$C_3H_7 + C_3H_5 \rightarrow 2C_3H_6$	3×10^{-18}		[259]
274	$C_3H_7 + C_3H_6 \rightarrow C_3H_5 + C_3H_8$	2.53×10^{-26}		[259]
275	$2C_3H_7 \rightarrow C_3H_6 + C_3H_8$	2.81×10^{-18}		[259]
276	$2NH \rightarrow N_2H + H$	$2.29 \times 10^{-17} \left(T_g/300\right)^{0.5} \exp\left(-5/T_g\right)$		[263]
277	$2NH \rightarrow N_2 + H_2$	1.7×10^{-17}		[6]
278	$2NH \rightarrow NH_2 + N$	$1.4 \times 10^{-20} \left(T_g/300\right)^{2.89} \exp\left(1015/T_g\right)$		[273]
279	$NH_2 + NH \rightarrow N_2H_2 + H$	$2.49 \times 10^{-15} \left(T_g/300\right)^{-0.5}$		[242]
280	$2NH_2 \rightarrow H_2 + N_2H_2$	8.31×10^{-17}		[274]
281	$2NH_2 \rightarrow NH_3 + NH$	$8.31 \times 10^{-17} \exp\left(-51/T_g\right)$		[275]
282	$N_2H_4 + NH_2 \rightarrow NH_3 + N_2H_3$	5.15×10^{-19}		[269]
283	$2N_2H_3 \rightarrow N_2H_4 + N_2H_2$	2×10^{-17}		[276]
284	$CH_2 + N \rightarrow CN + 2H$	1.6×10^{-17}		[265]
285	$NH_2 + N \rightarrow N_2 + 2H$	1.2×10^{-16}		[242]
286	$CH_3 + N_2^* \rightarrow CH_2 + H + N_2$	4.5×10^{-17}		[272]
287	$N_2^* + CH_4 \rightarrow N_2 + CH_2 + H_2$	1.35×10^{-19}		[265]
288	$N_2^* + C_2H_2 \rightarrow C_2H + H + N_2$	2×10^{-16}		[263]
289	$N_2^* + C_2H_4 \rightarrow C_2H_3 + H + N_2$	5.5×10^{-17}		[263]
290	$N_2^* + C_2H_4 \rightarrow C_2H_2 + H_2 + N_2$	5.5×10^{-17}		[263]
291	$N_2^* + C_2H_6 \rightarrow C_2H_4 + H_2 + N_2$	$1.8 \times 10^{-16} \exp\left(-198/T_g\right)$		[263]
292	$N_2^* + C_3H_6 \rightarrow C_3H_5 + H + N_2$	1.4×10^{-16}		[263]
293	$N_2^* + C_3H_6 \rightarrow C_2H_3 + CH_3 + N_2$	1.4×10^{-16}		[263]
294	$N_2^* + C_3H_8 \rightarrow C_3H_6 + H_2 + N_2$	1.3×10^{-18}		[263]
295	$N_2^* + HCN \rightarrow N_2 + CN + H$	6×10^{-18}		[265]
296	$2NH \rightarrow N_2 + 2H$	1.16×10^{-15}		[277]
297	$NH_2 + N_2H_2 \rightarrow N_2 + H + NH_3$	$1.53 \times 10^{-21} \left(T_g/300\right)^{4.05} \exp\left(81/T_g\right)$		[278]
298	$2N_2H_3 \rightarrow 2NH_3 + N_2$	5×10^{-18}		[279]
299	$H + H_2^+ \rightarrow H_2 + H^+$	6.4×10^{-16}		[237]
300	$N^+ + H \rightarrow N + H^+$	2×10^{-15}		[280]
301	$H^+ + C_2 \rightarrow C_2^+ + H$	3.09×10^{-15}		[237]
302	$H^+ + N \rightarrow N^+ + H$	5×10^{-17}		[6]
303	$H^+ + CH \rightarrow CH^+ + H$	1.89×10^{-15}		[237]
304	$H^+ + CH_2 \rightarrow CH_2^+ + H$	1.39×10^{-15}		[237]
305	$H^+ + CH_3 \rightarrow CH_3^+ + H$	3.32×10^{-15}		[237]
306	$H^+ + CH_4 \rightarrow CH_4^+ + H$	1.5×10^{-15}		[259]
307	$H^+ + C_2H \rightarrow C_2H^+ + H$	1.5×10^{-15}		[237]
308	$H^+ + C_2H_2 \rightarrow C_2H_2^+ + H$	2×10^{-15}		[237]
309	$H^+ + C_2H_3 \rightarrow C_2H_3^+ + H$	2×10^{-15}		[237]
310	$H^+ + C_2H_4 \rightarrow C_2H_4^+ + H$	1×10^{-15}		[237]
311	$H_2^+ + C_2 \rightarrow C_2^+ + H_2$	1.1×10^{-15}		[237]
312	$H_2^+ + N \rightarrow N^+ + H_2$	5×10^{-16}		[280]
313	$H_2^+ + CH \rightarrow CH^+ + H_2$	7.1×10^{-16}		[237]
314	$H_2^+ + CH_2 \rightarrow CH_2^+ + H_2$	1×10^{-15}		[237]
315	$H_2^+ + CH_4 \rightarrow CH_4^+ + H_2$	1.4×10^{-15}		[237]
316	$H_2^+ + C_2H \rightarrow C_2H^+ + H_2$	1×10^{-15}		[237]
317	$H_2^+ + C_2H_2 \rightarrow C_2H_2^+ + H_2$	4.82×10^{-15}		[237]
318	$H_2^+ + C_2H_4 \rightarrow C_2H_4^+ + H_2$	2.21×10^{-15}		[237]
319	$H_2^+ + C_2H_6 \rightarrow C_2H_6^+ + H_2$	2.94×10^{-16}		[259]
320	$C^+ + C_2H_4 \rightarrow C_2H_4^+ + C$	1.7×10^{-17}		[237]
321	$C^+ + C_2H_5 \rightarrow C_2H_5^+ + C$	5×10^{-16}		[237]
322	$C_2^+ + CH \rightarrow CH^+ + C_2$	3.2×10^{-16}		[237]
323	$C_2^+ + CH_2 \rightarrow CH_2^+ + C_2$	4.5×10^{-16}		[237]
324	$N_2^+ + N \rightarrow N^+ + N_2$	5×10^{-18}		[9][b]

Continued on next page

Table A.6 (*Continued*)

ID	Reaction	k	ΔE_e	Source
325	$N^+ + N_2 \rightarrow N + N_2^+$	1×10^{-15}		[9][b]
326	$N^+ + NH_3 \rightarrow NH_3^+ + N$	1.67×10^{-15}		[9][b]
327	$N_2^+ + NH_3 \rightarrow NH_3^+ + N_2$	1.95×10^{-15}		[9][b]
328	$CH_3^+ + CH_4 \rightarrow CH_4^+ + CH_3$	1.36×10^{-16}		[259]
329	$CH_3^+ + C_2H_3 \rightarrow C_2H_3^+ + CH_3$	3×10^{-16}		[237]
330	$CH_4^+ + C_2H_2 \rightarrow C_2H_2^+ + CH_4$	1.13×10^{-15}		[237]
331	$CH_4^+ + C_2H_4 \rightarrow C_2H_4^+ + CH_4$	1.38×10^{-15}		[237]
332	$C_2H_2^+ + C_2H_3 \rightarrow C_2H_3^+ + C_2H_2$	3.3×10^{-16}		[237]
333	$C_2H_2^+ + C_2H_4 \rightarrow C_2H_4^+ + C_2H_2$	4.14×10^{-16}		[237]
334	$C_2H_4^+ + C_2H_3 \rightarrow C_2H_3^+ + C_2H_4$	5×10^{-16}		[237]
335	$C_2H_6^+ + C_2H_4 \rightarrow C_2H_4^+ + C_2H_6$	1.15×10^{-15}		[259]
336	$NH^+ + NH_2 \rightarrow NH_2^+ + NH$	1.8×10^{-15}		[280]
337	$NH^+ + NH_3 \rightarrow NH_3^+ + NH$	1.8×10^{-15}		[280]
338	$NH_2^+ + NH_3 \rightarrow NH_3^+ + NH_2$	2.2×10^{-15}		[9][b]
339	$N_4^+ + N \rightarrow 2N_2 + N^+$	1×10^{-17}		[6]
340	$N_3^+ + NH_3 \rightarrow NH_3^+ + N + N_2$	2.1×10^{-15}		[9][b]
341	$CH^+ + H \rightarrow C^+ + H_2$	7.5×10^{-16}		[237]
342	$CH_4^+ + H \rightarrow CH_3^+ + H_2$	1.1×10^{-17}		[237]
343	$CH_5^+ + H \rightarrow CH_4^+ + H_2$	1.5×10^{-16}		[237]
344	$C_2H_3^+ + H \rightarrow C_2H_2^+ + H_2$	6.8×10^{-17}		[237]
345	$C_2H_4^+ + H \rightarrow C_2H_3^+ + H_2$	3×10^{-16}		[237]
346	$C_2H_5^+ + H \rightarrow C_2H_4^+ + H_2$	1×10^{-17}		[237]
347	$C_2H_6^+ + H \rightarrow C_2H_5^+ + H_2$	1×10^{-17}		[237]
348	$H^+ + CH_2 \rightarrow CH^+ + H_2$	1.39×10^{-15}		[237]
349	$H^+ + CH_4 \rightarrow CH_3^+ + H_2$	2.33×10^{-15}		[237]
350	$H^+ + C_2H \rightarrow C_2^+ + H_2$	1.5×10^{-15}		[237]
351	$H^+ + C_2H_3 \rightarrow C_2H_2^+ + H_2$	2×10^{-15}		[237]
352	$H^+ + C_2H_4 \rightarrow C_2H_2^+ + H_2 + H$	1×10^{-15}		[237]
353	$H^+ + C_2H_4 \rightarrow C_2H_3^+ + H_2$	3×10^{-15}		[237]
354	$H^+ + C_2H_5 \rightarrow C_2H_3^+ + H_2 + H$	3.06×10^{-15}		[237]
355	$H^+ + C_2H_5 \rightarrow C_2H_4^+ + H_2$	1.65×10^{-15}		[237]
356	$H^+ + C_2H_6 \rightarrow C_2H_4^+ + H_2 + H$	1.4×10^{-15}		[259]
357	$H^+ + C_2H_6 \rightarrow C_2H_3^+ + 2H_2$	2.8×10^{-15}		[259]
358	$H^+ + C_2H_6 \rightarrow C_2H_5^+ + H_2$	1.3×10^{-15}		[259]
359	$H_2^+ + H_2 \rightarrow H_2 + H^+ + H$	$1 \times 10^{-14} \exp\left(-841/T_g\right)$		[6]
360	$H_2 + H_2^+ \rightarrow H + H_3^+$	2.08×10^{-15}		[237]
361	$C_2^+ + H_2 \rightarrow C_2H^+ + H$	1.1×10^{-15}		[237]
362	$CH^+ + H_2 \rightarrow CH_2^+ + H$	1.2×10^{-15}		[237]
363	$CH_2^+ + H_2 \rightarrow CH_3^+ + H$	1.6×10^{-15}		[237]
364	$CH_4^+ + H_2 \rightarrow CH_5^+ + H$	3.3×10^{-17}		[237]
365	$C_2H^+ + H_2 \rightarrow C_2H_2^+ + H$	1.1×10^{-15}		[237]
366	$C_2H_2^+ + H_2 \rightarrow C_2H_3^+ + H$	1×10^{-17}		[237]
367	$NH_2^+ + H_2 \rightarrow NH_3^+ + H$	1×10^{-15}		[9][b]
368	$NH_3^+ + H_2 \rightarrow NH_4^+ + H$	4×10^{-19}		[9][b]
369	$H_2^+ + C \rightarrow CH^+ + H$	2.4×10^{-15}		[237]
370	$H_2^+ + C_2 \rightarrow C_2H^+ + H$	1.1×10^{-15}		[237]
371	$H_2^+ + CH \rightarrow CH_2^+ + H$	7.1×10^{-16}		[237]
372	$H_2^+ + CH_2 \rightarrow CH_3^+ + H$	1×10^{-15}		[237]
373	$H_2^+ + CH_4 \rightarrow CH_3^+ + H_2 + H$	2.3×10^{-15}		[237]
374	$H_2^+ + CH_4 \rightarrow CH_5^+ + H$	1.14×10^{-16}		[237]
375	$H_2^+ + C_2H \rightarrow C_2H_2^+ + H$	1×10^{-15}		[237]
376	$H_2^+ + C_2H_2 \rightarrow C_2H_3^+ + H$	4.8×10^{-16}		[237]
377	$H_2^+ + C_2H_4 \rightarrow C_2H_3^+ + H_2 + H$	1.81×10^{-15}		[237]
378	$H_2^+ + C_2H_4 \rightarrow C_2H_2^+ + 2H_2$	8.82×10^{-15}		[237]
379	$H_2^+ + C_2H_6 \rightarrow C_2H_3^+ + 2H_2 + H$	6.86×10^{-16}		[259]
380	$H_2^+ + C_2H_6 \rightarrow C_2H_5^+ + H_2 + H$	1.37×10^{-15}		[259]
381	$H_2^+ + C_2H_6 \rightarrow C_2H_2^+ + 3H_2$	1.96×10^{-16}		[259]
382	$H_2^+ + C_2H_6 \rightarrow C_2H_4^+ + 2H_2$	2.35×10^{-15}		[259]
383	$H_3^+ + C \rightarrow CH^+ + H_2$	2×10^{-15}		[237]
384	$H_3^+ + CH \rightarrow CH_2^+ + H_2$	1.2×10^{-15}		[237]

Continued on next page

Table A.6 (*Continued*)

ID	Reaction	k	ΔE_e	Source
385	$H_3^+ + CH_2 \rightarrow CH_3^+ + H_2$	1.7×10^{-15}		[237]
386	$H_3^+ + CH_3 \rightarrow CH_4^+ + H_2$	2.1×10^{-15}		[237]
387	$H_3^+ + CH_4 \rightarrow CH_5^+ + H_2$	2.4×10^{-15}		[237]
388	$H_3^+ + C_2H_2 \rightarrow C_2H_3^+ + H_2$	3.5×10^{-15}		[237]
389	$H_3^+ + C_2H_3 \rightarrow C_2H_4^+ + H_2$	2×10^{-15}		[237]
390	$H_3^+ + C_2H_4 \rightarrow C_2H_3^+ + 2H_2$	1.15×10^{-15}		[237]
391	$H_3^+ + C_2H_4 \rightarrow C_2H_5^+ + H_2$	1.15×10^{-15}		[237]
392	$H_3^+ + C_2H_5 \rightarrow C_2H_6^+ + H_2$	1.4×10^{-15}		[237]
393	$H_3^+ + C_2H_6 \rightarrow C_2H_5^+ + 2H_2$	2.4×10^{-15}		[259]
394	$CH^+ + C \rightarrow C_2^+ + H$	1.2×10^{-15}		[237]
395	$CH_2^+ + C \rightarrow C_2H^+ + H$	1.2×10^{-15}		[237]
396	$CH_3^+ + C \rightarrow C_2H^+ + H_2$	1.2×10^{-15}		[237]
397	$CH_5^+ + C \rightarrow CH^+ + CH_4$	1.2×10^{-15}		[237]
398	$C^+ + CH_3 \rightarrow C_2H_2^+ + H$	1.3×10^{-15}		[259]
399	$C^+ + CH_3 \rightarrow C_2H^+ + H_2$	1×10^{-15}		[259]
400	$C^+ + C_2H_4 \rightarrow C_2H_3^+ + CH$	8.5×10^{-17}		[237]
401	$C^+ + C_2H_6 \rightarrow C_2H_5^+ + CH$	2.31×10^{-16}		[259]
402	$C^+ + C_2H_6 \rightarrow C_2H_4^+ + CH_2$	1.16×10^{-16}		[259]
403	$C^+ + C_2H_6 \rightarrow C_2H_3^+ + CH_3$	4.95×10^{-16}		[259]
404	$C^+ + C_2H_6 \rightarrow C_2H_2^+ + CH_4$	8.25×10^{-17}		[259]
405	$CH_5^+ + C_2 \rightarrow C_2H^+ + CH_4$	9.5×10^{-16}		[237]
406	$C_2^+ + CH_4 \rightarrow C_2H_2^+ + CH_2$	1.82×10^{-16}		[237]
407	$C_2^+ + CH_4 \rightarrow C_2H^+ + CH_3$	2.38×10^{-16}		[237]
408	$N_3^+ + N \rightarrow N_2^+ + N_2$	6.6×10^{-17}		[6]
409	$N^+ + NH \rightarrow H + N_2^+$	3.7×10^{-16}		[6]
410	$N_2^+ + N_2 \rightarrow N_4^+$	8.26×10^{-16}		[7]
411	$N_2^+ + C_3H_8 \rightarrow C_2H_3^+ + CH_3 + H_2 + N_2$	5.2×10^{-16}		[263]
412	$N_2^+ + C_3H_8 \rightarrow C_2H_5^+ + CH_3 + N_2$	3.9×10^{-16}		[263]
413	$N_2^+ + C_3H_8 \rightarrow C_2H_4^+ + CH_4 + N_2$	2.2×10^{-16}		[263]
414	$N_3^+ + M \rightarrow M + N + N_2^+$	6.6×10^{-17}		[6]
415	$N_4^+ + C_3H_8 \rightarrow C_2H_5^+ + CH_3 + 2N_2$	6.7×10^{-16}		[263]
416	$N_4^+ + C_3H_8 \rightarrow C_2H_4^+ + CH_4 + 2N_2$	4.3×10^{-16}		[263]
417	$N_4^+ + M \rightarrow N_2^+ + M + N_2$	2.5×10^{-21}		[6]
418	$CH^+ + CH \rightarrow C_2^+ + H_2$	1×10^{-15}		[237]
419	$CH_3^+ + CH \rightarrow C_2H_2^+ + H_2$	7.1×10^{-16}		[259]
420	$CH_5^+ + CH \rightarrow CH_2^+ + CH_4$	6.9×10^{-16}		[237]
421	$C_2H^+ + CH \rightarrow CH_2^+ + C_2$	3.2×10^{-16}		[237]
422	$CH^+ + CH_2 \rightarrow C_2H^+ + H_2$	7.5×10^{-16}		[237]
423	$CH^+ + CH_4 \rightarrow C_2H_2^+ + H_2 + H$	1.43×10^{-16}		[237]
424	$CH^+ + CH_4 \rightarrow C_2H_4^+ + H$	6.5×10^{-17}		[237]
425	$CH_3^+ + CH_2 \rightarrow C_2H_3^+ + H_2$	1×10^{-15}		[259]
426	$CH_5^+ + CH_2 \rightarrow CH_3^+ + CH_4$	9.6×10^{-16}		[237]
427	$C_2H^+ + CH_2 \rightarrow CH_3^+ + C_2$	4.4×10^{-16}		[237]
428	$CH_2^+ + CH_4 \rightarrow C_2H_3^+ + H_2 + H$	2.31×10^{-16}		[259]
429	$CH_2^+ + CH_4 \rightarrow C_2H_5^+ + H$	3.6×10^{-16}		[237]
430	$CH_2^+ + CH_4 \rightarrow C_2H_2^+ + 2H_2$	3.97×10^{-16}		[259]
431	$CH_2^+ + CH_4 \rightarrow C_2H_4^+ + H_2$	8.4×10^{-16}		[237]
432	$CH_2^+ + CH_4 \rightarrow CH_3^+ + CH_3$	1.38×10^{-16}		[259]
433	$CH_3^+ + C_2H_4 \rightarrow C_2H_3^+ + CH_4$	3.5×10^{-16}		[237]
434	$CH_4^+ + CH_4 \rightarrow CH_5^+ + CH_3$	1.5×10^{-15}		[237]
435	$C_2H^+ + CH_4 \rightarrow C_2H_2^+ + CH_3$	3.74×10^{-16}		[237]
436	$C_2H_2^+ + CH_4 \rightarrow C_2H_3^+ + CH_3$	4.1×10^{-15}		[259]
437	$CH_4^+ + C_2H_2 \rightarrow C_2H_3^+ + CH_3$	1.23×10^{-15}		[237]
438	$CH_4^+ + C_2H_4 \rightarrow C_2H_5^+ + CH_3$	4.23×10^{-16}		[237]
439	$CH_4^+ + C_2H_6 \rightarrow C_2H_4^+ + CH_4 + H_2$	1.91×10^{-15}		[259]
440	$CH_5^+ + C_2H \rightarrow C_2H_2^+ + CH_4$	9×10^{-16}		[237]
441	$CH_5^+ + C_2H_4 \rightarrow C_2H_5^+ + CH_4$	1.5×10^{-15}		[237]
442	$CH_5^+ + C_2H_6 \rightarrow C_2H_5^+ + H_2 + CH_4$	2.25×10^{-16}		[259]
443	$C_2H_3^+ + C_2H \rightarrow C_2H_2^+ + C_2H_2$	3.3×10^{-16}		[237]
444	$C_2H_6^+ + C_2H_2 \rightarrow C_2H_5^+ + C_2H_3$	2.47×10^{-16}		[237]

Continued on next page

Table A.6 (*Continued*)

ID	Reaction	k	ΔE_e	Source
445	$C_2H_2^+ + C_2H_6 \rightarrow C_2H_5^+ + C_2H_3$	1.31×10^{-16}		[259]
446	$C_2H_2^+ + C_2H_6 \rightarrow C_2H_4^+ + C_2H_4$	2.48×10^{-16}		[259]
447	$C_2H_3^+ + C_2H_3 \rightarrow C_2H_5^+ + C_2H$	5×10^{-16}		[237]
448	$C_2H_4^+ + C_2H_3 \rightarrow C_2H_5^+ + C_2H_2$	5×10^{-16}		[237]
449	$C_2H_3^+ + C_2H_4 \rightarrow C_2H_5^+ + C_2H_2$	8.9×10^{-16}		[237]
450	$C_2H_3^+ + C_2H_6 \rightarrow C_2H_5^+ + C_2H_4$	2.91×10^{-16}		[259]
451	$NH^+ + NH_3 \rightarrow NH_4^+ + N$	1.8×10^{-15}		[9][b]
452	$NH_2^+ + NH_3 \rightarrow NH_4^+ + NH$	2.2×10^{-15}		[9][b]
453	$NH_3^+ + NH_3 \rightarrow NH_4^+ + NH_2$	2.2×10^{-15}		[9][b]
454	$H^- + M \rightarrow H + e + M$	$2.7 \times 10^{-16} \left(T_g/300\right)^{0.5} \exp\left(-559/T_g\right)$		[6]
455	$H^- + H \rightarrow H_2 + e$	1.8×10^{-15}		[280]
456	$H^- + C \rightarrow CH + e$	1×10^{-15}		[259]
457	$H^- + C_2 \rightarrow C_2H + e$	1×10^{-15}		[259]
458	$H^- + N \rightarrow NH + e$	1×10^{-15}		[6]
459	$H^- + CH \rightarrow CH_2 + e$	1×10^{-16}		[259]
460	$H^- + CH_2 \rightarrow CH_3 + e$	1×10^{-15}		[259]
461	$H^- + CH_3 \rightarrow CH_4 + e$	1×10^{-15}		[259]
462	$H^- + C_2H \rightarrow C_2H_2 + e$	1×10^{-15}		[259]
463	$H^- + H^+ \rightarrow 2H$	2×10^{-13}		[9][b]
464	$H^- + H_2^+ \rightarrow H + H_2$	2×10^{-13}		[9][b]
465	$C^+ + H^- \rightarrow C + H$	2.3×10^{-13}		[259]
466	$H^- + N_2^+ \rightarrow N_2 + H$	$2 \times 10^{-13} \left(T_g/300\right)^{-0.5}$		[6]
467	$H^- + N_3^+ \rightarrow NH + N_2$	$3 \times 10^{-12} \left(T_g/300\right)^{-0.5}$		[9][b]
468	$H^- + H_2^+ \rightarrow 3H$	1×10^{-13}		[6]
469	$H^- + H_3^+ \rightarrow H_2 + 2H$	1×10^{-13}		[9][b]
470	$H^- + N_2^+ \rightarrow 2N + H$	1×10^{-13}		[6]
471	$H^- + N_3^+ \rightarrow N + N_2 + H$	1×10^{-13}		[6]
472	$H^- + N_4^+ \rightarrow 2N_2 + H$	1×10^{-13}		[6]
473	$2H + H_2 \rightarrow 2H_2$	$4 \times 10^{-44} \left(T_g/300\right)^{-1}$		[6]
474	$2H + N_2 \rightarrow H_2 + N_2$	$9.11 \times 10^{-45} \left(T_g/300\right)^{-1.32}$		[266]
475	$2H + CH_4 \rightarrow H_2 + CH_4$	6×10^{-45}		[259]
476	$H^+ + H + M \rightarrow H_2^+ + M$	1×10^{-46}		[6]
477	$H + N + H_2 \rightarrow NH + H_2$	1×10^{-43}		[6]
478	$H + N + N_2 \rightarrow NH + N_2$	5×10^{-44}		[6]
479	$CH_4 + N + H \rightarrow NH + CH_4$	5×10^{-44}		[281]
480	$CH_3 + H + N_2 \rightarrow CH_4 + N_2$	$6 \times 10^{-41} \left(T_g/300\right)^{-1.8}$		[272]
481	$C_2H + H + N_2 \rightarrow C_2H_2 + N_2$	9.44×10^{-42}		[259]
482	$C_2H_2 + H + N_2 \rightarrow C_2H_3 + N_2$	$1.08 \times 10^{-37} \left(T_g/300\right)^{-7.27} \exp\left(-3623/T_g\right)$		[272]
483	$C_2H_3 + H + N_2 \rightarrow C_2H_4 + N_2$	8.26×10^{-42}		[259]
484	$C_2H_4 + H + N_2 \rightarrow C_2H_5 + N_2$	8.19×10^{-42}		[259]
485	$C_2H_5 + H + N_2 \rightarrow C_2H_6 + N_2$	9.2×10^{-42}		[259]
486	$C_3H_5 + H + N_2 \rightarrow C_3H_6 + N_2$	1.33×10^{-41}		[259]
487	$C_3H_6 + H + N_2 \rightarrow C_3H_7 + N_2$	3.79×10^{-45}		[259]
488	$C_3H_7 + H + N_2 \rightarrow C_3H_8 + N_2$	3.96×10^{-42}		[259]
489	$H + HCN + N_2 \rightarrow H_2CN + N_2$	$4.84 \times 10^{-42} \exp\left(-244/T_g\right)$		[263]
490	$CH_3 + H + CH_4 \rightarrow 2CH_4$	2.97×10^{-40}		[259]
491	$C_2H + H + CH_4 \rightarrow C_2H_2 + CH_4$	9.44×10^{-42}		[259]
492	$C_2H_2 + H + CH_4 \rightarrow C_2H_3 + CH_4$	2.81×10^{-43}		[259]
493	$C_2H_3 + H + CH_4 \rightarrow C_2H_4 + CH_4$	8.26×10^{-42}		[259]
494	$C_2H_4 + H + CH_4 \rightarrow C_2H_5 + CH_4$	3.66×10^{-42}		[259]
495	$C_2H_5 + H + CH_4 \rightarrow C_2H_6 + CH_4$	9.2×10^{-42}		[259]
496	$C_3H_5 + H + CH_4 \rightarrow C_3H_6 + CH_4$	1.33×10^{-41}		[259]
497	$C_3H_6 + H + CH_4 \rightarrow C_3H_7 + CH_4$	3.79×10^{-45}		[259]
498	$C_3H_7 + H + CH_4 \rightarrow C_3H_8 + CH_4$	3.96×10^{-42}		[259]
499	$H + NH_2 + M \rightarrow NH_3 + M$	6×10^{-42}		[282]
500	$H^+ + H^- + M \rightarrow 2H + M$	$2 \times 10^{-37} \left(T_g/300\right)^{-2.5}$		[6]
501	$H^+ + H_2 + M \rightarrow H_3^+ + M$	1.5×10^{-41}		[6]
502	$H^- + H_2^+ + M \rightarrow H + H_2 + M$	$2 \times 10^{-37} \left(T_g/300\right)^{-2.5}$		[6]
503	$H^- + N^+ + M \rightarrow NH + M$	$2 \times 10^{-37} \left(T_g/300\right)^{-2.5}$		[6]
504	$H^- + N_2^+ + M \rightarrow N_2 + H + M$	$2 \times 10^{-37} \left(T_g/300\right)^{-2.5}$		[6]

Continued on next page

Table A.6 (*Continued*)

ID	Reaction	k	ΔE_e	Source
505	$2N + H_2 \rightarrow N_2 + H_2$	$2.5 \times 10^{-46} \exp(5/T_g)$		[6]
506	$H_2 + N + NH_3 \rightarrow NH_2 + NH_3$	1×10^{-48}		[9]^b
507	$2N + N_2 \rightarrow 2N_2$	$1.38 \times 10^{-46} \exp(5/T_g)$		[6]
508	$N^+ + N + M \rightarrow N_2^+ + M$	1×10^{-41}		[6]
509	$N_2^+ + N + M \rightarrow M + N_3^+$	$9 \times 10^{-42} (T_g/300)^1 \exp(4/T_g)$		[6]
510	$N^+ + N_2 + M \rightarrow N_3^+ + M$	$9 \times 10^{-42} \exp(4/T_g)$		[6]
511	$CH + C_2H_6 + N_2 \rightarrow C_3H_7 + N_2$	1.14×10^{-41}		[259]
512	$2CH_3 + N_2 \rightarrow C_2H_6 + N_2$	$1.41 \times 10^{-41} (T_g/300)^{-0.78} \exp(-31/T_g)$		[263]
513	$CH_3 + C_2H_3 + N_2 \rightarrow C_3H_6 + N_2$	4.91×10^{-42}		[259]
514	$CH_3 + C_2H_5 + N_2 \rightarrow C_3H_8 + N_2$	1×10^{-40}		[259]
515	$CH + C_2H_6 + CH_4 \rightarrow C_3H_7 + CH_4$	1.14×10^{-41}		[259]
516	$2CH_3 + CH_4 \rightarrow C_2H_6 + CH_4$	$4.23 \times 10^{-41} (T_g/300)^{-0.78} \exp(-31/T_g)$		[263]
517	$CH_3 + C_2H_3 + CH_4 \rightarrow C_3H_6 + CH_4$	4.91×10^{-42}		[259]
518	$CH_3 + C_2H_5 + CH_4 \rightarrow C_3H_8 + CH_4$	1×10^{-40}		[259]
519	$2NH + M \rightarrow H_2 + N_2 + M$	1×10^{-45}		[265]
520	$2NH_3 + NH \rightarrow N_2H_4 + NH_3$	1×10^{-45}		[283]
521	$2NH_2 + NH_3 \rightarrow N_2H_4 + NH_3$	6.9×10^{-42}		[282]

Table A.7: Detailed chemistry set for all the Ar–NF_3–O_2 reduction cases. The kinetic data are taken directly from the corresponding pre-compiled chemistry set in QDB database [9] (QDB chemistry ID: C33). Primary sources are cited, if listed in QDB. The purpose of all the test chemistry sets extracted from QDB in this work is merely to provide input for testing of the presented chemistry reduction method, therefore the consistency of this chemistry set and the validity of the cited sources listed in QDB were not explicitly verified in this work.

[a] Fitted from a cross section on a grid of Maxwellian temperatures.

[b] Original source not listed in QDB.

ID	Reaction	k	ΔE_e	Source
1	$e + Ar \rightarrow e + Ar$	$2.66 \times 10^{-13} T_e^{-0.01} \exp(-3.15/T_e)$		[284]^a
2	$e + Ar^+ \rightarrow Ar^+ + e$	$1.61 \times 10^{-10} T_e^{-1.22} \exp(-0.04/T_e)$		[251]^a
3	$e + O_2 \rightarrow O_2 + e$	$3.93 \times 10^{-14} T_e^{0.63} \exp(0.02/T_e)$		[9]^a
4	$e + O_2^+ \rightarrow O_2^+ + e$	$1.61 \times 10^{-10} T_e^{-1.22} \exp(-0.04/T_e)$		[221]^a
5	$e + F \rightarrow e + F$	$3.3 \times 10^{-14} T_e^{0.5} \exp(-0.42/T_e)$		[285]^a
6	$e + F_2 \rightarrow F_2 + e$	$1.98 \times 10^{-13} T_e^{-0.02} \exp(-0.43/T_e)$		[206]^a
7	$e + NO \rightarrow NO + e$	$7.06 \times 10^{-14} T_e^{0.36} \exp(-0.06/T_e)$		[286]^a
8	$e + N_2O \rightarrow N_2O + e$	$1.01 \times 10^{-13} T_e^{0.32} \exp(-0.66/T_e)$		[9]^{a,b}
9	$e + NF_3 \rightarrow NF_3 + e$	$6.66 \times 10^{-14} T_e^{0.41} \exp(0.19/T_e)$		[225]^a
10	$e + NF_2 \rightarrow NF_2 + e$	$6.64 \times 10^{-14} T_e^{0.41} \exp(0.19/T_e)$		[225]^a
11	$e + NF \rightarrow NF + e$	$6.64 \times 10^{-14} T_e^{0.41} \exp(0.19/T_e)$		[225]^a
12	$e + Ar \rightarrow Ar^* + e$	$1.54 \times 10^{-15} T_e^{0.41} \exp(-12.1/T_e)$	11.6	[284]^a
13	$e + Ar \rightarrow Ar^{**} + e$	$1.82 \times 10^{-14} T_e^{0.19} \exp(-12.8/T_e)$	13.1	[284]^a
14	$e + Ar^* \rightarrow Ar^{**} + e$	$7.91 \times 10^{-13} T_e^{0.28} \exp(-1.9/T_e)$	1.57	[9]^{a,b}
15	$e + O \rightarrow e + O^*$	$1.06 \times 10^{-14} T_e^{-0.4} \exp(-3.44/T_e)$	1.95	[202]^a
16	$e + O \rightarrow e + O^*$	$1.16 \times 10^{-15} T_e^{-0.17} \exp(-5.08/T_e)$	4.17	[202]^a
17	$e + O_2 \rightarrow O_2^* + e$	$2.76 \times 10^{-15} T_e^{-0.34} \exp(-3.27/T_e)$	0.97	[9]^a
18	$e + N \rightarrow e + N^*$	$2.62 \times 10^{-14} T_e^{-0.3} \exp(-2.97/T_e)$	2.38	[254]^a
19	$e + N \rightarrow e + N^*$	$1.04 \times 10^{-14} T_e^{-0.33} \exp(-4.56/T_e)$	3.55	[254]^a
20	$e + N_2 \rightarrow e + N_2^*$	$9.43 \times 10^{-14} T_e^{-0.72} \exp(-8.8/T_e)$	6.15	[255]^a
21	$e + Ar^* \rightarrow Ar + e$	$1.96 \times 10^{-15} T_e^{0.32} \exp(-0.98/T_e)$	-11.6	[284]^a
22	$e + Ar^{**} \rightarrow Ar + e$	$2.26 \times 10^{-14} T_e^{0.1} \exp(-0.04/T_e)$	-13.1	[284]^a
23	$e + Ar^{**} \rightarrow Ar^* + e$	$6.86 \times 10^{-13} T_e^{0.34} \exp(-0.1/T_e)$	-1.57	[9]^{a,b}
24	$e + O^* \rightarrow O + e$	$5.82 \times 10^{-15} T_e^{-0.2} \exp(-1.08/T_e)$		[9]^{a,b}

Continued on next page

Table A.7 (*Continued*)

ID	Reaction	k	ΔE_e	Source
25	$e + Ar \rightarrow Ar^+ + 2e$	$3.09 \times 10^{-14} T_e^{0.45} \exp(-17/T_e)$	15.88	[284][a]
26	$e + Ar^* \rightarrow Ar^+ + 2e$	$1.42 \times 10^{-13} T_e^{0.2} \exp(-4.38/T_e)$	4.42	[287][a]
27	$e + Ar^{**} \rightarrow Ar^+ + 2e$	$3.45 \times 10^{-13} T_e^{-0.02} \exp(-4.11/T_e)$	2.9	[208][a]
28	$e + O \rightarrow O^+ + 2e$	$4.82 \times 10^{-15} T_e^{0.73} \exp(-13.1/T_e)$	13.6	[202][a]
29	$e + O^* \rightarrow O^+ + 2e$	$1.56 \times 10^{-14} T_e^{0.29} \exp(-13.3/T_e)$	11.65	[9][a,b]
30	$e + O_2 \rightarrow O_2^+ + 2e$	$7.08 \times 10^{-15} T_e^{0.76} \exp(-13.8/T_e)$	12.05	[9][a]
31	$e + O_2^* \rightarrow O_2^+ + 2e$	$1.3 \times 10^{-15} T_e^{1.1} \exp(-11.1/T_e)$	11.1	[208; 288][a]
32	$e + F \rightarrow F^+ + 2e$	$2.15 \times 10^{-15} T_e^{0.87} \exp(-16/T_e)$	17.27	[9][a,b]
33	$e + F_2 \rightarrow F_2^+ + 2e$	$2.96 \times 10^{-15} T_e^{0.84} \exp(-15.9/T_e)$	15.53	[206][a]
34	$e + NO \rightarrow NO^+ + 2e$	$7.31 \times 10^{-15} T_e^{0.74} \exp(-11.9/T_e)$	9.25	[289][a]
35	$e + N_2O \rightarrow N_2O^+ + 2e$	$1.08 \times 10^{-14} T_e^{0.57} \exp(-13.7/T_e)$	12.85	[9][a,b]
36	$e + NF_3 \rightarrow NF_3^+ + 2e$	$1.47 \times 10^{-15} T_e^{0.7} \exp(-12.8/T_e)$	13	[225][a]
37	$e + NF_2 \rightarrow NF_2^+ + 2e$	$1.16 \times 10^{-15} T_e^{1.16} \exp(-12/T_e)$	11.8	[225][a]
38	$e + NF \rightarrow NF^+ + 2e$	$2.11 \times 10^{-15} T_e^{0.82} \exp(-14.9/T_e)$	15.7	[225][a]
39	$e + O_2 \rightarrow O + O^+ + 2e$	$9.92 \times 10^{-16} T_e^{1.1} \exp(-20.3/T_e)$	16.93	[214][a]
40	$e + NO \rightarrow N^+ + O + 2e$	$1.34 \times 10^{-15} T_e^{0.86} \exp(-23.5/T_e)$	20.95	[289][a]
41	$e + NO \rightarrow N + O^+ + 2e$	$8.19 \times 10^{-17} T_e^{1.47} \exp(-21.5/T_e)$	20.07	[289][a]
42	$e + N_2O \rightarrow N_2^+ + O + 2e$	$3.14 \times 10^{-15} T_e^{0.56} \exp(-19.9/T_e)$	17.45	[9][a,b]
43	$N_2O + e \rightarrow 2e + N_2 + O^+$	$8.82 \times 10^{-16} T_e^{0.53} \exp(-15.9/T_e)$	15.18	[9][a,b]
44	$e + NF_3 \rightarrow NF_2^+ + F + 2e$	$1.21 \times 10^{-14} T_e^{0.43} \exp(-15.8/T_e)$	14	[225][a]
45	$e + NF_3 \rightarrow 2e + NF_2 + F^+$	$6.92 \times 10^{-16} T_e^{0.71} \exp(-16.7/T_e)$	15.46	[290][a]
46	$e + NF_2 \rightarrow 2e + F + NF^+$	$4.61 \times 10^{-16} T_e^{1.22} \exp(-15.1/T_e)$	14.9	[290][a]
47	$e + NF_2 \rightarrow 2e + NF + F^+$	$7.39 \times 10^{-17} T_e^{1.23} \exp(-15.1/T_e)$	14.9	[290][a]
48	$e + NF \rightarrow 2e + N + F^+$	$1.66 \times 10^{-15} T_e^{0.74} \exp(-15.6/T_e)$	15.2	[290][a]
49	$e + NF \rightarrow 2e + N^+ + F$	$2.39 \times 10^{-15} T_e^{0.74} \exp(-15.6/T_e)$	15.2	[290][a]
50	$e + O_2 \rightarrow O^- + O$	$6.74 \times 10^{-16} T_e^{-1.02} \exp(-5.78/T_e)$		[9][a]
51	$e + F_2 \rightarrow F + F^-$	$3.82 \times 10^{-15} T_e^{-1.16} \exp(-0.16/T_e)$		[206][a]
52	$e + N_2O \rightarrow O^- + N_2$	$6.92 \times 10^{-16} T_e^{-0.89} \exp(-1.18/T_e)$		[9][a,b]
53	$e + NF_3 \rightarrow NF_2 + F^-$	$2.08 \times 10^{-14} T_e^{-1.23} \exp(-1.28/T_e)$		[225][a]
54	$e + NF_2 \rightarrow NF + F^-$	$2.09 \times 10^{-14} T_e^{-1.23} \exp(-1.29/T_e)$		[225][a]
55	$e + O^- \rightarrow O + 2e$	$1.95 \times 10^{-18} T_e^{-0.5} \exp(-3.4/T_e)$	3.4	[288][a]
56	$e + Ar^+ \rightarrow Ar$	$4.83 \times 10^{-19} T_e^{-0.5} \exp(-0.01/T_e)$		[9][a,b]
57	$e + F^+ \rightarrow F$	$4.83 \times 10^{-19} T_e^{-0.5} \exp(-0.01/T_e)$		[9][a,b]
58	$e + O_2^+ \rightarrow 2O$	$1.53 \times 10^{-14} T_e^{-0.51} \exp(-0.01/T_e)$		[221][a]
59	$e + F_2^+ \rightarrow 2F$	$2.26 \times 10^{-13} T_e^{-0.5} \exp(-0.01/T_e)$		[222][a]
60	$NO^+ + e \rightarrow N + O$	$1.71 \times 10^{-14} T_e^{-0.51} \exp(-/T_e)$		[221][a]
61	$e + NF_3^+ \rightarrow NF_2 + F$	$1 \times 10^{-13} T_e^{-0.5}$		[291]
62	$e + NF_2^+ \rightarrow NF + F$	$1 \times 10^{-13} T_e^{-0.5}$		[291]
63	$e + NF^+ \rightarrow N + F$	$1 \times 10^{-13} T_e^{-0.5}$		[291]
64	$e + O_2 \rightarrow e + 2O$	$1.75 \times 10^{-14} T_e^{-1.28} \exp(-7.38/T_e)$	4.5	[9][a]
65	$e + N_2O \rightarrow N_2 + O + e$	$1.4 \times 10^{-15} \exp(-1.67/T_e)$	1.67	[9][b]
66	$e + NF_3 \rightarrow NF + 2F + e$	$9.68 \times 10^{-15} T_e^{0.53} \exp(-10.6/T_e)$	8.9	[225][a]
67	$e + NF_3 \rightarrow NF_2 + F + e$	$7.06 \times 10^{-14} T_e^{-0.37} \exp(-5.41/T_e)$	5.6	[225][a]
68	$e + NF_2 \rightarrow NF + F + e$	$3.97 \times 10^{-14} T_e^{-0.16} \exp(-7.48/T_e)$	5.6	[225][a]
69	$e + NF \rightarrow N + F + e$	$3.97 \times 10^{-14} T_e^{-0.16} \exp(-7.48/T_e)$	5.6	[225][a]
70	$O_2 + M \rightarrow 2O + M$	$1.31 \times 10^{-16} \exp(-5274/T_g)$		[9][b]
71	$O_3 + M \rightarrow O_2 + O + M$	$1.56 \times 10^{-15} \exp(-1149/T_g)$		[292]
72	$N_2 + M \rightarrow 2N + M$	$9.86 \times 10^{-11} (T_g/300)^{-3.33} \exp(-11322/T_g)$		[293]
73	$N_2^* + M \rightarrow N^* + N + M$	$9.86 \times 10^{-11} (T_g/300)^{-3.33} \exp(-69163/T_g)$		[294]
74	$F_2 + M \rightarrow 2F + M$	$7.6 \times 10^{-18} \exp(-143/T_g)$		[295]
75	$NO + M \rightarrow N + O + M$	$2.28 \times 10^{-16} \exp(-7468/T_g)$		[9][b]
76	$N_2O + M \rightarrow N_2 + O + M$	$2.36 \times 10^{-16} \exp(-2581/T_g)$		[9][b]
77	$NO_2 + M \rightarrow NO + O + M$	$1.88 \times 10^{-10} (T_g/300)^{-3.37} \exp(-3764/T_g)$		[296]
78	$FO + M \rightarrow F + O + M$	$1.31 \times 10^{-16} \exp(-5274/T_g)$		[294]
79	$NF_3 + M \rightarrow NF_2 + F + M$	$3.98 \times 10^{-16} \exp(-18417/T_g)$		[297]
80	$NF_2 + M \rightarrow NF + F + M$	$1.26 \times 10^{-15} \exp(-257/T_g)$		[9][b]
81	$NF + M \rightarrow N + F + M$	$1.31 \times 10^{-16} \exp(-5274/T_g)$		[294]
82	$FNO + M \rightarrow F + NO + M$	$1.31 \times 10^{-16} \exp(-53899/T_g)$		[294]
83	$O + O_3 \rightarrow O_2^* + O_2$	$1 \times 10^{-17} \exp(-23/T_g)$		[9][b]
84	$O^* + Ar \rightarrow O + Ar$	5×10^{-19}		[9][b]

Continued on next page

Table A.7 (*Continued*)

ID	Reaction	k	ΔE_e	Source
85	$O^* + O_3 \rightarrow 2O_2$	1.2×10^{-16}		[298]
86	$NO + O^* \rightarrow O_2 + N$	1.5×10^{-16}		[299]
87	$O^* + N_2O \rightarrow N_2 + O_2$	4.4×10^{-17}		[8]
88	$O^* + N_2O \rightarrow 2NO$	7.2×10^{-17}		[8]
89	$O^* + FO \rightarrow O_2 + F$	5×10^{-17}		[226]
90	$NF_3 + O^* \rightarrow NF_2 + FO$	1.1×10^{-17}		[300]
91	$O_2 + O_2^* \rightarrow O + O_3$	2.95×10^{-27}		[294]
92	$N^* + O_2 \rightarrow NO + O$	$1.22 \times 10^{-17} \exp\left(-317/T_g\right)$		[301]
93	$N_2^* + O_2 \rightarrow N_2O + O$	7.8×10^{-20}		[6]
94	$N + O_2^* \rightarrow NO + O$	$2 \times 10^{-20} \exp\left(-6/T_g\right)$		[6]
95	$N^* + O_2^* \rightarrow NO + O$	2×10^{-20}		[294]
96	$N^* + O_3 \rightarrow NO + O_2$	1×10^{-16}		[6]
97	$N^* + NO \rightarrow N_2 + O$	6.3×10^{-17}		[302]
98	$N_2O + N^* \rightarrow N_2 + NO$	$1.5 \times 10^{-17} \exp\left(-57/T_g\right)$		[9]^b
99	$N^* + NO_2 \rightarrow N_2O + O$	$1.5 \times 10^{-18} \exp\left(-57/T_g\right)$		[9]^b
100	$N^* + NO_2 \rightarrow N_2 + O_2$	1.41×10^{-18}		[294]
101	$N^* + NO_2 \rightarrow 2NO$	1.5×10^{-18}		[302]
102	$NF_3 + N^* \rightarrow NF + NF_2$	2.13×10^{-18}		[294]
103	$NF_2 + N^* \rightarrow 2NF$	3×10^{-18}		[294]
104	$NF + N^* \rightarrow N_2 + F$	2.5×10^{-16}		[303]
105	$O_2^* + M \rightarrow 2O + M$	$1.31 \times 10^{-16} \exp\left(-41146/T_g\right)$		[294]
106	$N_2^* + M \rightarrow 2N + M$	$9.86 \times 10^{-11} \left(T_g/300\right)^{-3.33} \exp\left(-41337/T_g\right)$		[294]
107	$Ar^* + O \rightarrow O^* + Ar$	4.1×10^{-17}		[304]
108	$2Ar^* \rightarrow Ar^+ + Ar + e$	1×10^{-16}		[249]
109	$Ar^* + Ar^{**} \rightarrow Ar^+ + Ar + e$	$1.2 \times 10^{-15} \left(T_g/300\right)^{0.5}$		[9]^b
110	$Ar^* + O_2^* \rightarrow O_2^+ + Ar + e$	$1.2 \times 10^{-15} \left(T_g/300\right)^{0.5}$		[294]
111	$2Ar^{**} \rightarrow Ar^+ + Ar + e$	5×10^{-16}		[249]
112	$O + O_3 \rightarrow 2O_2$	$8 \times 10^{-18} \exp\left(-206/T_g\right)$		[8]
113	$N_2 + O \rightarrow N + NO$	$1.26 \times 10^{-16} \exp\left(-3804/T_g\right)$		[9]^b
114	$F_2 + O \rightarrow F + FO$	$1.62 \times 10^{-17} \exp\left(-5233/T_g\right)$		[9]^b
115	$NO + O \rightarrow N + O_2$	$7.48 \times 10^{-19} \left(T_g/300\right)^{1} \exp\left(-195/T_g\right)$		[9]^b
116	$N_2O + O \rightarrow N_2 + O_2$	$1.66 \times 10^{-16} \exp\left(-141/T_g\right)$		[6]
117	$N_2O + O \rightarrow 2NO$	$1.15 \times 10^{-16} \exp\left(-134/T_g\right)$		[6]
118	$FO + O \rightarrow O_2 + F$	2.7×10^{-17}		[226]
119	$NF_2 + O \rightarrow F + FNO$	1.25×10^{-17}		[305]
120	$NF_2 + O \rightarrow NF + FO$	1.79×10^{-18}		[305]
121	$FNO + O \rightarrow F + NO_2$	3×10^{-19}		[9]^b
122	$2O_2 \rightarrow O_3 + O$	$1.11 \times 10^{-17} \exp\left(-498/T_g\right)$		[306]
123	$N + O_2 \rightarrow NO + O$	$1.5 \times 10^{-17} \exp\left(-36/T_g\right)$		[8]
124	$N_2 + O_2 \rightarrow N_2O + O$	$1 \times 10^{-16} \exp\left(-552/T_g\right)$		[6]
125	$N_2 + O_2 \rightarrow 2NO$	$9.85 \times 10^{-12} \exp\left(-6466/T_g\right)$		[9]^b
126	$N + O_3 \rightarrow NO + O_2$	5×10^{-22}		[307]
127	$F + O_3 \rightarrow FO + O_2$	$2.82 \times 10^{-17} \exp\left(-252/T_g\right)$		[9]^b
128	$NO + O_3 \rightarrow NO_2 + O_2$	$1.8 \times 10^{-18} \exp\left(-137/T_g\right)$		[8]
129	$N + NO \rightarrow N_2 + O$	$2.1 \times 10^{-17} \exp\left(1/T_g\right)$		[8]
130	$NF_3 + N \rightarrow NF + NF_2$	$2.13 \times 10^{-18} \left(T_g/300\right)^{1.97} \exp\left(-1512/T_g\right)$		[308]
131	$FO + F \rightarrow F_2 + O$	$6.61 \times 10^{-20} \exp\left(-9561/T_g\right)$		[9]^b
132	$F_2 + NO \rightarrow F + FNO$	1.2×10^{-20}		[9]^b
133	$NF_2 + F_2 \rightarrow F + NF_3$	$3 \times 10^{-20} \exp\left(-486/T_g\right)$		[9]^b
134	$2NO \rightarrow N_2O + O$	$7.22 \times 10^{-18} \exp\left(-33155/T_g\right)$		[6]
135	$2NO \rightarrow N_2 + O_2$	$1.35 \times 10^{-17} \exp\left(-2868/T_g\right)$		[9]^b
136	$N_2O + NO \rightarrow NO_2 + N_2$	$2.92 \times 10^{-19} \left(T_g/300\right)^{2.23} \exp\left(-23292/T_g\right)$		[6]
137	$NF_3 + NF \rightarrow 2NF_2$	1×10^{-20}		[309]
138	$2NF_2 \rightarrow NF + NF_3$	$1.66 \times 10^{-18} \exp\left(-186/T_g\right)$		[310]
139	$2NF \rightarrow F_2 + N_2$	4×10^{-18}		[309]
140	$Ar^* + O_2 \rightarrow Ar + O^* + O$	2.1×10^{-16}		[311]
141	$O^* + O_3 \rightarrow O_2 + 2O$	1.2×10^{-16}		[298]
142	$N_2O + O^* \rightarrow N_2 + O_2^*$	$2.43 \times 10^{-18} \left(T_g/300\right)^{2.3} \exp\left(-9645/T_g\right)$		[312]
143	$N^* + O_2 \rightarrow NO + O^*$	$6 \times 10^{-18} \left(T_g/300\right)^{0.5}$		[9]^b
144	$N_2^* + O_2 \rightarrow N_2O + O^*$	3×10^{-20}		[6]

Continued on next page

Table A.7 (*Continued*)

ID	Reaction	k	ΔE_e	Source
145	$2O_3 \rightarrow 3O_2$	$7.42 \times 10^{-18} \exp\left(-946/T_g\right)$		[9][b]
146	$NF_2 + N \rightarrow N_2 + 2F$	$1.4 \times 10^{-17} \exp\left(-95/T_g\right)$		[9][b]
147	$N^* + NO_2 \rightarrow N_2 + 2O$	1.12×10^{-18}		[294]
148	$NF_2 + N^* \rightarrow N_2 + 2F$	1.4×10^{-17}		[294]
149	$N_2O + N_2^* \rightarrow NO + N + N_2$	8×10^{-17}		[9][b]
150	$NF_2 + FO \rightarrow FNO + 2F$	3.8×10^{-18}		[9][b]
151	$2NF \rightarrow N_2 + 2F$	$6.88 \times 10^{-17} \exp\left(-1251/T_g\right)$		[9][b]
152	$Ar + Ar^+ \rightarrow Ar + Ar^+$	$5.66 \times 10^{-16} \left(T_g/300\right)^{0.5}$		[9][b]
153	$O + O^+ \rightarrow O^+ + O$	1×10^{-15}		[224]
154	$O_2^+ + O_2 \rightarrow O_2 + O_2^+$	1×10^{-15}		[249]
155	$N^+ + N \rightarrow N^+ + N$	1×10^{-15}		[9][b]
156	$N_2^+ + N_2 \rightarrow N_2^+ + N_2$	1×10^{-15}		[9][b]
157	$F^+ + F \rightarrow F^+ + F$	1×10^{-15}		[224]
158	$F_2^+ + F_2 \rightarrow F_2^+ + F_2$	1×10^{-15}		[224]
159	$NO^+ + NO \rightarrow NO + NO^+$	1×10^{-15}		[294]
160	$N_2O^+ + N_2O \rightarrow N_2O + N_2O^+$	1×10^{-15}		[294]
161	$NF_3^+ + NF_3 \rightarrow NF_3 + NF_3^+$	1×10^{-15}		[294]
162	$NF_2^+ + NF_2 \rightarrow NF_2 + NF_2^+$	1×10^{-15}		[294]
163	$NF^+ + NF \rightarrow NF + NF^+$	1×10^{-15}		[294]
164	$Ar + O^+ \rightarrow O + Ar^+$	2.1×10^{-17}		[313]
165	$Ar + O_2^+ \rightarrow O_2 + Ar^+$	2.1×10^{-17}		[313]
166	$F^+ + Ar \rightarrow F + Ar^+$	1×10^{-17}		[294]
167	$Ar^+ + O \rightarrow O^+ + Ar$	6.4×10^{-18}		[313]
168	$Ar^+ + O_2 \rightarrow O_2^+ + Ar$	1.2×10^{-17}		[129]
169	$Ar^+ + N \rightarrow N^+ + Ar$	1×10^{-17}		[280]
170	$Ar^+ + N_2 \rightarrow Ar + N_2^+$	5×10^{-16}		[314]
171	$Ar^+ + F_2 \rightarrow Ar + F_2^+$	1×10^{-17}		[294]
172	$Ar^+ + NO \rightarrow Ar + NO^+$	1×10^{-17}		[294]
173	$Ar^+ + N_2O \rightarrow Ar + N_2O^+$	1×10^{-17}		[294]
174	$Ar^+ + NF_3 \rightarrow Ar + NF_3^+$	1×10^{-17}		[294]
175	$Ar^+ + NF_2 \rightarrow NF_2^+ + Ar$	1×10^{-17}		[9][b]
176	$Ar^+ + NF \rightarrow NF^+ + Ar$	5×10^{-18}		[9][b]
177	$N^+ + O \rightarrow N + O^+$	1×10^{-17}		[294]
178	$N_2^+ + O \rightarrow N_2 + O^+$	9.8×10^{-18}		[315]
179	$F^+ + O \rightarrow F + O^+$	1×10^{-16}		[226]
180	$F_2^+ + O \rightarrow O^+ + F_2$	5×10^{-16}		[9][b]
181	$O^+ + O_2 \rightarrow O_2^+ + O$	$2 \times 10^{-17} \left(T_g/300\right)^{-0.4}$		[7]
182	$O^+ + N_2O \rightarrow O + N_2O^+$	6.3×10^{-16}		[9][b]
183	$O^+ + NF_3 \rightarrow O + NF_3^+$	1×10^{-17}		[294]
184	$O^+ + NF_2 \rightarrow O + NF_2^+$	1×10^{-17}		[294]
185	$O^+ + NF \rightarrow O + NF^+$	1×10^{-17}		[294]
186	$N_2^+ + O_2 \rightarrow O_2^+ + N_2$	$5 \times 10^{-17} \left(T_g/300\right)^{-0.8}$		[7]
187	$F^+ + O_2 \rightarrow F + O_2^+$	7.14×10^{-16}		[226]
188	$F_2^+ + O_2 \rightarrow O_2^+ + F_2$	5×10^{-16}		[9][b]
189	$N_2O^+ + O_2 \rightarrow N_2O + O_2^+$	2.24×10^{-16}		[9][b]
190	$NF_3^+ + O_2 \rightarrow NF_3 + O_2^+$	1×10^{-17}		[294]
191	$NF^+ + O_2 \rightarrow NF + O_2^+$	1×10^{-17}		[294]
192	$O_2^+ + NO \rightarrow NO^+ + O_2$	4.6×10^{-16}		[7]
193	$N_2^+ + N \rightarrow N^+ + N_2$	5×10^{-18}		[9][b]
194	$F^+ + N \rightarrow N^+ + F$	1×10^{-17}		[238]
195	$F_2^+ + N \rightarrow N^+ + F_2$	1×10^{-17}		[9][b]
196	$N^+ + NO \rightarrow N + NO^+$	4.72×10^{-16}		[315]
197	$N^+ + N_2O \rightarrow N + N_2O^+$	1×10^{-17}		[294]
198	$N^+ + NF_3 \rightarrow NF_3^+ + N$	1×10^{-17}		[316]
199	$F^+ + N_2 \rightarrow N_2^+ + F$	1×10^{-17}		[317]
200	$F_2^+ + N_2 \rightarrow N_2^+ + F_2$	5×10^{-18}		[9][b]
201	$N_2^+ + NO \rightarrow NO^+ + N_2$	3.9×10^{-16}		[7]
202	$N_2^+ + N_2O \rightarrow N_2 + N_2O^+$	6×10^{-16}		[9][b]
203	$N_2^+ + NF_3 \rightarrow N_2 + NF_3^+$	1×10^{-17}		[294]
204	$N_2^+ + NF_2 \rightarrow NF_2^+ + N_2$	1×10^{-17}		[316]

Continued on next page

Table A.7 (*Continued*)

ID	Reaction	k	ΔE_e	Source
205	$N_2^+ + NF \rightarrow N_2 + NF^+$	1×10^{-17}		[294]
206	$F^+ + F_2 \rightarrow F_2^+ + F$	7.94×10^{-16}		[238]
207	$F^+ + NO \rightarrow F + NO^+$	8.64×10^{-16}		[315]
208	$F^+ + N_2O \rightarrow F + N_2O^+$	1×10^{-17}		[294]
209	$F^+ + NF_3 \rightarrow F + NF_3^+$	1×10^{-17}		[294]
210	$F^+ + NF_2 \rightarrow NF_2^+ + F$	1×10^{-17}		[238]
211	$F^+ + NF \rightarrow NF^+ + F$	1×10^{-17}		[9][b]
212	$F_2^+ + NO \rightarrow F_2 + NO^+$	1×10^{-17}		[294]
213	$F_2^+ + N_2O \rightarrow F_2 + N_2O^+$	1×10^{-17}		[294]
214	$F_2^+ + NF_3 \rightarrow F_2 + NF_3^+$	1×10^{-17}		[294]
215	$F_2^+ + NF_2 \rightarrow NF_2^+ + F_2$	1×10^{-17}		[9][b]
216	$F_2^+ + NF \rightarrow NF^+ + F_2$	1×10^{-17}		[9][b]
217	$N_2O^+ + NO \rightarrow N_2O + NO^+$	2.3×10^{-16}		[294]
218	$NF_3^+ + NO \rightarrow NF_3 + NO^+$	1×10^{-17}		[294]
219	$NF_2^+ + NO \rightarrow NF_2 + NO^+$	1×10^{-17}		[294]
220	$NF^+ + NO \rightarrow NF + NO^+$	1×10^{-17}		[294]
221	$NF_3^+ + N_2O \rightarrow NF_3 + N_2O^+$	1×10^{-17}		[294]
222	$N_2O^+ + NF_2 \rightarrow N_2O + NF_2^+$	1×10^{-17}		[294]
223	$N_2O^+ + NF \rightarrow N_2O + NF^+$	1×10^{-17}		[294]
224	$NF_3^+ + NF_2 \rightarrow NF_3 + NF_2^+$	1×10^{-17}		[294]
225	$NF^+ + NF_2 \rightarrow NF_2^+ + NF$	1×10^{-17}		[318]
226	$NF_3^+ + NF \rightarrow NF_3 + NF^+$	1×10^{-17}		[294]
227	$Ar^+ + O^* \rightarrow O^+ + Ar$	6.4×10^{-18}		[311]
228	$N_2^+ + O \rightarrow N + NO^+$	1.4×10^{-16}		[9][b]
229	$N^+ + O_2 \rightarrow NO + O^+$	4.64×10^{-17}		[315]
230	$N_2^+ + O_2 \rightarrow NO + NO^+$	1×10^{-23}		[6]
231	$F^+ + O_2 \rightarrow O^+ + FO$	5.04×10^{-17}		[245]
232	$N_2O^+ + O_2 \rightarrow NO_2 + NO^+$	4.59×10^{-17}		[9][b]
233	$O_2^+ + N \rightarrow O + NO^+$	1.5×10^{-16}		[315]
234	$O_2^+ + N_2 \rightarrow NO + NO^+$	1×10^{-23}		[6]
235	$N^+ + NO \rightarrow O + N_2^+$	8.33×10^{-17}		[319]
236	$N^+ + N_2O \rightarrow N_2 + NO^+$	5.5×10^{-16}		[9][b]
237	$N_2^+ + N_2O \rightarrow N_2 + N + NO^+$	4×10^{-16}		[9][b]
238	$N_2^+ + NO_2 \rightarrow N_2O + NO^+$	5×10^{-17}		[9][b]
239	$F^+ + NO \rightarrow O + NF^+$	9.4×10^{-17}		[315]
240	$N_2O^+ + N_2O \rightarrow N_2 + NO + NO^+$	1.2×10^{-17}		[9][b]
241	$N_2O^+ + NO_2 \rightarrow N_2 + O_2 + NO^+$	4.29×10^{-16}		[9][b]
242	$NF^+ + NF_3 \rightarrow NF_2 + NF_2^+$	5.5×10^{-16}		[318]
243	$O_2^- + O \rightarrow O_2 + O^-$	3.3×10^{-16}		[14]
244	$O^- + O_2 \rightarrow O_2^- + O$	2.5×10^{-20}		[320]
245	$O^- + O_3 \rightarrow O_3^- + O$	5.3×10^{-16}		[9][b]
246	$O^- + F \rightarrow F^- + O$	5.5×10^{-16}		[294]
247	$O_2^- + O_3 \rightarrow O_2 + O_3^-$	4×10^{-16}		[14]
248	$O_2^- + F \rightarrow F^- + O_2$	1×10^{-13}		[224]
249	$O_3^- + F \rightarrow F^- + O_3$	5.5×10^{-16}		[294]
250	$O_3^- + O \rightarrow 2O_2 + e$	3×10^{-16}		[14]
251	$O^- + O_3 \rightarrow 2O_2 + e$	$3.01 \times 10^{-16} \left(T_g/300\right)^{0.5}$		[280]
252	$O^- + O \rightarrow O_2 + e$	$3 \times 10^{-16} \left(T_g/300\right)^{-0.5}$		[321]
253	$O_2^- + O \rightarrow O_3 + e$	1.5×10^{-16}		[14]
254	$O^- + O_2 \rightarrow O_3 + e$	5×10^{-21}		[14]
255	$O^- + N \rightarrow NO + e$	2.6×10^{-16}		[14]
256	$O^- + N_2 \rightarrow N_2O + e$	1×10^{-18}		[9][b]
257	$O^- + NO \rightarrow NO_2 + e$	2.6×10^{-16}		[14]
258	$O_2^- + N \rightarrow NO_2 + e$	5×10^{-16}		[14]
259	$F^- + F \rightarrow e + F_2$	1×10^{-16}		[242]
260	$O_3^- + O \rightarrow O_2^- + O_2$	3.2×10^{-16}		[9][b]
261	$O^- + O_3 \rightarrow O_2^- + O_2$	$1.02 \times 10^{-17} \left(T_g/300\right)^{0.5}$		[280]
262	$O_2^- + N_2O \rightarrow O_3^- + N_2$	1×10^{-18}		[14]
263	$Ar^+ + O^- \rightarrow Ar + O$	2.7×10^{-13}		[313]
264	$O_2^- + Ar^+ \rightarrow O_2 + Ar$	1×10^{-13}		[247]

Continued on next page

Table A.7 (*Continued*)

ID	Reaction	k	ΔE_e	Source
265	$O_3^- + Ar^+ \rightarrow O_3 + Ar$	1×10^{-13}		[247]
266	$F^- + Ar^+ \rightarrow F + Ar$	1×10^{-13}		[322]
267	$O_2^- + O^+ \rightarrow O_2 + O$	1×10^{-13}		[247]
268	$O_3^- + O^+ \rightarrow O_3 + O$	1×10^{-13}		[247]
269	$O^+ + F^- \rightarrow O + F$	1×10^{-13}		[9]^b
270	$O^- + O_2^+ \rightarrow O_2 + O$	1×10^{-13}		[247]
271	$O^- + F^+ \rightarrow O + F$	3×10^{-13}		[224]
272	$O^- + F_2^+ \rightarrow O + F_2$	1.5×10^{-13}		[224]
273	$O^- + NO^+ \rightarrow O + NO$	1×10^{-13}		[247]
274	$O^- + N_2O^+ \rightarrow O + N_2O$	1×10^{-13}		[247]
275	$O_2^- + O_2^+ \rightarrow 2O_2$	1×10^{-13}		[247]
276	$O_3^- + O_2^+ \rightarrow O_3 + O_2$	1×10^{-13}		[247]
277	$O_2^+ + F^- \rightarrow O_2 + F$	1×10^{-13}		[9]^b
278	$O_2^- + N^+ \rightarrow O_2 + N$	1×10^{-13}		[247]
279	$O_2^- + N_2^+ \rightarrow O_2 + N_2$	1×10^{-13}		[247]
280	$O_2^- + F^+ \rightarrow O_2 + F$	2×10^{-13}		[224]
281	$O_2^- + F_2^+ \rightarrow O_2 + F_2$	1.5×10^{-13}		[224]
282	$O_2^- + NO^+ \rightarrow O_2 + NO$	1×10^{-13}		[247]
283	$O_2^- + N_2O^+ \rightarrow O_2 + N_2O$	1×10^{-13}		[247]
284	$O_3^- + N^+ \rightarrow O_3 + N$	1×10^{-13}		[247]
285	$O_3^- + N_2^+ \rightarrow O_3 + N_2$	1×10^{-13}		[247]
286	$O_3^- + NO^+ \rightarrow O_3 + NO$	1×10^{-13}		[247]
287	$O_3^- + N_2O^+ \rightarrow O_3 + N_2O$	1×10^{-13}		[247]
288	$F^- + N^+ \rightarrow F + N$	2×10^{-13}		[9]^b
289	$F^- + N_2^+ \rightarrow F + N_2$	3×10^{-13}		[9]^b
290	$F^- + F^+ \rightarrow 2F$	1×10^{-13}		[242]
291	$F^- + N_2O^+ \rightarrow F + N_2O$	$2 \times 10^{-13} \left(T_g/300\right)^{-0.5}$		[294]
292	$O^- + N_2O^+ \rightarrow 2O + N_2$	1×10^{-13}		[9]^b
293	$O^- + NF_3^+ \rightarrow O + NF_2 + F$	2×10^{-13}		[294]
294	$O^- + NF_2^+ \rightarrow O + NF + F$	2×10^{-13}		[294]
295	$O_2^- + NO^+ \rightarrow O_2 + N + O$	1×10^{-13}		[9]^b
296	$O_2^- + N_2O^+ \rightarrow O_2 + N_2 + O$	1×10^{-13}		[9]^b
297	$O_2^- + NF_3^+ \rightarrow O_2 + NF_2 + F$	2×10^{-13}		[294]
298	$O_2^- + NF_2^+ \rightarrow O_2 + NF + F$	2×10^{-13}		[294]
299	$F^- + N_2O^+ \rightarrow F + N_2 + O$	1×10^{-13}		[294]
300	$F^- + NF^+ \rightarrow 2F + N$	1×10^{-13}		[294]
301	$2O + M \rightarrow O_2^* + M$	$1.9 \times 10^{-47} \left(T_g/300\right)^{-0.63}$		[323]
302	$O + O^+ + M \rightarrow O_2^+ + M$	1×10^{-41}		[323]
303	$F + O + M \rightarrow FO + M$	1×10^{-45}		[227]
304	$2N + M \rightarrow N_2^* + M$	1×10^{-44}		[266]
305	$N + F + M \rightarrow NF + M$	2.8×10^{-46}		[294]
306	$2F + M \rightarrow F_2 + M$	6.77×10^{-46}		[9]^b
307	$F + NO + M \rightarrow FNO + M$	$5.9 \times 10^{-44} \left(T_g/300\right)^{-1.7}$		[9]^b
308	$NF_2 + F + M \rightarrow NF_3 + M$	5×10^{-43}		[324]
309	$NF + F + M \rightarrow NF_2 + M$	1.03×10^{-42}		[294]
310	$Ar^{**} \rightarrow Ar^*$	1×10^5		[9]^b

Bibliography

[1] d'Agostino R, Favia P, Oehr C and Wertheimer M R 2005 *Plasma Processes and Polymers* **2** 7–15

[2] Weltmann K, Kolb J F, Holub M, Uhrlandt D, Šimek M, Ostrikov K K, Hamaguchi S, Cvelbar U, Černák M, Locke B, Fridman A, Favia P and Becker K 2019 *Plasma Processes and Polymers* **16** 1800118

[3] Berthelot A and Bogaerts A 2016 *Plasma Sources Science and Technology* **25** 045022

[4] Guerra V, Tejero-del Caz A, Pintassilgo C D and Alves L L 2019 *Plasma Sources Science and Technology* **28** 073001

[5] Hong J, Pancheshnyi S, Tam E, Lowke J J, Prawer S and Murphy A B 2017 *Journal of Physics D: Applied Physics* **50** 154005

[6] Gaens W V and Bogaerts A 2013 *Journal of Physics D: Applied Physics* **46** 275201

[7] Sieck L W, Heron J T and Green D S 2000 *Plasma Chemistry and Plasma Processing* **20** 235–258

[8] Herron J T and Green D S 2001 *Plasma Chemistry and Plasma Processing* **21** 459–481

[9] Tennyson J, Rahimi S, Hill C, Tse L, Vibhakar A, Akello-Egwel D, Brown D B, Dzarasova A, Hamilton J R, Jaksch D, Mohr S, Wren-Little K, Bruckmeier J, Agarwal A, Bartschat K, Bogaerts A, Booth J P, Goeckner M J, Hassouni K,

Itikawa Y, Braams B J, Krishnakumar E, Laricchiuta A, Mason N J, Pandey S, Petrovic Z L, Pu Y K, Ranjan A, Rauf S, Schulze J, Turner M M, Ventzek P, Whitehead J C and Yoon J S 2017 *Plasma Sources Science and Technology* **26** 055014

[10] Koelman P, Heijkers S, Tadayon Mousavi S, Graef W, Mihailova D, Kozak T, Bogaerts A and van Dijk J 2017 *Plasma Processes and Polymers* **14** 1600155

[11] Nagy T and Turanyi T 2009 *Combustion and Flame* **156** 417–428

[12] Tomlin A S, Pilling M J, Turányi T, Merkin J H and Brindley J 1992 *Combustion and Flame* **91** 107 – 130

[13] Bak M S and Cappelli M A 2015 *IEEE Transactions on Plasma Science* **43** 995–1001

[14] Kossyi I A, Kostinsky A Y, Matveyev A A and Silakov V P 1992 *Plasma Sources Science and Technology* **1** 207–220

[15] Gorban A 2018 *Current Opinion in Chemical Engineering* **21** 48–59

[16] Tomlin A S, Turányi T and Pilling M J 1997 Chapter 4 Mathematical tools for the construction, investigation and reduction of combustion mechanisms *Comprehensive Chemical Kinetics* vol 35 (Elsevier) pp 293–437

[17] Okino M S and Mavrovouniotis M L 1998 *Chemical Reviews* **98** 391–408

[18] Law C K 2007 *Proceedings of the Combustion Institute* **31** 1–29

[19] Lu T and Law C K 2009 *Progress in Energy and Combustion Science* **35** 192–215

[20] Turányi T and Tomlin A S 2014 *Analysis of kinetic reaction mechanisms* (Berlin: Springer) oCLC: 904443703

[21] Huang H, Fairweather M, Griffiths J, Tomlin A and Brad R 2005 *Proceedings of the Combustion Institute* **30** 1309–1316

[22] Turner M M 2015 *Plasma Sources Science and Technology* **24** 035027

[23] Zheng X, Lu T and Law C 2007 *Proceedings of the Combustion Institute* **31** 367–375

[24] Maas U and Pope S 1992 *Combustion and Flame* **88** 239–264

[25] Rehman T, Kemaneci E, Graef W and van Dijk J 2016 *Journal of Physics: Conference Series* **682** 012035

[26] Lam S and Goussis D 1989 *Symposium (International) on Combustion* **22** 931–941

[27] Lam S H and Goussis D A 1994 *International Journal of Chemical Kinetics* **26** 461–486

[28] Lam S H 2013 *Combustion and Flame* **160** 2707–2711

[29] Rabitz H, Kramer M and Dacol D 1983 *Annual Review of Physical Chemistry* **34** 419–461

[30] Ayilaran A, Hanicinec M, Mohr S and Tennyson J 2019 *Plasma Science and Technology* **21** 064006

[31] Wang H and Frenklach M 1991 *Combustion and Flame* **87** 365–370

[32] Oluwole O, Bhattacharjee B, Tolsma J, Barton P and Green W 2006 *Combustion and Flame* **146** 348–365

[33] Liu D X, Bruggeman P, Iza F, Rong M Z and Kong M G 2010 *Plasma Sources Science and Technology* **19** 025018

[34] Whitehouse L E, Tomlin A S and Pilling M J 2004 *Atmospheric Chemistry and Physics* **4** 2025–2056

[35] Valorani M, Creta F, Goussis D, Lee J and Najm H 2006 *Combustion and Flame* **146** 29–51

[36] Bellemans A, Deak N and Bisetti F 2020 *Plasma Sources Science and Technology* **29** 025020

[37] Lu T and Law C K 2005 *Proceedings of the Combustion Institute* **30** 1333–1341

[38] Lu T and Law C K 2006 *Combustion and Flame* **144** 24–36

[39] Lu T and Law C K 2006 *Combustion and Flame* **146** 472–483

[40] Pepiotdesjardins P and Pitsch H 2008 *Combustion and Flame* **154** 67–81

[41] Sankaran R, Hawkes E R, Chen J H, Lu T and Law C K 2007 *Proceedings of the Combustion Institute* **31** 1291–1298

[42] Bellemans A, Kincaid N, Deak N, Pepiot P and Bisetti F 2020 *Proceedings of the Combustion Institute* S1540748920304569

[43] Sun S R, Wang H X and Bogaerts A 2020 *Plasma Sources Science and Technology* **29** 025012

[44] Venot O, Bounaceur R, Dobrijevic M, Hébrard E, Cavalié T, Tremblin P, Drummond B and Charnay B 2019 *Astronomy & Astrophysics* **624** A58

[45] Obrusnik A, Bilek P, Hoder T, Simek M and Bonaventura Z 2018 *Plasma Sources Science and Technology* **27** 085013

[46] Lebedev A V, Okun M V, Chorkov V A, Tokar P M and Strelkova M 2013 *Journal of Mathematical Chemistry* **51** 73–107

[47] Pitchford L C, Alves L L, Bartschat K, Biagi S F, Bordage M C, Bray I, Brion C E, Brunger M J, Campbell L, Chachereau A, Chaudhury B, Christophorou L G, Carbone E, Dyatko N A, Franck C M, Fursa D V, Gangwar R K, Guerra V, Haefliger P, Hagelaar G J M, Hoesl A, Itikawa Y, Kochetov I V, McEachran R P, Morgan W L, Napartovich A P, Puech V, Rabie M, Sharma L, Srivastava R, Stauffer A D, Tennyson J, de Urquijo J, van Dijk J, Viehland L A, Zammit M C, Zatsarinny O and Pancheshnyi S 2017 *Plasma Processes and Polymers* **14** 1600098

[48] Celiberto R, Armenise I, Cacciatore M, Capitelli M, Esposito F, Gamallo P, Janev R K, Laganà A, Laporta V, Laricchiuta A, Lombardi A, Rutigliano M, Sayós R, Tennyson J and Wadehra J M 2016 *Plasma Sources Science and Technology* **25** 033004

[49] Wakelam V, Herbst E, Loison J C, Smith I W M, Chandrasekaran V, Pavone B, Adams N G, Bacchus-Montabonel M C, Bergeat A, Béroff K, Bierbaum V M, Chabot M, Dalgarno A, van Dishoeck E F, Faure A, Geppert W D, Gerlich D, Galli D, Hébrard E, Hersant F, Hickson K M, Honvault P, Klippenstein S J, Le Picard S, Nyman G, Pernot P, Schlemmer S, Selsis F, Sims I R, Talbi D, Tennyson J, Troe J, Wester R and Wiesenfeld L 2012 *The Astrophysical Journal Supplement Series* **199** 21

[50] Wakelam V, Loison J C, Herbst E, Pavone B, Bergeat A, Béroff K, Chabot M, Faure A, Galli D, Geppert W D, Gerlich D, Gratier P, Harada N, Hickson K M, Honvault P, Klippenstein S J, Picard S D L, Nyman G, Ruaud M, Schlemmer S, Sims I R, Talbi D, Tennyson J and Wester R 2015 *The Astrophysical Journal Supplement Series* **217** 20

[51] McElroy D, Walsh C, Markwick A J, Cordiner M A, Smith K and Millar T J 2013 *Astronomy & Astrophysics* **550** A36

[52] Dubernet M L, Alexander M H, Ba Y A, Balakrishnan N, Balança C, Ceccarelli C, Cernicharo J, Daniel F, Dayou F, Doronin M, Dumouchel F, Faure A, Feautrier N, Flower D R, Grosjean A, Halvick P, Kłos J, Lique F, McBane G C, Marinakis S, Moreau N, Moszynski R, Neufeld D A, Roueff E, Schilke P, Spielfiedel A, Stancil P C, Stoecklin T, Tennyson J, Yang B, Vasserot A M and Wiesenfeld L 2013 *Astronomy & Astrophysics* **553** A50

[53] Murakami I, Kato D, Kato M, Sakaue H A and Kato T 2007 *Fusion Science and Technology* **51** 138–140

[54] Park J H, Choi H, Chang W S, Chung S Y, Kwon D C, Song M Y and Yoon J S 2020 *Applied Science and Convergence Technology* **29** 5–9

[55] Hulse R A 1990 The ALADDIN atomic physics database system *AIP Conference Proceedings* vol 206 (Gaithersburg, Maryland (USA): AIP) pp 63–72 iSSN: 0094243X

[56] Brunger M J and Buckman S J 2002 *Physics Reports* **357** 215–458

[57] Trajmar S, Register D and Chutjian A 1983 *Physics Reports* **97** 219–356

[58] Itikawa Y, Hayashi M, Ichimura A, Onda K, Sakimoto K, Takayanagi K, Nakamura M, Nishimura H and Takayanagi T 1986 *Journal of Physical and Chemical Reference Data* **15** 985–1010

[59] Bartschat K and Kushner M J 2016 *Proceedings of the National Academy of Sciences* **113** 7026–7034

[60] Manthe U 2011 *Molecular Physics* **109** 1415–1426

[61] Harada N and Herbst E 2008 *The Astrophysical Journal* **685** 272–280

[62] Smith D, Church M J and Miller T M 1978 *The Journal of Chemical Physics* **68** 1224–1229

[63] Adamovich I, Baalrud S D, Bogaerts A, Bruggeman P J, Cappelli M, Colombo V, Czarnetzki U, Ebert U, Eden J G, Favia P, Graves D B, Hamaguchi S, Hieftje G, Hori M, Kaganovich I D, Kortshagen U, Kushner M J, Mason N J, Mazouffre S, Thagard S M, Metelmann H R, Mizuno A, Moreau E, Murphy A B, Niemira B A, Oehrlein G S, Petrovic Z L, Pitchford L C, Pu Y K, Rauf S, Sakai O, Samukawa S, Starikovskaia S, Tennyson J, Terashima K, Turner M M, van de Sanden M C M and Vardelle A 2017 *Journal of Physics D: Applied Physics* **50** 323001

[64] Little D A 2015 *Electron-N_2^+ scattering and dynamics* Ph.D. thesis University College London United Kingdom

[65] Car R and Parrinello M 1985 *Physical Review Letters* **55** 2471–2474

[66] Hutter J 2012 *Wiley Interdisciplinary Reviews: Computational Molecular Science* **2** 604–612

[67] Kohn W and Sham L J 1965 *Physical Review* **140** A1133–A1138

[68] Remler D K and Madden P A 1990 *Molecular Physics* **70** 921–966

[69] Galli G and Pasquarello A 1993 First-principles Molecular Dynamics *Computer Simulation in Chemical Physics* ed Allen M P and Tildesley D J (Dordrecht: Springer Netherlands) pp 261–313

[70] Marx D and Hutter J 2012 *Ab initio molecular dynamics: basic theory and advanced methods* first paperback edition ed (Cambridge: Cambridge University Press)

[71] Laidler K J and King M C 1983 *The Journal of Physical Chemistry* **87** 2657–2664

[72] Eyring H 1935 *The Journal of Chemical Physics* **3** 107–115

[73] Truhlar D G, Garrett B C and Klippenstein S J 1996 *The Journal of Physical Chemistry* **100** 12771–12800

[74] Pechukas P 1981 *Annual Review of Physical Chemistry* **32** 159–177

[75] Miller W H 1976 *Dynamics of molecular collisions* (New York: Plenum Press) oCLC: 681088701

[76] Charnley S 2011 Langevin Rate Coefficient *Encyclopedia of Astrobiology* ed Gargaud M, Amils R, Quintanilla J C, Cleaves H J, Irvine W M, Pinti D L and Viso M (Berlin, Heidelberg: Springer Berlin Heidelberg) pp 905–905

[77] Kim B and May G 1994 *IEEE Transactions on Semiconductor Manufacturing* **7** 12–21

[78] Kim B, Lee D W, Park K Y, Choi S R and Choi S 2004 *Vacuum* **76** 37–43

[79] Kim B and Kwon M 2009 *Journal of Materials Processing Technology* **209** 2620–2626

[80] Kim B and Kim S 2010 *Surface Engineering* **26** 224–228

[81] Himmel C and May G 1993 *IEEE Transactions on Semiconductor Manufacturing* **6** 103–111

[82] Rietman E and Lory E 1993 *IEEE Transactions on Semiconductor Manufacturing* **6** 343–347

[83] Han S, Ceiler M, Bidstrup S, Kohl P and May G 1994 *IEEE Transactions on Components, Packaging, and Manufacturing Technology: Part A* **17** 174–182

[84] Stokes D and May G 2000 *IEEE Transactions on Semiconductor Manufacturing* **13** 469–480

[85] Tudoroiu N, Patel R and Khorasani K 2006 *Neurocomputing* **69** 786–802

[86] Rosen I, Parent T, Cooper C, Chen P and Madhukar A 2001 *IEEE Transactions on Control Systems Technology* **9** 271–284

[87] Bhatikar S and Mahajan R 2002 *IEEE Transactions on Semiconductor Manufacturing* **15** 71–78

[88] Chen W, Lee A, Deng W and Liu K 2007 *Expert Systems with Applications* **32** 1148–1153

[89] Ko Y D, Moon P, Kim C E, Ham M H, Myoung J M and Yun I 2009 *Expert Systems with Applications* **36** 4061–4066

[90] Guessasma S, Montavon G and Coddet C 2004 *Computational Materials Science* **29** 315–333

[91] Jean M D, Lin B T and Chou J H 2008 *Journal of the American Ceramic Society* **91** 1539–1547

[92] Choudhury T, Berndt C and Man Z 2015 *Engineering Applications of Artificial Intelligence* **45** 57–70

[93] Krüger F, Gergs T and Trieschmann J 2019 *Plasma Sources Science and Technology* **28** 035002

[94] Kino H, Ikuse K, Dam H C and Hamaguchi S 2021 *Physics of Plasmas* **28** 013504

[95] Leparoux M, Loher M, Schreuders C and Siegmann S 2008 *Powder Technology* **185** 109–115

[96] Wang C, Wang X and He X 2007 Neural Networks Model of Polypropylene Surface Modification by Air Plasma *2007 IEEE International Conference on Automation and Logistics* (Jinan, China: IEEE) pp 20–24

[97] Abd Jelil R, Zeng X, Koehl L and Perwuelz A 2013 *Engineering Applications of Artificial Intelligence* **26** 1854–1864

[98] Rietman E A 1996 *Journal of Vacuum Science & Technology B: Microelectronics and Nanometer Structures* **14** 504

[99] Salam F, Piwek C, Erten G, Grotjohn T and Asmussen J 1997 *IEEE Transactions on Control Systems Technology* **5** 598–613

[100] Molga E 2003 *Chemical Engineering and Processing: Process Intensification* **42** 675–695

[101] Kim B and Park S 2001 *Chemometrics and Intelligent Laboratory Systems* **56** 39–50

[102] Kim B and Bae J 2005 *Solid-State Electronics* **49** 1576–1580

[103] Mesbah A and Graves D B 2019 *Journal of Physics D: Applied Physics* **52** 30LT02

[104] Dral P O, von Lilienfeld O A and Thiel W 2015 *Journal of Chemical Theory and Computation* **11** 2120–2125

[105] Komp E and Valleau S 2020 *The Journal of Physical Chemistry A* **124** 8607–8613

[106] Zhang Y 2009 *Chemometrics and Intelligent Laboratory Systems* **98** 162–172

[107] Hansen K, Montavon G, Biegler F, Fazli S, Rupp M, Scheffler M, von Lilienfeld O A, Tkatchenko A and Müller K R 2013 *Journal of Chemical Theory and Computation* **9** 3404–3419

[108] Goh G B, Hodas N O and Vishnu A 2017 *Journal of Computational Chemistry* **38** 1291–1307

[109] Ventura S, Silva M, Perez-Bendito D and Hervas C 1995 *Analytical Chemistry* **67** 1521–1525

[110] Galván I, Zaldívar J, Hernández H and Molga E 1996 *Computers & Chemical Engineering* **20** 1451–1465

[111] Baş D, Dudak F C and Boyacı H 2007 *Journal of Food Engineering* **79** 622–628

[112] Baş D, Dudak F C and Boyacı H 2007 *Journal of Food Engineering* **79** 1152–1158

[113] Valeh-e Sheyda P, Yaripour F, Moradi G and Saber M 2010 *Industrial & Engineering Chemistry Research* **49** 4620–4626

[114] Tumanov V E and Gaifullin B N 2015 Evaluation of the Rate Constants of Reactions of Phenyl Radicals with Hydrocarbons with the Use of Artificial Neural Network *Current Approaches in Applied Artificial Intelligence* vol 9101 ed Ali M, Kwon Y S, Lee C H, Kim J and Kim Y (Cham: Springer International Publishing) pp 394–403 series Title: Lecture Notes in Computer Science

[115] Allison T C 2016 *The Journal of Physical Chemistry B* **120** 1854–1863

[116] Choi S, Kim Y, Kim J W, Kim Z and Kim W Y 2018 *Chemistry - A European Journal* **24** 12354–12358

[117] Grambow C A, Pattanaik L and Green W H 2020 *The Journal of Physical Chemistry Letters* **11** 2992–2997

[118] Kuang D and Xu B 2018 *Thermochimica Acta* **669** 8–15

[119] Huang Y W, Chen M Q and Li Q H 2019 *Journal of Thermal Analysis and Calorimetry* **138** 451–460

[120] Vieira D and Krems R V 2017 *The Astrophysical Journal* **835** 255

[121] Amato F, González-Hernández J L and Havel J 2012 *Talanta* **93** 72–78

[122] Hanicinec M, Mohr S and Tennyson J 2021 *Plasma Sources Science and Technology* **29** 125024

[123] Lietz A M and Kushner M J 2016 *Journal of Physics D: Applied Physics* **49** 425204

[124] Kokkoris G, Panagiotopoulos A, Goodyear A, Cooke M and Gogolides E 2009 *Journal of Physics D: Applied Physics* **42** 055209

[125] Pancheshnyi S, Eismann B, Hagelaar G and Pitchford L 2008

[126] Turner M M 2016 *Plasma Sources Science and Technology* **25** 015003

[127] Hurlbatt A, Gibson A R, Schröter S, Bredin J, Foote A P S, Grondein P, O'Connell D and Gans T 2017 *Plasma Processes and Polymers* **14** 1600138

[128] Stoffels E, Stoffels W W, Vender D, Haverlag M, Kroesen G M W and de Hoog F J 1995 *Contributions to Plasma Physics* **35** 331–357

[129] Lee C and Lieberman M A 1995 *Journal of Vacuum Science & Technology A: Vacuum, Surfaces, and Films* **13** 368–380

[130] Lieberman M A and Lichtenberg A J 2005 *Principles of plasma discharges and materials processing* 2nd ed (Hoboken, N.J: Wiley-Interscience) oCLC: ocm56752658

[131] Harris C R, Millman K J, van der Walt S J, Gommers R, Virtanen P, Cournapeau D, Wieser E, Taylor J, Berg S, Smith N J, Kern R, Picus M, Hoyer S, van Kerkwijk M H, Brett M, Haldane A, del Río J F, Wiebe M, Peterson P, Gérard-Marchant P, Sheppard K, Reddy T, Weckesser W, Abbasi H, Gohlke C and Oliphant T E 2020 *Nature* **585** 357–362

[132] Jones E, Oliphant T, Peterson P *et al.* 2001–2021 SciPy: Open source scientific tools for Python URL `http://www.scipy.org/`

[133] Shampine L F and Reichelt M W 1997 *SIAM Journal on Scientific Computing* **18** 1–22

[134] Dijkstra E W 1959 *Numerische Mathematik* **1** 269–271

[135] Pollack M 1960 *Operations Research* **8** 733–736

[136] Bellman R 1958 *Quarterly of Applied Mathematics* **16** 87–90

[137] Edmonds J and Karp R M 1972 *Journal of the ACM (JACM)* **19** 248–264

[138] Morris M D 1991 *Technometrics* **33** 161–174

[139] Campolongo F, Cariboni J and Saltelli A 2007 *Environmental Modelling & Software* **22** 1509–1518

[140] Schulz-von der Gathen V, Buck V, Gans T, Knake N, Niemi K, Reuter S, Schaper L and Winter J 2007 *Contributions to Plasma Physics* **47** 510–519

[141] Gordiets B, Ferreira C M, Pinheiro M J and Ricard A 1998 *Plasma Sources Science and Technology* **7** 363–378

[142] Gordiets B, Ferreira C M, Pinheiro M J and Ricard A 1998 *Plasma Sources Science and Technology* **7** 379–388

[143] Murphy A B 2012 *Chemical Physics* **398** 64–72

[144] Colombo V, Ghedini E and Sanibondi P 2009 *Journal of Physics D: Applied Physics* **42** 055213

[145] Sackheim R L 2006 *Journal of Propulsion and Power* **22** 1310–1332

[146] Wang H X, Geng J Y, Chen X, Pan W X and Murphy A B 2010 *Plasma Chemistry and Plasma Processing* **30** 707–731

[147] Ageorges H, Megy S, Chang K, Baronnet J M, Williams J K and Chapman C 1993 *Plasma Chemistry and Plasma Processing* **13** 613–632

[148] Ananthapadmanabhan P, Taylor P R and Zhu W 1999 *Journal of Alloys and Compounds* **287** 126–129

[149] Chang Y, Young R M and Pfender E 1987 *Plasma Chemistry and Plasma Processing* **7** 299–316

[150] Yamamoto H, Kuroda H, Ito M, Ohta T, Takeda K, Ishikawa K, Kondo H, Sekine M and Hori M 2012 *Japanese Journal of Applied Physics* **51** 016202

[151] Nayebpashaee N, Soltanieh M and Kheirandish S 2016 *Materials and Manufacturing Processes* **31** 1192–1200

[152] Oberkofler M, Alegre D, Aumayr F, Brezinsek S, Dittmar T, Dobes K, Douai D, Drenik A, Köppen M, Kruezi U, Linsmeier C, Lungu C, Meisl G, Mozetic M, Porosnicu C, Rohde V and Romanelli S 2015 *Fusion Engineering and Design* **98-99** 1371–1374

[153] Carrasco E, Jiménez-Redondo M, Tanarro I and Herrero V J 2011 *Physical Chemistry Chemical Physics* **13** 19561

[154] Heidner R and Kasper J V 1972 *Chemical Physics Letters* **15** 179–184

[155] Black G, Wise H, Schechter S and Sharpless R L 1974 *The Journal of Chemical Physics* **60** 3526–3536

[156] Nagai H, Takashima S, Hiramatsu M, Hori M and Goto T 2002 *Journal of Applied Physics* **91** 2615–2621

[157] Knoops H C M, Langereis E, van de Sanden M C M and Kessels W M M 2012 *Journal of Vacuum Science & Technology A: Vacuum, Surfaces, and Films* **30** 01A101

[158] Vos M F J, van Straaten G, Kessels W M M E and Mackus A J M 2018 *The Journal of Physical Chemistry C* **122** 22519–22529

[159] Géron A 2019 *Hands-on machine learning with Scikit-Learn, Keras, and TensorFlow: concepts, tools, and techniques to build intelligent systems* second edition ed (Beijing [China] ; Sebastopol, CA: O'Reilly Media, Inc)

[160] Mitchell T M 2013 *Machine learning* nachdr. ed McGraw-Hill series in Computer Science (New York: McGraw-Hill)

[161] Witten I H 2017 *Data mining: practical machine learning tools and techniques* fourth edition ed (Amsterdam: Elsevier)

[162] Domingos P 2012 *Communications of the ACM* **55** 78

[163] Banko M and Brill E 2001 Scaling to very very large corpora for natural language disambiguation *Proceedings of the 39th Annual Meeting on Association for Computational Linguistics - ACL '01* (Toulouse, France: Association for Computational Linguistics) pp 26–33

[164] Halevy A, Norvig P and Pereira F 2009 *IEEE Intelligent Systems* **24** 8–12

[165] Wigner E P 1960 *Communications on Pure and Applied Mathematics* **13** 1–14

[166] Sejnowski T J 2020 *Proceedings of the National Academy of Sciences* **117** 30033–30038

[167] Fabbri M and Moro G 2018 Dow Jones Trading with Deep Learning: The Unreasonable Effectiveness of Recurrent Neural Networks *Proceedings of the 7th International Conference on Data Science, Technology and Applications* (Porto, Portugal: SCITEPRESS - Science and Technology Publications) pp 142–153

[168] Wolpert D H 1996 *Neural Computation* **8** 1341–1390

[169] Pedregosa F, Varoquaux G, Gramfort A, Michel V, Thirion B, Grisel O, Blondel M, Prettenhofer P, Weiss R, Dubourg V, Vanderplas J, Passos A, Cournapeau D, Brucher M, Perrot M and Duchesnay E 2011 *Journal of Machine Learning Research* **12** 2825–2830

[170] Boser B E, Guyon I M and Vapnik V N 1992 A training algorithm for optimal margin classifiers *Proceedings of the fifth annual workshop on Computational learning theory - COLT '92* (Pittsburgh, Pennsylvania, United States: ACM Press) pp 144–152

[171] Breiman L, Friedman J, Olshen R and Stone C J 1983 Classification and regression trees

[172] Breiman L (ed) 1998 *Classification and regression trees* 1st ed (Boca Raton, Fla.: Chapman & Hall/CRC)

[173] Breiman L 2001 *Machine Learning* **45** 5–32

[174] Breiman L 1997 Arcing the edge

[175] Friedman J H 2001 *The Annals of Statistics* **29** 1189–1232 ISSN 00905364

[176] An K and Meng J 2010 Voting-Averaged Combination Method for Regressor Ensemble *Advanced Intelligent Computing Theories and Applications* vol 6215 ed Huang D S, Zhao Z, Bevilacqua V and Figueroa J C (Berlin, Heidelberg: Springer Berlin Heidelberg) pp 540–546 series Title: Lecture Notes in Computer Science

[177] Alwosheel A, van Cranenburgh S and Chorus C G 2018 *Journal of Choice Modelling* **28** 167–182

[178] Kouzis-Loukas D 2016 *Learning Scrapy* (Packt Publishing Ltd)

[179] Woon D E and Herbst E 2009 *The Astrophysical Journal Supplement Series* **185** 273–288

[180] Wakelam V, Smith I W M, Herbst E, Troe J, Geppert W, Linnartz H, Öberg K, Roueff E, Agúndez M, Pernot P, Cuppen H M, Loison J C and Talbi D 2010 *Space Science Reviews* **156** 13–72

[181] Hill C 2020 Pyvalem: Open source python package for parsing, validating, manipulating and interpreting the chemical formulas, quantum states and labels of atoms, ions and small molecules. URL `https://github.com/xnx/pyvalem`

[182] Chase M 1998 *NIST-JANAF Thermochemical Tables, 4th Edition* (American Institute of Physics, -1)

[183] Ruscic B, Pinzon R E, Morton M L, von Laszevski G, Bittner S J, Nijsure S G, Amin K A, Minkoff M and Wagner A F 2004 *The Journal of Physical Chemistry A* **108** 9979–9997

[184] Lu B 2020 Master's thesis University College London United Kingdom

[185] Tipping M E 2001 *J. Mach. Learn. Res.* **1** 211–244 ISSN 1532-4435 URL `https://doi.org/10.1162/15324430152748236`

[186] MacKay D J C 1992 *Neural Computation* **4** 415–447

[187] Russell S J, Norvig P and Davis E 2010 *Artificial intelligence: a modern approach* 3rd ed Prentice Hall series in artificial intelligence (Upper Saddle River: Prentice Hall)

[188] Berrar D 2019 Cross-Validation *Encyclopedia of Bioinformatics and Computational Biology* (Elsevier) pp 542–545

[189] Kluyver T, Ragan-Kelley B, Pérez F, Granger B, Bussonnier M, Frederic J, Kelley K, Hamrick J, Grout J, Corlay S, Ivanov P, Avila D, Abdalla S and Willing C 2016 Jupyter notebooks – a publishing format for reproducible computational workflows *Positioning and Power in Academic Publishing: Players, Agents and Agendas* ed Loizides F and Schmidt B (IOS Press) pp 87 – 90

[190] Harada N, Herbst E and Wakelam V 2010 *The Astrophysical Journal* **721** 1570–1578

[191] Hickson K M, Wakelam V and Loison J C 2016 *Molecular Astrophysics* **3** 1–9

[192] McKinney W *et al.* 2010 Data structures for statistical computing in python *Proceedings of the 9th Python in Science Conference* vol 445 (Austin, TX) pp 51–56

[193] Itikawa Y 2006 *Journal of Physical and Chemical Reference Data* **35** 31–53

[194] Yoon J S, Song M Y, Han J M, Hwang S H, Chang W S, Lee B and Itikawa Y 2008 *Journal of Physical and Chemical Reference Data* **37** 913–931

[195] Smith A C H, Caplinger E, Neynaber R H, Rothe E W and Trujillo S M 1962 *Physical Review* **127** 1647–1649

[196] Tarnovsky V, Deutsch H and Becker K 1997 *International Journal of Mass Spectrometry and Ion Processes* **167-168** 69–78

[197] Hayashi M 1979 *Le Journal de Physique Colloques* **40** C7–45–C7–46

[198] Ehrhardt H, Langhans L, Linder F and Taylor H S 1968 *Physical Review* **173** 222–230

[199] Rauf S and Kushner M J 1999 *Journal of Applied Physics* **85** 3460–3469

[200] Gougousi T, Johnsen R and Golde M 1995 *International Journal of Mass Spectrometry and Ion Processes* **149-150** 131–151

[201] Rogoff G L, Kramer J M and Piejak R B 1986 *IEEE Transactions on Plasma Science* **14** 103–111

[202] Laher R R and Gilmore F R 1990 *Journal of Physical and Chemical Reference Data* **19** 277–305

[203] Ganas P S 1988 *Journal of Applied Physics* **63** 277–279

[204] Kushner M J 2009 *Journal of Physics D: Applied Physics* **42** 194013

[205] Brook E, Harrison M F A and Smith A C H 1978 *Journal of Physics B: Atomic and Molecular Physics* **11** 3115–3132

[206] Hayashi M and Nimura T 1983 *Journal of Applied Physics* **54** 4879–4882

[207] Aydil E S 1993 *Journal of The Electrochemical Society* **140** 1471

[208] Vriens L 1964 *Physics Letters* **8** 260–261

[209] Itikawa Y and Mason N 2005 *Journal of Physical and Chemical Reference Data* **34** 1–22

[210] Hayashi M 1987 Electron Collision Cross-Sections for Molecules Determined from Beam and Swarm Data *Swarm Studies and Inelastic Electron-Molecule Collisions* ed Pitchford L C, McKoy B V, Chutjian A and Trajrnar S (New York, NY: Springer New York) pp 167–187

[211] Deutsch H, Märk T, Tarnovsky V, Becker K, Cornelissen C, Cespiva L and Bonacic-Koutecky V 1994 *International Journal of Mass Spectrometry and Ion Processes* **137** 77–91

[212] Tarnovsky V, Kurunczi P, Rogozhnikov D and Becker K 1993 *International Journal of Mass Spectrometry and Ion Processes* **128** 181–194

[213] Thorsteinsson E G and Gudmundsson J T 2010 *Plasma Sources Science and Technology* **19** 055008

[214] Krishnakumar E and Srivastava S 1992 *International Journal of Mass Spectrometry and Ion Processes* **113** 1–12

[215] Christophorou L G, Olthoff J K and Rao M V V S 1997 *Journal of Physical and Chemical Reference Data* **26** 1–15

[216] Goto M, Nakamura K, Toyoda H and Sugai H 1994 *Japanese Journal of Applied Physics* **33** 3602–3607

[217] Bardsley J N and Wadehra J M 1983 *The Journal of Chemical Physics* **78** 7227–7234

[218] Morgan W L 1992 *Plasma Chemistry and Plasma Processing* **12** 449–476

[219] Zhao S X, Gao F, Wang Y N and Bogaerts A 2012 *Plasma Sources Science and Technology* **21** 025008

[220] Chan C F, Burrell C F and Cooper W S 1983 *Journal of Applied Physics* **54** 6119–6137

[221] Brian J 1990 *Physics Reports* **186** 215–248

[222] Bretagne J, Godart J and Puech V 1982 *Journal of Physics D: Applied Physics* **15** 2205–2225

[223] Yang Y and Kushner M J 2010 *Plasma Sources Science and Technology* **19** 055011

[224] Vasenkov A V, Li X, Oehrlein G S and Kushner M J 2004 *Journal of Vacuum Science & Technology A: Vacuum, Surfaces, and Films* **22** 511

[225] Meeks E 1997 *Journal of The Electrochemical Society* **144** 357

[226] Song S H and Kushner M J 2012 *Plasma Sources Science and Technology* **21** 055028

[227] Burgess D, Zachariah M, Tsang W and Westmoreland P 1995 *Progress in Energy and Combustion Science* **21** 453–529

[228] Harding L B, Guadagnini R and Schatz G C 1993 *The Journal of Physical Chemistry* **97** 5472–5481

[229] Mao M and Bogaerts A 2010 *Journal of Physics D: Applied Physics* **43** 205201

[230] Kushner M J 1993 *Journal of Applied Physics* **74** 6538–6553

[231] Hack W, Wagner H G and Zasypkin A 1994 *Berichte der Bunsengesellschaft für physikalische Chemie* **98** 156–164

[232] Tsai C P, Belanger S M, Kim J T, Lord J R and McFadden D L 1989 *The Journal of Physical Chemistry* **93** 1916–1922

[233] Wang H and Frenklach M 1997 *Combustion and Flame* **110** 173–221

[234] Efremov A, Kim D P and Kim C I 2004 *Vacuum* **75** 237–246

[235] Bradley J N, Whytock D A and Zaleski T A 1973 *Journal of the Chemical Society, Faraday Transactions 1: Physical Chemistry in Condensed Phases* **69** 1251

[236] Voloshin D G, Klopovskiy K S, Mankelevich Y A, Popov N A, Rakhimova T V and Rakhimov A T 2007 *IEEE Transactions on Plasma Science* **35** 1691–1703

[237] Tian C and Vidal C R 1998 *Journal of Physics B: Atomic, Molecular and Optical Physics* **31** 895–909

[238] Font G I, Morgan W L and Mennenga G 2002 *Journal of Applied Physics* **91** 3530–3538

[239] Tinck S and Bogaerts A 2016 *Journal of Physics D: Applied Physics* **49** 195203

[240] Subramonium P and Kushner M J 2002 *Journal of Vacuum Science & Technology A: Vacuum, Surfaces, and Films* **20** 325–334

[241] Tinck S, Boullart W and Bogaerts A 2008 *Journal of Physics D: Applied Physics* **41** 065207

[242] Sommerer T J and Kushner M J 1992 *Journal of Applied Physics* **71** 1654–1673

[243] Almeida D P, Fontes A C and Godinho C F L 1995 *Journal of Physics B: Atomic, Molecular and Optical Physics* **28** 3335–3345

[244] Babcock L M and Streit G E 1981 *The Journal of Chemical Physics* **74** 5700–5706

[245] Mayhew C A and Smith D 1990 *International Journal of Mass Spectrometry and Ion Processes* **100** 737–751

[246] Morris R A, Viggiano A A, Van Doren J M and Paulson J F 1992 *The Journal of Physical Chemistry* **96** 2597–2603

[247] Hickman A P 1979 *The Journal of Chemical Physics* **70** 4872–4878

[248] Shuman N S, Wiens J P, Miller T M and Viggiano A A 2014 *The Journal of Chemical Physics* **140** 224309

[249] Eckstrom D J, Nakano H H, Lorents D C, Rothem T, Betts J A, Lainhart M E, Triebes K J and Dakin D A 1988 *Journal of Applied Physics* **64** 1691–1695

[250] Banks P 1966 *Planetary and Space Science* **14** 1085–1103

[251] Choi S J and Kushner M J 1993 *Applied Physics Letters* **62** 2197–2199

[252] Geltman S 1973 *Journal of Quantitative Spectroscopy and Radiative Transfer* **13** 601–613

[253] Nakamura Y 2010 *Journal of Physics D: Applied Physics* **43** 365201

[254] Henry R J W, Burke P G and Sinfailam A L 1969 *Physical Review* **178** 218–225

[255] Phelps A V and Pitchford L C 1985 *Physical Review A* **31** 2932–2949

[256] Chutjian A, Cartwright D C and Trajmar S 1977 *Physical Review A* **16** 1052–1060

[257] Chatham H, Hils D, Robertson R and Gallagher A 1984 *The Journal of Chemical Physics* **81** 1770–1777

[258] Kushner M J 1988 *Journal of Applied Physics* **63** 2532–2551

[259] Snoeckx R, Aerts R, Tu X and Bogaerts A 2013 *The Journal of Physical Chemistry C* **117** 4957–4970

[260] Winters H F 1975 *The Journal of Chemical Physics* **63** 3462–3466

[261] Nicholas J E, Spiers A I and Martin N A 1986 *Plasma Chemistry and Plasma Processing* **6** 39–51

[262] Pagsberg P B, Eriksen J and Christensen H C 1979 *The Journal of Physical Chemistry* **83** 582–590

[263] Moreau N, Pasquiers S, Blin-Simiand N, Magne L, Jorand F, Postel C and Vacher J R 2010 *Journal of Physics D: Applied Physics* **43** 285201

[264] Teng L and Winkler C A 1973 *Canadian Journal of Chemistry* **51** 3771–3773

[265] Pintassilgo C D, Jaoul C, Loureiro J, Belmonte T and Czerwiec T 2007 *Journal of Physics D: Applied Physics* **40** 3620–3632

[266] Dorai R and Kushner M J 2003 *Journal of Physics D: Applied Physics* **36** 666–685

[267] Rohrig M and Wagner H G 1994 *Berichte der Bunsengesellschaft fur Physikalische Chemie* **98** 858–863

[268] Corchado J C and Espinosa-Garcia J 1997 *The Journal of Chemical Physics* **106** 4013–4021

[269] Gehring V M, Hoyermann K, Wagner H G and Wolfram J 1971 *Berichte der Bunsengesellschaft für physikalische Chemie* **75** 1287–1294

[270] Vaghjiani G L 1995 *International Journal of Chemical Kinetics* **27** 777–790

[271] Yoshimura M, Tamura F, Koshi M and Matsui H 1990 *NIPPON KAGAKU KAISHI* 589–593

[272] Laufer A H and Fahr A 2004 *Chemical Reviews* **104** 2813–2832

[273] Xu Z F, Fang D C and Fu X Y 1997 *Chemical Physics Letters* **275** 386–391

[274] Stothard N, Humpfer R and Grotheer H H 1995 *Chemical Physics Letters* **240** 474–480

[275] Zhen-Feng X, De-Cai F and Xiao-Yuan F 1998 *International Journal of Quantum Chemistry* **70** 321–329

[276] Stief L J 1970 *The Journal of Chemical Physics* **52** 4841–4845

[277] Meaburn G M and Gordon S 1968 *The Journal of Physical Chemistry* **72** 1592–1598

[278] Linder D P, Duan X and Page M 1996 *The Journal of Chemical Physics* **104** 6298–6307

[279] Schiavello M and Volpi G G 1962 *The Journal of Chemical Physics* **37** 1510–1513

[280] Hamden M 1989 *Rapid Communications in Mass Spectrometry* **3** iii–iii

[281] Arakoni R A, Bhoj A N and Kushner M J 2007 *Journal of Physics D: Applied Physics* **40** 2476–2490

[282] Kushner M J 1992 *Journal of Applied Physics* **71** 4173–4189

[283] Zetzsch C and Stuhl F 1981 *Berichte der Bunsengesellschaft für physikalische Chemie* **85** 564–568

[284] Tachibana K 1986 *Physical Review A* **34** 1007–1015

[285] Gedeon V, Gedeon S, Lazur V, Nagy E, Zatsarinny O and Bartschat K 2014 *Physical Review A* **89** 052713

[286] Josić L, Wróblewski T, Petrović Z, Mechlińska-Drewko J and Karwasz G 2001 *Chemical Physics Letters* **350** 318–324

[287] McFarland R H and Kinney J D 1965 *Physical Review* **137** A1058–A1061

[288] Meeks E, Larson R S, Ho P, Apblett C, Han S M, Edelberg E and Aydil E S 1998 *Journal of Vacuum Science & Technology A: Vacuum, Surfaces, and Films* **16** 544–563

[289] Lindsay B G, Mangan M A, Straub H C and Stebbings R F 2000 *The Journal of Chemical Physics* **112** 9404–9410

[290] Hamilton J R, Tennyson J, Huang S and Kushner M J 2017 *Plasma Sources Science and Technology* **26** 065010

[291] Greenberg K E and Verdeyen J T 1985 *Journal of Applied Physics* **57** 1596–1601

[292] Stafford D S and Kushner M J 2004 *Journal of Applied Physics* **96** 2451–2465

[293] Thielen K and Roth P 1986 *AIAA Journal* **24** 1102–1105

[294] Huang S, Volynets V, Hamilton J R, Lee S, Song I C, Lu S, Tennyson J and Kushner M J 2017 *Journal of Vacuum Science & Technology A: Vacuum, Surfaces, and Films* **35** 031302

[295] Lloyd A C 1971 *International Journal of Chemical Kinetics* **3** 39–68

[296] Tsang W and Herron J T 1991 *Journal of Physical and Chemical Reference Data* **20** 609–663

[297] Doroshchenko V, Kudriavtsev N, Sukhov A and Shamshev D 1992 *Chemical Physics Letters* **193** 258–260

[298] Atkinson R, Baulch D L, Cox R A, Hampson R F, Kerr J A, Rossi M J and Troe J 1997 *Journal of Physical and Chemical Reference Data* **26** 521–1011

[299] Young R A, Black G and Slanger T G 1968 *The Journal of Chemical Physics* **49** 4758–4768

[300] Sorokin V I, Gritsan N P and Chichinin A I 1998 *The Journal of Chemical Physics* **108** 8995–9003

[301] González M, Miquel I and Sayós R 2001 *Chemical Physics Letters* **335** 339–347

[302] Person J C and Ham D O 1988 *International Journal of Radiation Applications and Instrumentation. Part C. Radiation Physics and Chemistry* **31** 1–8

[303] Herron J T 1999 *Journal of Physical and Chemical Reference Data* **28** 1453–1483

[304] King D L, Piper L G and Setser D W 1977 *Journal of the Chemical Society, Faraday Transactions 2* **73** 177

[305] Cheah C T, Clyne M A A and Whitefield P D 1980 *J. Chem. Soc., Faraday Trans. 2* **76** 711–728

[306] Benson S W and Axworthy A E 1957 *The Journal of Chemical Physics* **26** 1718–1726

[307] Stief L J, Payne W A, Lee J H and Michael J V 1979 *The Journal of Chemical Physics* **70** 5241–5243

[308] Barreto P R, Vilela A F, Gargano R, Ramalho S S and Salviano L R 2006 *Journal of Molecular Structure: THEOCHEM* **769** 201–205

[309] Weiller B H, Heidner R F, Holloway J S and Koffend J B 1992 *The Journal of Physical Chemistry* **96** 9321–9328

[310] Corbin W and Levy J B 1975 *International Journal of Chemical Kinetics* **7** 679–688

[311] Rauf S and Kushner M J 1997 *Journal of Applied Physics* **82** 2805–2813

[312] González M, Sayós R and Valero R 2002 *Chemical Physics Letters* **355** 123–132

[313] Bogaerts A 2009 *Spectrochimica Acta Part B: Atomic Spectroscopy* **64** 1266–1279

[314] Moravej M, Yang X, Barankin M, Penelon J, Babayan S E and Hicks R F 2006 *Plasma Sources Science and Technology* **15** 204–210

[315] Anicich V G 1993 *Journal of Physical and Chemical Reference Data* **22** 1469–1569

[316] Smith D, Adams N G and Miller T M 1978 *The Journal of Chemical Physics* **69** 308

[317] Hamdan M, Copp N, Birkinshaw K, Jones J and Twiddy N 1986 *International Journal of Mass Spectrometry and Ion Processes* **69** 191–195

[318] Armentrout P, Berman D and Beauchamp J 1978 *Chemical Physics Letters* **53** 255–259

[319] Johnsen R and Biondi M A 1980 *The Journal of Chemical Physics* **73** 190–193

[320] Snuggs R M, Volz D J, Gatland I R, Schummers J H, Martin D W and McDaniel E W 1971 *Physical Review A* **3** 487–493

[321] Motapon O, Fifirig M, Florescu A, Tamo F O W, Crumeyrolle O, Varin-Bréant G, Bultel A, Vervisch P, Tennyson J and Schneider I F 2006 *Plasma Sources Science and Technology* **15** 23–32

[322] Olson R E, Peterson J R and Moseley J 1970 *The Journal of Chemical Physics* **53** 3391–3397

[323] Gordiets B, Ferreira C, Guerra V, Loureiro J, Nahorny J, Pagnon D, Touzeau M and Vialle M 1995 *IEEE Transactions on Plasma Science* **23** 750–768

[324] Koffend J B, Gardner C E and Heidner R F 1985 *The Journal of Chemical Physics* **83** 2904–2912